Geologic Studies in Alaska by the U.S. Geological Survey, 1993

U.S. GEOLOGICAL SURVEY BULLETIN 2107

AVAILABILITY OF BOOKS AND MAPS OF THE U.S. GEOLOGICAL SURVEY

Instructions on ordering publications of the U.S. Geological Survey, along with prices of the last offerings, are given in the current-year issues of the monthly catalog "New Publications of the U.S. Geological Survey." Prices of available U.S. Geological Survey publications released prior to the current year are listed in the most recent annual "Price and Availability List." Publications that are listed in various U.S. Geological Survey catalogs (**see back inside cover**) but not listed in the most recent annual "Price and Availability List" are no longer available.

Reports released through the NTIS may be obtained by writing to the National Technical Information Service, U.S. Department of Commerce, Springfield, VA 22161; please include NTIS report number with inquiry.

Order U.S. Geological Survey publications **by mail** or **over the counter** from the offices given below.

BY MAIL

Books

Professional Papers, Bulletins, Water-Supply Papers, Techniques of Water-Resources Investigations, Circulars, publications of general interest (such as leaflets, pamphlets, booklets), single copies of Earthquakes & Volcanoes, Preliminary Determination of Epicenters, and some miscellaneous reports, including some of the foregoing series that have gone out of print at the Superintendent of Documents, are obtainable by mail from

U.S. Geological Survey, Information Services
Box 25286, Federal Center
Denver, CO 80225

Subscriptions to periodicals (Earthquakes & Volcanoes and Preliminary Determination of Epicenters) can be obtained ONLY from the

Superintendent of Documents
Government Printing Office
Washington, DC 20402

(Check or money order must be payable to Superintendent of Documents.)

Maps

For maps, address mail orders to

U.S. Geological Survey, Map Distribution
Box 25286, Bldg. 810, Federal Center
Denver, CO 80225

Residents of Alaska may order maps from

U.S. Geological Survey, Earth Science Information Center
101 Twelfth Ave., Box 12
Fairbanks, AK 99701

OVER THE COUNTER

Books and Maps

Books and maps of the U.S. Geological Survey are available over the counter at the following U.S. Geological Survey offices, all of which are authorized agents of the Superintendent of Documents.

- **ANCHORAGE, Alaska**—4230 University Dr., Rm. 101
- **LAKEWOOD, Colorado**—Federal Center, Bldg. 810
- **MENLO PARK, California**—Bldg. 3, Rm. 3128, 345 Middlefield Rd.
- **RESTON, Virginia**—National Center, Rm. 1C402, 12201 Sunrise Valley Dr.
- **SALT LAKE CITY, Utah**—Federal Bldg., Rm. 8105, 125 South State St.
- **SPOKANE, Washington**—U.S. Post Office Bldg., Rm. 135, W. 904 Riverside Ave.
- **WASHINGTON, D.C.**—Main Interior Bldg., Rm. 2650, 18th and C Sts., NW.

Maps Only

Maps may be purchased over the counter at the U.S. Geological Survey offices:

- **FAIRBANKS, Alaska**—New Federal Building, 101 Twelfth Ave.
- **ROLLA, Missouri**—1400 Independence Rd.
- **STENNIS SPACE CENTER, Mississippi**—Bldg. 3101

Geologic Studies in Alaska by the U.S. Geological Survey, 1993

Alison B. Till *and* Thomas E. Moore, *Editors*

U.S. GEOLOGICAL SURVEY BULLETIN 2107

UNITED STATES GOVERNMENT PRINTING OFFICE, WASHINGTON : 1994

U.S. DEPARTMENT OF THE INTERIOR
BRUCE BABBITT, Secretary

U.S. GEOLOGICAL SURVEY
Gordon P. Eaton, Director

For sale by
U.S. Geological Survey, Map Distribution
Box 25286, MS 306, Federal Center
Denver, CO 80225

Any use of trade, product, or firm names in this publication is for descriptive purposes only and does not imply endorsement by the U.S. Government.

COVER: Dead trees at tidewater, Kenai Fjords National Park, south-central Alaska. Trees died as a result of land subsidence during the 1964 Alaska earthquake. Photograph by Alison B. Till.

CONTENTS

Introduction
Alison B. Till and Thomas E. Moore, Editors 1

ENVIRONMENT AND CLIMATE

Mercury in the environment and its implications, Kuskokwim River region, southwestern Alaska
John Gray, Peter Theodorakos, Jim Budahn, and Richard O'Leary 3

High arsenic content in sediments from the Koyukuk National Wildlife Refuge, west-central Alaska
Robert G. Eppinger, J.M. Motooka, and S.J. Sutley 15

Environmental geochemistry of mesothermal gold deposits, Kenai Fjords National Park, south-central Alaska
Barrett A. Cieutat, Richard J. Goldfarb, J. Carter Borden, John McHugh, and Cliff D. Taylor 21

Paleowind directions for late Holocene dunes on the western Arctic coastal plain, northern Alaska
John P. Galloway and L. David Carter 27

Methane in the Fox Permafrost Tunnel near Fairbanks, Alaska
Keith A. Kvenvolden, Thomas D. Lorenson, and Valerie Barber 31

HAZARDS AND RELATED STUDIES

The 1993 Nelson Mountain Landslide, Chitina Valley, southern Alaska, an aerial view
Lynn A. Yehle and Danny Rosenkrans 39

Importance of landslides in the geomorphic development of the upper Caribou Creek area, Talkeetna Mountains, Alaska
Steven W. Nelson 43

Possible active fault traces on or near the Castle Mountain Fault between Houston and the Hatcher Pass Road
Peter J. Haeussler 49

High stand and catastrophic draining of intracaldera Surprise Lake, Aniakchak volcano, Alaska
R.G. McGimsey, C.F. Waythomas, and C.A. Neal 59

RESOURCES

Isotopic constraints on the genesis of base-metal-bearing mineral occurrences near Columbia Glacier, Northern Prince William Sound, Alaska
Richard J. Goldfarb, Carol A. Gent, John E. Gray, and Steven W. Nelson 73

Gold in heavy-mineral-concentrate samples from the Howard Pass quadrangle, Brooks Range, Alaska
K.D. Kelley, E.A. Bailey, B.A. Cieutat, and J.C. Borden 83

RESOURCES—*Continued*

Calculated gold resource in Circle and Fortymile placers
Warren Yeend 91

Miocene coal-bearing strata of the Tyonek Formation: braided-stream deposits in the Chuit Creek-Chuitna River drainage basin, southern Alaska
R.M. Flores, G.D. Stricker, and S.B. Roberts 95

GEOLOGIC FRAMEWORK

Preliminary results of a tectonic subsidence analysis of the central North Slope, Alaska
Frances Cole, Kenneth Bird, and David Howell 115

Cyrtospirifer from Upper Devonian rocks of the Endicott Group, west-central Brooks Range, Alaska
J. Thomas Dutro, Jr., Robert B. Blodgett, and Charles G. Mull 133

New Late(?) Proterozoic-age formations in the vicinity of Lone Mountain, McGrath quadrangle, west-central Alaska
Loren E. Babcock, Robert B. Blodgett, and James St. John 143

Possible occurrence of lower to middle Paleozoic rocks south of the Denali fault, Denali National Park, Alaska, and implications for Denali fault displacement
Béla Csejtey, Jr., Phil F. Brease, Arthur B. Ford, and Willis H. Nelson 157

Chemical characteristics of major plutonic belts of the Coast plutonic-metamorphic complex near Juneau, southeastern Alaska
James L. Drinkwater, David A. Brew, and Arthur B. Ford 161

Geochemical reconnaissance of alkalic plutons on Prince of Wales Island, southeastern Alaska
James L. Drinkwater and James P. Calzia 173

Evaluation and application of garnet amphibolite thermobarometry, western metamorphic belt near Juneau, Alaska
Glen R. Himmelberg, David A. Brew, and Arthur B. Ford 185

METHODS

GPS versus template—Simple field and office experiments concerning GPS-determined positions and template-scaled map locations
David A. Brew, Arthur B. Ford, Richard D. Koch, Michael F. Diggles, James L. Drinkwater, Robert A. Loney, and James G. Smith 199

BIBLIOGRAPHIES

U.S. Geological Survey reports on Alaska released in 1993
Ellen R. White 207

Reports about Alaska in non-USGS publications released in 1993 that include USGS authors
Ellen R. White 211

CONTRIBUTORS TO THIS BULLETIN

Anchorage

U.S. Geological Survey
4200 University Drive
Anchorage, Alaska 99508-4667

Bailey, E.A.
Carter, L. David
Haeussler, Peter J.
McGimsey, Robert G.
Neal, C.A.
Nelson, Steven W.
Waythomas, C.F.

Denver

U.S. Geological Survey MS-
Box 25046 Denver Federal Center
Lakewood, Colorado 80225-0046

Borden, J. Carter MS 973
Budahn, Jim MS 424
Cieutat, Barrett A. MS 973
Eppinger, Robert G. MS 973
Flores, Romeo M. MS 972
Gent, Carol A. MS 973
Goldfarb, Richard J. MS 973
Gray, John E. MS 973
Kelley, K.D. MS 973
McHugh, John MS 973
Motooka, J.M. MS 973
O'Leary, Richard MS 973
Roberts, S.B. MS 972
Stricker, Gary D. MS 972
Sutley, S. MS 973
Taylor, Cliff D., MS 973
Theodorakos, Peter M. MS 973
Yehle, Lynn A. MS 966

Menlo Park

U.S. Geological Survey
345 Middlefield Rd.
Menlo Park, California 94025

Barber, Valerie MS 999
Bird, Kenneth J. MS 999
Brew, David A. MS 904
Calzia, James P. MS 901
Cole, Frances MS 955
Csejtey, Béla MS 904
Diggles, Michael F. MS 901
Drinkwater, James L. MS 904
Ford, Arthur B. MS 904
Galloway, John P. MS 904

Menlo Park—Continued

Howell, David G., MS 902
Koch, Richard D. MS 904
Kvenvolden, Keith A. MS 999
Loney, Robert A. MS 904
Lorenson, Thomas D. MS 999
Nelson, Willis H. MS 904
Smith, James G. MS 910
White, Ellen R. MS 955
Yeend, Warren MS 904

Reston

U.S. Geological Survey
National Center, MS-
12201 Sunrise Valley Drive
Reston, Virginia 22092

Blodgett, Robert. MS 970

Others

Babcock, Loren E.
Department of Geological Sciences
Orton Hall
The Ohio State University
155 S. Oval Mall
Columbus, Ohio 43210

Brease, Phil F.
Denali National Park and Preserve
P.O. Box 9
Denali Park, Alaska 99755

Dutro, J. Thomas, Jr.
U.S. Geological Survey
Rm E308, Museum of Natural History, MRC-137
10th and Constitution NW
Washington, D.C. 20560

Himmelberg, G.R.
Department of Geological Sciences
University of Missouri-Columbia
Columbia, MO 65211

Mull, Charles G.
Alaska State Division of Geologic and Geophysical Surveys
794 University Avenue Suite 200
Fairbanks, Alaska 99709

Rosenkrans, Danny
Wrangell-St. Elias National Park and Preserve
P.O. Box 29
Glenallen, Alaska 99588

Geologic Studies in Alaska by the U.S. Geological Survey, 1993

Alison B. Till *and* Thomas E. Moore, *Editors*

INTRODUCTION

This collection of 19 papers continues the annual series of U.S. Geological Survey reports on geologic investigations in Alaska. Contributions include 14 *Articles* and 5 shorter *Geologic Notes* that report results from all corners of the State.

USGS activities in Alaska cover a broad spectrum of earth science topics, including the environment, hazards, resources, and geologic framework studies. Three articles focus on the environmental geochemistry of parts of south-central, west-central, and southwestern Alaska. An article on methane released from permafrost near Fairbanks and a note on paleowind direction indicators on the Arctic coastal plain contribute to ongoing climate and paleoclimate investigations. Landslide hazards in the Talkeetna Mountains and Wrangell-St. Elias National Park are discussed in two notes. Possible active fault traces near Alaska's main population center are described in an article on the Castle Mountain fault. An article on Aniakchak volcano presents evidence for a previously unrecognized catastrophic flooding event. Resources and resource assessment on gold, base metals, and coal are discussed in several articles and a note. Geologic framework studies cover tectonics, paleontology, stratigraphy, and metamorphic petrology. One contribution involves field methods; it evaluates the relative accuracy of global positioning systems and topographic map-based methods for deriving location data for field stations.

Two bibliographies at the end of the volume list reports about Alaska in USGS publications released in 1993 and reports about Alaska by USGS authors in non-USGS publications in 1993.

Manuscript approved for publication July 19, 1994.

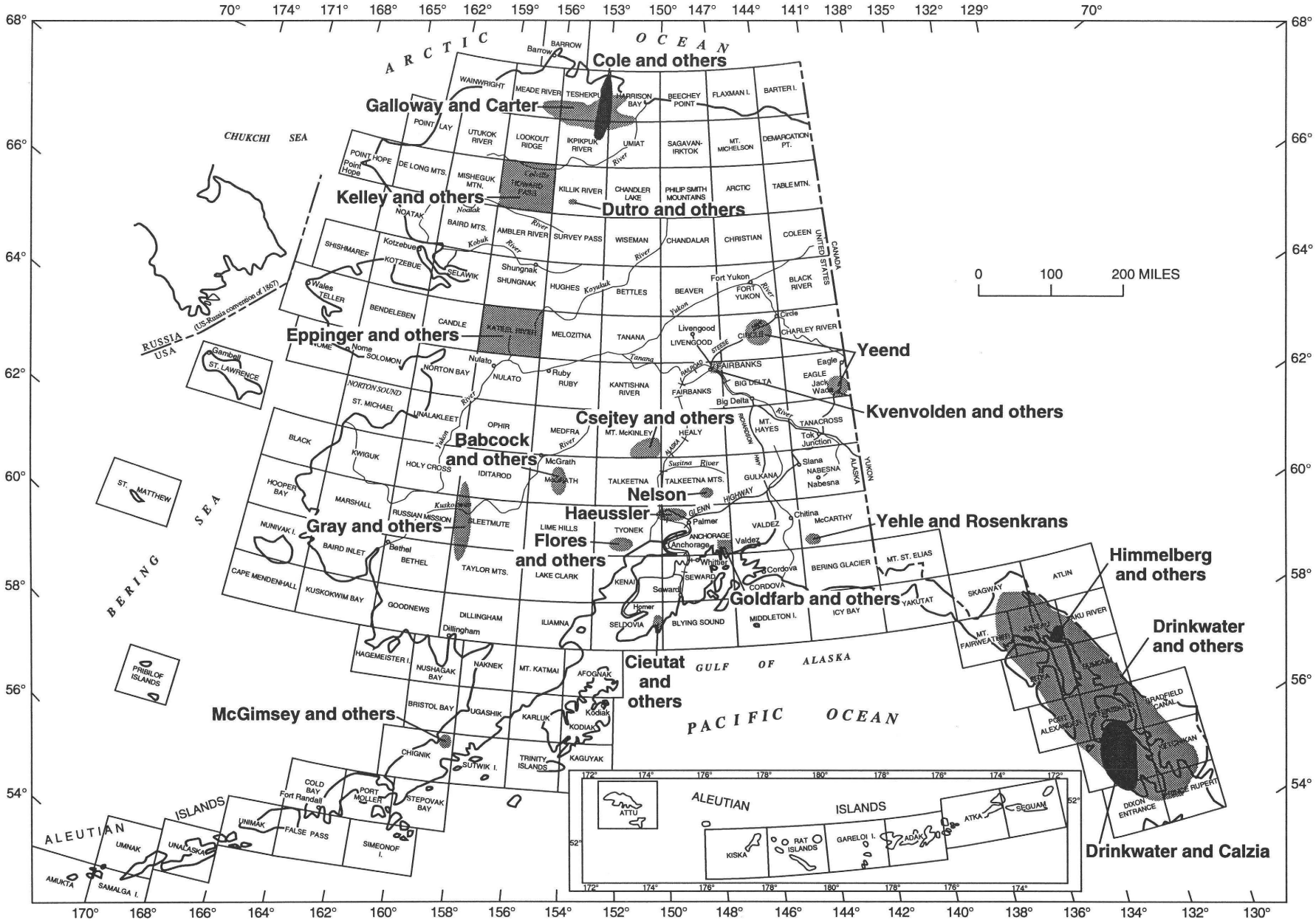

Figure 1. Index map of Alaska showing 1:250,000-scale quadrangles and locations of study areas discussed in this bulletin.

Mercury in the Environment and Its Implications, Kuskokwim River Region, Southwestern Alaska

By John Gray, Peter Theodorakos, Jim Budahn, *and* Richard O'Leary

ABSTRACT

Potential mercury contamination was evaluated downstream from an abandoned mercury mine and a site downstream from placer mines in the Kuskokwim River region of southwestern Alaska. Mercury and other heavy-metal concentrations were measured in liver, muscle, and whole fish samples of Arctic grayling, as well as in stream-sediment, heavy-mineral-concentrate, and stream-water samples. Results indicate that mercury is most concentrated in samples collected below the mercury mine, where stream-sediment samples contain in excess of 36 ppm and samples of muscle and whole fish from Arctic grayling range from 0.24 to 0.55 ppm wet weight. Mercury concentrations in whole fish and muscle samples of grayling collected downstream from placer mines range from 0.067 to 0.30 ppm wet weight. Although mercury concentrations in fish are elevated with respect to those in fish from a control site, the mercury concentrations in fish samples do not exceed the Food and Drug Administration (FDA) action level of 1 ppm wet weight for edible fish. Results for other heavy-metals in samples collected in this study are not in concentrations high enough to be of concern.

INTRODUCTION

Major mineral commodities in the Kuskokwim River region of southwestern Alaska are gold, silver, and mercury. Most of the gold and silver have been recovered from placer mines, some of which are presently operating. Numerous epithermal mercury-rich vein deposits are scattered over several thousand square kilometers in southwestern Alaska. Ore mineralogy is dominated by cinnabar, but stibnite, realgar, orpiment, native mercury, pyrite, limonite, hematite, and gold are found locally (Sainsbury and MacKevett, 1965; Gray and others, 1990). Vein gangue is typically quartz, carbonate, and dickite. Several of the mercury deposits have been developed into mines. The Red Devil mine, located about 6 miles (10 km) northwest of Sleetmute, is the largest mercury deposit in Alaska; about 36,000 flasks of mercury (1 flask = 76 lbs or 34.5 kg) have been recovered from Red Devil (Miller and others, 1989). However, other mercury mines developed in the region are much smaller, for example the Cinnabar Creek mine, that produced several hundred flasks (Sainsbury and MacKevett, 1965). Total mercury production in southwestern Alaska is about 41,000 flasks (Bundtzen and others, 1986), but no mercury mines are currently operating.

Although the region has been exploited for gold, silver, and mercury, few studies have been conducted in the region to evaluate the environmental impact of toxic compounds related to surface weathering of naturally occurring mineral deposits, mercury mining, or placer mining activity. Due to the presence of numerous mercury-rich deposits in the region, evaluation of potential hazards related to environmental mercury contamination is of primary concern to inhabitants in the area; other heavy metals are of lesser concern, but are still important.

Mercury is a heavy-metal pollutant of great concern that can be life threatening to humans and aquatic organisms when concentrations are high. Most forms of mercury are poisonous to some degree; however, most mercury toxicity problems are related to organic mercury compounds (Eisler, 1987; Baeyens, 1992), methylmercury being the most toxic to humans (Friberg and Vostal, 1972). Methylmercury is volatile, water soluble, and accumulates in tissues of fish and other aquatic organisms (Fenchel and Blackburn, 1979; Manahan, 1991). Various forms of mercury in the aquatic environment are converted into mercuric ion and then methylated (Manahan, 1991). Conversion to methylmercury is largely dependent on biological processes and may be produced by aerobic or anaerobic bacteria (Wood, 1974). Concentration of methylmercury in fish provides an easy pathway for mercury to enter the food chain.

One of the most extreme cases of acute mercury toxicity occurred in the 1950's at Minamata, Japan, and resulted in the poisoning of hundreds and the death of numerous persons who ate mercury-contaminated fish and shellfish (Irukayama, 1967; Manahan, 1991). These mercury contaminants were associated with the effluent from a local chemical factory (Kurland and others, 1960). More recently, over 60 persons in the Amazon region of Brazil were found to have mercury concentrations above the 6-ppm limit in humans set by the World Health Organization (World Press Review, 1993). In addition, fish collected in this area contain up to 2.7 ppm mercury (Pfeiffer and others, 1989; Nriagu and others, 1992). Mercury contamination in the Amazon region is related to the use of native mercury for gold amalgamation in placer mining. Estimates indicate that from 1980 to 1992, over 2,000 tons of mercury contaminated watersheds in the Amazon region (World Press Review, 1993). Mercury contaminated freshwater fish and airborne mercury vapor pollution related to amalgam roasting are known in the Amazon region (Nriagu and others, 1992). In both the Minamata and Amazon region cases, a major part of the mercury poisoning was directly linked to the consumption of mercury-contaminated fish. The widespread occurrence of mercury deposits and placer mining in southwestern Alaska suggest that concentrations of mercury should be investigated in several sample media.

The objective of this study is to (1) report concentrations of mercury and other heavy-metals in fish, stream-sediment, heavy-mineral-concentrate, and stream-water samples collected downstream from an abandoned mercury mine, gold-placer mines, and a control site, and (2) evaluate the effects of possible metal toxicity on the food chain at these sites. This study is an important outgrowth of the U.S. Geological Survey's Alaska Mineral Resource Assessment Program (AMRAP) in southwestern Alaska that was undertaken to examine how mineral deposits in the region affect the environment.

STUDY AREAS AND SAMPLE COLLECTION

Sites selected for study included (1) Cinnabar Creek, located in the northwestern Taylor Mountains quadrangle about 60 miles (100 km) southeast of Aniak, (2) Crooked Creek, located in the western Sleetmute quadrangle about 50 miles (80 km) northwest of Aniak, and (3) a site on the Buckstock River about 30 miles (50 km) southeast of Aniak (fig. 1). Samples collected for study included fish, stream-sediment, heavy-mineral-concentrate, and stream-water. All samples were collected from the active stream channel. Fish samples collected included whole fish, fish muscle (edible fillets), and fish livers. Fish collected were Arctic grayling (Thymallus arcticus) because this species was the primary freshwater fish observed at the sites studied.

CINNABAR CREEK

Cinnabar Creek was selected for study because the abandoned Cinnabar Creek mercury mine is located upstream. This has been a site of previous geochemical studies (Gray and others, 1991) and is ideal for the present study due to its proximity to the mercury mine. For this study, fish were collected from two sites on Cinnabar Creek to address possible metal contamination. All of the Arctic grayling collected from Cinnabar Creek were small, weighing less than 45 grams (table 1). The first site was about 1 mile (1.6 km) downstream from the mine and second site was about 3 miles (4.8 km) from the mine. Muscle samples were collected from two fish from the second site. Liver samples were not collected from Cinnabar Creek due to the small size of the fish.

Geochemical and mineralogical dispersion was previously studied on Cinnabar Creek (Gray and others, 1991). In their study, stream-sediment, heavy-mineral-concentrate, and stream-water samples were collected from six sites downstream from the Cinnabar Creek mine; these sample sites were located about 0.8, 1.3, 1.8, 2.9, 3.6, and 4.3 miles from the mine. Geochemical and mineralogical results from these samples were evaluated for this study.

CROOKED CREEK

Two sites were studied on Crooked Creek, located about 5 and 8 miles (8 and 13 km) below the placer mining in the Donlin Creek area (fig. 1). Placer gold mining has been conducted in this area since 1910; placer gold has been recovered from several drainages and placer mining is ongoing at Snow Gulch (Cady and others, 1955; Bundtzen and others, 1988). All of these drainages are upstream from Crooked Creek (fig. 1). This creek was chosen for study because placer cinnabar has been reported in heavy-mineral concentrates from placer mines in the area (Cady and others, 1955); in addition, native mercury was commonly used for placer gold recovery in Alaska in the early 1900's (Smith and Maddren, 1915) and was probably used during placer mining in the Donlin Creek area. One stream-sediment, heavy-mineral-concentrate, and stream-water sample was collected from each site. Nine Arctic grayling were sampled from both localities; five grayling from each site were dissected and liver and muscle samples were collected.

BUCKSTOCK RIVER

A baseline or control site was selected on the Buckstock River for the study because no mercury sources are known upstream. One stream-sediment, heavy-mineral-concentrate, and stream-water sample was collected from this site; in addition, 11 Arctic grayling were collected. Five Arctic grayling were dissected for fish muscle and liver samples.

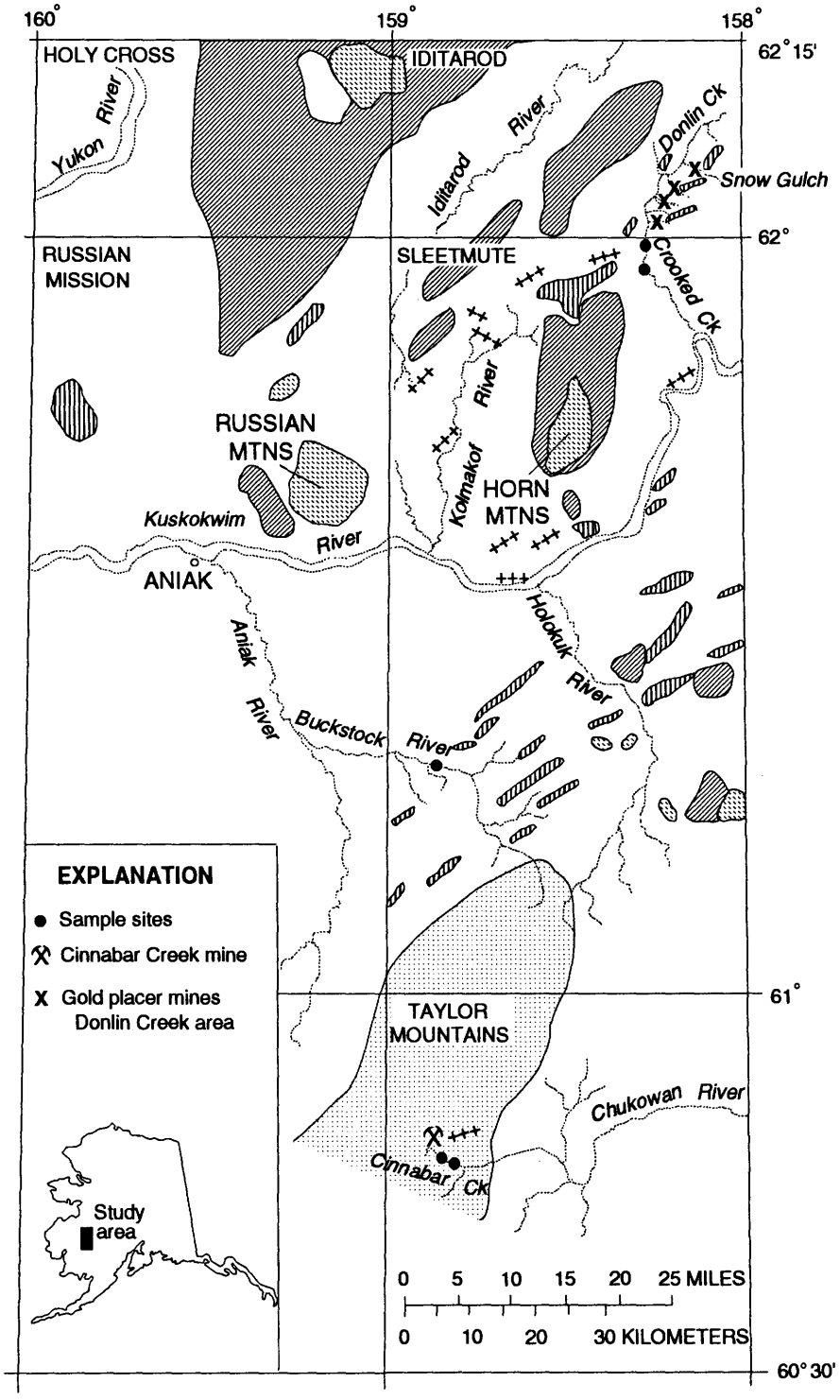

Figure 1. Location map of study area. Geology generalized from Cady and others (1955), Hoare and Coonrad (1959), Miller and others (1989), and Miller and Bundtzen (1994).

EXPLANATION

- Kuskokwim Group (Cretaceous)--Sedimentary rocks
- Granite porphyry (Tertiary and Late Cretaceous)
- Mafic to felsic volcanic rocks (Tertiary and Late Cretaceous)
- Intermediate to felsic intrusive rocks (Tertiary and Late Cretaceous)
- +++ Intermediate to mafic dikes (Tertiary and Late Cretaceous)
- Gemuk Group (Cretaceous and Triassic)--Sedimentary and volcanic rocks

Table 1. Data for Arctic grayling collected from the Buckstock River (BR), Crooked Creek (CR), and Cinnabar Creek (CC).

[Analysis of Hg by cold-vapor atomic absorption spectrophotometry (CVAAS); Pb, Cu, Ag, and Sn by inductively coupled plasma-mass spectrometry (ICP-MS); and As, Cd, Zn, Cr, Ni, and Se by instrumental neutron activation analysis (INAA); concentrations are in parts per million wet weight; methylmercury values are given in parentheses; n.d., not determined]

Sample	Tissue	Wet weight	Condition factor (K)[1]	Percent moisture	Hg		As	Cd	Pb	Zn	Cu	Cr	Ni	Ag	Se	Sn
BR1F01M	muscle	159 g	1.04	72	0.084		<0.1	<0.25	<0.3	15	<1	0.1	<0.5	<0.2	1.1	<1
BR1F02M	muscle	115	.771	74	.10		n.d.	n.d.	n.d.	n.d.	n.d.	n.d.	n.d.	n.d.	n.d.	n.d.
BR1F03M	muscle	108	.771	73	.068		n.d.	n.d.	n.d.	n.d.	n.d.	n.d.	n.d.	n.d.	n.d.	n.d.
BR1F05M	muscle	223	.975	68	.077	(0.074)	< .1	< .25	< .3	12	<1	< .1	< .5	< .2	1.6	<1
BR1F10M	muscle	151	1.02	77	.071		n.d.	n.d.	n.d.	n.d.	n.d.	n.d.	n.d.	n.d.	n.d.	n.d.
BR1F06W	whole fish	159	.913	74	.057		.1	< .25	< .3	21	2	.2	2.0	< .2	1.7	<1
BR1F08W	whole fish	276	.951	75	.038		< .1	< .25	< .3	24	<1	.1	< .5	< .2	1.5	<1
BR1F01L	liver	3.6	1.04	73	.13		< .1	.32	< .3	21	2	.1	< .5	< .2	4.3	<1
BR1F02L	liver	1.4	.771	75	.10		< .1	< .25	< .3	13	2	.4	< .5	< .2	4.6	<1
BR1F03L	liver	0.99	.771	72	.10		< .1	.87	< .3	23	2	2	< .5	< .2	8.7	<1
BR1F05L	liver	3.3	.975	72	.13		< .1	< .25	< .3	24	2	< .1	< .5	< .2	12	<1
BR1F10L	liver	2.3	1.02	73	.14		< .1	< .25	< .3	23	2	.3	< .5	< .2	4.3	<1
CR1F02M	muscle	93	1.08	76	.11	(.11)	< .1	< .25	< .3	14	<1	.1	< .5	< .2	.6	<1
CR1F04M	muscle	88	.932	78	.20	(.20)	< .1	< .25	< .3	15	<1	.1	< .5	< .2	.6	<1
CR1F13M	muscle	88	.904	74	.30		n.d.	n.d.	n.d.	n.d.	n.d.	n.d.	n.d.	n.d.	n.d.	n.d.
CR2F08M	muscle	139	.892	74	.18		n.d.	n.d.	n.d.	n.d.	n.d.	n.d.	n.d.	n.d.	n.d.	n.d.
CR2F16M	muscle	143	.802	72	.12	(.11)	< .1	< .25	< .3	9.2	<1	.1	< .5	< .2	.7	1
CR2F18M	muscle	86	.841	74	.30		n.d.	n.d.	n.d.	n.d.	n.d.	n.d.	n.d.	n.d.	n.d.	n.d.
CR1F15W	whole fish	131	.673	75	.075		.3	< .25	< .3	21	<1	.2	< .5	< .2	1.2	<1
CR2F06W	whole fish	85	.921	71	.067		.1	< .25	< .3	25	<1	.1	< .5	< .2	1.4	<1
CR1F02L	liver	1.4	1.08	73	.17		.1	.28	< .3	21	3	.3	< .5	< .2	4.4	<1
CR1F04L	liver	1.1	.932	75	.43		.1	.30	< .3	21	4	.3	.6	< .2	3.9	<1
CR1F13L	liver	1.8	.904	73	.32		< .1	1.0	< .3	22	2	.2	< .5	< .2	2.7	<1
CR1F16L	liver	1.2	.940	74	.11		< .1	< .25	< .3	21	2	.6	< .5	< .2	4.2	<1
CR1F18L	liver	0.68	.909	74	.36		< .1	.46	< .3	22	2	.6	< .5	< .2	3.9	<1
CR2F08L	liver	1.7	.829	72	.28		< .1	.53	< .3	22	2	< .1	< .5	< .2	4.4	<1
CR2F09L	liver	1.4	1.04	75	.18		< .1	.28	< .3	20	2	.1	.5	< .2	4.9	<1
CR2F13L	liver	1.0	.785	72	.22		< .1	.33	< .3	23	3	.2	1.4	< .2	3.8	<1
CR2F16L	liver	2.1	.802	75	.18		.1	< .25	< .3	34	2	< .1	< .5	< .2	3.0	8
CR2F18L	liver	1.7	.841	72	.53		.1	1.2	< .3	21	3	.5	< .5	< .2	4.1	<1
CC2F04M	muscle	3.1	.728	74	.47		.2	< .25	< .3	16	<1	< .1	< .5	< .2	1.8	<1
CC2F07M	muscle	2.5	.970	76	.38		.1	< .25	< .3	30	<1	< .1	.6	< .2	1.1	<1
CC2F01W	whole fish	45	.979	74	.52	(.49)	.2	< .25	< .3	25	1	.4	< .5	< .2	1.5	<1
CC2F02W	whole fish	41	1.08	75	.48		.5	< .25	< .3	19	<1	.5	1.0	< .2	1.7	<1
CC2F03W	whole fish	10	.848	75	.35		.2	< .25	< .3	31	<1	.2	< .5	< .2	1.0	<1
CC2F05W	whole fish	8.9	1.03	78	.24		.1	< .25	< .3	26	<1	.3	< .5	< .2	.8	<1
CC2F06W	whole fish	11	1.13	76	.34		.5	< .25	< .3	25	<1	.4	< .5	< .2	1.0	<1
CC1F01W	whole fish	38	1.00	71	.55		.3	< .25	< .3	20	<1	.1	< .5	< .2	1.9	<1

[1] $K = \text{weight (g)} \times 10^5 / \text{fork length (mm)}^3$

GEOLOGY

The Cinnabar Creek area is underlain by Triassic and Cretaceous rocks of the Gemuk Group. The Gemuk Group consists of massive siltstone interbedded with lesser amounts of chert, volcanic rocks, graywacke, and limestone (Cady and others, 1955). Rocks of the Gemuk Group are interpreted as part of a volcanic-arc complex (Box, 1985). Late Cretaceous and Tertiary mafic dikes cut rocks of the Gemuk Group near the Cinnabar Creek mine (Sainsbury and MacKevett, 1965). Ore at the mine is high-grade cinnabar found as massive replacements, disseminations, and vug fillings within small quartz-carbonate veins cutting siltstone and graywacke. Native mercury, and lesser stibnite and pyrite are associated with the cinnabar (Sainsbury and MacKevett, 1965). Native mercury is common within sheared and brecciated sedimentary rocks and is visible in streams in the area (Gray and others, 1991). Several hundred flasks of mercury were recovered from the Cinnabar Creek mine (Sainsbury and MacKevett, 1965).

Cretaceous sedimentary rocks of the Kuskokwim Group are the dominant bedrock in the Crooked Creek area (Miller and Bundtzen, 1994). These rocks consist of thick sequences of intercalated sandstones, shales, and conglomerates (Cady and others, 1955). The Kuskokwim Group is primarily made-up of deep-water turbidite facies, with lesser amounts of shallow-shoreline-facies rocks (Miller and Bundtzen, 1987). In the Crooked Creek area, small Late Cretaceous and Tertiary granite porphyry intrusions cut sedimentary rocks of the Kuskokwim Group at several localities, most notably along Snow Gulch (Miller and Bundtzen, 1994). Epithermal stibnite-rich veins are found near Snow Gulch (Cady and others, 1955). These lodes consist of small quartz-carbonate veins and vug fillings that contain stibnite. These veins are hosted in granite porphyry dikes, enclosed within the adjacent siltstone and graywacke of the Kuskokwim Group, or at contacts between the two rock types. About 25,000 oz of gold have been produced from placer mines in the Donlin-Crooked Creek area (Bundtzen and others, 1988).

The Buckstock River dissects rocks of the Kuskokwim Group and the Gemuk Group. Small Late Cretaceous and Tertiary granite porphyry intrusions cut the sedimentary rocks at several localities (Cady and others, 1955; Miller and others, 1989). No mineral deposits that might be sources of mercury are known in the Buckstock River drainage basin.

METHODS OF STUDY

Samples used in this study were collected from the stream channel at each site. Fish were collected using fly and spinning rods equipped with artificial flies and lures. A subset of whole fish, fish muscle, and fish liver tissues were air dried at room temperature and ground. Whole fish and muscle samples were ground in borosilicate glass or stainless steel blenders. Fish livers were hand-ground using an agate mortar and pestle. Mercury was measured in each ground-fish sample using a cold-vapor atomic absorption spectrophotometry (CVAAS) method modified from Adeloju and others (1994). Fish tissues were also analyzed for a multielement suite by inductively coupled plasma-mass spectrophotometry (ICP-MS) (Lichte and others, 1987) and by instrumental neutron activation analysis (INAA) using a technique similar to that described by Baedecker and McKown (1987). Five fish-tissue samples were analyzed for methylmercury using the method of Bloom (1989) to confirm the approximate ratio of methylmercury to total mercury. Data for the Arctic grayling are shown in table 1.

In the laboratory, stream-sediment samples were dried below 50°C, sieved to minus-80 mesh, pulverized, and chemically analyzed. The sediments were analyzed for mercury by CVAAS following the technique of Kennedy and Crock (1987). Concentrations of Ag, Au, As, Sb, Bi, Cd, Cu, Mo, Pb, and Zn were determined in the minus-80-mesh stream-sediment samples by an inductively coupled plasma-atomic emission spectrometry (ICP-AES) technique developed by Motooka (1988). In addition, the stream-sediment samples were analyzed for a multielement suite by a semiquantitative, direct-current arc-emission spectrographic technique adapted from Grimes and Marranzino (1968).

The heavy-mineral-concentrate samples were air-dried, separated in bromoform, and then separated magnetically. The nonmagnetic fractions of the heavy-mineral-concentrate samples were ground and analyzed chemically and mineralogically. The nonmagnetic heavy-mineral-concentrate samples were analyzed for a multielement suite by emission spectrography. The mineralogical content of the nonmagnetic fraction of the heavy-mineral-concentrate samples was determined using a binocular microscope. The nonmagnetic heavy-mineral-concentrates contain sulfide minerals, gold, and some oxides and silicates; the abundance of cinnabar was the most useful for this study.

Stream-water samples collected for mercury analysis were filtered through a 0.45-µm membrane into glass bottles and preserved with a nitric acid and sodium dichromate solution. Mercury in the stream-water samples was determined by CVAAS using a modified version of the method of Kennedy and Crock (1987). A separate stream-water sample filtered through a 0.45-µm membrane was acidified with nitric acid and used for analysis of other metals. Concentrations of As and Sb were determined in the stream-water samples by atomic absorption spectrophotometry following a procedure adapted from Perkin-Elmer Corporation (1977). Concentrations of Cd, Pb, Zn, Cu, Cr, Ni, Ag, and Sn in samples of stream water were determined by an ICP-AES technique modified from

Lichte and others (1987). The analytical results for stream-sediment, heavy-mineral-concentrate, and stream-water samples are shown in table 2.

RESULTS

FISH SAMPLES

All biogeochemical data from fish tissues are reported on a wet-weight basis (table 1). Arctic grayling samples collected from the Buckstock River contain the lowest concentrations of mercury in the study. For fish collected from the Buckstock River, average mercury concentrations are about 0.05 ppm in whole fish, 0.08 ppm in muscle, and 0.12 ppm in liver. The low mercury concentrations in fish collected from this site are consistent with the lack of known mercury sources in the Buckstock River basin. Therefore, the Buckstock River site represents an adequate control for this study.

Fish with the highest mercury concentrations were collected from Cinnabar Creek; these results are consistent with the presence of the abandoned Cinnabar Creek mercury mine upstream. Due to the small size of the fish obtained from Cinnabar Creek, samples analyzed were limited to whole fish and muscle tissue. Mercury contents average about 0.43 ppm in whole fish and muscle samples obtained from Cinnabar Creek (table 1). Mercury results for grayling collected downstream from gold placer mines on Crooked Creek average about 0.07 ppm in whole fish, 0.20 ppm in muscle, and 0.28 ppm in liver samples. Comparison of the range in mercury concentrations in grayling from the three sites studied is shown in figure 2. The data indicate that mercury is most concentrated in liver tissue. Methylmercury determinations for four muscle samples and one whole fish sample suggest that methylmercury comprises greater than 90 percent of the total mercury in Arctic grayling in this region. Similar methylmercury/total mercury ratios have been observed in studies of other freshwater fish (Hildebrand and others, 1980; Bloom, 1989).

In addition to Hg, other heavy-metals investigated included As, Pb, and Cd because these metals can be toxic to the environment. Anomalous concentrations of As have been observed in mercury-rich mineral deposits in southwestern Alaska (Sainsbury and MacKevett, 1965). Anomalous concentrations of arsenic are found in stream-sediment samples collected from Cinnabar Creek (Gray and others, 1991). Arsenic concentrations are highest in whole-body and muscle samples of grayling collected from Cinnabar Creek, averaging about 0.26 ppm, whereas whole-body and muscle samples from Crooked Creek and the Buckstock River average about 0.10 ppm As (table 1). In this study, all arsenic concentrations are well below the recommended FDA action level of 50 ppm wet weight in fish muscle (Crayton, 1990). Concentrations of Cd and Pb in the grayling samples in this study are also low. Most muscle samples are below detection limits for Cd (0.06 ppm), although liver samples from Crooked Creek and the Buckstock River average about 0.4 ppm (table 1). All grayling samples contain Pb below detection limits (0.3 ppm).

Heavy-metals such as Cu, Cr, Ni, Ag, Se, Sn, and Zn can be of environmental concern. However, grayling samples in this study typically contain low concentrations of these elements (table 1). Although zinc is an essential element to humans, it can be toxic to fish (Nriagu, 1980). Zinc concentrations observed in the Arctic grayling in this study range from about 9 to 34 ppm. The concentrations for all these heavy-metals are similar to those reported in other freshwater fish in Alaska (Crayton, 1990; Snyder-Conn and others, 1992). These heavy-metals are often more concentrated in liver samples, but are below FDA action levels.

STREAM-SEDIMENT SAMPLES

Minus-80-mesh stream-sediment samples collected below Cinnabar Creek are anomalous in Hg, Sb, and As. All stream-sediment samples collected from Cinnabar Creek contain greater than 36 ppm Hg, which is the upper limit of determination for Hg (table 2). Background mercury concentrations vary up to about 0.8 ppm in stream-sediment samples collected from the region (Gray and others, 1992); thus, the stream-sediment samples collected from Cinnabar Creek are highly anomalous in mercury. Geochemical dispersion patterns are observed for Sb and As in stream-sediment samples collected from Cinnabar Creek; the stream-sediment sample collected nearest the mine contains 23 ppm Sb and 500 ppm As, and concentrations for both elements decrease in stream-sediment samples collected further downstream (table 2). The stream-sediment samples do not contain anomalous concentrations of Au, Ag, Cu, Pb, Zn, or Mo, indicating the precious- and base-metal-poor nature of these epithermal mercury-rich deposits.

Mercury concentrations are below background in the two stream-sediment samples collected from Crooked Creek. Stream-sediment sample 3062 contains 0.18 ppm Hg and 3063 contains 0.13 ppm Hg (table 2). No geochemical anomalies were identified in the stream-sediment sample collected from the Buckstock River.

HEAVY-MINERAL-CONCENTRATE SAMPLES

Cinnabar is abundant in the nonmagnetic fraction of the heavy-mineral-concentrate samples collected from Cinnabar Creek. The concentration of cinnabar in nonmagnetic heavy-mineral-concentrate samples collected from Cinnabar Creek decrease downstream from the mine, where concentrate samples collected closest to the mine contain greater than 50 percent cinnabar (table 2), and concentrate samples

Table 2. Geochemical data for stream-sediment, heavy-mineral-concentrate, and stream-water samples collected from the Buckstock River (BR), Crooked Creek (CR), and Cinnabar Creek (CC).

[Analysis of Hg in stream-sediment and stream-water samples by cold-vapor atomic absorption spectrophotometry (CVAAS); Hg in heavy-mineral-concentrate samples is an estimated percentage of cinnabar (cinn) determined microscopically; Sb, As, Cd, Pb, Zn, Cu, and Ag in stream-sediment samples and Cd, Pb, Zn, Cu, Cr, Ni, Ag, and Sn in stream-water samples determined by inductively coupled plasma-atomic emission spectrometry (ICP-AES); Cr, Ni, and Sn in stream-sediment samples and Sb, As, Cd, Pb, Zn, Cu, Cr, Ni, Ag, and Sn in heavy-mineral-concentrates determined by semiquantitative emission spectrography; Sb and As in stream-water samples determined by atomic absorption spectrophotometry; concentrations are in ppm, unless otherwise listed; n.d., not determined]

Sample	Media	Hg	Sb	As	Cd	Pb	Zn	Cu	Cr	Ni	Ag	Sn
BR3069S	sediment	<0.05	1.3	34	0.13	6.3	63	18	30	15	<0.067	<10
BR3069C	concentrate	no cinn	<200	<500	<50	<20	500	<10	200	10	<1	<20
BR3069W	stream water	< .05 ppb	n.d.	n.d.	<1 ppb	<10 ppb	29 ppbb	44 ppb	<1 ppb	<5 ppb	<2 ppb	<6 ppb
CR3062S	sediment	.18	1.1	14	.11	6.1	75	15	100	30	< .067	<10
CR3063S	sediment	.12	1.4	20	.12	6.1	77	16	200	50	< .067	<10
CR3062C	concentrate	< 1% cinn	<200	<500	<50	<20	500	<10	200	10	<1	<20
CR3063C	concentrate	< 1% cinn	<200	<500	<50	<20	500	<10	200	10	<1	<20
CR3062W	stream water	< .05 ppb	n.d.	n.d.	<1 ppb	<10 ppb	7 ppb	<10 ppb	<1 ppb	<5 ppb	<2 ppb	<6 ppb
CR3063W	stream water	< .05 ppb	n.d.	n.d.	<1 ppb	<10 ppb	<3 ppb	<10 ppb	<1 ppb	<5 ppb	<2 ppb	<6 ppb
CC072S	sediment	>36	23	500	.17	9.8	110	38	100	20	.12	<10
CC122S	sediment	>36	18	110	.17	8.2	110	39	150	20	.08	<10
CC020S	sediment	>36	5	79	.18	9.8	110	42	150	30	.12	<10
CC073S	sediment	>36	3	61	.17	8.6	110	43	150	50	.09	<10
CC123S	sediment	>36	2	37	.17	8.2	100	33	100	30	.12	<10
CC021S	sediment	>36	1	31	.13	6.7	97	34	150	50	< .05	<10
CC072C	concentrate	>50% cinn	300	<500	<50	50	<500	100	2000	200	<1	<20
CC122C	concentrate	>50% cinn	300	<500	<50	70	<500	70	500	100	<1	<20
CC020C	concentrate	>50% cinn	300	<500	<50	70	<500	50	700	70	<1	<20
CC073C	concentrate	>20% cinn	<200	<500	<50	30	<500	50	500	100	<1	<20
CC123C	concentrate	> 5% cinn	<200	<500	<50	20	<500	50	500	50	<1	<20
CC021C	concentrate	> 1% cinn	<200	<500	<50	30	<500	30	1500	100	<1	<20
CC072W	stream water	.10 ppb	3.8 ppb	12 ppb	< .1 ppb	<2 ppb	< .01	2 ppb	n.d.	n.d.	.4 ppb	n.d.
CC122W	stream water	.20 ppb	1.1 ppb	3.5 ppb	< .1 ppb	<2 ppb	.01	<2 ppb	n.d.	n.d.	.2 ppb	n.d.
CC020W	stream water	.65 ppb	1.0 ppb	4.5 ppb	< .1 ppb	<2 ppb	< .01	<2 ppb	n.d.	n.d.	.3 ppb	n.d.
CC073W	stream water	.30 ppb	.40 ppb	2.6 ppb	< .1 ppb	<2 ppb	< .01	<2 ppb	n.d.	n.d.	.3 ppb	n.d.
CC123W	stream water	.10 ppb	1.0 ppb	2.4 ppb	< .1 ppb	<2 ppb	.01	<2 ppb	n.d.	n.d.	.2 ppb	n.d.
CC021W	stream water	.75 ppb	.20 ppb	2.0 ppb	< .1 ppb	<2 ppb	< .01	<2 ppb	n.d.	n.d.	.2 ppb	n.d.
CC931W	stream water	< .05 ppb	n.d.	n.d.	<1 ppb	<10 ppb	4 ppb	<10 ppb	<1 ppb	<5 ppb	<2 ppb	<6 ppb

collected farthest from the mine contain as little as 1 percent cinnabar (table 2). Other sulfide minerals are uncommon in these concentrate samples. The three nonmagnetic heavy-mineral-concentrate samples closest to the mine contain anomalous Sb (300 ppm), but the other concentrate samples contain less than 200 ppm Sb. Other element anomalies were not observed in concentrates collected from Cinnabar Creek.

Minor cinnabar, less than one percent, was observed in both of the nonmagnetic heavy-mineral-concentrate samples collected from Crooked Creek. Two small gold grains were identified in the concentrate collected about 8 miles (13 km) below the placer mining; no gold was found in the other concentrate. No geochemical anomalies were identified in the data from the concentrates collected from Crooked Creek. No sulfide minerals or geochemical anomalies were found in the nonmagnetic heavy-mineral-concentrate sample collected from the Buckstock River.

STREAM-WATER SAMPLES

Mercury contents in the stream-water samples collected from Cinnabar Creek vary erratically, ranging from less than 0.05 to 0.75 ppb (table 2). The inconsistent mercury results are probably related to the highly volatile nature of mercury or possibly due to mercury sorption onto iron and manganese hydroxides or organic matter. Stream-water samples collected from Cinnabar Creek contain as much as 12 ppb As and as much as 3.8 ppb Sb. Geochemical dispersion patterns were observed for these elements at Cinnabar Creek, although the concentrations decrease rapidly downstream from the mine.

Mercury was below the detection limit of 0.05 ppb in the two samples of stream water collected from Crooked Creek, as well as in the stream-water sample collected from the control site on the Buckstock River.

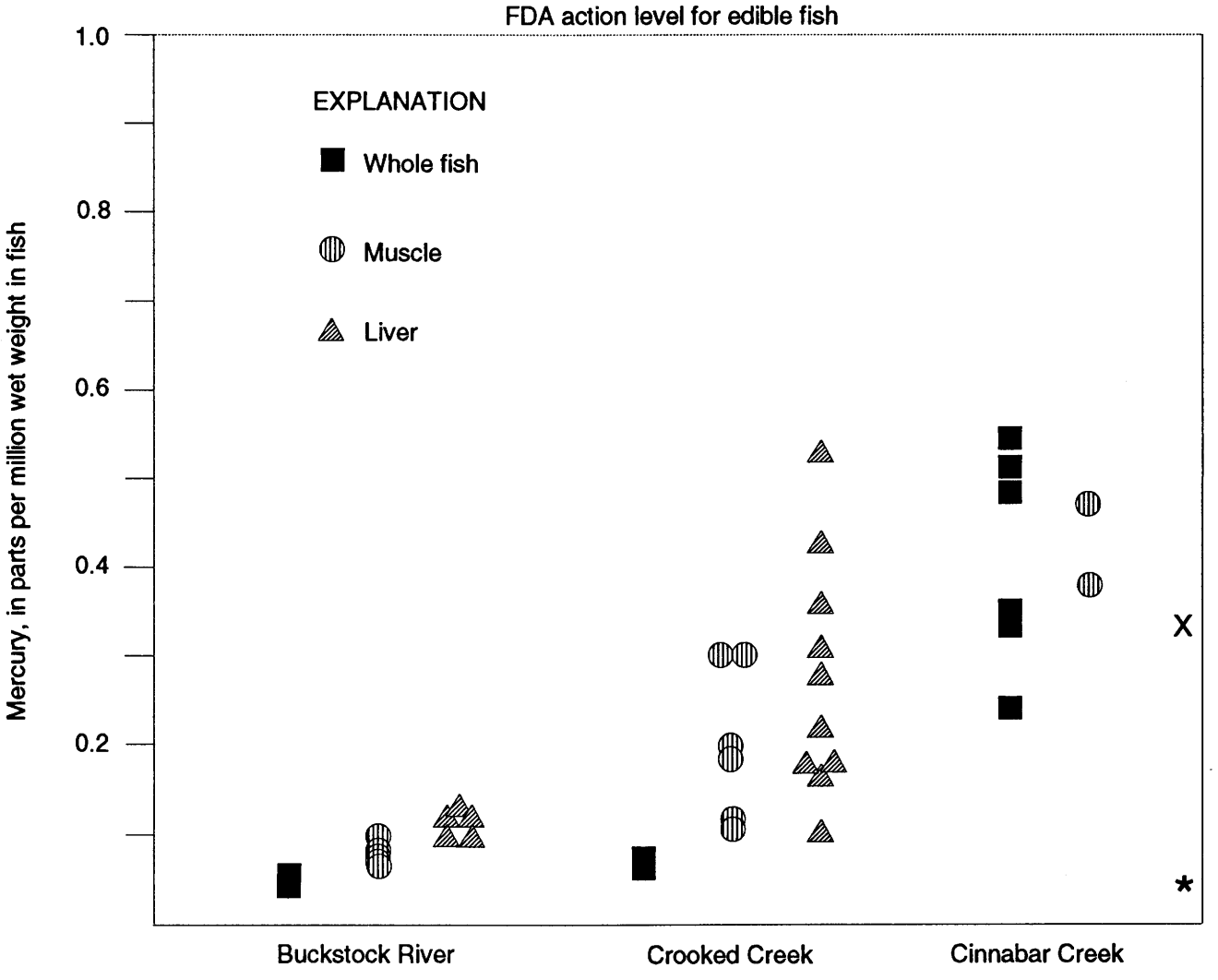

Figure 2. Comparison of mercury concentrations in tissues of Arctic grayling collected from three study sites. Average values shown for reference are Alaskan Arctic grayling (*) whole fish samples (Snyder-Conn and others, 1992) and (X) liver samples (Crayton, 1990).

IMPLICATION OF THE MERCURY RESULTS

Sample media collected from Cinnabar Creek have the highest mercury concentrations observed in this study. The creek drains the abandoned Cinnabar Creek mine that contains abundant cinnabar and native mercury; this ore is the source of the mercury in Cinnabar Creek. Mercury concentrations in Arctic grayling collected from Cinnabar Creek are as much as 10 times higher than mercury concentrations in grayling collected from the Buckstock River that drains an area with no known mineral deposits (fig. 2). However, the mercury concentrations found in the fish from Cinnabar Creek (0.24–0.55 ppm in whole body and muscle) do not exceed the FDA action limit of 1 ppm wet weight for edible fish (Federal Register, 1979). In addition, it is important to note that the grayling sampled from Cinnabar Creek were small; all fish weighed less than 45 grams. The small fish size could be related to adverse environmental conditions affecting the fish habitat and the long-term survivability of the grayling. The general condition of fish was estimated using a condition factor (k), which is a ratio of weight to length (table 1). The condition factors do not vary significantly for grayling between the three sites, and argues against adverse conditions affecting fish health. These results suggest that the small fish may not overwinter at Cinnabar Creek. The condition factors for the fish studied here are similar to those determined for other grayling in Alaska (Glesne and others, 1985).

At Cinnabar Creek, the highest mercury concentrations are found in the larger fish (probably the oldest fish), suggesting increasing concentration of mercury in fish with age (biomagnification); this is a commonly observed pattern (Huckabee and others, 1979; Rada and others, 1986). The approximate correlation of fish weight with higher mercury concentrations suggests that if there are larger fish in Cinnabar Creek, they may contain higher mercury concentrations; however, fish larger than those sampled could not be located. Additional studies should be conducted on Cinnabar Creek farther downstream to determine if larger fish, perhaps with higher mercury concentrations, are present.

Mercury concentrations in Arctic grayling (0.11 to 0.30 ppm in muscle samples) collected from Crooked Creek are as much as three times those of the control site on the Buckstock River (0.077 to 0.10 ppm). However, similar to fish from Cinnabar Creek, the mercury concentrations in grayling collected from Crooked Creek are significantly less than the FDA action level for edible fish. Grayling from Crooked Creek were collected below placer mines. Mercury results presented in this study suggest no significant adverse effects on fish in this drainage basin.

Although southwestern Alaska is sparsely populated, subsistence fishing and hunting are common. Mercury concentrations in grayling collected from the Buckstock River, Crooked Creek, and Cinnabar Creek do not exceed levels considered to be toxic to humans or aquatic organisms, but any possible effect on higher order organisms was not investigated here. Also of note is that Cinnabar Creek, which contains fish with the highest mercury concentrations, is distant from human populations and is an unlikely site for subsistence or sport fishing.

The pathway of mercury to the fish is unresolved at the study sites. Stream-sediment samples collected from Cinnabar Creek are highly anomalous in Hg, but all stream-water samples contain less than 1 ppb Hg. Stream-water samples collected from Crooked Creek and the Buckstock River contain less than 0.05 ppb Hg (table 2). These results suggest that the transfer of mercury to fish in this region may not be through stream water. Other possible mechanisms of Hg transport to fish are adherence of particulate sediment to mucus coverings and Hg absorbance through gill membranes, or ingestion of Hg contaminated food or sediment (Huckabee and others, 1979). Transfer of mercury to fish through food sources has been noted in freshwater ecosystems (Boudou and others, 1991). Insects, larvae, or small fish are probable food sources. In several of the dissected grayling, the stomach contents were predominately insects (mostly flies), but these contents were not analyzed for Hg. A food source pathway of Hg to the fish is likely assuming that the larval stage of resident flies develops in place within sediment enriched in Hg.

CONCLUSIONS

Mercury concentrations are found to be highest in all sample media collected downstream from the Cinnabar Creek mercury mine. Stream-sediment samples collected from Cinnabar Creek exceed 36 ppm Hg and samples of Arctic grayling whole fish and muscle range from 0.24 to 0.55 ppm Hg. Samples from Cinnabar Creek were collected below an abandoned mercury mine, which is the source of the mercury in this drainage basin. Samples collected from a control site on the Buckstock River generally contain the lowest concentrations of mercury.

Samples of fish-liver tissue contain the highest concentrations of Hg and other heavy-metals; samples of whole fish generally contain the lowest concentrations of heavy-metals. All mercury concentrations determined for fish in this study are below the FDA action level of 1 ppm wet weight for edible parts of fish. Heavy-metals such as Cd, Pb, Zn, Cu, Cr, Ni, As, Ag, Se, and Sn were also measured in samples collected for this study. Concentrations for these heavy-metals are typically low in the three areas studied.

Methylmercury is the most toxic form of mercury to humans and aquatic organisms. Mercury analyses indicate that at least 90 percent of the total mercury is methylmercury, a form that accumulates in fish.

Acknowledgments.—The authors thank John Bullock, Paul Briggs, Phil Hageman, Al Love, Al Meier, Mollie Malcolm, Craig Motooka, and Jerry Motooka for chemical analyses. Greg Lee and Jimmy Carter Borden assisted with sample collection. Discussions with Elizabeth Bailey, Jim Crock, Larry Gough, Elaine Snyder-Conn, and Steve Wilson were helpful in the development of many of ideas presented here. Calista Corporation is also recognized for providing permission to access their lands and encouraging these studies.

REFERENCES CITED

Adeloju, S.B., Dhindsa, H.S., and Tandon, R.K., 1994, Evaluation of some wet decomposition methods for mercury determination in biological and environmental materials by cold vapour atomic absorption spectroscopy: Analytica Chimica Acta, v. 285, p. 359–364.

Baedecker, P.A., and McKown, D.M., 1987, Instrumental neutron activation analysis of geochemical samples, *in* Baedecker, P.A., ed., Methods for Geochemical Analysis: U.S. Geological Survey Bulletin 1770, p. H1–H14.

Baeyens, W., 1992, Speciation of mercury in different compartments of the environment: Trends in Analytical Chemistry, v. 11, no. 7, p. 245–254.

Bloom, N., 1989, Determination of picogram levels of methylmercury by aqueous phase ethylation, followed by cryogenic gas chromatography with cold vapor atomic fluorescence detection: Canadian Journal of Fisheries and Aquatic Science, v. 46, p. 1131–1136.

Boudou, A., Delnomdedieu, M., Georgescauld, D., Ribeyre, F., and Saouter, E., 1991, Fundamental roles of biological barriers in mercury accumulation and transfer in freshwater ecosystems (analysis at organism, organ, cell, and molecular levels): Water, Air, and Soil Pollution: v. 56, p. 807–822.

Box, S.E., 1985, Terrane analysis, northern Bristol Bay region, southwestern Alaska, Development of a Mesozoic interoceanic arc and its collision with North America: Santa Cruz, California, University of California, Ph.D. dissertation, 163 p.

Bundtzen, T.K., Cox, B.C., and Veach, N.C., 1988, Heavy mineral provenance studies in the Iditarod and Innoko districts, western Alaska, *in* Process Mineralogy VII: Metallurgical Society, SME/AIME joint meeting, Denver, Colorado, proceedings, p. 221–245.

Bundtzen, T.K., Kline, J.T., Clautice, K.H., and Adams, D.D., 1986, Minerals potential, Department of Natural Resources Kuskokwim planning block, Alaska: Alaska Division of Geological and Geophysical Surveys, Public Data File 86-53e, 44 p.

Cady, W.M., Wallace, R.E., Hoare, J.M., and Webber, E.J., 1955, The central Kuskokwim region, Alaska: U.S. Geological Survey Professional Paper 268, 132 p.

Crayton, W.M., 1990, Report of findings, placer mining impacts—Tuluksak River: U.S. Fish and Wildlife Service, Anchorage, Alaska, unpublished report, 20 p.

Eisler, R., 1987, Mercury hazards to fish, wildlife, and invertebrates: A synoptic review: Fish and Wildlife Service Biological Report 85(1.10), 90 p.

Federal Register, 1979, Action level for mercury in fish, shellfish, crustaceans, and other aquatic animals: Comment from the Department of Health, Education, and Welfare, Food and Drug Administration, v. 44, no. 14, p. 3990–3993.

Fenchel, T., and Blackburn, T.H., 1979, Bacteria and mineral cycling: London, England, Academic Press, 225 p.

Friberg, L., and Vostal, J., 1972, Mercury in the environment: CRC Press, Cleveland, Ohio, 215 p.

Glesne, R.S., Deschermeier, S.J., and Rost, P.J., 1985, Final report, fisheries and aquatic habitat survey of the Hodzana River, Yukon Flats National Wildlife Refuge, 1983 and 1984: Fairbanks Fishery Resources Report, no. FY-85/3.

Gray, J.E., Frost, T.P., Goldfarb, R.J., and Detra, D.E., 1990, Gold associated with cinnabar- and stibnite-bearing deposits and mineral occurrences in the Kuskokwim River region, southwestern Alaska, *in* Goldfarb, R.J., Nash, T.J., and Stoeser, J.W., eds., Geochemical studies in Alaska by the U.S. Geological Survey, 1989: U.S. Geological Survey Bulletin 1950, p. D1–D6.

Gray, J.E., Goldfarb, R.J., Detra, D.E., and Slaughter, K.E., 1991, Geochemistry and exploration criteria for epithermal cinnabar and stibnite vein deposits in the Kuskokwim River region, southwestern Alaska: Journal of Geochemical Exploration, v. 41, p. 1–24.

Gray, J.E., Hageman, P.L., and Ryder, J.L., 1992, Comparison of the effectiveness of stream-sediment, heavy-mineral-concentrate, aquatic-moss, and stream-water geochemical sample media for the mineral assessment study of the Iditarod quadrangle, Geologic Studies in Alaska by the U.S. Geological Survey during 1991: U.S. Geological Survey Bulletin 2041, p. 49–59.

Grimes, D.J., and Marranzino, A.P., 1968, Direct-current arc and alternating-current spark emission spectrographic field methods for the semiquantitative analysis of geological materials: U.S. Geological Survey Circular 591, 6 p.

Hildebrand, S.G., Strand, R.H., and Huckabee, J.W., 1980, Mercury accumulation in fish and invertebrates of the North Fork Holson River, Virginia and Tennessee: Journal of Environmental Quality, v. 9, no. 3, p. 393–400.

Hoare, J.M., and Coonrad, W.L., 1959, Geology of the Russian Mission quadrangle, Alaska: U.S. Geological Survey Miscellaneous Geologic Investigations Map I–292, scale 1:250,000.

Huckabee, J.W., Elwood, J.W., and Hildebrand, S.G., 1979, Accumulation of mercury in freshwater biota, *in* Nriagu, J.O., ed., The Biogeochemistry of Mercury in the Environment: Elsevier/North-Holland Biomedical Press, New York, p. 277–302.

Irukayama, K., 1967, Mercury and Minamata: Proceedings of the 3rd International Conference, Advances in Water Pollution Research, Washington, D.C., v. 3, p. 153–180.

Kennedy, K.R., and Crock, J.G., 1987, Determination of mercury in geological materials by continuous flow, cold-vapor, atomic-absorption spectrophotometry: Analytical Letters, v. 20, p. 899-908.

Kurland, L.T., Faro, S.N., and Siedler, H., 1960, Minamata disease: World Neurology, v. 1, p. 370–391.

Lichte, F.E., Golightly, D.W., and Lamothe, P.J., 1987, Inductively coupled plasma-atomic emission spectrometry, *in* Baedecker, P.A., ed., Methods for Geochemical Analysis: U.S. Geological Survey Bulletin 1770, p. B1–B10.

Manahan, S.E., 1991, Environmental chemistry (5th ed.): Lewis Publishers, Chelsea, Michigan, 583 p.

Miller, M.L., Belkin, H.E., Blodgett, R.B., Bundtzen, T.K., Cady, J.W., Goldfarb, R.J., Gray, J.E., McGimsey, R.G., and Simpson, S.L., 1989, Pre-field study and mineral resource assessment of the Sleetmute quadrangle, southwestern Alaska: U.S. Geological Survey Open-File Report 89-363, 115 p., 3 plates, scale 1:250,000.

Miller, M.L., and Bundtzen, T.K., 1987, Geology and mineral resources of the Iditarod quadrangle, west-central Alaska [abs.], *in* Sachs, J.S., ed., U.S.G.S. research on mineral resources, 1987—Programs and abstracts: U.S. Geological Survey Circular 995, p. 46–47.

———1994, Geologic map of the Iditarod quadrangle, Alaska: U.S. Geological Survey Miscellaneous Field Studies Map MF–2219–A, 1 plate, scale 1:250,000.

Motooka, J.M., 1988, An exploration geochemical technique for the determination of preconcentrated organometallic halides by ICP-AES: Applied Spectroscopy, v. 42, no. 7, p. 1293–1296.

Nriagu, J.O., 1980, Zinc in the environment, part II, Health effects: John Wiley and Sons, New York, 480 p.

Nriagu, J.O., Pfeiffer, W.C., Malm, O., Magalhaes de Souza, C.M., and Mierle, G., 1992, Mercury Pollution in Brazil: Nature, v. 356, no. 6368, p. 389.

Perkin-Elmer Corporation, 1977, Analytical methods for atomic-absorption spectrophotometry, using the HGA graphite furnace: Norwalk, Connecticut, Perkin-Elmer Corporation, 208 p.

Pfeiffer, W.C., Drude de Lacerda, L., Malm, O., Souza, C.M.M., Gloria da Silveira, E.G., and Bastos, W.R., 1989, Mercury concentrations in inland waters of gold-mining areas in Rondônia, Brazil: The Science of the Total Environment, v. 87/88, p. 233–240.

Rada, R.C., Findley, J.E., and Wiener, J.G., 1986, Environmental fate of mercury discharged into the upper Wisconsin River: Water, Air, and Soil Pollution, v. 29, p. 57–76.

Sainsbury, C.L., and MacKevett, E.M., Jr., 1965, Quicksilver deposits of southwestern Alaska: U.S. Geological Survey Bulletin 1187, 89 p.

Smith, P.S., and Maddren, A.G., 1915, Quicksilver deposits of the Kuskokwim region: U.S. Geological Survey Bulletin 622, p. 272–291.

Snyder-Conn, E., Patton, T., Bertram, M., Scannell, P., and Anthony, C., 1992, Contaminant baseline data for water, sediments, and fish of the Nowitna National Wildlife Refuge, 1985–1988: U.S. Fish and Wildlife Service, Fairbanks, Alaska, Ecological Services Technical Report NAES-TR-92-02.

Wood, J.M., 1974, Biological cycles for toxic elements in the environment: Science, v. 183, no. 4129, p. 1049–1052.

World Press Review, 1993, Brazil's Minamata?: World Press Review, v. 40, no. 12, p. 44.

Reviewers: Geoffrey S. Plumlee and Stephen A. Wilson

High Arsenic Content in Sediments from the Koyukuk National Wildlife Refuge, West-Central Alaska

By Robert G. Eppinger, J.M. Motooka, *and* S.J. Sutley

ABSTRACT

An area with anomalously high arsenic in pond- and stream-sediments was discovered during examination of geochemical data for a large region of west-central Alaska. The area lies within the Kateel River 1°×3° quadrangle, and includes much of the Koyukuk Wilderness, within the western part of the Koyukuk National Wildlife Refuge. The samples were collected and analyzed in the late 1970's during the U.S. Department of Energy's National Uranium Resource Evaluation. A subset of the samples was reanalyzed, and these new data confirm the presence of high concentrations of arsenic in the samples.

The Kateel River quadrangle lies near the center of the Yukon-Koyukuk basin. Most of the Kateel River quadrangle is covered by Quaternary flood plain and eolian deposits. Bedrock exposures include Cretaceous marine and nonmarine sandstone, mudstone, siltstone, graywacke, and shale, Jurassic to Cretaceous andesitic volcanic rocks, and Cretaceous to Tertiary minor syenite and granite bodies. There are no reported mineral deposits or prospects in the quadrangle.

Thirty-four stream- and pond-sediment samples in the quadrangle contained As concentrations above the 30 ppm threshold value. All but nine of these samples define a large As anomaly that encloses and extends south and east of the Koyukuk Wilderness. Ten samples within the anomaly had As values from 129 to 846 ppm. High Fe concentrations, ranging from 8 to 33 percent, were found in 16 samples, most lying within the area of the As anomaly. Samples within the As anomaly also contain slightly anomalous Pb (13 samples, 24 to 372 ppm) and possibly anomalous Cd (8 samples, 5 to 28 ppm). However, these high Cd concentrations from the original NURE data were not reproduced in our new analyses and work is underway to resolve the discrepancy. X-ray diffraction studies of samples with high As content identified amorphous iron-oxides and organic material, but no As-bearing species were found.

Arsenic is strongly adsorbed to iron-oxides, particularly in areas of poor drainage, moderate to high precipitation, and cool climate, where waterlogged soils and bogs are present. Much of the Kateel River quadrangle fits this description. The As may have been mobilized by reducing ground water and precipitated onto iron-oxides in the surface water. The present data preclude identifying the source of the As. However, the As anomaly may reflect underlying base- or precious-metal mineralization. Felsic intrusions are present to the north, west, and east of the As anomaly. Geophysical evidence suggests that additional intrusions probably underlie the extensive Quaternary cover in the area of the As anomaly.

It is unclear whether the anomalous As, slightly anomalous Pb, and possibly anomalous Cd in sediments pose an environmental hazard to the area. The remoteness of the area minimizes impact on humans by these elements. However, the area should be investigated further with respect to bioavailability of these elements to fish and wildlife within the Koyukuk National Wildlife Refuge, and to determine metal concentrations in vegetation, surface water, and groundwater.

INTRODUCTION

Examination of data from stream- and pond-sediment samples collected throughout west-central Alaska has revealed the presence of high arsenic concentrations in many samples from the Kateel River 1°×3° quadrangle. The area with high arsenic in sediments includes much of the Koyukuk Wilderness and surrounding area, which lie within the western part of the Koyukuk National Wildlife Refuge (fig. 1).

The area of anomalously high arsenic was discovered during an examination of existing geochemical data for 20 1°×3° quadrangles in west-central Alaska. These data were retrieved from the U.S. Geological Survey's National Geochemical Database and examined as part of a large-scale assessment of the United States for undiscovered non-fuel mineral resources (Barton and others, 1994). The stream- and pond-sediment samples were collected in the late 1970's

during the U.S. Department of Energy's National Uranium Resource Evaluation (NURE). A subset of the NURE samples from the Kateel River quadrangle was reanalyzed as part of this study, and these new data confirm the presence of high concentrations of arsenic in the samples. The purpose of this report is to document the presence of the large arsenic anomaly and to suggest possible origins for it.

GEOLOGIC SETTING

The Kateel River quadrangle lies near the center of the large, wedge-shaped Yukon-Koyukuk basin, which extends from the Ruby geanticline westward to the Seward Peninsula. The Yukon-Koyukuk basin has five major geological components: (1) an arcuate belt of Middle Jurassic to Early Cretaceous island arc-type volcanic and lesser intrusive rocks (Koyukuk terrane) exposed on structural highs; (2) mid-Cretaceous terrigenous sedimentary rocks filling smaller sub-basins that flank these volcanic and intrusive rocks; (3) large, mid- and Late Cretaceous, alkalic to calc-alkalic, granitoid bodies that intrude both components (1) and (2) in the northern part of the basin; (4) Late Cretaceous and early Tertiary calc-alkalic volcanic rocks distributed over all but the northwestern part of the region; and (5) two Tertiary to Quaternary tholeiitic and alkali olivine basalt fields that crop out in the western margin of the basin (Patton and Box, 1989; Patton and others, in press). The volcanic rocks in components (4) and (5) transgress basin boundaries.

Most of the Kateel River quadrangle is covered by Quaternary flood plain and eolian deposits (fig. 1). Bedrock exposures are confined largely to the western third of the quadrangle (Patton, 1966). The southwestern quadrant is composed of Cretaceous marine and nonmarine sandstone, mudstone, siltstone, graywacke, and shale. In the

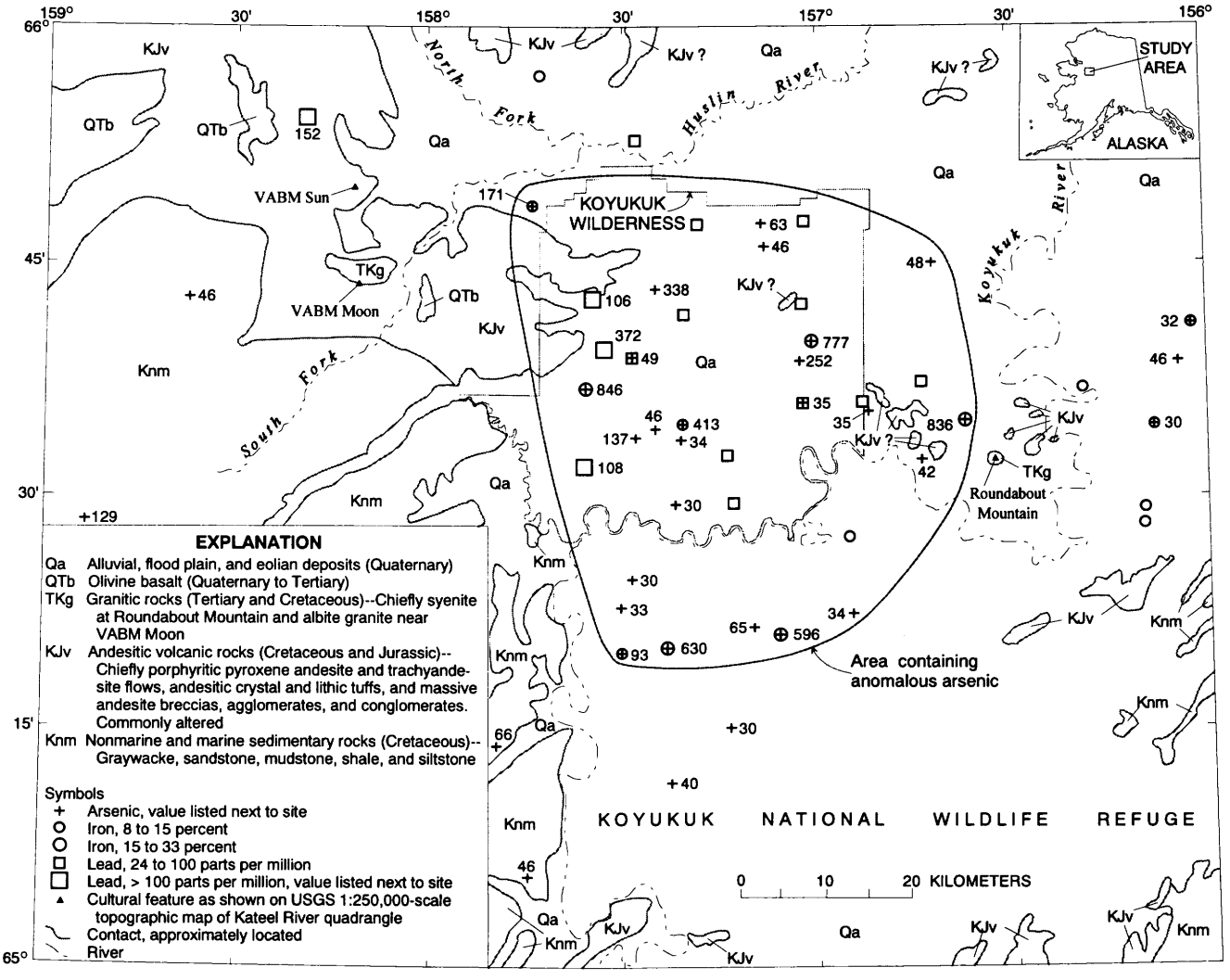

Figure 1. Simplified geology and distribution of samples with anomalous arsenic, lead, and iron concentrations in minus-100-mesh stream- and pond-sediment samples, Kateel River quadrangle, Alaska. Chemical analyses are by Los Alamos Scientific Laboratories (Hardy and others, 1982). Geology from Patton (1966).

southeastern corner of the quadrangle are isolated exposures of undifferentiated nonmarine sedimentary rocks. Jurassic to Cretaceous andesitic volcanic rocks crop out in a large area in the northwestern part and as small isolated bodies throughout the eastern half of the quadrangle. Two intrusions, both of Cretaceous to Tertiary age, are exposed in the quadrangle, a syenite at Roundabout Mountain, and an albite granite near VABM Moon. Other unmapped granitic bodies may intrude andesitic volcanic rocks (Patton, 1966). Immediately north of the Kateel River quadrangle are several large granitic intrusions that are part of a 500-km-long plutonic belt of varied age and composition (Patton and others, 1968; Miller, 1989). Tertiary to Quaternary olivine basalt crops out in the northwestern corner of the quadrangle and is part of the Buckland River field (Patton and Box, 1989).

There are no reported mineral deposits or prospects in the Kateel River quadrangle. However, several small base- and precious-metal lodes and one gold placer are found peripheral to granitic intrusions immediately north of the quadrangle (Cobb, 1972).

METHODS

In 1976, sediments were collected throughout west-central Alaska from streams and ponds as part of the NURE program. These samples were collected and analyzed under the direction of the Los Alamos Scientific Laboratory (LASL). A total of 254 stream- and 399 pond-sediment samples were collected in the Kateel River quadrangle. These samples were subsequently sieved to minus-100-mesh and analyzed for over 50 elements (including Ag, As, Au, Ba, Bi, Cd, Cu, Fe, Mn, Pb, Sb, Se, Sn, Th, U, W, and Zn) by neutron activation, emission spectrography, and X-ray fluorescence. Details on the techniques used for sample collection and field measurements are found in Sharp and Aamodt (1978) and Sharp (1978). Hardy and others (1982) provide a statistical summary and data listing for sediment samples from the Kateel River quadrangle.

As part of the NURE program, unfiltered, acidified stream, lake, and pond water samples were collected at sediment sample sites. However, the water samples were not analyzed for As, and no coherent patterns were observed in plots of other elements. Thus, the water data are not discussed here. A description of analytical techniques and a listing of water data for the Kateel River quadrangle are found in Arendt and others (1980) and Arendt (1981), respectively.

After recognition of the high arsenic concentrations in many of the NURE sediments, a subset of the original samples was retrieved and reanalyzed. Thirty-three stream- and pond-sediment samples, with LASL As concentrations ranging from 30 to 846 ppm (parts per million), were reanalyzed for Ag, As, Au, Bi, Cd, Cu, Mo, Pb, Sb, and Zn by inductively-coupled-plasma atomic-emission spectrometry (ICP-AES) using the procedure of Motooka (1988). These new analyses, along with the original As, Cd, Fe, and Pb analyses by LASL for the same samples, are provided in table 1. Additional analyses for Hg, low-level Au, Cd, and several additional elements are in progress.

RESULTS

After inspection of histograms and percentiles from the Kateel River LASL sediment data, single-element spatial distribution maps were generated for As, Cd, Fe, and Pb. Table 2 lists thresholds, concentration ranges, and percentiles for these elements. For comparison, the table also lists world-wide average concentrations of these elements in igneous and sedimentary rocks.

Thirty-four stream- and pond-sediment samples in the quadrangle contained As concentrations above the 30 ppm threshold value. All but nine of these samples define a large (about 2,400 km^2) As anomaly that encloses and extends south and east of the Koyukuk Wilderness (fig. 1). Eleven samples contained As concentrations of 129 ppm or higher, and eight of these samples had values above 250 ppm, the highest value being 846 ppm. Only 1 of the 11 samples, with an As value of 129 ppm, was collected outside the large As anomaly.

Contained within the As anomaly are several samples with slightly anomalous concentrations of Pb. Sixteen samples contained Pb concentrations from 24 to 372 ppm, and all but three are from sites within the As anomaly (fig. 1). However, only two samples contained anomalous concentrations of both As and Pb. While the absolute Pb values are not excessively high, the fact that nearly all the samples with anomalous Pb concentrations lie within the As anomaly is noteworthy.

High Fe concentrations, ranging from 8 to 33 percent, were found in 16 samples; most of these samples lie within the As anomaly (fig. 1). Iron is the only element analyzed by LASL which correlates strongly with As (correlation coefficient 0.75 based on 556 samples). All the samples collected within 15 km of the Koyukuk Wilderness with Fe contents greater than 11 percent also contained anomalous As in the hundreds of ppm.

High As concentrations in the sediment samples were confirmed in this study by ICP-AES (table 1). As expected, the precise As values differ between LASL and our analyses. However, the magnitudes of concentrations are the same for all the samples that were reanalyzed. Similarly, the two LASL samples containing anomalous concentrations of both As and Pb (table 1, nos. 424761 and 424791) contained comparable As and Pb concentrations in the reanalysis. No other high-Pb samples were included in the reanalyzed set of samples.

Table 1. Analytical data for selected minus-100-mesh stream- and pond-sediment samples containing anomalous As concentrations in analyses by Los Alamos Scientific Laboratories (LASL) and reanalyzed in this study.

[All values in parts per million, except Fe (percent); N, not detected; LASL analyses by energy-dispersive X-ray fluorescence, except Fe (instrumental neutron-activation); USGS analyses by inductively-coupled plasma atomic-emission spectrometry; detection limits listed below element; elements not detected in this study: Au (detection limit, 0.30 ppm) and Bi (2.0 ppm)]

Sample	Latitude	Longitude	Ag, USGS	As, LASL	As, USGS	Cd, LASL	Cd, USGS	Fe, LASL	Cu, USGS	Mo, USGS	Pb, LASL	Pb, USGS	Sb, USGS	Zn, USGS
			0.20	5	2.0	5	0.15	0.05	0.06	0.18	5	2.0	2.0	0.06
403742	65.2133	158.1	N	66	52	N	0.76	6.697	23	1.1	6	19	N	95
403895	65.4733	158.8967	N	129	110	5	0.69	4.19	24	3.8	N	13	N	37
406492	65.7139	158.6236	N	46	30	N	0.52	5.906	20	1.5	N	15	N	76
424478	65.0958	157.7547	N	46	47	N	0.33	6.057	27	0.64	N	9.4	N	64
424495	65.1989	157.3817	N	40	30	N	0.47	3.253	27	2.5	11	13	N	43
424590	65.5764	156.1322	0.22	30	24	N	0.77	9.241	62	1.5	13	23	N	110
424594	65.6406	156.0703	0.22	46	34	N	0.92	7.925	61	4.0	17	26	N	110
424596	65.6822	156.0325	0.22	32	21	N	0.67	11.06	54	2.3	10	23	N	110
424657	65.7528	156.7039	N	48	35	N	0.82	5.903	27	1.5	N	10	N	62
424706	65.6175	157.5961	N	846	670	10	3.1	22.74	7.4	1.5	N	26	N	22
424717	65.8128	157.7367	N	171	160	5	4.1	11.66	21	1.3	14	36	N	57
424746	65.7683	157.1278	N	46	38	N	1.5	2.427	15	2.7	7	12	N	25
424747	65.7931	157.1378	N	63	48	N	1.2	3.088	12	1.5	7	13	N	32
424761	65.6492	157.4778	N	49	41	N	7.1	1.997	8.2	3.4	62	58	N	32
424763	65.5794	157.3456	N	413	340	N	0.2	11.15	6.0	1.4	N	2.5	N	24
424764	65.5617	157.3503	N	34	27	N	0.79	6.561	46	1.6	13	18	N	92
424765	65.5636	157.4694	N	137	110	N	0.2	5.34	10	1.7	N	6.2	N	36
424766	65.5739	157.4203	N	46	37	N	0.19	3.864	11	1.7	N	4.0	N	38
424767	65.4944	157.3697	N	30	17	N	0.62	5.365	47	1.7	14	19	2.3	99
424783	65.7247	157.4181	N	338	260	N	0.67	7.348	5.6	1.8	N	2.2	N	11
424789	65.6692	157.0106	N	777	690	13	0.88	18.05	6.4	1.5	N	4.2	N	24
424790	65.6478	157.0439	N	252	190	N	0.78	4.186	7.6	6.0	N	7.3	N	45
424791	65.6022	157.0417	0.24	35	25	N	1.5	4.528	86	2.9	24	28	2	130
424794	65.59	156.8717	N	35	24	N	0.72	5.396	56	1.8	22	24	2.3	110
424803	65.5825	156.625	N	836	860	13	0.37	25.47	11	4.2	N	N	N	22
424824	65.5414	156.7322	N	42	36	N	0.56	4.095	30	1.6	5	15	N	72
424836	65.4122	157.4831	N	30	24	N	0.51	4.53	41	1.7	9	21	N	91
424840	65.3358	157.5103	N	93	84	N	0.48	8.442	37	6.2	N	12	N	73
424841	65.3836	157.5064	N	33	28	N	0.54	3.771	43	4.6	N	13	N	55
424842	65.3414	157.3836	N	630	540	N	N	15.18	2.7	1.1	N	N	N	42
424847	65.3619	157.1669	N	65	63	N	0.38	3.615	19	2.4	5	10	N	38
424848	65.3544	157.1003	N	596	670	21	N	32.78	3.0	0.86	N	N	N	17
424851	65.3761	156.9192	N	34	29	N	0.86	3.073	62	4.5	11	19	N	100

Table 2. Thresholds, ranges in concentration, and percentiles for As, Cd, Fe, and Pb in NURE stream- and pond-sediment samples, compared to world-wide average concentration ranges for igneous and sedimentary rocks.

[NURE samples collected and analyzed by Los Alamos Scientific Laboratories; *n* indicates the number of unqualified values for each element; As, Cd, and Pb analyzed by energy-dispersive X-ray fluorescence; Fe analyzed by instrumental neutron activation; N(5), not detected at 5 ppm lower detection limit; average range in igneous rocks is for ultramafic, mafic, and granitic rocks; average range in sedimentary rocks is for limestone, shale, and sandstone; average ranges are from Rose and others, 1979]

Element	*n*	Threshold	Equivalent percentile	Number of anomalous samples	Anomalous concentration range	Percentiles			Average range in igneous rocks	Average range in sedimentary rocks
						50th	75th	95th		
As, ppm	556	30	95th	34	30–846	10	14	30	1–2	1–12
Cd, ppm	13	5	98th	13	5–28	N(5)	N(5)	N(5)	0.1–0.2	0.03–0.3
Fe, pct	651	8	97.5th	16	8–33	4	4.6	6.7	1.4–9.4	0.3–4.7
Pb, ppm	442	24	97.5th	16	24–372	7	10	19	1–18	5–25

Anomalous Cd, ranging from 5 to 28 ppm, was found by LASL in 13 samples; 8 were within the As anomaly. Six of these eight samples were included in the group for reanalysis. There is generally poor agreement for Cd between LASL and our analyses (table 1). The reason for this analytical discrepancy is unclear; possibilities include analytical interference (high Fe?), sample digestion problems, or total versus partial analytical methods. The samples are being reanalyzed for Cd to resolve this problem.

Eight sediment samples containing the highest As content were analyzed by X-ray diffraction to determine mineral phases. Generally, all the patterns were poor, due to the predominance of amorphous organic material and iron-oxides. Minerals identified include quartz, siderite, calcite, orthoclase, albite, kaolinite, maghemite, and possibly goethite. No As-bearing species were found.

CONCLUSIONS

The strong association between high Fe content and anomalous As is not unusual. Arsenic is strongly adsorbed to iron-oxides, more so than many other elements affected by sorption (Nowlan, 1976). This process is enhanced in areas of poor drainage, moderate to high precipitation, and cool climate, where waterlogged soils and bogs are present (Rose and others, 1979). More than half of the Kateel River quadrangle fits this description. The As may have been mobilized by reducing ground water and precipitated onto iron-oxides in the surface water. A similar mechanism was postulated for natural arsenic enrichment in sediments from Scotland by Farmer and Lovell (1986).

The present data preclude identifying the source of the As. Arsenic is associated with a variety of base- and precious-metal deposits and is commonly used as a pathfinder element because of its mobility under a variety of conditions. The As anomaly and the coincident, albeit lower-level, Pb anomaly may reflect underlying base- or precious-metal mineralization. The ferromagnetic ferric oxide maghemite is found principally as an alteration product after magnetite. Interestingly, maghemite is commonly, although not exclusively, found in gossans (Palache and others, 1944).

Bodies of granite, quartz monzonite, granodiorite, alaskite, and syenite are present to the north, west, and east of the large As anomaly. A total magnetic intensity map of the Kateel River quadrangle (Union Carbide Corporation, 1981) reveals numerous high-amplitude, high and low magnetic anomalies underlying areas of exposed Jurassic and Cretaceous volcanic rocks and the large area of Quaternary cover, including the As anomaly. In this part of the Yukon-Koyukuk basin, Cady (1989) interprets magnetic highs as indicators of magnetic andesitic rocks and magnetic lows as indicators of granitic plutons. Thus, additional concealed igneous bodies probably underlie the extensive Quaternary cover and could have provided heat and metal sources for deposits manifested by the surface As anomaly.

The Environmental Protection Agency lists several toxic elements, including As, Pb, and Cd, as of particular concern for health and environmental issues. While highly anomalous As, slightly anomalous Pb, and possibly anomalous Cd have been found in pond and stream sediments from the Koyukuk Wilderness and surrounding areas, it is presently unclear whether these elements pose an environmental hazard to the area. Certainly, the remoteness of the area minimizes impact on humans by these elements. However, the area should be investigated further with respect to bioavailability of these elements to fish and wildlife within the Koyukuk National Wildlife Refuge, and to determine metal concentrations in vegetation, surface water, and groundwater. This area may be useful as a natural laboratory containing elevated As concentrations in sediments.

REFERENCES CITED

Arendt, J.W., 1981, Hydrogeochemical and stream sediment reconnaissance basic data for Kateel River Quadrangle, Alas-

ka: Oak Ridge Gaseous Diffusion Plant, Oak Ridge National Laboratory, Oak Ridge Tennessee, U.S. Department of Energy Report GJBX-360(81), 73 p.

Arendt, J.W., Butz, T.R., Cagle, G.W., Kane, V.E., and Nichols C.E., 1980, Hydrogeochemical and stream sediment reconnaissance procedures of the uranium resource evaluation project: Oak Ridge Gaseous Diffusion Plant, Oak Ridge National Laboratory, Oak Ridge Tennessee, U.S. Department of Energy Report GJBX 32(80), 56 p.

Barton, P.B., Ayuso, R.A., Brew, D.A., Force, E.R., Gamble, B.M., Goldfarb, R.J., John, D.A., Johnson, K.M., Lindsey, D.A., and Ludington, S.D., 1994, Quantitative assessment of undiscovered, non-fuel mineral resources, *in* Carter, L.M.H., Toth, M.I., and Day, W.C., eds., USGS research on mineral resources-1994, part A, program and abstracts: U.S. Geological Survey Circular 1103–A, p. 4–5.

Cady, J.W., 1989, Geologic implication of topographic, gravity, and aeromagnetic data in the northern Yukon-Koyukuk province and its borderlands, Alaska: Journal of Geophysical Research, v. 94, no. B11, p. 15,821–15,841.

Cobb, E.H., 1972, Metallic mineral resource map of the Shungnak quadrangle, Alaska: U.S. Geological Survey Miscellaneous Field Studies Map MF–448, scale 1:250,000.

Farmer, J.G., and Lovell, M.A., 1986, Natural enrichment of arsenic in Loch Lomond sediments: Geochimica et Cosmochimica Acta, v. 50, p. 2059–2067.

Hardy, L.C., D'Andrea, R.F., Jr., Zinkl, R.J., Minor, M.M., McInteer, C., Hansel, J.N., and Broxton, D.E., 1982, Uranium hydrogeochemical and stream sediment reconnaissance of the Kateel River NTMS quadrangle, Alaska: Los Alamos Scientific Laboratory, Los Alamos, New Mexico, U.S. Department of Energy Report GJBX 182(82).

Miller, T.P., 1989, Contrasting plutonic rock suites of the Yukon-Koyukuk basin and the Ruby geanticline, Alaska: Journal of Geophysical Research, v. 94, no. B11, p. 15,969–15,987.

Motooka, J.M., 1988, An exploration geochemical technique for the determination of preconcentrated organometallic halides by ICP-AES: Applied Spectroscopy, v. 42, no. 7, p. 1293–1296.

Nowlan, G.A., 1976, Concretionary manganese-iron oxides in streams and their usefulness as a sample medium for geochemical prospecting: Journal of Geochemical Exploration, v. 6, p. 193–210.

Palache, C., Berman, H., and Frondel, C., 1944, Dana's System of Mineralogy, v. 1, 7th ed.: New York, John Wiley and Sons, 834 p.

Patton, W.W., Jr., 1966, Regional geology of the Kateel River quadrangle, Alaska: U.S. Geological Survey Miscellaneous Geologic Investigations Map I–437, scale 1:250,000.

Patton, W.W., Jr., Miller, T.P., and Tailleur, I.L., 1968, Regional geologic map of the Shungnak and southern part of the Ambler River quadrangles, Alaska: U.S. Geological Survey Miscellaneous Geologic Investigations Map I–554, scale 1:250,000.

Patton, W.W., Jr., and Box, S.E., 1989, Tectonic setting of the Yukon-Koyukuk basin and its borderlands, western Alaska: Journal of Geophysical Research, v. 94, no. B11, p. 15,807–15,820.

Patton, W.W., Jr., Box, S.E., Moll-Stalcup, E.J., and Miller, T.P., in press, Geology of west-central Alaska, *in* Plafker, G., and Berg, H.C., eds., Geology of Alaska: Boulder, Colo., Geological Society of America, The Geology of North America, v. G-1.

Rose, A.W., Hawkes, H.E., and Webb, J.S., 1979, Geochemistry in Mineral Exploration, 2nd ed.: New York, Academic Press, 657 p.

Sharp, R.R., Jr., 1978, Uranium hydrogeochemical and stream sediment reconnaissance data from the area of the Teller, Bendeleben, Candle and Kateel River quadrangles, Seward Peninsula and vicinity, Alaska: Los Alamos Scientific Laboratory, Los Alamos, New Mexico, U.S. Department of Energy Report GJBX 85(78), 161 p.

Sharp, R.R., Jr., and Aamodt, P.L., 1978, Field procedures for the uranium hydrogeochemical and stream sediment reconnaissance as used by the Los Alamos Scientific Laboratory: Los Alamos Scientific Laboratory, Los Alamos, New Mexico, U.S. Department of Energy Report GJBX 68(78).

Union Carbide Corporation, 1981, Kateel River quadrangle; total intensity magnetic anomaly profile map: Computer Sciences Division, Union Carbide Corporation, Oak Ridge National Laboratory, Oak Ridge, Tennessee, U.S. Department of Energy Report GJM 005(81).

Reviewers: Karen D. Kelley and David L. Leach, Jr.

Environmental Geochemistry of Mesothermal Gold Deposits, Kenai Fjords National Park, South-Central Alaska

By Barrett A. Cieutat,[1] Richard J. Goldfarb, J. Carter Borden, John McHugh, *and* Cliff D. Taylor

ABSTRACT

Stream water samples were collected at 16 sites below and near 3 developed, mesothermal gold vein occurrences of the Nuka Bay mining district in Kenai Fjords National Park. Occurrences are largely hosted by metagraywacke of the Valdez Group; one prospect is located in a felsic dike. The ore veins typically contain 1 to 3 percent by volume pyrite and arsenopyrite, and range from thin stringers to 3 m in width. They have been developed by a number of small adits and surface diggings.

Background metal concentrations of <0.05 ppb Ag, ≤2 ppb As, <1 ppb Cd, ≤1 ppb Cu, ≤10 ppb Fe, <1 ppb Sb, and 3 to 6 ppb Zn characterize waters that drain metasedimentary rocks of the Valdez Group. In a small basin containing undeveloped sulfide-bearing quartz veins, arsenic concentrations are elevated to 6 ppb. Immediately downstream of surface workings and at the mouth of the adits, metal concentrations are as great as 130 ppb As, 2 ppb Sb, and 40 ppb Fe. These anomalous concentrations are rapidly diluted downstream to background levels; no elevated metal values are detected beyond 500 m from any of the three occurrences. Small-scale lode gold mining in the Kenai Mountains may not have significant impact on water quality.

INTRODUCTION

During the summer of 1993, hydrogeochemical samples were collected from surface waters near three developed mesothermal gold vein deposits within Kenai Fjords National Park. The purpose of this sample collection was to detect any effect on water quality directly resulting from small-scale mining activity. A second objective of the study is to determine natural baseline levels for environmentally sensitive metals in surface waters that have reacted with such metal-bearing vein systems.

Mesothermal gold vein occurrences are widespread within the accreted and regionally metamorphosed terranes of the southern Alaskan Cordillera (Goldfarb and others, 1986). Small gold mines (generally less than 5,000 to 10,000 ounces of total production), such as those in the Nuka Bay area of Kenai Fjords National Park, are common throughout much of the Kenai and Chugach Mountains of south-central Alaska and the Alexander Archipelago of southeastern Alaska. The results of this site-specific study could aid environmental assessment and land use planning decisions within the mountainous regions rimming the Gulf of Alaska, including lands of the Tongass and Chugach National Forests.

GEOLOGIC SETTING

The Nuka Bay gold district is located on the eastern side of the southern Kenai Mountains, approximately 55 km east of the town of Homer (fig. 1). Gold-bearing quartz veins in the district have most recently been described by Richter (1970) and Borden and others (1992). The veins were discovered in the early 1900's, and peak mining activity occurred in the 1930's. Dollar estimates by Richter (1970) suggest that combined gold production totaled about 5,000 to 6,000 oz. from 5 mines. There has been no recorded production from any of the mines for the past 50 years. However, recent claim work has been conducted at the Goyne prospect, Sonny Fox mine, and Little Creek prospect (fig. 1). These claims remain active within the Kenai Fjords National Park because they existed prior to the 1980 establishment of the park. A large dump exists adjacent to the adit at the Sonny Fox mine; numerous structures occur adjacent to the workings at both the Sonny Fox mine and Little Creek prospects.

[1]Present address: ERM-Southwest Inc., 3501 N. Causeway Blvd., Suite 200, Metairie, Louisiana 70002.

The Nuka Bay mining district is mainly underlain by metagraywacke and slate of the Upper Cretaceous Valdez Group. Tertiary granodioritic dikes and, less commonly, sills, cut the metasedimentary rocks in many areas of the district. Most gold-bearing quartz veins in the region are preferentially hosted by the metagraywacke, although veins at the Goyne prospect are largely restricted to a chloritized granodiorite dike (Richter, 1970).

The largest gold-bearing quartz veins in the district are about 100 m long and 3 m wide. Veins typically contain 1 to 3 percent sulfides and a few percent carbonate minerals. Samples of the most sulfide-rich vein material from the district have a metal content of up to 30 percent Fe, 8.7 percent As, 2 percent Pb, 0.65 percent Zn, 0.10 percent Cu, 300 ppm Sb, 304 ppm Au, 200 ppm Ag, 200 ppm Co, 220 ppm Cd, 19 ppm Te, and 7.6 ppm Hg (Borden and others, 1992). These analyses reflect an arsenopyrite- and pyrite-dominant sulfide assemblage in the veins. Lesser chalcopyrite, sphalerite, galena, and free gold, with rare tetrahedrite, covellite, chalcocite, sylvanite, native silver, and native copper, have also been noted in veins in the district (Smith, 1938; Borden and others, 1992). Carbonatization and silicification of wallrocks adjacent to the auriferous veins is a common alteration feature.

FIELD AND ANALYTICAL METHODS

Water samples were collected in drainage basins containing the three recently active mines and prospects in the Nuka Bay district (fig. 2*A*, *B*). At the Little Creek prospect, samples were collected in (1) a 2-m-wide stream located 100 m west of the prospect and containing mineralized vein float but no upstream workings (sample site 1, fig. 2), (2) a small, less than 0.5-m-wide rill located about 6 m downstream from a large, decaying building that sits against the south edge of the mineral deposit (sample site 2, fig. 2), and (3) Ferrum Creek, at locations approximately 200 m upstream (sample site 3, fig. 2) and 500 m downstream (sample site 4) from the junction with the channel draining the prospect. Ferrum Creek is 8 to 10 m wide, with depths of up to 1 m. The creek has a high velocity and carries a moderate suspended load, reflecting upstream glacial erosion. Near the Sonny Fox mine, five samples were collected over a distance of 0.5 km along a small, unnamed creek between the mine portal and Babcock Creek (sample sites 5–8 and 10, fig. 2), one sample was collected on an adjacent rill (sample site 9, fig. 2), and two samples were located on Babcock Creek (sample sites 11 and 12, fig. 2). Babcock Creek is 5 to 7 m wide, up to 1 m deep, and contains little suspended material. At

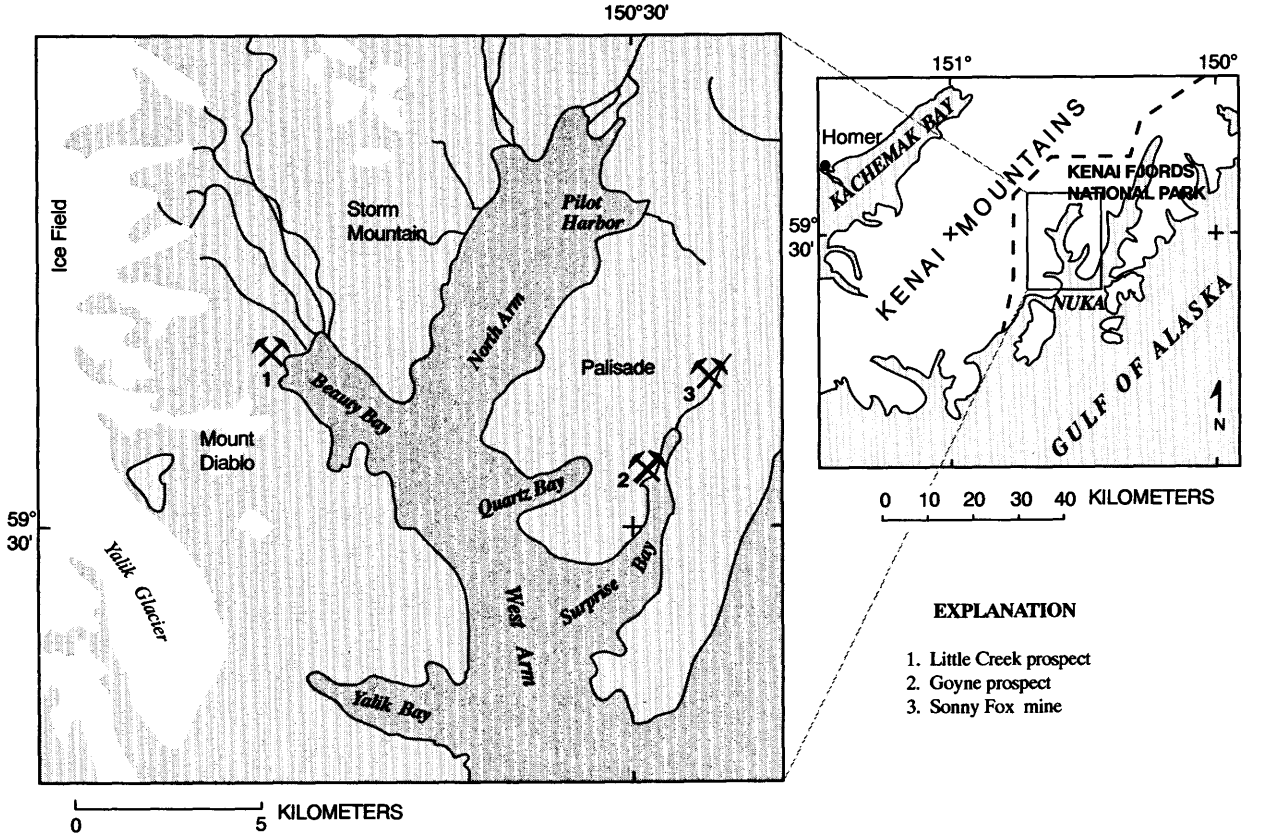

Figure 1. Location of studied gold occurrences of the Nuka Bay district, Kenai Fjords National Park.

the Goyne prospect, samples collected included effluent dripping from a sulfide-rich fracture within the adit (sample site 13, fig. 2), a small stream flowing directly over the top of the adit (sample site 14, fig. 2), and two small streams about 200 m north and spatially removed from the deposit (sample sites 15 and 16, fig. 2).

Water temperature and pH were measured at each site. Two 60-ml water samples were collected in polyethylene bottles at all locations; both stream-water samples were filtered through a 0.45-micron membrane filter, and one was acidified with reagent-grade concentrated nitric acid to a pH of less than 2.

Each acidified-water sample was analyzed for calcium, iron, magnesium, potassium, manganese, sodium, and zinc, using flame atomic-absorption spectrophotometry (Perkin-Elmer Corp., 1976). The samples were analyzed for antimony, arsenic, cadmium, cobalt, copper, lead, and silver, using flameless atomic-absorption spectrophotometry (Perkin-Elmer Corp., 1977). Chloride, nitrate, and sulfate concentrations were determined in unacidified water samples using ion chromatography (Fishman and Pyen, 1979). These samples were also analyzed for conductivity using a standard meter and for alkalinity by titration. The results of these analyses are given in table 1. All measurements were below the lower determination limits for Ag (50 ppt), Cd (1 ppb), Co (1 ppb), and Mn (10 ppb) and, therefore, have been omitted from the table of results.

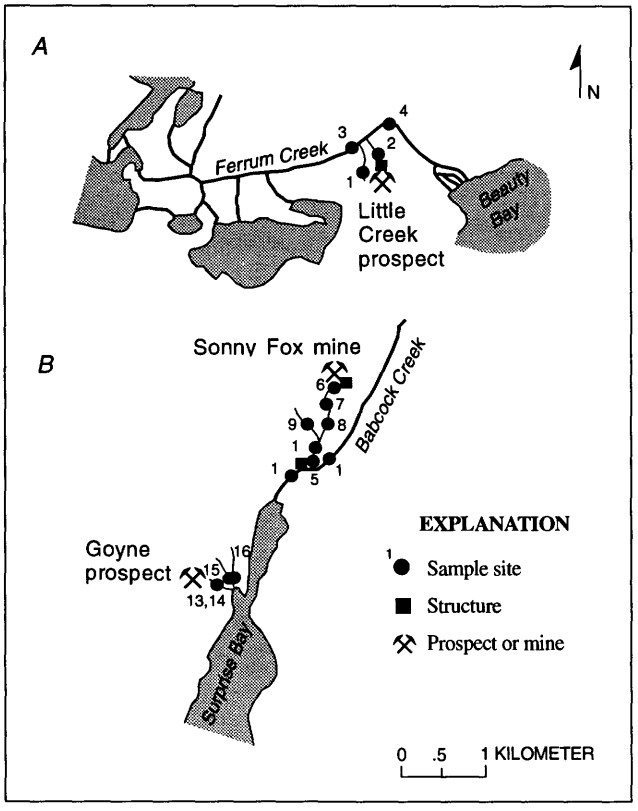

Figure 2. Location of stream-water sample sites near (*A*) Little Creek prospect and (*B*) Sonny Fox mine and Goyne prospect.

RESULTS OF ANALYSES

LITTLE CREEK PROSPECT

Water chemistry at site 3 on Ferrum Creek, upstream from any influx due to known mineral occurrences, characterizes local background metal concentrations for this area. The resulting data indicate that surface waters in drainage basins underlain by rocks of this part of the Valdez Group may contain background concentrations of about <0.05 ppb Ag, 2 ppb As, <10 ppb Fe, 6 ppb Zn, <1 ppb Pb, Cd, Sb, and nitrate, 0.4 ppm chloride, and 0.7 ppm sulfate. The conductivity and alkalinity were 37 ppm and <10 mg/l as $CaCO_3$, respectively, and the water pH was 7.43. As with many of the streams in this part of the Kenai Mountains, a large percentage of the discharge is derived from glacial melt. Therefore, concentrations are significantly lower for many elements in Ferrum Creek in comparison to waters from other streams near the Little Creek prospect (such as at sites 1 and 2) that have mainly formed via ground water discharge.

Water collected from site 1, located immediately west of the prospect, drains a small watershed that contains no mine workings but some auriferous veins. The resulting data (table 1) provide a baseline chemical signature for waters that have interacted with small and undeveloped vein occurrences. The sample from site 1 contains 6 ppb As and is enriched relative to a baseline concentration of 2 ppb in Ferrum Creek (site 3). This reflects interaction between waters and arsenopyrite in the quartz veins and in adjacent, altered wall rocks. None of the base-metal concentrations at site 1 were elevated above background levels defined at site 3. However, at site 1, concentrations of the major cations (Ca, K, Mg, Na) and anions (Cl, NO_3, SO_4) were notably higher, and the pH of 7.98 was slightly higher. The increased pH may have resulted in part from an increased alkalinity in the water due to its reaction with the carbonate-dominant alteration assemblage surrounding the quartz veins. Much of the difference, though, is believed to reflect the different water sources. Glacial-melt water clearly accounts for most of the discharge at site 3, whereas at site 1 it is largely a product of ground water influx from higher elevations.

The water sample collected immediately downstream from the main workings (site 2) is characterized by concentrations of 130 ppb As and 2 ppb Sb. The arsenic concentration is the highest arsenic value detected in this study. Surprisingly, although both arsenopyrite and pyrite are abundant upstream, there is no iron enrichment in the water at site 2. Perhaps iron is rapidly precipitated as Fe-hydroxides subsequent to dissolution of sulfide minerals,

Table 1. Analytical data for hydrogeochemical samples.

[As, Cu, Fe, Pb, Sb, and Zn are in ppb; other dissolved species are in ppm except for alkalinity which was measured as mg/l as $CaCO_3$. T, temperature in degrees Celsius]

Site	T	pH	As	Cu	Fe	Pb	Sb	Zn	Ca	K	Mg	Na	Conductivity	Chloride	Nitrate	Sulfate	Alkalinity
Little Creek Prospect																	
1	8	7.98	6	<1	<10	<1	<1	8	10	0.1	0.1	1.7	120	1.44	0.62	3.61	27
2	12	7.81	130	<1	<10	<1	2	6	15	0.2	0.3	2.0	85	2.05	2.64	4.23	19
3	4	7.43	2	<1	<10	<1	<1	6	2.3	0.1	<0.1	0.6	37	0.43	<1.0	0.76	<10
4	4	7.35	2	<1	<10	<1	<1	3	2.3	0.1	<0.1	0.6	24	0.40	<1.0	0.73	<10
Sonny Fox Mine																	
5	11	7.74	2	<1	<10	<1	<1	4	8.4	0.1	<0.1	1.4	50	0.96	<1.0	3.03	25
6	4	7.72	10	<1	<10	<1	2	5	15	0.1	<0.1	1.7	64	1.44	0.71	5.27	40
7	6	7.43	6	<1	<10	<1	1	5	14	0.1	<0.1	1.7	52	1.30	0.60	4.57	35
8	7	7.14	4	<1	10	<1	<1	2	11	0.1	<0.1	1.7	61	1.30	<1.0	3.86	33
9	12	7.39	1	<1	<10	<1	<1	4	8.8	0.1	<0.1	1.3	74	0.87	<1.0	3.08	21
10	12	7.38	1	<1	10	<1	<1	4	9.0	0.1	<0.1	1.4	65	0.90	<1.0	3.18	25
11	6	7.08	1	<1	10	<1	<1	3	3.0	<0.1	<0.1	0.7	46	0.65	<1.0	0.88	15
12	6	7.28	<1	<1	10	<1	<1	3	3.0	0.1	<0.1	0.8	20	0.65	<1.0	0.79	13
Goyne Prospect																	
13	8	7.04	40	2	20	1	<1	8	2.9	0.1	<0.1	1.1	19	0.42	0.85	0.75	13
14	12	6.39	<1	<1	40	1	<1	6	0.8	<0.1	<0.1	0.9	14	0.32	0.54	<1.0	<10
15	12	7.26	3	<1	<10	<1	<1	6	5.4	0.1	<0.1	1.2	33	0.62	0.70	1.13	19
16	12	7.67	<1	1	<10	<1	<1	4	10	0.1	<0.1	1.8	62	0.84	0.71	2.82	40

whereas arsenic remains soluble. Major ion concentrations and pH values in water from site 2 are similar to those in water from site 1 and are notably greater than values in water collected from Ferrum Creek (site 3).

The high arsenic and antimony values found in the water samples collected below the Little Creek prospect (site 2) are no longer detectable when flow enters the main valley drainage. Data for a sample collected on Ferrum Creek downstream from the confluence (site 4) are essentially identical to those from the sample upstream from the confluence (site 3). These data indicate that the mine effluent is diluted to background levels after entering Ferrum Creek.

SONNY FOX MINE

Data from samples collected below the Sonny Fox mine (sites 5-12) show the same general trends as noted for those from the Little Creek prospect. Maximum values of 10 ppb As and 2 ppb Sb were determined for the sample of effluent collected from the mine portal (site 6). Anomalous arsenic can be traced downstream for about 500 m before dilution causes concentrations to drop to background levels of 1 to 2 ppb As (sites 7, 8, and 10). The highest values for Na, Ca, pH, chloride, nitrate, sulfate, and alkalinity were found in the sample of effluent collected nearest the mine (site 6). Dilution from the influx of unexchanged surface water occurs downstream. Glaciers are not present in the headwaters of Babcock Creek; however, an influx of water from snow melt was observed throughout the drainage basin. The concentrations of most dissolved species in the two water samples collected from Babcock Creek (sites 11 and 12) are identical to those in Ferrum Creek (sites 3 and 4), suggesting similar background concentrations of metals in water from both areas.

GOYNE PROSPECT

Different trends were noted in the data from water samples collected near the Goyne prospect (sites 13-16). Water emanating directly out of the main vein in the adit (site 13) contains 40 ppb As. But unlike waters collected nearest the Little Creek prospect and Sonny Fox mines (sites 2 and 6), water collected at the Goyne prospect (site 13) lacks anomalous concentrations of Sb and contains higher concentrations of Fe (20 ppb) and Pb (1 ppb). In addition, a stream flowing directly on top of the ore (site 14) contains 40 ppb Fe. The iron and lead enrichments possibly reflect the greater solubility of these species due to the slightly lower pH of the water at sites 13 and 14 (7.04 and 6.39, respectively). Two small creeks about 200 m north of the Goyne prospect (sites 15 and 16) con-

tain background amounts of arsenic (<1–3 ppb), lead (<1 ppb), and iron (<10 ppb).

Data also indicate a very low content of total dissolved species in the two water samples from the Goyne prospect (sites 13 and 14). The reason for the relatively low cation and anion content, as well as the acidic pH, in waters at this prospect is uncertain. These results are possibly related to the host igneous dike, whereas the veins at the Little Creek prospect and Sonny Fox mine are hosted by metasedimentary rocks. The igneous host rocks may have a somewhat lower acid-buffering capacity than the sedimentary rocks. The dike at the Goyne prospect is composed of at least 50 percent sodic andesine, with lesser potassium feldspar and quartz (Richter, 1970). Such a composition may not have been as amenable as that of the metagraywackes to extensive formation of Fe-, Mg-, and Ca-rich carbonate alteration.

ENVIRONMENTAL IMPLICATIONS

The hydrogeochemical data show that mine drainage waters below mesothermal gold veins in Kenai Fjords National Park have compositions that are in part a function of ore deposit geology. In a small drainage basin with undeveloped vein occurrences, the surface waters show an increase in arsenic from ≤3 ppb to 6 ppb. Concentrations of as much as 130 ppb arsenic in waters draining mine workings of this mineral deposit type reflect the arsenopyrite-dominant mineral assemblage. This extremely high arsenic value in one of the most alkaline waters in this study is believed to reflect a decreased sorption of arsenic on particulates at high pH (Smith and others, 1993). Alternatively, especially given the large volume of suspended matter noted during collection of this sample, arsenic might have been adsorbed onto colloidal material of <0.45 microns. Slight increases in antimony concentrations in alkaline waters and iron and lead in more acidic waters is also characteristic of the mine drainage.

The mesothermal gold deposits in south-central Alaska, although of high grade, are typically of low tonnage. Therefore, the chemical signatures of the ore deposit are very localized. Anomalous concentrations of arsenic and other heavy-metals in waters were found in small drainages immediately below mineral occurrences; mine drainage effluent is diluted rapidly downstream. During the summer, when glacial and snow melt runoff are at their maximum, no significant input of heavy-metals was detected in stream waters beyond about 500 m from the mine workings. Even where abundant metallic debris litters the landscape adjacent to mine workings and mine dump materials have been spread out along stream valleys, no adverse effects on dissolved stream load were detected in higher-order trunk streams. Unless significantly higher percentages of sulfide materials are present in veins or in associated dumps, or lesser carbonate minerals are available to prevent buffering of effluent from the deposits, our data suggest that small-scale mining of mesothermal gold veins along the northern Gulf of Alaska may not have a significant effect on surface-water quality. However, additional data collected during the fall and winter are required to determine if little impact is also characteristic of periods of low surface discharge.

REFERENCES CITED

Borden, J.C., Goldfarb, R.J., Gent, C.A., Burruss, R.C., and Roushey, B.H., 1992, Geochemistry of lode-gold deposits, Nuka Bay district, southern Kenai Peninsula, *in* Bradley, Dwight, and Dusel-Bacon, Cynthia, Geologic studies in Alaska by the U.S. Geological Survey, 1991: U.S. Geological Survey Bulletin 2041, p. 13–22.

Fishman, M.J., and Pyen, G., 1979, Determination of selected anions in water by ion chromatograph: U.S. Geological Survey Water Resources Investigation Report 79-101, 30 p.

Goldfarb, R.J., Leach, D.L., Miller, M.L., and Pickthorn, W.J., 1986, Geology, metamorphic setting, and genetic constraints of epigenetic lode-gold mineralization within the Cretaceous Valdez Group, south-central Alaska, *in* Keppie, J.D., Boyle, R.W., and Haynes, S.J., eds., Turbidite-hosted gold deposits: Geological Association of Canada Special Paper 32, p. 87–105.

Perkin-Elmer Corporation, 1976, Analytical methods for atomic-absorption spectrophotometry: Norwalk, Conn., Perkin-Elmer Corporation, 586 p.

Perkin-Elmer Corporation, 1977, Analytical methods for atomic-absorption spectrophotometry, using the HGA graphite furnace: Norwalk, Conn., Perkin-Elmer Corporation, 208 p.

Richter, D.H., 1970, Geology and lode-gold deposits of the Nuka Bay area, Kenai Peninsula, Alaska: U.S. Geological Survey Professional Paper 625G, 16 p.

Smith, K.S., Ficklin, W.H., Plumlee, G.S., and Meier, A.L., 1993, Computer simulations of the influence of suspended iron-rich particulates on trace-metal removal from mine-drainage waters: Sixth Billings Symposium on Planning, Rehabilitation, and Treatment of Disturbed Lands, Billings, Montana, March 21–27, 1993, Proceedings, Volume II, p. 107–115.

Smith, P.S., 1938, Mineral industry of Alaska in 1936: U.S. Geological Survey Bulletin 897–A, p. 1–107.

Reviewers: Johnny Gray and Helen Folger

Paleowind Directions for Late Holocene Dunes on the Western Arctic Coastal Plain, Northern Alaska

By John P. Galloway *and* L. David Carter

Late Holocene stabilized longitudinal and parabolic dunes occur across much of the western Arctic Coastal Plain except for river flood plains and terraces (fig. 1, Galloway and Carter, 1993). Parabolic dunes are excellent indicators of wind direction, because they form downwind of a local sand source and do not migrate (Pye and Tsoar, 1990). The approximate direction of the wind that formed a parabolic dune can be determined by measuring the orientation of the dune's long axis, which is a line that bisects the angle formed by the dune arms. The open end of the parabolic dune indicates the upwind direction. Longitudinal dunes are linear sand ridges aligned parallel with the predominant winds; they usually have longitudinal axes within 15° of the strongest wind direction. The utility of longitudinal dunes for determination of wind direction is controversial (Tseo, 1993). For the Arctic Coastal Plain, however, the orientation of longitudinal dunes generally parallels the long axes of parabolic dunes. Thus, we assume that the orientations of longitudinal dunes in this region are parallel to the winds that formed them. This paper uses measurements of the

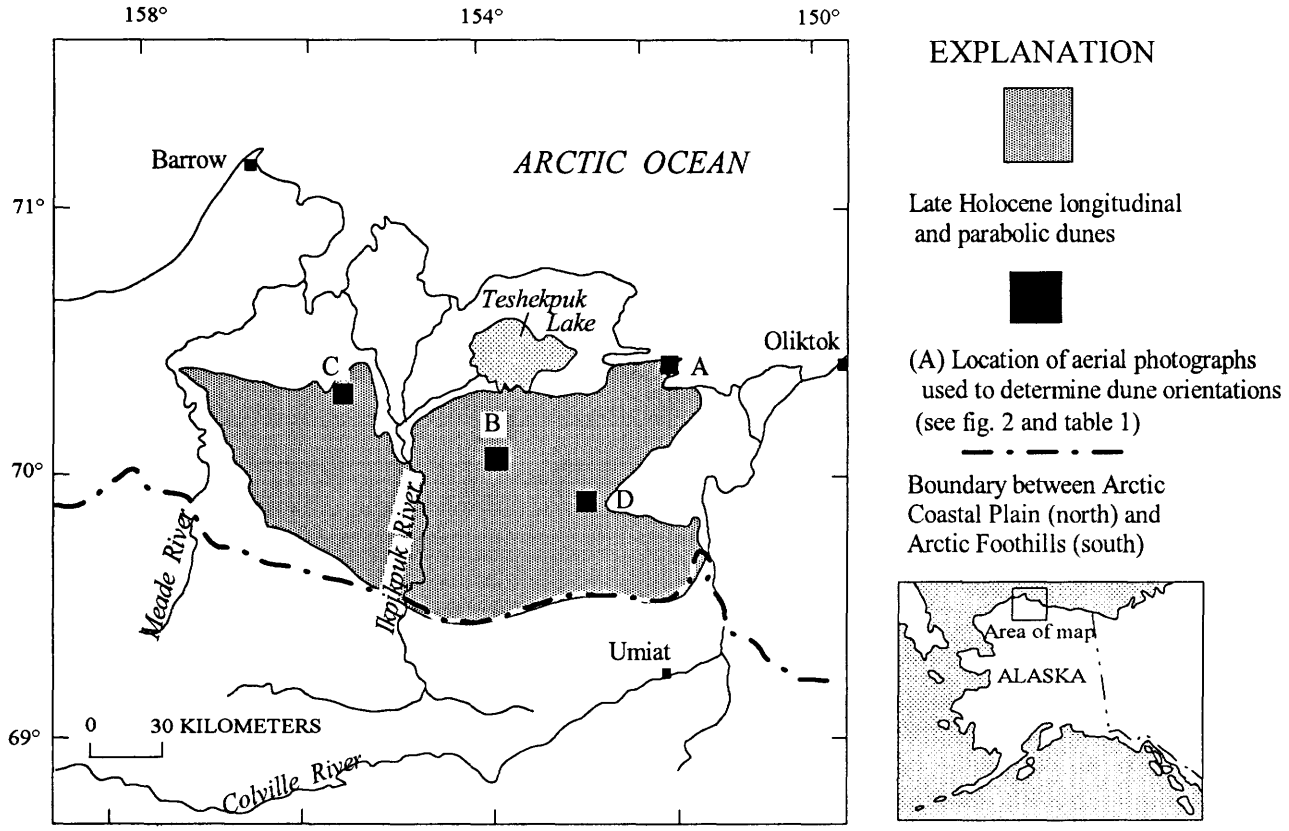

Figure 1. Distribution of stabilized longitudinal and parabolic dunes and locations mentioned in text.

Table 1. Summary of mean azimuth for stabilized parabolic and longitudinal dunes.

Location (see fig. 1)	Types of Dunes: Parabolic Dunes: East opening: Number	Mean azimuth	Outside 1σ	West opening: Number	Mean azimuth	Outside 1σ	Longitudinal Dunes: Number	Mean azimuth	Outside 1σ
A	16	69°± 9°	3	1	73°	–	44	70°± 14°	13
B	50	76°± 9°	12	4	75° ± 12°	1	75	70°± 11°	17
C	3	79°± 2°	1	1	82°	–	36	78°± 6°	10
D	12	71 ± 7°	6	–	–	–	127	71°± 7°	27
Total or average azimuth	81	74 ± 9°	22	6	76 ± 10°	1	282	71 ± 10	67

orientations of longitudinal dunes and the line that bisects the arms of parabolic dunes to determine late Holocene wind directions, and compares these orientations to those of modern sand-moving winds.

A description of the dunes, together with radiocarbon ages for paleosols associated with them, was given by Galloway and Carter (1993). They described the dunes as 15 to 40 m wide, and averaging 600 to 835 m long, depending on location within the dune field. Most dunes are 1 to 3 m thick, and the density of dunes ranges from a few to more than 275 per 100 km^2. Radiocarbon ages for the associated paleosols show that the dunes were active during several late Holocene episodes of landscape instability.

Three hundred and sixty-nine measurements (table 1) were made of dune axes for stabilized parabolic and longitudinal dunes in four areas that we judged to be representative of the dune field (fig. 1). The measurements were made on black and white aerial photographs taken in 1955. Eighty-seven (24 percent) of the measured dunes are parabolic dunes that give unequivocal evidence for the direction of the winds that formed them. Ninety-three percent of these parabolic dunes were formed by northeasterly winds and have long axes whose azimuths average 74 degrees (fig. 2). This azimuth is nearly identical (76°) to the average azimuth for the remainder of the parabolic dunes, but these dunes were formed by southwesterly winds that were approximately 180 degrees opposed to the northeasterly winds. This indicates a bimodal regime of sand moving winds, with most sand movement being accomplished by the northeasterly winds.

The mean azimuth for the long axes of all 282 of the longitudinal dunes is 71 degrees, which is essentially parallel to the long axes of the parabolic dunes (fig. 2). Twenty-four percent of the longitudinal dunes have long axes that are not encompassed by 1σ from the mean azimuth. The longitudinal dunes could have been formed by northeasterly winds, southwesterly winds, or winds from both directions. Their orientations are therefore compatible with the bimodal wind regime indicated by the parabolic dunes.

To compare this late Holocene, bimodal dune-forming wind regime with modern winds that are capable of moving sand, we used surface wind observations obtained from the National Climatic Data Center, Asheville, North Carolina. Surface wind data are available for two coastal locations on the Arctic Coastal Plain in the vicinity of our study area; Barrow and Oliktok (fig. 1). To determine the potential for eolian sand movement at these two locations we used the method described by Fryberger (1979), which determines potential sand drift for the 16 compass directions. This method considers only wind speeds greater than 5.7 m/s, which is the threshold wind velocity for the movement of medium sand. Cumulative curves for 20 samples of eolian sand from the Pleistocene dunes that underlie and are the main source of sand for the late Holocene dunes (Galloway, 1982) indicate that 90 percent of the sand is capable of being transported at a velocity of 5.7 m/s.

Our calculations from annual percentage frequency of wind directions for the two coastal sites (Barrow and Oliktok) show east-northeast (ENE.) and east (E.) as the dominant sand-moving winds, followed by northeast winds (NE.) with west-southwest (WSW.) as a secondary minor wind direction (fig. 3). In an earlier study, Black (1951, p. 93) stated that "numerous oriented lakes and dunes throughout the coastal plain show that these maximum winds are just as consistent and effective inland and that slightly more erosion is produced by the easterly (65° to 80°) than by the westerly winds (245° to 260°)." Modern blowouts (deflation hollows) in the region also indicate a bimodal wind regime of ENE.–WSW., with the majority of the blowouts produced by easterly winds.

These measurements, calculations, and observations indicate that the paleowinds responsible for formation and modification of the now stabilized, late Holocene dunes had the same directional regime as the modern sand-moving winds. Earlier studies showed that these late Holocene dunes

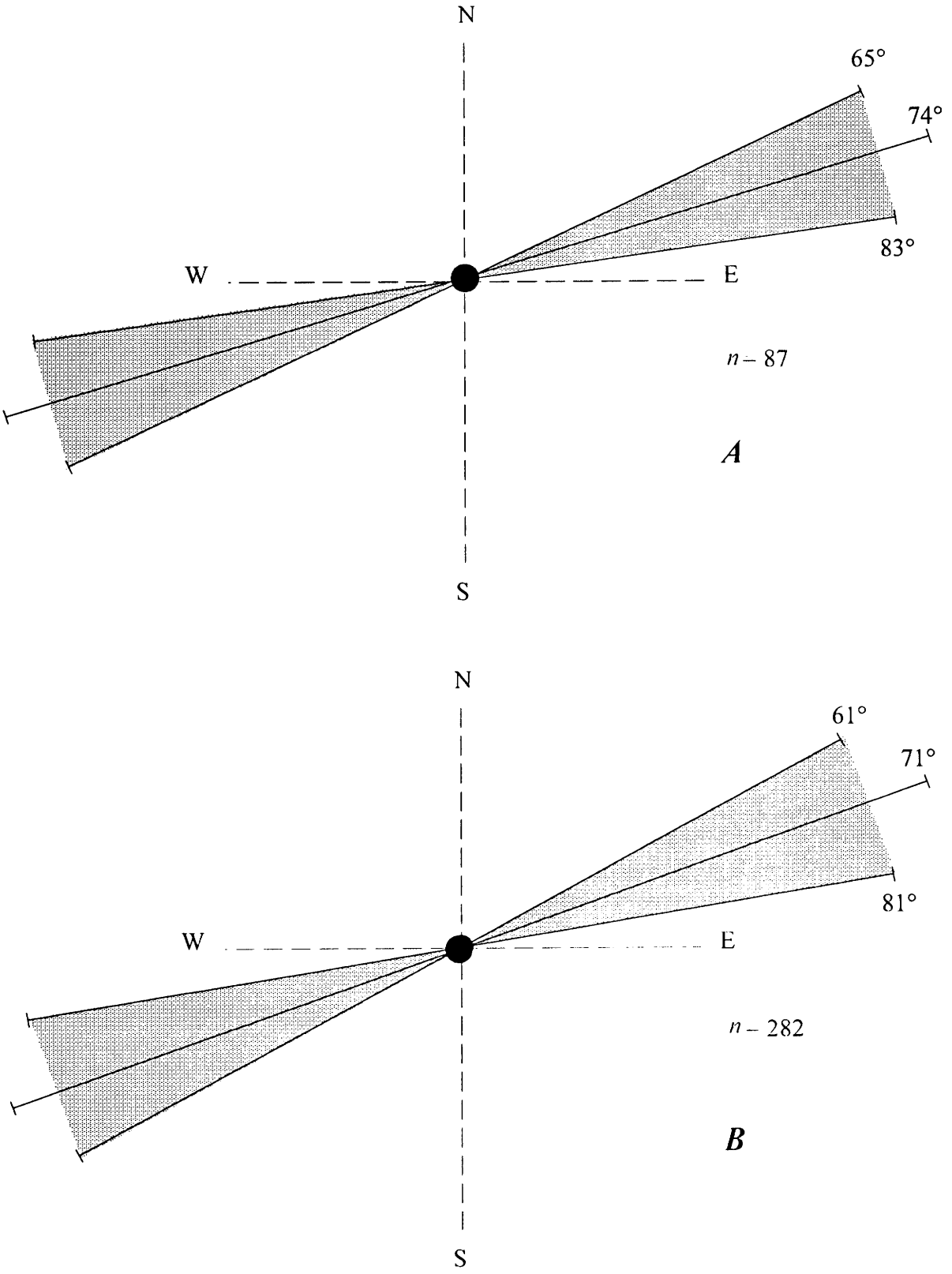

Figure 2. Diagrams showing mean azimuth with one standard deviation for stabilized parabolic dunes (*A*) and longitudinal dunes (*B*). *n*, total number of measurements.

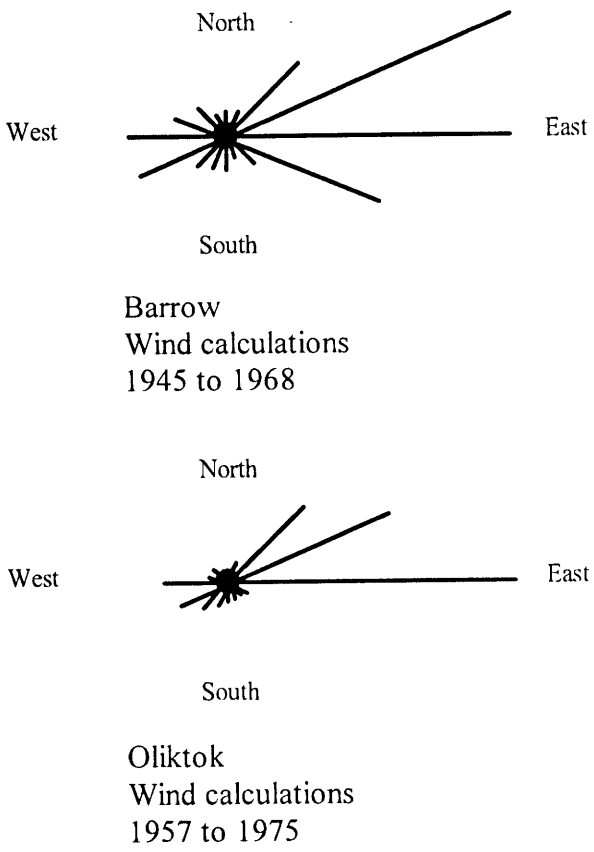

Figure 3. Wind rose diagrams depicting annual distribution of wind directions calculated for wind speeds greater than 5.7 m/s. (see fig. 1 for location).

were active during cooler climates and drier surface conditions than those of today, which broadly coincided with episodes of Neoglacial expansions of cirque glaciers in the Brooks Range (Galloway and Carter, 1993).

REFERENCES CITED

Black, R.F., 1951, Eolian deposits of Alaska: Arctic, v. 4, no. 2, p. 89–111.

Fryberger, S.G., 1979, Dune forms and wind regime, *in* McKee, E.D., ed., A study of global sand seas: U.S. Geological Survey Professional Paper 1052, p. 137–169.

Galloway, J.P., 1982, Grain-size analysis of 20 eolian sand samples from northern Alaska, *in* Coonrad, Warren, ed., The United States Geological Survey in Alaska—Accomplishments during 1980: U.S. Geological Survey Circular 844, p. 51–53.

Galloway, J.P., and Carter, L.D., 1993, Late Holocene longitudinal and parabolic dunes in northern Alaska: Preliminary interpretations of age and paleoclimatic significance, *in* Dusel-Bacon, Cynthia, and Till, A.B., eds., Geologic studies in Alaska by the U.S. Geological Survey, 1992: U.S. Geological Survey Bulletin 2068, p. 3–11.

Pye, Kenneth, and Tsoar, Haim, 1990, Aeolian sand and sand dunes: Boston, Unwin Hyman, 396 p.

Tseo, George, 1993, Two types of longitudinal dune fields and possible mechanisms for their development: Earth and Surface Processes and Landforms, v. 18, no. 7, p. 627–643.

Reviewed by David Mouat and Warren Yeend

Methane in the Fox Permafrost Tunnel Near Fairbanks, Alaska

By Keith A. Kvenvolden, Thomas D. Lorenson, *and* Valerie Barber

ABSTRACT

As part of a study to assess the methane content of permafrost, we have examined the Fox permafrost tunnel, located about 16 km north of Fairbanks, near the town of Fox, Alaska. The tunnel, excavated by CRREL (Cold Regions Research and Engineering Laboratory) and the U.S. Bureau of Mines, penetrates about 110 m of perennially frozen silts of late Pleistocene and early Holocene age. We measured methane in the tunnel air and in selected samples of ice and frozen silt, cored from the walls of the tunnel. The methane content of the tunnel air was measured at several sites within the tunnel at nine different times between 1990 and 1993 and compared with the methane content of atmospheric air outside the tunnel. Methane is generally well-mixed throughout the tunnel; however, seasonal variations do occur. The largest methane concentrations were observed in October 1992 (41.5±0.22 parts per million by volume [ppmv]) and the smallest in February 1993 (5.15±0.66 ppmv). On the same dates, the outside atmosphere contained 2.06±0.00 and 2.05±0.01 ppmv, respectively. Thus, the air in the tunnel has 2.5 to 20 times more methane than the outside atmosphere. Permafrost in the tunnel sublimates because of moisture loss to very dry air that circulates through the tunnel. During sublimation methane is released from the permafrost.

Core samples of ice and frozen silt contain varying quantities of methane: pond ice (0–1.8 μg/kg); thaw bulb under pond ice (58–120 μg/kg); wedge ice (0–15 μg/kg); pore ice with silt (2,100–2,400 μg/kg); and silt with pore ice (4,000–9,700 μg/kg). The carbon isotopic composition of methane from the pond ice and silt with pore ice averages −86.9±0.4 per mil (relative to the PDB standard), indicating that the methane results from the microbial decomposition of sediment organic material. The methane contents of tunnel air and core samples from the tunnel walls indicate that permafrost, when destabilized by sublimation and melting, can be a high-latitude source of atmospheric methane.

INTRODUCTION

Between 1963 and 1969, a tunnel was excavated by the U.S. Army Corps of Engineers, Cold Regions Research and Engineering Laboratory (CRREL) into permafrost near the community of Fox (64°57′ N., 147°37′ W.), about 16 km north of Fairbanks, Alaska (fig. 1). The tunnel penetrates into the north-facing side of Goldstream Valley about 110 m, providing a continuous exposure of undisturbed, perennially frozen, ice-rich, fossil-bearing silt and alluvium above schistose bedrock (Sellmann, 1967, 1972). The age of the frozen sediments ranges from late Pleistocene to early Holocene (~46,000 to ~7,000 yr B.P.) (Hamilton and others, 1988). Originally, the tunnel was used to evaluate various methods of excavating and stabilizing underground openings in frozen ground. Now it serves as an underground laboratory for basic and applied research related to the permafrost environment and as a tourist attraction.

The 110-m-long horizontal tunnel, called an adit, was dug by CRREL during 1963–1966 (fig. 1). A vertical ventilation shaft, which allows winter air circulation to cool and stabilize the tunnel, was completed in 1965. In 1969 the U.S. Bureau of Mines excavated a 61-m-long inclined passage, called a winze, that slopes downward at 12° from the main tunnel near the entrance (fig. 1). Currently, the operation of the facility is jointly supported by CRREL, the Bureau of Mines, and the University of Alaska. Besides being used to evaluate underground excavation techniques in frozen ground, the tunnel has been used for the study of engineering properties of permafrost (standard index parameters, compressive and tensile strengths, modulus of deformation), acoustic and electrical properties, sublimation processes, and geologic and paleoecological histories (summarized by Hamilton and others, 1988).

Our study of the methane content of the tunnel air and of core samples of frozen materials from the tunnel walls was designed to evaluate permafrost as a possible source of atmospheric methane in global warming (Kvenvolden and Lorenson, 1991; Lorenson and others, 1992; Kvenvolden and Lorenson, 1993; Kvenvolden and others,

1993). Our objective is to quantitatively evaluate the unsubstantiated statement by the United Nations Intergovernmental Panel on Climate Change (IPCC) that permafrost is an important high-latitude source of atmospheric methane (Houghton and others, 1990). The permafrost tunnel provides an accessible and well-described site where we were able to (1) measure the methane content of tunnel air at several locations within the tunnel and at different times of the year over a span of 3 years, (2) compare the methane content of tunnel air with the atmospheric concentrations, and (3) measure the methane content of cores taken from the walls of the tunnel. Preliminary results have been reported previously (Kvenvolden and others, 1992, 1993).

GEOLOGY

Hamilton and others (1988) have provided a comprehensive description of the geology of the permafrost tunnel, and much of this section summarizes their observations. A generalized geologic section of the tunnel is shown in figure 1. The lowest part of the winze penetrates frozen bedrock, which is a weathered schist of the Yukon crystalline terrane (Templeman-Kluit, 1976). Overlying the bedrock is a 3- to 4-m-thick deposit of sandy gravel and gravelly sand containing lenses of organic silt, silty fine sand, and sandy fine gravel. The gravel is perennially frozen and bonded with ice. Generally unstratified and well-sorted silt, 14- to 17-m thick, overlies the gravel and is the most widespread lithologic type in the tunnel. The silt is divided into two depositional units separated by an unconformity. Both units are characterized by high organic carbon contents with average values reaching 6.3 and 6.8 percent. Ground ice in the silt includes pore ice, wedge ice, and pond ice, samples of which were collected for methane analysis (locations shown in fig. 2), and segregated ice. Near the tunnel entrance are debris-fan deposits composed of subangular pebbles and cobbles in a matrix of silty sand and sandy silt. Animal macrofossils and plant remains occur throughout the sediment exposed in the tunnel. Radiocarbon ages indicate that the frozen sediments within the tunnel span a period of geologic time ranging from <46,000 to ~7,000 yr B.P.

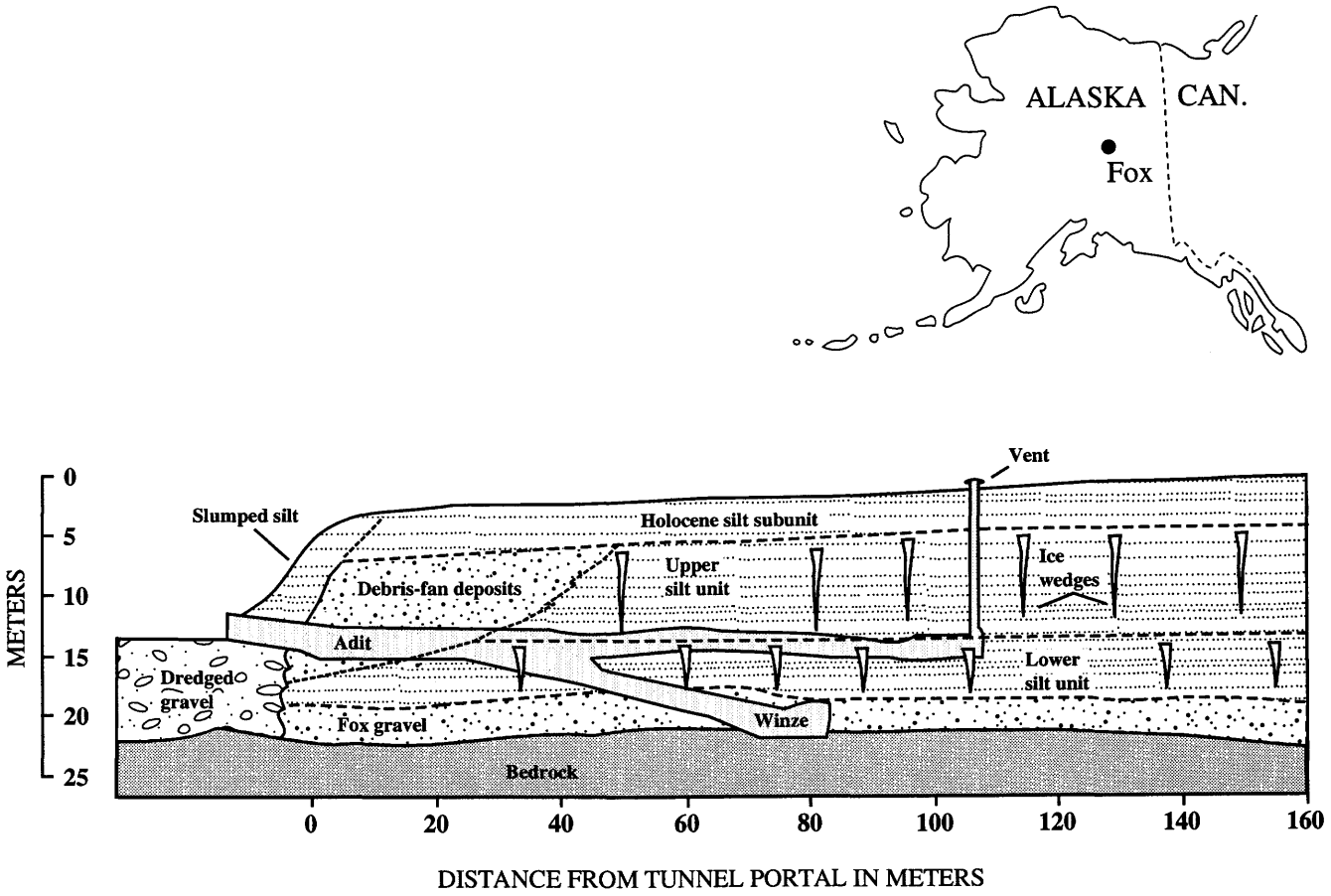

Figure 1. Location map and generalized geologic section of the Fox permafrost tunnel. Slightly modified from Hamilton and others (1988).

METHODS

For the purpose of obtaining air samples within and outside of the permafrost tunnel at various times during the year, 11 sampling sites were designated as shown on figure 2. Site 1 was outside the tunnel, where air samples were collected to determine the atmospheric content of methane. Site 2 was located in the air lock that separates the tunnel from the outside. The other sites were positioned throughout the tunnel to determine the extent of mixing of methane within the tunnel system. Some or all of the sites were sampled nine times between 1990 and 1993.

Air samples were collected at each of the sites in 40-cc syringes, usually in duplicate or triplicate, and analyzed within 24 hours by gas chromatography on a 1-m-long, 5-Å, molecular sieve (60/80 mesh) column. Results are reported in parts per million by volume (ppmv). Samples of the frozen tunnel walls were obtained in the adit by means of a SIPRE ice corer (7.6-cm internal diameter). The recovered core segments, approximately 10 cm in length, were sealed in gas-tight containers and weighed. Procedures for extraction and analysis of methane follow those of Kvenvolden and Lorenson (1993). Degassed water was added to most of the samples to establish a 100-cc headspace, which was purged with helium through septa-covered ports after the container was sealed. For methane analysis, the samples were thawed, the container shaken, and a portion of the headspace was analyzed by gas chromatography. Results are reported in micrograms of methane per kilogram of sample. In most cases, except for silt with pore ice, the samples were predominantly ice. Carbon isotopic composition of methane in selected tunnel-wall samples were obtained through Global Geochemical Company, Canoga Park, California, and reported in per mil relative to the Peedee Belemnite Standard.

RESULTS

Methane was measured in tunnel air and in the atmosphere outside the tunnel on nine occasions during a

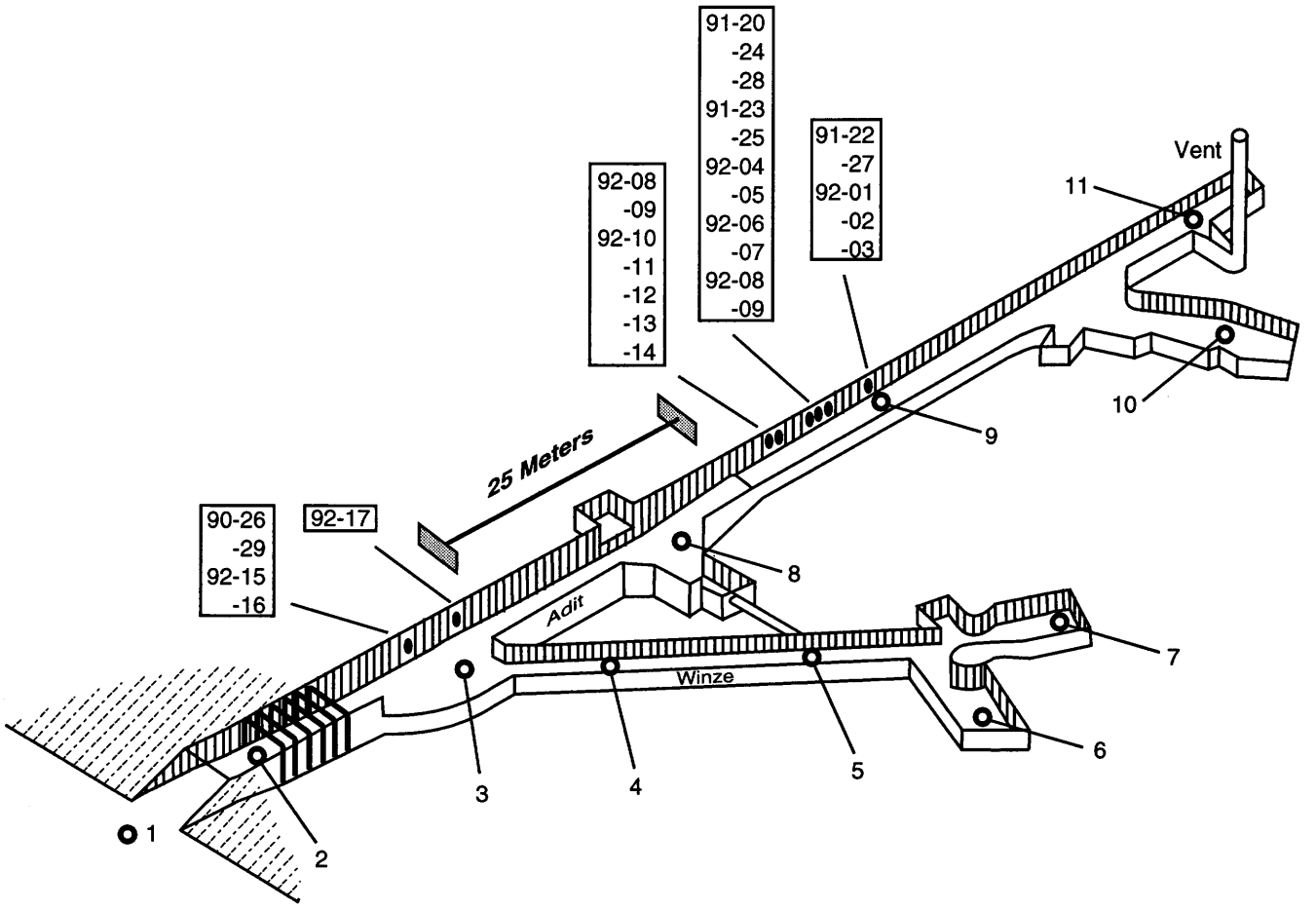

Figure 2. Isometric view of the Fox permafrost tunnel showing sites where air samples (open circles) and permafrost cores (solid circles) were collected for methane analysis. Adit and winze are 110-m and 61-m long, respectively. Numbers in boxes refer to core samples listed in table 2. No core samples were collected in the winze. Samples from different core materials are listed in sets designated by year (90-, 91-, and 92-). Modified from Kvenvolden and others (1993).

Table 1. Concentrations of methane (ppmv) within and outside the Fox permafrost tunnel measured at 11 sites on 9 days between 1990 and 1993.

[Numbers in parentheses are the number of samples measured. nd, not determined]

Site	06/15/90	04/04/91	05/21/91	07/17/91	08/14/91	04/02/92	07/17/92	10/16/92	02/26/93
1	1.71±0.01 (4)	1.84±0.01 (3)	1.79±0.02 (2)	1.75±0.04 (2)	1.81±0.01 (2)	1.96±0.00 (2)	1.75±0.04 (2)	2.06±0.0 (2)	2.05±0.01 (2)
2	4.24 (1)	13.19±1.04 (3)	7.75±0.66 (2)	nd	11.37±0.05 (2)	6.58±0.11 (2)	nd	41.2±0.0 (2)	4.26±0.25 (2)
3	12.87±0.07 (2)	35.75±0.73 (3)	15.60±1.75 (2)	15.04±0.11 (2)	10.94±0.30 (2)	26.89±0.08 (4)	15.04±0.11 (2)	41.8±0.0 (2)	4.26±0.25 (2)
4	13.07±0.10 (3)	35.24±0.08 (3)	16.61±0.10 (2)	14.95±0.04 (2)	10.87±0.52 (2)	27.02±0.21 (2)	14.95±0.42 (2)	41.6±0.1 (2)	4.98±0.23 (2)
5	12.80±0.06 (3)	35.15±0.04 (3)	16.50±0.50 (2)	15.04±0.13 (2)	11.30±0.28 (2)	nd (2)	15.04±0.13 (2)	41.8±0.2 (2)	5.12±0.13 (2)
6	nd	35.09±0.36 (3)	nd	15.11±0.11 (2)	11.30±0.27 (2)	26.62±0.69 (3)	15.11±0.11 (2)	41.5 (1)	5.14±0.26 (2)
7	nd	35.32±0.11 (3)	nd	nd	nd	nd	nd	41.5 (1)	4.91±0.31 (2)
8	nd	35.51±0.13 (3)	15.21±0.01 (2)	14.18±0.12 (2)	11.22±0.25 (2)	27.13±0.04 (2)	14.18±0.12 (2)	41.5 (1)	5.05±0.02 (2)
9	nd	35.40±0.06 (3)	16.06±0.38 (2)	15.10±0.12 (2)	10.89±0.81 (2)	27.05±0.05 (2)	15.10±0.12 (2)	41.3 (1)	4.62 (2)
10	nd	35.46±0.07 (3)	nd	14.90±0.04 (2)	11.06±0.02 (2)	25.63±1.79 (2)	14.90±0.04 (2)	41.5 (1)	5.16±0.07
11	nd	35.46 (1)	nd	nd	nd	27.21±0.24 (2)	nd	41.5 (1)	6.74±0.57 (2)
Average 3-11		35.37±0.32 (24)	15.99±0.84 (10)	14.90±0.32 (14)	11.08±0.36 (14)	26.80±0.70 (16)	14.90±0.33 (14)	41.6±0.2 (12)	5.26±0.61 (17)

period between June 15, 1990, and February 26, 1993. The results are listed in table 1 and summarized in figure 3. As an example of the methane distribution in the tunnel on a given day, results obtained on April 4, 1991, are shown at the eleven sampling sites (fig. 4), demonstrating that on this date the methane was apparently well-mixed within the tunnel system. At the sample site outside the tunnel, methane concentrations increased from 1.71 ppmv in 1990 to 2.05 ppmv in 1993. At the sample site inside the air lock, methane concentrations usually were intermediate between tunnel air and the outside atmosphere; however, on three occasions (August 1991, October 1992, and February 1993) the air lock was open to the tunnel, and methane concentrations in the air lock were similar to the concentrations measured within the main tunnel system.

Methane concentrations in samples of frozen materials sampled from the adit wall were variable, with the highest values (9,700 μg/kg) found in samples of silt with pore ice, and the lowest values (<2 μg/kg) in pond ice (table 2). The tunnel was sampled in two consecutive years (1991 and 1992), and quantitatively similar results were obtained from the same kinds of frozen materials from the same sample locations. Carbon isotopic compositions of methane from pond ice and silt with pore ice average −86.9±0.4 per mil, which is consistent with organic matter as the source of methane carbon and methanogenesis as the mediating process.

DISCUSSION

Our results clearly demonstrate that methane is present in the air of the permafrost tunnel at concentrations ranging from 2.5 to 20 times greater than its atmospheric concentration (table 1). On any given day, methane within the tunnel is usually well mixed (fig. 3); that is, measurements taken from air samples throughout the tunnel are within ±1 ppmv. Only in February 1993 was the concentration of methane significantly higher at the end of the tunnel (site 11, 6.74±0.57 ppmv) relative to the average concentration that same day of 5.26±0.61 ppmv. A ventilation shaft is located near site 11 (fig. 2), and air circulation through this shaft must have an effect on methane concentrations in this region of the tunnel.

The air lock at the entrance to the tunnel separates the main tunnel system from the outside atmosphere, and methane concentrations within the air lock reflect the mixing of air from the tunnel with the air from outside. On 3 days when measurements were made, the internal door of the air lock was open and the external door was closed for a time that was sufficient for the methane concentrations in the air lock to be similar to those measured within the tunnel (table 1). In all cases, the methane concentrations in the air lock were 2 to 20 times greater than in the outside atmosphere.

The variability of the methane content of the tunnel air during the year (fig. 2, table 1) is due in part to the

history of usage of the tunnel. During the winter, the tunnel is chilled naturally by cold outside air that is circulated by convection through the ventilation shaft at the rear of the tunnel and an opening at the entrance. Some excess moisture in this air is condensed as frost on the cold ceiling. During the summer, air is not circulated, and a refrigeration system is used to cool the tunnel to compensate for the warming that takes place when hundreds of visitors come to observe the features and properties of the permafrost environment. Refrigeration in the summer also lowers the relative humidity of the air. We sampled tunnel air at random opportunities that were not coordinated with the usage events of the tunnel. Our results (fig. 2, table 1) suggest that methane concentrations in the tunnel air are high in spring and decrease during the summer. The highest methane concentrations (41.6±0.2 ppmv) were recorded in October 1992, but unfortunately, methane measurements were not made in October of the previous two years. The lowest methane values (5.26±0.61 ppmv) were obtained during the winter (February 1993), but only one set of measurements could be made at this time of year during the study period. Although the concentrations of methane in the tunnel vary during the year, the source of this methane must be within the tunnel itself. We believe that the methane comes from the permafrost and is released by the process of sublimation.

Ice in the exposed frozen walls of the tunnel is sublimating because of contact with relatively dry air (Johansen and others, 1981). Winter cooling by outside air circulation and summer cooling by refrigeration act together to maintain the thermal regime. Exposed permafrost is sublimating due to the relative dryness of the tunnel air both in winter and in summer. The sublimation of ice in silt exposed in the walls has produced a large amount of dust that is ubiquitously present throughout the tunnel. As a result of sublimation, methane which has been dissolved in the ice and trapped by the silt is apparently released from the permafrost.

Analyses of core samples of ice and silt with pore ice (table 2) confirm the presence of methane in the walls of the tunnel, with the highest concentrations (up to 9,700 µg/kg) being found in silt with pore ice. This silt is organic-rich,

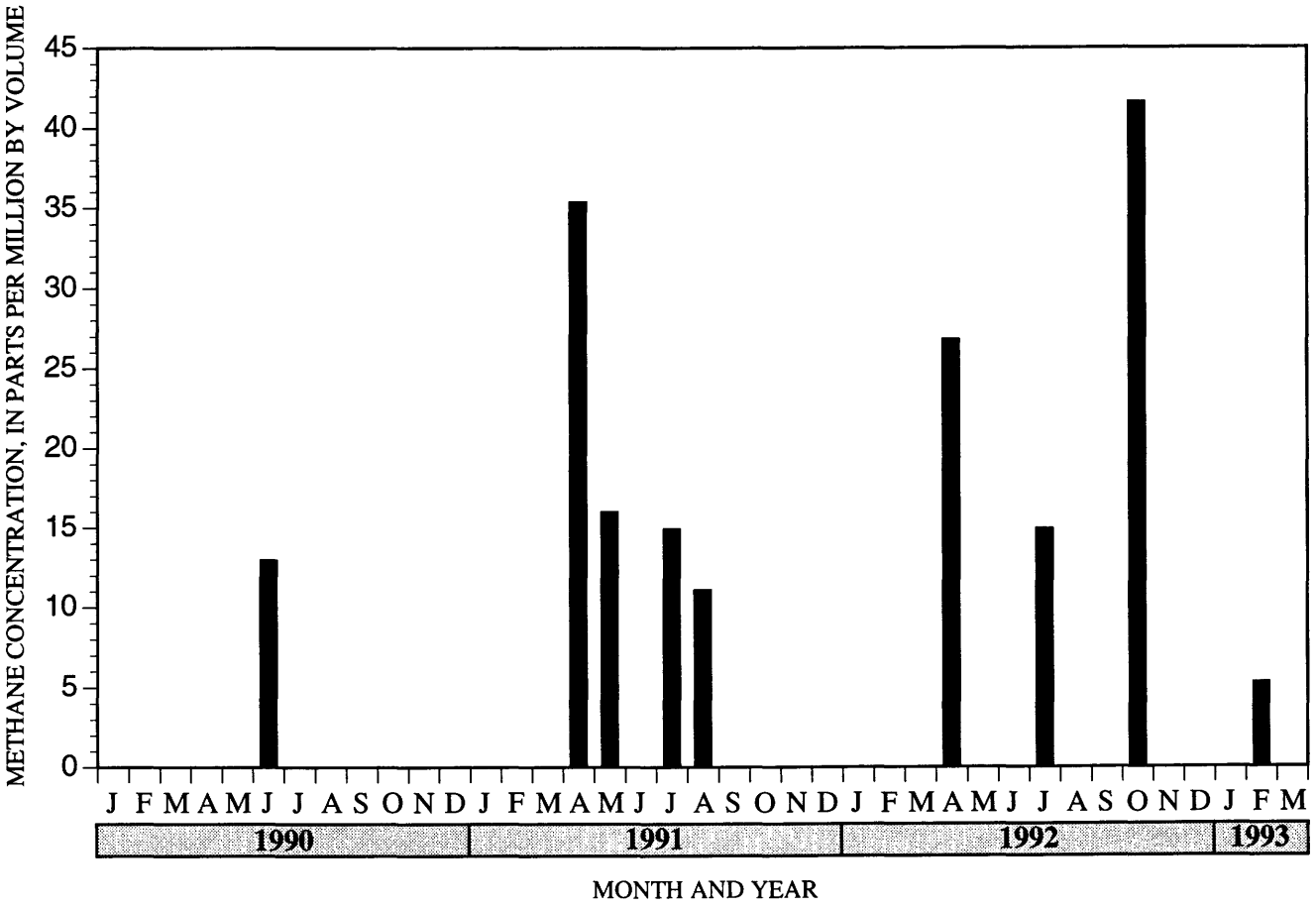

Figure 3. Average methane concentrations (ppmv) measured 9 times at 5 to 10 stations during 1990–1993 in the air of the Fox permafrost tunnel.

Table 2. Methane concentrations (μg/kg) in core samples of permafrost from the walls of the Fox permafrost tunnel.

Sample	Distance*	Description	Wt. (g)	Methane (μg/kg)	$\delta^{13}C$ (per mil)
91-22	78	Pond ice	402.8	0.8	
27	78	Pond ice	411.0	0.8	
20	74	Wedge ice	381.2	3.3	
24	74	Wedge ice	445.6	2.4	
28	74	Wedge ice	279.5	5.4	
23	71	Pore ice with silt	450.1	2,400	
25	71	Pore ice with silt	566.7	2,100	–86.7
26	28	Silt with pore ice	558.1	4,100	–87.5
29	28	Silt with pore ice	505.5	9,200	–86.6
92- 1	78	Pond ice	374.4	0.0	
2	78	Pond ice	373.8	3.6	
3	78	Pond ice	456.8	1.8	
4	74	Thaw bulb under pond ice	347.6	58	
5	74	Thaw bulb under pond ice	298.8	120	
6	72	Wedge ice	339.3	0.0	
7	72	Wedge ice	321.5	3.2	
8	69	Paleosol	441.7	1,100	
9	69	Paleosol	470.8	1,600	
10	66	Wedge ice	334.4	0.0	
11	66	Wedge ice	333.8	15	
12	66	Paleosol	450.4	390	
13	66	Paleosol	408.2	200	
14	66	Holocene permafrost	449.8	230	
15	28	Silt with pore ice	428.8	9,700	–87.0
16	28	Silt with pore ice	470.3	4,000	–86.9
17	36	Groundwater ice	269.6	170	

* Distance measured from each sample site to the inner portal of the tunnel.

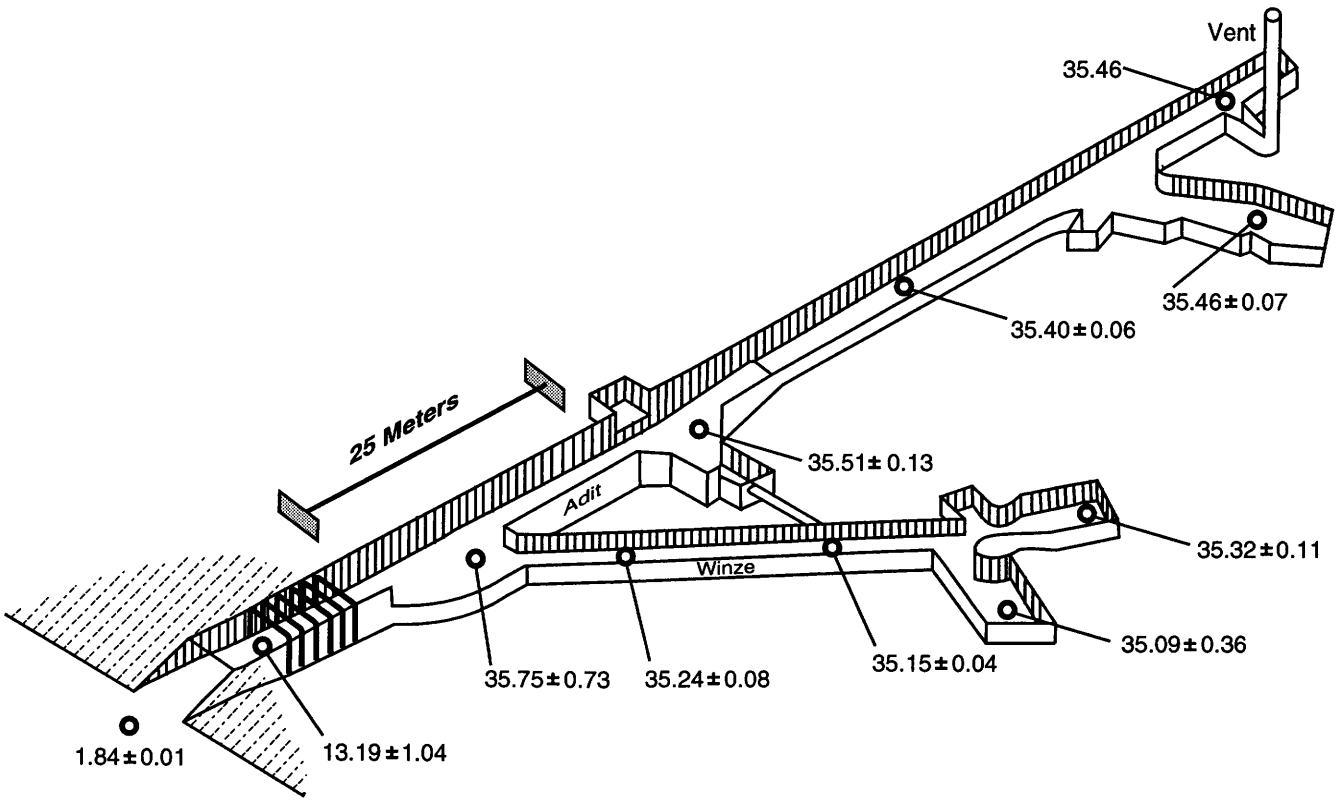

Figure 4. Isometric view of the Fox permafrost tunnel showing methane concentrations (ppmv) in tunnel air at 11 stations, sampled on April 4, 1991.

containing up to 6.8 percent organic carbon (Hamilton and others, 1988). Carbon isotopic composition of methane ($\delta^{13}C_1 = -86.9 \pm 0.4$ per mil) from the frozen material of the tunnel walls suggests that the methane is likely to be derived from the microbial decomposition of the abundant organic matter in the permafrost. Such an isotopically light methane composition is indicative of microbial processes (Schoell, 1988).

We have clearly demonstrated that methane is present in permafrost and can be released when permafrost is destabilized. In the case of the permafrost tunnel, sublimation provides an efficient, direct process for methane release into the atmosphere. More commonly, however, melting of ice is the dominant process of permafrost destabilization. This process leads to dissolution and possible oxidation of methane in the water, rather than to direct release of methane into the atmosphere (Kvenvolden and Lorenson, 1993). Thus, our results provide evidence for the maximum amount of methane that could reach the atmosphere during the destabilization of permafrost caused by, for example, global warming.

CONCLUSIONS

This paper demonstrates that methane is present in permafrost, especially in silt with pore ice, in the Fox permafrost tunnel. The methane is probably derived from the microbial decomposition of organic matter that is common in the silt. Methane is released from the permafrost in the tunnel by sublimation processes that occur because of the air exchange that takes place during tunnel operations. The air inside the tunnel contains 2.5 to 20 times more methane than does the air outside the tunnel. The amount of methane observed in the tunnel provides a guide to the maximum amount that can be expected to come from the destabilization of permafrost during global warming.

Acknowledgments.—We thank B. Brockett, W. Olson, D. Dillingham, and S. Wagner, CRREL, for assistance in gaining access to the permafrost tunnel and for coring equipment; N. Johansen, University of Alaska, Fairbanks, and M. Lilly, U.S. Geological Survey, Fairbanks, Alaska, for guidance and assistance in sampling; and W. Reeburgh and S. Whalen, University of Alaska, Fairbanks, for logistical and laboratory support. This research is supported in part by the U.S. Geological Survey's Global Change and Climate History Program.

REFERENCES CITED

Hamilton, T.D., Craig, J.L., and Sellmann, P.V., 1988, The Fox permafrost tunnel: A late Quaternary geologic record in central Alaska: Geological Society of America Bulletin, v. 100, p. 948–969.

Houghton, J.T., Jenkins, G.J., and Ephraums, J.J., eds., 1990, Climate Change: Cambridge, Cambridge University Press, 365 p.

Johansen, N.I., Chalich, P.C., and Wellen, E.W., 1981, Sublimation and its control in the CRREL permafrost tunnel: Hanover, New Hampshire, U.S. Army CRREL Special Report 81-8, 12 p.

Kvenvolden, K.A., Collett, T.S., and Lorenson, T.D., 1993, Studies of permafrost and gas-hydrates as possible sources of atmospheric methane at high latitudes, *in* Oremland, R.S., ed., Biogeochemistry of Global Change: New York, Chapman & Hall, p. 487–501.

Kvenvolden, K.A., and Lorenson, T.D., 1991, Varying amounts of methane in shallow permafrost cores from Alaska: Eos, Transactions, American Geophysical Union, v. 72, no. 44, Supplement, p. 162.

———1993, Methane in permafrost—Preliminary results from coring at Fairbanks, Alaska: Chemosphere, v. 26, p. 609–616.

Kvenvolden, K.A., Lorenson, T.D., and Reeburgh, W.S., 1992, Methane in permafrost—preliminary studies of the CRREL permafrost tunnel near Fox, Alaska: Eos, Transactions, American Geophysical Union, v. 73, no. 14, Supplement, p. 119.

Lorenson, T.D., Kvenvolden, K.A., and Lilly, M.R., 1992, Methane in permafrost—comparison of frozen and thawed ground: Eos, Transactions, American Geophysical Union, v. 73, no. 43, Supplement, p. 182–183.

Schoell, M., 1988, Multiple origins of methane in the earth: Chemical Geology, v. 71, p. 1–10.

Sellmann, P.V., 1967, Geology of the USA CRREL permafrost tunnel, Fairbanks, Alaska: Hanover, New Hampshire, U.S. Army CRREL Technical Report 199, 22 p.

———1972, Geology and properties of materials exposed in the USA CRREL permafrost tunnel: Hanover, New Hampshire, U.S. Army CRREL Special Report 177, 16 p.

Templeman-Kluit, D.J., 1976, The Yukon crystalline terrane—enigma in the Canadian Cordillera: Geological Society of America Bulletin, v. 87, p. 1343–1357.

Reviewers: Thomas D. Hamilton and Ronald S. Oremland

The 1993 Nelson Mountain Landslide, Chitina Valley, Southern Alaska, an Aerial View

By Lynn A. Yehle *and* Danny Rosenkrans

INTRODUCTION

A very large landslide, 4.5 km long and 1.1 km wide at its toe, coursed down the steep northeast flank of Nelson Mountain (61.33° N. latitude 143.75° W. longitude) and slid about one-third of the way (0.6 km) across the flood plain of the Chitina River (fig. 1). The event apparently occurred at 12:10 p.m., January 4, 1993, when several seismological stations of the U.S. Geological Survey, Alaska Earthquake Information Center, recorded signals centered in this region area that were uncharacteristic of earthquakes of the region (W.R. Hammond, oral commun., November 2, 1993). No eye witnesses are known and the following observations are

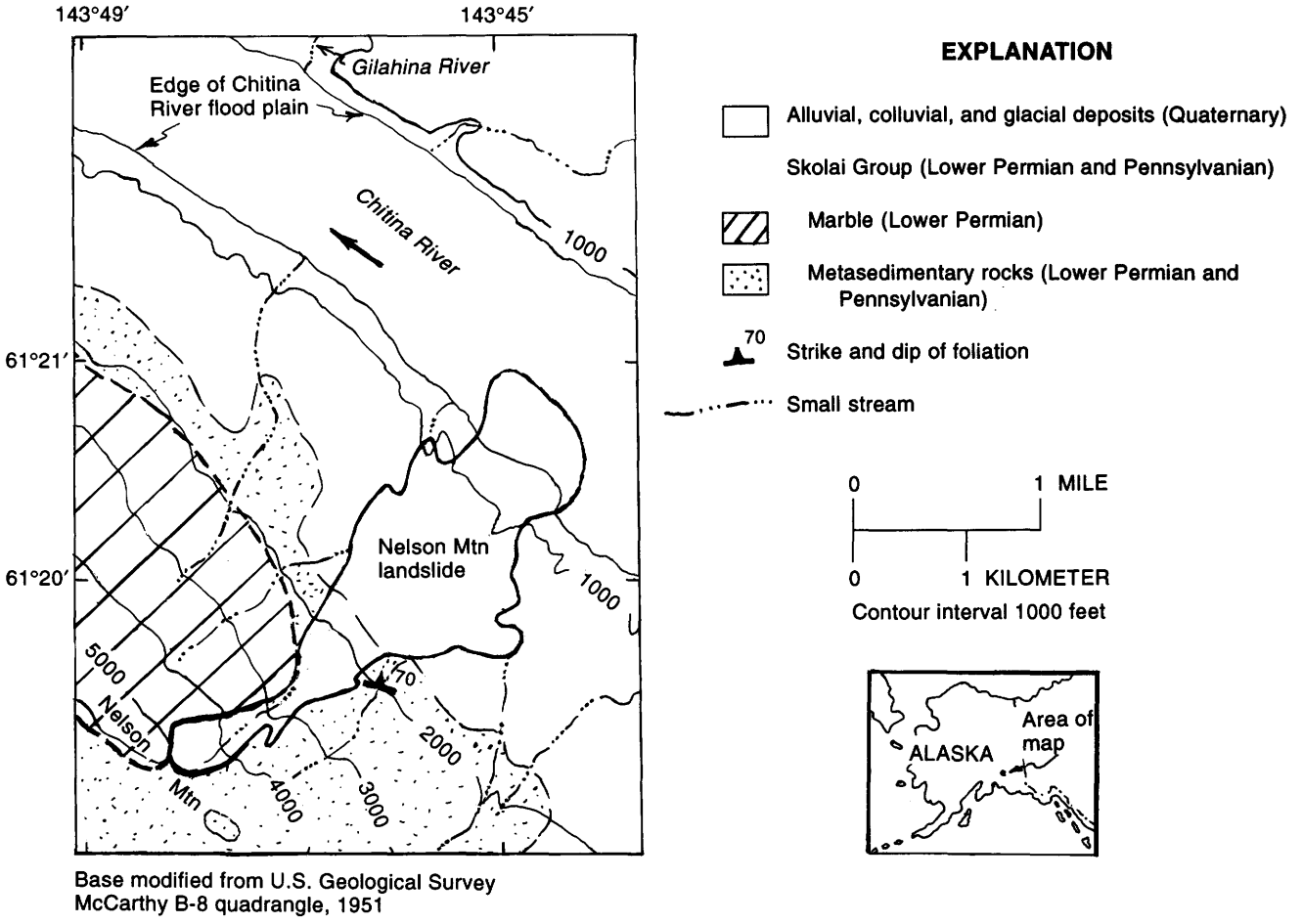

Figure 1. Sketch map showing location of 1993 Nelson Mountain landslide, Chitina Valley, southern Alaska.

based upon air reconnaissance on March 30 and July 11, 1993.

The purpose of this note is to provide a preliminary description of this landslide. We believe it is one of the more spectacular, far reaching, and dynamic geologic events to have occurred in this region in the last several years.

GEOLOGIC SETTING

Nelson Mountain is underlain by bedrock of the Pennsylvanian and Lower Permian Skolai Group (MacKevett, 1978). The Skolai consists predominantly of schistose, metasedimentary rocks including thin-to-thick discontinuous beds of marble, one of which underlies much of the northwest part of Nelson Mountain. Surficial deposits (Yehle, unpub. map, 1964) on the middle and lower slopes of the mountain form a series of Pleistocene glacial deposits and Holocene alluvial and landslide deposits. Upper slopes seem to host several types of colluvial deposits situated between angular to smooth bedrock outcroppings.

DESCRIPTION OF SLIDE

The landslide has the form of an irregular cone or narrow fan that includes a breakaway scarp zone heading at the rim of the saddle along the crestline of Nelson Mountain, and an accumulation zone heading at 870 m, extending about 3 km northeastward, and crossing about one-third of the Chitina River flood plain. Total relief of the slide is 1,300 m. The central part of the accumulation zone is dominated by lumpy cobble- and boulder-strewn ground. Near the margins of the central part, some elongate, concentrically lobed (nested) sectors are marked by different rock types. The slide's lower, outer rim is marked by a berm of broken tree trunks that give the appearance of being plowed up. On the Chitina River flood plain most of the slide debris consists of lumpy piles of material. Longitudinal grooving is evident in the middle lowermost part of the slide. Some sectors of slope-parallel cracks (not evident during observations in March) cut across part of the slide, especially in the central part of the accumulation zone.

The total area affected by the slide (accumulation zone and breakaway headscarp zone) is estimated at 3.8 km^2. Thickness of the slide in the middle reach of the central deposition area is roughly estimated at about 6 m, along the lower, distal margins at about 1.5 m. We conservatively estimate that the original volume of the slide was 3.1×10^6 m^3, using 1.5 m as the average thickness of the deposition zone. No water was seen issuing from the surface of the slide, although a few short dendritic paths exist, possibly from snow-melt concentrations.

SEQUENCE OF SLIDE ACTIVITY

The landslide probably started as a massive fall of jointed, weathered bedrock along part of the saddle rim heading the minor valley bearing the present slide. Comparing pre-slide, 1962 ground photographs and 1957 vertical aerial photographs of the valley head with post-slide, July 11, 1993, oblique aerial photographs strongly suggests that the breakaway zone involved (1) valley headwall enlargement due to a massive rock fall, (2) removal of some of the more angular outcroppings of bedrock, and (3) stripping of colluvium that overlay some of the bedrock, especially marble. Fall-induced fragmentation of bedrock apparently evolved into a debris slide that entrained trees and other vegetation, snow, ice, and unfrozen subsurface pockets of water. The above noted events, whose deposits now rest in the middle of the accumulation zone, seem to have been followed by much smaller debris flows near the topographically lower, outer margins of the slide, possibly where more moisture was available. The nested segregation of different rock types comprising parts of some of these flows cannot be explained at present.

Speed of the landslide in its latter phase is categorized as being in the slow-to-moderate category, not in the fast (debris) avalanche category. We feel that a low-speed flow is required to maintain the observed segregation of different rock types. In addition, there is no apparent evidence of the airblast effects that characterize some debris avalanches. Trees that stood directly in the apparent line of airblast at outermost, land-based parts of the slide were not uniformly downed but had the irregularly downed appearance noted previously. Additionally, shore features such as uprooted brush along the opposing Chitina River flood plain margin show no obvious airblast effects.

ORIGIN OF THE SLIDE

We feel that the cause of the slide probably is related to (1) above-average precipitation and an above average number of extreme freeze-thaw cycles in November and December 1992 (National Oceanic and Atmospheric Administration, 1993), (2) steep, upper-mountain slopes, and (3) bedrock that is oriented subparallel to slopes, and bedrock dips of as much as 70° measured nearby (MacKevett, 1978).

FUTURE ACTIVITY OF THE SLIDE

Landslide activity at the Nelson Mountain locality probably will recur because the headwall breakaway zone of the slide still contains bedrock that has a favorable orientation for additional slope failures. Small landslide deposits mapped in this locality (Yehle, unpub. map, 1964) indicate that slides occurred prior to the 1993 landslide event. The

January 4, 1993 slide mass will continue to differentially settle and crack as it did between March and July, as the deposit further adjusts to the pre-existing ground surface. The outermost part of the slide (that is, the part lying on the floor of Chitina River channels) is being eroded and cut through by river channels. Most of the slide probably will be eroded down below summer-time river level within about 20 years, judging from the erosion rate of other slides along the edge of active channels of the Chitina River in the area.

REFERENCES CITED

MacKevett, E.M., Jr., 1978, Geologic map of the McCarthy quadrangle, Alaska: U.S. Geological Survey Miscellaneous Investigations Series Map I–1032, scale 1:250,000.

National Oceanic and Atmospheric Administration, 1993, Climatologic data, Alaska, November, December, 1992.

Reviewers: Rex L. Baum and Richard Van Horn

Importance of Landslides in the Geomorphic Development of the Upper Caribou Creek Area, Talkeetna Mountains, Alaska

By Steven W. Nelson

INTRODUCTION

This report describes several landslides in the upper Caribou Creek area of the Talkeetna Mountains. These landslides are important to the geomorphic development of the area, and they constitute a potential hazard to development and mining activity. The landslides have produced a topography that is strikingly similar to the landslide-produced topography of some of the Hawaiian Islands. However, the geologic processes producing the landslides in Alaska are different than in Hawaii.

The easiest access to the area is by single-engine (Super Cub) fixed-wing aircraft. Alternatively, an all-terrain vehicle (ATV) trail from mile 106 on the Glenn Highway follows Caribou Creek to Mazuma Creek, and continues a short distance up Mazuma Creek. From here, one can take a five-mile walk to the area. The ATV trail was established to facilitate access to several active placer gold claims on Caribou Creek, the highest of which is located at the mouth of Mazuma Creek.

The upper Caribou Creek area, including Mazuma Creek, is located in the southern Talkeetna Mountains approximately 150 km northeast of Anchorage, Alaska (fig. 1). The area described is located in the southern Talkeetna Mountains A-1 and A-2 quadrangles. Reconnaissance mapping was done at a scale of 1:63,350 during an eight-day period in August 1993. Additions to the field mapping were made from false-color, infrared aerial photographs taken in July 1982. Earlier mapping by Grantz (1960) and Csejtey and others (1978) was also incorporated.

LOCAL GEOLOGY

The upper Caribou Creek area is underlain by a thick sequence (600 m) of shallowly dipping (<10°), undifferentiated, mafic to felsic subaerial lava flows and related hypabyssal intrusive rocks of Paleocene to Miocene age; the upper part of the sequence may be as young as Pleistocene (Csejtey and others, 1978). Additional units include a pink rhyolite (tuff?) and several thin (<10 m thick), discontinuous horizons of poorly consolidated, fluvial or lacustrine deposits (fig. 2) with rare petrified trees and carbonized plant fragments interlayered with the flows. These sedimentary units are composed of poorly indurated shale and very fine-grained sandstone with thin pebble horizons. During rainy weather, some of these sedimentary horizons absorb water and turn into a sticky, greasy mass of clay that suggests they may be bentonitic. The lava flows are usually dark brown, 3 to 4 m thick, aphanitic, massive, and contain moderate to well-formed columnar jointing. Abundant quartz-filled amygdules, ranging in size from <1 cm to 10 cm across, are found in some flows.

The oldest rocks in the area are sedimentary rocks (figs. 1, 3) assigned to the Matanuska Formation (Early and Late Cretaceous) and are exposed in an erosional window in Mazuma Creek (Grantz, 1960). A stratigraphically equivalent unit on Caribou Creek has yielded a single dinosaur skull, which is the subject of current study by staff of the University of Alaska (Anne Pasch, written commun., Aug. 1993).

The area was extensively glaciated during the late Pleistocene (Welsch and others, 1982), and small remnants of these glaciers are still present at higher elevations at the head of Caribou Creek and to the north. In the study area, no glacial deposits are visible beyond the immediate vicinity of present day glaciers. R.D. Reger (oral commun., 1993) believes that these valleys were ice-free about 9,500 years ago. Péwé and Reger (1983) suggest that most of the existing nonglacial features, such as landslides and rock glaciers, developed during or after the last glaciation in middle to late Holocene time. On this basis, the landslides could be 9,500 years old, but are more likely to be 5,000 years old and younger. Lichen chronology could be undertaken for more precise dating of the landslides.

Landslides were also observed 8 km to the north near the headwaters of the Oshetna River, and some are

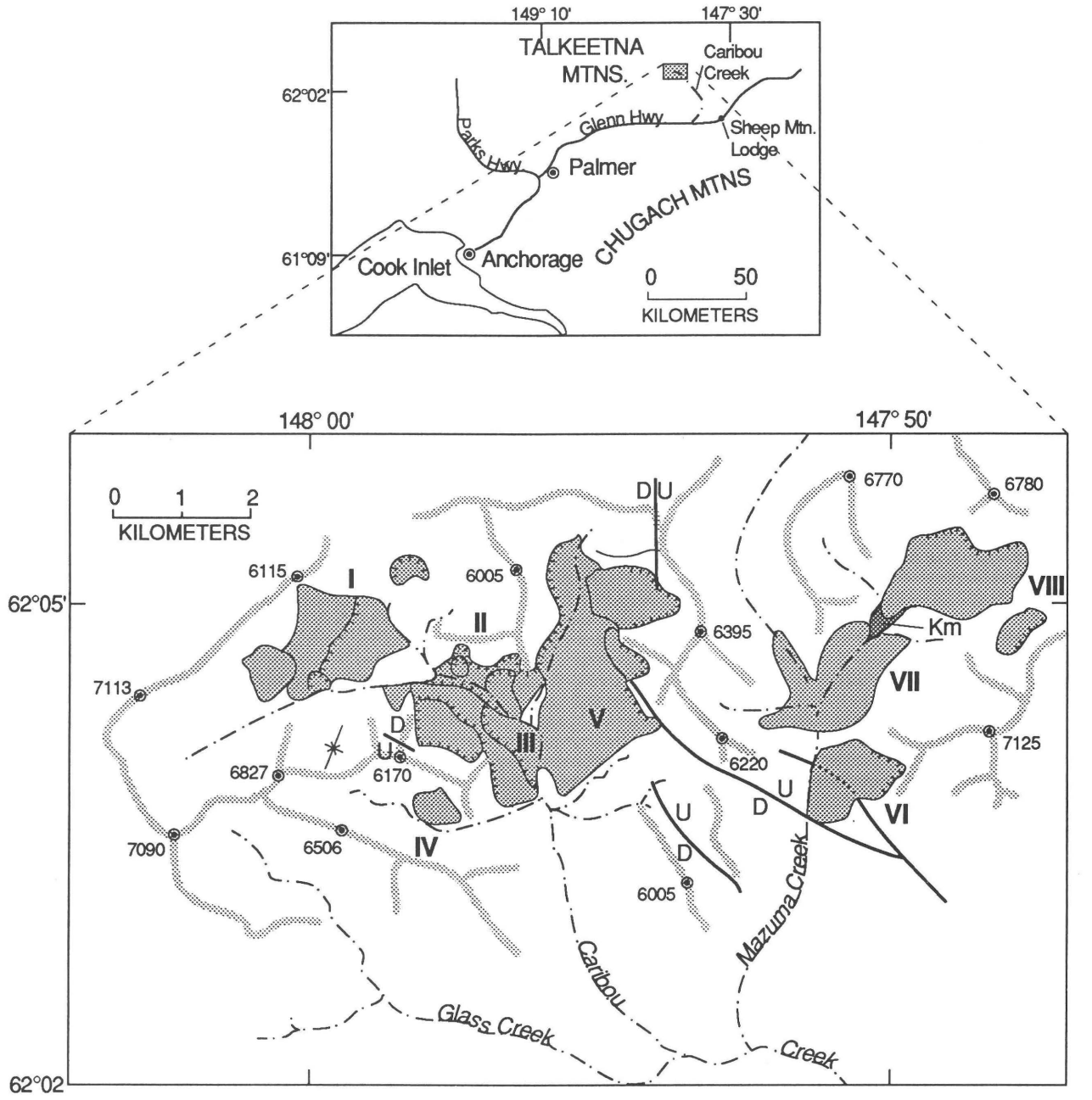

EXPLANATION

III — Landslide deposits--Hachures demark landslide scarp. Roman numeral refers to landslide type discussed in text

Tertiary volcanic rocks, undivided

Km — Matanuska Formation outcrop

6005 — Ridgeline--Topographic highs in feet

Syncline axis

U / D ..... Fault--Concealed where dotted; U, up thrown side; D, down thrown side

Creek

Figure 1. Caribou Creek area, landslides, and other geologic features.

mapped in Glass Creek and other areas by Grantz (1960). These landslides are prominently formed in the Tertiary undivided volcanic rocks unit (Tv) of Csejtey and others (1978), which covers an area of about 200 km^2. If landslides are found throughout this outcrop area, they would constitute a significant regional geomorphic feature.

GEOMORPHOLOGY OF THE LANDSLIDES

Eight landslides were mapped in upper Caribou Creek and Mazuma Creek (fig. 1; labeled I–VIII). The landslides are of two kinds: rotational block slides and debris slides (nomenclature after Varnes, 1958; Selby, 1982). Rotational block slides are characterized by a failure surface that is produced by rotation of a block in a down-slope direction. Rotational block slides can be further divided into two types: single or multiple (Brunsden, 1979), based on the number of rotational blocks. Most of the rotational block slides in the Caribou Creek area are multiple types characterized by more than one rotational block, a major scarp, and minor scarps with their heads marked by depressions commonly containing small ponds or meadows. Landslides II and III (fig. 1) have these features well developed. Debris slides have only a main scarp and are made up of large, poorly sorted boulder fields (Selby, 1982). In this paper, the general term landslide refers to both landslides and debris slides. Other mass-wasting features observed include individual rock slides similar to the one described by Brew (1962), rock glaciers, talus aprons, and channel-restricted debris flows with levees.

The landslides are irregular in shape, usually having widths which exceed their lengths. They range in area from <100 m^2 to over 2.6 km^2 (fig. 1). The total area occupied by landslides is about 20 km^2. All have a main scarp, which usually forms a spectacular headwall several hundred meters or more high (fig. 2). Minor scarps are approximately less than one-half of the height of the main scarps. One Mazuma Creek debris slide is separated from its main scarp by a talus apron (fig. 3).

Many of the rotational landslide surfaces are marked by hummocky topography and boulders of lava. It is

Figure 2. View looking west across Caribou Creek drainage to multiple type rotational block landslide location III, in fig. 1. Main scarp (300 m high) is cliff face below peak 6170. Minor scarps shown by "ms"; light-colored layers on left are bentonitic sedimentary rock horizon.

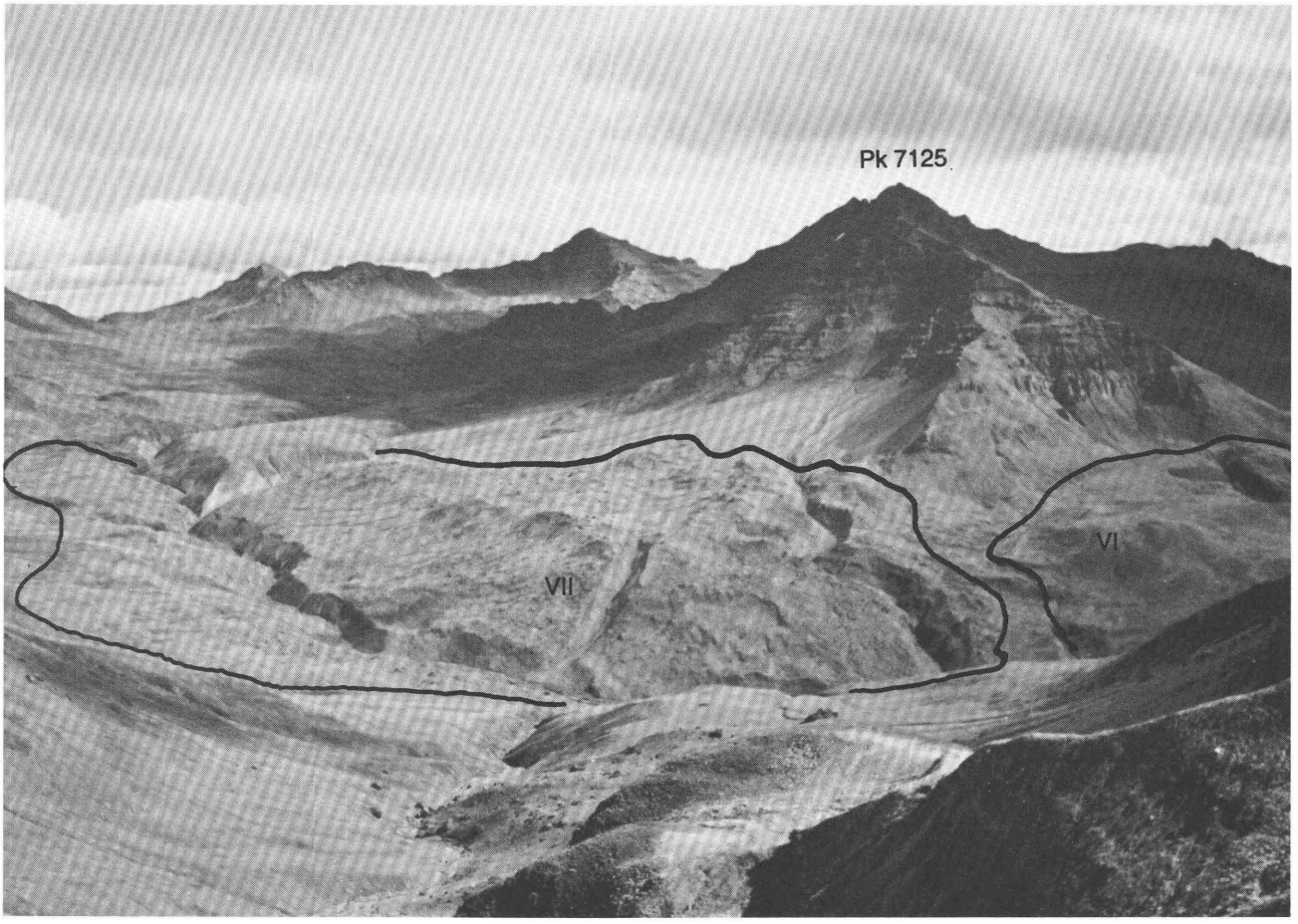

Figure 3. View looking east to the head of Mazuma Creek showing debris slides (VI and VII) right center, center, and left center. Light colored-rocks in Mazuma Creek are outcrops of the Matanuska Formation.

suspected that the well-developed columnar jointing of the volcanic flows contributed to the break-up during emplacement and to the numerous boulders presently seen on the slide surfaces.

The slide complexes VI and VII in Mazuma Creek (fig. 1) are different in morphology from those described in Caribou Creek. The Mazuma Creek slides are large rock falls, or debris slides, which appear to have resulted from single catastrophic events. These slides are large boulder fields (fig. 3) that do not have minor scarps.

Several factors may have contributed to the morphological differences in these two areas. In Mazuma Creek the lava flows appear to be thicker, with better developed columnar jointing, and there is greater topographic relief. A possible interpretation of the influence of these factors is that well-developed jointing and greater relief resulted in the landslide disintegrating more completely before coming to rest.

Other factors which may have facilitated the downslope movement include glaciation, bentonitic sedimentary horizons, which are interlayered with the volcanic rocks, and faults and joints parallel to the main scarps. In many of the landslides the bentonitic horizon is located near the base of the main scarp (fig. 2). These layers are weaker layers composed of soft, expandable, easily deformed material lying between the more competent volcanic flows. Moisture seeping through fractures would contribute to the potential for failure in the bentonitic horizons and would turn them into slip surfaces.

Some slides are presently active and are creeping into Caribou Creek (landslide I). The next older slides have scarps which lack vegetation and still display transverse fractures in the crown area. The oldest slides have vegetated scarps and a more subdued surface, which is probably the result of weathering, solifluction, and vegetation cover.

Numerous faults are recognized in the area and may contribute to the localization of scarps, but only two are in the main scarp area of two landslides (fig. 1). Additional mapping may find others. There may be more factors which account for these landslides and the contrasting morphologies. The issue needs further work.

The main geomorphic features of the landslides overall are the steep escarpments that cut subhorizontal layering in the volcanic rocks. In several cases the slides have created mountains with steep pyramidal forms and sharp ridges radiating from the center. These features have a remarkable

similarity to the larger landslide-produced topography in the Hawaiian Islands. In that area, mass wasting is an important process in the evolution of the island volcanoes (Moore and others, 1989). The Hawaiian landslides occur throughout the shield-building stage and are facilitated by rift-zone parallel faults and seismic, magmatic, and hydrothermal activity (Moore and Clague, 1992).

Despite the topographic similarity, the Caribou Creek landslides represent a different history than those in Hawaii. The Caribou Creek slides occurred long after volcanic activity ceased and after the area had undergone extensive valley glaciation (Welsch and others, 1982; Péwé and Reger, 1983). Glaciers typically produce oversteepened slopes, which probably contributed to the high landslide potential of the area (Selby, 1982).

HAZARD EVALUATION

The landslides in this area are probably of only seasonal concern as geologic hazards. The area surrounding upper Caribou Creek has no year-round population. During summer months most visitors in the vicinity are present for recreational or scientific purposes. There are several placer gold operations, which are active only on a seasonal basis. Two possible hazards of concern are (1) a landslide blockage of Caribou Creek, which might result in formation of a lake, and subsequently, a catastrophic flood downstream due to dam failure, or (2) a landslide impacting a placer operation directly. However, no evidence for previous landslide-dammed lakes was seen, and only a few placer operations exist in the outcrop area that is prone to landslides.

CONCLUSIONS

Several conclusions can be made about the landslides in the area.

1. Landslides are an important geomorphic feature of the upper Caribou Creek area.

2. Bentonitic horizons, fractures in bedrock, the movement of ground water, and oversteepened slopes due to glaciation are important factors that have contributed to the development of landslides.

3. The landslides have produced rugged and stepped topography, which is remarkably similar to landslide-produced topography in the Hawaiian Islands.

4. The landslides are a potential hazard in the area.

Acknowledgments.—I thank Mike Meekins of Meekins Air Service for his skilled aircraft piloting to access the upper Caribou Creek area, and T.K. Hyer for his patience on our hunting trips, when I pursue geologic interests instead of wild animals.

REFERENCES CITED

Brew, D.A., 1962, Description and mechanics of a small landslide block in the Wattener Lizum, Austria: Geological Society of America Bulletin, v. 73, p. 1277–1280.

Brunsden, Denys, 1979, Mass movements, *in* Tembleton, Clifford and Thornes, John, eds., Processes in Geomorphology: John Wiley and Sons, New York, p. 130–186.

Csejtey, Béla, Jr., Nelson, W.H., Jones, D.L., Siberling, N.J., Dean, R.M., Morris, M.S., Lanphere, M.A., Smith, J.G., and Silberman, M.L., 1978, Reconnaissance geologic map and geochronology, Talkeetna Mountains quadrangle, northern part of Anchorage quadrangle, and southwest corner of Healy quadrangle, Alaska: U.S. Geological Survey Open-File Report OF 78-558A, scale 1:250,000, 60 p.

Grantz, Arthur, 1960, Geologic map of the Talkeetna Mountains A-2 quadrangle, Alaska and the contiguous area to the north and northwest: U.S. Geological Survey Miscellaneous Geologic Investigations Map I–313, scale 1:48,000.

Moore, J.G., Clague, D.A., Holcomb, R.T., Lipman, P.W., Normark, W.R., and Thorreson, M.E., 1989, Prodigious landslides on the Hawaiian Ridge: Journal of Geophysical Research, v. 94, p. 17465–17484.

Moore, J.G., and Clague, D.A., 1992, Volcano growth and evolution of the Island of Hawaii: Geological Society of America Bulletin, v. 104, p. 1471–1484.

Péwé, T.L., and Reger, R.D., 1983, Guidebook to permafrost and Quaternary geology along the Richardson and Glenn Highways between Fairbanks and Anchorage, Alaska: Fourth International Conference on Permafrost, Guidebook 1, University of Alaska, Fairbanks, 263 p.

Selby, M.J., 1982, Hillslope materials and processes: Oxford University Press, Oxford, 264 p.

Varnes, D.L., 1958, Landslide types and processes, *in* Eckel, E.B., ed., Landslides and engineering practice: Highway Research Board Special Report 29, NAS-NRC Publication 544, p. 20–47.

Welsch, Dennis, Goodwin, Robert, and Ten Brinks, Norman, 1982, Late Quaternary glaciations of the Talkeetna Mountains, Alaska [abs.]: Geological Society of America Abstracts with Programs, v. 14, no. 6, p. 353–354.

Reviewers: Tina Neal and Anne Pasch

Possible Active Fault Traces on or near the Castle Mountain Fault between Houston and the Hatcher Pass Road

By Peter J. Haeussler

ABSTRACT

The Castle Mountain fault is one of several major east-northeast-striking faults in southern Alaska, and it has had historical seismicity and Holocene surface faulting. The Castle Mountain fault was delineated on a regional scale by Detterman and others (1974, 1976), who divided it into two physiographic segments. Mapping in a 30-km-long region between the two segments (from Houston to the Hatcher Pass Road) is the subject of this study. I found two faults in the central part of the study area, north of the inferred trace of the Castle Mountain fault, which have experienced late Quaternary surface-faulting. I also traced the Castle Mountain fault in the Houston area about 3 km farther east than previously recognized. The age of faulting in the study area is constrained by the glacial history to be younger than approximately 10,000 yr B.P. on several faults and younger than approximately 40,000 yr B.P. on another fault. However, because prior work on the Castle Mountain fault west of the study area has recognized surface faulting younger than 1,860 yr B.P., it is likely that the age of faulting within the study area is substantially younger than 10,000 or 40,000 yr B.P.

INTRODUCTION

The Castle Mountain fault is one of several major east-northeast-striking faults in southern Alaska, and unlike other faults with a similar orientation, the Castle Mountain fault has been active in historical time and surface faulting has occurred during the Holocene (Lahr and others, 1986; Detterman and others, 1974). Martin and Katz (1912) first noted the fault, but it was delineated on a regional scale by Detterman and others (1974, 1976), who divided it into two physiographic segments—the western Susitna Lowland and the eastern Talkeetna Mountains segments (fig. 1). Detterman and others (1974, 1976) found no trace of the Castle Mountain fault in the 30-km-long region between Houston on the west and Hatcher Pass Road on the east (figs. 1, 2), and they did not include this area in either of their maps (G. Plafker, oral commun., 1993). This study re-examines the area and reports possible active fault traces in it.

The total length of the Castle Mountain fault in the Talkeetna Mountains and eastern Susitna Lowland is approximately 200 km. Correlation of the Castle Mountain fault with the Bruin Bay fault or Lake Clark fault, each of which lies to the southwest, seems likely because the faults are aligned, but such a connection is complicated by lack of an exposed fault trace in a critical 15- to 20-km-long area where the Lake Clark, Bruin Bay, and Castle Mountain faults join together (fig. 1) (Detterman and others, 1974). In addition, neither the Lake Clark nor the Bruin Bay faults is known to be active, whereas the Castle Mountain fault is active (Detterman and others, 1975; Plafker and others, 1975). The northeastern extent of the Castle Mountain fault is unknown because the fault disappears beneath Pleistocene glacial deposits of the Copper River Lowland (which lies just northeast of the area of fig. 1).

The Castle Mountain fault has had a long and complicated history. Detterman and others (1974) argued that the fault existed in Mesozoic time, and Grantz (1966) and Fuchs (1980) gave evidence for more than 14 km of Tertiary dextral slip along the eastern part of the fault. However, there is also substantial evidence for vertical displacement with the north side relatively up. North-side-up vertical displacement has been inferred to be 500-650 m in the Susitna Lowland based on offset reflectors in reflection seismic profiles (Kelley, 1963). Also, Clardy (1974, p. 46) states, "There is a minimum of several thousand feet of vertical separation (up to the north) of Miocene and Oligocene (?) sediments between [two wells that straddle the Castle Mountain fault near Houston]" (see well locations, fig. 2). In addition, more than 3 km of north-side-up vertical displacement on the Castle Mountain fault is indicated in the upper Matanuka Valley from offsets of Tertiary strata (Grantz, 1966; Detterman and

others, 1976). At the eastern end of the Castle Mountain fault system, the fault divides into the Caribou fault and the Castle Mountain fault splay (fig. 1) (Detterman and others, 1976). The Talkeetna Mountains segment of the Castle Mountain fault dips steeply to the north, and both Bruhn and Pavlis (1981) and Detterman and others (1976) concluded that the most recent offset on the fault was post-Oligocene reverse motion. Along the Susitna Lowland segment, Bruhn (1979) reported north-side-up normal faults in two trenches located southwest of Houston (figs. 1, 2), and Detterman and others (1974) found a north-side-up reverse fault in a third trench about 10 km to the west (fig. 1).

Recent motion along the Castle Mountain fault is demonstrated by a discontinuous series of linear south-facing scarps in the Susitna Lowland. These scarps are generally less than 2 m high, but are up to 4 m high, and cut late Quaternary glacial deposits and Holocene fluvial deposits associated with the Susitna and Little Susitna rivers (Wahrhaftig, 1965; Detterman and others, 1974; Reger, 1981a, b). In a trench across the fault in the Susitna Lowland, Detterman and others (1974) found an offset peat horizon, which was dated at 1,860 radiocarbon yr B.P. The oldest age of a tree on the scarp was 225 yr, which suggests that a surface-faulting event occurred between 225 and 1,860 yr B.P. In contrast, no unambiguous evidence for Quaternary offset has been recognized along the Talkeetna Mountains segment (Detterman and others, 1976; Bruhn and Pavlis, 1981). However, a surface-wave magnitude 5.2 earthquake that occurred along this part of the fault in 1984 demonstrates that it is still active at depth (Lahr and others, 1986). No surface breaks were observed during an aerial reconnaissance investigation immediately after the earthquake (S. Nelson, oral commun., 1993). However, the hypocenter of the main shock and aftershocks was relatively deep—between 13 and 20 km—and thus the fault might not have ruptured the surface. The focal mechanism for the earthquake, and locations of aftershocks indicated a steeply north-dipping fault plane, which is in agreement with field observations for the geometry of the fault (Martin and Katz, 1912; Detterman and others, 1976). However, the inferred motion of the event from earthquake focal-mechanism studies was right-lateral strike-slip, which is in contrast to field-based geological inferences of recent reverse motion on the fault (Bruhn and Pavlis, 1981; Detterman and others, 1976). A short-period magnitude 7.0 event in 1933 that caused Modified Mercalli intensity VII effects at Anchorage was possibly also associated with the Castle Mountain fault (Lahr and others, 1986).

The Quaternary geology of the Matanuska Valley in the vicinity of the Castle Mountain fault is dominated by repeated glacial advances and retreats. The oldest recognized glaciation may have occurred in late Pliocene time, and the most recent retreat took place within approximately the last 10,000 years (Reger and Updike, 1983). In general, the ice flowed from east to west down the Matanuska Valley toward Cook Inlet (fig. 1). The Naptowne glaciation is the youngest in the Matanuska Valley (Reger and Updike, 1983), and drift of Naptowne age blankets the study area. There are at least two stades within the Naptowne (Reger and Updike, 1983), and the oldest stade is

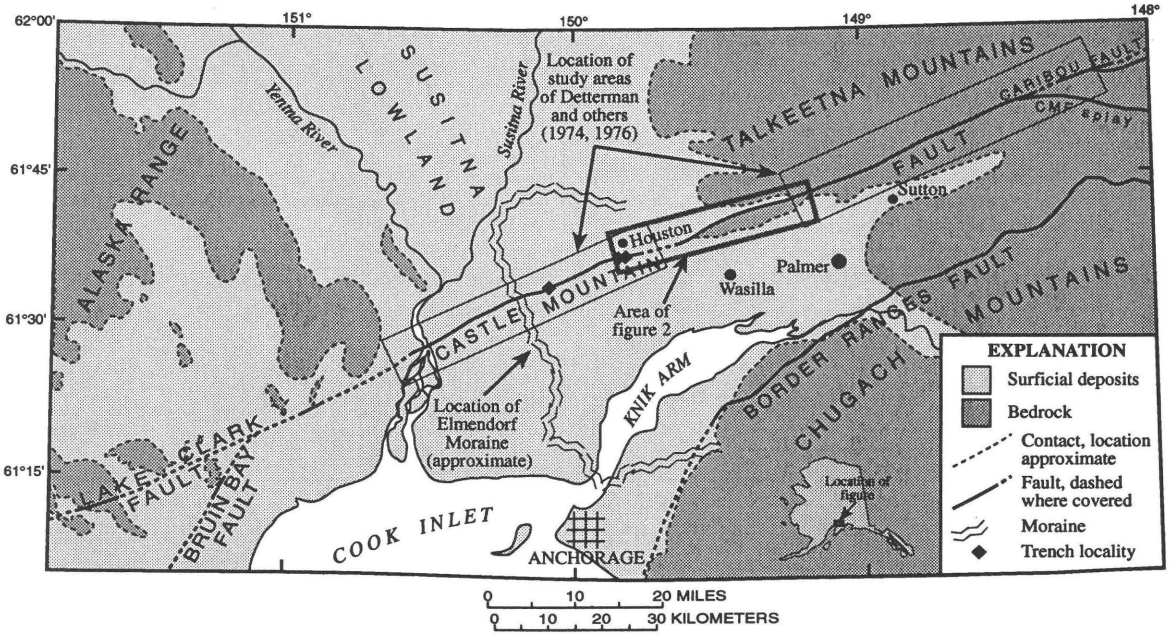

Figure 1. Simplified geologic map of upper Cook Inlet region, showing regional extent of Castle Mountain fault and location of study area (see fig. 2). Castle Mountain fault splay, CMF splay.

poorly dated because it predates, or is at the limit of, the radiocarbon dating technique. Reger and Updike (1983) estimate that the oldest glacial advance began no earlier than 47,000 yr B.P, but possibly just after 39,000 yr B.P. The youngest glacial advance in the upper Cook Inlet area formed the arcuate Elmendorf Moraine (fig. 1), which is about 5 to 10 km northeast of Anchorage at the southern limit, and about 10 km north of Houston at its northern limit. Reger and Updike (1983) bracketed the age of this moraine at between 11,690 and 13,690 yr B.P. Following deposition of the Elmendorf Moraine, the ice stagnated and the main glacier lying in the Matanuska Valley rapidly retreated. Many ice-stagnation features are found in the Palmer and Wasilla area (fig. 1), including kames, kettle lakes and ponds, crevasse-fill-ridge complexes, and subglacial channels (Reger and Updike, 1983). The Wasilla area was deglaciated by 9,155 yr B.P., and a location near the terminus of the modern Matanuska Glacier (which lies about 10 km east of the eastern edge of fig. 1) was deglaciated prior to 8,000 yr B.P. (Reger and Updike, 1983), which suggests that the glacier retreated approximately 56 km in about two thousand years.

However, radiocarbon ages from a bog section 2 km from the end of the Matanuska Glacier show that these peat deposits have not been covered by ice in the last 13,000 years (Williams, 1986), and therefore there may be some problems with the timing of deglaciation proposed by Reger and Updike (1983). An alternative explanation is that deglaciation in the Matanuska Valley region occurred just prior to 13,000 yr B.P. and that other minimum ages of deglaciation underestimate the timing of deglaciation by approximately 3,000 to 4,000 years. Support for this idea comes from deglaciation histories of other parts of southern Alaska, which indicate that deglaciation occurred prior to 10,000 to 14,000 years ago (Williams, 1986). In any case, the Castle Mountain fault in the study area has been deglaciated since late Quaternary time.

METHODOLOGY

I first examined stereographic pairs of vertical color aerial photographs (scale 1:18,000) for linear features within several miles of the projected trace of the Castle Mountain fault. The projected trace of the fault in the study area was determined by drawing a line between its surface expression in the Houston area with the location of the Castle Mountain fault along the Hatcher Pass Road, which is the next known location of the fault to the east. I subsequently examined linear features identified on air photos in the field in order to better characterize them and assess their origins.

With the hope of better constraining the location of the Castle Mountain fault, I also examined proprietary seismic-reflection data from the vicinity of the fault in the western one-quarter of the study area. The seismic profiles exhibit well-defined reflectors south of the inferred trace of the fault and noise to the north, but no feature on the profiles could be associated with the Castle Mountain fault. In addition, a gap in the seismic lines where they crossed the Little Susitna River (fig. 2), and the unconsolidated sediments adjacent to the river, made it impossible to resolve the location of the Castle Mountain fault using the seismic-reflection profiles.

OBSERVATIONS AND INTERPRETATIONS

HOUSTON AREA

About one to one-and-a-half kilometers south of Houston there are three or four faults that define the main trace of the Castle Mountain fault (fig. 2). To the southwest of the study area, the Castle Mountain fault is easily seen as a very linear scarp with the northwestern side upthrown (Detterman and others, 1974). As the fault enters the study area (from the southwest), the fault bends from a strike of approximately 070° to almost 090° (fig. 2, location A). At this point, the fault divides into two splays and the main trace of the fault follows the northern splay (fig. 2, loc. B). The southern splay dies out 2 km east of the split (fig. 2, loc. C). About four kilometers east of the bend to the 090° strike, the fault resumes its 070° strike and continues eastward on the alluvial terrace of the Little Susitna River (fig. 2, loc. B). Along the east-west-striking part of the fault, there are two more faults, one to the north of the main trace of the Castle Mountain fault (fig. 2, loc. D), and the other is a splay to the south (fig. 2, loc. E). It appears likely the additional faults in this area accommodate strain along the bend. I infer there is one more fault in the Houston area, about a kilometer north of the town (fig. 2, loc. F). This fault is indicated by a linear drainage and an elongate pond subparallel to the Castle Mountain fault.

CENTRAL PART OF STUDY AREA

In the central part of the study area there are two linear features that are visible on vertical aerial photographs (fig. 3) that I interpret as faults with surface expression. These features are (1) the more northerly and longer Bench Lake fault, which is named for Bench Lake—the only named geographic feature lying near the inferred trace of the fault, and (2) the southern and shorter Lost-in-the-woods fault, which is informally named for what usually happened to me when I tried to find it. There are no named geographic features in the vicinity of this fault. The Bench Lake fault offsets glacial deposits at its eastern end and has a well-defined linear north-facing

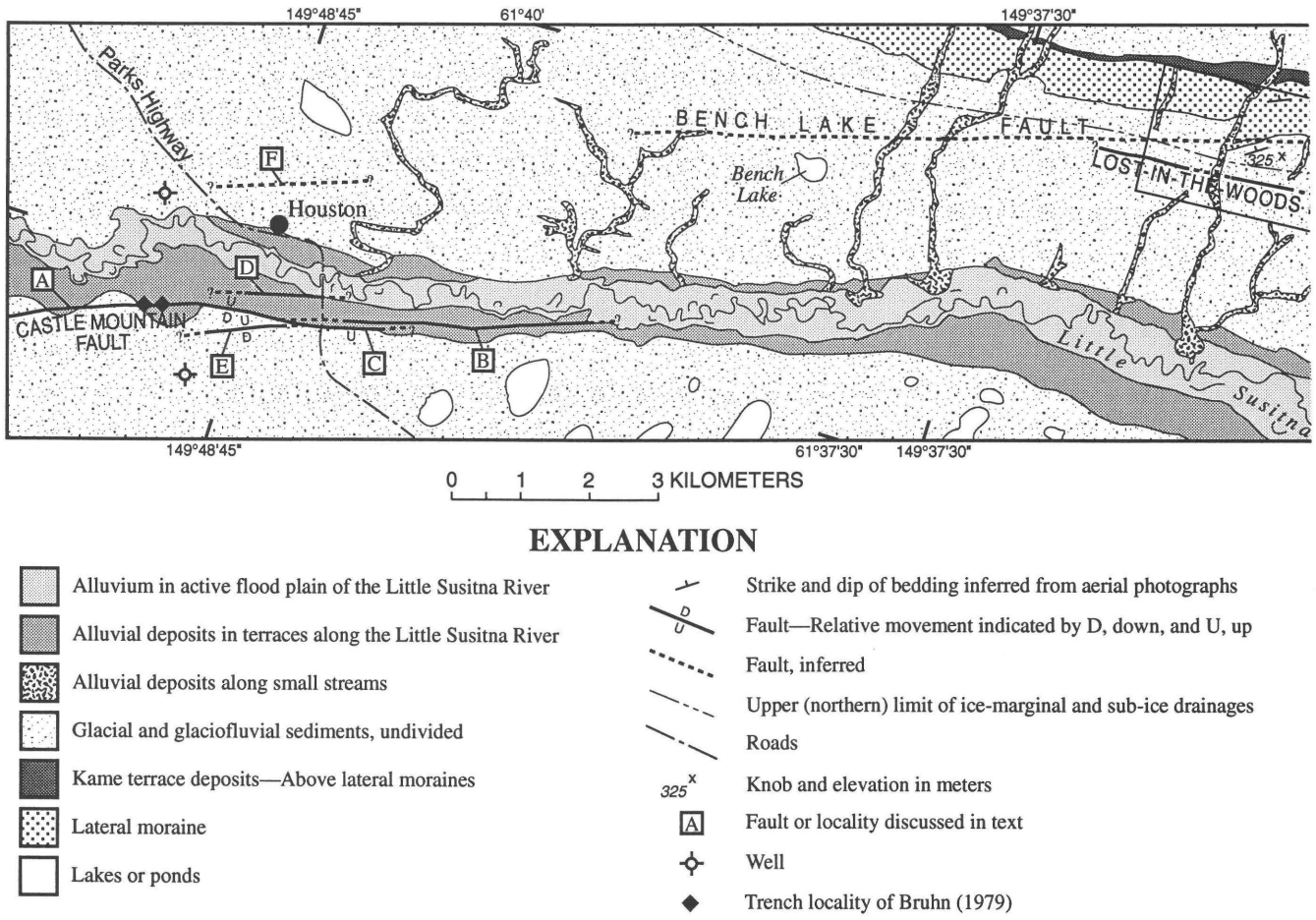

Figure 2. Quaternary geologic map of study area. Sources include Detterman and others (1974, 1976), Reger (1981a, b), and P. Haeussler (unpublished mapping, 1993).

scarp 1.5 m high (figs. 3, 4). Soil pits dug into the top of the scarp, up to 60 cm deep, exhibited a podzolic O-A soil horizon up to 20 cm thick, dominated by peat and underlain by 40 cm of brownish-red fine-grained silty clay (fig. 5). The bottom of the soil pits had cobbles of hornblende tonalite and sandstone within the silty clay. The tonalite cobbles looked similar to rocks of the Cretaceous Willow Creek pluton (Winkler, 1992) in the Hatcher Pass area, and the sandstone cobbles appeared similar to sandstone found in outcrops of the nearby Wishbone Formation. This sequence may be interpreted as a youthful soil profile developed on unconsolidated sediments of glacial or glaciofluvial origin derived from nearby sources. A soil pit in the trough on the north side of the scarp had a thick (>40 cm) O-A soil horizon also dominated by peat (fig. 5). About 25 cm beneath the surface there were numerous hornblende tonalite cobbles up to 15 cm across. Because the tonalite cobbles were within the O-A horizon, and because of the scarp topography adjacent to the soil pit, it is likely the cobbles rolled into a pre-existing trough from the scarp. The scarp and all of the surrounding area were covered by vegetation (dominantly grasses with minor trees), and there were no exposed unconsolidated sediments. Therefore, I infer that the cobbles fell into the peat during a surface-faulting event, during south-side-up motion that exposed unconsolidated glacially derived cobbles, which then rolled into the trough on the scarp's north side. Another possibility is that the tonalite cobbles were pulled out of underlying till by the roots of large trees that fell over. Although this process, called "tree windthrow" (Birkeland, 1984), is commonly observed at lower elevations in the study area, I saw no cases of this in the vicinity of the scarp. In addition, this process would bring to the surface clasts of all grain sizes, not just cobbles.

The trough on the north side of the scarp, at its eastern end, is a wet area that drains toward the east. If the scarp was not related to surface faulting, but was instead a bedrock feature that predated glaciation, it is unlikely that the feature would have been preserved, principally because this area was glaciated, and also because the feature has an orientation that would not be favorable to preservation. A small and angular topographic feature that drains to the east, such as the trough on the north side of the escarpment, probably would have been removed by the

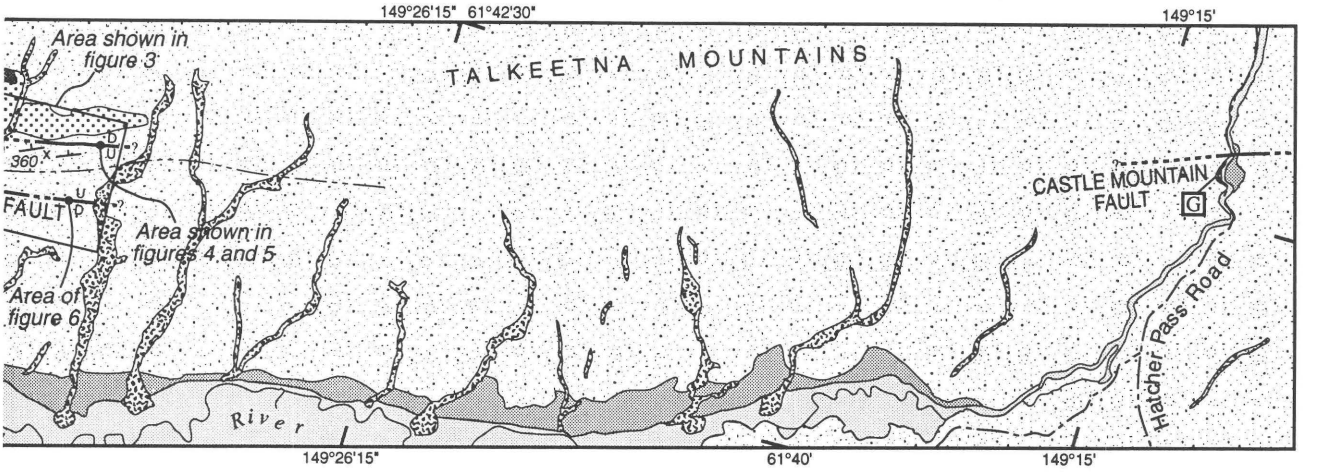

Figure 2.—Continued.

westward flow of ice (Reger and Updike, 1983) down the Matanuska Valley. More importantly, because no bedrock was encountered in deep soil pits located on top of, or on the side of, the scarp, it is unlikely that the feature is cored by bedrock. The scarp would also be expected to be more rounded if it was glacial in origin. Finally, the trough on the north side of the scarp is unusually wet, despite the small amount (about 5 m) of topography uphill from the trough. This suggests that the flow of groundwater along the trough may be controlled by a fault.

Only the easternmost 1 km of the Bench Lake fault has evidence of surface faulting. The majority of the fault lies to the west and is inferred by the trace of linear paleodrainages, which probably developed beneath stagnating ice. There are two prominent knobs (labelled with elevations of 325 m and 360 m on the USGS 1:25,000-scale topographic map) of conglomerate near the eastern end of the Bench Lake fault (see fig. 2). The conglomerate at these knobs is massive and contains approximately 80 to 85 percent well-rounded intermediate-composition volcanic pebbles and cobbles. About 5 percent of the clasts are sedimentary in origin, and the remaining 10 to 15 percent are granitic. Based on a comparison of the cobble compositions with that of sandstones and conglomerates of the Wishbone Formation (Clardy, 1974), I correlate this conglomerate with the Wishbone Formation because both rock units are dominated by volcanic clasts. Clardy (1974) interpreted similar massive conglomerates in the Wishbone Formation to have been deposited by sheet floods in alluvial fans. Because of the massive nature of the conglomerate, I was unable to discern the bedding orientation in the field. However, bedding can be distinguished from aerial photographs, striking N. 67° E. and dipping steeply (possibly 60°–70°) to the north. The Bench Lake fault in the vicinity of knobs 325 m and 360 m strikes N. 77° E., and thus the fault is at a 10° angle to bedding. Conglomerate of the Wishbone Formation near the Bench Lake fault was found in outcrops on both sides of the inferred fault.

The Lost-in-the-woods fault was observed on aerial photographs as a slightly discontinuous linear feature (fig. 3), but is difficult to find on the ground because there are no significant topographic features near it. Where I observed the fault at its eastern end, it consisted of a south-facing scarp with an average height of 3.6 meters, but its height ranged from 2.4 to 4.4 m. Minor low-discharge streams that connect bogs within the spruce and birch forest cut across the escarpment without a significant change in gradient. In a soil pit at the base of the scarp, there was a 25-cm-thick A soil horizon dominated by humus, and 10-20 cm downward into this horizon there were large cobbles up to 15 cm across (fig. 6). Beneath the A horizon was 35 cm of poorly-sorted reddish-buff-brown sand, silt, and clay. The remaining 5+ cm of the pit consisted of striated pebbles and cobbles in the poorly sorted sand, silt, and clay, which was probably till. Because of the cobbles in the A horizon, and because of the topography of the scarp adjacent to the soil pit, it is likely that the cobbles rolled into the humus during a surface-faulting event. It is unlikely that the cobbles were washed into the peat by a nearby low-discharge stream because the largest clasts being transported by the stream were silt-to-sand size, and because a high-velocity stream would have removed the humus layer. Alternatively, tree windthrow may have introduced the cobbles into the humus. There were uprooted trees from blowdowns nearby, but only cobbles were seen in the soil pit, not clasts of all sizes, as would be expected from tree windthrow.

HATCHER PASS ROAD AREA

The Castle Mountain fault in the vicinity of the Hatcher Pass Road juxtaposes the Paleocene and Eocene Arkose Ridge Formation on the north against the Eocene Wishbone Formation to the south. The actual fault zone is

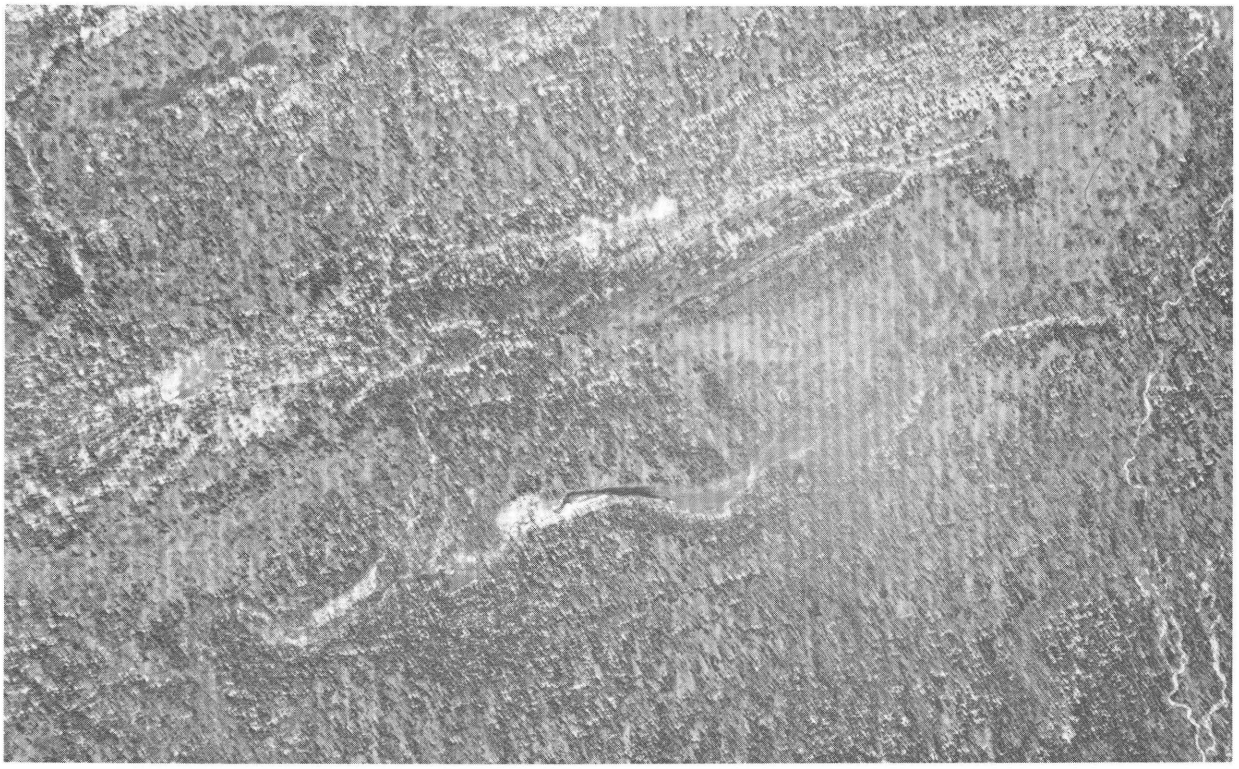

A

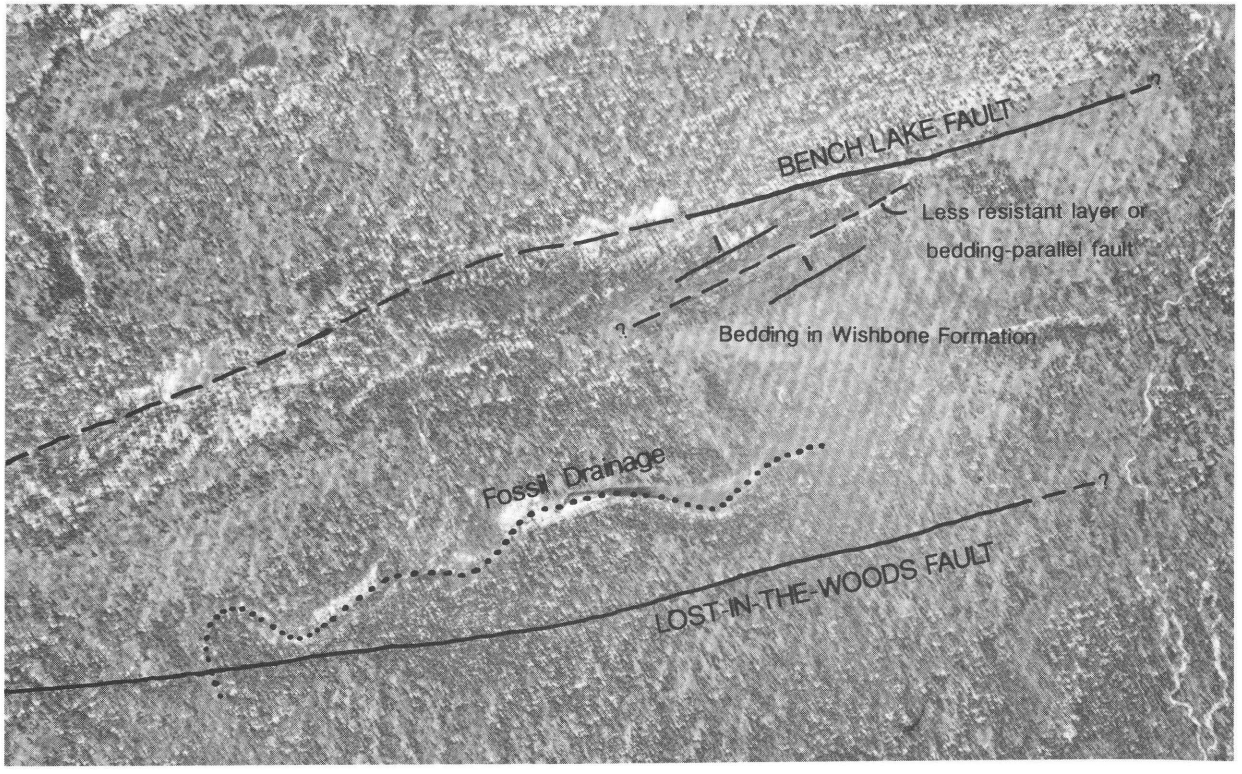

B

Figure 3. *A*, Uninterpreted vertical aerial photograph in the vicinity of Bench Lake and Lost-in-the-woods faults. *B*, Same aerial photograph showing interpreted locations of Bench Lake and Lost-in-the-woods faults, and bedding orientation in conglomerate of the Wishbone Formation.

Figure 4. View due south toward 1.5-m-tall scarp at eastern end of Bench Lake fault.

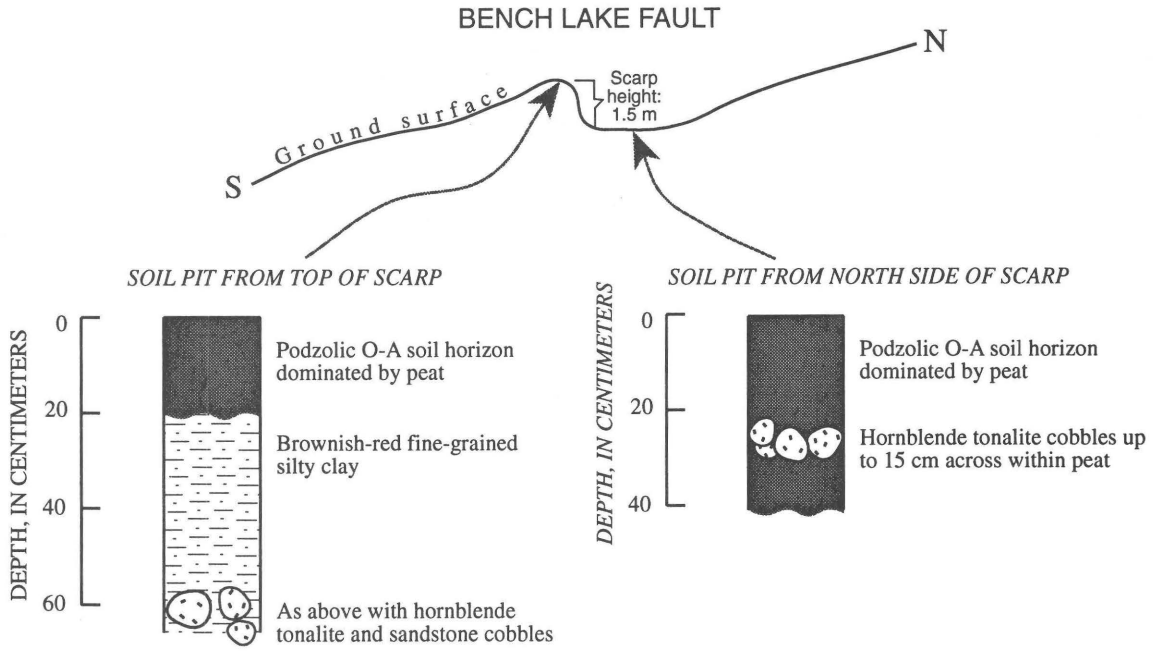

Figure 5. Profile of scarp and soil pit stratigraphy at Bench Lake fault.

not exposed; however, outcrops of the Wishbone Formation and Arkose Ridge Formation are separated from each other by a distance perpendicular to the fault of about 200 m. In the course of this study, an outcrop of the Wishbone Formation was found 200 m north of the mapped trace of the Castle Mountain fault (Detterman and others, 1976), suggesting that the fault (fig. 2, loc. G) is located slightly north of its previously mapped position in the center of the bend of the Little Susitna River. Detterman and others (1976) indicated that the Castle Mountain fault consists of two strands that ran through the two prominent bends in the canyon that the Little Susitna River has carved. I did not find evidence for the southern strand, although I saw nothing to preclude its presence.

There is virtually no evidence for deformation of the Wishbone Formation, but the Arkose Ridge Formation is almost pervasively deformed along anastomosing subvertical brittle faults with muddy gouge. Faulting was especially common along shale horizons. I noted numerous subvertical and subhorizontal slickenside striae on slip surfaces, as did Bruhn and Pavlis (1981), but I found that steps on the slickensides were rare. As a result, I was unable to make any conclusions of the fault's history, other than that both dip-slip and strike-slip motion has occurred on it. I did not notice any increase in intensity of deformation approaching the Castle Mountain fault, although David Doherty (ARCO Alaska, Inc., oral commun., 1993) stated from his observations over a larger area that the pervasive faulting of the Arkose Ridge Formation is limited to the vicinity of the fault.

I found no unambiguous geomorphic expression of the Castle Mountain fault in the vicinity of the Hatcher Pass Road. However, Detterman and others (1976) claimed that there were elongate ponds along one of the traces of the fault east of the Little Susitna River. I observed two ponds on aerial photographs, but both were elongate roughly perpendicular to the strike of the fault. Therefore, I conclude that these two ponds are not related to the fault. I did observe several broad (50–200 m wide) subparallel linear features weakly defined by vegetation to the east of the Little Susitna River. One of the vegetation lineaments is near the trace of the Castle Mountain fault, and it may be related to the fault, but the remainder of the linear features may be bedrock ridges mantled by glacial sediments. West of the Hatcher Pass Road, there is one linear feature subparallel to the trace of the Castle Mountain fault, although it is located approximately 100 m to the south of the fault. This feature is defined by an 8-m-high, north-facing escarpment. From aerial photographs, it appears that this feature is related to an ancient drainage that flowed to the west and then to the south. If there was south-side-up faulting along the Castle Mountain fault prior to, or during, the time the drainage was active, the stream may have been constrained by a fault scarp of the Castle Mountain fault at its southern bank.

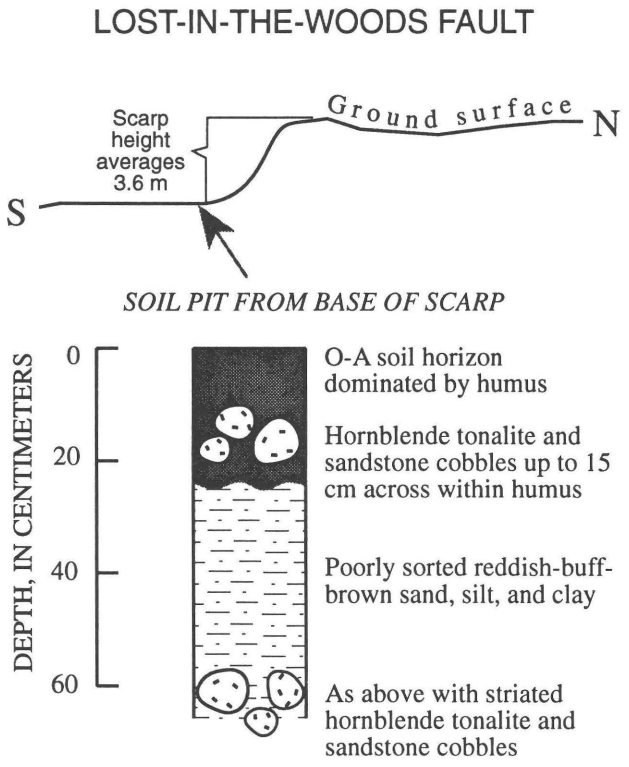

Figure 6. Profile of scarp and soil pit stratigraphy at Lost-in-the-woods fault.

AGE OF SURFACE FAULTING IN THE STUDY AREA

All faulting in the vicinity of Houston certainly postdates glacial stagnation and retreat of the late Naptowne stade glaciers, which occurred prior to 9,000 to 13,000 yr B.P. Faulting is further constrained to post-date formation of the alluvial terrace south of the Little Susitna River (fig. 2). There are no radiocarbon dates to better limit the age of surface faulting in the area; this will be a focus of future work.

The age of faulting along the Bench Lake fault and the Lost-in-the-woods fault is more speculative because lateral moraines of unequivocal late Naptowne age are not present. There is an undated lateral moraine and adjacent kame terrace on the south flank of the Talkeetna Mountains at elevations between 300 and 400 m, which lies to the north of the Bench Lake fault and the Lost-in-the-woods fault (fig. 2) (Haeussler, unpublished mapping, 1993; Reger and Updike, 1983). This moraine may be as old as approximately 40,000 yr B.P. because it is the lowest pre-late Naptowne-age moraine (Reger and Updike, 1983); however, it could be substantially younger, as Richard Reger (Alaska Division of Geological and Geophysical Surveys, oral commun., 1993) contends. To the south of

this moraine, there are numerous ice-marginal and subglacial channels in the study area (fig. 3) (P. Haeussler, unpublished mapping). The upper (or northern) limit of these drainages is shown on figure 2, and it may approximate the late Naptowne ice limit. If so, then surface faulting on the Lost-in-the-woods fault and the western (inferred) part of the Bench Lake fault postdates the most recent glaciation. The eastern part of the Bench Lake fault may lie above the late Naptowne ice limit, and surface faulting may predate the late Naptowne stade and postdate the early Naptowne stade. However, I suggest that movement on the Bench Lake fault is younger than that on the Lost-in-the-woods fault because (1) the Lost-in-the-woods fault is dissected by minor streams that do not change gradient as they cross the scarp, whereas the Bench Lake fault is not dissected, (2) the scarp on the Bench Lake fault is more clearly defined and steeper than the scarp on the Lost-in-the-woods fault, and (3) the soil profile on the Bench Lake fault is dominated by peat and thus may be more youthful than the soil profile adjacent to the Lost-in-the-woods fault, which is dominated by humus. Further study will attempt to place tighter limits on the age of surface faulting in this area.

DISCUSSION

The principal conclusion of this study is that late Quaternary surface faulting has occurred more extensively on or near the Castle Mountain fault than previously recognized. The identification of the Castle Mountain fault on the alluvial terrace of the Little Susitna River extends the eastward limit of its known location near Houston by 3 km (fig. 2). In addition, there is evidence for late Quaternary faulting along the Bench Lake and Lost-in-the-woods faults—two previously unrecognized features. Both the Bench Lake and Lost-in-the-woods faults lie north of the inferred trace of the Castle Mountain fault, and thus they may not be part of the Castle Mountain fault. Where previously studied, the Castle Mountain fault consists of one trace (Detterman and others, 1974, 1976). However, because the Bench Lake and Lost-in-the-woods faults lie within 1 to 3 km of the inferred trace of the Castle Mountain fault, and because all three faults have had late Quaternary surface faulting, the Bench Lake and Lost-in-the-woods faults may be associated with the Castle Mountain fault. Also, because the age of surface faulting on the Castle Mountain fault in the Susitna Lowland is younger than 1,860 yr B.P. (Detterman and others, 1974), the age of faulting on the Bench Lake and Lost-in-the-woods faults may be substantially younger than the approximately 10,000- to 40,0000-yr-B.P. constraints on the maximum age of faulting.

The large-scale geometry of the late Quaternary faults in the study area is indicated by the sense of slip on faults in trenches (Detterman and others, 1974; Bruhn, 1979) and by scarp topography (for example, a north-facing scarp indicates south-side-up motion). Using this data, most faults in the study area have north-side-up motion, although there are two cases of south-side-up motion. On the Castle Mountain fault in the Susitna Lowland, the north side is up (fig. 2, fault segment A), but the trenches of Bruhn (1979) had normal faults, whereas the trench of Detterman and others (1974) had a reverse fault. Just east of where the Castle Mountain fault crosses the Parks Highway near Houston, the south side is up (fig. 2, fault segment C). The Bench Lake fault is south side up, whereas the Lost-in-the-woods fault is north side up (figs. 5, 6). The opposing senses of relative offset may be indicative of strike-slip motion on a system of faults with a simplified palm tree structure (Sylvester, 1988). However, because earthquake and most field data (Lahr and others, 1986; Detterman and others, 1974, 1976) indicate the fault is steeply north-dipping, the north-side-up offset may be indicative of contractional deformation, which is expected from North American-Pacific relative plate motions. Neither end-member explanation is entirely satisfactory, and perhaps a combination of right-slip and contractional deformation is involved.

Acknowledgments.—I appreciate the encouragement of George Plafker to undertake a study of the Castle Mountain fault, as well as his technical review. Discussions with, and a technical review by, Oscar Ferrians were also very helpful. Tom Hamilton provided valuable input into interpreting a critical outcrop. Discussions with Dick Reger and Dave Doherty were also insightful. Chuck Moore helped in drafting, and Lucita Haeussler provided faithful field assistance.

REFERENCES CITED

Birkeland, P.W., 1984, Soils and geomorphology, Oxford University Press, New York, 372 p.

Bruhn, R.L., 1979, Holocene displacements measured by trenching the Castle Mountain fault near Houston, Alaska, *in* Short Notes on Alaskan Geology—1978: Alaska Division of Geological and Geophysical Surveys, Geologic Report 61, p. 1–13.

Bruhn, R.L., and Pavlis, T.L., 1981, Late Cenozoic deformation in the Matanuska Valley, Alaska: three dimensional strain in a forearc region: Geological Society of America Bulletin, v. 92, p. 282–293.

Clardy, Bruce I., 1974, Origin of the lower and middle Tertiary Wishbone and Tsadaka Formations, Matanuska Valley, Alaska: unpublished M.S. thesis, University of Alaska, Fairbanks, 74 p.

Detterman, R.L., Plafker, G., Hudson, T., Tysdal, R.G., and Pavoni, N., 1974, Surface geology and Holocene breaks along the Susitna segment of the Castle Mountain fault, Alaska: U.S. Geological Survey Miscellaneous Field Studies Map MF–618, 1 sheet.

Detterman, R.L., Hudson, T., and Hoare, J.M., 1975, Bruin Bay fault inactive during the Holocene, *in* Yount, M. E., ed., U.S. Geological Survey Alaska Program, 1975: U.S. Geological Survey Circular 722, p. 45.

Detterman, R.L., Plafker, G., Russell, G.T., and Hudson, T., 1976, Features along part of the Talkeetna segment of the Castle Mountain-Caribou fault system, Alaska: U.S. Geological Survey Miscellaneous Field Studies Map MF–738, 1 sheet.

Fuchs, W.A., 1980, Tertiary tectonic history of the Castle Mountain-Caribou fault system in the Talkeetna Mountains, Alaska: unpublished Ph.D dissertation, University of Utah.

Grantz, A., 1966, Strike-slip faults in Alaska: U.S. Geological Survey Open-File Report, 92 p.

Kelley, T.E., 1963, Geology and hydrocarbons in Cook Inlet Basin, Alaska: American Association of Petroleum Geologists Memoir 2, p. 278–296.

Lahr, J.C., Page, R.A., Stephens, C.D., and Fogleman, K.A., 1986, Sutton, Alaska, earthquake of 1984: evidence for activity on the Talkeetna segment of the Castle Mountain fault system: Bulletin of the Seismological Society of America, v. 76, p. 967–983.

Martin, G.C., and Katz, F.J., 1912, Geology and coal fields of the lower Matanuska Valley, Alaska: U.S. Geological Survey Bulletin 500, 98 p.

Plafker, G., Detterman, R.L., and Hudson, T., 1975, New data on the displacement history of the Lake Clark fault, *in* Yount, M.E., ed., U.S. Geological Survey Alaska Program, 1975: U.S. Geological Survey Circular 722, p. 44–45.

Reger, R.D., 1981a, Geology and geologic-materials maps of the Anchorage C-8 SE Quadrangle, Alaska: Alaska Division of Geological and Geophysical Surveys Geologic Report 65, scale 1:25,000, 2 sheets.

Reger, R.D., 1981b, Geology and geologic-materials maps of the Anchorage C-8 SW Quadrangle, Alaska: Alaska Division of Geological and Geophysical Surveys Geologic Report 68, scale 1:25,000, 2 sheets.

Reger, R.D., and Updike, R.G., 1983, Upper Cook Inlet region and the Matanuska Valley, p. 185–263, *in* Péwé, T.L., and Reger, R.D., editors, Guidebook to permafrost and Quaternary geology along the Richardson and Glenn Highways between Fairbanks and Anchorage, Alaska: Fourth International Conference on Permafrost, Fairbanks, July 18–22, 1983, Field Trip Guidebook 1: Alaska Department of Natural Resources, Division of Geological and Geophysical Surveys, 263 p.

Sylvester, A.G., 1988, Strike-slip faults, Geological Society of America Bulletin, v. 100, p. 1666–1703.

Wahrhaftig, C., 1965, Physiographic divisions of Alaska: U.S. Geological Survey Professional Paper 482, 52 p.

Williams, J.R., 1986, New radiocarbon dates from the Matanuska Glacier bog section, *in* Bartsch-Winkler, S., and Reed, K. M., ed., U.S. Geologic Studies in Alaska by the U.S. Geological Survey During 1985: U.S. Geological Survey Circular 978, p. 85–88.

Winkler, G.R., 1992, Geologic map and summary geochronology of the Anchorage 1°×3° quadrangle, southern Alaska, U.S. Geological Survey Miscellaneous Investigations map I–2283.

Reviewers: Oscar Ferrians and George Plafker

High Stand and Catastrophic Draining of Intracaldera Surprise Lake, Aniakchak Volcano, Alaska

By R.G. McGimsey, C.F. Waythomas, *and* C.A. Neal

ABSTRACT

Wave-cut terraces and multiple exposures of lacustrine sediment indicate a former, more extensive stand of intracaldera Surprise Lake in the crater of Aniakchak volcano. The lake once covered nearly half of the caldera floor and had an estimated volume of about 3.7×10^9 m^3. A terrace that marks the high stand of the lake is traceable along the north caldera wall to a break in slope near the top of a v-shaped notch (The Gates) in the caldera rim. Downstream from The Gates, the Aniakchak River flows through a broad, terraced, and boulder-strewn valley. Results from our preliminary investigations suggest that Surprise Lake may have been at its high stand during the explosive destruction of an intracaldera stratocone sometime after 464 yr B.P. Stratigraphic relations suggest that the lake may have drained during this eruptive episode. We speculate that the eruptive activity caused water in the lake to overtop the caldera rim at The Gates, initiating failure of the caldera-rim dam and subsequent catastrophic drainage of Surprise Lake.

INTRODUCTION

Because of their basin-like shape, calderas on many Alaskan volcanoes are geomorphic repositories for water, ice, and snow. The heat flux associated with these volcanoes enhances melting of ice and snow, and caldera lakes commonly result. The caldera rim is a type of natural dam that may impound a substantial amount of water depending on the size of the caldera and the integrity of the bedrock that forms the rim. Failure of a caldera dam and subsequent catastrophic drainage of the intracaldera lake can pose a serious hazard to life and property situated in the flood path (Bolt and others, 1977, p. 94–95). In this report of our preliminary observations, we present geomorphic and stratigraphic evidence for (1) a former extensive intracaldera lake at Aniakchak volcano, (2) catastrophic drainage of this lake by failure of the caldera rim dam, and (3) possible linkages between dam failure and the recent eruptive history of the volcano.

SETTING

Aniakchak volcano is a late Holocene caldera located 670 km southwest of Anchorage on the Alaska Peninsula in Aniakchak National Monument and Preserve (fig. 1). Surprise Lake covers 2.75 km^2 of the northeast floor of the caldera (Cameron and Larson, 1992).

First reported by Smith (1925), the caldera is 10 km wide, about 1 km deep, and circular in plan-view (figs. 2, 3). It formed about 3,400 yr B.P. during a cataclysmic eruption that produced more than 50 km^3 (bulk volume) of pyroclastic material (Miller and Smith, 1987; Beget and others, 1992). An extensive ashflow sheet, originally covering an area of about 2,500 km^2, extends up to 80 km beyond the caldera rim and fills glacial valleys of the pre-caldera stratovolcano to a depth of up to 75 m (Miller and Smith, 1987; Miller and Smith, 1977).

The highest point in the crater is Vent Mountain, a prominent 670-m-high stratocone, located in the southern half of the caldera (figs. 2, 3). Vent Mountain has been active repeatedly since the caldera formed and may be one of the oldest features in the caldera (C.A. Neal and R.G. McGimsey, unpublished field data).

Along the west wall of the caldera is a spectacularly exposed cross section of a young intracaldera stratocone called Half Cone (fig. 3). Our work indicates that this was the site of the most voluminous and explosive post-caldera eruptive activity. Half Cone was destroyed during a violent eruption that produced massive intracaldera pyroclastic-flow and pyroclastic-surge deposits. These deposits extend about 5 km eastward from the vent across the northern floor of the caldera. A wide-spread pumice-fall deposit, of stratigraphic significance to this study, also originated from Half Cone. Field relations indicate that this deposit, informally referred to as the "pink pumice," was formed just prior to

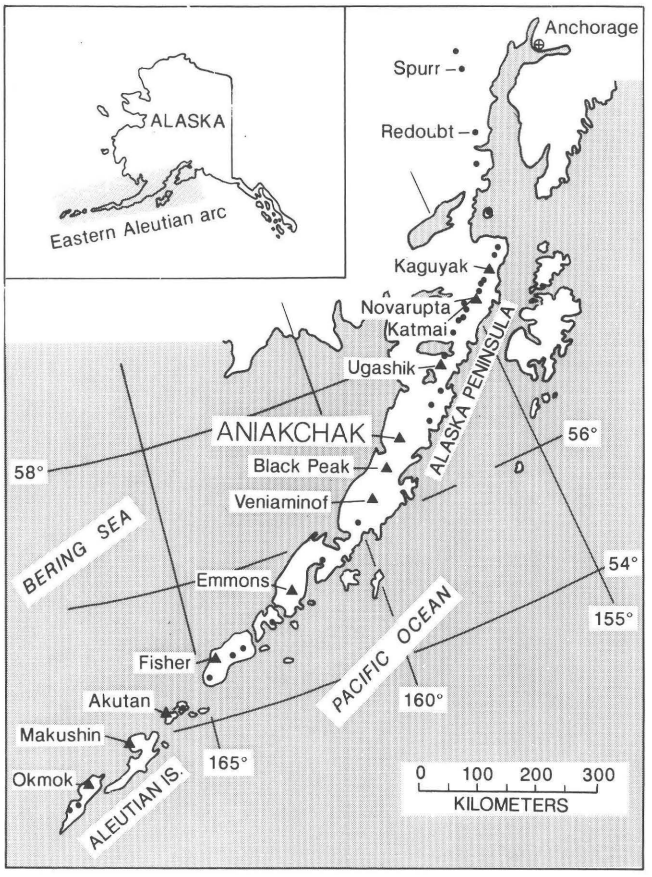

Figure 1. Location of Aniakchak caldera and other major Holocene volcanoes of the eastern Aleutian arc. Triangles denote calderas and circles denote stratovolcanoes. From Miller and Smith, 1987.

Figure 2. Aerial oblique view from west of Aniakchak caldera. Surprise Lake is located adjacent to northeast rim of caldera. The Gates is prominent notch in east caldera wall in center of view. Vent Mountain is snow-covered cone in south half of caldera, and 1931 vent is circular crater at bottom center of photograph. Photograph by M. Woodbridge Williams, National Park Service, 1986.

the eruptive cycle that destroyed Half Cone. Organic matter immediately beneath this deposit yielded a radiocarbon age of about 464 yr B.P. (table 1; fig. 3, point D); this is the only post-caldera tephra unit that has been dated. The deposit is exposed along much of the caldera rim where it is up to 1 m thick, and it is also exposed at Half Cone, the flanks of Vent Mountain, and on the tops of Surprise cone and other tuff cones north and east of Vent Mountain (fig. 3). In low areas in the northern half of the caldera, the deposit is unusually discontinuous and poorly preserved.

Surprise cone is the westernmost of at least three clustered tuff cones that pre-date Half Cone (fig. 3). Surprise cone is about 150 m high and the entire western half of the cone has been removed by erosion, exposing the eastern inner wall and limbs (fig. 3). The topography of all three tuff cones is rounded and subdued.

Aniakchak volcano last erupted in 1931 (Hubbard, 1931; Jagger, 1932). The 1931 eruption produced a tephra cone along the west caldera wall about 4 km northwest of Vent Mountain and 2.5 km south of Half Cone (fig. 3).

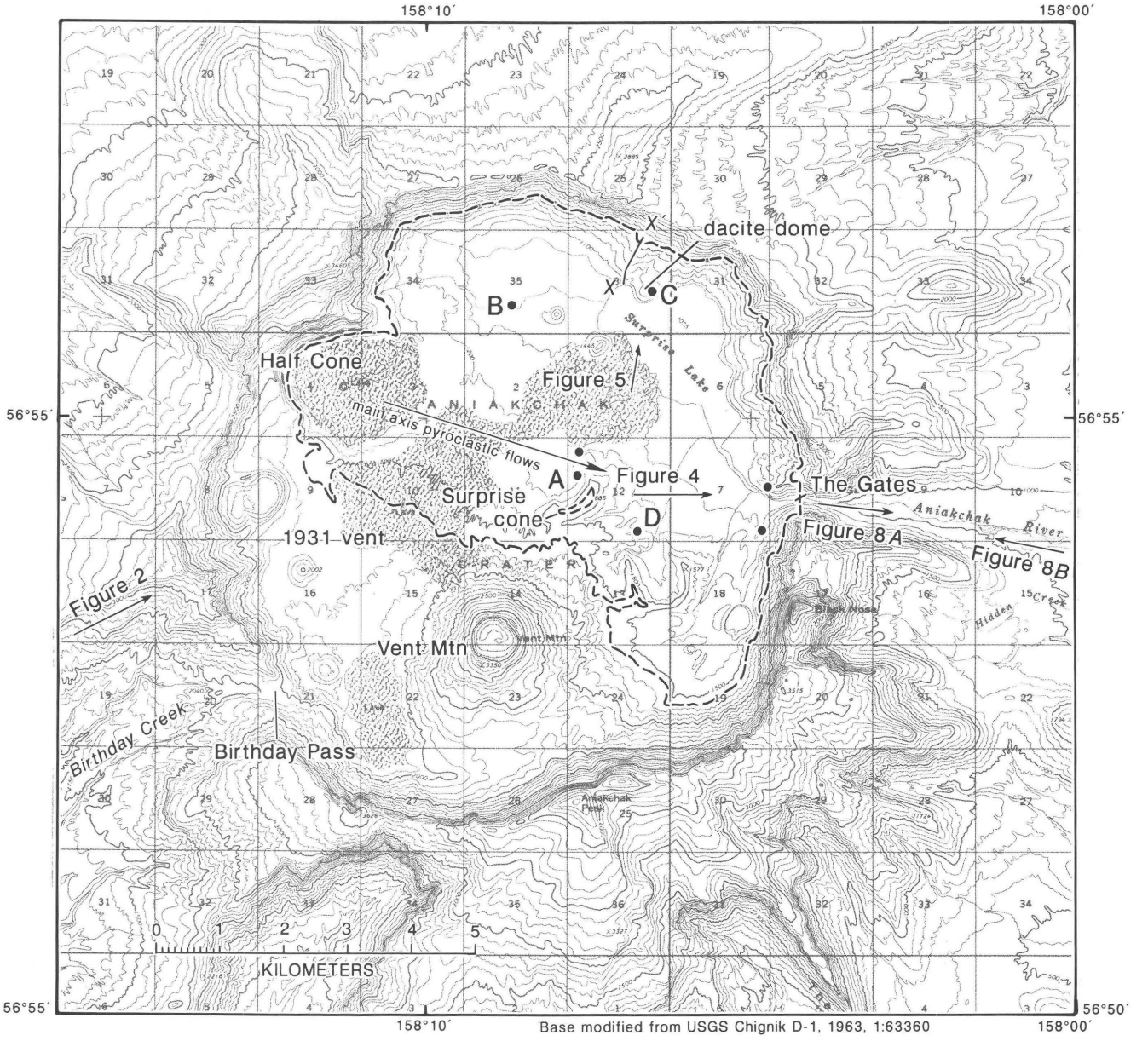

Figure 3. Topographic map of Aniakchak Crater. Large arrow shows main emplacement direction of pyroclastic-flow deposits produced during explosive destruction of Half Cone. Small arrows show direction of view in other figures. Solid circles are locations of lake sediments discussed in text, and points A–C mark specific outcrops referred to in text. Point D is location for radiocarbon-dated organic material underlying Half Cone pumice-fall deposit, which predates destruction of Half Cone. Line *X*-*X*' marks location of traverse across wave-cut terraces on north caldera wall. Heavy dashed line depicts the maximum area that would be covered by the proposed last high stand of the lake (38 km^2).

This eruption deposited tens of meters of tephra adjacent to the vent, and spread ash over much of southwestern Alaska (Jaggar, 1932).

Table 1. Radiocarbon age of organic sediment underlying prominent pumice-fall deposit from Half Cone (sample location on figure 3).

Sample number and material dated	Reported age (^{14}C years B.P.)[1]	Calibrated age[2]	
		Year B.P.	Year AD
CAMS-9851 organic matter	390±60	510, 464, 319	1440, 1486, 1631

[1]Age reported in years before present (B.P.) with respect to year AD 1950.
[2]Ages calibrated using method of Stuiver and Reimer (1993); reported as: -1σ, age, $+1\sigma$.

GEOMORPHIC RELATIONS NEAR THE GATES

The elevation of the caldera rim ranges from 1,341 m at Aniakchak Peak to 320 m at the bottom of The Gates (fig. 3). The caldera floor is highest (700 m) between Vent Mountain and the south wall and generally slopes northward toward Surprise Lake (321 m). A prominent v-shaped notch in the east wall of the caldera, The Gates, is the only drainage outlet from the caldera (fig. 4*A*). The maximum width of The Gates is about 700 m and the depth is about 600 m. The caldera rim on either side of The Gates is one of the two lowest points on the entire rim (excluding the bottom of The Gates); the other is Birthday Pass on the south rim. Exposed in the south wall of The Gates is an undisturbed sequence of pre-caldera lava flows and pyroclastic deposits that overlie light- to medium-gray and greenish-yellow basement rocks of Jurassic, Cretaceous, and Tertiary age (Detterman and others, 1981). From a distance, the north wall of The Gates appears to contain reddish-orange basement rocks that are fractured, faulted, and webbed with whitish-gray veins. The alteration

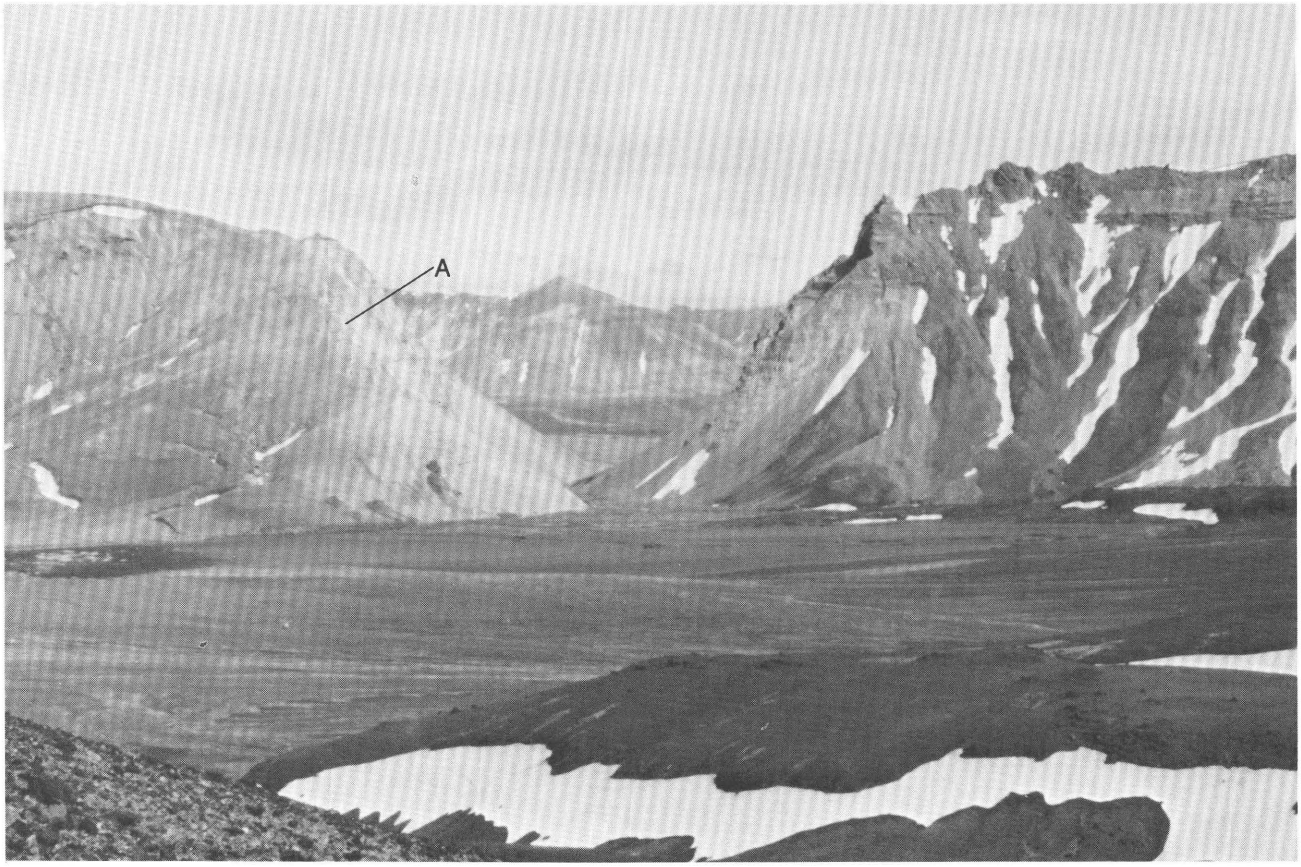

A

Figure 4. *A*, View east of The Gates from within caldera. Point A marks altitude of the highest of several lake terraces above Surprise Lake. *B*, Large slump blocks in north wall of The Gates. Point A marks altitude of the highest of several lake terraces.

of these rocks likely has a hydrothermal origin. This altered zone extends for perhaps 0.5 km along the east wall north of The Gates. On the inside wall of the caldera adjacent to the north wall of The Gates is a chaotic assemblage of tilted slump blocks composed of the same altered bedrock as that in the north wall of The Gates, as well as pre-caldera lava flows and volcaniclastic rocks (fig. 4*B*). The contact between the inner caldera wall and the first slump block forms a small notch (point A, fig. 3). The crest of this and an adjacent slump block form a ridge that extends down toward the caldera floor. The lower several hundred meters of the ridge is truncated by a horizontal erosion surface (fig. 4*B*). Other parts of the caldera wall have veins, dikes, and landslide debris at the base; however, alteration and veining are particularly pervasive and numerous only along the caldera wall that encompasses The Gates.

HIGH STAND OF SURPRISE LAKE

Most geological studies at Aniakchak volcano to date have focused on the caldera-forming eruption and post-caldera eruptive activity (Smith, 1925; Hubbard, 1931; Miller and Smith, 1977, Miller and Smith, 1987; Neal and others, 1992). However, the history of Surprise Lake and a possible relation between the lake and the latest Holocene eruptive history of the volcano has not been addressed. Smith (1925, p. 142) conjectured that "Surprise Lake may have formerly covered a much larger area...but terraces or high-water marks could not be detected on the wall at the few places examined." Subsequent workers (T.P. Miller, oral commun., 1992) noted possible evidence of a higher stand of the lake such as the ~4-km^2 flat, featureless caldera floor that extends west of the lake, and an erosion surface that truncates the top of a pumiceous dacite dome about 52 m above present lake level (fig. 3).

During field investigations in 1993, we discovered lake sediments at several localities on the caldera floor and lower walls of the caldera above Surprise Lake (fig. 3). Where best exposed, the lake sediments are laminated, clayey silt with sandy intervals. Exposures are located in stream banks on the caldera floor, in gullies on the caldera wall, and in the breach of Surprise cone. All exposures of the lake sediments are overlain by pumiceous pyroclastic deposits from Half Cone. At localities where a complete sequence of lacustrine sediment was exposed, the deposits

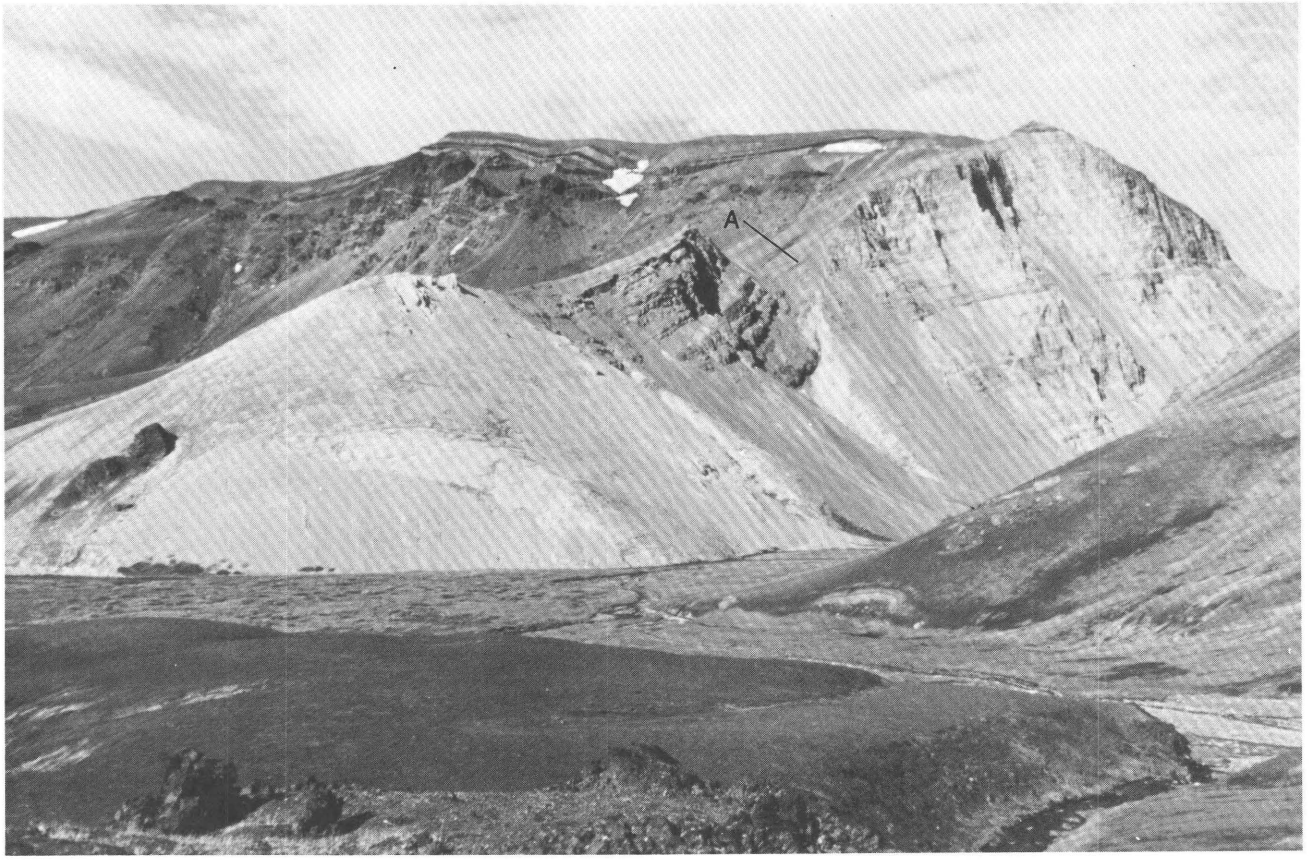

B

Figure 4.—Continued.

are about 0.5 m thick and overlie poorly sorted, sandy to pebbly, reworked volcaniclastic material. At the other localities, the lacustrine sediments were frozen below about 40 cm, and we could not determine the thickness of these deposits. One of the 0.5-m-thick sequences of lacustrine sediment occurs on the lowest of three prominent wave-cut terraces (point C, fig. 3).

We identified at least three wave-cut terraces on the northeast wall of the caldera above Surprise Lake (fig. 5). The terraces are present along the lower half of the northeast wall of the caldera, which generally has a more gentle slope than the rest of the inner wall of the caldera (fig. 6). About 1 meter of primary and reworked tephra, principally from the eruption of Half Cone, mantles the lower slopes, including the terraces. The topography along this northeast section of the caldera wall appears more rounded and subdued in contrast to the remainder of the caldera wall (fig. 6).

Starting at the northwest end of Surprise Lake, we measured the altitude of the terraces using a Jacob Staff and Abney Level (fig. 3). The lowest terrace is approximately 52 m above the lake and is accordant with an erosion surface on the top of a pumiceous dacite dome (figs. 5, 6). The second terrace is located about 82 m above the lake, and is at the same level as the top of one of the slump blocks adjacent to The Gates. The top of this slump block also appears truncated by an erosion surface. The highest terrace is 166 m above the lake (elevation 488 m). Although none of these terraces can be traced continuously along the northeast caldera wall, matching segments are preserved intermittently along the wall from our measuring point southeastward to The Gates. A search for lake sediments on the highest terrace was abandoned when we encountered frozen ground at about 40-cm depth. Other terrace segments along the wall were not examined.

Lacustrine terraces typically form during prolonged, stable stands of a lake when there is sufficient time for storm waves to batter the coastline. Although wave-cut terraces can form when the lake is either rising or falling, lacustrine deposits on top of the lowest terrace above Surprise Lake indicate that this terrace probably formed during the filling cycle of the lake. Because we found no evidence to the contrary, we have made the assumption that all of the terraces on the northeast wall of Aniakchak caldera formed as the lake rose. Assuming otherwise—that the terraces formed as lake level fell—is inconsistent with a single, catastrophic draining of the lake. Future examination of the other terrace segments on the northeast caldera wall should help us determine whether our assumption is correct.

From the highest terrace, prominent geographic points within the caldera at the same altitude were located by hand leveling to determine areas that were submerged when the lake was at this position. Among the points that would have been at or below the highest stand of the lake were a break in slope above one of the slump blocks adjacent to the north

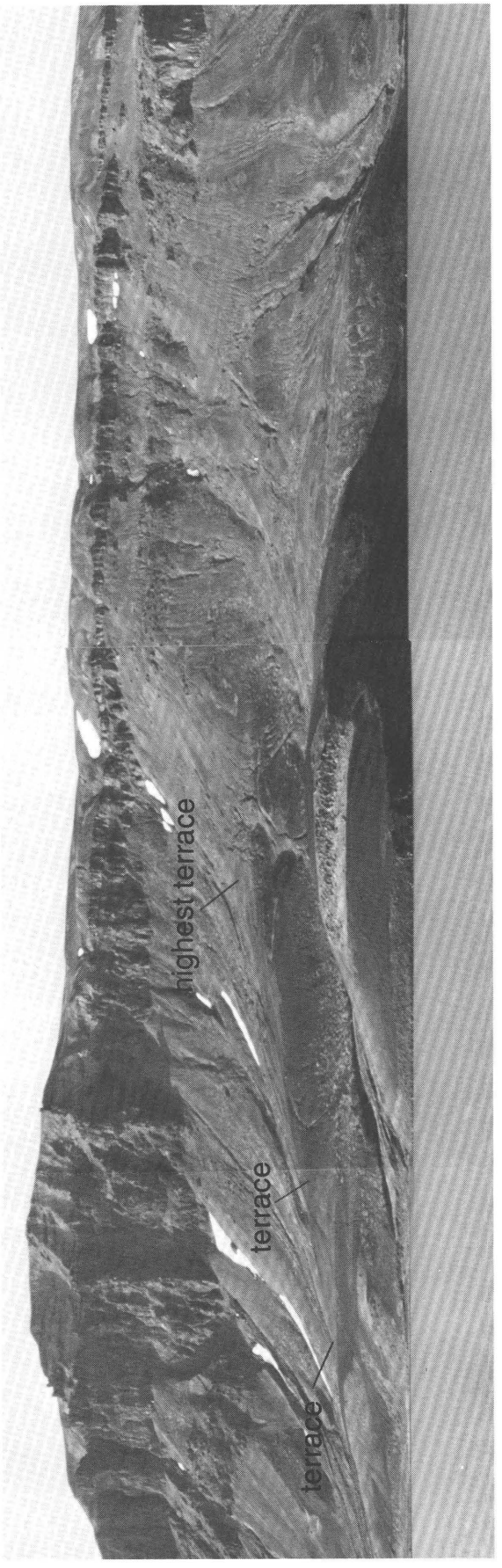

Figure 5. Northeast caldera wall and remnants of 3 wave-cut terraces formed during higher stands of Surprise Lake.

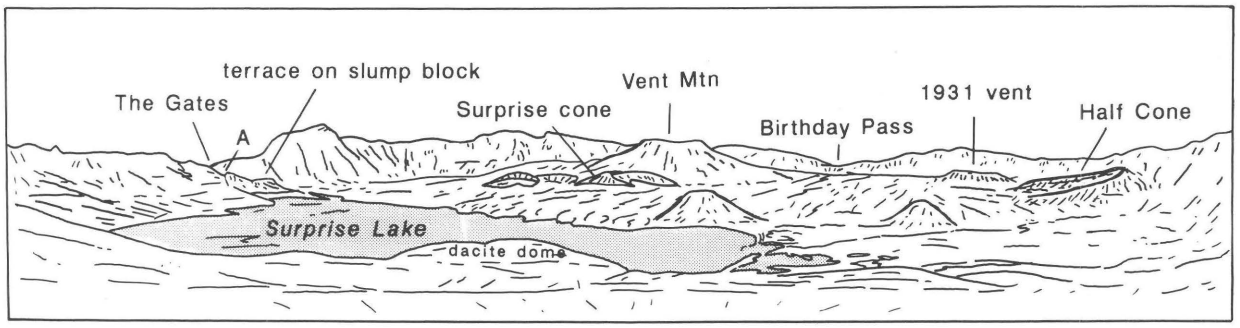

Figure 6. Panoramic view south of Aniakchak caldera from highest lake terrace on north wall above Surprise Lake (*X'*, fig. 3). Surprise cone in center view is breached on the west, facing Half Cone.

wall of The Gates (point A on fig. 4*A*, *B*), and the summit of Surprise cone (fig. 3). At this stand, the lake would have covered about 38 km^2—more than half of the caldera floor (fig.3)—and would have had an average depth of about 98 m and a volume of about 3.7×10^9 m^3.

NATURAL DAM FAILURE AT THE GATES

At the high stand of the lake, we estimate from topography and hand leveling that the low point on the caldera rim was within the area now occupied by The Gates. In its present configuration, formation of The Gates must post-date the existence of the lake because the bottom of the breach would have been 400 to 600 m below the lake surface.

The geometry of The Gates is indicative of erosion by water because the breach is v-shaped and narrow (700 m wide, 600 m deep) and has a low width-depth ratio (about 1.2). In contrast, Birthday Creek valley, the next lowest point on the rim (fig. 3), was formed by pre-caldera glacial erosion and has a width-depth ratio of 12. Thus, it is unlikely that The Gates were formed by glacial erosion. Incision of The Gates could not have happened by slow spillover of water from the lake because the boundary shear stress at the low point on the caldera rim would be so small that erosion of bedrock could not occur. Erosion of bedrock by flowing water is governed by the shear stress at the rock-water boundary. The boundary shear stress (τ) is a function of the depth of water (D), the specific weight of water (γ), and the energy slope (S; approximately equal to the water surface slope), as indicated by the following relation (Baker and Costa, 1987):

$$\tau = \gamma DS \qquad (1)$$

If water begins to flow over the low point in the caldera rim because of excess inflow, such as an overflowing bathtub, both D and S and the resulting τ are so small that erosion cannot occur. Thus, formation of The Gates by fluvial erosion requires a significant increase in flow depth and energy slope. In contrast, if the caldera rim failed, both flow depth and energy slope would increase, almost instantaneously, resulting in a flow with significant erosive capacity. Erosion of the caldera rim will commence when τ exceeds the resistance of the boundary. In bedrock fluvial systems not subject to rapid tectonic uplift, large-scale erosion of bedrock is nearly always the result of catastrophic water floods where bedrock is entrained by plucking or cavitation (Baker and Komar, 1987).

We surmise that water was, by some mechanism, discharged rapidly from the intracaldera lake, causing fluvial erosion of the caldera rim to produce The Gates. Furthermore, we suggest that incision of the breach was initiated by failure of the caldera rim at The Gates because this part of the caldera rim appears to be structurally weak. If we consider the catastrophic outflow from the intracaldera lake to be the result of a natural dam failure, we can estimate the peak discharge at The Gates using the method of Costa and Schuster (1988). For earth and rockfill dams, the empirical expression used to predict peak discharge from dimensions of the reservoir and dam is:

$$Q = 0.0184(E_v)^{0.42} \qquad (2)$$

where Q is the peak discharge in meters per second, and E_v is the potential energy of the lake behind the dam in joules (Costa and Schuster, 1988). Potential energy is determined from the relation:

$$E_v = (h)(v)(g) \qquad (3)$$

where h is the dam height in meters, v is the volume of the lake, and g is the specific weight of water in newtons per cubic meter. For h=183 m, $v=3.7\times10^9$ m^3, and g=9,800 N/m^3 the resulting peak discharge is about 81,000 cubic meters per second. The regression equation used to develop the relation between peak discharge and potential energy has a standard error of 91 percent (Costa and Schuster, 1988). This large standard error results from uncertainties in the indirect estimates of peak discharge from dam failures used to develop the relation (Costa, 1985; Costa and Schuster, 1988).

A context for the postulated Aniakchak caldera flood is established by comparing the potential energy and peak discharge of this flood with other dam-break floods (fig. 7). This plot indicates that even with the large standard error, the Aniakchak caldera flood would be a significant event, exceeded by few known dam-break floods. If our hypothesis of a catastrophic caldera rim dam failure is correct, telltale flood evidence should exist outside the caldera.

DOWNSTREAM OBSERVATIONS

We have not yet directly examined the area downstream from The Gates, and the following observations and interpretations are based on brief aerial reconnaissance, analysis of air photographs and topographic maps, and photographs taken by Smith (1925) and during the 1931 Hubbard expedition to Aniakchak (Hubbard, 1931).

Downstream from The Gates, the Aniakchak River flows in a broad valley about 1 km wide and is flanked by at least two terraces (Smith, 1925, plate XLIII-C) that stand an estimated 50 meters above the valley floor and extend downvalley for several kilometers (figs. 8, 9). A cursory air-photo survey of other rivers and streams in the area revealed that none had similar terraces. River terraces can form in response to a wide range of fluvial, sedimentologic, and tectonic conditions, one of which is catastrophic flooding (Bull, 1990). At present, we do not know if the terraces along the Aniakchak River are fluvial terraces; however, incision of the Aniakchak River valley to form these features would be a likely consequence of a catastrophic flood. The apparent absence of similar-scale terraces on other local rivers and streams suggests that the terraces along the Aniakchak River have a unique origin. Also, it seems unlikely that the present Aniakchak River could have incised such a broad and deep valley since the time of caldera formation.

Large boulders (estimated from Hubbard photographs to be up to about 5 m across) of a distinctive volcanic rock-type are strewn about the valley floor outside The Gates and for several kilometers downstream (fig. 8). The same, or similar rocks are exposed in the caldera wall and rim immediately adjacent to the north wall of The Gates. The blocks seemingly are evidence of vigorous sediment transport from the caldera. We interpret the boulders as representing flood deposits; however, without additional field data, other explanations for the origin of the large boulders are possible. For example, an alternative hypothesis is that the blocks were excavated from the deposit in which the valley is cut and were too large to be carried downstream by the Aniakchak River.

About 20 kilometers downstream from The Gates, the Aniakchak River flows out of a rolling upland area onto a low-relief alluvial plain. A large fan-shaped feature is present along the Aniakchak River in the zone where the river debouches from the upland onto the alluvial plain (fig. 9). The feature is topographically identical to alluvial and outwash fans elsewhere in Alaska and the Western United States. Streams crossing the "fan," including the Aniakchak River, are too small to have formed it. This suggests that the fan could be the product of a larger, more competent Aniakchak River. Where the Aniakchak River

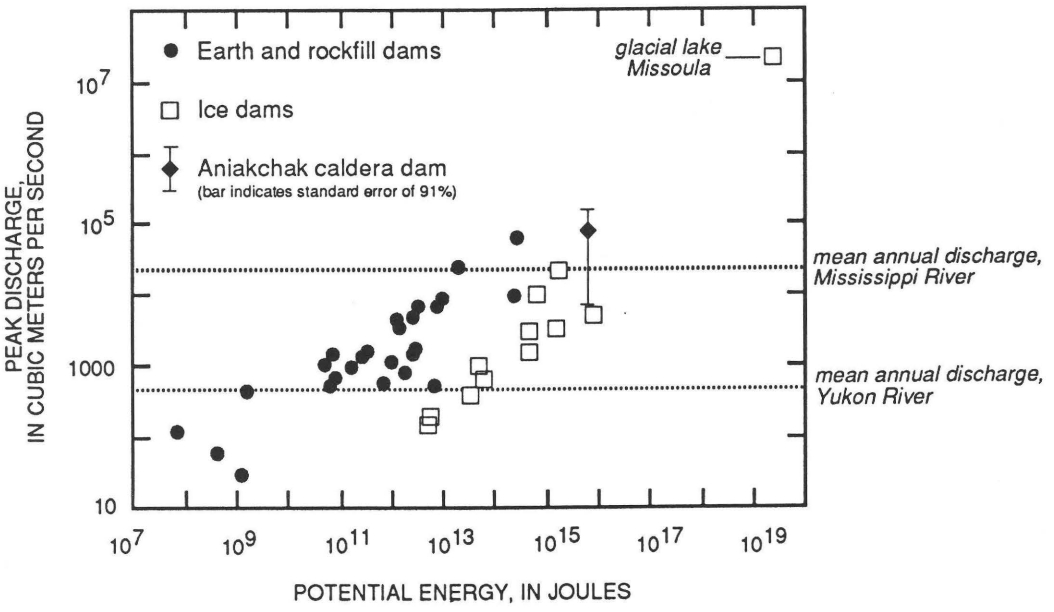

Figure 7. Potential energy of lake water versus peak discharge for natural dam failures, including Aniakchak caldera (data from Costa, 1985, and Costa and Schuster, 1988). Mean annual discharge for the Mississippi and Yukon Rivers shown for comparison.

crosses the fan, the channel is braided and straight. The braided pattern and straight channel of the river indicate, in part, that the channel is formed in coarse, noncohesive sedimentary deposits. Based on its geometry, location, and probable sediment type, and with consideration of the terraces and boulders upstream, our preliminary interpretation is that the fan also is a flood deposit.

TIMING AND CAUSE OF PROPOSED CATASTROPHIC FLOOD

If Surprise Lake drained catastrophically, what mechanism or circumstances might have triggered the event? Eruptive activity has been documented as one method of evacuating water from an intracaldera lake (Bolt and others, 1977; Major and Newhall, 1989). Another possibility is structural failure of the caldera-rim dam, perhaps unrelated to eruptive activity. Either scenario might apply to the draining of Surprise Lake. Based on our preliminary studies we have developed the working hypothesis that Half Cone erupted during the high stand of the lake, that the eruptive activity in some way initiated the catastrophic draining of the lake and concurrent formation of The Gates, and that the eruption continued after the lake level was lowered to near its present position. This hypothesis is founded primarily on three lines of evidence: (1) isolated exposures of pyroclastic surge deposits on the summit of Surprise cone, (2) poorly preserved and laterally discontinuous occurrence of the Half Cone pink pumice deposit in the northern half of the caldera, and (3) the stratigraphic relation of pyroclastic deposits and lake sediments at the base of Surprise cone and on the north floor of the caldera.

Exposed for about 300 m along the summit rim of Surprise cone (ranging vertically over 25 m) is a 2-m-thick section of pyroclastic-surge deposits overlain by less

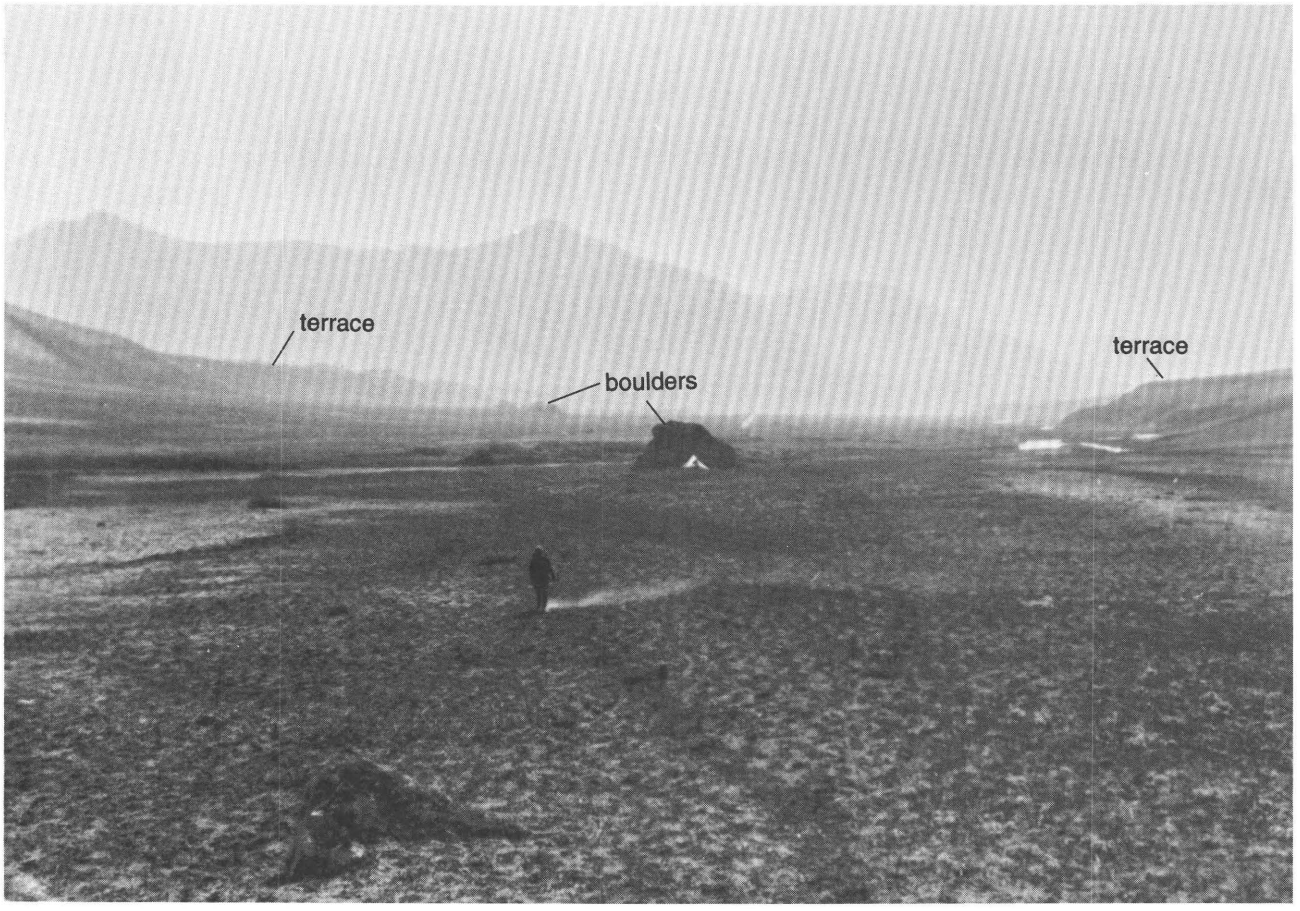

A

Figure 8. Large (up to 5-m-diameter) boulders in terraced valley immediately outside The Gates may be evidence of catastrophic draining of Surprise Lake. *A*, View downvalley from The Gates, showing large boulders strewn about valley bottom between paired terraces that flank the valley. *B*, View toward The Gates from top of terrace on south side of Aniakchak River. Note large boulders in valley bottom. Photographs from the Bernard R. Hubbard S.J. Collection, Santa Clara University Archives.

than a meter of pumiceous fallout deposits originating from Half Cone. In contrast, massive pyroclastic-flow debris and bombs from Half Cone occur on the flanks of Surprise cone. The eroded west flank of Surprise cone faces Half Cone, about 4.5 km to the northwest. The horizontally laminated, clayey lake sediments we discovered at the northwest base of Surprise cone (fig. 3), about 115 m below the summit and about 75 m above present lake level (point A, fig. 3), are overlain by massive pyroclastic-flow deposits derived from Half Cone.

The distribution, bedforms, and geomorphology of Half Cone pyroclastic-flow deposits indicate that the main flow direction of pyroclastic flows and surges was toward The Gates (fig. 3). However, pyroclastic-flow deposits also extend radially from Half Cone across the caldera floor. On the flat floor of the caldera, 1.5 km west of Surprise Lake (point B, fig. 3), yellowish, clayey lake sediments are present only a few meters above Surprise Lake. In one exposure, the sediments have been invaded and upended by at least one tongue of Half Cone pyroclastic-flow deposits that are at least several meters thick (fig. 10). The imbrication direction of the upended lake sediments indicates that the pyroclastic flow was directed from the southwest, which is consistent with an origin from Half Cone. The lake sediments in contact with the pyroclastic-flow deposits are orange-colored and oxidized, consistent with thermal alteration. Fossil fumaroles, with oxidized alteration halos, occur on the surface of Half Cone pyroclastic-flow deposits a few kilometers south and about 60 m above these lake sediments (fig. 3). Pyroclastic-surge deposits are located near the fossil fumaroles on the caldera floor. In summary, we observed isolated pyroclastic surge deposits on the summit of Surprise cone, Half Cone pyroclastic flow debris overlying lake sediments at the base of Surprise cone and invasively disturbing lake sediments lower on the caldera floor, and fossil fumaroles and pyroclastic surge deposits located on the caldera floor between Surprise cone and Half Cone.

We suggest that pyroclastic surge deposits on the summit of Surprise cone are discontinuous with other surge deposits because the final eruption of Half Cone occurred during the high stand of the lake when only the

B

Figure 8.—Continued.

summit of Surprise cone was aerially exposed. According to Cas and Wright (1987, p. 283) when a subaerially erupted pumice flow enters water, an ash-cloud surge continues over the water surface. If an ash cloud of this type encountered an "island" and surge deposits formed, these would later appear, when lake level dropped, as isolated deposits, similar to those observed on Surprise cone. In this model, the pyroclastic-flow and pyroclastic-surge deposits on the floor of the caldera would have been emplaced subaerially after the lake level had dropped during the eruption.

An alternative explanation for the surge deposits on the summit of Surprise cone is that they are not related to lake level, but are instead a spatially limited primary deposit, or an exposure isolated by erosion. This explanation requires (1) Surprise Lake be near its present level during the final eruption of Half Cone (this accounts for Half Cone pyroclastic-flow deposits on the lower floor of the caldera), and (2) a pyroclastic flow, or flows, advanced across the caldera floor from Half Cone, up the 150-m-high eroded face of Surprise cone to deposit about 2 meters of surge deposits. This interpretation also requires the lake sediments, located at the base of Surprise cone and conformably overlain by Half Cone pyroclastic-flow deposits, to have been subaerially exposed during the eruption. We found no evidence for subaerial exposure of these lake sediments (mudcracks, soil development, erosional unconformity).

The foregoing alternative explanation is consistent with many of our observations. However, the discontinuous, poorly preserved character of the ca. 464-yr-B.P. pink pumice deposit in the northern half of the caldera—the same area that would have been submerged during high stand of the lake—is difficult to explain in the absence of a higher lake. We suggest that in the northern half of the caldera the limited distribution and poor preservation of this deposit, which is so uniform and continuously exposed elsewhere in the caldera and along the rim, is a result of reworking by water and deposition through a water column. Thus, a higher stand of Surprise Lake could account for the observed character of the pink pumice.

Accepting the foregoing arguments for a high stand of Surprise Lake during the final eruption of Half Cone, we interpret the Half Cone pyroclastic-flow deposits that immediately overlie the lake sediments at the base of Surprise cone and on the caldera floor west of Surprise Lake to indicate that the lake drained to near its present level during that eruption. The orange-colored, oxidized condition of the invaded lake sediments in contact with Half Cone pyroclastic deposits indicates that the pyroclastic material was probably hot when emplaced, causing alteration of the lake sediments.

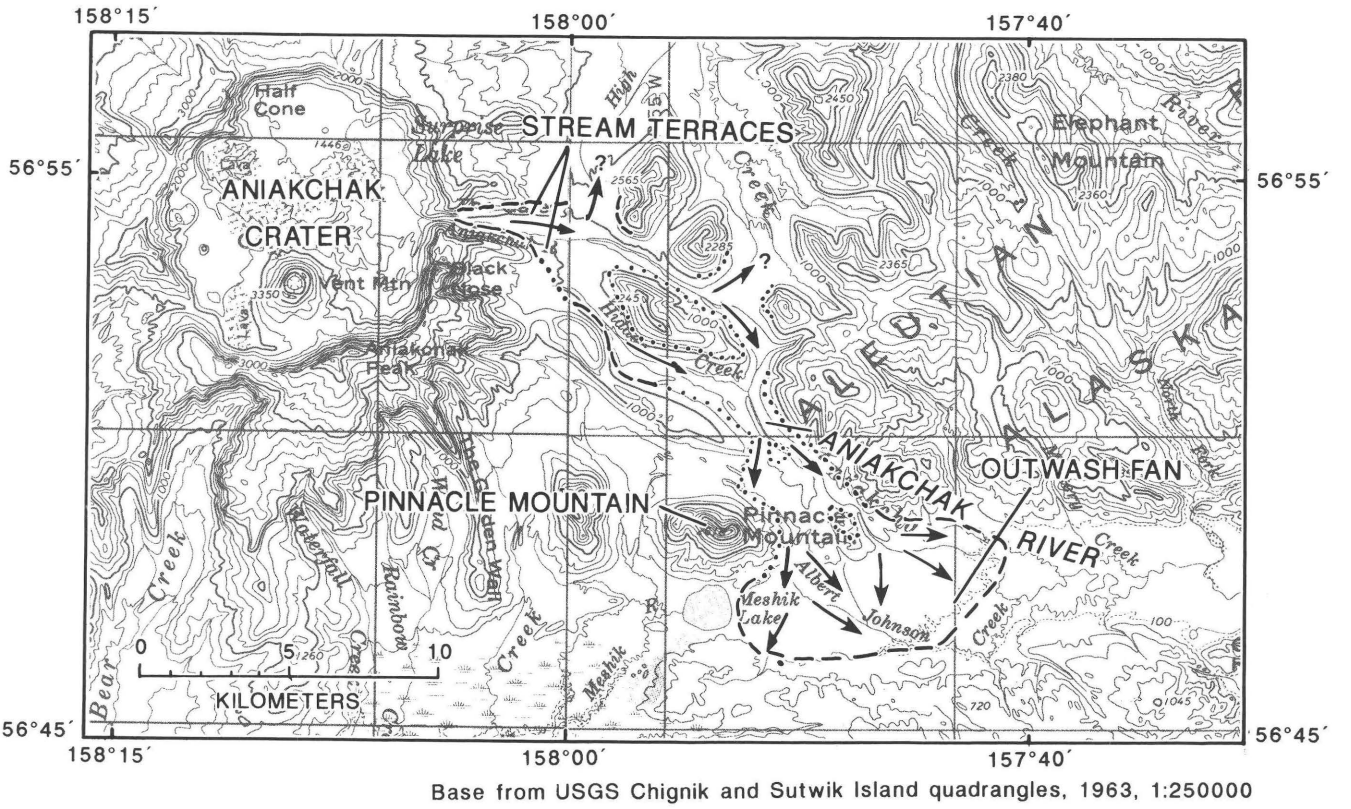

Figure 9. Course of the Aniakchak River eastward from caldera. Large, south-facing alluvial fan is delineated by topography southeast of Pinnacle Mountain. We suggest this fan formed during catastrophic draining of Surprise Lake in Aniakchak caldera. Arrows indicate possible routes for floodwaters, and dashed and dotted lines delineate probable extent of floodwaters.

If this interpretation is correct, the lake could not have been more than a few meters deep, because it is unlikely that pyroclastic flows can maintain their heat and physical integrity upon entering water (Cas and Wright, 1987). However, the behavior of subaqueously emplaced pyroclastic flows is controversial (Cas and Wright, 1987). Fossil fumaroles and alteration halos observed in Half Cone pyroclastic-flow deposits on the caldera floor are similar to those in the 1912 ashflow sheet in the Valley of Ten Thousand Smokes near Mt. Katmai, Alaska, which were emplaced subaerially, and some of which still retain heat. Thus, rapid draining of the lake, just prior to the cessation of eruptive activity, could account for the pyroclastic-flow deposits with fossil fumaroles, and would allow for the lake sediments on the low north floor of the caldera to be disrupted and overlain by hot pyroclastic-flow deposits.

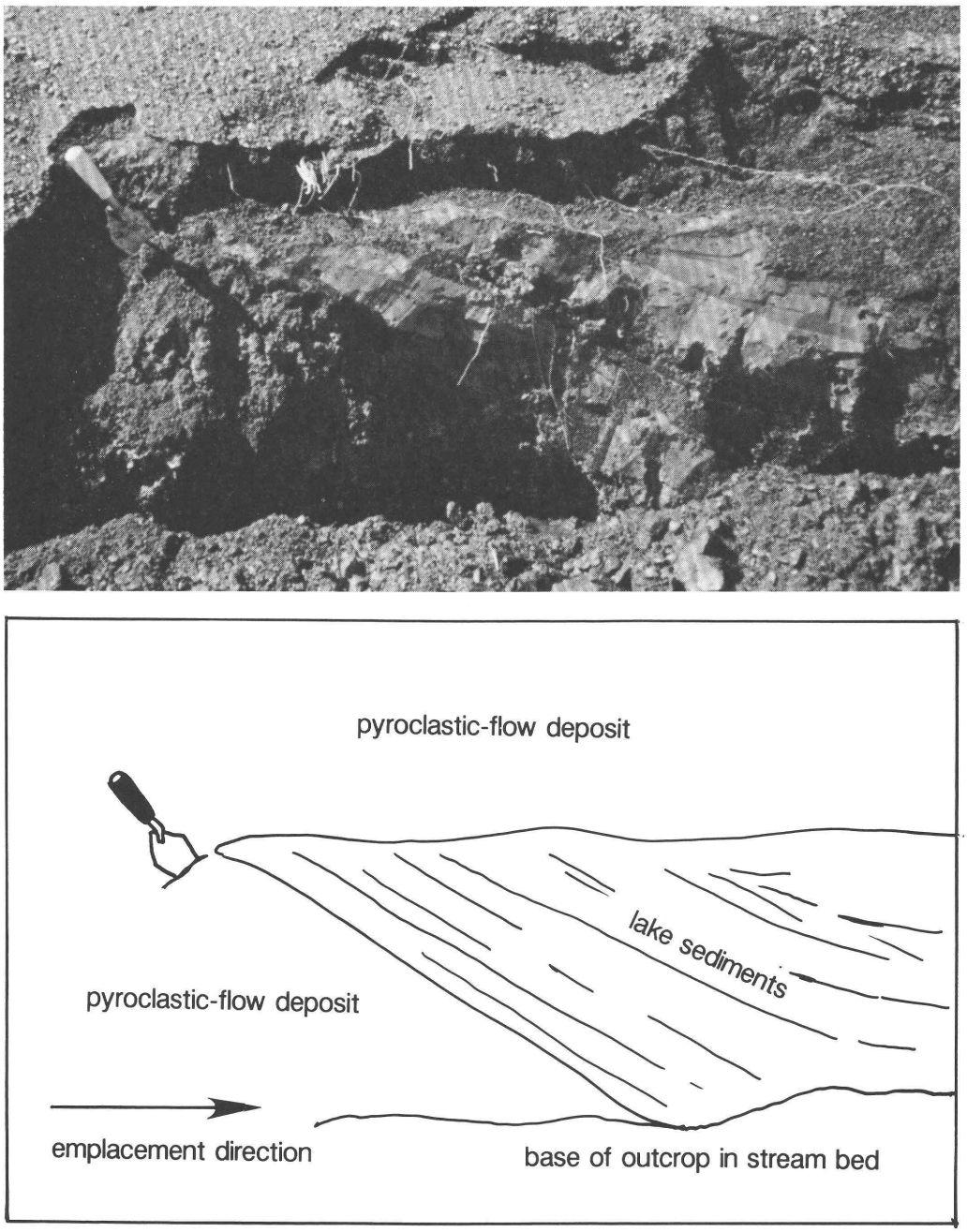

Figure 10. Lake sediments that are displaced and overlain by Half Cone pyroclastic-flow deposits (point B, fig. 3). Tongue of pyroclastic-flow deposits bulldozed into and beneath soft lake sediments, thereby upturning, truncating, and baking the beds.

Eruption of Half Cone during the high stand of Surprise Lake also provides a plausible mechanism for initiating the catastrophic drainage of the lake. If the lake was at its high stand when Half Cone explosively erupted, pyroclastic flows and debris avalanches(?) entering and displacing water in the lake likely would generate large waves (Latter, 1981). Additionally, strong seismicity that is typically associated with eruptive activity might also generate waves in the lake. Assuming that the low point on the caldera rim was at or near water level, we suggest that waves could have produced a rush of water over the low point of the rim, initiating dam failure, subsequent erosion of The Gates, and catastrophic drainage of the lake.

The timing of the destruction of Half Cone, and the subsequent catastrophic draining of Surprise Lake, is in part constrained by the 464-yr-B.P. age of the distinctive pink pumice, that was deposited just prior to the final eruption of Half Cone.

During field studies planned for 1994, we will test the catastrophic flood hypothesis by investigating possible flood deposits identified on topographic maps and aerial photographs and by collecting additional samples for radiocarbon dating to better constrain the timing of events.

Acknowledgments.—Aniakchak National Monument is administered by staff at Katmai National Park in King Salmon. We thank Rick Potts and Susan Savage of the National Park Service for their help with permits and logistics. We thank Tom Miller for introducing us to Aniakchak.

REFERENCES CITED

Baker, V.R., and Costa, J.E., 1987, Flood power, *in* Mayer, L.D., and Nash, D., eds., Catastrophic flooding: Allen and Unwin, Boston, p. 1–21.

Baker, V.R., and Komar, P.D., 1987, Cataclysmic flood processes and landforms, *in* Baker, V.R., Greely, R., Komar, P.D., Swanson, P.D., and Waitt, R.B., Jr., The Columbia and Snake River Plains, *in* Graf, W.L., ed., Geomorphic systems of North America: Boulder, Colorado, Geological Society of America, The Geology of North America, Centennial Special Volume 2, p. 423–443.

Beget, J., Mason, O., and Anderson, P., 1992, Age, extent and climatic significance of the c. 3400 BP Aniakchak tephra, western Alaska, USA: The Holocene, v. 2, no. 1, p. 51–56.

Bolt, B.A., Horn, W.L., Macdonald, G.A., and Scott, R.F., 1977, Geologic hazards: Springer-Verlag, New York, 330 p.

Bull, W.B., 1990, Stream-terrace genesis—Implications for soil development, *in* Knvepfer, P.L.K., and McFadden, L.D., eds., Soils and landscape evolution: Geomorphology, v. 3, p. 351–368.

Cameron, W.A., and Larson, G.L., 1992, Baseline inventory of the aquatic resources of Aniakchak National Monument, Alaska: National Park Service Technical Report NPS/PNROSU/NRTR–92/03, 243 p.

Cas, R.A.F., and Wright, J.V., 1987, Volcanic successions—modern and ancient: Allen and Unwin Ltd., London, 528 p.

Costa, J.E., 1985, Floods from dam failures: U.S. Geological Survey Open-File Report 85-560, 54 p.

Costa, J.E., and Schuster, R.L., 1988, The formation and failure of natural dams: Geological Society of America Bulletin, v. 100, p. 1054–1068.

Detterman, R.L., Miller, T.P., Yount, M.E., and Wilson, F.H., 1981, Quaternary geologic map of the Chignik and Sutwik Island quadrangles, Alaska: U.S. Geological Survey Miscellaneous Investigations Series Map 1292, scale 1:250,000.

Hubbard, B.R., 1931, A world inside a mountain, the new volcanic wonderland of the Alaska Peninsula, is explored: National Geographic Society, v. 60, no. 9, p. 319–345.

Jaggar, T.A., 1932, The Volcano Letter, v. 375, p. 1–3.

Latter, J.H., 1981, Tsunamis of volcanic origin: Bulletin of Volcanology, v. 44, p. 467–490.

Major, J.J., and Newhall, C.G., 1989, Snow and ice perturbation during historical volcanic eruptions and the formation of lahars and floods—A global review: Bulletin of Volcanology, v. 52, p. 1–27.

Miller, T.P., and Smith, R.L., 1977, Spectacular mobility of ash flows around Aniakchak and Fisher calderas, Alaska: Geology, v. 5, p. 173–176.

Miller, T.P., and Smith, R.L., 1987, Late Quaternary caldera-forming eruptions in the eastern Aleutian arc, Alaska: Geology, v. 15, p. 434–438.

Neal, C.A., McGimsey, R.G., Braitseva, O., Miller, T.P., Eichelberger, J.C., and Nye, C., 1992, Post-caldera eruptive history of Aniakchak Caldera, Alaska: Eos, Transactions, American Geophysical Union, v. 73, no. 43, p. 645.

Smith, W.R., 1925, Aniakchak Crater, Alaska Peninsula: U.S. Geological Survey Professional Paper 132–J, p. 139–149.

Stuiver, M., and Reimer, P.J., 1993, Extended ^{14}C database and revised CALIB radiocarbon calibration program: Radiocarbon, v. 35, p. 215–230.

Reviewers: Willie Scott, Steve Nelson, and Tom Miller

Isotopic Constraints on the Genesis of Base-Metal-Bearing Mineral Occurrences near Columbia Glacier, Northern Prince William Sound, Alaska

By Richard J. Goldfarb, Carol A. Gent, John E. Gray, *and* Steven W. Nelson

ABSTRACT

Sulfide-bearing veins, breccias, and silicified replacement zones occur in metasedimentary rocks of the Orca Group and in felsic intrusive rocks within a 900-km^2 area of northern Prince William Sound. Fluid $\delta^{18}O$ values calculated to be in equilibrium with hydrothermal quartz range between –4.2 per mil and +2.8 per mil and are consistent with values for evolved meteoric water. The δD compositions of fluid inclusion waters are generally about –90 per mil to –100 per mil, providing no evidence of any significant magmatic component to the ore fluids. Values of $\delta^{34}S_{sulfide}$ are generally between 0 per mil and –6 per mil where occurrences are hosted by metasedimentary rocks, but range from +4 per mil to +10 per mil where hosted by igneous rocks. These data are best interpreted as indicating two distinct sulfur sources, one igneous and one sedimentary, that interacted with the metal-bearing ore fluids.

Intrusion of felsic plutons into shallow levels of the Prince William terrane may have been the driving force for formation of the mineral deposits during the Tertiary. Magma emplacement may have locally initiated convective flow of surface waters. Highly radiogenic lead isotope values for sulfides from the mineral occurrences indicate that metals were leached from either metasedimentary rocks or granites. Few other metallic mineral deposits in southern Alaska have been recognized as having formed from convecting meteoric water, perhaps because shallow-level hydrothermal systems are rapidly eroded during regional uplift.

INTRODUCTION

Small, base-metal-rich mineral occurrences are abundant throughout the area between Columbia Glacier and Unakwik Inlet in northern Prince William Sound (fig. 1). Sulfide minerals occur as veins in fractures with variable amounts of quartz gangue, as blebs and massive pods in silicified and brecciated igneous and metasedimentary country rocks, and as disseminated grains within country rocks. Low tonnages and inaccessibility have hampered production from the occurrences. Prospecting activity, generally consisting of shallow, surface diggings or the construction of short adits, has taken place at about half a dozen of the occurrences. Jansons and others (1984) indicate inferred reserves of less than 50,000 short tons of ore in six occurrences containing resources of copper, lead, zinc, silver, and fluorite.

These base-metal-bearing occurrences are, however, significant because they reflect a mineral deposit type (epigenetic base-metal veins and replacement zones) that has not been widely recognized in the terranes of south-central Alaska. Low-sulfide, gold-bearing quartz veins (Goldfarb and others, 1986) and volcanogenic massive sulfide deposits (Crowe and others, 1992) are widespread within the Chugach and Prince William terranes. In contrast, numerous, generally gold-poor, copper-silver-zinc-(±lead)-rich, epigenetic occurrences have only been recognized in this part of the Prince William terrane (Nelson and others, 1984). It is possible that these occurrences were formed by remobilization of metals from syngenetic massive sulfides, by metamorphic processes similar to those that formed the regionally widespread epigenetic gold deposits, or by some other type of localized hydrothermal fluid-flow event within the forearc of southern Alaska. To aid in assessing the possibilities, stable and radiogenic isotopic studies were conducted to define fluid, sulfur, and metal sources.

GEOLOGY

A composite accretionary prism extends for more than 2,000 km along the Gulf of Alaska, from Baranof Island in the southeast to Sanak Island in the southwest (Plafker and others, 1977). The prism is composed of marine sedimentary and oceanic crustal rocks of the Chugach and Prince William terranes. In south-central Alaska, the youngest and most seaward part of the Chugach terrane is

made up of Upper Cretaceous volcaniclastic flysch and basalt of the Valdez Group. These rocks were accreted and deformed by latest Cretaceous or earliest Tertiary time (Plafker and others, 1989). The Prince William terrane, made up of upper Paleocene through middle Eocene turbidites and lesser basalt of the Orca Group, was accreted onto the Chugach terrane by middle Eocene time along the Contact fault system (Winkler and Plafker, 1981).

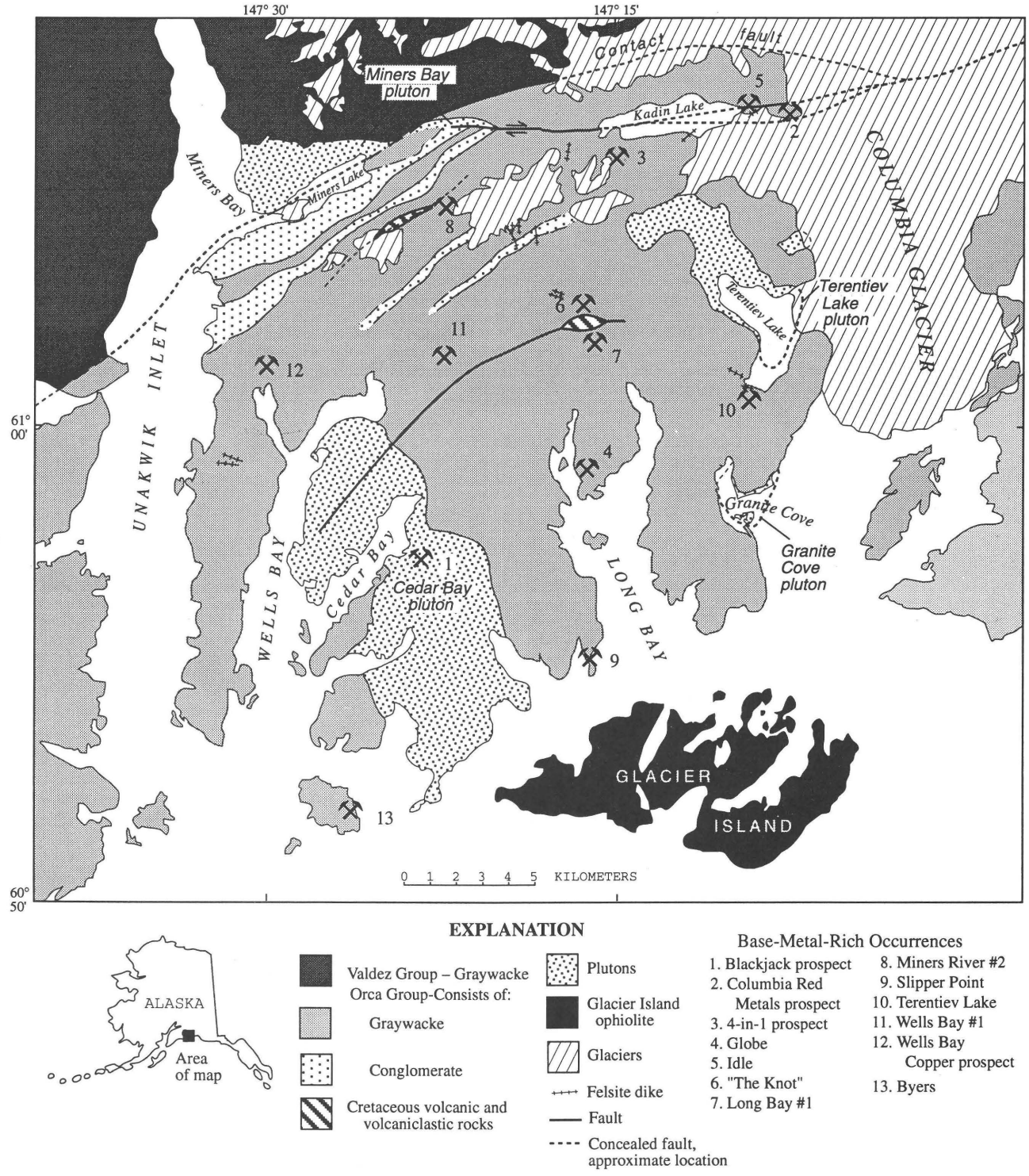

Figure 1. Geology and location of base-metal-bearing mineral occurrences, northern Prince William Sound. Geology is generalized from Haeussler and Nelson (1993).

Siliceous plutons and sills of the Sanak-Baranof plutonic belt intruded rocks of both the Orca and Valdez Groups at about 50–53 Ma in the Prince William Sound area (Hudson and others, 1979; Nelson and others, 1985). A second pulse of magmatism intruded both groups at about 34–38 Ma (Lanphere and others, 1966; Nelson and others, 1985). Igneous rocks formed during this later event, localized in western Prince William Sound, consist of composite bodies of gabbro and granite.

Base-metal-bearing mineral occurrences crop out in an area of approximately 900 km^2, immediately south of the Contact fault system, underlain mainly by sedimentary rocks of the Orca Group and undated felsic igneous rocks. Sedimentary units include conglomerate, massive sandstone, turbidites, shale, mixtures of massive sandstone and rhythmite, and chaotic deposits. The range of lithofacies in this area suggests the deposition of these materials in deep sea fans and submarine canyons at the base of the continental slope (Plafker and others, 1989). Additionally, two small areas in the study area, at the occurrence called "The Knot" and just south of Miners Bay (fig. 1), contain basaltic flows, pillow basalts, and tuff that are interbedded with the sedimentary rocks. Both volcanic rock-bearing sections contain carbonate rocks with mid-Cretaceous microfossils (Rashel Rosen, written commun., 1993). A complex folding history of rocks of the Orca Group, in part reflecting the oroclinal bending of southern Alaska between about 65 and 45 Ma, has been documented in the study area (Haeussler and Nelson, 1993). The rocks have been regionally metamorphosed to low grades during early Tertiary subduction, with facies ranging between laumontite and lower greenschist (Marti Miller, written commun., 1985). Locally, upper greenschist- to amphibolite-facies rocks of the Orca Group occur in the 2- to 2.5-km-wide contact aureoles of the larger plutons (Haeussler and Nelson, 1993).

In the northwest corner of the study area, composite bodies of the Miners Bay pluton have intruded sedimentary rocks on both sides of the Contact fault system. The 38-Ma gabbroic and dioritic bodies of the pluton intrude rocks of the Valdez Group immediately north of the Contact fault system. A large body of biotite granite subsequently intruded rocks of both the Orca and Valdez Groups, along with the older mafic igneous rocks, sometime before 32 Ma (Nelson and others, 1985). Since this time, the granite has been offset by a few kilometers of sinistral movement along the north strand of the Contact fault system (Winkler, 1992).

Numerous felsic dikes and three large granitic to granodioritic plutons—located at Terentiev Lake, Granite Cove, and Cedar Bay—are found in the study area. Tysdal and Case (1979) originally correlate these plutons with those of the Eocene Sanak-Baranof belt based on major-oxide chemistry. Winkler (1992), however, indicates that the low color indices and abundance of K-bearing minerals in these plutons are more characteristic of the Oligocene bodies in western Prince William Sound. A $^{40}Ar/^{39}Ar$ age of 30 Ma was determined for K-feldspar from the Granite Cove body (Larry Snee, unpub. data). Because the feldspar blocking temperature for argon loss is about 150°C, the intrusive event may have occurred (1) close to 30 Ma with rapid cooling from crystallization down to 150°C, or (2) between about 38 and 34 Ma and then cooled relatively slowly.

New chemical data from the igneous rocks from the study area are also more suggestive of a correlation with the Oligocene magmatic suite or possibly the existence of a third magmatic event (Steve Nelson, unpub. data). These data show the plutons in the study area to be relatively enriched in silica and alkali elements. The spatial association of the base-metal-rich mineral occurrences solely with the group of undated plutons and dikes is supportive of a third, distinct magmatic event.

MINERAL OCCURRENCES

Base-metal-bearing mineral occurrences are scattered throughout the metasedimentary and lesser metavolcanic rocks of the Orca Group and the felsic igneous rocks (fig. 1). The occurrences consist of north-trending and sulfide-bearing vein and breccia fracture-fillings and silicified replacement zones. The zones of silicified and sulfidized rock are generally less than 1 m in width, but at the Blackjack occurrence they reach widths of 2 to 3 m. Little evidence for shearing is present, and the host structures are simple brittle fractures (Haeussler and Nelson, 1993). Very fine grained, barren, quartz stockworks are located in wall rocks adjacent to many of the occurrences. Where the occurrences are hosted by igneous rocks, such as at the Blackjack prospect, the wall rocks are commonly bleached and altered to clay. No coarse-grained alteration phases are present. Also, unlike the epigenetic gold-bearing quartz veins found elsewhere in south-central Alaska, Fe-Mg-carbonate alteration is not common adjacent to the occurrences. This indicates that relatively low-CO_2 hydrothermal fluids were involved in the deposition of the base-metal-rich occurrences.

Many of the occurrences are briefly described in Jansons and others (1984). During our field investigations in 1992 and 1993, additional occurrences were discovered including Slipper Point, those at "The Knot," and numerous, recently exposed mineralized zones along the south shore of rapidly draining Terentiev Lake. Occurrences throughout the study area are either Pb-Zn-dominant (Long Bay #1, Miners River #2), Cu-dominant (Columbia Red Metals, Slipper Point, Globe, Wells Bay Copper, 4-in-1), or Zn-dominant (Byers, Blackjack) (table 1). Chalcopyrite, sphalerite, galena, arsenopyrite, and pyrite are the most common sulfide phases. Ore grades are variable, with Cu, Pb, or Zn concentrations

Table 1. Stable isotope data for silicate, carbonate, and sulfide minerals from base-metal-bearing mineral occurrences, northern Prince William Sound. Also shown are data ranges for other mineral deposits types in south-central Alaska summarized from Crowe and others (1992), Goldfarb and others (1986, 1993), Pickthorn (1982), and Pickthorn and Nelson (1984).

[Oxygen measurements are for quartz except where noted "cc" for calcite. Hydrogen measurements are for waters released during thermal decrepitation of fluid inclusions in quartz. Sulfur measurements are for pyrite (py), pyrrhotite (po), chalcopyrite (cp), galena (gn), sphalerite (sl), and intergrown sphalerite and galena (sl/gn). All data are in per mil]

	$\delta^{18}O$	δD	$\delta^{34}S$
Columbia Red Metals	13.6	−97	−5.7 (py)
	13.7		−6.5 (cp)
			−4.9 (sl/gn)
Slipper Point	12.8	−100	+0.2 (py)
Miners River #2	7.5		−2.0 (sl)
			−1.2 (py)
Wells Bay #1	12.0	−88	+7.4 (py)
Wells Bay Copper	8.3		−1.1 (sl)
			−1.6 (cp)
Blackjack	9.1	−139	+10.2 (sl)
			+7.6 (cp)
Globe	10.4		+1.6 (py)
4-in-1 (East Vein)	13.6		−4.7 (cp)
	10.6 (cc)		−5.0 (py)
Long Bay #1	10.8		−8.0 (sl)
Byers	14.5		−3.3 (py)
	11.7 (cc)		−3.6 (sl)
			−2.1 (py)
			−4.9 (po)
			−3.2 (sl)
Terentiev Lake	10.8		+5.1 (sl/gn)
	9.8		+7.8 (py)
	10.4		+3.8 (sl)
			+0.3 (sl/gn)
			+4.1 (py)
"The Knot"	12.7		−4.2 (py)
	11.7		
Idle	11.8		−4.1 (py)
			−5.9 (py)
Miners Bay pluton			−0.6 (po)
Barren vein, 2 km S of Miners Lake	13.6		
Barren vein, 1.5 km SE of Billy's Hole	11.5		
Barren vein, S shore Eickelberg Bay	10.9		
Barren vein, 3 km S of Kadin Lake	5.2		
Gold-bearing quartz veins, Chugach Mts.	13.9–17.0	−53 to −117	−2.3 to +2.2
Volcanogenic massive sulfides, Prince William Sound	9.8–16.9		+2.7 to +11.0

often exceeding 1 to 2 percent in high-grade grab samples. Iron concentrations in these samples generally range between 10 and 15 percent. Barite has not been identified in any of the occurrences and barium concentrations are generally at background levels of 1,000 ppm or less. However, a few samples of mineralized igneous float surrounding the Miners River #2 prospect contain 5,000 ppm Ba and a quartz vein from The Knot occurrence contains >5,000 ppm Ba, suggesting at least local barite precipitation.

Most grab samples of base-metal-rich material contain 10 to 100 ppm Ag. The highest silver concentrations, consistently ranging from 500 to 1,000 ppm, characterize samples from the Columbia Red Metals and Wells Bay Copper prospects. Most occurrences are notably gold-poor, with concentrations below the 0.05 ppm lower determination limit of chemical analysis. Sulfide-rich material, however, from "the Knot", Idle, Columbia Red Metals, and Wells Bay Copper occurrences contain 0.1 to 0.6 ppm Au. The Byers occurrence on Fairmont Island is notably anomalous in gold and mercury, especially relative to the other polymetallic occurrences, with grab samples of a sphalerite-rich vein containing as much as 4.4 ppm Au and 30 ppm Hg. Tellurium enrichments are common in occurrences near Long Bay; grab samples from Long Bay #1 contain 11 to 14 ppm Te and those from the Globe prospect contain 2.9 to 4.9 ppm Te. Other common trace element enrichments in the occurrences include Bi (10 to 150 ppm), Hg (0.4 to 1 ppm), Cd (20 to greater than 500 ppm), Sb (4 to 160 ppm), and Sn (20 to 30 ppm). The sandstone-hosted Wells Bay #1 occurrence consists of a quartz-fluorite vein with minor pyrite and hematite. Chemical analysis of two samples indicates about 15 percent F.

ISOTOPIC ANALYSES

Oxygen and hydrogen isotope studies were carried out to help identify possible sources for the hydrothermal fluids responsible for the ore formation. Sulfide-bearing quartz from 14 occurrences was separated and analyzed for $\delta^{18}O$. In addition, $\delta^{18}O$ was determined for calcite intergrown with the quartz at the 4-in-1 and Byers occurrences. A number of barren quartz veins were also analyzed for $\delta^{18}O$. Coarse-grained, hydrogen-bearing, hydrothermal minerals are not characteristic of the mineral occurrences. Therefore, hydrogen isotope analyses could only be conducted on thermally extracted fluid inclusion waters. Pickthorn and others (1987) discuss the problems that may arise using such an approach, which incorporates fluids from multiple generations of inclusions. Sulfide minerals were separated from many of the occurrences in an attempt to determine the sulfur sources by measurement of $\delta^{34}S$. Also, sulfides from the Blackjack and Miners River #2 prospects were analyzed for Pb isotopes to aid in the identification of the metal sources.

Oxygen for isotopic analysis was liberated by reaction of quartz with bromine pentafluoride in nickel bombs at 580°C as described by Clayton and Mayeda (1963). Calcite samples were reacted at 25°C with 100% phosphoric acid following a procedure developed by McCrea (1950). The evolved carbon dioxide is separated from

water vapor and then analyzed for $\delta^{18}O$. For δD analysis of fluid inclusion waters, quartz samples were outgassed at 150°C, decrepitated by heating at 850°C for one hour, and then the released waters were converted to hydrogen gas by the method of Godfrey (1962). The $\delta^{34}S$ values of sulfide minerals were determined following oxidation to sulfur dioxide by combustion with vanadium pentoxide using a modification of a method by Yanagisawa and Sakai (1983). The reproducibility of each analysis is ±0.2 per mil for sulfur and oxygen and ±3.0 per mil for hydrogen. The values are expressed relative to V-SMOW (Vienna Standard Mean Ocean Water) and Canyon Diablo troilite. Oxygen and hydrogen analyses were carried out on a Finnigan MAT 252 mass spectrometer; sulfur analyses were performed on a modified Nuclide 6-60 RMS. Results from the stable isotope analyses are included in table 1. Lead isotope measurements were determined using the methods described in Gaccetta and Church (1989). Results are discussed below. The Pb isotope measurements are reproducible to within ±0.1%.

OXYGEN AND HYDROGEN ISOTOPES

The $\delta^{18}O$ values for the base-metal-rich quartz range between 7.5 per mil and 14.5 per mil. There is apparently no variation in composition with host rock-type, as the isotopically lightest and heaviest values are both for vein quartz in sedimentary rocks of the Orca Group. Intermediate $\delta^{18}O_{quartz}$ values characterize greenstone-hosted occurrences at Long Bay #1 and felsic pluton-hosted occurrences at Blackjack and Terentiev Lake. Barren quartz veins within sedimentary rocks have $\delta^{18}O_{quartz}$ values ranging between 5.2 per mil and 13.6 per mil. These data suggest that much of the barren quartz is of similar origin to the base-metal-rich quartz.

Calcite is intergrown with quartz gangue at the 4-in-1 and Byers occurrences. Using the experimental equation presented by Kyser (1987) for quartz-calcite fractionation and assuming the two oxygen-bearing phases to be in equilibrium, precipitation temperatures of 174°C and 190°C are estimated for the two occurrences, respectively. Such relatively low formation temperatures are in agreement with data from numerous other sources. Sulfide geothermometry, discussed below, also yields relatively low temperatures for metal deposition. Microscopic examination of fluid inclusions in quartz in doubly polished thin-sections from many of these occurrences indicates that vapor phases never exceed 1 to 2 volume percent of the inclusion. Homogenization temperatures for such inclusions are certainly less than 200°C, and given the low metamorphic grade of and absence of high-pressure indicators in rocks of the Orca Group, it is doubtful that significant corrections for pressure are required for determination of trapping temperatures. Also, the lack of high-temperature alteration phases, such as tourmaline and muscovite, even adjacent to the igneous rock-hosted occurrences, provides evidence that these were relatively low-temperature fluids at the time of mineral precipitation.

The range of $\delta^{18}O$ values for the epigenetic base-metal occurrences are significantly lighter than that of epigenetic gold-bearing quartz veins in south-central Alaska. Auriferous deposits, hypothesized to have been deposited by fluids of a metamorphic origin, show a range of $\delta^{18}O_{quartz}$ between 15.0 per mil and 16.5 per mil in the Port Wells district (30 km west of the study area) and between 13.9 per mil and 17.0 per mil in the Port Valdez district (30 km northeast of the study area) (Goldfarb and others, 1986). For such metamorphic fluids to have deposited the base-metal-bearing quartz, higher temperatures than the 250–300°C estimates for the gold deposits (Goldfarb and others, 1986) are required to account for the lighter $\delta^{18}O$ values. But, as discussed above, stable isotope geothermometry indicates that temperatures of base metal deposition were less than 200°C. Therefore, the base metal occurrences within the study area document the circulation of a largely non-metamorphic fluid. A genetically distinct type of fluid is also suggested by the lack of intense carbonate alteration that is diagnostic of the gold systems.

The experimentally-derived equation of Clayton and others (1972), applicable for temperatures as low as 200°C, was used to calculate $\delta^{18}O_{fluid}$ values in equilibrium with measured $\delta^{18}O$ for vein quartz. Assuming quartz precipitation at 200°C, $\delta^{18}O_{fluid}$ for the base-metal-transporting fluid ranged between –4.2 per mil and +2.8 per mil (fig. 2). Extrapolating the equation down to a possible precipitation temperature of 175°C, fluid values would

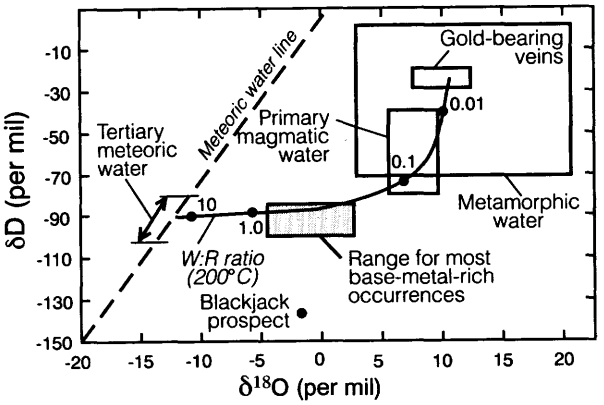

Figure 2. Plot of $\delta^{18}O$ vs. δD showing the estimated composition for the ore fluids. $\delta^{18}O_{fluid}$ calculated using measurements from quartz and a temperature of 200°C; δD determined for fluids released from thermal decrepitation of fluid inclusion in quartz. A meteoric-water-evolution path, calculated for Tertiary waters at 200°C, indicates water:rock (W:R) ratios required to reach estimated ore-fluid isotopic compositions. Calculations assume metasedimentary rocks to have an average $\delta^{18}O$ of +16 per mil and δD of –60 per mil.

have ranged between −5.9 per mil and +1.1 per mil. The range of 7 per mil for the fluid values can be interpreted to reflect temperature variations, mixing of different fluids, or variable interaction between isotopically light fluids with relatively heavy rocks. Major temperature variation is the least likely of the three possibilities because a spread of more than 100°C would be required to explain the spread in $\delta^{18}O$.

The calculated fluid values suggest that the ore-forming fluids contained a large meteoric component. If the fluids were largely of magmatic (+5.5 per mil to +9.5 per mil) or metamorphic (+4 per mil to +20 per mil) origin, $\delta^{18}O$ values would have been heavier than the calculated values of −4.2 per mil to +2.8 per mil. Tertiary meteoric waters in south-central Alaska had $\delta^{18}O$ values of about −13 per mil (Taylor, 1974). This is an additional indication that hydrothermal fluids predominantly of meteoric origin either variably mixed with ^{18}O-enriched water or reacted to variable degrees with isotopically heavier wall rocks. If wall rock exchange was predominant, then water:rock mass ratios (Field and Fifarek, 1985) would range between 0.1 and 1 for a fluid equilibrated with sedimentary rocks of the Orca Group (fig. 2).

The δD values for fluid inclusion waters from three occurrences ranged between −88 per mil and −100 per mil; that for the Blackjack prospect was −139 per mil. The three former values are consistent with meteoric water that was about −95 per mil in the Tertiary and −110 per mil today (Taylor, 1974). If reliable, these data suggest that water-rock interaction, rather than mixing of two fluids, is responsible for the oxygen isotope shift (fig. 2). Because crustal rocks are enriched in oxygen relative to hydrogen, such rocks will have a greater capacity for oxygen exchange than for hydrogen exchange with fluids. If mixing with magmatic or metamorphic fluids had occurred, then δD fluid inclusion water values significantly heavier than −95 per mil would be expected, and none were measured. However, as discussed by Pickthorn and others (1987), bulk extractions from fluid inclusions can contain waters from numerous events and not just from the main hydrothermal event that was responsible for deposition of the host mineral. Observations of fluid inclusions within the quartz samples that were used for δD analyses consistently indicate the presence of fluid inclusion with very small vapor:liquid ratios or no vapor phase at all. Thus, at least in this situation, bulk extraction of fluid inclusion waters may yield accurate estimates of the δD_{fluid}.

The anomalously light δD value for the Blackjack prospect is difficult to explain. Possibilities include some post-entrapment fractionation of the hydrogen in the fluid inclusions, or a spurious analysis. If, however, the value actually approximates a true, original-fluid composition, then the sources for such light hydrogen are very restricted. Waters modified by interaction with organic material are likely to be D-depleted relative to local meteoric water. Such a fluid could have been produced through contact metamorphism of any organic-bearing material in rocks of the Orca Group or by hydrogen isotope exchange between convecting meteoric water and organic hydrogen. Carbonized plant fragments that possibly could contribute to a high-organic content have been noted in parts of the study area (Lethcoe, 1990, p. 119). Glacial meltwater and snow melt also will be D-depleted relative to local rain water, and could contribute to the light value at the Blackjack prospect. However, most of the surface water throughout the study area is derived from snow melt and glacially-fed ground waters. It is thus hard to justify a more D-depleted ice and snow melt contribution to fluid δD solely at one location.

SULFUR ISOTOPES

Sulfur isotope data show a remarkable correlation with host rock type (fig. 3). Sulfide minerals from occurrences hosted by granitic rocks at Terentiev Lake and at the Blackjack prospect have a range of $\delta^{34}S$ that is generally between +4 per mil and +10 per mil. Those from occurrences hosted by sedimentary rocks are notably more depleted in ^{34}S, with $\delta^{34}S$ values of about 0 per mil to −6 per mil. These data could reflect two distinct sulfur sources. Alternatively, the variation in $\delta^{34}S$ compositions may be a function of kinetic effects associated with redox reactions as fluids reacted with different wall rocks.

The $\delta^{34}S$ values of 0 per mil to −6 per mil are interpreted to represent sulfur derived from sedimentary rocks of the Orca Group. Both the dissolution of pyrite and the decomposition of organic material are possible sources for

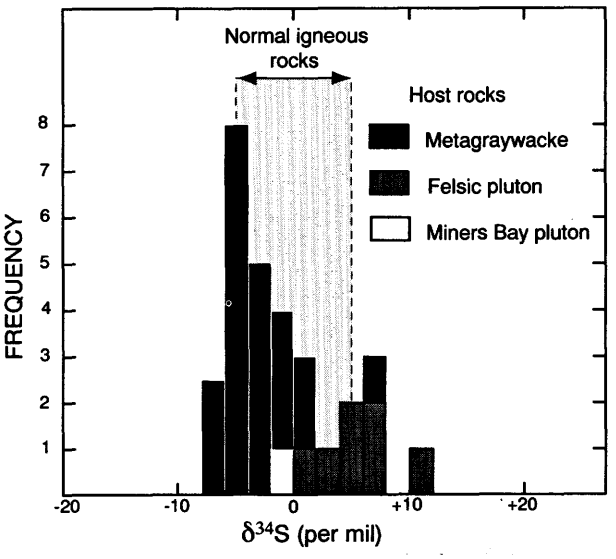

Figure 3. Distribution of sulfur isotope data from igneous and sedimentary rock-hosted base-metal-rich occurrences. Range for typical igneous rocks is also shown.

the sulfur. An overlapping range of +2.2 per mil to –2.3 per mil was determined for sulfide minerals in auriferous quartz veins hosted by rocks of the Valdez Group in the Port Valdez district (Pickthorn, 1982) and indicate a similar sedimentary rock source for the sulfur. Sulfur isotope data from deposits in the study area are significantly different from those for volcanogenic massive sulfide deposits hosted by sedimentary rocks of the Orca Group. The massive sulfides, with some sulfur contribution undoubtedly derived from isotopically heavy seawater sulfate, range between +2.7 per mil and +11.0 per mil in $\delta^{34}S$ (Pickthorn and Nelson, 1984; Crowe and others, 1992). It is, therefore, highly unlikely that the sedimentary rock-hosted base-metal-rich systems near Columbia Glacier are related to the massive sulfide deposits hosted by rocks of the Orca Group.

Values of $\delta^{34}S$ of about 0±5 per mil generally have been accepted as indicative of magmatic sulfur (Ohmoto, 1986). The $\delta^{34}S_{pyrrhotite}$ composition (–0.6 per mil) for a disseminated sulfide occurrence in mafic rocks of the Miners Bay pluton is certainly characteristic of magmatic sulfur. However, compositions of up to +10 per mil for granite-hosted sulfides in the study area are atypical of most magmatic sources.

One possible explanation for the heavy sulfur enrichments at the Blackjack prospect and Terentiev Lake is that sedimentary rock-derived sulfur reacted with the granites during hydrothermal activity. A ^{34}S enrichment would result if the fluids underwent a decrease in fO_2 or an increase in pH as the hydrothermal fluids interacted with the igneous rocks (Ohmoto and Rye, 1979). There is no reason to suspect significant redox shifts, but shifts to more alkaline pH values could have occurred when a fluid in equilibrium with sedimentary rocks reacted with the granitic bodies. The evidence for such a pH change includes clay formation in the wall rocks at the Blackjack prospect that reflects an exchange of H^+ ions in the fluid for base cations in the granite. But, it is doubtful that changes in pH could lead to such large changes in $\delta^{34}S_{fluid}$.

The more likely explanation for the high $\delta^{34}S$ values for sulfide minerals from igneous-hosted occurrences is that the granites themselves were anomalous in ^{34}S. A high fO_2 during magma fractionation could result in a shift to greater $\delta^{34}S$ within the magmatic fluid, and a very strong negative Eu anomaly for the granites (Steve Nelson, unpub. data) supports such a highly evolved fractionation episode. It is also possible that, unlike the 50-Ma granites from Prince William Sound (Barker and others, 1992), these granites do not represent simple melts of flysch. The relatively heavy sulfur data, if not solely a function of extreme magmatic fractionation, suggest a significant contribution of isotopically heavy, reduced seawater sulfate in the magmas. The melting of sulfide-bearing submarine basalts, such as those that crop out elsewhere in the Orca Group, would provide such a sulfur composition.

An additional ^{34}S-enriched sample was collected from the Wells Bay #1 occurrence. A pyrite separate was obtained from a quartz-calcite-fluorite vein hosted by slate of the Orca Group. The measured $\delta^{34}S$ value of +7.4 per mil is similar to those for sulfide minerals from the Blackjack and Terentiev Lake pluton-hosted occurrences, rather than the base-metal-rich occurrences hosted by sedimentary rocks. This suggests that the vein-forming fluids for Wells Bay #1 may have been in isotopic equilibrium with unexposed igneous rocks. Three felsic dikes crop out within 1 km of the occurrence, and it is therefore credible that more extensive bodies of the granite occur at shallow depths. The only fluorite observed in the study area occurs at the Wells Bay #1 occurrence. It probably was leached from an igneous rock body, and is therefore indicative of fluid-igneous rock interaction.

Galena-sphalerite or galena-pyrite pairs make the best sulfide geothermometers because of the relatively high temperature dependence of the isotopic fractionation factors. Unfortunately, where fine-grained galena was observed to be intergrown with other sulfide minerals in the Miners River #2, Columbia Red Metals, and Terentiev Lake occurrences, pure sulfide separates were unobtainable. Pyrite-chalcopyrite pairs often yield unreasonable temperature estimates due to complex and perhaps distinct mineral precipitation mechanisms (Ohmoto, 1986). Using the equation of Ohmoto and Rye (1979), co-existing chalcopyrite and pyrite yield a temperature of almost 500°C. Such an estimate is extremely unreasonable given much of the previous discussion favoring mineral precipitation at ≤200°C. Microscopically, pyrite and sphalerite appear to be coeval in sections from the Byers occurrence. A temperature of deposition of 144°C is calculated from these minerals using the relationship of Kajiwara and Krouse (1971) and measured $\delta^{34}S$ values of –2.1 per mil for pyrite and –3.6 per mil for sphalerite. This temperature is in general agreement with the 190°C value calculated from silicate geothermometry.

LEAD ISOTOPES

Lead isotope compositions were determined for two sulfide samples, one from the granite-hosted Blackjack prospect and the other from the sedimentary rock-hosted Miners River #2 prospect (Gray and others, 1986; Gaccetta and Church, 1989). The isotopic compositions of the samples vary within the limits of analytical uncertainty for $^{207}Pb/^{204}Pb$ (15.627–15.635) and $^{208}Pb/^{204}Pb$ (38.722–38.759). The $^{206}Pb/^{204}Pb$ values (19.060–19.096) differ by 0.2% and are slightly outside the limit of analytical uncertainty. We interpret this difference to reflect minor heterogeneities in the lead source areas.

The Pb isotope data for the base metal occurrences overlap with Pb isotope compositions measured by Farmer

and others (1993) for argillite and graywacke of both the Valdez and Orca Groups (fig. 4). These data are therefore permissive of lead in the base-metal-rich deposits having been derived from the sedimentary rocks. Isotopic compositions are also similar to those reported by Gray and others (1986) for gold-bearing quartz veins in the accreted terranes of south-central Alaska. This allows for the possibility that lead in both epigenetic deposit types was leached from the same crustal source. The Pb data are, however, significantly different than those from mafic volcanic rocks in the accretionary prism (Barker and others, 1992). This indicates little or no leaching of lead from the volcanic rocks during epigenetic hydrothermal events. Additionally, contribution of mantle lead is unlikely because such lead, like that in the volcanic rocks, will be significantly less radiogenic than that of the mineral occurrences.

Unfortunately, it is not possible to determine from the Pb isotope data whether the lead was actually derived from the sedimentary rocks or from the felsic igneous rocks. Isotopic data are not available for the igneous rocks from the study area and, without such data, it cannot be determined if the measured values are compatible with leaching of the igneous rocks. Barker and others (1992) present isotopic data for the Eocene granodiorites that intruded the accretionary prism and conclude that these plutonic bodies were largely derived from melted flysch. As a result, Pb isotopic compositions of some of the igneous rocks entirely overlap those of the sedimentary rocks of the Orca Group at 50 Ma (Barker and others, 1992). If future studies indicate a large sedimentary rock component also within the granitic rocks that are spatially associated with the base-metal-rich occurrences, then specific identification of the crustal lead source will remain unlikely.

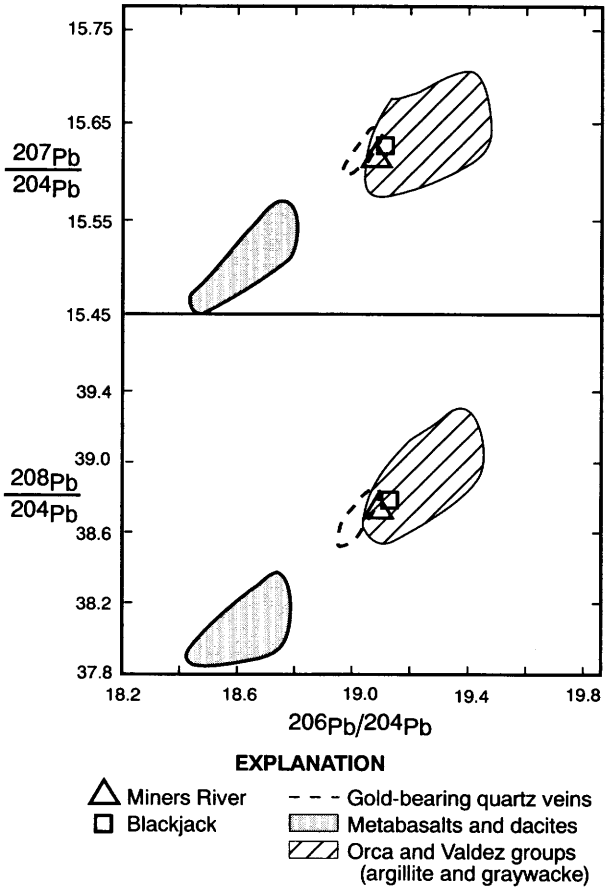

Figure 4. Plots of $^{206}Pb/^{204}Pb$ vs. $^{207}Pb/^{204}Pb$ and $^{206}Pb/^{204}Pb$ vs. $^{208}Pb/^{204}Pb$ for sulfide minerals from Miners River #2 and Blackjack prospects and sedimentary and volcanic rocks from the accretionary prism as defined in Farmer and others (1993). Field for sulfide minerals from gold-bearing quartz veins in accretionary prism from Gray and others (1986) is also shown.

DISCUSSION

Oxygen and hydrogen isotope data from the base-metal-rich occurrences indicate that the metals were transported by a fluid of largely meteoric origin. Lead isotope data are compatible with lead, and possibly other metals, being leached from the sedimentary rocks of the Orca Group, but felsic igneous source rocks cannot be excluded. Similarly, the sulfur isotope data are consistent with both sedimentary and igneous rocks providing sulfur to the hydrothermal fluids. During convection of the meteoric fluids, $\delta^{18}O$ values were shifted by reaction with wall rocks. Hence the lightest values at the Miners River #2, Wells Bay Copper, and Blackjack prospects likely identify the largest, or at least the most channelized, flow systems where exchange with isotopically heavy country rocks was minimized. Relatively ^{18}O-enriched fluids at the Columbia Red Metals, 4-in-1, and Byers occurrences suggest lower water:rock ratios and less extensive convection of the meteoric fluids.

The dominantly base-metal-rich nature of the hydrothermal systems is compatible with metal transport by chloride complexing. Whereas daughter minerals are not observed in fluid inclusions from any of the mineral occurrences, it is nevertheless likely, given the abundance of base metals, that at least moderate salinities characterize the ore fluids. The reason for the anomalous gold and mercury at the Byers occurrence is uncertain. Perhaps this reflects one area where bisulfide complexing was also significant within the hydrothermal cells.

The spatial association of the base-metal-rich occurrences and the felsic intrusive rocks favors fluid convection driven by igneous activity. The δD data, however, provide no evidence for magmatic water input into the hydrothermal fluids. Anomalous concentrations of Bi, F, Sn, and Te in some of the occurrences are suggestive of a magmatic-fluid phase, but based on the stable isotope data it is more probable that these elements were just enriched in the ore fluids by leaching of the igneous rocks. Deuteri-

um-depleted fluid inclusion waters from the Blackjack prospect support some of the hydrogen in the fluid being derived by breakdown of organic material. Such decomposition could have been initiated by heat from the magmatic episode.

The base-metal-bearing occurrences in northern Prince William Sound are the only recognized mineral deposit systems in the southern Alaskan accretionary prism in which meteoric fluids have conclusively been recognized as important components. To a great extent, this likely reflects the relatively limited amount of uplift and erosion of rocks of the Orca Group or a relatively shallow emplacement depth of the plutons in the study area, or both. Obviously, without geobarometry studies of the igneous rocks, emplacement depths cannot be estimated. Most of the exposed parts of the Orca Group, however, have only been metamorphosed to low grades and represent shallow parts of the accretionary prism. In such an environment, epigenetic mineral deposits developed within a few kilometers of the surface are likely to be preserved.

Higher grade metamorphosed rocks of the Valdez Group, uplifted from deeper crustal levels, are exposed farther landward within the southern Alaska fore-arc. Any mineral deposits that might have formed during shallow circulation of meteoric fluids would have been eroded during uplift of the Chugach and Kenai Mountains. The dominance of contractional and strike-slip tectonic regimes in this fore-arc region generally is not conducive to deep (>5–10 km) convection of meteoric fluid. Therefore, a crustal fluid source is more likely for hydrothermal ore deposits formed in these rocks of largely greenschist facies.

Acknowledgments.—This area is currently being evaluated by the U.S. Geological Survey for the Chugach National Forest as part of their forest management plan. The U.S.G.S. appreciates the financial support for these studies by the Chugach National Forest.

REFERENCES CITED

Barker, F., Farmer, G.L., Ayuso, R.A., Plafker, G., and Lull, J.S., 1992, The 50 Ma granodiorite of the eastern Gulf of Alaska—Melting in an accretionary prism in the forearc: Journal of Geophysical Research, v. 97, p. 6757–6778.

Clayton, R.N., and Mayeda, T.K., 1963, The use of bromine pentafluoride in the extraction of oxygen from oxides and silicates for isotopic analysis: Geochimica et Cosmochimica Acta, v. 27, p. 43–52.

Clayton, R.N., O'Neil, J.R., and Mayeda, T.K., 1972, Oxygen isotope fractionation between quartz and water: Journal of Geophysical Research, v. 77, p. 3057–3067.

Crowe, D.E., Nelson, S.W., Shanks, W.C., Brown, P.E., and Valley, J.W., 1992, Geology and geochemistry of volcanogenic massive sulfide deposits, Prince William Sound district, south-central Alaska: Economic Geology, v. 87, p. 1722–1746.

Farmer, G.L., Ayuso, R., and Plafker, G., 1993, A Coast Mountains provenance for the Valdez and Orca groups, southern Alaska, based on Nd, Sr, and Pb isotopic evidence: Earth and Planetary Science Letters, v. 116, p. 9–21.

Field, C.W., and Fifarek, R.H., 1985, Light stable-isotope systematics in the epithermal environment, *in* Berger, B.R., and Bethke, P.M., eds., Geology and geochemistry of epithermal systems: Society of Economic Geologists, Reviews in Economic Geology, v. 2, p. 99–128.

Gaccetta, J.D., and Church, S.E., 1989, Lead isotope data base for sulfide occurrences from Alaska, December, 1989: U.S. Geological Survey Open-File Report 89-688, 59 p.

Godfrey, J.D., 1962, The deuterium content of hydrous minerals from the east-central Sierra Nevada and Yosemite National Park: Geochimica et Cosmochimica Acta., v. 26, p. 1215–1245.

Goldfarb, R.J., Leach, D.L., Miller, M.L., and Pickthorn, W.J., 1986, Geology, metamorphic setting and genetic constraints of epigenetic lode-gold mineralization within the Cretaceous Valdez Group, south-central Alaska, *in* Keppie, J.D., Boyle, R.W., and Haynes, S.J., eds., Turbidite-hosted gold deposits: Geological Association of Canada Special Paper 32, p. 87–105.

Goldfarb, R.J., Snee, L.W., and Pickthorn, W.J., 1993, Orogenesis, high-T thermal events, and gold vein formation within metamorphic rocks of the Alaskan Cordillera: Mineralogical Magazine, v. 57, p. 375–394.

Gray, J.D., Church, S.E., and Delevaux, M.H., 1986, Lead-isotope results from gold-bearing quartz veins from the Valdez and Orca Groups, Chugach National Forest, *in* Bartsch-Winkler, Susan, and Reed, K.M., eds., The U.S. Geological Survey in Alaska—Accomplishments during 1985: U.S. Geological Survey Circular 978, p. 45–49.

Haeussler, P.J., and Nelson, S.W., 1993, Structural evolution of the Chugach-Prince William terrane at the hinge of the orocline in Prince William Sound, and implications for ore deposits, *in* Dusel-Bacon, Cynthia, and Till, A.B., eds., Geologic studies in Alaska by the U.S. Geological Survey, 1992: U.S. Geological Survey Bulletin 2068, p. 143–162.

Hudson, Travis, 1979, Calc-alkaline plutonism along the Pacific rim of southern Alaska: U.S. Geological Survey Open-File Report 79-953, 30 p.

Jansons, Uldis, Hoekzema, R.B., Kurtak, J.M., and Fechner, S.A., 1984, Mineral occurrences in the Chugach National Forest, south-central Alaska: U.S. Bureau of Mines Mineral Land Assessment Report 5-84, 43 p., 2 map sheets.

Kajiwara, Y., and Krouse, H.R., 1971, Sulfur isotope partitioning in metallic sulfide systems: Canadian Journal of Earth Sciences, v. 8, p. 1397–1408.

Kyser, T.K., 1987, Equilibrium fractionation factors for stable isotopes, *in* Kyser, T.K., ed., Short course in stable isotope geochemistry of low temperature fluids: Mineralogical Association of Canada Short Course Handbook, v. 13, p. 1–84.

Lanphere, M.A., 1966, Potassium-argon ages of Tertiary plutons in the Prince William Sound region, Alaska: U.S. Geological Survey Professional Paper 550–D, p. D195– D198.

Lethcoe, J., 1990, An observer's guide to the geology of Prince William Sound, Alaska: Prince William Sound Books, Valdez, Alaska, 224 p.

McCrea, J.M., 1950, On the isotopic chemistry of carbonates and a paleotemperature scale: Journal of Chemical Physics, v. 18, p. 848–857.

Nelson, S.W., Dumoulin, J.A., and Miller, M.L., 1985, Geologic map of the Chugach National Forest, Alaska: U.S. Geological Survey Miscellaneous Field Studies Map MF–1645–B, 18 p., 1 sheet, scale 1:250,000.

Nelson, S.W., Miller, M.L., Barnes, D.F., Dumoulin, J.A., Goldfarb, R.J., Koski, R.A., Mull, C.G., Pickthorn, W.J., Jansons, Uldis, Hoekzema, R.B., Kurtak, J.M., and Fechner, S.A., 1984, Mineral resource potential map of the Chugach National Forest, Alaska: U.S. Geological Survey Miscellaneous Field Studies Map MF–1645–A, scale 1:250,000.

Ohmoto, H., 1986, Stable isotope geochemistry of ore deposits, *in* Valley, J.W., Taylor, H.P., Jr., and O'Neil, J.R., eds., Stable isotopes in high temperature geologic processes: Mineralogical Society of America, Reviews in Mineralogy, v. 16, p. 491–555.

Ohmoto, H., and Rye, R.O., 1979, Isotopes of sulfur and carbon, *in* Barnes, H.L., ed., Geochemistry of hydrothermal ore deposits, 2nd edition: John Wiley and Sons, New York, p. 509–567.

Pickthorn, W.J., 1982, Stable isotope and fluid inclusion study of the Port Valdez district, southern Alaska: University of California at Los Angeles, M.S. thesis, 66 p.

Pickthorn, W.J., Goldfarb, R.J., and Leach, D.L., 1987, Comment on "Dual origin of lode gold deposits in the Canadian Cordillera": Geology, v. 15, p. 471–472.

Pickthorn, W.J., and Nelson, S.W., 1984, Preliminary reconnaissance sulfur isotope study of massive sulfide occurrences in the Prince William Sound district, *in* Reed, K.M., and Bartsch-Winkler, Susan, eds., The United States Geological Survey in Alaska—Accomplishments during 1982: U.S. Geological Survey Circular 939, p. 70–71.

Plafker, George, Jones, D.L., and Pessagno, E.A., Jr., 1977, A Cretaceous accretionary flysch along the Gulf of Alaska margin, *in* Blean, K.M., ed., U.S. Geological Survey in Alaska—Accomplishments during 1976: U.S. Geological Survey Circular 751–B, p. B41–B43.

Plafker, George, Nokleberg, W.J., and Lull, J.S., 1989, Bedrock geology and tectonic evolution of the Wrangellia, Peninsular, and Chugach terranes along the Trans-Alaska Crustal Transect in the Chugach Mountains and southern Copper River Basin, Alaska: Journal of Geophysical Research, v. 94, no. B4, p. 4255–4295.

Taylor, H.P., Jr., 1974, The application of oxygen and hydrogen isotope studies to problems of hydrothermal alteration and ore deposition: Economic Geology, v. 69, p. 843–883.

Tysdal, R.G., and Case, J.E., 1979, Geologic map of the Seward and Blying Sound quadrangles, Alaska: U.S. Geological Survey Miscellaneous Field Studies Map I–1150, 12 p., 1 sheet, scale 1:250,000.

Winkler, G.R., 1992, Geologic map and summary geochronology of the Anchorage 1°×3° quadrangle, southern Alaska: U.S. Geological Survey Miscellaneous Investigations Map I–2283, 1 sheet, scale 1:250,000.

Winkler, G.R., and Plafker, G., 1981, Geologic map and cross sections of the Cordova and Middleton Island quadrangles, southern Alaska: U.S. Geological Survey Open-File Report 81-1164, scale 1:250,000.

Yanagisawa, F., and Sakai, H., 1983, Thermal decomposition of barium sulfate-vanadium accretionary-silica glass mixtures for preparation of sulfur dioxide in sulfur isotope ratio measurements: Analytical Chemistry, v. 55, p. 985–987.

Reviewers: Wayne Shanks and Cliff Taylor

Gold in Heavy-Mineral-Concentrate Samples from the Howard Pass Quadrangle, Brooks Range, Alaska

By K.D. Kelley, E.A. Bailey, B.A. Cieutat,[1] *and* J.C. Borden

ABSTRACT

A reconnaissance geochemical survey was conducted in the Howard Pass quadrangle in the central Brooks Range as part of the Alaska Mineral Resource Assessment Program (AMRAP). Twelve heavy-mineral-concentrate samples were found to contain visible gold; three additional samples contained anomalous concentrations of gold (30 to more than 1,000 ppm). The presence of gold-bearing samples is of interest because of the general lack of gold deposits in this part of the Brooks Range.

In the southwestern part of the quadrangle, concentrate samples containing anomalous gold are spatially associated with Upper Devonian and Lower Mississippian(?) clastic sedimentary rocks. These sedimentary rocks are host to several Ag-Pb-Zn vein-breccia mineral occurrences in the Howard Pass and adjacent quadrangles. Mineralized rocks from some of these vein-breccias yield anomalous concentrations of gold. The gold-bearing concentrate samples were collected near, but not directly downstream from, two vein-breccia occurrences. The geochemical data indicate the potential for the presence of additional Ag-Pb-Zn vein-breccia mineral occurrences in this area.

Most of the gold-bearing concentrate samples from the Howard Pass quadrangle were collected in the foothills north of the mountains in the central and northern parts of the quadrangle. Cretaceous sedimentary rocks are exposed in this area, but much of it is covered by Quaternary surficial deposits. The geochemistry of these gold-bearing samples indicates a different source than that postulated for the gold-bearing samples in the southwestern part of the quadrangle. Anomalous concentrations of Sn and W in these samples indirectly suggest the presence of scheelite and cassiterite, and a possible felsic igneous source. Gold-bearing quartz vein and placer deposits that are spatially associated with Devonian granitic rocks are located in the metamorphic belt of rocks south of the Howard Pass quadrangle. Geologic, geochemical, and mineralogical data suggest that these gold deposits may be the source of the gold (and cassiterite and scheelite?) in sediment samples collected from the foothills area.

INTRODUCTION

The Howard Pass quadrangle is located in the central Brooks Range of northern Alaska (fig. 1). Reconnaissance geochemical studies were conducted in the quadrangle as part of the Alaska Mineral Resource Assessment Program (AMRAP). The overall objectives of the studies were to define geochemical variations within the quadrangle and to provide geochemical data for use in delineating favorable areas for hosting mineral deposits.

As part of the reconnaissance geochemical studies, panned concentrate samples were obtained by panning bulk stream-sediment samples. After panning, each sample was examined in the field with a hand lens. Twelve samples were found to contain visible gold. Subsequent chemical analysis in the laboratory indicated that three additional samples contain anomalous concentrations of gold. The presence of gold in concentrate samples from the Howard Pass quadrangle is of interest because of the general lack of gold deposits in this part of the Brooks Range. This paper presents the locations and the results of chemical analyses of the Au-bearing concentrate samples and discusses possible sources for these unusual occurrences in the region.

PHYSIOGRAPHIC AND GEOLOGIC SETTING

The Howard Pass quadrangle is located in the central part of the Brooks Range and Arctic Foothills physiographic provinces (Wahrhaftig, 1965), along the northern flank and foothills of the Endicott Mountains (fig. 1). Topography varies from moderately steep in the southern part of the

[1]Present address: ERM-Southwest Inc., 3501 N. Causeway Blvd., Suite 200, Metairie, Louisiana 70002.

quadrangle to nearly flat with some low rolling hills and broad open valleys in the northern part of the quadrangle.

The quadrangle lies within the Brooks Range fold and thrust belt, which spans northern Alaska from west to east. Deformation in the western and central parts of the orogen was north directed and apparently occurred in Late Jurassic to Late Cretaceous time (Mayfield and others, 1988). The metamorphic core of the Brooks Range (fig. 1) is composed of Proterozoic and Paleozoic continental-margin sedimentary and igneous rocks that were metamorphosed to blueschist facies during the orogenic episode (Mull, 1982; Till, 1992). North of the metamorphic core is a belt of intensively thrust-faulted middle Paleozoic to Lower Cretaceous sedimentary rocks; allochthons of Late Jurassic ultramafic and middle Paleozoic to Triassic mafic rocks sit above these thrust sheets (Mayfield and others, 1988). Rocks of the foreland basin are exposed in the foothills north of the mountains. These rocks are predominantly siliciclastic rocks of Early Cretaceous to Tertiary age that were derived from the Brooks Range and prograded northward and eastward (Mull, 1982).

Only Devonian through Cretaceous sedimentary rocks and lesser mafic and ultramafic igneous rocks of Mississippian(?) through Jurassic age are exposed in the Howard Pass quadrangle. These rocks have been involved in large-scale thrust faulting which have obscured their original stratigraphic relations. They are overlain by Upper Tertiary and Quaternary glacial and alluvial sedimentary deposits.

MINERAL DEPOSITS

The Brooks Range hosts a number of different deposit types, most of which are base metal deposits hosted by sedimentary and volcanic rocks of Devonian to Mississippian age. The only known gold deposits in the region are found in the regionally metamorphosed rocks in the core of the Brooks Range (fig. 1). The most significant of these are the placer gold and auriferous vein deposits of the Chandalar and Upper Koyukuk districts, which have yielded at least 320,000 oz of gold (Dillon and others, 1989). Gold-bearing quartz veins are also reportedly found in the Cosmos Hills of the Ambler district (Cobb, 1975; Einaudi and Hitzman, 1986), and gold has been recovered from small placer operations in the Klery Creek-Timber Creek area in the Baird Mountains (Cobb, 1975). The veins in the Chandalar-Koyukuk region occur within high-angle shear zones that clearly developed subsequent to regional metamorphism of the host pelitic sedimentary rocks. Dillon and others (1989) suggest that the gold was originally deposited by magmatic processes in cupolas of Devonian granites and remobilized into host structures by metamorphic fluids. Rose and others (1988) suggest that the gold-bearing fluids were derived by devolatization of pelitic sedimentary deposits.

The deposit types known in the Howard Pass quadrangle are listed in table 1 and shown in figure 2. They can be

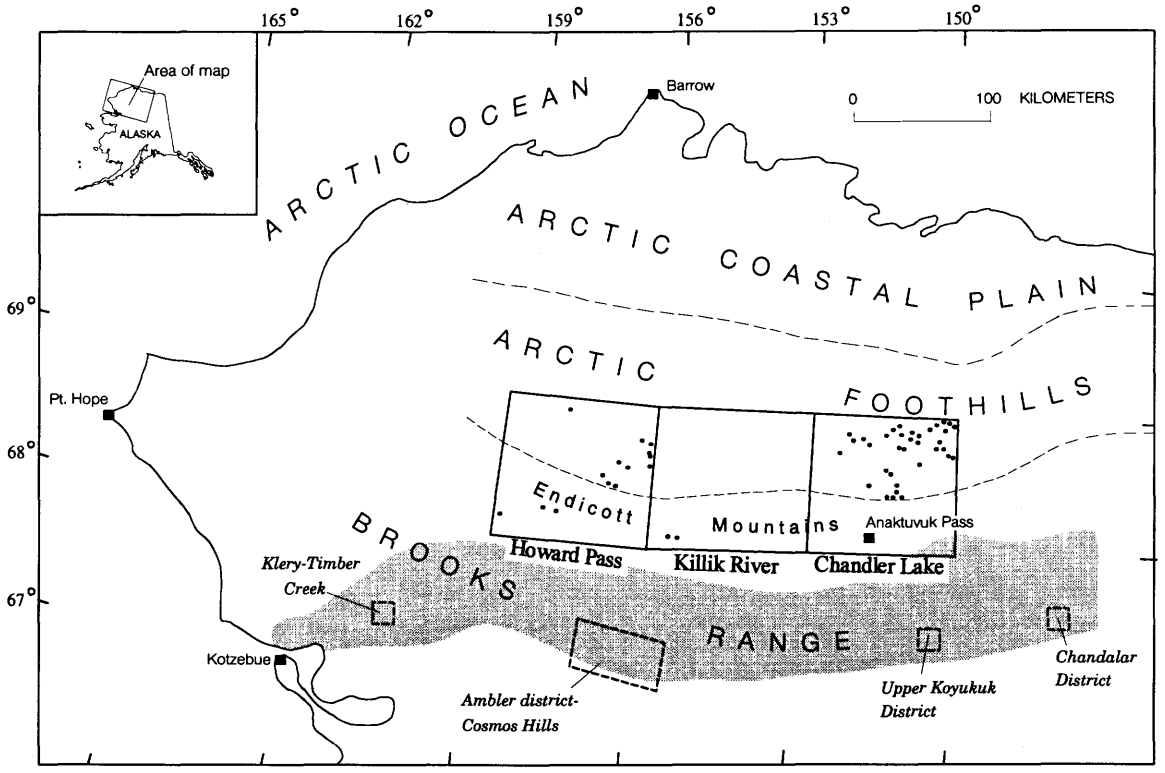

Figure 1. Location of Howard Pass quadrangle. Solid circles show locations of gold-bearing stream sediment or nonmagnetic heavy-mineral-concentrate samples. Shaded area shows location of metamorphic core of the Brooks Range (from Till, 1992).

Table 1. Mineral occurrences in the Howard Pass quadrangle.

[Numbers in parentheses following mineral occurrence or deposit names refer to figure 2]

Deposit type	Age	Host rock type/host rock unit (if known)	Name	References
Sedimentary exhalative Ag-Pb-Zn massive sulfide.	Mississippian and Pennsylvanian.	Black chert/Kuna Fm. or its stratigraphic equivalent.	Drenchwater Creek (1)	Jansons (1982), Nokleberg and Winkler (1982), Lange and others (1985), Lange and Nokleberg (1987), Young and Moore (1987).
Banded Ag-Pb-Zn vein-breccias.	Devonian and Mississippian.	Siltstone, sandstone, or conglomerate/Hunt Fork Shale, Kanayut Conglomerate, or Kayak Shale.	Story Creek (2)	Ellersieck and others (1982), Jansons (1982).
			Whoopee Creek (3)	Ellersieck and others (1982), Jansons (1982).
			Kivliktort Mountain (4)	Jansons and Parke (1981), Jansons (1982).
			Koiyoktot Mountain (5)	Jansons and Parke (1981).
			Safari Creek (6)	Meyer and others (1993).
			Unnamed (7)	Unpublished data (K.D. Kelley).
			Ipnavik River (8)	Unpublished data (K.D. Kelley).
Sulfide-bearing concretions (Ag-Pb-Zn).	Mississippian	Shale/Kayak Shale	Unnamed (9)	Unpublished data (K.D. Kelley).
Massive barite lenses	Mississippian and Pennsylvanian.	Chert, limestone, or shale	Abby Creek (10), Bion (11), Tuck (12), Stack (13), Lakeview (14), Longview (15), Ekakevik (16).	Kelley and others (1993).
Barite nodules and discontinuous veins and lenses.	Permian to Jurassic	Gray and green chert, siltstone, mudstone/Siksikpuk(?) Formation.	Rolling Pin Creek (17)	Jansons and Baggs (1980).
			Zhar (18)	Unpublished data (K.D. Kelley).
Podiform chromite	Mississippian(?) to Jurassic.	Mafic-ultramafic igneous rocks	Siniktanneyak Mtn (19)	Jansons and Baggs (1980), Nelson and Nelson (1982), Foley and others (1986).

categorized into six base metal, barite, and chromite deposit types. There are no known gold occurrences or deposits within the quadrangle. However, some of the chromite deposits and (or) base metal deposits have been found to contain anomalously high concentrations of Au. For instance, some Cr-rich samples of dunite from the mafic-ultramafic complex at Siniktanneyak Mountain (No. 19, table 1; fig. 2) contain anomalous concentrations of Au (J.Y. Foley, oral commun., 1991), and anomalous gold (up to 336 parts per billion) was detected in two stream-sediment samples from that area (J.Y. Foley, written communication, 1991). In addition, sphalerite- and galena-rich quartz vein samples from two vein-breccia occurrences (Nos. 2 and 7, table 1; fig. 2) contain detectable Au (0.05 to 0.15 ppm). Similar vein-breccia occurrences outside the Howard Pass quadrangle also commonly yield anomalous concentrations of Au; quartz veins and breccias

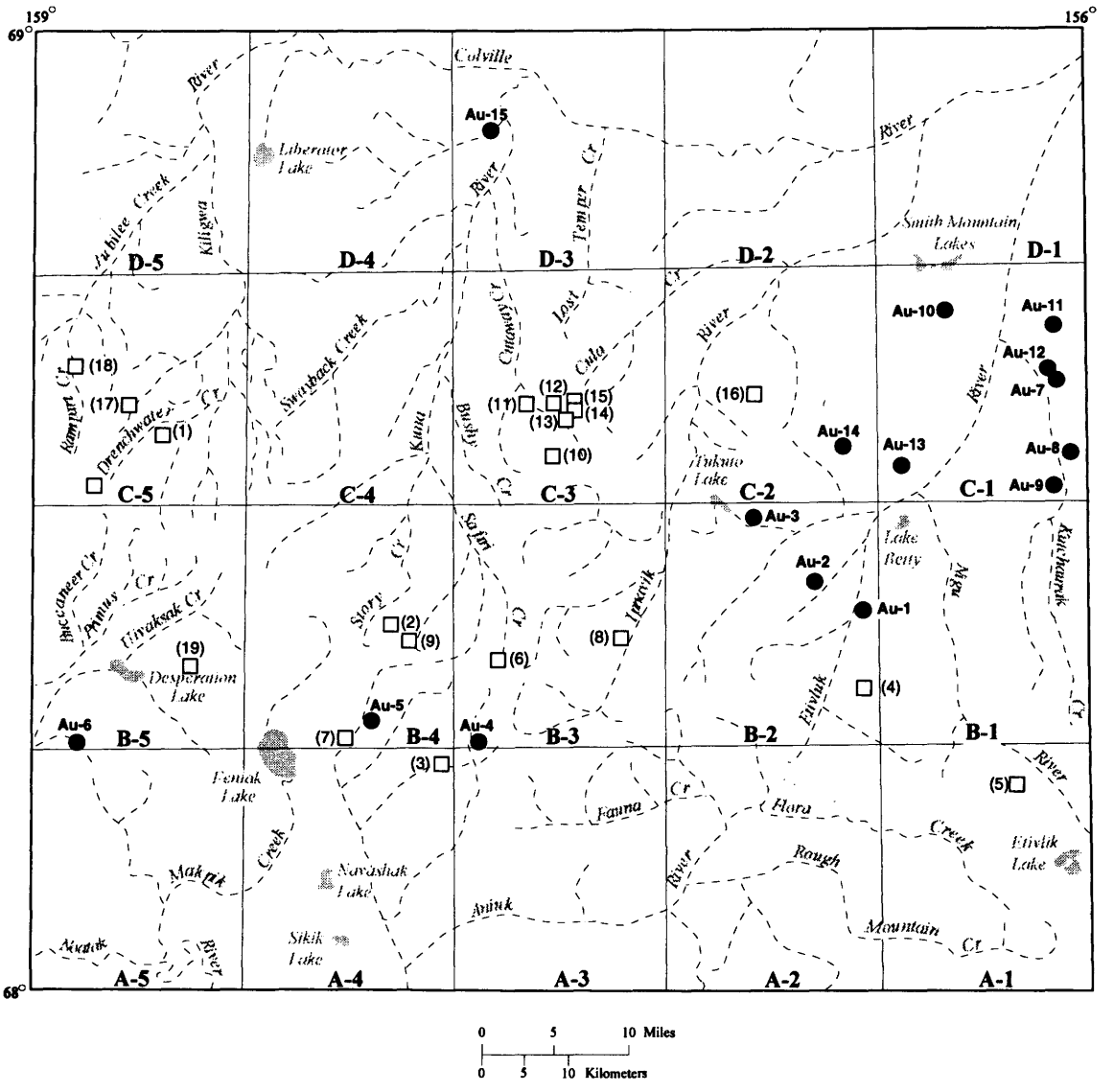

EXPLANATION

□ (2) Mineral occurrence or deposit; number in parentheses refers to table 1

● Au-4 Heavy-mineral concentrate sample containing visible gold or anomalous concentrations of gold; number refers to table 2

Figure 2. Howard Pass quadrangle showing locations of known mineral occurrences and deposits and heavy-mineral-concentrate samples containing visible gold or anomalous concentrations of gold.

Table 2. Geochemical data for gold-bearing heavy-mineral-concentrate samples.

[Sample number refers to figure 2; all analyses by semiquantitative emission spectrography; values in parts per million (ppm); N, not detected at the lower detection limit shown in parentheses; <, less than the lower detection limit; >, greater than the upper detection limit]

Sample No.	Field No.	Quadrangle	Ag	Au	Cd	Pb	Sn	W	Zn
Au-1	2HP864C	B-2	5	N(20)	N(50)	<20	200	N(50)	N(500)
Au-2	2HP866C	B-2	N(1)	N(20)	N(50)	20	300	200	N(500)
Au-3	2HP868C	B-2	N(1)	N(20)	N(50)	<20	300	100	N(500)
Au-4	2HP562C	B-3	200	>1,000	<50	5000	<20	70	1,000
Au-5	2HP614C	B-4	<1	50	N(50)	<20	N(20)	150	3,000
Au-6	2HP506C	B-5	N(1)	30	N(50)	N(20)	N(20)	N(50)	N(500)
Au-7	2HP659C	C-1	N(1)	N(20)	N(50)	20	N(20)	N(50)	N(500)
Au-8	2HP662C	C-1	N(1)	N(20)	N(50)	20	N(20)	N(50)	700
Au-9	2HP663C	C-1	N(1)	N(20)	N(50)	<20	70	N(50)	N(500)
Au-10	2HP667C	C-1	N(1)	N(20)	N(50)	70	N(20)	N(50)	N(500)
Au-11	2HP883C	C-1	N(1)	N(20)	N(50)	N(20)	N(20)	N(50)	N(500)
Au-12	2HP884C	C-1	N(1)	N(20)	<50	30	200	N(50)	500
Au-13	2HP896C	C-1	N(1)	N(20)	N(50)	N(20)	>2,000	500	500
Au-14	2HP673C	C-2	N(1)	N(20)	N(50)	200	300	<50	700
Au-15	2HP957C	D-3	3	N(20)	<50	N(20)	N(20)	N(50)	7,000

containing abundant pyrite, sphalerite, and galena from the Kady vein-breccia occurrence in the southwestern part of the Killik River quadrangle contain 0.05 to 0.20 ppm Au, and those from the Vidlee occurrence contain 0.05 to 0.75 ppm Au (Duttweiler, 1987; Kelley and others, 1994).

METHODS

A total of 761 concentrate samples were collected in the Howard Pass quadrangle during the 1990 through 1992 field seasons. Sample sites were selected on first- and second-order drainages as shown on 1:63,360-scale topographic maps. At most sites, sediment was composited from several locations along approximately 8 m (25 ft) of active alluvium. Each bulk sample was passed through a 2.0-mm (10-mesh) screen to remove coarse material. The sediment passing through the screen was panned using a standard 14-in gold pan to remove most of the quartz, feldspar, organic material, and clays. The resulting panned concentrate sample was examined in the field to determine the minerals easily identifiable by hand lens.

In the laboratory, each panned concentrate was air-dried and the strongly magnetic minerals were removed with a hand magnet. Any remaining material of low specific gravity (such as quartz and feldspar) was removed using a heavy-liquid (bromoform, 2.8 specific gravity) separation technique. The resulting heavy-mineral fraction was then separated into nonmagnetic and magnetic fractions. The nonmagnetic fraction obtained was split into two fractions: one split was stored for future mineralogical analysis and the other was submitted for chemical analysis. Each nonmagnetic heavy-mineral-concentrate sample was analyzed for 31 elements using a direct-current arc emission spectrographic method (Grimes and Marranzino, 1968).

RESULTS

The locations of gold-bearing concentrate samples are shown on figure 2, and selected analytical data for these samples are listed in table 2. Twelve panned concentrate samples contained visible gold (samples Au-1 through Au-3 and Au-7 through Au-15; fig. 2). Three additional nonmagnetic heavy-mineral-concentrate samples (Au-4 through Au-6) contained anomalous concentrations of Au (30 to more than 1,000 parts per million [ppm]). Most of the gold observed in the panned concentrates consisted of shiny, flat flakes that did not appear to be etched or rounded. With the exception of one sample (Au-13), which contained 3 large flakes, all samples contained only 1 to 2 flakes of gold.

None of the twelve concentrate samples that contained visible gold were found to have detectable Au when analyzed by emission spectrography (lower determination limit of 20 ppm). This could be partly due to the relatively high detection limit for gold by this method (for instance, 1 or 2 small flakes of gold may result in concentrations of less than 20 ppm). It may also be due to the loss of gold during the laboratory magnetic, heavy liquid, and splitting procedures. The relatively fine gold flakes could have been caught up with the magnetic grains or held up in the light material in the heavy liquid separation. Also, some gold grains may have been preferentially split into the fractions for mineralogical study. For example, if only 1 or 2 flakes of gold are in the nonmagnetic heavy-mineral-concentrate sample prior to splitting, it is possible that the flakes could be incorporated into the mineralogical split rather than the split used for chemical analysis. These factors illustrate the particulate nature of gold and the common difficulty of repeating Au analyses. Clearly, it is important to conduct field examinations of panned concentrate samples and

subsequent mineralogical studies of nonmagnetic heavy-mineral-concentrate samples. Mineralogical studies are currently underway, and therefore, the distribution of gold-bearing samples shown on figure 2 may not be entirely complete; there may be additional gold in mineralogical splits from samples that did not yield gold by field or chemical methods.

The Au-bearing concentrate samples are distributed primarily in the east-central part of the Howard Pass quadrangle, but there are a few samples located in the southwestern and one in the northern part of the quadrangle (fig. 2). The three samples that were collected from the southwestern part of the quadrangle (Au-4 through Au-6) contain analytical gold. Two of these gold-bearing samples (Au-4 and Au-5) were collected from streams underlain primarily by Upper Devonian and Lower Mississippian(?) clastic sedimentary rocks, including the Hunt Fork Shale and Kanayut Conglomerate (C.G. Mull, unpublished mapping, 1992). They are near, but not directly downstream from, Ag-Pb-Zn vein-breccia occurrences (Nos. 3 and 7; fig. 2). In the southwestern part of the adjacent Killik River quadrangle, two stream-sediment samples that were collected in the vicinity of a vein-breccia occurrence also yielded anomalous (0.05 to 0.1 ppm) gold (fig. 1; Kelley and others, 1994). Since mineralized rocks from this type of occurrence have been found to contain anomalous concentrations of gold, it is likely that the source of the gold in concentrate samples Au-4 and Au-5 may be additional Ag-Pb-Zn vein-breccia occurrences in this area. Geochemical data for these samples support this conclusion; they contain anomalous concentrations of Ag, Pb, and Zn in addition to Au (table 2), which suggests the presence of sulfide minerals such as galena and sphalerite. Furthermore, the presence of analytical gold, but not visible gold, suggests that the source of gold in these samples may be gold-bearing sulfide minerals.

Most of the gold-bearing concentrate samples from the Howard Pass quadrangle were collected in the foothills north of the mountains (fig. 1), from the tributaries of the Etivluk River and Kutchaurak Creek in the C-1, C-2, and B-2 quadrangles (fig. 2). All of these samples contained visible, but not analytical, gold. Cretaceous sedimentary rocks and a few small exposures of Upper Paleozoic sedimentary rocks, as well as some minor mafic igneous rock bodies, are the primary rock units exposed in this area. However, much of the area is covered by Quaternary surficial deposits (C.G. Mull, unpublished mapping, 1992). Similar lithologies characterize the central and northern parts of the adjacent Killik River and Chandler Lake quadrangles. Although gold was not found (either visually or analytically) in stream-sediment or nonmagnetic heavy-mineral-concentrate samples from the foothills of the Killik River quadrangle (Kelley and others, 1994; Kelley and Mull, 1994), 35 gold-bearing (0.05 to 2.4 ppm) sediment samples and 1 concentrate sample containing anomalous gold (20 ppm) were collected from the northern part of the Chandler Lake quadrangle (fig. 1) (Kelley and Sutley, 1993). As in the Howard Pass quadrangle, most of these gold-bearing sediment samples are spatially associated with Cretaceous sedimentary rocks or Quaternary surficial deposits.

The source of the gold in concentrate samples collected from the foothills is not easily explained. Anomalous concentrations of Sn and W in many of these samples (table 2) and the general lack of anomalous concentrations of base metals indicate a different source than that postulated for the gold-bearing samples in the southwestern part of the quadrangle. The anomalous concentrations of Sn and W indirectly suggest the presence of cassiterite and scheelite, respectively, and a possible felsic igneous source.

The close spatial association between gold-bearing sediment samples collected from the Howard Pass and adjacent quadrangles, and Cretaceous and Quaternary sedimentary rocks suggests that the gold may exist as a detrital mineral in the Cretaceous units, or in Quaternary alluvial deposits formed by reworking of Cretaceous sedimentary rocks containing detrital heavy minerals. The Cretaceous rocks in the foothills of the Brooks Range are composed of sediments derived from the Brooks Range and prograded northward and eastward during the Late Jurassic to Late Cretaceous Brooks Range orogeny (Mull, 1982). In the Howard Pass quadrangle, most of the Cretaceous rocks exposed in the foothills belong to the Okpikruak, Torok, and Fortress Mountain Formations (C.G. Mull, unpublished mapping, 1992), whereas in the northern parts of the Killik River and Chandler Lake quadrangles, rocks of the Lower and Upper Cretaceous Nanushuk Group and Upper Cretaceous Colville Group predominate (Kelley, 1990; Mull and others, 1994). Detrital metamorphic minerals identified in heavy mineral separates from the Torok Formation and Nanushuk Group indicate that the orogenic sediments were derived, in part, from the blueschist-facies rocks that now occupy the metamorphic core (schist belt) of the Brooks Range (Till, 1992). Based on outcrop observations and petrographic studies, rocks of the Fortress Mountain Formation may also have been derived from the schist belt.

Gold-bearing quartz vein and placer deposits in the metamorphic core (fig. 1) are the only known gold deposits in the region; many of these deposits are spatially associated with Devonian granitic rocks. It is possible that these may be the source of gold (and cassiterite and scheelite) in sediment samples collected from the foothills area.

REFERENCES CITED

Cobb, 1975, Summary of references to mineral occurrences (other than mineral fuels and construction materials) in northern Alaska: U.S. Geological Survey Open-File Report 75-628, 106 p.

Dillon, J.T., Lamal, K.K., and Huber, J.A., 1989, Gold deposits in the Upper Koyukuk and Chandalar mining districts, *in* Mull, C.G., and Adams, K.E., eds., Dalton Highway, Yukon River to Prudhoe Bay, Alaska; Bedrock geology of the eastern Koyukuk basin, central Brooks Range, and eastcentral Arctic Slope: Guidebook—Alaska Division of Geological and Geophysical Surveys, Report no. 7, v. 2, p.195–201.

Duttweiler, K.A., 1987, Use of factor analysis in locating base metal mineralization in the Killik River quadrangle, Alaska, *in* Hamilton, T.D., and Galloway, J.P., eds., Geologic studies in Alaska by the U.S. Geological Survey during 1986: U.S. Geological Survey Circular 998, p. 27–30.

Ellersieck, Inyo, Jansons, Uldis, Mayfield, C.F., and Tailleur, I.L., 1982, The Story Creek and Whoopee Creek lead-zinc-silver occurrences, western Brooks Range, Alaska, *in* Coonrad, W.L., ed., U.S. Geological Survey in Alaska—Accomplishments during 1980: U.S. Geological Survey Circular 844, p. 35–38.

Einaudi, M.T., and Hitzman, M.W., 1986, Mineral deposits in northern Alaska—Introduction: Economic Geology, v. 81, no. 7, p. 1583–1591.

Foley, J.Y., Barker, J.C., and Brown, L.L., 1986, Chromite resources in Alaska, *in* Daellenbach, C.C., ed., Chromium-chromite: Proceedings of USBM briefing—U.S. Bureau of Mines Information Circular 9087, p. 23–29.

Grimes, D.J., and Marranzino, A.P., 1968, Direct-current arc and alternating-current spark emission spectrographic field methods for the semiquantitative analysis of geologic materials: U.S. Geological Survey Circular 591, 6 p.

Jansons, Uldis, 1982, Zinc-lead occurrences in and near the National Petroleum Reserve in Alaska: U.S. Bureau of Mines Mineral Lands Assessment Report MLA 121-82, 55 p.

Jansons, Uldis, and Baggs, D.W., 1980, Mineral investigations of the Misheguk Mountain and Howard Pass quadrangles, Alaska: U.S. Bureau of Mines Open-File Report 38-80, 76 p.

Jansons, Uldis, and Parke, M.A., 1981, Mineral investigations in the Misheguk Mountain and Howard Pass quadrangles, Alaska: U.S. Bureau of Mines Open-File Report 26-81, 195 p.

Kelley, J.S., 1990, Generalized geologic map of the Chandler Lake quadrangle, north-central Alaska: U.S. Geological Survey Miscellaneous Field Studies Map MF–2144–A, scale 1:250,000.

Kelley, J.S., Tailleur, I.L., Morin, R.L., Reed, K.M., Harris, A.G., Schmidt, J.M., and Brown, F.M., 1993, Barite deposits in the Howard Pass quadrangle and possible relations to barite elsewhere in the northwestern Brooks Range, Alaska: U.S. Geological Survey Open-File Report 93-215, 13 p.

Kelley, K.D., and Mull, C.G., 1994, Maps showing the distribution of selected elements in minus-100-mesh stream- and lake-sediment samples from the northern part of the Killik River quadrangle, Alaska: U.S. Geological Survey Miscellaneous Field Studies Map MF–2225–B, in press.

Kelley, K.D., Mull, C.G., and Barton, H.N., 1994, Maps showing the distribution of selected elements in minus-30-mesh stream-sediment samples from the southern part of the Killik River quadrangle, Alaska: U.S. Geological Survey Miscellaneous Field Studies Map MF–2225–C, scale 1:250,000, in press.

Kelley, K.D., and Sutley, S.J., 1993, Maps showing the geochemistry of sediment samples from the northern part of the Chandler Lake quadrangle, Alaska: U.S. Geological Survey Miscellaneous Field Studies Map MF–2144–D, scale 1:250,000.

Lange, I.M., Nokleberg, W.J., Plahuta, J.T., Krouse, H.R., and Doe, B.R., 1985, Geologic setting, petrology, and geochemistry of stratiform sphalerite-galena-barite deposits, Red Dog Creek and Drenchwater Creek areas, northwestern Brooks Range, Alaska: Economic Geology, v. 80, no. 7, p. 1896–1926.

Lange, I.M., and Nokleberg, W.J., 1987, Geologic setting, petrology, and geochemistry of stratiform sphalerite-galena-barite deposits, Red Dog Creek and Drenchwater Creek areas, northwestern Brooks Range, Alaska—A reply to discussion by Young, L.E., and Moore, D.W., 1987: Economic Geology, v. 82, no. 4, p. 1077–1079.

Mayfield, C.F., Tailleur, I.L., and Ellersieck, Inyo, 1988, Stratigraphy, structure, and palinspastic synthesis of the western Brooks Range, northwestern Alaska, *in* Gryc, George, ed., Geology and exploration of the National Petroleum Reserve in Alaska, 1974 to 1982: U.S. Geological Survey Professional Paper 1399, p. 143–186.

Meyer, M.P., Kurtak, J.M., and Hicks, R.W., 1993, Results of the 1992 U.S. Bureau of Mines Colville Mining District study: U.S. Bureau of Mines Open File Report 12-93, 35 p.

Mull, C.G., 1982, The tectonic evolution and structural style of the Brooks Range, Alaska—An illustrated summary, *in* Powers, R.B., ed., Geological studies of the Cordilleran thrust belt: Denver, Colorado, Rocky Mountain Association of Geologists, v. 1, p. 1–45.

Mull, C.G., Tailleur, I.L., and Harris, E.E., 1994, Preliminary geologic map of the Killik River quadrangle, central Brooks Range, Alaska: U.S. Geological Survey Open-File Report, scale 1:125,000, in press.

Nelson, S.W., and Nelson, W.H., 1982, Geology of the Siniktaneyak Mountain ophiolite, Howard Pass quadrangle, Alaska: U.S. Geological Survey Miscellaneous Field Studies Map MF–1441, scale 1:63,360.

Nokleberg, W.J., and Winkler, G.R., 1982, Stratiform zinc-lead deposits in the Drenchwater Creek area, Howard Pass quadrangle, northwestern Brooks Range, Alaska: U.S. Geological Survey Professional Paper 1209, 22 p.

Rose, S.C., Pickthorn, W.J., and Goldfarb, R.J., 1988, Gold mineralization by metamorphic fluids in the Chandalar district, southern Brooks Range-Fluid inclusion and oxygen-isotopic evidence: U.S. Geological Survey Circular 1016, p. 81–84.

Till, A.B., 1992, Detrital blueschist-facies metamorphic mineral assemblages in Early Cretaceous sediments of the foreland basin of the Brooks Range, Alaska, and implications for orogenic evolution: Tectonics, v. 11, no. 6, p. 1207–1223.

Wahrhaftig, Clyde, 1965, Physiographic divisions of Alaska: U.S. Geological Survey Professional Paper 482, 52 p.

Young, L.E., and Moore, D.W., 1987, A discussion of "Geologic setting, petrology, and geochemistry of stratiform sphalerite-galena-barite deposits, Red Dog Creek and Drenchwater Creek areas, northwestern Brooks Range, Alaska": Economic Geology, v. 82, no. 4, p. 1077–1079.

Reviewers: Robert G. Eppinger and Richard J. Goldfarb

Calculated Gold Resource in Circle and Fortymile Placers

By Warren Yeend

In general, lode sources of magnitudes sufficient to supply the gold found in placer districts are not identified. The Circle and Fortymile Districts in east central Alaska (fig. 1) are two examples of this. Over the past 100 years approximately 1,000,000 ounces (31.2 tons) of gold have been recovered from placers in the Circle District (Yeend, 1991), and 500,000 ounces (15.6 tons) from the Fortymile area (Yeend, in press).

Prindle (1905) thought that the gold found in creeks in the Circle region was derived from large areas of almost uniformly mineralized bedrock and that there were probably no zones or pockets especially rich in the metal. McConnell (1905) studied the gold placers in the Klondike and suggested that the lode gold content of the bedrock quartz veins was probably no more than a few cents to the ton and hence the veins might not be productive even if discovered. Similar conclusions were reached by Loen (1992) almost 90 years later from studies of the mass balance constraints on gold placers of varying ages and in a variety of locations, including Fairbanks, Alaska (Pliocene and Quaternary), Sierra Nevada, California (Eocene to Quaternary), and Witwatersrand, South Africa (Archean).

Several of Loen's conclusions are presented here as they bear on the Circle District and Fortymile River area placers, neither of which has an identified rich lode source:

1. Cenozoic gold placers develop from the gradual erosion of large volumes (10^1 to 10^4 km^3) of source rocks with gold contents at mean background values;

2. No correlation exists between mean source-rock gold content and amount of gold in placers, indicating that other factors (degree of weathering of source rocks, volume of rock eroded, efficiency of concentration processes, and so on) are of greater importance than the richness of source regions;

3. The concentration of gold into placers is inefficient because of incomplete release of gold from source rocks and transport of gold out of the system in solution, suspension, and chemical complexes (in other words, an estimated 50 to 90 percent of the gold that was present in source rocks is not recovered from placers).

Calculating the expected amount of placer gold deposited in the Circle and Fortymile River area using Loen's (1992) mass balance equation and making some assumptions on the efficiency of the gold release system, erosion rates, and time duration of erosion is an instructive exercise. The mass balance equation (Loen, 1992) is:

$$P = \frac{(D \times Ad \times C \times t \times R)}{100} \times E$$

where P is total mass of heavy mineral in the placer deposit (tons Au), D is mean density of the source rocks (tons/m^3), A_d is drainage basin area (km^2), C is mean abundance of gold in source rock (ppb), R is mean denudation rate (cm/ka), t is time constraint on erosion of source rocks (Ma), and E is efficiency of weathering and concentration processes (percent).

Efficiencies of placer-forming systems are expected to be low because a substantial portion of the heavy minerals are either not released by weathering or are chemically and mechanically lost from the system (Loen, 1992). It is recognized that trace gold (ppb) is not directly recovered or even concentrated in the placers; rather, it must have been concentrated into particulate gold in epigenetic deposits such as quartz veins prior to erosion to eventually be concentrated in placers (Henley and Adams, 1979).

Solving for P for the Fortymile River area:

D is 2.65 tons/m^3, the mean density of rocks (Loen, 1992);

A_d is 2,000 km^2, the approximate area of the metamorphic rock unit that is the suspected gold source rock in the drainage basins of the gold-rich creeks in the Fortymile River area (Yeend, in press);

C is 6.5 ppb, the average gold content of 560 worldwide samples of greenschist and amphibolite (Crocket, 1991);

t is 5 Ma, the time available to erode the source rocks and deposit the Pliocene and Pleistocene age gold-bearing gravel deposits in the Fortymile River area. A Pliocene age is obtained from a tuff in some high terrace gravels so this figure is an estimate; it could be older, but probably not much younger;

R is 30 cm/ka, a relatively high rate resulting from the periglacial processes (Péwé, 1975) that produced high denudation rates in the unglaciated part of central Alaska. Loen used a range of 10 to 50 cm/ka for the Fairbanks area;

E is 10 percent (this, of course, is an estimate based on figures given by others and on my knowledge of placer formation; Henley and Adams (1979) present evidence suggesting very low efficiencies of 1 to .01 percent, whereas Boyle (1979) presents data indicating up to 50 percent of gold release; Loen (1992), uses 10 to 50 percent in his calculations.)

Substituting these values in the above equation, *P* is 5,167 tons of gold, the amount that should have been available for concentration in placers in the Fortymile River area. Since only 15.6 tons of gold have been recovered, which is less than 1 percent of 5,167 tons, the calculations suggest that either there is an abundance of gold remaining or *E* is too high, or *t* is too high, or both. A much greater volume of gravel is present in the high terrace gravels of the Fortymile River system than is in the present flood plains. These high-level gravels have been selectively mined, but much of the deposit contains gold

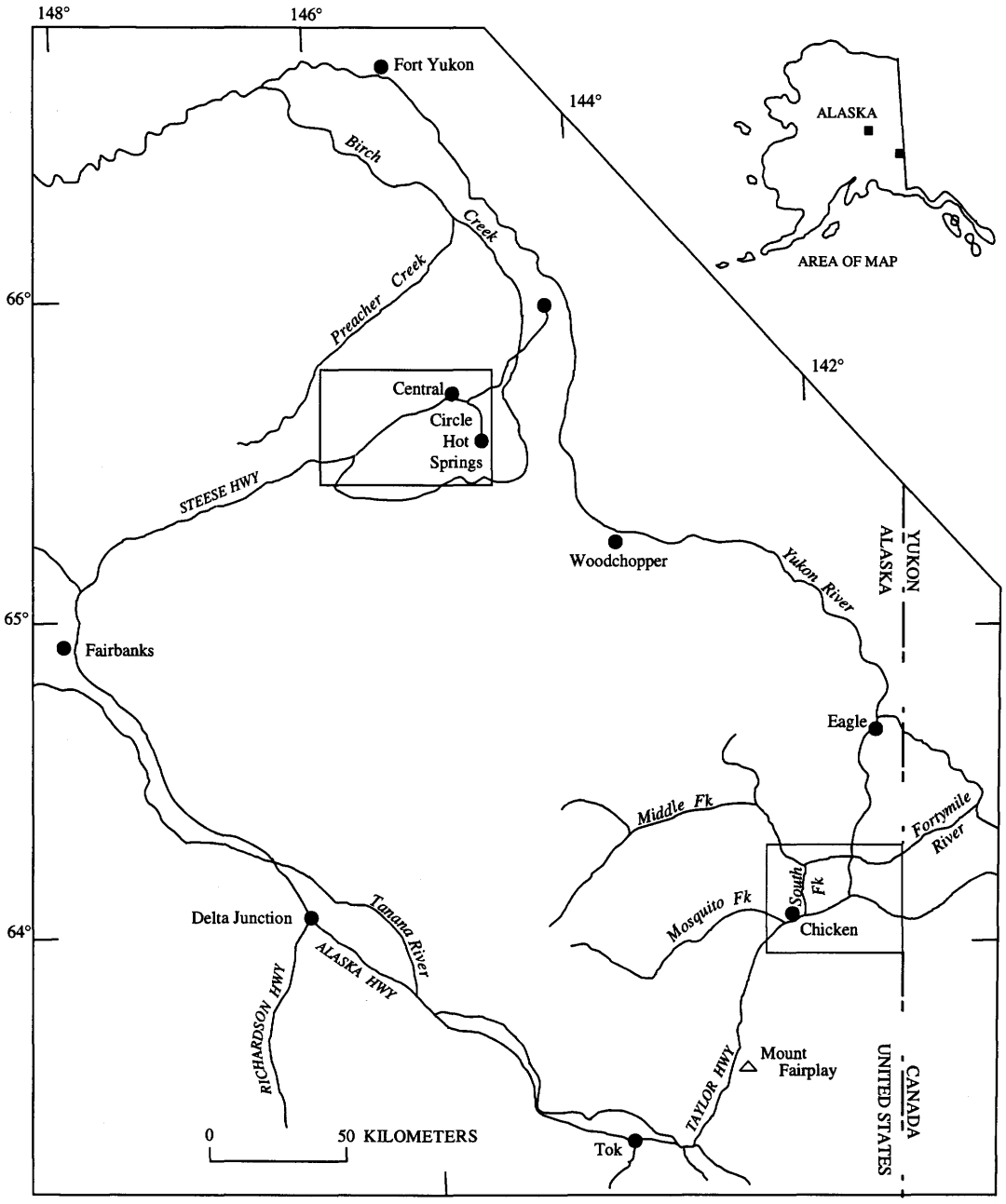

Figure 1. Index map showing location of the Circle and Fortymile mining districts in east-central Alaska.

in subeconomic amounts and is difficult to prospect and mine (Yeend, 1990; Yeend, in press).

The following calculations apply to the Circle area: Solving for P:

D is 2.65 tons/m^3, the mean density of rocks;

A_d is 316 km^2, the approximate area of the mafic schist unit, the suspected gold source rock in the drainage basins of the gold-rich creeks in the Circle District (Yeend, 1991);

C is 6.5 ppb, as described above;

t is 5 Ma, the estimated time available to erode the source rocks and recycle the gold into the Pleistocene and Holocene age gold-bearing deposits in the Circle area; t could be as small as 2 Ma or as much as 30 Ma;

R is 30 cm/ka, as described above;

E is 10 percent, as described above.

Substituting these values in the equation, P is 816 tons of gold, the amount that should have been available for concentration in the Circle district. Since only 31.2 tons of gold have been recovered, which is less than 3.8 percent of 816 tons, the calculations suggest that either there is an abundance of gold remaining, or that E is off by an order of magnitude, or t is too high, or both. A substantial portion of this gold is probably present in the gravel fill within the Tintina Fault trench adjacent to the Circle area placers, as previously suggested (Yeend, 1991); however, this gold resource is not currently economic for mining because the high clay content of the placer deposit makes separation of the gold difficult.

REFERENCES CITED

Boyle, R.W., 1979, The geochemistry of gold and its deposits: Geological Survey of Canada Bulletin 280, 584 p.

Crocket, J.H., 1991, Distribution of gold in the earth's crust, *in* Foster, R.P. ed., Gold metallogeny and exploration: London, Blackie, p. 1–36.

Henley, R.W., and Adams, J., 1979, On the evolution of giant gold placers: Institute of Mining Metallurgy Transactions, v. 88, p. B41–B50.

Loen, J.S., 1992, Mass balance constraints on gold placers: Possible solutions to "source area problems": Economic Geology, v. 87, p. 1624–1634.

McConnell, R.G., 1905, Report on the Klondike Gold Fields: Geological Survey of Canada, Annual Report vol. XIV, pt. B, 71 p.

Péwé, T.L., 1975, Quaternary geology of Alaska: U.S. Geological. Survey Professional. Paper 835, 145 p.

Prindle, L.M., 1905, The gold placers of the Fortymile, Birch Creek and Fairbanks regions, Alaska: U.S. Geological Bulletin 251, 89 p.

Yeend, Warren, 1990, Gold placers, gold source and high terrace gravels in the Fortymile River area, Alaska, *in* Bradley, D.C., and Ford, A.G., eds., Geologic studies in Alaska by the U.S. Geological Survey, 1990: U.S. Geological Survey Bulletin 1999, p. 228–230.

———1991, Gold placers of the Circle District, Alaska—Past, present, and future: U.S. Geological Survey Bulletin 1943, 42 p.

———in press, Gold placers of the Fortymile River region, Alaska, an historic mining area: U.S. Geological Survey Bulletin.

Reviewers: David A. Brew and John P. Galloway

Miocene Coal-Bearing Strata of the Tyonek Formation: Braided-Stream Deposits in the Chuit Creek-Chuitna River Drainage Basin, Southern Alaska

By R.M. Flores, G.D. Stricker, *and* S.B. Roberts

ABSTRACT

Coal beds and hydrocarbons in the Tyonek Formation are targets for exploration and development by coal and oil companies. Sandstones of the formation are important oil and gas reservoirs, as indicated by their recent discovery in the offshore of upper Cook Inlet. Thus, sandstone characterization in outcrops will provide two-dimensional properties of these subsurface reservoirs.

Stratigraphic and sedimentologic studies of the upper part of the Tyonek Formation in the Chuit Creek-Chuitna River drainage basin suggest deposition in an alluvial plain. The alluvial plain was drained by braided streams, which were flanked by overbank-flood plains and mires. Braided-stream deposits consist mainly of erosional-based, conglomeratic sandstones that are subdivided by multiple, internal scour surfaces. Between scour surfaces, the conglomeratic sandstones are in turn partitioned by grain size and sedimentary structures. The sedimentary structures are governed by the variations in flow regimes of the braided streams. The overbank-flood plain mudstones, siltstones, and sandstones were formed during bankfull discharge of the braided streams, by overtopping and breaching river banks. Breached river banks resulted in crevasse splays, which transported fine-grained sediments into overbank-flood plains and peat-forming mires. Thick coal beds mainly accumulated on raised platforms formed on abandoned braidbelts.

INTRODUCTION

During the past two decades, coal companies have been exploring and development-drilling in the Beluga coal field, in general, and in the Chuitna River drainage basin, in particular (figs. 1, 2). These activities have focused on Miocene strata of the Tyonek Formation of the Kenai Group, which contains numerous thick coal beds (Barnes, 1966; Adkison and others, 1975). A large part of the Kenai Group is exposed along the margins, and north of, the Cook Inlet basin (fig. 1). The Chuitna River drainage basin has been targeted for its shallow Tyonek coal beds, which are located within 20 km of the tidewater of Cook Inlet. Exploration drilling programs have outlined surface minable coal reserves in the Chuitna River drainage basin, where two leases were obtained by coal companies (Ramsey, 1981; McFarland, 1987; Stiles and Franklin, 1987). Coal companies are mainly interested in marketing electricity generated from mine-mouth, coal-fired power plants.

In addition to the economic coal beds of the Tyonek Formation, a 1991 oil and gas discovery (Sunfish ARCO No. 1 well) in reservoir sandstones of the Tyonek in the northwestern Cook Inlet Basin and 65 km west-southwest of Anchorage (fig. 1) has spurred additional interest in the formation (Petroleum Information Corporation, 1991). This major discovery well, which was in an area many explorationists believed to be depleted, flowed 1,100 barrels per day of oil and 1 million cubic feet of gas (Oil and Gas Journal, 1993) from Tyonek sandstone reservoirs. Two other wells (Sunfish ARCO Nos. 2 and 3) will be drilled near the discovery well to determine how much oil is present in the area. Preliminary estimates by ARCO indicate that the Sunfish prospect may contain 750 million barrels of gross oil reserves (Petroleum Information Corporation, 1993). Thus, characterization of the Tyonek sandstone reservoirs will assist in development of the hydrocarbon reserves. The Sunfish petroleum discovery adds to the economic importance of the Tyonek Formation as a source of multiple fossil-fuel commodities.

In response to the various economic interests in the Tyonek Formation, detailed stratigraphic and sedimentologic studies were made on the coal-bearing strata exposed along the Chuit Creek-Chuitna River drainage basin in the upper reaches of the Chuitna River (fig. 2). The study area is at the southwest and northeast boundaries of the coal-company leases (Ramsey, 1981; McFarland, 1987; Stiles and Franklin, 1987) and about 70 km west of Anchorage.

The purpose of this study is to establish the stratigraphic- and sedimentologic-facies framework of coal-bearing strata in the Tyonek Formation. Ten stratigraphic sections were measured and described. These sections include detailed characterization of the lithology, grain size, sedimentary structures, and nature of contacts of the rock units. In addition, photomosaics of continuous outcrops (50 to 75 percent rock exposure) were used to compliment the measured sections. This information, in combination with stratigraphic data from earlier studies (Barnes, 1966; McGee, 1972; Adkison and others, 1975; Odum and others, 1983), was used to construct stratigraphic cross sections and sedimentologic facies profiles to determine lateral and vertical variability of the rock units. Analyses of internal facies architecture were made to determine the reservoir characteristics of the sandstone units in the Tyonek Formation. Stratigraphic reconstructions, sedimentologic facies profiles, and facies-architecture analysis, in turn, reflect the geomorphic and depositional settings of the Tyonek in the study area.

PREVIOUS STUDIES AND GEOLOGIC SETTING

The Tyonek Formation in the Beluga and Capps Glacier coal fields (the latter is approximately 18 km northwest of our study area; see fig. 3) consists of interbedded conglomerate, sandstone, siltstone, mudstone, carbonaceous shale, and coal beds. Barnes (1966) referred to the lower conglomeratic interval as the lower (conglomerate) member and the coal-bearing interval as the middle member of what was then called the Kenai Formation. Calderwood and Fackler (1972) elevated the Kenai Formation to group status and the rocks comprising the above mentioned lower and middle members were reassigned to form part of the Tyonek Formation (see also, Magoon and others, 1976). Adkison and others (1975) described the lower part of the Tyonek Formation as consisting of conglomerates and sandstones and the upper part as composed of sandstones, siltstones, shales, and coals.

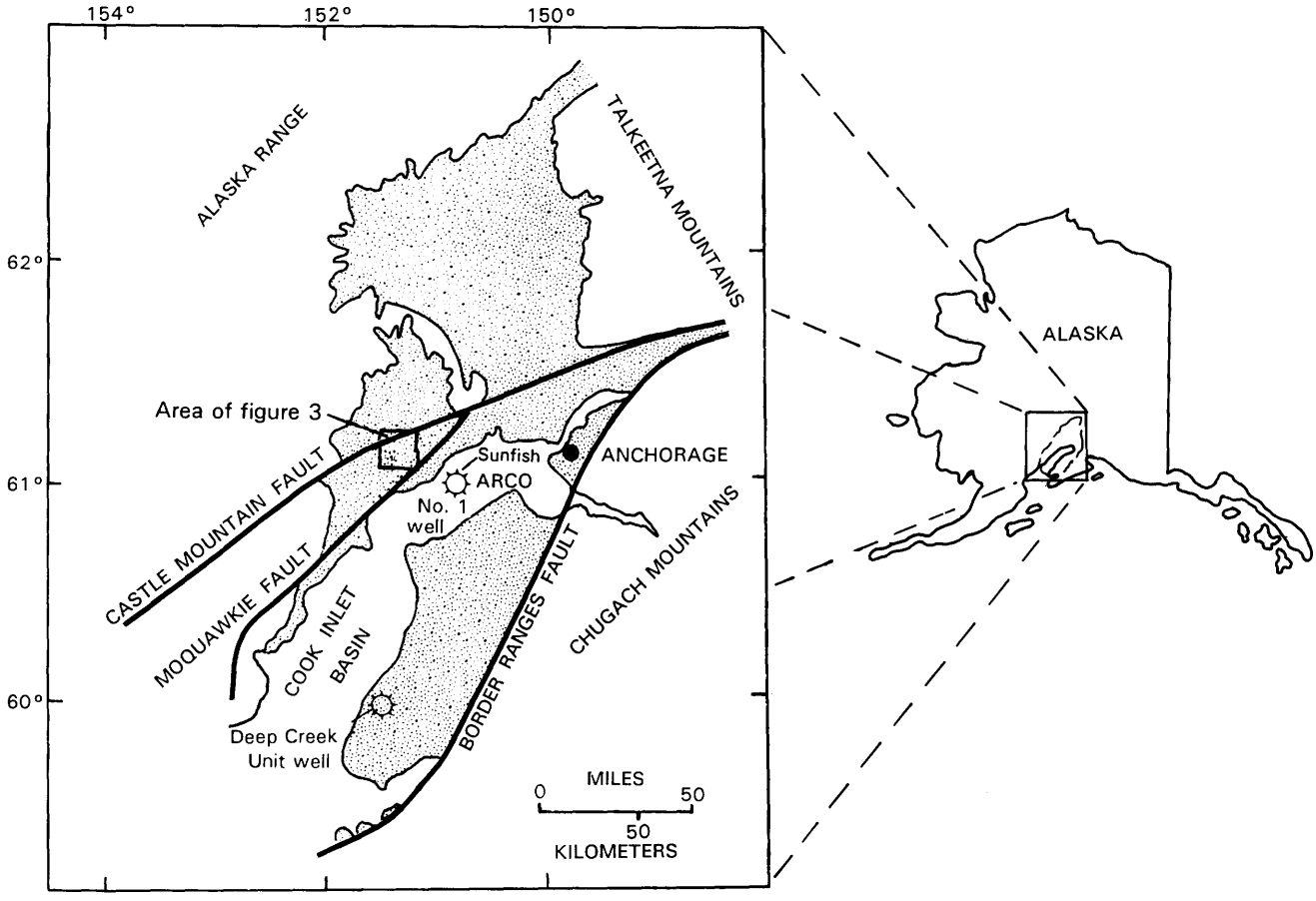

Figure 1. Locality map showing areal distribution of the coal-bearing Kenai Group (stipple pattern) along margins of Cook Inlet basin and location of study area (see fig. 3).

Palynomorph analysis (Adkison and others, 1975) indicates that the Tyonek Formation in the Beluga and Capps Glacier coal fields is stratigraphically equivalent to the middle part of the Tyonek in the Deep Creek Unit well on the Kenai Peninsula (Adkison and Newman, 1973). Biostratigraphic analysis of the Tyonek Formation in the Beluga and Capps Glacier coal fields yielded macroflora of the Seldovian and Homerian Stages (early to late Miocene) (Wolfe and others, 1966). More specifically, the Tyonek in the Chuit Creek-Chuitna River drainage basin yielded primarily Seldovian-Homerian macroflora (early to late Miocene) (Wolfe and others, 1966; Adkison and others, 1975).

Correlation of lithologic units in the Tyonek Formation, in general, and the coal beds, in particular, between the Beluga and Capps Glacier coal fields is tenuous, because of structural complications. Barnes (1966) indicated that coal beds in the Capps Glacier area rise structurally and are eroded to the southeast. In addition, the Castle Mountain fault (fig. 3), a major southwest-trending structure, lies at

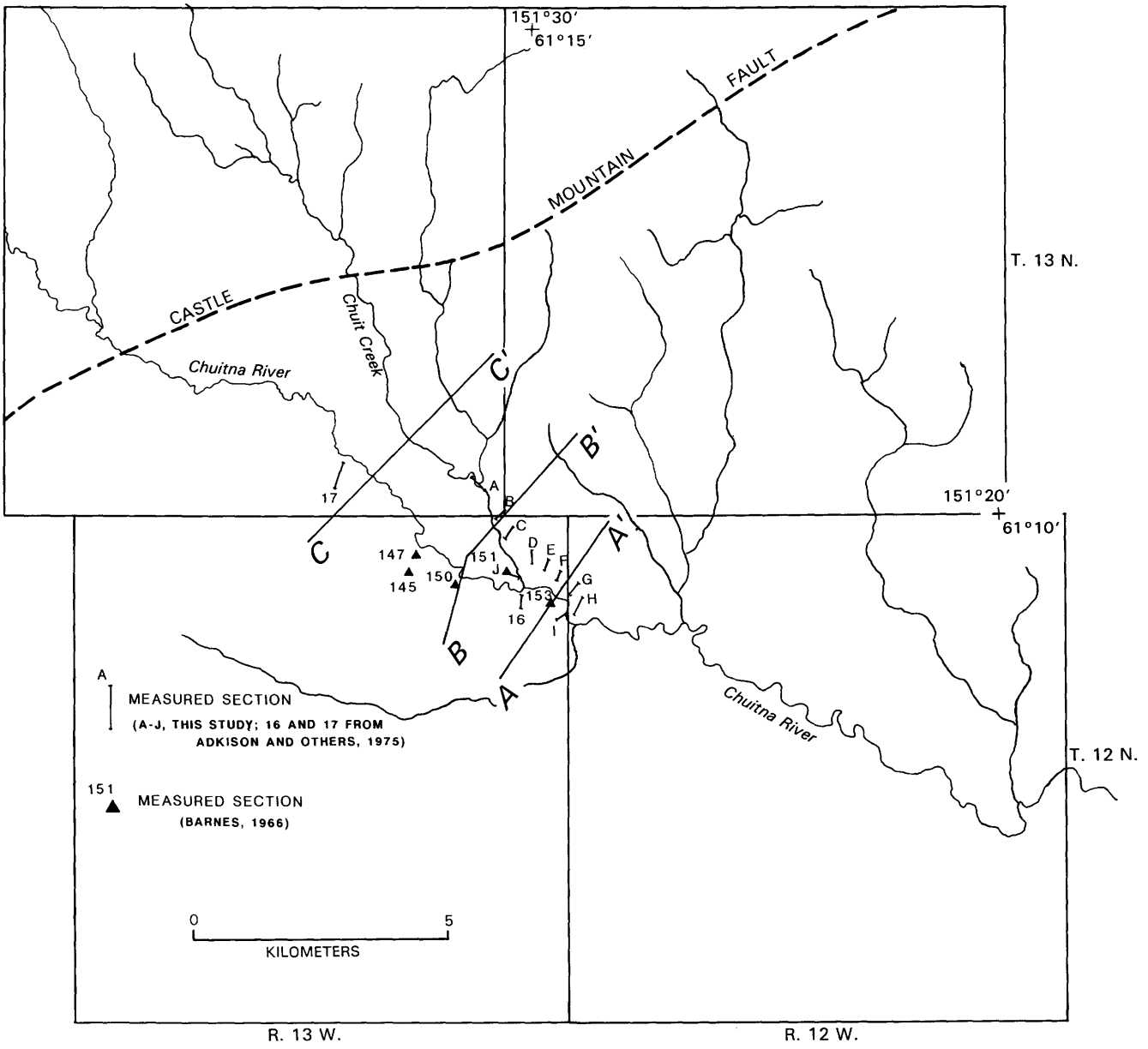

Figure 2. Chuitna River drainage basin and localities of measured sections for this study, for Adkison and others (1975), and for Barnes (1966). Lines of cross sections (*A–A′*, *B–B′*, and *C–C′*) adopted from McGee (1972) are also shown.

the northern boundary of the Beluga coal field and the Chuitna River drainage basin. Rocks on the southeast side of the fault are downthrown. This fault, which extends for several hundred kilometers, was interpreted by Grantz (1966) to be a right-lateral, strike-slip fault from Mesozoic through early Tertiary time and a steep reverse fault from Oligocene time to the present. Kirschner and Lyon (1973) suggested a large component of right-lateral movement along this fault. Detterman and others (1976) and Fuchs (1980) indicated that the Castle Mountain fault has been active for millions of years and has recorded at least several kilometers of net displacement. A secondary fault, the Moquawkie fault zone, with rocks downthrown on the southeast side, splays southwestward from the Castle Mountain fault (see fig. 1) and extends into the southern end of the Chuitna River drainage basin. This fault and the Castle Mountain fault define a pie-shaped structural block that contains the Tyonek outcrops of the study area. Within this structural block are other minor, northeast-southwest-trending faults displaying rocks downthrown on the southeast side. Thus, assuming that active vertical net displacement of the Castle Mountain fault occurred from Oligocene time to the present, and that the Tyonek Formation is early through middle Miocene in age in the area of this report, we suggest that the Tyonek is a syntectonic deposit.

In general, the Tyonek Formation is interpreted to contain non-marine strata mainly deposited in channels (McGee, 1972: Adkison and others, 1975; Dickinson and others, in press). Hite (1976) indicated that these channel fills were developed in a poorly-drained alluvial plain. A study of the Kenai Group (Tyonek and Beluga Formations) in the northwestern Cook Inlet area by Dickinson and Campbell (1978) revealed three fluvial depositional facies: (1) proximal-braided, (2) distal-braided, and (3) distal facies. The proximal-braided facies, which consists of medium- to thick-bedded clayey or sandy conglomerates with low-angle foresets in lenticular channel forms, was interpreted to be deposited by mudflows and near-source braided streams. The distal-braided facies, which consists of interbedded conglomerates, sandstones, and coals particularly well exposed near the toe of the Capps Glacier, was interpreted to have been deposited by braided and meandering fluvial systems. The distal facies contains predominantly mudstones, sandstones and lesser amounts of conglomerates and coals. This facies was interpreted as braided streams, which reworked earlier sediment of proximal-braided and distal-braided streams that was deposited on a broad plain. In the Capps Glacier and Chuitna drainage basin, the West Foreland Formation, dominated by conglomerates, and the Tyonek Formation, dominated by

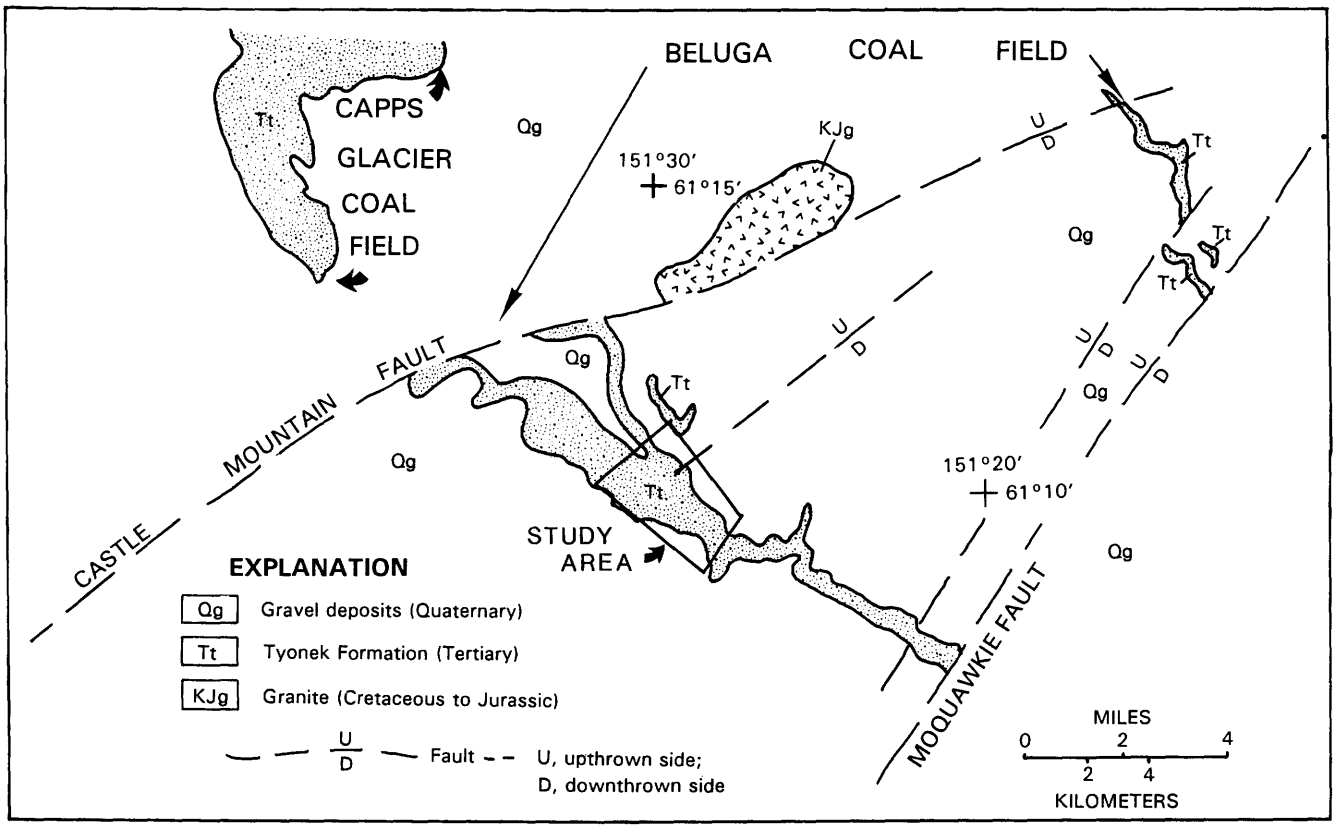

Figure 3. Study area and outcrops of the Tyonek Formation, located between the Castle Mountain and Moquawkie faults. Modified from Ramsey (1981).

sandstone, siltstones, shales, and coals (Adkison and others, 1975, pl. 1), may represent the proximal- and distal-braided and distal facies, respectively.

STRATIGRAPHIC-LITHOLOGIC FRAMEWORK OF STUDY INTERVAL

A composite stratigraphic section of the Tyonek Formation exposed in the Chuit Creek-Chuitna River drainage basin is shown in figure 4. This stratigraphic section, which is only 225 m thick, probably represents the upper part of the Tyonek Formation, because Calderwood and Fackler (1972) report the Tyonek to be 1.2 to 2.3 km thick. Our study focused on the rocks from above the Lower Chuitna (coal) bed to the unnamed coal beds above the Chuitna (coal) bed (fig. 4). Stratigraphic cross sections (fig. 5) of these coal beds (without interburden lithology) constructed by McGee (1972) show that our study interval is stratigraphically younger upstream. Additional cross sections by McGee (1972) indicate that the Chuitna (coal)

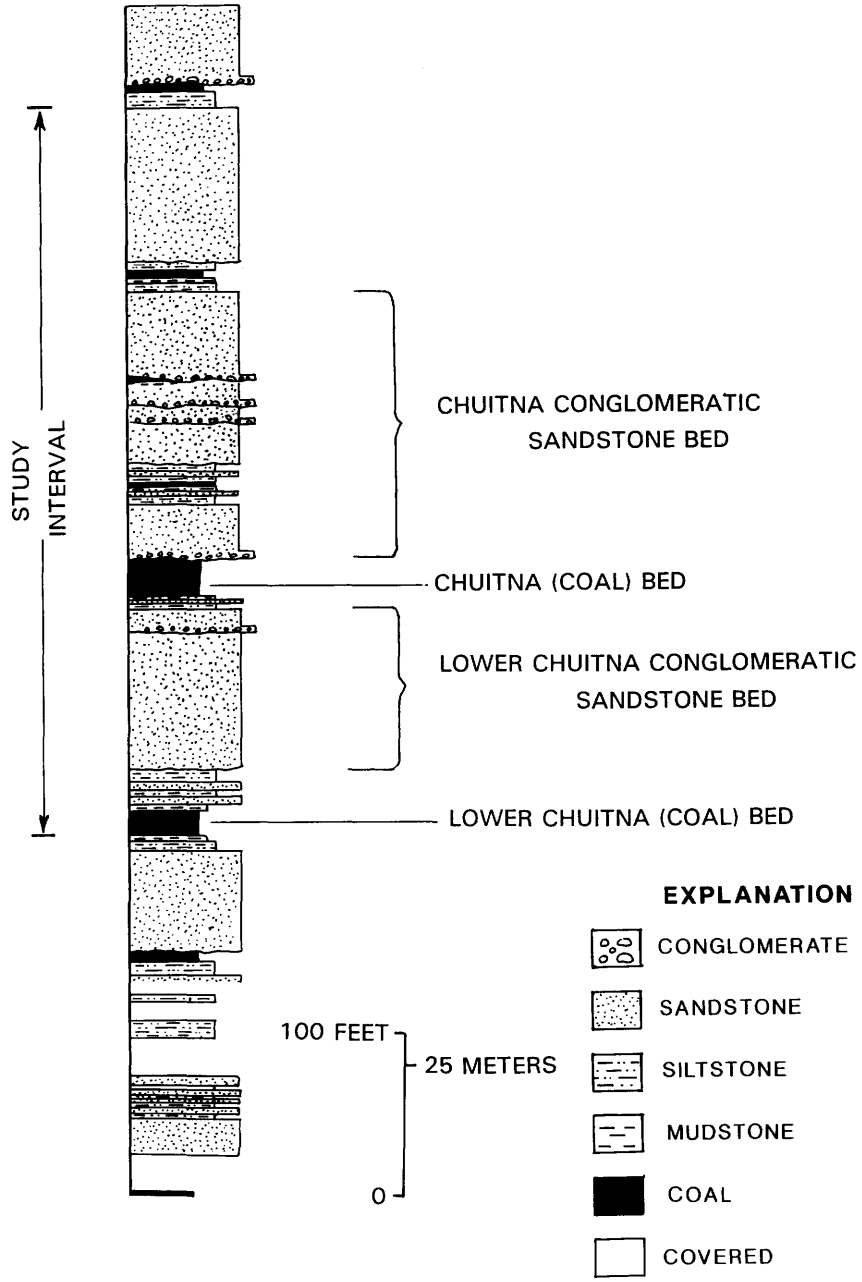

Figure 4. Composite stratigraphic column of the Tyonek Formation and position of study interval in the Chuitna River drainage basin.

bed is exposed for 11 km along the Chuit Creek-Chuitna River valley walls. The Chuitna (coal) bed and five lower coal beds within 91 m of the surface comprise the bulk of the coal reserves within nearby coal leases (Ramsey, 1980).

Lithologies of these coal-bearing strata consist of abundant conglomeratic sandstones and subordinate siltstones, mudstones, carbonaceous shales, and coals. Variability in the stratigraphic framework of these lithologies for the study is shown in figure 6.

CONGLOMERATIC SANDSTONES

The conglomeratic sandstones comprise as much as 75 percent of the total rock volume of the study interval. The sandstones are gray, fine-grained to very coarse grained and granule-size, fining-upward units. These sandstones, which are generally friable, are quartzose and micaceous, and are poorly to moderately sorted; case-hardened, iron-cemented intervals are present locally. Sandstone bodies exhibit flat-bottomed to concave-upward erosional bases marked by lag conglomerates. These lag conglomerates consist of subrounded to rounded, pebble- to cobble-sized fragments of chert, limestone, shale, ironstone, quartz (some vein quartz), and granite, as well as coal spar fragments. Conglomerates are framework supported and exhibit crude-to well-developed imbrication.

Conglomeratic sandstones are amalgamated beds with an aggregate thickness of as much as 45 m. Vertical and lateral variations of the conglomeratic sandstones (fig. 6) indicate rapid changes in thickness and lithology within a 10-km^2 area. Along the eastern valley walls of the Chuit Creek and Chuitna River, southeast of their confluence, an amalgamated conglomeratic sandstone is exposed above the Chuitna (coal) bed (fig. 6, see sections A to H). At

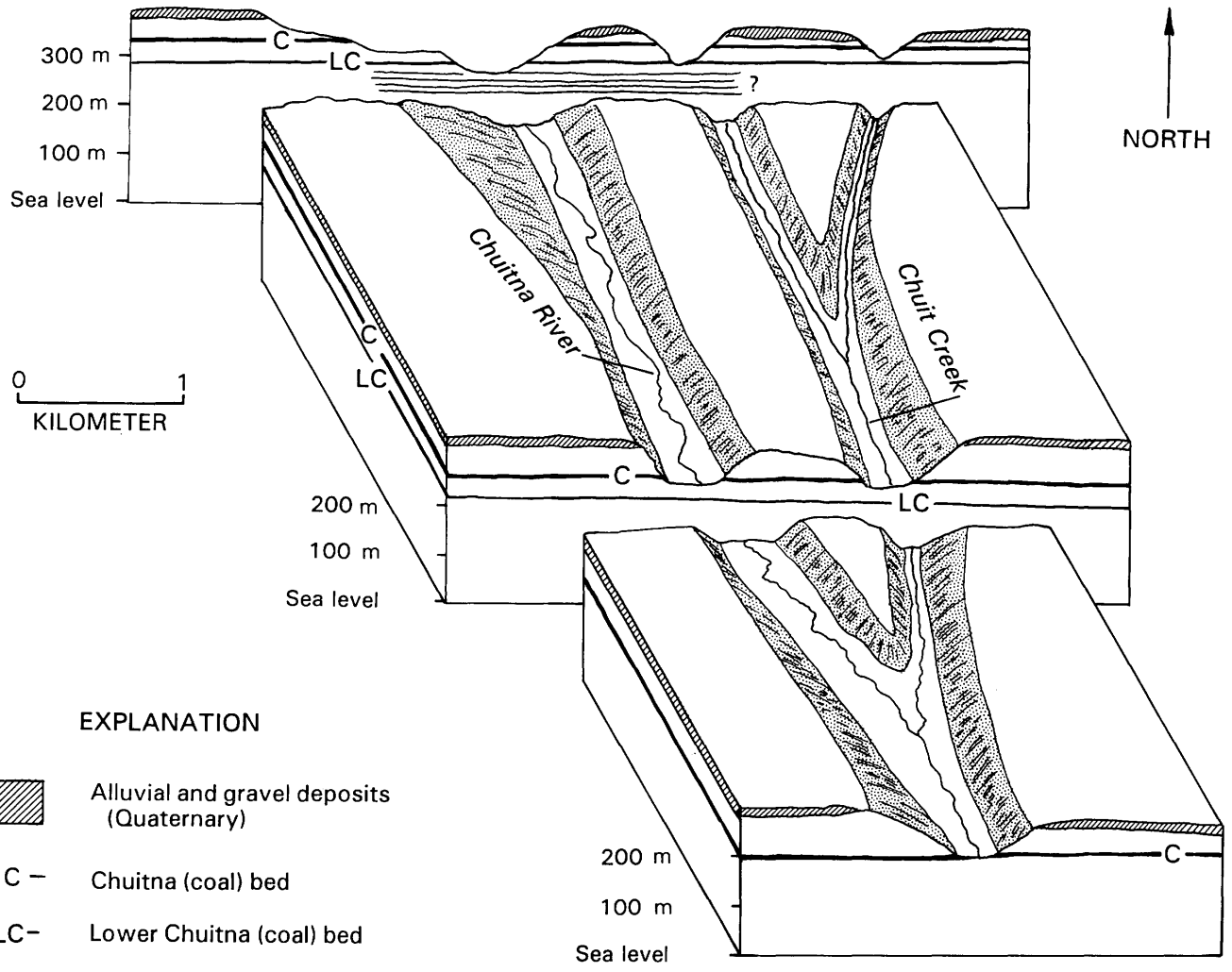

Figure 5. Stratigraphic cross sections showing positions of the Chuitna, Lower Chuitna, and unnamed (coal) beds in the study area. Modified from McGee (1972).

section H (fig. 6), this sandstone attains a maximum of 45 m thick but thins to 30 to 40 m. This sandstone bed, which is informally designated here as the Chuitna conglomeratic sandstone bed (fig. 7), is 42 m thick along the western wall of the Chuitna River Valley near the confluence with Chuit Creek (fig. 6, see sections 16, J, and 151). However, southward (within 1.6 km) along the western Chuitna River Valley wall (fig. 6, see sections 145, 147, 150, 16, and 153), the Chuitna conglomeratic sandstone bed interfingers with a local, thin coal bed (TCB) that splits the Chuitna conglomeratic sandstone bed into a lower, 32-m-thick bed and an upper 8-m-thick bed. Although the Chuitna conglomeratic sandstone bed is composed of two bodies in the southwest part of the study area, the bed is a sheet-like body that extends beyond the 10-km^2 study area.

Conglomeratic sandstones, generally less than 33 m thick, underlie and overlie the Chuitna conglomeratic sandstone bed (fig. 6). Amalgamated conglomeratic sandstones above the Lower Chuitna (coal) bed, informally designated here as the Lower Chuitna conglomeratic sandstone bed (see figs. 6, 7), are as much as 30 m thick in the northwestern part of the study area. Thus, this sandstone bed at sections 17 and B is directly overlain by the Lower Chuitna (coal) bed. However, at section A, the sandstone bed is laterally replaced by mudstones, siltstones, and sandstones, which are directly underlain by the Lower Chuitna (coal) bed, indicating thinning of the sandstone. This trend of sandstone thinning is similar to that shown on sections 17 through 16 (see fig. 6). The Lower Chuitna conglomeratic sandstone bed thins to the east-northeast and west-southwest indicating a generally west to east direction of elongation. Thinning of the Lower Chuitna conglomeratic sandstone bed toward the east-northeast and west-southwest directions indicates that the bed is probably less laterally extensive than the Chuitna conglomeratic sandstone bed.

The conglomeratic sandstone overlying the Chuitna conglomeratic sandstone bed is as much as 29 m thick along the Chuitna River Valley wall (see fig. 6). This unnamed conglomeratic sandstone is partly exposed along the Chuit Creek and Chuitna River Valleys in the eastern and western parts of the drainage basin.

Areas of thinning of the conglomeratic sandstones appear to exist where overlying sandstone bodies are thickened and vertically stacked. That is, the area of thinning of the Lower Chuitna conglomeratic sandstone bed in

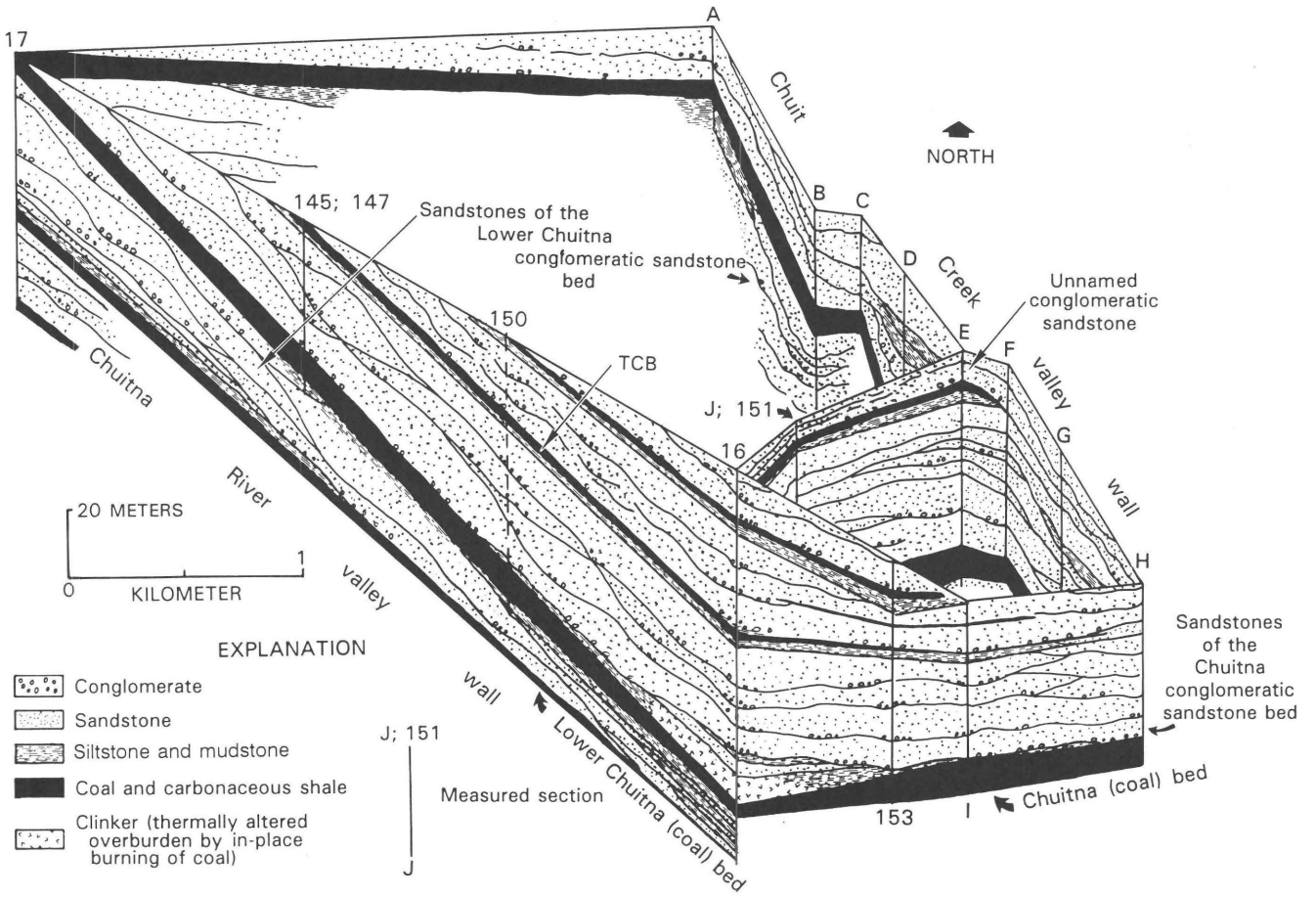

Figure 6. Stratigraphic three-dimensional fence diagram of the study interval in the Chuit Creek and Chuitna River drainage basin. TCB, thin coal bed. See figure 2 for explanation of measured section.

the southern part of the study area corresponds to where the overlying Chuitna conglomeratic sandstone bed is stacked, and locally split by thin coal beds (fig. 6, see sections 16, 153, I, and 4). In addition, the unnamed conglomeratic sandstone that overlies the overthickened Chuitna conglomeratic sandstone bed is thin in this area (fig. 6, see section 16).

SILTSTONES AND MUDSTONES

Siltstones and mudstones make up approximately 20 percent of the total rock volume in the study area. These lithologies form individual beds displaying sharp and (or) gradational contacts. Siltstone beds, which are as much as 7 m thick, are also interbedded with silty to very fine-grained sandstones. These siltstones are micaceous and light to dark gray or greenish gray; dark hues are related to a high content of very finely macerated plant remains. Greenish hues may be due to staining from reduced iron minerals. In addition, the siltstones contain large coalified wood fragments (stems and trunks), carbonized root marks, and carbonaceous plant stems and leaves. Trace-fossils in this lithology are sparse, nondescript vertical and horizontal animal burrows. Ripple and subparallel laminations are common sedimentary structures in siltstone, where bedding is not destroyed by root and animal bioturbation.

Mudstone beds are as thick as 2.5 m and contain mica, quartz grains, and smectitic clay minerals, the latter inferred from "popcorn" weathering. Mudstone is light to dark gray and yellow with darker hues corresponding to high organic content; the yellow is caused by staining from oxidized iron minerals. Coalified roots, trunks, stems, and leaves are common in the mudstones. Vertical and horizontal animal burrows are abundant locally, and where bioturbation is not present, sparse, isolated starved ripple laminae and lenticular bedding occur in intercalated siltstones and silty sandstones. Ironstone nodules and concretions are common diagenetic features in the mudstones.

As shown in figure 6, the siltstones and mudstones commonly underlie, overlie, and grade laterally into the conglomeratic sandstones. Thick (6 m) successions of siltstone interbedded with sandstone merge with the conglomeratic sandstone bodies. This merging represents the transition of conglomeratic sandstone bodies into finer-grained sequences. This transition is best displayed by the Lower Chuitna conglomeratic sandstone bed in the southern part of the study area (see fig. 6, section 16). Farther from the margin of the Lower Chuitna conglomeratic sandstone bed (see fig. 6, toward section A from section 16), the siltstone-sandstone succession is replaced by a thick (>4.5 m) mudstone-dominated interval in the northeastern part of the study area. Thick (7 m) siltstone and mudstone successions that underlie and overlie the conglomeratic sandstones (see Chuitna conglomeratic sandstone bed in fig. 6) thin laterally where the sandstone bodies thicken (fig. 6, sections 16 through H). In addition, siltstones and mudstones are commonly interbedded with thin coal and carbonaceous shale beds.

Figure 7. Outcrop of informally named Lower Chuitna conglomeratic sandstone bed (LC) overlain by informally named Chuitna conglomeratic sandstone bed (C); both separated by thick Chuitna (coal) bed (CB). Outcrop of LC on photo is approximately 8 m high.

COALS AND CARBONACEOUS SHALES

Coal and carbonaceous shale beds comprise less than 5 percent of the total rock-volume of the study interval. Coal beds range from a few centimeters to 9.8 m thick and are commonly interbedded with carbonaceous shale. The coals are generally black, although weathering imparts a dark-gray color and brings out the woody (vitrain) bands and a splintery, plywood-like texture. Sparse tonsteins (volcanic ash), up to a few centimeters thick, are present in some coal beds. The Chuitna and Lower Chuitna (coal) beds are subbituminous C in apparent rank, range from 3,770 to 4,360 kilocalories/kg, and range from 10.13 to 18.19 percent ash and 0.28 to 0.33 percent sulfur (Ramsey, 1981). McGee (1972) estimated the coal reserves in the Chuitna River area for beds greater than 2.5 m thick and within 300 m of overburden to be about 1.41 billion metric tons.

Carbonaceous shales are mixtures of mud and macerated organic matter. They are black to dark gray (related to high organic content) or gray brown (weathered), fissile or platy, and contain abundant plant stems and leaves. The carbonaceous shale beds range from less than 2.5 cm to 59 cm in thickness, are intercalated with lenses of bright coal (vitrain) and contain flattened coalified logs and other woody fragments.

The coal beds, particularly the thin beds (see fig. 6), merge laterally with the carbonaceous shale beds. The thickest coal bed in the study area is the Chuitna (coal) bed; it is 9.8 m thick in the southern part of the study area and 6.5 m thick in the northeastern part. The Chuitna (coal) bed is a single bed along the Chuit Creek and the Chuitna River Valley wall; however, in the southern part of the study area where it consists of two beds (Barnes, 1966), it may be split by a 2.5-m-thick mudstone parting. This Lower Chuitna (coal) bed is partially exposed in the southern part of the study area; in the northeastern part, the coal bed is as much as 6.5 m thick. The Chuitna and Lower Chuitna (coal) beds, which are the most continuous beds in the study interval, extend 6.5 km or more beyond the study area. Unnamed coal beds, which are as much as 1.3 m thick, are concentrated in the southern part of the study area (fig. 6, sections E and 16).

SEDIMENTOLOGIC-FACIES FRAMEWORK OF THE STUDY INTERVAL

Sedimentologic-facies framework analysis of the study interval concentrated on the vertical variations in grain size and sedimentary structures of the Chuitna and Lower Chuitna conglomeratic sandstone beds. These basally erosional, coarse-grained deposits were analyzed for internal architecture, which emphasizes the hierarchy of internal scours in the conglomeratic sandstone bodies. In addition, facies-sequence analysis was done on the siltstones and mudstones (fine-grained deposits), and the carbonaceous shales and coals (organic deposits). Vertical and lateral relationships of the sandstones and siltstone-mudstone-carbonaceous shale-coal facies sequences are used to interpret their depositional environments.

FACIES PROFILES OF THE CONGLOMERATIC SANDSTONES

Vertical-facies profiles of the conglomeratic sandstones (figs. 8–10) were constructed to compare the variations in grain size, sedimentary structures, and patterns of change in these facies characteristics between sandstone bodies. Paleocurrent data measured from trough crossbeds (n=28) and pebble-cobble orientations (n=6) are integrated with the facies profiles to determine paleoflow direction and type of fluvial processes reflected by the deposits.

The facies profile of the Lower Chuitna conglomeratic sandstone bed (fig. 8) in the Chuit Creek Valley wall in the northeastern part of the study area shows a general fining-upward sequence. The lower 18 m of this sequence is conglomerate-rich and the upper 6.5 m is sandstone-rich; the sequence is capped by a siltstone. The conglomeratic sandstone bed is composed of interbeds of pebble to cobble conglomerates ranging from 15 to 46 cm in thickness; the conglomerates are lenses ranging from a few cm to 4.5 m in lateral extent (fig. 11). Conglomeratic lenses are found in scour bases with erosional relief of as much as a meter. These lenses are in the lower parts of 1- to 3-m-thick, fining-upward, multistory, conglomerate-sandstone units. The internal scour surfaces are shallow to deep, and cut into each other along a 30-m-wide outcrop; thus, they are discontinuous and have a low order of lateral magnitude (a relatively short length). Clast-imbrication measurements show an east-northeast dip.

Conglomerate lenses grade upward into medium-grained to very coarse grained and gritty sandstones that are as much as 2.5 m thick. They are trough crossbedded, and trough amplitudes range from 15 cm to 1 m (see fig. 11). The lower part of the sandstone-facies sequence consists mainly of small-scale trough crossbeds ranging from 15 to 45 cm high. In contrast, the upper part contains mainly large-scale trough crossbeds ranging from 0.6 to 1 m high. Steep foresets of these large-scale, trough crossbeds contain convolute laminations that are as much as 30 cm high. Dip directions of foresets of the trough crossbeds range from northwest to southwest.

A facies profile of the Chuitna conglomeratic sandstone bed, which overlies the facies profile of the Lower Chuitna conglomeratic sandstone bed described above is shown in

the upper part of the section in figure 8. Here, the exposed lower part of the Chuitna conglomeratic sandstone bed consists mainly of medium- to coarse-grained sandstone interbedded with two pebble- to cobble-conglomerate lenses of up to 1.5 m thick (fig. 12). The lowermost part of the sandstone bed, although partly weathered, consists mainly of large-scale trough crossbeds (0.45 to 1 m high) with steep foresets. This sequence of sedimentary structures is capped by 30-cm-thick, ripple laminated, fine-grained to silty sandstone. This fine-grained sandstone, which is in turn overlain by coarse-grained sandstone, contains small-scale trough crossbeds ranging from 30 to 45 cm high (see fig. 12). Sparse large-scale trough crossbeds (up to 1 m high) are present among these small-scale trough crossbeds. Contact between the coarse- and fine-grained sandstone beds is an erosional surface. Other erosional surfaces are observed in the Chuitna conglomeratic sandstone bed as continuous internal scour surfaces within a 90- to 120-m-wide outcrop (see fig. 13); thus, these surfaces are continuous or have a high order of lateral magnitude. The internal scour surfaces separate the thinning-upward, 4- to 20-m-thick, conglomerate-sandstone units in the Chuitna conglomeratic sandstone bed (fig. 13). Foresets of the trough crossbeds in the Chuitna conglomeratic sandstone bed are dominantly southwest dips.

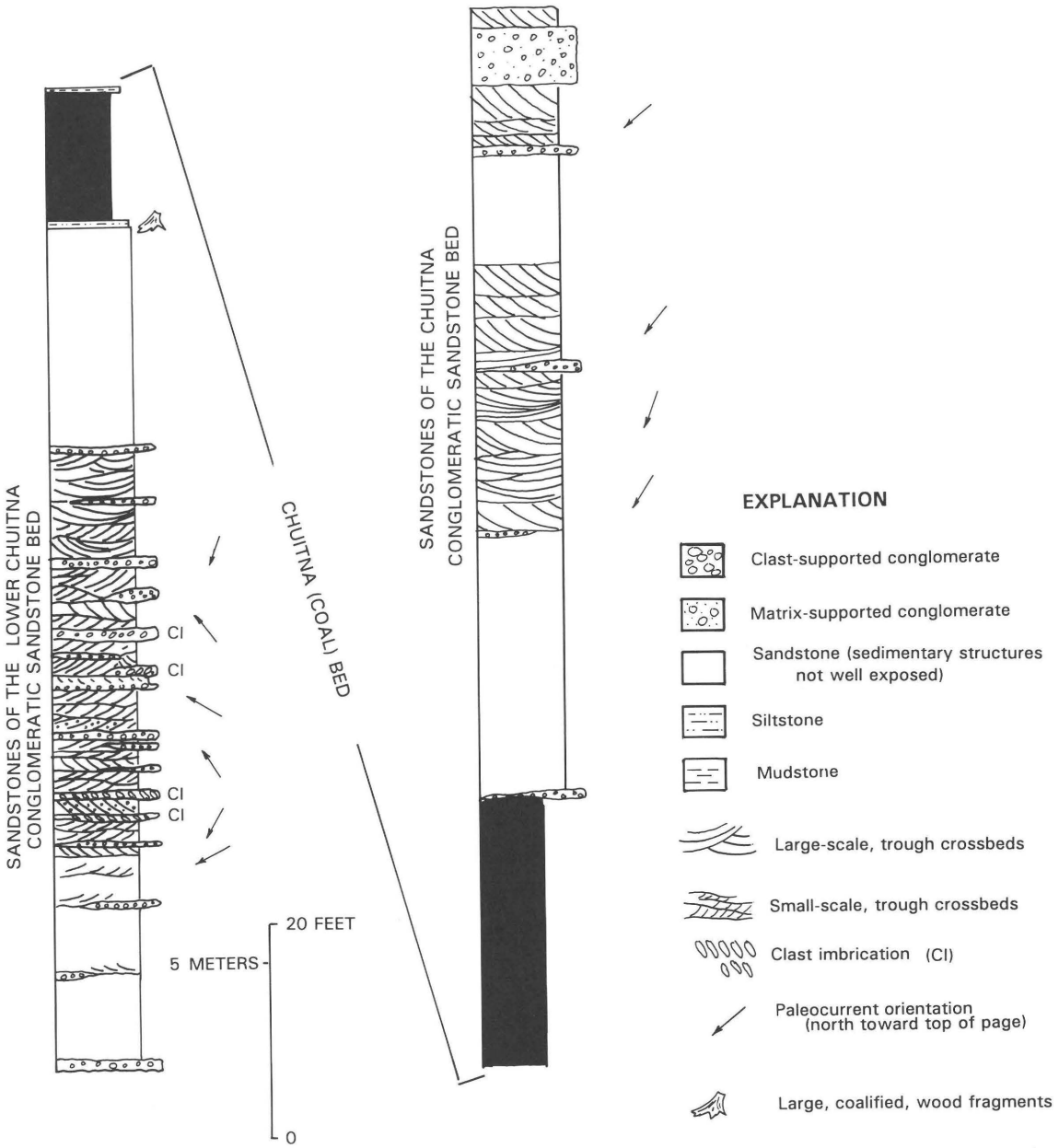

Figure 8. Facies profile of informally named Lower Chuitna and Chuitna conglomeratic sandstone beds and intervening Chuitna (coal) bed. Reconstructed from measured section B (see fig. 2 for location).

Diagrammatic field sketches of the vertical and lateral variations in sedimentary structures of the Chuitna conglomeratic sandstone bed display a complicated and heterogeneous architecture (see figs. 9, 10). A diagrammatic sketch showing a cross section of the 23- to 28-m-thick Chuitna conglomeratic sandstone bed at the confluence of the Chuit Creek and Chuitna River (fig. 9) shows divergent patterns of vertical organization of sedimentary structures between internal scour surfaces. The Chuitna conglomeratic sandstone bed can be subdivided into four, 4.5- to 6.7-m-thick sandstone bodies separated by three internal scour surfaces (IS_1, IS_2, and IS_3), which are present above the basal scour surface (BS) on top of the Chuitna (coal) bed. The lower sandstone body above the BS, which is partly covered, contains large-scale trough crossbeds (about 0.6 m high and 3 m long) in its upper part. The sandstone body above IS_1

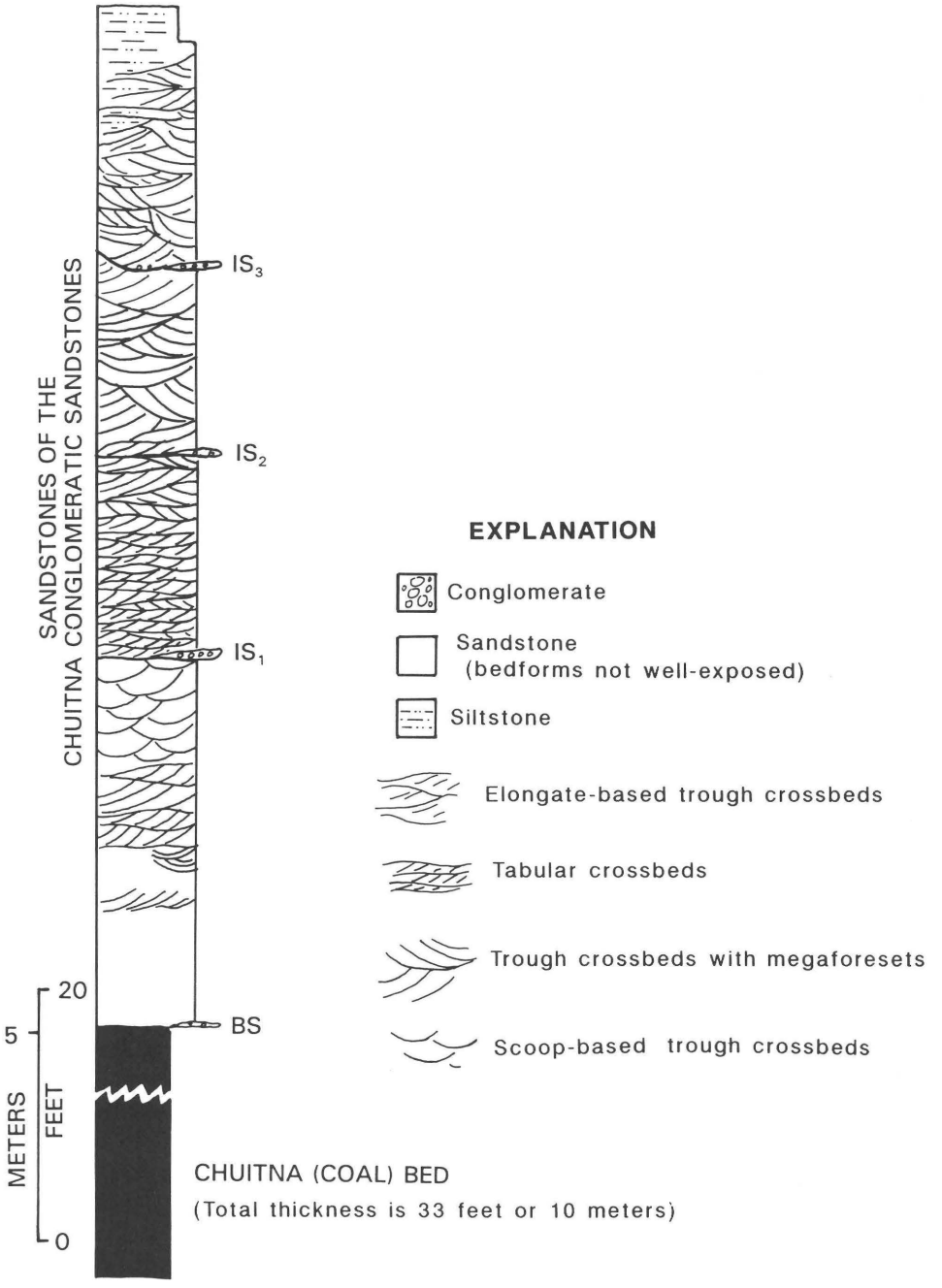

Figure 9. Facies profile of informally named Chuitna conglomeratic sandstone bed above Chuitna (coal) bed in the Chuit Creek-Chuitna River confluence. Reconstructed from measured section J (see fig. 2 for location). BS, basal scour surface; (IS_1, IS_2 and IS_3), three internal scour surfaces.

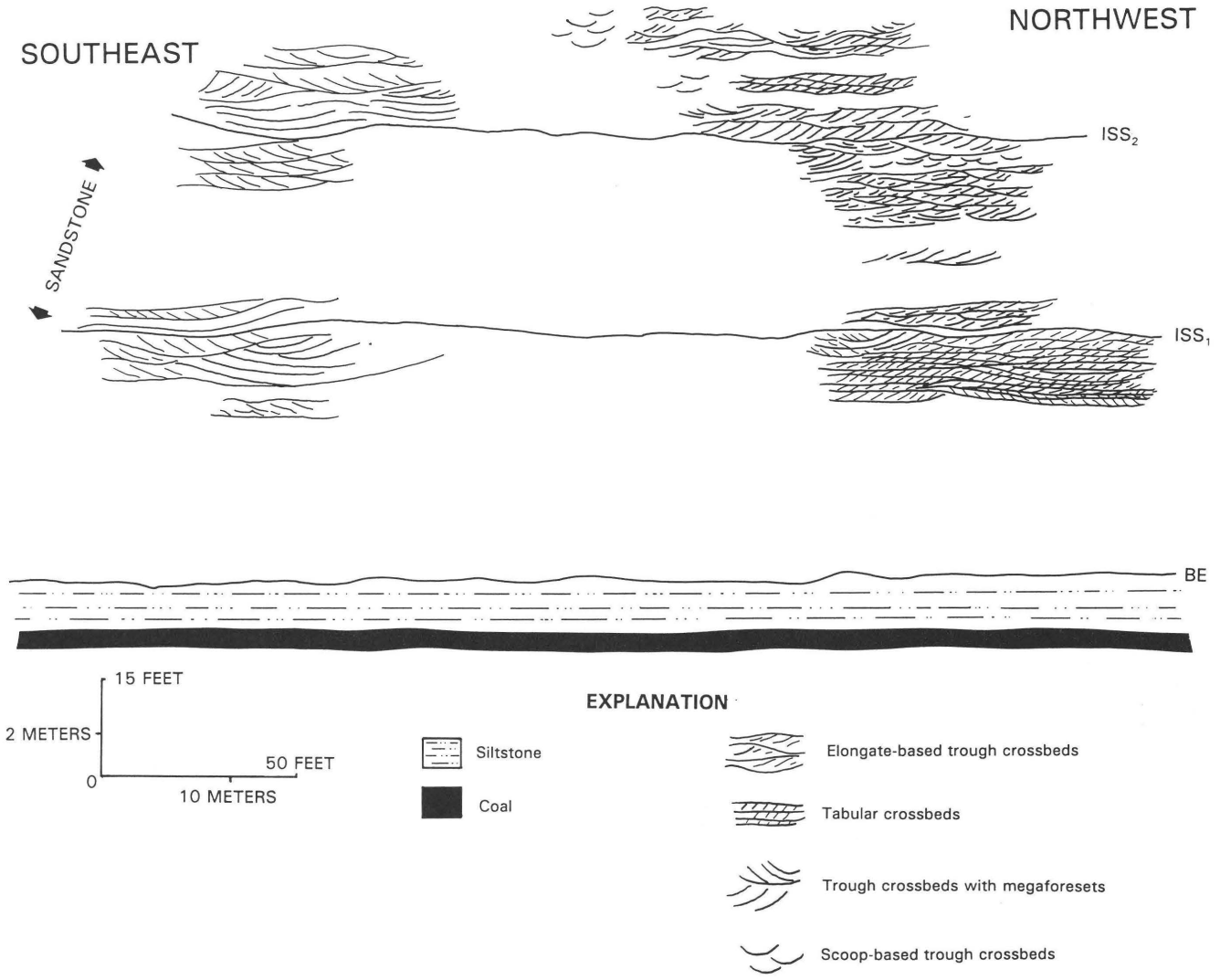

Figure 10. Two-dimensional facies profile of upper informally named Chuitna conglomeratic sandstone bed immediately south of the Chuit Creek-Chuitna River confluence. Same locality as measured section 16 of Adkison and others (1975). See figure 2 for location of measured section. BE, basal erosional surface; (ISS_1 and ISS_2), two internal scour surfaces.

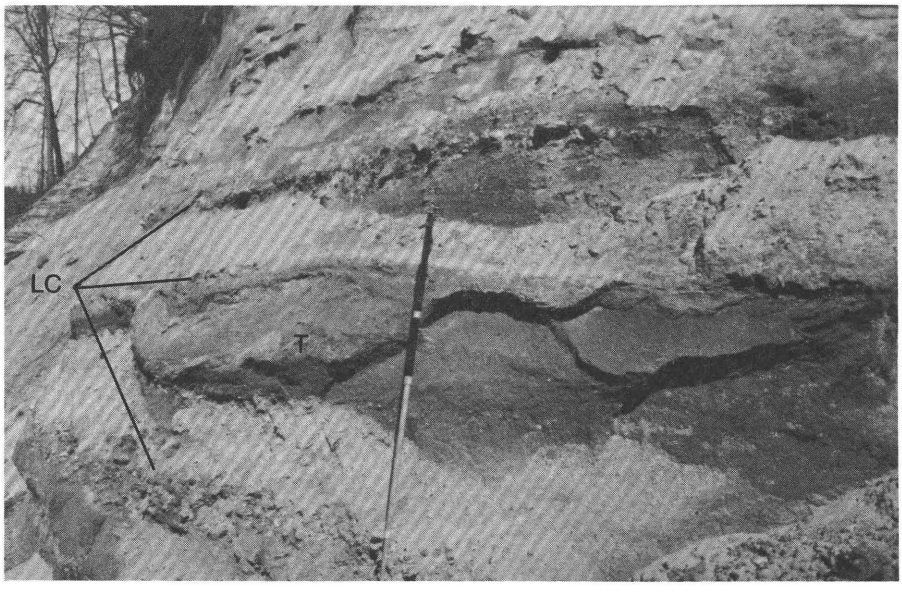

Figure 11. Closely spaced, pebble-lag-conglomerate lenses (LC) and intervening trough crossbeds (T) in informally named Lower Chuitna conglomeratic sandstone bed. Jacob's staff in center of photo is 1.5 m tall.

consists of a lower unit of large-scale, elongate-based trough crossbeds (about 1 m high to >7 m long). The upper unit of this sandstone body contains large-scale (about 0.6 m high and 1.5 m long), scoop-based, trough crossbeds. The sandstone body above IS_2 comprises small-scale (about 0.3 m high and 3 m long), tabular crossbed sets to medium-scale (about 0.3 to 0.6 m high and 3 to 4.5 m long), elongate-based, trough crossbeds. The sandstone body above IS_3 consists mainly of very large-scale trough crossbeds (about 1 to 1.3 m high and 1.5 to 3 m long). Large foresets are well developed within these trough crossbeds. Locally, the large-scale trough crossbeds grade laterally into small, elongate-based, trough crossbeds (about 0.6 to 1 m high and >3 m long).

Figure 12. Large-scale trough crossbeds (T) and lag conglomerate (LC) in informally named Chuitna conglomeratic sandstone bed. Pen below LC is 11 cm tall.

Figure 13. Outcrop of sandstones of informally named Chuitna conglomeratic sandstone bed showing internal scour surfaces (dark units between sandstone bodies) that separate sandstone bodies, which thin upward. Bottom width of photo represents approximately 25 m.

A diagrammatic field sketch (fig. 10) of the upper 15- to 18-m-thick Chuitna conglomeratic sandstone bed along the valley wall southwest of the confluence of the Chuit Creek and Chuitna River depicts lateral variations of the crossbed types within a 90-m-wide outcrop. Here, the Chuitna conglomeratic sandstone bed consists of three sandstone bodies (approximately 4.5 to 7.5 m thick), separated by a basal erosional surface (BE) and two internal scour surfaces (ISS_1 and ISS_2). The BE directly overlies the first unnamed coal bed, and ISS_1 is where the second unnamed coal bed pinches out. Both coal beds split the upper Chuitna conglomeratic sandstone bed in the northern part of the study area (see fig. 6). The upper part of the sandstone body above the BE consists, from base to top, of large-scale (0.6- to 1-m-thick) and small-scale (15- to 30-cm-thick), elongate-based trough crossbeds. This sequence of sedimentary structures grades laterally southward into very large-scale (0.6 to 1.5 m), elongate-based, trough crossbeds that are internally partitioned by cross laminae. The sandstone body above ISS_1 consists of small-scale (16 cm high) elongate-based, trough crossbeds and tabular crossbeds overlain by ripple lamination, which grade southward into large-scale (1.5 m high), elongate-based, trough crossbeds. The sandstone body above ISS_2 consists of large-scale (about 0.6 m high and 6 m long), elongate-based, trough crossbeds grading upward into large-scale (about 1.2 to 1.5 m high and >3 m long), scoop-based, trough crossbeds. These sedimentary sequences grade southward to large-scale (0.6 to 2.5 m high), elongate-based, trough crossbeds.

FACIES PROFILES OF THE SILTSTONES, MUDSTONES, CARBONACEOUS SHALES, AND COALS

Vertical-facies profiles (figs. 14, 15) of the fine-grained deposits (siltstones and mudstones) were constructed in combination with the organic deposits (carbonaceous shales and coals). Description of facies sequences in the fine-grained and organic deposits represents facies associations (facies which tend to occur together). Facies of these two types of deposits are linked because they are found either as matrix between the coarse-grained deposits (conglomeratic sandstones) or marginal to the conglomeratic sandstones, or both. Facies sequences in these deposits are described here as proximal and distal to the conglomeratic sandstones. This concept, in turn, facilitates interpretations of the temporal depositional environments of the combined coarse- and fine-grained and organic deposits.

PROXIMAL-FACIES PROFILE

A facies profile proximal to the Lower Chuitna conglomeratic sandstone bed (fig. 14) shows a generally coarsening-upward sequence of siltstones and mudstones that are interbedded with thin to thick, silty sandstones south of the Chuit Creek-Chuitna River confluence. Although the facies sequence is dominated by siltstone and sandstone, the upper, sandy part of the sequence contains siltstone and mudstone interbeds. The sandstones are partly parallel laminated to platy bedded and ripple laminated. Laminations of the sandstones are commonly enhanced by micaceous concentrates, thin coaly stringers, and carbonaceous plant fragments. Locally, sedimentary structures have been destroyed by root bioturbations or destroyed by compaction during coalification of tree trunks and wood fragments. Siltstones are horizontally laminated and rippled; laminae are highlighted by abundant, macerated, carbonaceous, plant fragments and leaf impressions. Coaly stringers and lenses are commonly interbedded with the siltstones. The mudstones are very thin, subordinate, carbonaceous, and contain root impressions.

DISTAL-FACIES PROFILE

The distal-facies profile (fig. 15) is represented by a mudstone-dominated sequence, which is laterally distant (see section A, fig. 6) from the Chuitna conglomeratic sandstone bed exposed in the Chuit Creek valley wall in the northeastern part of the study area. Here, the facies sequence, from its lower part (partly exposed above the Chuit Creek) to its upper part, is subdivided into three subfacies: (1) mudstone-silty sandstone, (2) siltstone-silty sandstone, and (3) mudstone-siltstone subfacies.

The lower mudstone-silty sandstone subfacies consists of heavily bioturbated, dark-gray mudstones interbedded with bioturbated, ripple-laminated, silty sandstones. The mudstones exhibit vertical and horizontal, irregular, smooth-walled, animal burrows that are as much as 0.6 cm across and 3 cm long (fig. 16). Burrowed horizons extend into the silty sandstone interbeds, disrupting their asymmetrical ripple laminations. The silty sandstones range from less than 2.5 cm to 15 cm in thickness and occur in the mudstones from 10 cm to 30 cm apart. They are laterally discontinuous and commonly pinch out in mudstones over distances of a meter or less (fig. 17).

The middle siltstone-silty sandstone subfacies consists of sparsely bioturbated, micaceous, rippled siltstones interbedded with bioturbated, rippled, silty sandstones. Horizontal, smooth-walled animal burrows that are 1.5 cm in diameter and a few centimeters long are common trace fossils in both rock types. The silty sandstones range from 7 to 15 cm in thickness and are laterally continuous for more than 1.5 m. These sandstones are more commonly interbedded with the siltstones than those of the lower mudstone-silty sandstone subfacies; both subfacies represent a generally coarsening-upward interval.

The upper mudstone-siltstone subfacies comprises interbedded, sparsely bioturbated and commonly rooted mud-

stone and siltstone. The mudstone is dark gray because of abundant carbonaceous plant fragments. The siltstone units are thin (as much as 1 cm thick), lenticular, discontinuous, and partly ripple laminated. The uppermost part of this subfacies consists of a carbonaceous mudstone with abundant coaly stringers and root traces. This subfacies is directly overlain by the partly exposed Chuitna (coal) bed, which contains a 2.5-cm-thick mudstone parting.

INTERPRETATIONS AND CONCLUSIONS

The fluvial origin of the Tyonek Formation had been established by early workers (Barnes, 1966; McGee, 1972; Adkison and others, 1975; Hite, 1976) and, in particular, the braided-stream origin of this formation was determined by Dickinson and Campbell (1978). Our study presents facies sequences and associations that provide evidence for more specific alluvial settings in a continuum of river, overbank-flood plain, and mire depositional environments. The following discussion focuses on interpretations of the stratigraphic- and sedimentologic-facies frameworks.

The basal erosional surfaces of the conglomeratic sandstones and their vertical change in grain size indicate that deposition occurred in waning channelized flow following an initial erosive stage. The internal-facies architecture (Miall, 1978; 1993) suggests that waning flow was interrupted by spatial separation of flow regimes in smaller

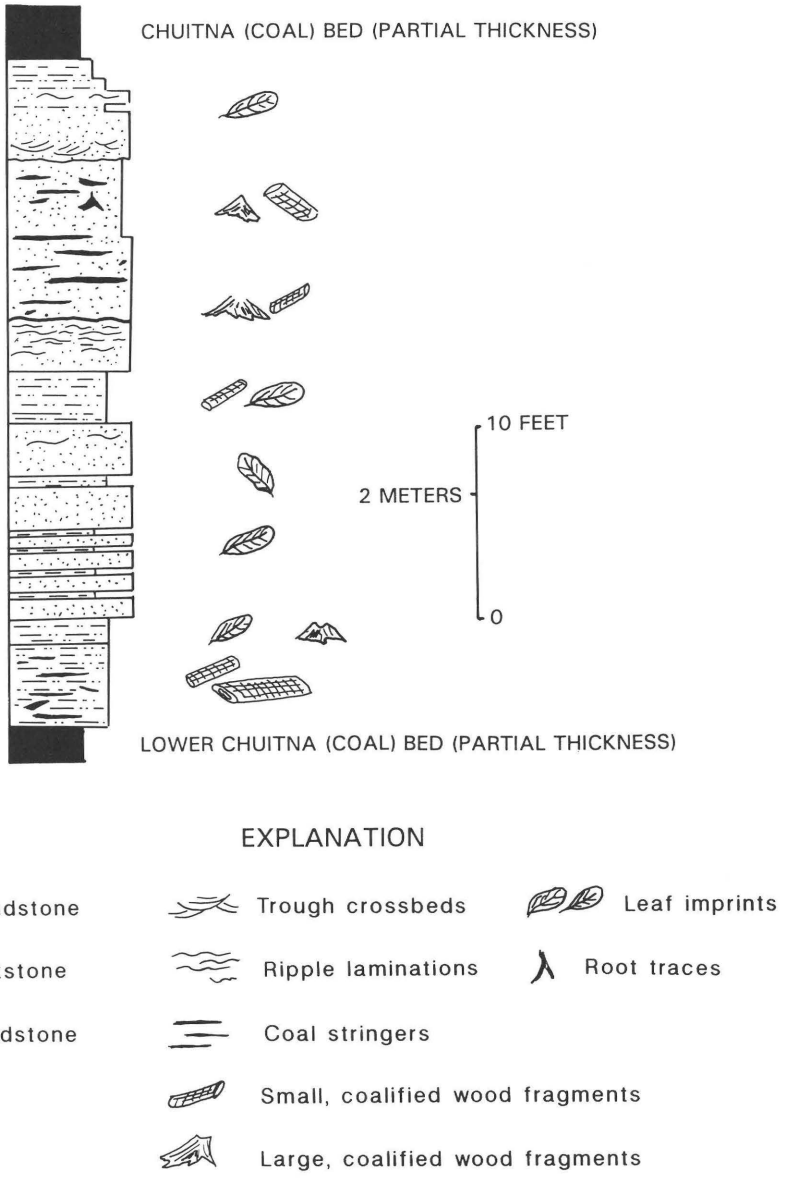

Figure 14. Facies profile proximal to informally named Lower Chuitna conglomeratic sandstone bed and adopted from measured section 16 (see fig. 2 for location) of Adkison and others (1975).

channelized flows. The highly discontinuous internal scour surfaces of the sandstones of the Lower Chuitna conglomeratic sandstone bed indicate deposition by multiple, narrow, shallow, channelized flows. The multistory channel conglomerate-sandstone units, which cut into each other vertically and laterally, are typical of braided stream deposits (Williams and Rust, 1969; Smith, 1970, 1974; Ramos and Sopena, 1983). In gravelly braided streams, such as those that formed the sandstones of the Lower Chuitna sandstone bed, the bedload gravels are transported during high-flow regime (that is, high discharge or flood event; Smith, 1974), whereas longitudinal bars with crude horizontal to imbricate clast stratification are developed during waning flow. During waning flow, the coarse clastic materials act as traps for finer sediments, such as sands, which are transported in suspension above the gravel. As flow discharge is reduced, bar development stops and the bar top emerges. Continued reduction of discharge diverts active channelized-flow and sand infilling into narrow, shallow channels lateral to the bar, thus permitting distinction of individual bars.

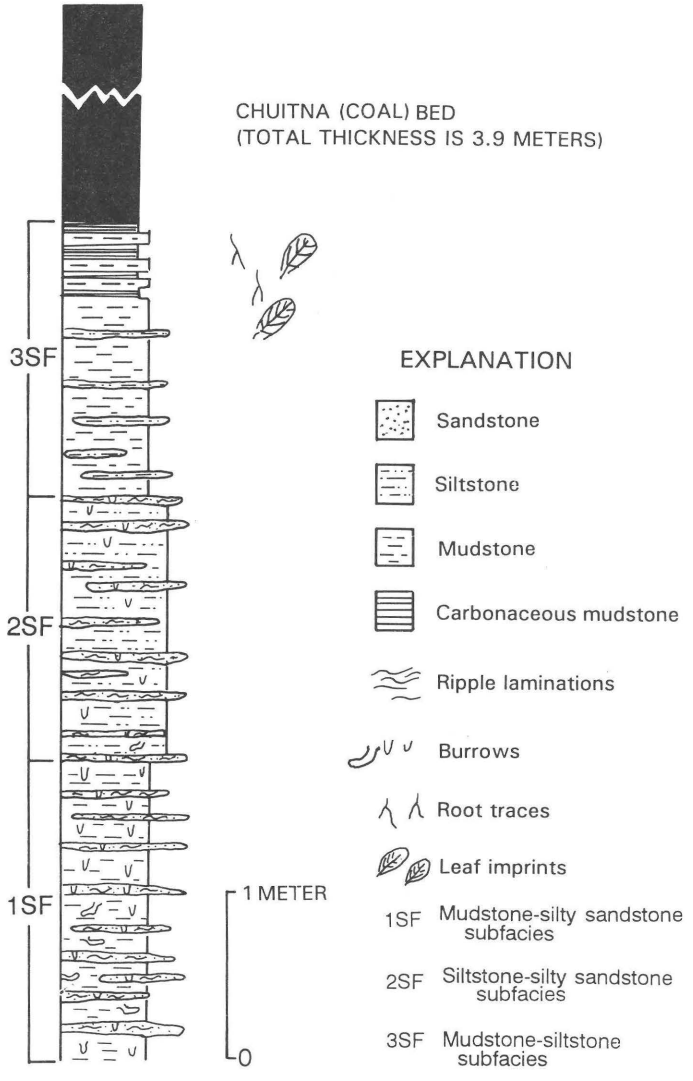

Figure 15. Facies profile distal to sandstones of informally named Lower Chuitna conglomeratic sandstone bed reconstructed from measured section A (see fig. 2 for location).

Trough crossbeds of the conglomerate-sandstone units may have formed by the downstream migration of in-channel dunes and megaripples. These in-channel dunes and megaripples may have developed downstream on submerged longitudinal bars. Large trough crossbeds of wider and deeper channels were probably deposited during near-bankfull discharge, when much of the braidbelt acted as one channel. The lag conglomerates between successive bars reflect flood gravels or remnant lags formed during increased flow that was strong enough to retransport the sand, or both. The channelized flows in these braided streams are interpreted as divergent because the paleocurrent measurements and clasts imbrication indicate bimodal northwest and southwest directions. That is, paleoflow directions changed alternately between northwest and southwest in response to channel migration.

The sandstones of the Chuitna conglomeratic sandstone bed, based on the multiple internal scours overlain by lag conglomerates, were also deposited by braided streams. However, unlike the braided stream sandstones of the Lower Chuitna braided stream sandstones, the Chuitna conglomeratic sandstone beds were deposited in wide and deep channels. This interpretation is indicated by continuous internal scour surfaces. The conglomerate-sandstone units between the internal scour surfaces are increasingly thinner from bottom to top, indicating an upward-shoaling-channel condition. However, local upward thickening of the conglomerate-sandstone units between the internal scour surfaces was also observed, suggesting temporal deepening of the channel condition. This deepening in channel depths indicates that the braidbelt may be subdivided into a passive belt drained by narrow and shallow channels and an active belt drained by wide and deep channels similar to those observed in modern braided rivers (Smith, 1971, 1974; Boothroyd and Ashley, 1975; Bristow, 1987).

Vertical and lateral variations (architectural framework) of the sedimentary structures (see figs. 8-10) of the conglomerate-sandstone units between the internal scour surfaces reflect very highly variable fluctuations of channelized flow discharges. As in the Lower Chuitna braided deposits, transportation and deposition of the bimodal sediment loads (gravels versus sands) occurred during separation of flow regimes. High-flow regime during high discharge governed transportation and deposition of gravel bars. This regime was succeeded by low-flow regime at low discharge, which governed sand accumulation on the gravel bars. However, unlike the primarily downstream sand dune and bar migrations in the Lower Chuitna braided streams, the presence of tabular crossbeds in the Chuit-

na braided streams reflect both downstream and transverse migration of bars. Thickening-upward sedimentary structures in conglomeratic sandstones between the internal scour surfaces probably indicates deepening, high-flow regime, presumably at bankfull discharge (Jackson, 1975). The thickness variations of cross sets within the Chuitna and Lower Chuitna conglomeratic sandstone beds suggest rise and fall of water levels due to discharge fluctuations.

Tabular crossbed sets with flat bottoms traceable for a few meters may be found simultaneously over longitudinal and transverse bars. These crossbed sets may be produced during high-flood stage when water was not restricted by channelized flow (Ramos and Sopena, 1983). A decrease in energy from this high-flood stage may have caused sands to move as dunes and megaripples, thus forming the scoop- and elongate-based, trough crossbeds (Harms and Fahnestock, 1965; Harms, 1969). The difference in the basal shape of the crossbeds is a function of migration of sands parallel to, or at angle to, local flow directions (Harms and others, 1982). The large-scale, trough crossbeds with

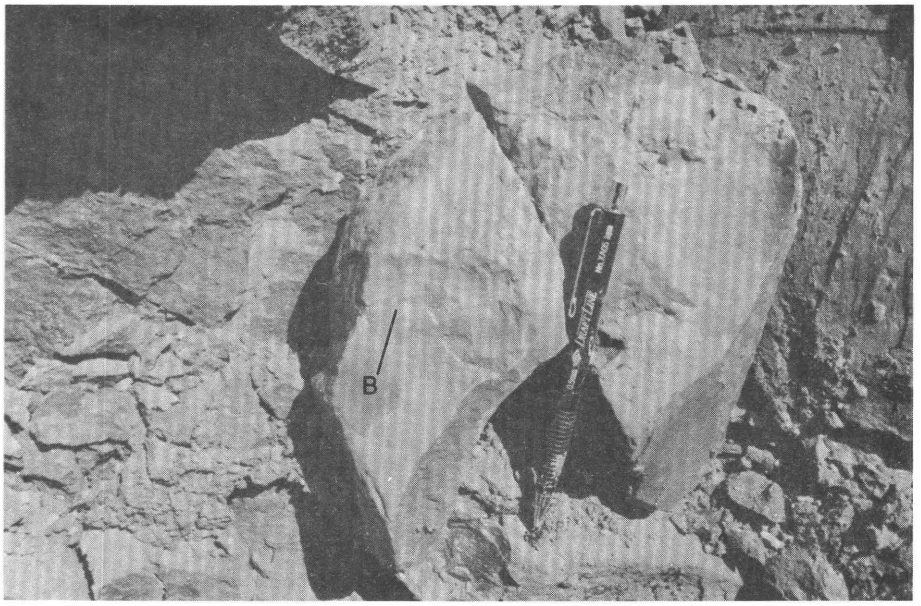

Figure 16. Vertical burrows (B) in mudstone of the distal-facies profile.

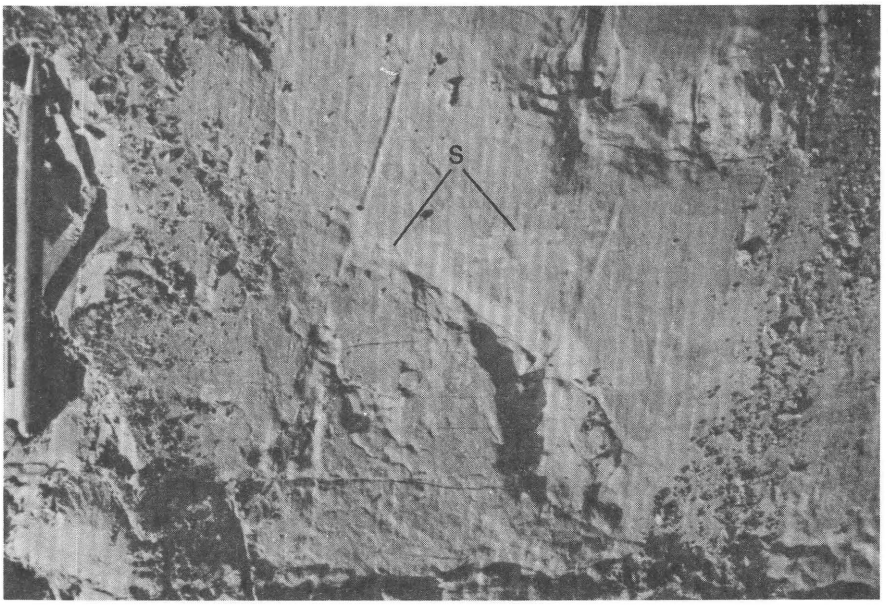

Figure 17. Lenticular, discontinuous, ripple-burrowed, silty sandstone (S) of the distal-facies profile.

megaforesets are overlain by small, elongate-based, trough crossbeds in the upper part of the sedimentary-structure sequences (see fig. 9). This succession indicates infilling of channels by megaripples at bankfull stage and by dunes following a reduced-flow discharge.

The vertical sequence of sedimentary structures in the conglomeratic sandstones, which are bounded by internal scour surfaces (see fig. 9), and which are probably widely separated in time, may be interpreted in space (fig. 10). Variations of the crossbed types within the same channelized (between internal scour surface) conglomeratic sandstones reflect bar development in the braided streams. For example, the trough crossbeds of the conglomeratic sandstones between BE, ISS_1, and ISS_2 in figure 10, which are dominantly small to medium scale, and elongate-based, are locally overlain by ripple laminations (see sandstone above ISS_1). The ripple laminations grade laterally southeastward to large-scale, scoop-based, trough-crossbed sets. This organization suggests that stacking of small bedforms (dunes and transverse bars and bar-top ripple laminae) provided a single slip face on which large bedforms developed (see fig. 10). Similar bar formation is observed of medium- to large-scale, trough crossbeds in the conglomeratic sandstone above ISS_2. Such bar evolution is commonly observed in flood cycles in the modern Brahmaputra River (Coleman, 1969). That the Chuitna braided streams displayed less divergent flows as compared with the Lower Chuitna braided streams is indicated by interpreted paleoflows suggesting a dominantly southwest orientation of flow.

The Lower Chuitna and Chuitna braided streams are confined by fine-grained sediments of levee-overbank and flood plain environments, and organic deposits of mires as represented by the proximal- and distal-facies profiles, respectively. The siltstone-sandstone-dominated facies profile reflect levee-overbank sedimentation lateral to the sandstones of the Lower Chuitna conglomeratic sandstone bed (see fig. 14). Intercalation of mudstones, siltstones, and silty sandstones in this facies indicates that deposition of suspended and bedload sediments occurred repeatedly during bankfull river stages. Root marks, coalified tree trunks, and wood fragments, and coaly stringers in this facies suggest riparian vegetal growth and localized accumulation of vegetal remains.

The mudstone-dominated distal-facies profile represents flood plain sedimentation. These are present lateral to the upper part of the Lower Chuitna conglomeratic sandstone bed and directly underlying the Chuitna (coal) bed (see fig. 15). The heavily bioturbated, mudstone-silty sandstone subfacies records sedimentation in a flood plain lake far removed from active channel activity. The burrowed silty sandstone lenses encased in mudstone resemble tidal flat deposits. These fine-grained sediments were probably deposited by sheet flows during overtopping, and channelized flows during breaching of the levee-overbank at bankfull river discharges, or both. The overlying sparsely bioturbated siltstone-silty sandstone subfacies indicates sedimentation in a shoaling flood plain lake. The coarsening-upward characteristic of the mudstone-silty sandstone and siltstone-silty sandstone subfacies suggests vertical accretion of suspended overbank-flood sediments and lateral accretion of prograding sand-laden overbank and (or) crevasse splay currents. The mudstone-siltstone subfacies overlying this coarsening-upward facies represents a return to vertical accretion of overbank flood sediments that were gradually occupied by vegetation. Subsequently, the region was permanently transformed into a mire, as indicated by the overlying Chuitna (coal) bed.

The presence of coaly units in the proximal- and distal-facies profiles suggest that mires extended from the levee-overbank areas well into the flood plain lateral to the braided streams. However, the presence of the thick Chuitna (coal) bed immediately above the sandstones of the Lower Chuitna conglomeratic sandstone bed suggests that the mire encroached on the channelized region after abandonment of the channels. Development of the uniformly thick Chuitna (coal) bed (Barnes, 1966, pl. 7), oriented northwest-southeast, is parallel to the direction of elongation of the underlying Lower Chuitna conglomeratic sandstone bed. This relation suggests that the abandoned braided stream sands served as a platform on which a raised mire formed and was protected from influx of flood detritus. The stratigraphic framework of the deposits of the Lower Chuitna conglomeratic sandstone bed, Chuitna conglomeratic sandstone bed, and unnamed conglomeratic sandstone suggests that the direction of abandonment of the braided streams was toward topographically low areas. These areas are typically underlain by thin, river-flood plain-mire deposits.

Data on local channel and flood plain-mire sedimentation provide a better insight to the regional setting of the braided streams of the Tyonek Formation. The west-northwest to east-southeast direction of elongation of the conglomeratic sandstones (that is, Lower Chuitna conglomeratic sandstone bed), combined with the northwest and southwest directions of transport of sediments based on the paleocurrent measurements and pebble-cobble imbrications, suggest an overall west- to southwest-flowing, braided, fluvial system. This fluvial system probably drained a paleovalley immediately south of, and constrained by, the southwest-northeast-trending (downthrown south side) Castle Mountain fault. This fault, which was active during deposition of the strata in the study interval, also controlled Paleocene and Eocene paleodrainages in the Matanuska Valley (Flores and Stricker, 1993, in press) 200 km northeast of the Chuit Creek-Chuitna River drainage basin. Jurassic to Cretaceous granitic rocks north of the fault may have served as local source of the Tyonek sediments. However, other Jurassic to Cretaceous greenstone, diorite, and interbedded slate and graywacke basement rocks in the Chugach uplift, and Jurassic to Cre-

taceous marine and nonmarine sedimentary rocks intruded by volcanic and plutonic rocks in the Talkeetna uplift (Barnes and Payne, 1956; Grantz and Jones, 1960; Barnes, 1962; Winkler, 1992), may be the main provenance, which was located 160 to 210 km east-northeast of the study area. Dickinson and others (in press) suggest that the ancestral drainages of the Matanuska and Susitna Rivers were possible point sources of the sedimentary deposits of the Tyonek Formation.

REFERENCES CITED

Adkison, W.L., and Newman, K.R., 1973, Lithologic characteristics and palynology of Upper Cretaceous and Tertiary rocks in the Deep Creek Unit well, Kenai Peninsula, Alaska: U.S. Geological Survey open-file report, 271 p., 1 pl.

Adkison, W.L., Kelley, J.S., and Newman, K.R., 1975, Lithology and palynology of Tertiary rocks exposed near Capps Glacier and along Chuitna River, Tyonek quadrangle, southern Alaska: U.S. Geological Survey Open-File Report 75-21, 58 p., 1 pl.

Barnes, F.F., 1962, Geologic map of lower Matanuska Valley, Alaska: U.S. Geological Survey Miscellaneous Investigations Series Map I–359, scale 1:63,360.

———1966, Coal resources of the Beluga-Yentna region, Alaska: U.S. Geological Survey Bulletin 1202–C, p. 1–54.

Barnes, F.F., and Payne, T.G., 1956, The Wishbone Hill district, Matanuska coal field, Alaska: U.S. Geological Survey Bulletin 1016, 88 p.

Boothroyd, J.C., and Ashley, G.M., 1975, Process, bar morphology and sedimentary structures on braided outwash fans, Northeastern Gulf of Alaska, *in* Jopling, A.V., and McDonald, B.C., eds., Glaciofluvial and glaciolacustrine sedimentation: Society of Economic Paleontologists and Mineralogists Special Publication No. 23, p. 193–222.

Bristow, C.S., 1987, Brahmaputra River—Channel migration and deposition, *in* Ethridge, F.G., Flores, R.M., and Harvey, M.D., eds., Recent developments in fluvial sedimentology: Society of Economic Paleontologists and Mineralogists Special Publication No. 39, p. 63–74.

Calderwood, K.W., and Fackler, W.C., 1972, Proposed stratigraphic nomenclature for Kenai Group, Cook Inlet Basin, Alaska: American Association of Petroleum Geologists Bulletin, v. 56, p. 739–754.

Coleman, J.M., 1969, Brahmaputra River—Channel processes and sedimentation: Sedimentary Geology, v. 3, p. 129–239.

Detterman, R.L., Plafker, George, Tysdal, R.G., and Hudson, Travis, 1976, Geology and surface features along part of the Talkeetna segment of the Castle Mountain-Caribou fault system: U.S. Geological Survey Miscellaneous Field Studies Map MF–738, scale 1:1,000,000.

Dickinson, K.A., and Campbell, J.A., 1978, Sedimentary facies in Tertiary rocks in the Tyonek quadrangle, *in* Geological Survey Research 1978: U.S. Geological Survey Professional Paper 1100, p. 84.

Dickinson, K.A., Campbell, J.A., and Dula, W.F., Jr., in press, Reconnaissance geology and geochemistry and uranium potential of the Tertiary continental sedimentary rocks in the northwestern part of the Cook Inlet area, Alaska: U.S. Geological Survey Bulletin.

Flores, R.M., and Stricker, G.D., 1993, Early Cenozoic depositional systems, Wishbone Hill district, Matanuska coal field, Alaska, *in* Dusel-Bacon, Cynthia, and Till, A.B., eds., Geologic Studies in Alaska by the U.S. Geological Survey, 1992: U.S. Geological Survey Bulletin 2068, p. 101–117.

———in press, Responses of coal splitting and associated drainage pattern to syntectonism in the Paleocene and Eocene Chickaloon Formation, Matanuska coal field, Alaska, *in* Rao, P.D., ed., Focus on Alaska coal '93: Proceedings, American Institute of Mining Engineers Conference, Anchorage, AK, May 5–8, 1993.

Fuchs, W.A., 1980, Tertiary tectonic history of the Castle Mountain-Caribou fault system in the Talkeetna Mountains, Alaska: Ph.D. dissertation, Salt Lake City, University of Utah, 152 p.

Grantz, Arthur, 1966, Strike-slip faults in Alaska: U.S. Geological Survey open-file report 267, 82 p.

Grantz, Arthur, and Jones, D.L., 1960, Stratigraphy and age of the Matanuska Formation, south central Alaska: American Association of Petroleum Geologists Bulletin, v. 45, p. 1762–1765.

Harms, J.C., 1969, Hydraulic significance of some sand ripple: Geological Society of America Bulletin, v. 80, p. 363–396.

Harms, J.C., and Fahnestock, R.K., 1965, Stratification, bedforms, and flow phenomena (with example from the Rio Grande), *in* Middleton, G.V., ed., Primary sedimentary structures and their hydrodynamic interpretation: Society of Economic Paleontologists and Mineralogists Special Publication No. 12, p. 84–115.

Harms, J.C., Southard, J.B., and Walker, R.G., 1982, Structures and sequences in clastic rocks: Society of Economic Paleontologists and Mineralogists Short Course No. 9, 249 p.

Hite, D.M., 1976, Some sedimentary aspects of the Kenai Group, Cook Inlet, Alaska, *in* Miller, T.P., ed., Recent and ancient sedimentary environments in Alaska: Alaska Geological Society Proceedings, Anchorage, Alaska, April 2–4, 1975, p. I1–I22.

Jackson, R.G., 1975, Velocity-bed-form-texture patterns of meander belts in the Lower Wabash River of Illinois and Indiana: Geological Society of America Bulletin, v. 86, p. 1511–1522.

Kirschner, C.E., and Lyon, C.A., 1973, Stratigraphic and tectonic development of Cook Inlet Petroleum Province, *in* Pitcher, M.G., ed., Arctic geology: American Association of Petroleum Geologists Memoir 19, p. 396–407.

Magoon, L.B., Adkison, W.L., and Egbert, R.M., 1976, Map showing geology, wildcat wells, Tertiary plant fossil localities, K-Ar age dates, and petroleum operations, Cook Inlet area, Alaska: U.S. Geological Survey Miscellaneous Investigations Map I–1019, scale 1:250,000.

McGee, D.C., 1972, Coal reserves Beluga and Chuitna Rivers and Capps Glacier areas, Alaska: Alaska Geological and Geophysical Surveys, Open-File Report 35, 5 p., 2 pls.

McFarland, C.E., 1987, Placer's Beluga coal project-Mining and marketing plans, *in* Rao, P.D., ed., Focus on Alaska's Coal '86: Mineral Industry Research Laboratory Report Number 72, p. 127–131.

Miall, A.D., 1978, Lithofacies types and vertical profile models in braided river deposits—A summary, *in* Miall, A.D., ed.,

Fluvial sedimentology: Canadian Society of Petroleum Geologists, p. 597–604.

———1993, The architecture of fluvial-deltaic sequences in the upper Mesaverde Group (Upper Cretaceous), Book Cliffs, Utah: Geological Society Special Publication, No. 75, p. 305–332.

Odum, J.K., Gardner, C.A., Yehle, L.A., Schmoll, H.R., and Dearborn, L.L., 1983, Preliminary lithologic, geotechnical, and geophysical data from drill hole CW-81-2, Chuitna west coal field, Cook Inlet region, Alaska: U.S. Geological Survey Open-file Report 83-78, 12 p.

Oil and Gas Journal, 1993, ARCO'S Cook Inlet, Beaufort strikes possible giants: v. 91, p 20.

Petroleum Information Corporation, 1991, ARCO completes Upper Cook Inlet oil discovery: Alaska Report, v. 37, p. 1.

Petroleum Information Corporation, 1993, Phillips stakes stepout from Sunfish discovery: Alaska Report Section I, v. 39, p. 4–5.

Ramos, A., and Sopena, A., 1983, Gravel bars in low-sinuosity streams (Permian and Triassic, central Spain), *in* Collinson, J.D., and Lewin, J., eds., Modern and ancient fluvial systems: International Association of Sedimentologists Special Publication No. 6, p. 301–312.

Ramsey, J.P., 1981, Geology-coal resources and mining plan for the Chuitna River field, Alaska, *in* Rao, P.D., ed., Focus on Alaska's coal '80: Mineral Industry Research Laboratory Report Number 50, p. 111–121.

Stiles, R.B., and Franklin, L.C., 1987, Diamond Chuitna project summary, *in* Rao, P.D., ed., Focus on Alaska's coal '86: Mineral Industry Research Laboratory Report Number 72, p. 132–141.

Smith, N.D., 1970, The braided stream depositional environment: Comparison of the Platte River with some Silurian clastic rocks, North-Central Appalachians: Geological Society of America Bulletin, v. 81, p. 2993–3014.

Smith, N.D., 1971, Transverse bars and braiding in the Lower Platte River, Nebraska: Geological Society of America Bulletin, v. 82, p. 3407–3420.

Smith, N.D., 1974, Sedimentology and bar formation in the Upper Kicking Horse River, a braided outwash stream: Journal of Geology, v. 82, p. 205–224.

Williams, P.F., and Rust, B.R., 1969, The sedimentology of a braided river: Journal of Sedimentary Petrology, v. 39, p. 649–679.

Winkler, G.R., 1992, Geologic map and summary geochronology of the Anchorage 1°×3° quadrangle, southern Alaska: U.S. Geological Survey Miscellaneous Investigations Map I–2283, 1 sheet, scale 1:250,000.

Wolfe, J.A., Hopkins, D.M., and Leopold, E.B., 1966, Tertiary stratigraphy and paleobotany of the Cook Inlet region, Alaska: U.S. Geological Survey Professional Paper 398–A, A1–A29.

Reviewers: Kendell A. Dickinson and Russell G. Tysdal

Preliminary Results of a Tectonic Subsidence Analysis of the Central North Slope, Alaska

By Frances Cole, Kenneth Bird, *and* David Howell

ABSTRACT

Subsidence histories in five wells in a 155-km-long transect across the central Colville basin were constructed using 1-dimensional backstripping, in order to resolve the timing of tectonic events in the central Brooks Range and North Slope. All wells show grossly similar tectonic subsidence histories that begin with slow, decelerating subsidence during late Paleozoic and early Mesozoic time, consistent with a passive margin style of subsidence resulting from thermal contraction. Renewed but moderate subsidence in Early Jurassic time may be related to the onset of failed rifting north of our transect (offshore) or to flexural effects of the southward-prograding Kingak Shale. Increased tectonic subsidence in earliest Cretaceous time, observed in several wells in the southern part of our transect, may signal stacking of allochthons in the distant, early-developed Brooks Range orogen. This is followed by uplift and erosion in Hauterivian time, related to development of the regional pebble shale unconformity. Hauterivian uplift is strongest in the north, and is most likely a result of thermal uplift of the rift shoulder along the southern margin of the Canada basin. Uplift is followed by roughly 600 to 700 m of tectonic subsidence in Barremian to Aptian time, signalling thrust loading in the Brooks Range orogen. Subsidence is recorded by a profound increase in water depth that preceded the main episode of sedimentary infilling in the foreland basin. Maximum subsidence occurred soon after Hauterivian uplift, suggesting a possible genetic linkage between rifting in the Canada basin and thrust loading in the Brooks Range orogen. Rifting may have weakened the plate, making it more responsive to foredeep deflection under a crustal load, while spreading in the Canada basin may have influenced compressional deformation in the Brooks Range orogen by increasing convergence rates along the Brookian margin. Barremian to Aptian subsidence is followed by suppressed tectonic uplift in Albian time, during the main episode of sediment progradation and basin infilling. This tectonic uplift may be a response to post-orogenic collapse of the orogen and reduction of the foreland deflection. Alternatively, Albian uplift may signal the northward propagation of compressional deformation into the foreland basin. Late Cretaceous and early Tertiary time is represented by moderate subsidence which, on the basis of regional evidence, is followed by uplift and erosion in Eocene(?) to Holocene time.

INTRODUCTION

The North Slope foreland basin (Colville basin) is a Mesozoic and Cenozoic foreland basin that occupies most of the North Slope of Alaska and extends offshore to the Chukchi platform (fig. 1; Bird and Molenaar, 1992). It is interpreted as a flexural basin that formed in response to crustal loading in the Brooks Range orogen to the south (Hawk, 1986; Nunn and others, 1987; Coakley and Watts, 1991; Bird and Molenaar, 1992; Flemings, 1992). The North Slope foreland basin is unusual in that continental rifting occurred along its northern margin concurrent with early compressional deformation in the Brooks Range to the south. Coakley and Watts (1991) successfully modeled the geometry of the Colville basin, taking into account the thermal effects of rifting along the Arctic margin and emplacement of tectonic and sedimentary loads in and adjacent to the Brooks Range.

The Colville basin is filled with a thick accumulation of deep-marine to deltaic clastic rocks of the Brookian sequence, of Early Cretaceous through Tertiary age. These strata overlie pre-foreland basin deposits of the Ellesmerian sequence, including Upper Devonian through Lower Cretaceous nonmarine to marine clastic and carbonate strata (Kirschner and Rycerski, 1988). The Ellesmerian sequence represents passive margin sedimentation from a northern source area, while the overlying Brookian sequence represents orogenic deposition from a southern source area (Lerand, 1973). Seismic reflection profiles clearly show a thick succession of northeastward-prograding clinoforms of the Brookian sequence, onlapping uppermost deposits of the south-dipping, southward-prograding Ellesmerian shelf (fig. 2).

The lithospheric mechanisms that drive basin subsidence and uplift include thermal upwelling and cooling, crustal thickening and thinning, and flexure by crustal loading (Angevine and others, 1990). Because of the linkage between flexural subsidence and crustal loading in the adjacent fold and thrust belt, the magnitude and timing of subsidence in a foreland basin reflect migration and growth of the tectonic load (Beaumont, 1981). In effect, the subsidence history can be viewed as a proxy to constrain the timing of thrusting in the orogen. In this study, we examine the subsidence history across the Colville basin in an effort to resolve the timing of tectonic events in the north-central Brooks Range and North Slope.

BROOKIAN OROGENESIS

The structural evolution of the Brooks Range orogen is thought to be related to Mesozoic underthrusting of northern Alaska beneath an ocean basin that lay to the south. In this scenario, the compressional deformation in the Brooks Range orogen represents shortening of detached upper crustal rocks above the underthrusted continental lithosphere. An estimated 400 to 600 km of shortening was accomplished through the stacking of relatively thin thrust sheets (Oldow and others, 1987; Mayfield and others, 1988), but the timing of shortening is not well-resolved.

Thrusting probably began in the Middle Jurassic, according to $^{40}Ar/^{39}Ar$ hornblende ages obtained from metamorphic rocks beneath northward-obducted ophiolitic rocks in the western Brooks Range (for example, Wirth and Bird, 1992). Blueschist-facies metamorphism in the southern Brooks Range may represent subduction and regional contraction in the orogen. The age of blueschist metamorphism is poorly-constrained, but is generally regarded as Late Jurassic to Early Cretaceous (Armstrong and others, 1986), with a minimum age of 149 Ma (Tithonian) according to Till (1992).

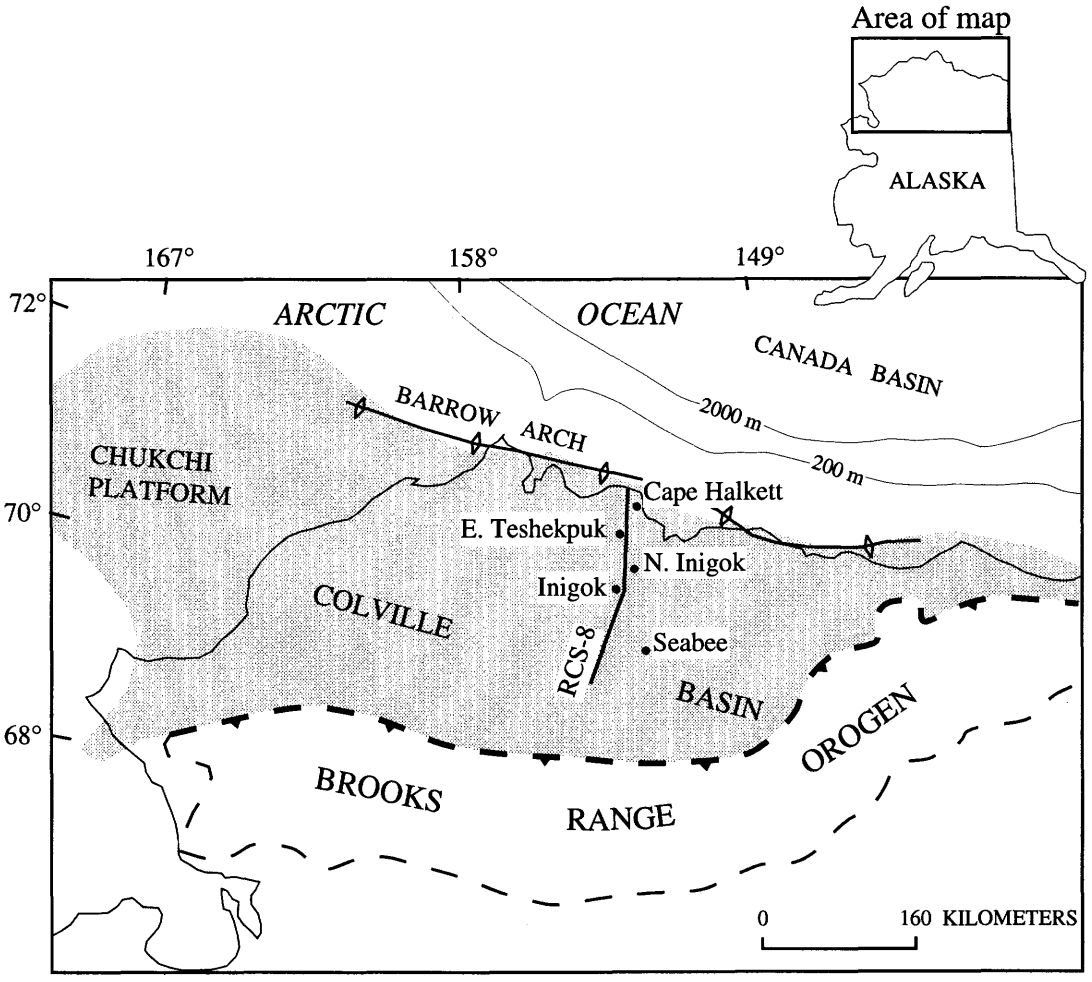

Figure 1. Index map for the North Slope foreland basin (shaded area), Brooks Range orogen (inside dashed line), Barrow arch (solid line with open arrows), and Canada basin. Bathymetry in meters. Seismic line RCS-8 (solid line) and well locations shown. From Bird and Molenaar (1992).

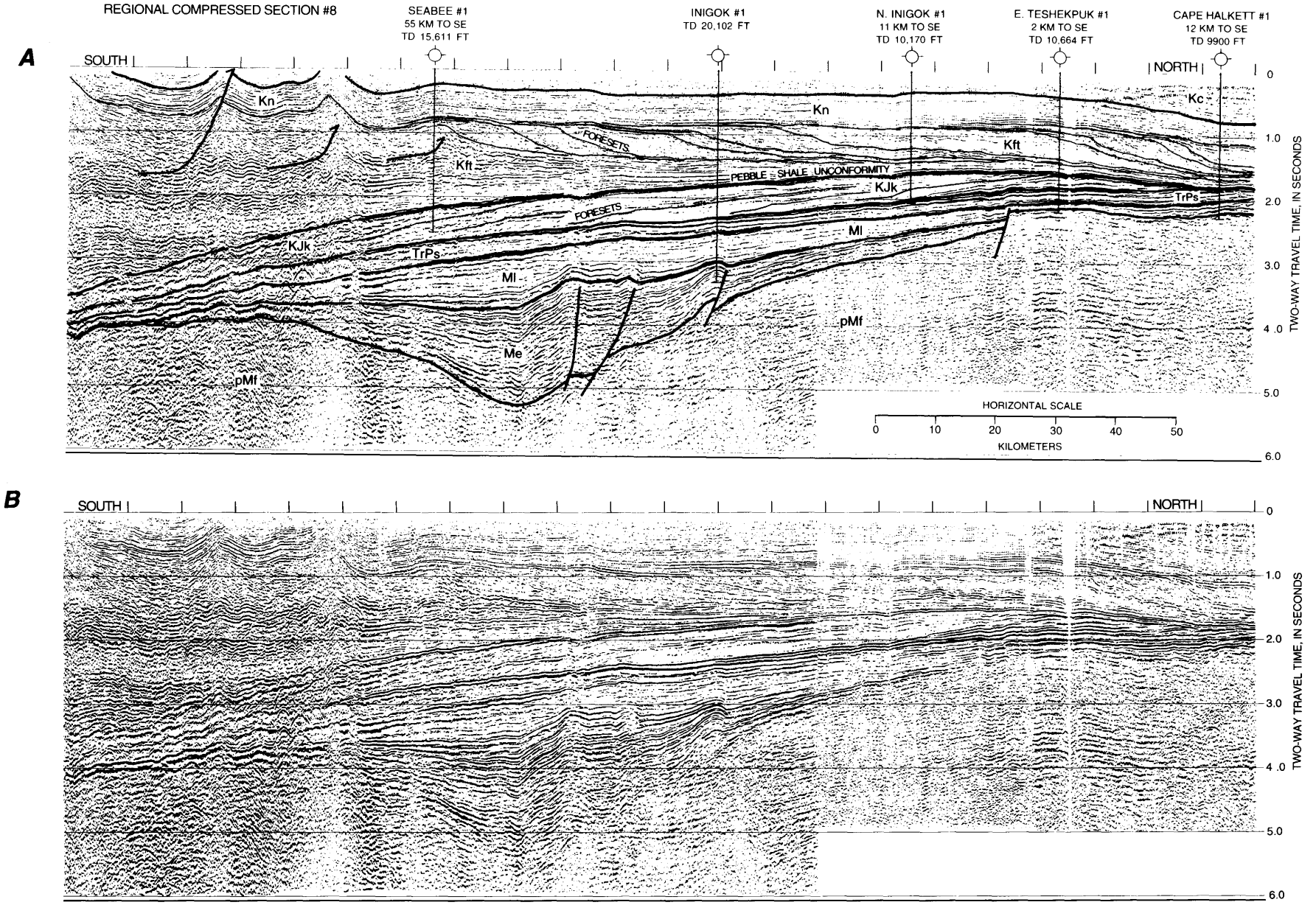

Figure 2. Interpreted *(A)* and uninterpreted *(B)* seismic line RCS-8, showing projected locations of wells used in this study, and major stratigraphic units: pMf, pre-Mississippian Franklinian sequence; Me, Mississippian Endicott Group; Ml, Mississippian Lisburne Group; TrPs, Permian and Triassic rocks of the undivided Sadlerochit Group and Shublik Formation; KJk, Jurassic and Cretaceous Kingak Shale; Kft, Cretaceous rocks of undivided Fortress Mountain and Torok Formations; Kn, Albian and Cenomanian Nanushuk Group; Kc, Upper Cretaceous Colville Group. TD, total depth.

The oldest stratigraphic evidence for convergence and orogenesis is the Okpikruak Formation, which occurs in allochthonous thrust sheets in the northern Brooks Range. These deposits are highly deformed turbidites with a poorly known stratigraphy, interpreted as syntectonic deposits shed northward from an advancing early Brookian thrust front. They are mostly early Neocomian (Berriasian and Valanginian) in age, except for one locality in the western Brooks Range with latest Jurassic (Tithonian) fossils (Curtis and others, 1984). In several localities in the northern Brooks Range, highly folded and imbricated rocks of the Okpikruak and older units are inferred by Mull (1989) to be overlain in angular unconformity by less deformed strata of the Fortress Mountain Formation of Aptian to Albian age. According to this stratigraphic interpretation, the most intense compressional deformation in the orogen was complete by Aptian or Albian time.

However, some of the highly telescoped turbidites in the foreland fold and thrust belt that were previously mapped as Okpikruak Formation have recently yielded probable Aptian to early Albian palynomorphs (Mickey and Haga, unpublished report), indicating that they belong to the Fortress Mountain Formation and were deformed after Aptian or early Albian time. In addition, some workers propose a passive roof thrust beneath the Fortress Mountain Formation in a tectonic triangle zone at the northern edge of the foreland fold and thrust belt (for example, Oldow and others, 1987; Howell and others, 1992), an interpretation that also requires some degree of continued thrusting after deposition of the Fortress Mountain Formation.

Because no post-Aptian to Albian strata have been identified in the thrust belt, there is no strict limit on the end of Brookian thrusting. North of the main thrust belt, in our study area, foreland basin strata as young as Maastrichtian age are involved in relatively minor folding and faulting (Brosgé and Whittington, 1966; Frederiksen and others, 1988), and in the northeastern Brooks Range contraction is active today. Some workers argue for ongoing compressional deformation from the Late Jurassic to the present-day (Oldow and others, 1987; J.S. Oldow, oral commun., 1993), while others envision a more episodic history of thrusting-versus-quiescence (Mull, 1989; O'Sullivan, 1993). Results of apatite fission track studies from the core of the Brooks Range to the North Slope foreland basin seem to support the latter view (O'Sullivan, 1993; O'Sullivan and others, in press).

A major cooling episode affected the southern and axial part of the Brooks Range in mainly Albian time, based on a clustering of K/Ar, $^{40}Ar/^{39}Ar$, and apatite and zircon fission track ages between 120 and 90 Ma (Dillon, 1989; Blythe and others, 1990; Moore and others, 1992). Cooling in the mid-Cretaceous probably resulted from erosion and tectonic denudation of the thickened, high-standing orogen. More than 5 km of foreland basin fill were deposited in the Colville basin at this time, indicating rapid erosion of an emergent source area. In addition, extensional structures of inferred mid-Cretaceous age occur in the southern Brooks Range (for example, Gottschalk and Oldow, 1988; Miller and Hudson, 1991; Little and others, in press), suggesting unroofing by down-to-the-south normal faulting on the south flank of the orogen. This extension may have been concurrent with some of the shortening in the foreland, but the timing constraints are too imprecise to demonstrate this.

Our subsidence analysis is aimed at resolving these timing questions by looking at the paleobathymetric and sedimentologic response of the Colville basin to deformation in the Brooks Range orogen. In this study we analyze the subsidence histories for five wells: Seabee #1, Inigok #1, North Inigok #1, East Teshekpuk #1, and Cape Halkett #1. These are located along a transect from the Umiat area to the coastline (figs. 1, 2). The wells, spaced 30 to 80 km apart, are located relatively close to regional seismic line RCS-8 (available from U.S. Geological Survey), which provides regional stratigraphic and paleobathymetric control on the north flank of the Colville basin. All wells penetrate the entire Brookian sequence and several penetrate all or most of the Ellesmerian sequence. We plan to supplement this work with additional transects to the west and east to see variations in the subsidence history along the axis of the basin, parallel to the present-day Brooks Range.

STRATIGRAPHY

The stratigraphy along our transect is illustrated in figure 3. The Ellesmerian stratigraphy begins with continental clastic strata, part of the Endicott Group, deposited in and adjacent to rift grabens and sags during Mississippian time. These lie unconformably on pre-Mississippian metasedimentary, and, locally, granitic basement rocks. The continental clastic rocks grade upward into marine shales and eventually into a very broad and continuous carbonate platform of Mississippian to Permian age (Lisburne Group). The Lisburne Group is overlain unconformably by a series of regressive and transgressive sandstones, shales, and carbonate rocks of Permian and Triassic age (the Sadlerochit Group, the Shublik Formation, and the Sag River Sandstone of Fackler and others, 1970). These are buried beneath the Kingak Shale—a thick marine sequence representing a southward-prograding Jurassic and Cretaceous shelf (figs. 2, 3).

Passive-margin sedimentation was interrupted in Early Cretaceous time by regional uplift and erosion represented by the pebble shale unconformity, also known as the Lower Cretaceous unconformity. This unconformity is considered the break-up unconformity related to opening of the Canada basin at the present-day site of the Beaufort

Sea (Grantz and others, 1990). From the Seabee well to the north, the unconformity is overlain by the pebble shale unit, a mostly Hauterivian to Barremian transgressive marine shale named for its rare but distinctive frosted quartz grains and chert pebbles. Widespread but discontinuous sandstones, composed primarily of quartz and chert grains, are associated with the basal part of the pebble shale unit (Moore and others, 1992; Schenk and Bird, 1993). The sandstones, as well as the pebbles, are evidently derived from a northern source area, probably from the emergent rift shoulder on the southern margin of the newly formed Canada basin. The pebble shale unit appears to die out south of the Seabee well (fig. 2, south end). At this location the unconformity is onlapped by lowermost strata of the Torok Formation, which are imaged seismically on RCS-8.

From the Seabee well to the north, the pebble shale unit is overlain by a condensed section of organic-rich, tuffaceous clay shale known as the Hue Shale (Molenaar and others, 1987). In the subsurface along our transect it is represented by a highly radioactive shale interval known as the gamma ray or highly radioactive zone. This is a prominent reflective horizon in North Slope seismic images (fig. 2). The Hue Shale, composed of pelagic and hemipelagic deposits, may be considered a transitional unit between Ellesmerian and Brookian rocks (Grantz and others, 1990) or as distal Brookian deposits (Molenaar and others, 1987; Moore and others, 1992), coeval in part with the lowermost strata of the Torok Formation south of the Seabee well. The Hue Shale is thought to represent the loss of northern (Ellesmerian) sediment sources and the beginning of Brookian deposition from a southern source area (Molenaar and others,

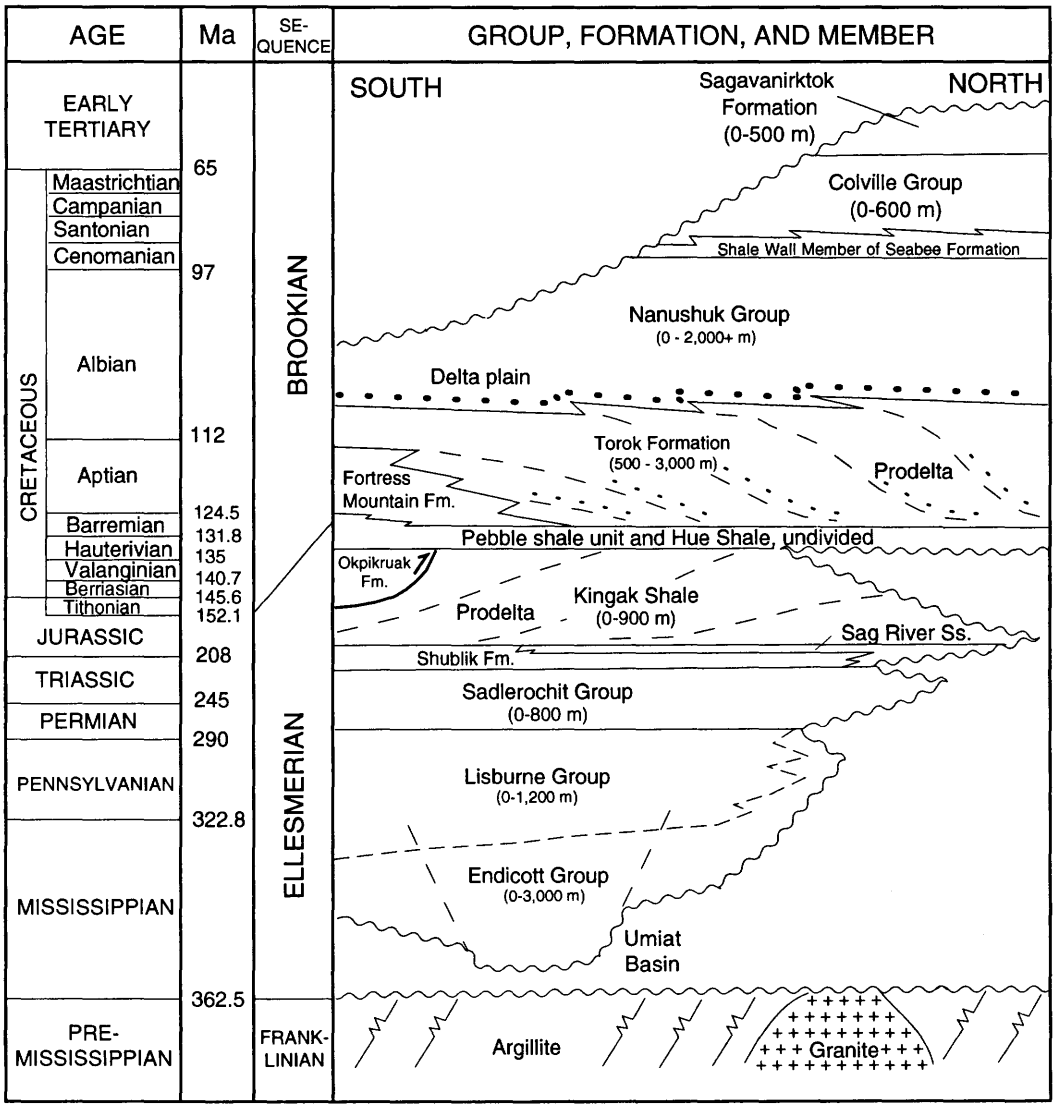

Figure 3. Generalized stratigraphy of the North Slope (modified from Kirschner and Rycerski, 1988). Radiometric ages are from Harland and others (1990).

1987; Moore and others, 1992). The Hue Shale is time transgressive, ranging from Barremian and Aptian in age in the western part of the Colville basin to Aptian and early Albian near the northern end of our transect, according to Mickey (oral commun., 1993).

The Hue Shale grades upward and southward into the Torok Formation, which is considered, in part, to be the northern, subsurface equivalent of the Fortress Mountain Formation that crops out in the foothills (Molenaar, 1988). The Torok Formation is a thick sequence of deep-water shale and turbidite sandstones with a distinct seismic geometry of sigmoidal clinoforms in its upper part. It represents the basinal, slope, and outer shelf facies deposited in advance of a northeastward-prograding shelf margin (Molenaar, 1985). The basal part of the Torok Formation is also time transgressive. In the Seabee well at the south end of our transect, it is possibly as old as Barremian (Haga and Mickey, 1983b), whereas at the north end of our transect in the Cape Halkett well, the basal part of the Torok is Aptian, most likely late(?) Aptian in age (Witmer and others, 1981b; Mickey and Haga, 1990).

The uppermost part of the Torok Formation is time transgressive and gradational into deltaic deposits of the Nanushuk Group, of mostly Albian to early Cenomanian age (Witmer and others, 1981a,b; Mickey and Haga, 1990). In seismic line RCS-8 (fig. 2), the Nanushuk Group forms most of the reflective topsets (shelf and delta plain facies) that grade laterally and downward into Torok foresets and bottomsets (slope and basinal facies). The Nanushuk is overlain by a transgressive marine shale, the Cenomanian and Turonian Shale Wall Member of the Seabee Formation. This shale sequence represents the youngest major marine transgression recorded in the stratigraphy along our transect. The remainder of Late Cretaceous time is represented by shallow-marine and nonmarine sandstones, shales, conglomerates, and coal beds of the Colville Group. At the northern end of our transect, the uppermost few hundred meters of strata near the coastline may be early Tertiary in age and thus assigned in this area to the Sagavanirktok Formation (Molenaar and others, 1986).

METHOD

To generate the subsidence histories that follow, we used the delithification and one-dimensional backstripping program "decem2," provided to us by M. Kominz at the University of Texas at Austin. The program delithifies sedimentary units by making corrections for compaction, according to the method of Van Hinte (1978), and for cementation according to Bond and Kominz (1984) and Bond and others (1989). The delithified sedimentary units are backstripped using the one-dimensional (Airy) isostatic adjustment developed by Steckler and Watts (1978) and illustrated in figure 4. Each sedimentary unit, beginning with the lowest unit, is first restored to its initial thickness and density. Then the isostatic subsidence of the basement caused by the weight of the sedimentary unit is removed, giving the elevation of the basement in the absence of the sedimentary load. This basement elevation is shifted downward to include the estimated water depth at the time of the base of the sedimentary unit. This is iterated upward through the stratigraphic column until all the sedimentary units are delithified and backstripped. The result is a tectonic subsidence history of the basement, viewed as the subsidence caused by mechanisms other than local sedimentary loading. One-dimensional backstripping is limited to the effects of local sedimentary loads in a vertical column at each well site; it does not take into account the two-dimensional effects of adjacent sedimentary loads. In general, one-dimensional backstripping underestimates tectonic subsidence near basin depocenters, and overestimates it near the edges (Kominz, written commun., 1994). For a two-dimensional treatment of the Colville basin, see Flemings (1992).

The subsidence histories are constructed principally from stratigraphic thickness, stratigraphic age, and paleobathymetry estimates. Stratigraphic thicknesses for the major units in the Seabee, Inigok, North Inigok, East Teshekpuk, and Cape Halkett wells, and other NPRA wells, are provided in Bird (1988, table 15.3). At the Seabee well, where some thickening in the Torok Formation is evident beneath the Umiat anticline, we used Molenaar's (1985, fig. 22) estimate of 3200 m for its pre-deformed thickness. Biostratigraphy for each well, summarized in Magoon and others (1988), is based primarily on foraminifers and palynology reported in Witmer and others (1981b), and Haga and Mickey (1983a,b). For detailed Jurassic to Early Cretaceous biostratigraphy, we relied heavily on Haga and Mickey (1983b) and on the original paleontology reports in the NPRA well files located at the USGS offices in Menlo Park, CA. We used the Harland and others (1990) time scale for numerical age assignments. These chronometric ages have variable uncertainties depending on the duration of the foraminifer and palynology zones (on the order of 10-m.y. duration for Mesozoic zones, giving an error of 5 m.y.), and the uncertainty on the chronostratigraphic stage boundaries in the Harland and others (1990) time scale (roughly 2 m.y. for Cretaceous stages, increasing to roughly 10 m.y. for Carboniferous stages). They are accurate and useful for relative age correlations between wells, but they have limited significance in terms of absolute time.

Estimates of paleobathymetry were based on lithofacies and to a lesser extent on biofacies (Witmer and others, 1981a) for all units except the Kingak Shale and Torok Formation. We did not make corrections for eustatic sea-level changes in any of our paleobathymetry estimates, but we consider some possible effects of eustacy in the discussion that follows.

From the Endicott Group to the top of the Sag River Sandstone, our water depth estimates carry small uncer-

tainties, less than 100 m. These are mostly nonmarine to shallow-marine carbonate and clastic strata, deposited in a continental shelf environment.

For the Kingak Shale and the Torok Formation, we made detailed water depth estimates based on clinoform geometries imaged on seismic line RCS-8 (fig. 5). The clinoforms are thought to represent depositional profiles of the prograding shelf, slope, and basin floor (Molenaar, 1988). We measured the amplitudes of numerous clinoforms at each well-site, converting two-way travel time to depth according to existing velocity data for each well. Treating each clinoform as a time line, we were able to construct fairly detailed paleobathymetry curves for most of the Jurassic and middle Cretaceous. For the Kingak Shale, most of our paleodepth estimates are accurate to within 150 m. At the north end of our transect, where most of the Kingak Shale is eroded beneath the pebble shale unconformity, water depth estimates carry a larger uncertainty—on the order of 250 m.

The water depth during deposition of the pebble shale unit and the Hue Shale increases from near sea level at the base of the pebble shale unit (pebble shale unconformity) to roughly 900 m during deposition of the lowest clinoforms in the Torok Formation. The intervening paleodepth history is not well constrained; the fauna are mostly basinal according to Witmer and others (1981b). The pebble shale unit is a transgressive marine sequence, and the Hue Shale is mostly hemipelagic and pelagic shale representing bathyal depths, so we assume a simple linear increase in water depth upsection. Onlap patterns in lowermost Torok strata south of the Seabee well are further

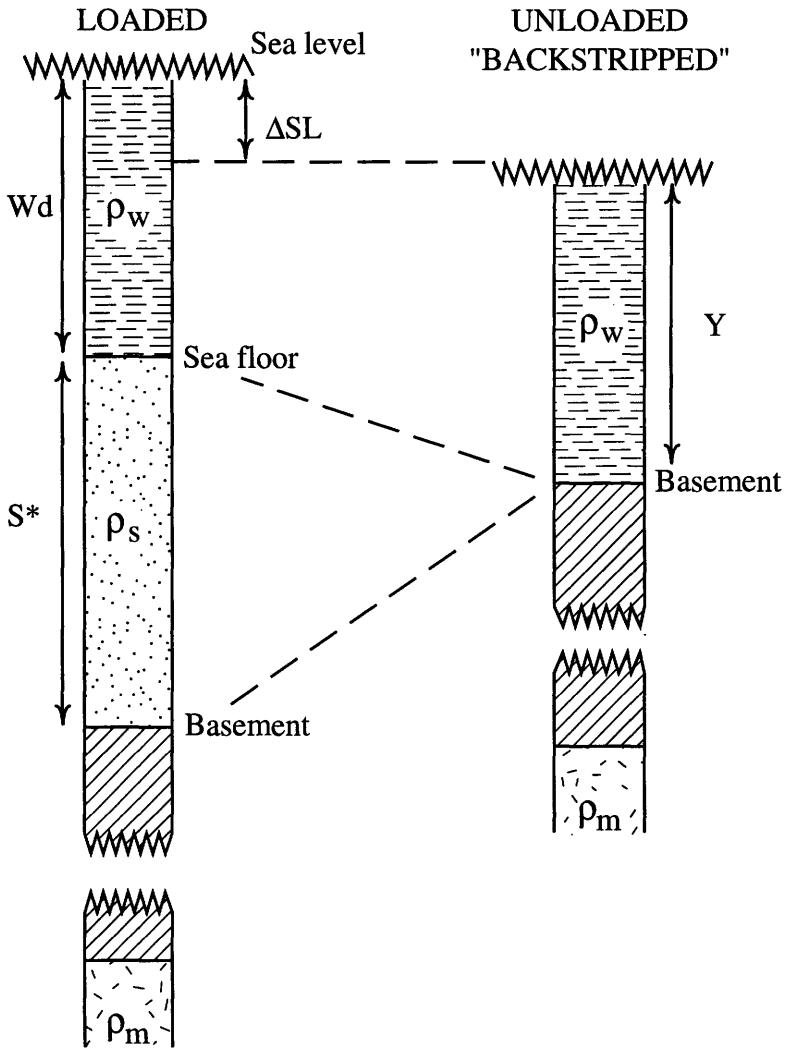

Figure 4. Schematic diagram of a reconstructed (loaded) sedimentary column and a backstripped (unloaded) column. S*, delithified sedimentary thickness; Wd, water depth; ΔSL, change in sea level; Y, depth to basement in the absence of sedimentary load; ρ_w, density of water; ρ_s, density of sediment; ρ_m, density of mantle. From Steckler and Watts (1978).

evidence of a relative sea level rise after flooding of the pebble shale unconformity (fig. 2, south end).

The clinoforms in the Torok Formation are well preserved and provide very good water depth control between the five wells (accurate to roughly 100 m), but precise chronostratigraphic control for each clinoform is lacking. We assigned numerical ages to clinoforms by assuming a constant rate of deposition between the oldest part of the Torok (Barremian(?), ca. 126 Ma, in the Seabee well) and the youngest part of the Torok (late Albian, ca. 100 Ma, in the Cape Halkett well). Water depth estimates for the overlying Nanushuk and Colville Groups are based on nearshore lithofacies and low-amplitude clinoforms and are accurate to within 100 m.

Several important assumptions were made regarding the pebble shale unconformity. First, the minimum age of the unconformity is taken as intra-Hauterivian, based on (1) the presence of Hauterivian to Barremian microfossils above the unconformity in all wells of our study (Haga and Mickey, 1983b), and (2) probable Hauterivian microfossils below the unconformity in the southernmost wells of our transect, Inigok and Seabee, where seismic and well data indicate minimal or no erosion of the upper part of the Kingak Shale (Haga and Mickey, 1983b). According to the Harland (1990) time scale, Hauterivian spans the interval from 135 Ma to 131.8 Ma, so we assigned an age of 135 to 133 Ma to the unconformity, giving it a duration of 2 million years. Given the uncertainty of the paleontologic dates for the overlying pebble shale unit, it could be as young as Barremian at the Inigok and Seabee wells; uncertainty also exists in the age of the onset of erosion at the north end of our transect where all of the Late Jurassic and earliest Cretaceous stratigraphic record below the unconformity is missing. Here the maximum age of the unconformity could be much older, possibly as old as Late Jurassic. Owing to the lack of precise age constraints in the northern part of the study area, we treat the unconformity as a nominally synchronous intra-Hauterivian event along the transect.

The thickness of section of the Kingak Shale eroded beneath the pebble shale unconformity in the Inigok, North Inigok, East Teshekpuk, and Cape Halkett wells was estimated from the morphology of the Kingak shelf interpreted from regional seismic line RCS-8 (Bird, 1987, fig. 7; Bird, in press, fig. QQ-7). We projected the uneroded top of the Kingak shelf from the Seabee well-site northward over the Barrow arch, using the gentle dip observed at the latitude of Seabee; we measured the thickness of missing Kingak beneath this surface. This projection yields 50 meters of missing Kingak section at Inigok and about 200 meters missing at Cape Halkett. These are minimum estimates of missing section, based on the assumption of a northward-tapering Kingak wedge. The amount of eroded Kingak could be much greater if its upper surface steepened toward the north, over the Barrow arch (Bird, 1987, fig. 13).

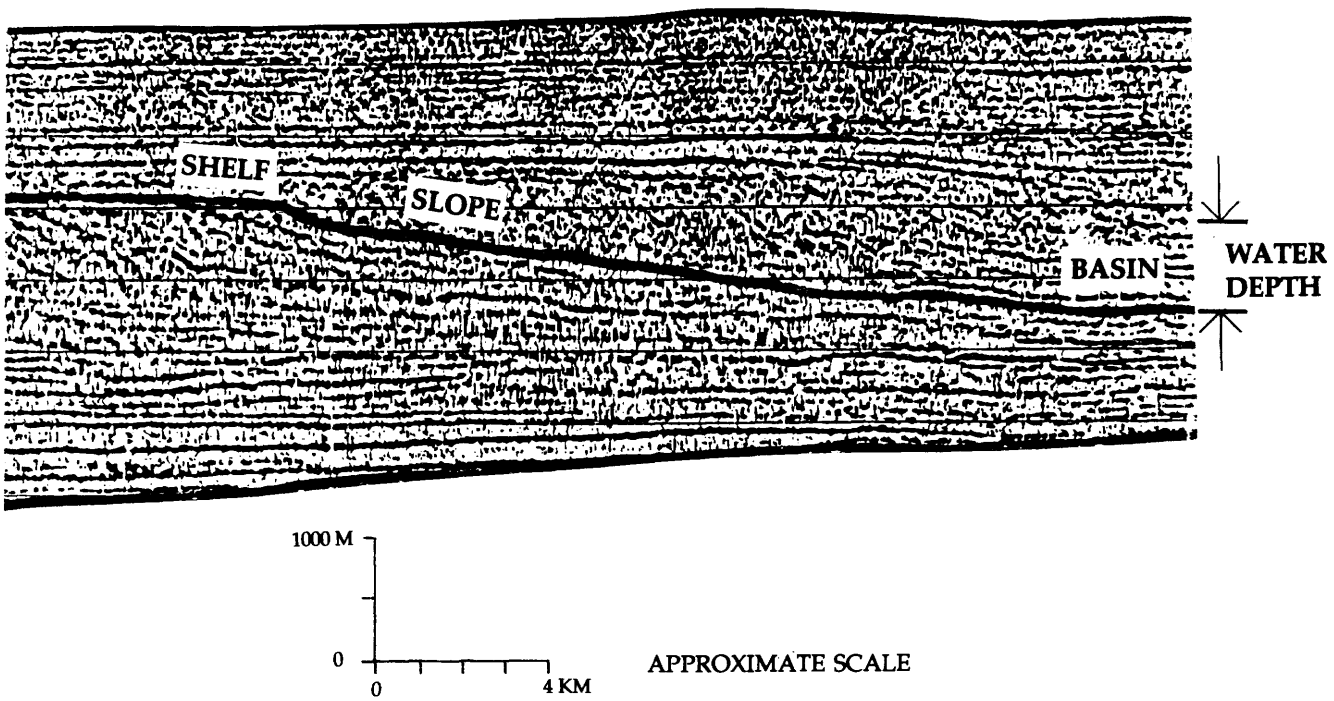

Figure 5. Detail of seismic line RCS-8 showing clinoforms in the Torok Formation used for estimating paleobathymetry. Approximate vertical scale in meters, horizontal scale in kilometers

RESULTS

For each well analyzed, three curves are presented (fig. 6*A*). The upper curve in each diagram is a plot of estimated paleobathymetry through time, based on sedimentary facies and clinoform amplitudes. The bottom curve is the total basement subsidence curve for the well; it is the delithified sediment thickness above basement combined with paleobathymetry. It models the burial history of the basement at each well. The middle curve is the tectonic residual subsidence curve that results when the local (Airy) isostatic effects of sediment loading are removed. This curve represents upward and downward motion of the basement that would have occurred in the absence of the local sedimentary load.

The tectonic residual subsidence curves for all five wells show two main subsidence events (fig. 6): (1) slow, decelerating subsidence during Paleozoic time, corresponding to deposition of the rock units of the Endicott and Lisburne Groups, and (2) rapid subsidence in the Early Cretaceous corresponding to a rapid increase in water depth prior to northward progradation of the Torok Formation. A third subsidence event of short duration and low magnitude occurs in the northern part of the transect in Early Jurassic time (ca. 200 Ma), corresponding to the base of the Kingak Shale. A fourth subsidence event is seen in the Late Cretaceous to early Tertiary parts of the tectonic subsidence curves; this corresponds to long-lived progradation of deltaic deposits of the Colville Group and Sagavanirktok Formation.

The Paleozoic subsidence event is consistent with thermal contraction of the south-facing passive margin, although it may represent more local effects of subsidence in the Umiat basin (fig. 2). The Paleozoic segments of the tectonic subsidence curves between about 350 Ma and 270 Ma are concave up, typical of well-known passive margins (Dickinson, 1976). This shape represents the exponential decay in the elevation of hot crust as it cools (Van Hinte, 1978). The magnitude of subsidence during this interval is highest in the south (seaward), decreasing from a maximum of 1200 m at the Inigok well to a minimum of 230 m at the Cape Halkett well. This gradient is consistent with subsidence patterns along well-known passive margins (Bond and Kominz, 1984). The tectonic subsidence curves are fairly flat for the remainder of Paleozoic and Triassic time, indicating an interval of continued thermal decay and tectonic quiescence until Early Jurassic time.

The Inigok, North Inigok, East Teshekpuk, and Cape Halkett wells all show an Early Jurassic (ca. 200 Ma) tectonic subsidence event corresponding to marine transgression and deposition of the basal part of the Kingak Shale (the Seabee well does not penetrate deeply enough to encounter this part of the Kingak). The magnitude of Early Jurassic subsidence appears to increase southward, from 75 m of subsidence at Cape Halkett, to 200 m of subsidence at the Inigok well. These values depend largely on Kingak clinoform amplitudes, which are partly eroded and therefore poorly known at the north end of our transect.

Subsidence in the Early Jurassic may have resulted from tectonic activity, although no compressional deformation of this age is recognized in the Brooks Range orogen. North of our transect (offshore), seismic reflection records show that extension occurred in Jurassic time (Hubbard and others, 1987; Grantz and others, 1990). The onset of extensional deformation, as inferred from seismic stratigraphy, is Middle Jurassic (Hubbard and others, 1987), whereas regional evidence (summarized in Grantz and others, 1990, p. 285) suggests that it could be Early Jurassic. This extensional episode could be responsible for the Early Jurassic (ca. 200 Ma) increased subsidence that we observe. The tectonic subsidence curves, particularly for the North Inigok, East Teshekpuk, and Cape Halkett wells, indicate a rapid decay in the rate of subsidence after 200 Ma, possibly reflecting thermal subsidence.

Alternatively, subsidence in the Early Jurassic may have resulted from sedimentary loading as the Kingak shelf prograded southward. The one-dimensional method of backstripping used in this analysis takes into account only the sedimentary load in a vertical column at each well-site, not the possible flexural effects of adjacent sedimentary loads. The sedimentary wedge comprising the Kingak Shale may have produced progressive subsidence as it prograded southward, in which case we should see a southward younging of the Early Jurassic subsidence event. However, it is not possible to resolve such a southward progression because of limitations on the age control of the basal part of the Kingak Shale. A eustatic sea level rise in the Early Jurassic can account for only 50 m of the observed subsidence (Haq and others, 1986).

At the Inigok, North Inigok, East Teshekpuk, and Cape Halkett wells, Jurassic quiescence is followed by Hauterivian uplift (ca. 135 Ma; fig. 7), corresponding to the pebble shale unconformity. The magnitude of tectonic uplift decreases from 90 m at Cape Halkett to 25 m at the Inigok well. The tectonic curves show synchronous uplift along our transect, but the timing of this event in the north is not well resolved. In the Cape Halkett area the unconformity has removed all but 53 m of the Kingak Shale section, cutting down to the presumed Early Jurassic (foraminiferal zone JEM4, the oldest of four zones that span Early and Middle Jurassic) resulting in at least 200 m of missing section there. The amount of missing section decreases systematically toward the south until, in the Seabee area, no Kingak section is missing, and its upper part contains probable Hauterivian fossils. These relations raise the possibility that uplift and erosion occurred earliest and lasted longest in the Cape Halkett area.

Hauterivian uplift has been attributed to regional thermal uplift of the rift shoulder along the southern margin of the Canada basin (which follows the present-day

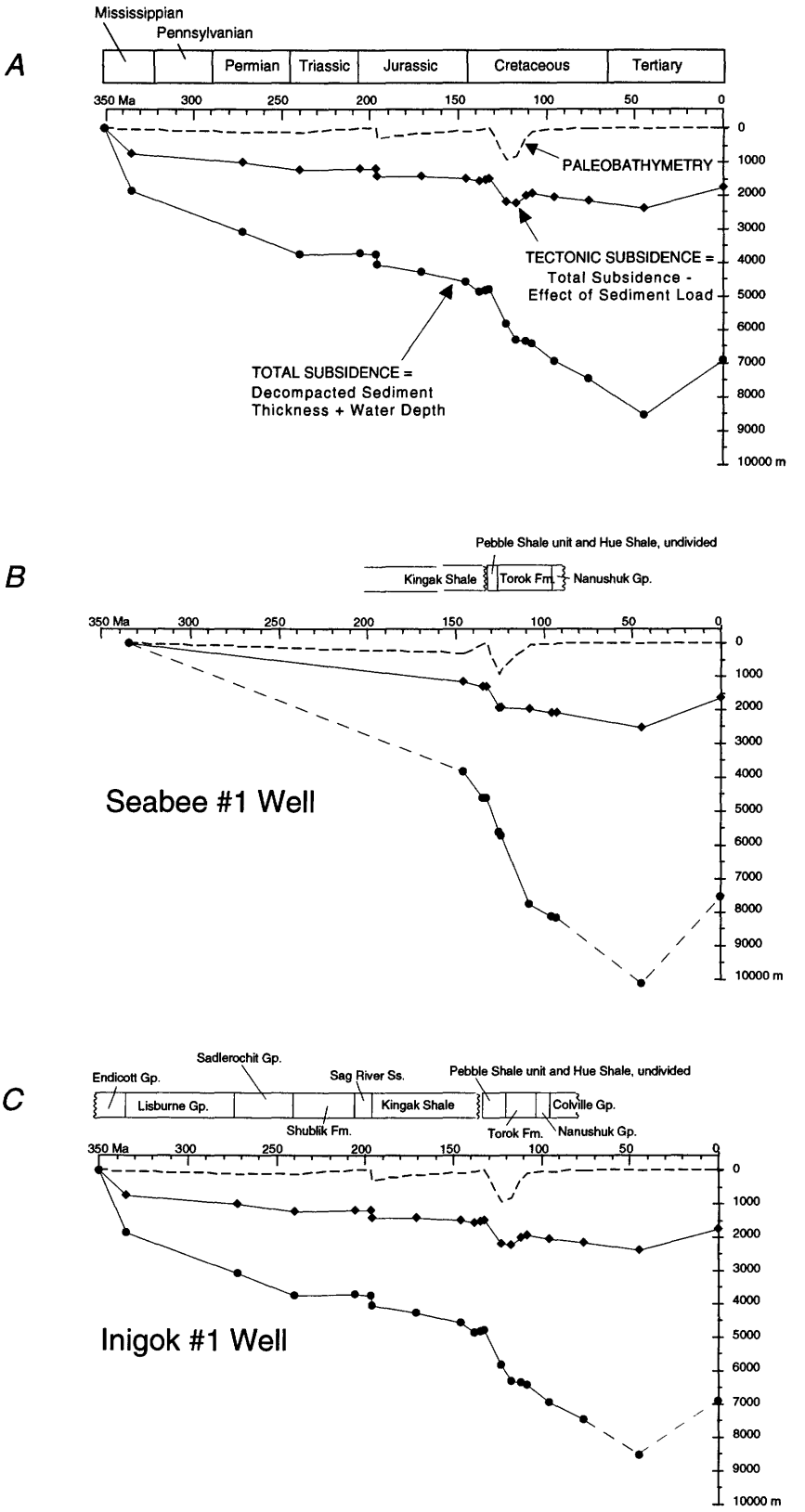

Figure 6. Subsidence curves for the North Slope foreland basin. Explanation *(A)* showing total and tectonic subsidence curves and paleobathymetry curve; subsidence and paleobathymetry curves for Seabee #1 well *(B)*, Inigok #1 well *(C)*, North Inigok #1 well *(D)*, East Teshekpuk #1 well *(E)*, and Cape Halkett #1 well *(F)*. Total subsidence curves are solid where constrained by well data; dashed where inferred from regional stratigraphy and seismic data. Absolute time scale is from Harland and others (1990).

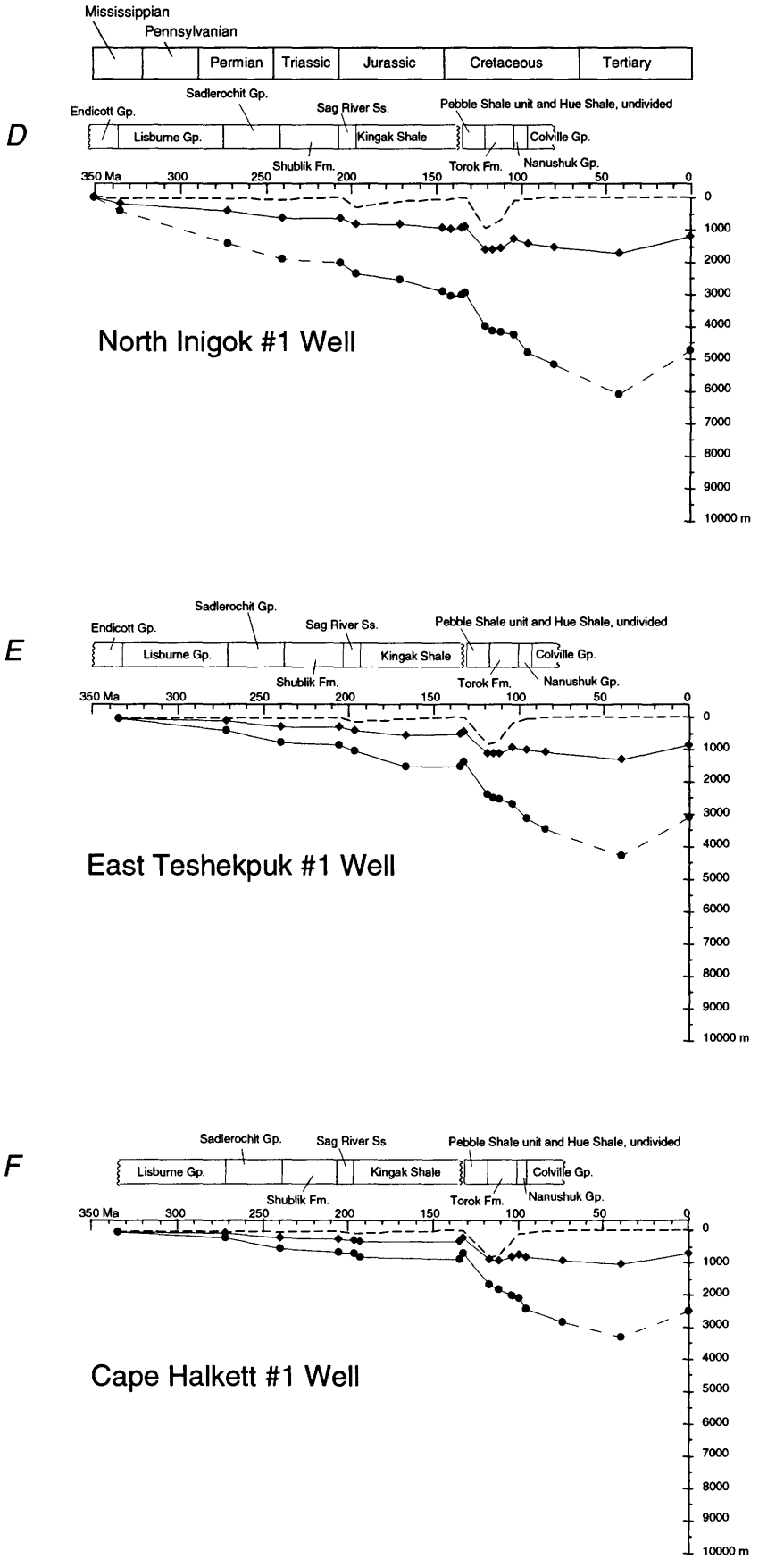

Figure 6.—Continued.

Barrow arch) (Hubbard and others, 1987; Grantz and others, 1990), and this model agrees well with our analysis. This uplift has also been interpreted as a flexural bulge associated with tectonic loading in the Brooks Range orogen (Nunn and others, 1987; Coakley and Watts, 1991), but our results do not support this model. In the case of a flexural bulge, Hauterivian uplift should progress from south to north, reflecting the direction of overthrusting in the orogen. Such a northward progression is unlikely according to the timing constraints discussed above.

Hauterivian uplift is followed by rapid subsidence in Barremian and Aptian time, involving roughly 600 to 770 m of tectonic subsidence in 15 million years (fig. 7). We attribute most of this subsidence to flexural loading in the ancestral Brooks Range, but a small part is presumably the result of thermal contraction of the uplifted Hauterivian rift shoulder. The component of subsidence due to cooling should simply counterbalance Hauterivian thermal uplift. This accounts for 90 m of thermal subsidence at Cape Halkett, 68 m at East Teshekpuk, 46 m at North Inigok, 24 m at Inigok, and no thermal subsidence (because no thermal uplift) at the Seabee well. Subtracting this thermal component from total Barremian and Aptian tectonic subsidence values leaves 766 m of remaining tectonic subsidence at the Seabee well, 717 m at Inigok, 652 m at North Inigok, 605 m at East Teshekpuk, and 602 m at Cape Halkett. This is the component of tectonic subsidence that can be ascribed to lithospheric flexure under a tectonic load. The magnitude of subsidence and the subsidence rates decrease with distance from the Brooks Range orogen, as expected for a flexural basin (Kominz and Bond, 1986; Homewood and others, 1986).

At the Seabee well (fig. 6*B*), where the effects of Hauterivian uplift are smallest, a convex-up pattern of subsidence is apparent in the earliest Cretaceous, typical of foredeep subsidence accelerating ahead of an advancing thrust load (Allen and others, 1986). The Inigok and North Inigok wells also show evidence of increased tectonic subsidence in earliest Cretaceous time (fig. 7, ca. 145-135 Ma). As in the case of the Early Jurassic event, this increased rate of subsidence could be related to rifting or two-dimensional effects of sedimentary loading. However, the fact that it precedes and is continuous with more rapid Barremian and Aptian subsidence at the Seabee well suggests that it represents early flexure of the lithosphere, related to tectonic loading in the orogen. At Inigok and

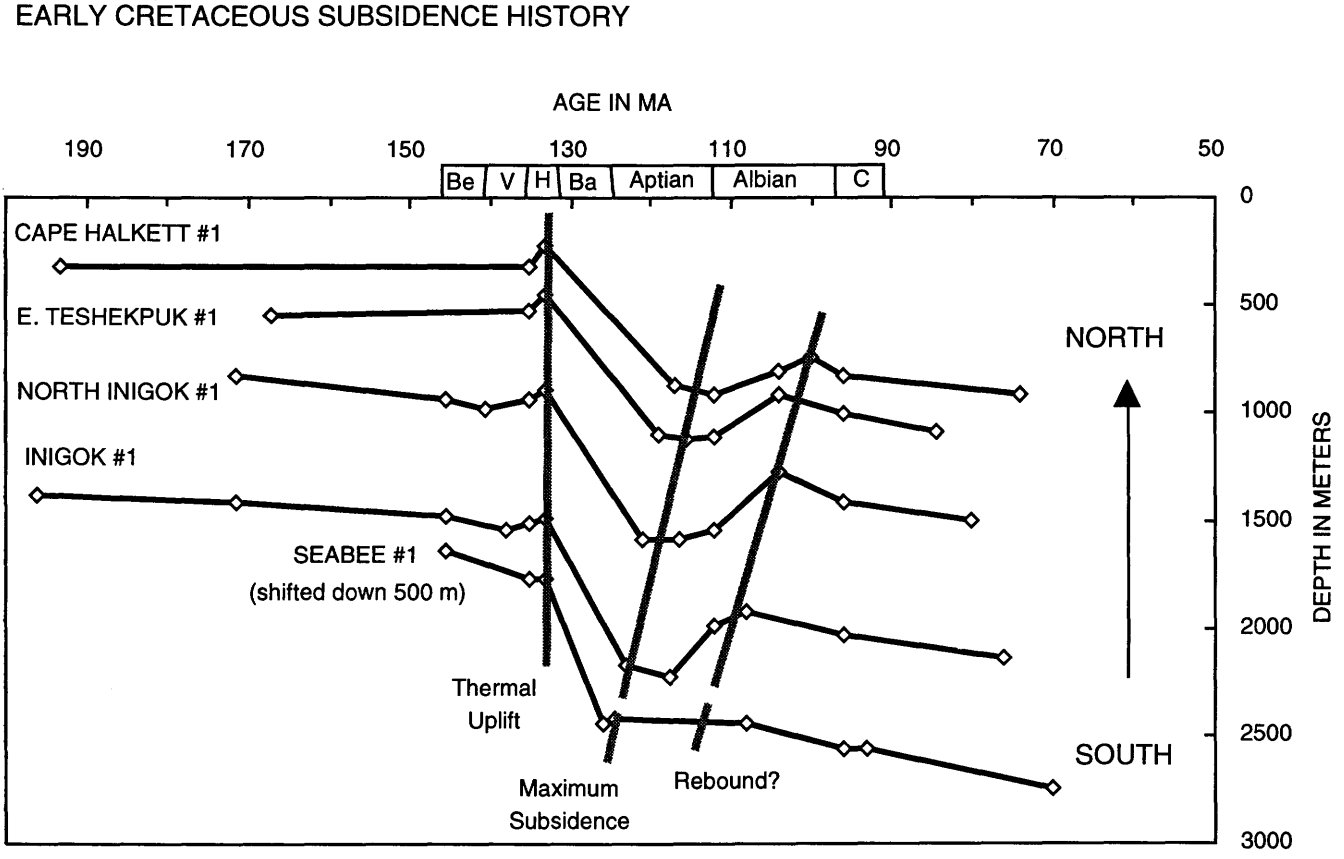

Figure 7. Tectonic subsidence curves for Inigok #1, North Inigok #1, East Teshekpuk #1, Cape Halkett #1, and Seabee #1 wells, enlarged for the Jurassic and Cretaceous time interval to see Brookian sequence events. Symbols: Be, Berriasisan; V, Valanginian; H, Hauterivian; B, Barremian; C, Cenomanian. Seabee #1 curve is shifted down 500 meters for comparison.

North Inigok, this initial increase in subsidence in Berriasian to Valanginian time is interrupted by Hauterivian uplift. If not for the superimposed effects of uplift, a convex-up pattern of accelerating subsidence may have been preserved at these sites also. Thus, the rapid tectonic subsidence after the Hauterivian may have begun as a gradual increase as far back as earliest Cretaceous time.

The exact timing of the rapid, post-Hauterivian subsidence is not well constrained, due to a lack of good paleobathymetric data between the Hauterivian pebble shale unconformity and the Barremian(?) to Aptian basal Torok Formation. The intervening, mostly Hauterivian to Barremian pebble shale unit and Barremian to Albian Hue Shale, record a major marine transgression and a reversal in sedimentary polarity, signalling subsidence of the basin and emergence of a southern source terrain. But neither the age of the sediment polarity reversal nor the age of the onset of the marine transgression is precisely known. In the Seabee well, basal Torok strata of possible Barremian age (Mickey and Haga, 1987) are observed in seismic images to onlap the south-dipping shelf formed by the Kingak Shale. This requires subsidence and southward tilting of a nearly flat Kingak shelf prior to the arrival of northward-directed Barremian(?) Torok strata. This argues for the onset of subsidence at Seabee sometime between deposition of the pebble shale unit and the basal part of the Torok Formation; that is, Hauterivian to Barremian time. Assuming that the basal part of the Torok is Barremian in age at this location, then rapid subsidence had begun by Barremian time.

The relative timing of maximum tectonic subsidence (corresponding to maximum water depth) between the five wells on the transect is better resolved. At Seabee, maximum tectonic subsidence occurs in late Barremian(?) time (ca. 126 Ma), while at Cape Halkett maximum subsidence does not occur until about the beginning of the Albian (ca. 112 Ma). Although these absolute ages contain uncertainties on the order of 5 m.y., a northward decrease in age of maximum subsidence is evident, presumably reflecting the northward migration of the tectonic load.

Barremian to Aptian tectonic subsidence is followed by suppressed tectonic uplift in Albian time, particularly evident in the Inigok and North Inigok wells (figs. 6, 7). This event is not resolved in our analysis of the Seabee well; because of structural thickening in the Torok Formation beneath the Seabee anticline, we were unable to divide its lower part into small intervals for detailed paleobathymetry measurements. Instead, we treated it as a single stratigraphic unit with a restored thickness of 3200 m (Molenaar, 1985, fig. 22).

Unlike the Hauterivian uplift event, which corresponds to true uplift and regional erosion, this Albian uplift event does not correspond to actual erosion or emergent topography in the foreland basin. It corresponds to the rapid shoaling of water depth (fig. 6) during the main episode of northeastward progradation of the sediments comprising the Torok Formation and Nanushuk Group. The dominance of lateral progradation over vertical aggradation at this time (fig. 2) suggests that vertical accommodation space was limited, and sediments were required to bypass the continental shelf to find space to accumulate. Shoaling bathymetry during sedimentation suggests that the basin substrate had ceased to subside even though the sedimentary load was very large. This requires an upward tectonic force to counteract the weight of the sedimentary load. The Albian suppressed uplift (fig. 7) represents this upward tectonic force.

At Inigok, 740 m of Barremian to middle Aptian tectonic subsidence is followed by nearly 400 m of early to middle Albian suppressed uplift. As with Aptian subsidence, Albian suppressed uplift is younger in the north than in the south, culminating toward the end of the Albian at Cape Halkett (fig. 7). The cause of this event is not obvious, but it may be related to a reduction in the size of the tectonic load affecting the foredeep, or to forward propagation of contraction into the foreland basin.

Both the Barremian to Aptian subsidence and the Albian suppressed uplift events are recorded in large part by rapid changes in bathymetry, which raises the question of eustacy. Could the Barremian to Aptian relative sea level rise, or the Aptian to Albian sea level drop be accounted for by global changes in sea level rather than local tectonics? The amplitude of sea level fluctuation in the Colville basin is too great (900 m or more) to be attributed to eustacy alone, and the timing of the major deepening and shoaling episodes does not correlate with Haq's (1986) global eustatic chart. In fact, Haq's curve shows a eustatic sea level fall during the Hauterivian to Aptian, and a gradual eustatic rise during late Aptian to Late Albian time, the reverse of what we see in the Colville basin. Kauffman and Caldwell's (1993) sea-level curves for the Cretaceous Western Interior Basin of North America also show a long-term rise during the Albian, but this is punctuated by several major short-term falls, one of which may correlate with the major shoaling episode in the Colville basin. However, the magnitude of sea level change is much smaller than that observed in the Colville basin. We conclude that the major rise and fall of relative sea level in Early to mid-Cretaceous time in the Colville basin is driven largely by local geodynamics rather than global eustacy.

Suppressed tectonic uplift in the Albian is followed by an episode of tectonic subsidence in Cenomanian to early Tertiary time, and finally by true uplift and erosion since Eocene(?) time. The magnitude and timing of the uplift event is poorly constrained because it is based on regional stratigraphic correlations; the Latest Cretaceous and Tertiary sedimentary sections along our transect are fragmentary and poorly preserved. However, the Cenomanian subsidence event is well dated and has been recognized elsewhere in the North Slope (Flemings, 1992). It may represent resumed

thrusting in the Brooks Range orogen, possibly related to the long-wavelength folding of middle and Upper Cretaceous foreland basin deposits.

DISCUSSION AND CONCLUSIONS

The subsidence histories for the five wells along our transect provide a detailed history of foreland basin subsidence and uplift that can be used to infer tectonic events in the Brooks Range orogen. The major orogenic events are summarized in figure 8. The tectonic subsidence history begins with passive-margin subsidence in the Carboniferous and Permian, corresponding to the clastic rocks of the Endicott Group and the carbonate platform rocks of the Lisburne Group. Subsidence during this time is greatest in the southern part of our transect, towards the ancient continental margin. This subsidence shows the exponential decay typical of thermal contraction in a rifted-margin setting. This protracted period of subsidence is followed by a second phase of minor subsidence in Early Jurassic time, possibly related to initial phases of rifting in the Canada basin, north of the Barrow arch (Hubbard and others, 1987; Grantz and others, 1990).

The earliest evidence of Brookian deformation is a subtle increase in tectonic subsidence in earliest Cretaceous time (Berriasian to Valanginian) in the Seabee, Inigok, and North Inigok wells (figs. 6, 7). This corresponds to the age of orogenic sedimentary deposits in the Okpikruak Formation (Mull, 1989), and may signal early stacking of allochthons hundreds of kilometers south of the Colville basin (Moore and others, 1992) (fig. 8*A*). This initial convergence may correspond to blueschist-facies metamorphism in the southern Brooks Range, although the age of this metamorphic event is not well constrained (Armstrong and others, 1986; Till, 1992).

In Hauterivian time, we observe regional uplift and erosion concentrated at the north end of our transect (fig. 8*B*). This uplift corresponds to the opening of the Canada basin and the thermal rise of the rift shoulder along the Barrow arch (Grantz and others, 1990). We see no evidence of a northward progression of uplift, as would be expected for a flexural bulge created ahead of a northward-advancing tectonic load.

Rapid subsidence in Barremian to Aptian time corresponds to a dramatic increase in relative sea level, and a reversal in sedimentary polarity. This is the flexural response to the main episode of overthrusting in the Brooks Range orogen (fig. 8*C*). It probably dates the main compressional structures in the orogen, and it corresponds well to the inferred post-Valanginian, pre-Albian folding observed in the Okpikruak Formation and older rock units in the northern Brooks Range (Mull, 1989). Barremian to Aptian subsidence predates the main pulse of foreland basin filling, suggesting that much of the orogen was still submerged at this time. A similar pattern of foreland basin subsidence preceding sediment infilling has been recognized in the Alberta Basin, in the Canadian Cordillera (Cant and Stockmal, 1993).

These results suggest a genetic link between Hauterivian uplift and Barremian to Aptian subsidence. The initiation of seafloor spreading in the Canada basin may have directly influenced foreland basin evolution by (1) increasing the mobility of the Arctic Alaska plate (North Slope and Brooks Range), causing accelerated convergence along the Brookian margin and more rapid emplacement of the tectonic load, and (2) weakening the plate, making it more responsive to foredeep deflection under a crustal load. These mechanisms are consistent with the rotational models invoked by previous workers to explain the temporal association between spreading in the Canada basin and convergent deformation in the Brooks Range orogen (Tailleur, 1973; Mull, 1982; Mayfield and others, 1988).

Barremian to Aptian subsidence was followed by suppressed tectonic uplift (not actual uplift) in the late Aptian and Albian (ca. 115–100 Ma) (fig. 8*D*), during progradation of the Torok and Nanushuk Formations. This corresponds to the major cooling episode in the Brooks Range orogen, which has been dated by K/Ar, $^{40}Ar/^{39}Ar$, and apatite and zircon fission track analyses as 130 to 90 Ma, culminating between 120 and 100 Ma (Dillon, 1989; Blythe and others, 1990; Moore and others, 1992). Cooling signals the removal of overburden from the orogen, through erosion and/or tectonic denudation. Rapid erosion is evidenced in the foreland basin, where more than 5 km of Albian sediments accumulated, and tectonic denudation of this age is supported by the presence of extensional structures of inferred mid-Cretaceous age on the southern flank of the Brooks Range (for example, Gottschalk and Oldow, 1988; Little and others, in press). Erosion and normal faulting may have reduced the size of the orogenic load and resulted in lithospheric rebound of the foredeep. Reducing the orogenic load requires that Albian contraction, which is recognized in the southwestern Brooks Range (Till and Snee, in press), did not keep pace with crustal thinning by erosion or normal faulting, possibly because of an increase in erosion rates or a relaxation of the far-field compressional stresses. Relaxed compression and diminished convergence might also allow thermal equilibration of the underthrusted, cold continental lithosphere beneath the orogen; warming the lithosphere would raise the orogenic load and further contribute to rebound in the foreland basin. Alternatively, tectonic uplift in the foreland basin in Albian time may represent northward propagation of compressional deformation into the foreland basin.

The strength of these results is that they show both temporal and spatial (north-to-south) variations in subsidence and uplift events affecting the North Slope, and they

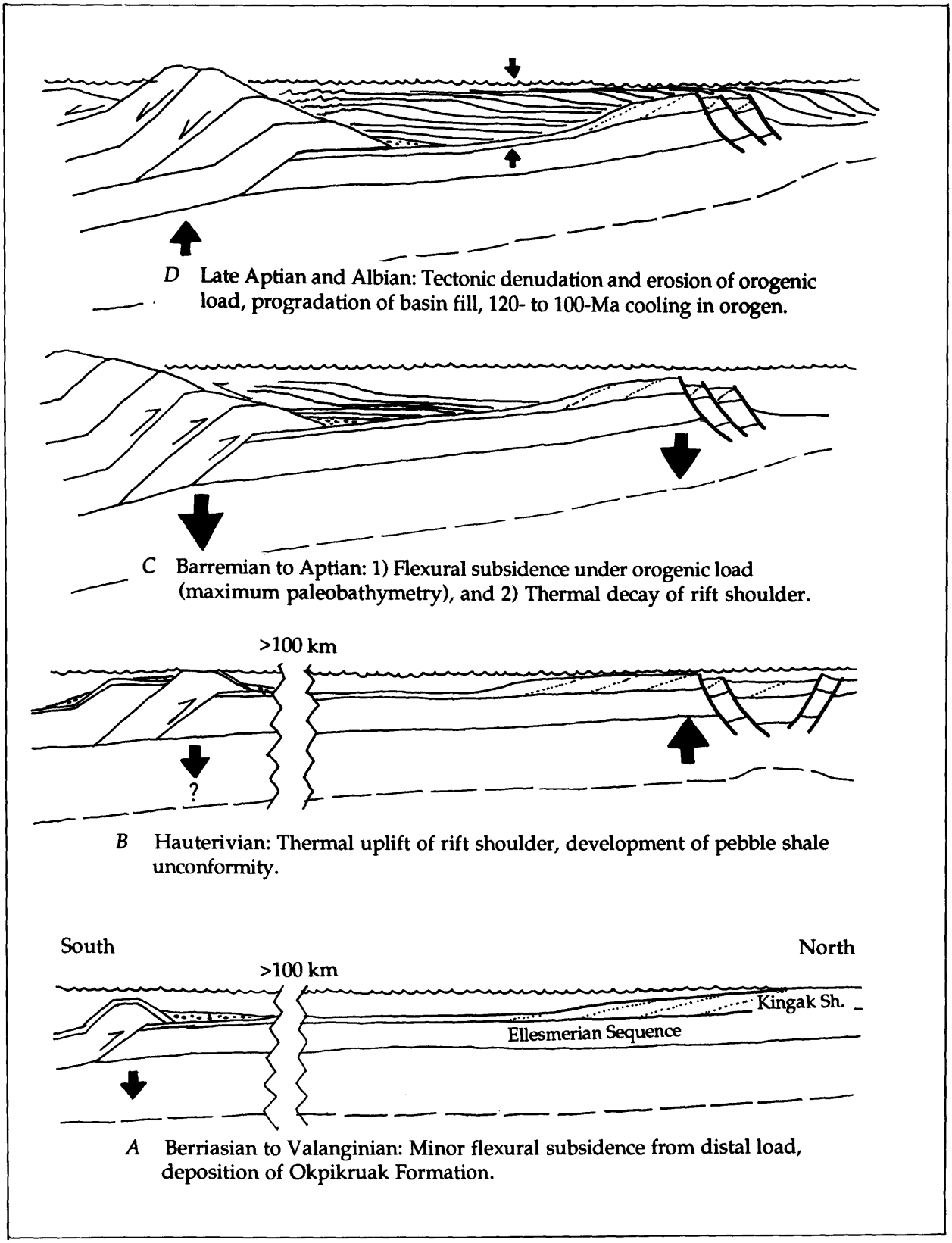

Figure 8. Schematic cross-sections showing Early Cretaceous tectonic evolution of central Brooks Range orogen and North Slope foreland basin, inferred from tectonic subsidence histories along our transect. Relative magnitude and direction of inferred vertical motions indicated by size of black arrows.

account for paleobathymetric as well as sedimentologic indicators of basin subsidence. Our preliminary results from the central Colville basin support an episodic style of Brookian deformation (for example, Mull, 1989; O'Sullivan, 1993), but additional analyses to the east and west are required to track the timing and importance of these events along the length of the Colville basin and the Brooks Range orogen. Ultimately, these studies will lead to a more precise reconstruction of the tectonic history of the foreland and the orogen.

Acknowledgments.—This work was initiated by N. Fehri (Fehri, 1990). We are very grateful to Michelle Kominz for sharing the backstripping program with us, and to Myung Lee and Warren Agena for producing plots of seismic lines on short notice. The manuscript benefited from careful reviews by Marc Hendrix, Gil Mull, Jaime Toro, Alison Till, Tom Moore, and Michelle Kominz.

REFERENCES CITED

Allen, P.B., Homewood, P., and Williams, G.D., 1986, Foreland basins: An introduction: Special Publications of the International Association of Sedimentologists, v. 8, p. 3–12.

Angevine, C.L., Heller, P.L., and Paola, C., 1990, Quantitative sedimentary basin modeling: American Association of Petroleum Geologists, 133 p.

Armstrong, R.L., Harakal, J.E., Forbes, R.B., Evans, B.W., and Thurston, S.P., 1986, Rb-Sr and K-Ar study of metamorphic rocks of the Seward Peninsula and southern Brooks Range, *in* Evans, B.W., and Brown, E.H., eds., Blueschists and eclogites: Boulder, Colorado, Geological Society of America Memoir 164, p. 185–203.

Beaumont, C., 1981, Foreland basins: Geophysical Journal of the Royal Astronomical Society, v. 65, p. 291–329.

Bird, K.J., 1987, The framework geology of the North Slope of Alaska as related to oil-source rock correlations, *in* Tailleur, I., and Weimer, P., eds., Alaskan North Slope Geology: Bakersfield, California, Pacific Section, Society of Economic Paleontologists and Mineralogists, p. 121–143.

Bird, K.J., 1988, Alaskan North Slope stratigraphic nomenclature and data summary for government-drilled wells, *in* Gryc, G., ed., Geology and exploration of the National Petroleum Reserve in Alaska, 1974 to 1982: U.S. Geological Survey Professional Paper 1399, p. 317–354.

Bird, K.J., in press, The Ellesmerian(!) petroleum system, North Slope of Alaska, USA, *in* Magoon, L.B., and Dow, W., eds., The petroleum system—From source to trap: American Association of Petroleum Geologists Memoir 59.

Bird, K.J., and Molenaar, C.M., 1992, The North Slope foreland basin, Alaska, *in* Macqueen, R., and Leckie, D., eds., Foreland basins and foldbelts: American Association of Petroleum Geologists Memoir 55, p. 363–393.

Blythe, A.E., Wirth, K.R., and Bird, J.M., 1990, Fission track and $^{40}Ar/^{39}Ar$ ages of metamorphism and uplift, Brooks Range, northern Alaska [abs.]: Geological Association of Canada, Program and Abstracts, v. 15, p. A-12.

Bond, G.C., and Kominz, M.A., 1984, Construction of tectonic subsidence curves for the early Paleozoic miogeocline, southern Canadian Rocky Mountains: Implications for subsidence mechanisms, age of breakup, and crustal thinning: Geological Society of America Bulletin, v. 95, no. 2, p. 155–173.

Bond, G.C., Kominz, M.A., Steckler, M.S., and Grotzinger, J.P., 1989, Role of thermal subsidence, flexure and eustacy in the evolution of early Paleozoic passive-margin carbonate platforms: Society of Economic Paleontologists and Mineralogists, Special Publication 44.

Brosgé, W.P., and Whittington, C.L., 1966, Geology of the Umiat-Maybe Creek region, Alaska: U.S. Geological Survey Professional Paper 303–H, p. 501–638.

Cant, D.J., and Stockmal, G.S., 1993, Some controls on sedimentary sequences in foreland basins: examples from the Alberta Basin, *in* Frostick, L.E., and Steel, R.J., eds., Tectonic controls and signatures in sedimentary successions: Special Publication, No. 20, International Association of Sedimentologists, Oxford, Blackwell Scientific Publications, p. 49–65.

Coakley, B.J., and Watts, A.B., 1991, Tectonic controls on the development of unconformities—The North Slope, Alaska: Tectonics, v. 10, no. 1, p. 101–130.

Curtis, S.M., Ellersieck, I., Mayfield, C.F., and Tailleur, I.L., 1984, Reconnaissance geologic map of the DeLong Mountains A1 and B1 quadrangles and part of the C2 quadrangle, Alaska: U.S. Geological Survey Miscellaneous Investigations Series Map I–1930, scale 1:63,360.

Dickinson, W.R., 1976, Plate tectonic evolution of sedimentary basins: American Association of Petroleum Geologists, Continuing Education Short Course Note Series, v. 1, p. 1–62.

Dillon, J.T., 1989, Structure and stratigraphy of the southern Brooks Range and northern Koyukuk basin near the Dalton Highway, *in* Mull, C.G., and Adams, K.E., eds., Dalton Highway, Yukon River to Prudhoe Bay, Alaska: Bedrock geology of the eastern Koyukuk basin, central Brooks Range, and east central Arctic Slope: Fairbanks, Alaska, Alaska Division of Geological and Geophysical Surveys Guidebook 7, v. 2, p. 157–187.

Fehri, N., 1990, Histoire de la subsidence du bassin de Colville (North Slope Alaska): Universite Pierre et Marie Curie, Paris, Labaratoire de Geologie, M.S. thesis.

Flemings, P.B., 1992, Three-dimensional foreland basin stratigraphic geometry and subsidence history: Colville trough, Alaska [abs]: Annual meeting of the American Association of Petroleum Geologists, Calgary, p. 41.

Frederiksen, N.O., Ager, T.A., and Edwards, L.E., 1988, Palynology of Maastrichtian and Paleocene rocks, lower Colville River region, North Slope of Alaska: Canadian Journal of Earth Science, v. 25, p. 512–527.

Gottschalk, R.R., Jr., and Oldow, J.S., 1988, Low-angle normal faults in the south-central Brooks Range fold and thrust belt, Alaska: Geology, v. 16, p. 395–399.

Grantz, A., May, S.D., and Hart, P.E., 1990, Geology of the Arctic continental margin of Alaska, *in* Grantz, A., Johnson, L., and Sweeney, J.F., eds., The geology of North America; The Arctic ocean region: Geological Society of America, p. 257–288.

Haga, H., and Mickey, M.B., 1983a, Jurassic-Neocomian seismic stratigraphy, NPRA: A report of work performed for the U.S. Geological Survey: San Diego, Biostratigraphics, Inc., unpublished report.

Haga, H., and Mickey, M.B., 1983b, South Barrow area Neocomian biostratigraphy: A report of work performed for the U.S. Geological Survey: San Diego, Biostratigraphics, Inc., unpublished report.

Haq, B.U., and others, 1986, Mesozoic-Cenozoic Cycle Chart: Houston, TX, Exxon.

Harland, W.B., Armstrong, R.L, Cox, A.V., Craig, L.E., Smith, A.G., and Smith, D.G., 1990, A geologic time scale: Cambridge University Press, 263 p.

Hawk, J.M., 1986, Lithospheric flexure, overthrust timing, and stratigraphic modeling of the central Brooks Range and Colville foredeep: Houston, TX, M.S. thesis, Rice University, 179 p.

Homewood, P., Allen, P.A., and Williams, G.D., 1986, Dynamics of the Molasse Basin of western Switzerland: Special Publications of the International Association of Sedimentologists, v. 8, p. 199–217.

Howell, D.G., Bird, K.J., Huafu, L., and Johnsson, M.J., 1992, Tectonics and petroleum potential of the Brooks Range fold and thrust belt—A progress report, *in* Bradley, D.C., and Ford, A.B., eds., Geological Studies in Alaska by the U.S. Geological Survey, 1990: U.S. Geological Survey Bulletin 1999, p. 112–126.

Hubbard, R.J., Edrich, S.P., and Rattey, R.P., 1987, Geologic evolution and hydrocarbon habitat of the 'Arctic Alaska Microplate', *in* Tailleur, I., and Weimer, P., eds., Alaskan North Slope Geology: Bakersfield, California and Anchorage, Alaska, Pacific Section, Society of Economic Paleontologists and Mineralogists and Alaska Geological Society, p. 797–830.

Kauffman, E.G., and Caldwell, W.G.E., 1993, The Western Interior Basin in space and time, *in* Caldwell, W.G.E., and Kauffman, E.G., eds., Evolution of the Western Interior Basin: Geological Association of Canada Special Paper 39, p. 1–30.

Kirschner, C.E., and Rycerski, B.A., 1988, Petroleum potential of representative stratigraphic and structural elements in the National petroleum Reserve in Alaska, *in* Gryc, G., ed., Geology and exploration of the National Petroleum Reserve in Alaska, 1974 to 1982: U.S. Geological Survey Professional Paper 1399, p. 191–208.

Kominz, M.A., and Bond, G.C., 1986, Geophysical modelling of the thermal history of foreland basins: Nature, v. 320, p. 252–256.

Lerand, M., 1973, Beaufort Sea, *in* McCrossam, R.G., ed., The future petroleum provinces of Canada—Their geology and potential: Canadian Society of Petroleum Geology Memoir 1, p. 315–386.

Little, T.A., Miller, E.L., Lee, J., and Law, R.D., in press, Extensional origin of ductile fabrics in the schist belt, central Brooks Range, Alaska—I. Geologic and structural studies: Tectonics.

Magoon, L.B., Bird, K.J., Claypool, G.E., Weitzman, D.E., and Thompson, R.H., 1988, Organic geochemistry, hydrocarbon occurrence, and stratigraphy of government-drilled wells, North Slope, Alaska, *in* Gryc, G., ed., Geology and exploration of the National Petroleum Reserve in Alaska, 1974 to 1982: U.S. Geological Survey Professional Paper 1399, p. 483–487.

Mayfield, C.F., Tailleur, I.L., and Ellersieck, I., 1988, Stratigraphy, structure, and palinspastic synthesis of the western Brooks Range, northwestern Alaska, *in* Gryc, G., ed., Geology and exploration of the National Petroleum Reserve in Alaska, 1974 to 1982: U.S. Geological Survey Professional Paper 1399, p. 143–186.

Mickey, M.B., and Haga, H., 1987, Report on the Neocomian biostratigraphy of the NPRA: San Diego, Micropaleo Consultants, Inc., unpublished report.

Mickey, M.B., and Haga, H., 1990, North Slope data base biostratigraphy summaries: San Diego, Micropaleo Consultants, Inc., unpublished report.

Mickey, M.B., and Haga, H., 1994, Biostratigraphy Report: 12 12Encinitas, CA, Micropaleo Consultants, Inc., unpublished report.

Miller, E.L., and Hudson, T.L., 1991, Mid-Cretaceous extensional fragmentation of a Jurassic-Early Cretaceous compressional orogen, Alaska: Tectonics, v. 10, p. 781–796.

Molenaar, C.M., 1985, Subsurface correlation and depositional history of the Nanushuk Group and related strata, North Slope, Alaska, *in* Huffman, A.C., Jr., ed., Geology of the Nanushuk Group and related rocks, North Slope, Alaska: U.S. Geological Survey Bulletin 1614, p. 37–58.

———1988, Depositional history and seismic stratigraphy of Lower Cretaceous rocks in the National Petroleum Reserve in Alaska and adjacent areas, *in* Gryc, G., ed., Geology and exploration of the National Petroleum Reserve in Alaska, 1974 to 1982: U.S. Geological Survey Professional Paper 1399, p. 593–621.

Molenaar, C.M., Bird, K.J., and Collett, T.S., 1986, Regional correlation sections across the North Slope of Alaska: U.S. Geological Survey Miscellaneous Geologic Studies Map MF-1907.

Molenaar, C.M., Bird, K.J., and Kirk, A.R., 1987, Cretaceous and Tertiary stratigraphy of northeastern Alaska, *in* Tailleur, I., and Weimer, P., eds., Alaskan North Slope Geology: Bakersfield, California and Anchorage, Alaska, Pacific Section, Society of Economic Paleontologists and Mineralogists and Alaska Geological Society, p. 513–528.

Moore, T.E., Wallace, W.K., Bird, K.J., Karl, S.M., Mull, C.G., and Dillon, J.T., 1992, Stratigraphy, structure, and geologic synthesis of northern Alaska: U.S. Geological Survey, Open-File Report, No. 92-330, 183 p.

Mull, C.G., 1982, The tectonic evolution and structural style of the Brooks Range, Alaska: An illustrated summary, *in* Powers, R.B., ed., Geological studies of the cordilleran thrust belt: Denver, Colo., Rocky Mountain Association of Geologists, v. 1, p. 1–45.

———1989, Summary of structural style and history of Brooks Range deformation, *in* Mull, C.G., and Adams, K.E., eds., Dalton Highway, Yukon River to Prudhoe Bay, Alaska: Bedrock geology of the eastern Koyukuk basin, central Brooks Range, and east central Arctic Slope: Fairbanks, Alaska, Alaska Division of Geological and Geophysical Surveys Guidebook 7, p. 47–56.

Nunn, J.A., Czerniak, M., and Pilger, R.H., 1987, Constraints on the structure of Brooks Range and Colville Basin, northern

Alaska, from flexure and gravity analysis: Tectonics, v. 6, no. 5, p. 603–617.

Oldow, J.S., Seidensticker, C.M., Phelps, J.C., Julian, F.E., Gottschalk, R.R., Boler, K.W., Handschy, J.W., and Avé Lallement, H.G., 1987, Balanced cross sections through the central Brooks Range and North Slope, Arctic Alaska: American Association of Petroleum Geologists publication, 19 p., 8 plates, scale 1:200,000.

O'Sullivan, P.B., 1993, Late Mesozoic to Cenozoic thermal and uplift history of the North Slope foreland basin, northern Alaska and northwestern Canada: La Trobe University, Bundoora, Victoria, Australia, Ph.D. dissertation, 419 p.

O'Sullivan, P.B., Moore, T.E., Murphy, J.M., in press, Tertiary uplift of the Mt. Doonerak antiform, central Brooks Range, Alaska: Apatite fission track evidence from the trans-Alaska crustal transect: Geological Society of America Memoir.

Schenk, C.J., and Bird, K.J., 1993, Depositional sequences in Lower Cretaceous rocks, Atigun syncline and Slope Mountain areas, Alaskan North Slope, *in* Dusel-Bacon, C., and Till, A.B., eds., Geologic studies in Alaska by the U.S. Geological Survey, 1992: U.S. Geological Survey Bulletin 2068, p. 48–58.

Steckler, M.S., and Watts, A.B., 1978, Subsidence of the Atlantic type continental margin off New York: Earth and Planetary Science Letters, v. 42, p. 1-13.

Tailleur, I.L., 1973, Probable rift origin of Canada basin, *in* Pitcher, M.G., ed., Arctic geology: American Association of Petroleum Geologists Memoir 19, p. 526–535.

Till, A.B., 1992, Detrital blueschist-facies metamorphic mineral assemblages in Early Cretaceous sediments of the foreland basin of the Brooks Range, Alaska, and implications for orogenic evolution: Tectonics, v. 11, no. 6, p. 1207–1223.

Till, A.B., and Snee, L.W., in press, $^{40}Ar/^{39}Ar$ evidence that formation of blueschists in continental crust was synchronous with foreland fold and thrust belt deformation, western Brooks Range, Alaska: Journal of Metamorphic Geology.

Van Hinte, J.E., 1978, Geohistory analysis—Application of micropaleontology in exploration geology: American Association of Petroleum Geologists Bulletin, v. 62, p. 201–222.

Wirth, K.R., and Bird, J.,M., 1992, Chronology of ophiolite crystallization, detachment, and emplacement—Evidence from the Brooks Range, Alaska: Geology, v. 20, no. 1, p. 75–78.

Witmer, R.J., Haga, H., and Mickey, M.B., 1981a, Biostratigraphic report of thirty-three wells drilled from 1975 to 1981 in National Petroleum Reserve in Alaska: U.S. Geological Survey, Open-File Report, No. 81-1166.

Witmer, R.J., Mickey, M.B., and Haga, H., 1981b, Biostratigraphic correlations of selected test wells of National Petroleum Reserve in Alaska: U.S. Geological Survey, Open-File Report, No. 81-1165.

Reviewers: C. Gil Mull and Marc Hendrix

Cyrtospirifer from Upper Devonian Rocks of the Endicott Group, West-Central Brooks Range, Alaska

By J. Thomas Dutro, Jr., Robert B. Blodgett, *and* Charles G. Mull

ABSTRACT

Fossils from beds mapped as the Noatak Sandstone (Endicott Group) in the Killik River quadrangle, west-central Brooks Range, indicate a Late Devonian (early Famennian) age. Both megafossils (mainly brachiopods) and microfossils (conodonts) suggest a time equivalence with the upper part of the Hunt Fork Shale of the eastern Endicott Mountains and the type Noatak Sandstone of the Nimiuktuk Valley. Correlation with the *Eoparaphorhynchus* Zone of Sartenaer (1969) in the Sassenach Formation of Alberta and the Three Forks Formation of Montana is suggested.

INTRODUCTION

This paper presents biostratigraphic interpretations and taxonomic descriptions of two collections of well-preserved invertebrate fossils (brachiopods) from the Noatak Sandstone of the Endicott Group in the western Endicott Mountains. The collections were made during the course of a collaborative geologic mapping project by the Alaska Division of Geological and Geophysical Surveys (ADGGS) and the U.S. Geological Survey (USGS) in the southeastern part of the National Petroleum Reserve in Alaska (NPRA), funded in part by the U.S. Bureau of Mines. The fossil collections were made by C.G. Mull and R.R. Reifenstuhl of the ADGGS in 1991 during their mapping of the Killik River A-5 and B-5 quadrangles. The locality from which both collections were made is on a ridge crest about 10 km (6 miles) south of the Brooks Range mountain front and 3 km (1.8 miles) northwest of the junction of two prominent forks of Ivotuk Creek (fig. 1) at an elevation of 1,450 m (4,500 feet); this is in the center of sec. 30, T. 33 N., R. 14 E., Kateel River Meridian (lat 68°13.66′ N., long 155°42.5′ W.). The regional geologic setting of the Devonian and Lower Mississippian rocks in the Killik River quadrangle is given by Brosgé and others (1979b) and by C.G. Mull and others (unpublished mapping, 1994).

STRATIGRAPHY

The fossil collections were made from two exposures of thin, silty limestone beds near one another in a 5-meter-thick phyllitic shale unit that immediately overlies a conspicuous, massive, 20-meter-thick (approximately 60 feet) marker unit of quartzitic sandstone and conglomerate. These strata are apparently within the lower part of the Noatak Sandstone of the Endicott Group (fig. 2). The massive unit is partly limonite-cemented quartzitic sandstone in 1- to 3-meter-thick, upward-thickening cycles and contains rounded, matrix-supported clasts of quartz and black chert up to 2 cm in diameter. The unit is both overlain and underlain by thin-bedded micaceous and limonitic sandstone and phyllitic siltstone, here provisionally mapped as the Noatak Sandstone. In the eastern Endicott Mountains, lithologically similar thin-bedded rocks are known as the informally named wacke member of the Hunt Fork Shale (Brosgé and others, 1979a, b). The massive marker unit can be traced more than 5 km westward as a nearly continuous belt of outcrops that partly defines the flanks of a regional west-plunging antiform. The quartzite and conglomerate unit, the fossiliferous horizon, and both the overlying and underlying sandy beds of the Noatak Sandstone overlie thick phyllitic siltstone and shale of the Hunt Fork Shale. All these units are part of a package of rocks that, in turn, overlies a regional thrust fault that is probably a splay of the Toyuk thrust mapped by Brosgé and others (1979a, b) in the Chandler Lake and Philip Smith Mountains quadrangles in the eastern Endicott Mountains.

This fossiliferous locality is significant because it apparently constrains the age of the underlying quartzite and conglomerate unit in the Noatak Sandstone in the Endicott Group of the western Endicott Mountains. The conglomeratic unit contrasts sharply with the generally thinner and finer grained quartzitic sandstone beds of the Kanayut Conglomerate, exposed both above and below the Toyuk thrust. In contrast to its type area where interbedded shale is common, the Kanayut in the western Endicott Mountains consists mostly of fine- to medium-grained quartzitic sandstone in beds up to about 1 m thick, forming units up to

3 m thick. Although the Kanayut forms resistant outcrops in the Ivotuk Creek area, it is not as coarse-grained as the massive conglomeratic unit in the Noatak Sandstone.

Both the Noatak Sandstone and Kanayut Conglomerate in the western Endicott Mountains contrast markedly in grain size and thickness with their laterally equivalent counterparts exposed in the eastern Endicott Mountains. In the Ivotuk Creek area, the Kanayut is about 200 m (approx. 600 ft) thick whereas, in its type area in the Chandler Lake quadrangle, it is as much as 3,000 m (9,300 ft) thick and contains many massive conglomerate beds with clasts up to 22 cm (9 in) in diameter (Nilsen and Moore, 1984). Although the Noatak Sandstone is reported to contain some conglomeratic beds in the eastern Endicott Mountains (Nilsen and Moore, 1984) none is as thick as the resistant unit in the Ivotuk Creek area of the western Endicott Mountains.

AGE AND CORRELATION

A Late Devonian (Famennian) age is indicated by both the megafauna and conodonts from the samples collected at this locality. The low-diversity brachiopod assemblage was collected at both places (Loc. numbers USGS 12247-SD and 12248-SD, field numbers 91AMu 25 and 91ARR 62a, respectively). Cyrtospirifers and rhynchonellids are the most abundant forms, accompanied by the distinctive athyrid *Crinisarina*. The association is the same as that found in parts of the Three Forks Formation of Montana and the Sassenach Formation of Alberta; this part of the early Famennian was designated the *Eoparaphorhynchus* Zone by Sartenaer (1969) and, from place to place, it contains one or more distinctive rhynchonellid genera. In these Alaskan collections, two species of *Eoparaphorhynchus* are present.

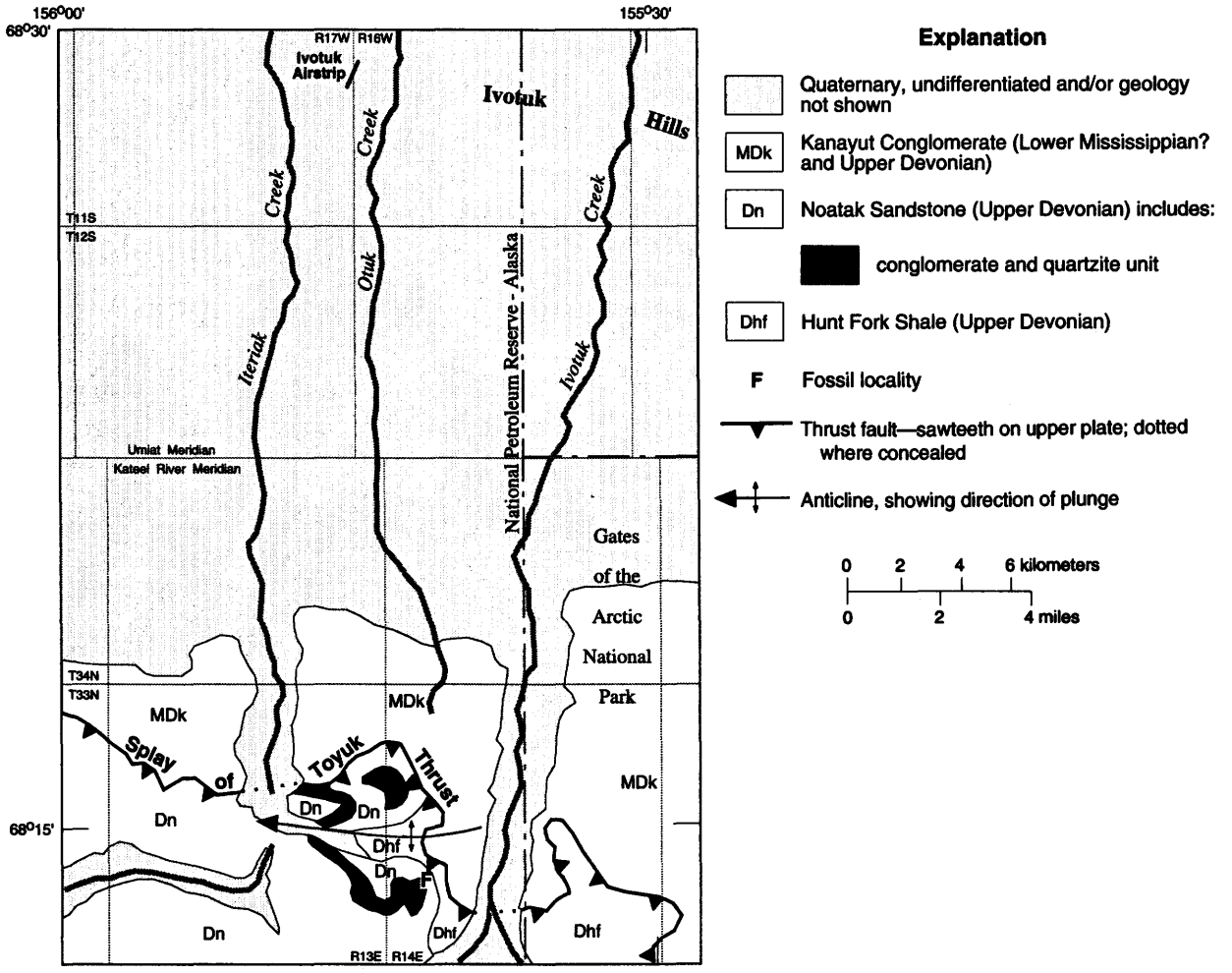

Figure 1. Geologic index map of Ivotuk Creek area, western Killik River quadrangle, showing location of fossil collections and generalized distribution of the Hunt Fork Shale, Noatak Sandstone, and Kanayut Conglomerate.

Conodonts were studied by Anita Harris of the U.S. Geological Survey. Both collections yielded species that indicate an early Famennian age, ranging from the Lower *triangularis* Subzone to the Lower *crepida* Subzone of Ziegler and Sandberg (1990), according to Harris (written commun., 1992).

There is no question, then, about the early Famennian age of these beds. The Noatak Sandstone, in its type area in the lower Nimiuktuk valley, contains Cyrtospirifers of probable Famennian age and, in the eastern Endicott Mountains, the unit identified and mapped as the wacke member of the Hunt Fork Shale contains a great variety of early Famennian brachiopods, along with rare mollusks and tentaculitids (Brosgé and others, 1979a). All these units are regionally correlative and we consider them to represent megafacies variants of the Noatak Sandstone.

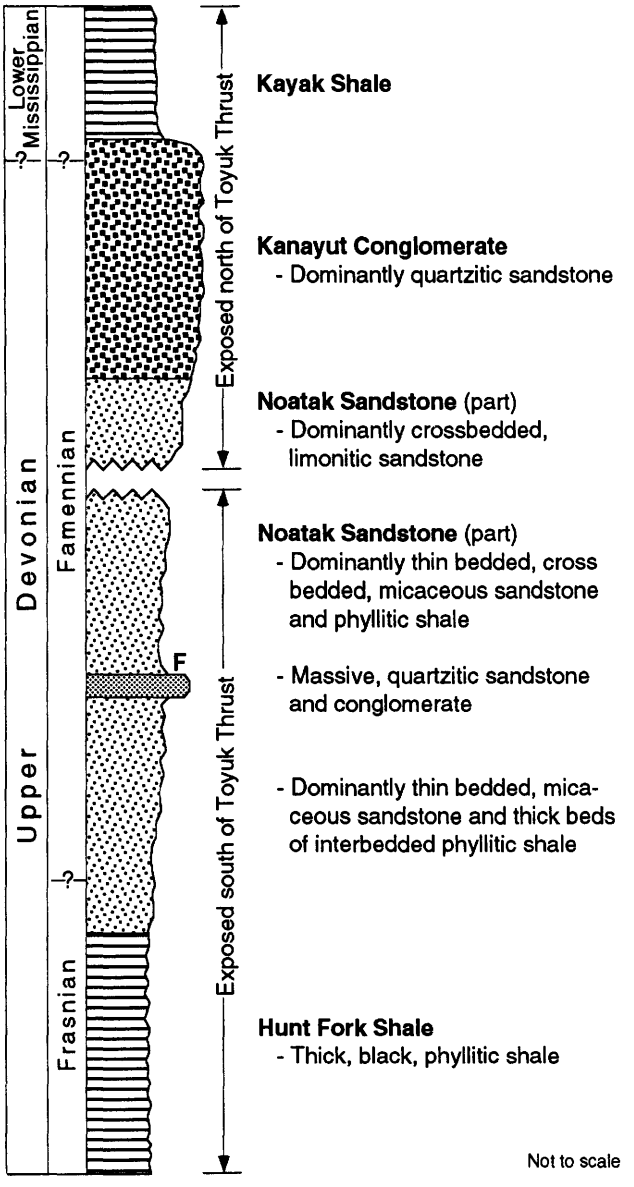

Figure 2. Generalized stratigraphic column of the Endicott Group in Ivotuk Creek area. F, approximate level of fossil collections.

PALEONTOLOGY

Although the brachiopods in these collections can be identified to genus, there is not enough material available to provide the variability needed to establish new species. However, all the forms can be readily assigned to closely related species from western Canada and the United States, and the morphological similarities and contrasts are given in the following discussion. Ultimately, each of these morphologic entities will probably represent species limited to the central and western Brooks Range.

RHYNCHONELLACEANS

Eoparaphorhynchus cf. *E. maclareni* Sartenaer (fig. 3*J–N*). Our single specimen falls well within the limits of morphologic variability established by Sartenaer (1969) for the Canadian species. It is a fairly large shell, measuring 21 mm long, 23 mm wide, and 18 mm thick. By way of comparison, the holotype specimen is 20.7 mm long, 24.3 mm wide, and 16.6 mm thick. Specimens measured by Sartenaer ranged from 17.5 to 26.3 mm long, 20.7 to 28.8 mm wide, and 13.9 to 22.3 mm thick.

The shoulder angle of the Alaskan specimen is about 110 degrees, whereas the range in the Canadian material is from 100 to 125 degrees and, for the holotype, the angle is 115 degrees. There are three costae on the fold and two in the sulcus of the Alaskan specimen; each flank has two indistinct costae. The costal formulae of the type material show that nearly three-quarters of the specimens have the same costal arrangement as our specimen.

Eoparaphorhynchus cf. *E. walcotti* (Merriam) (fig. 3*E–I*, *O–S*). These specimens are smaller than the single shell described above. The two Alaskan specimens are 15.5 and 14.5 mm long, 18.0 and 17.5 mm wide and 12.5 and 14.0 mm thick, respectively. There are four costae on the fold and three in the sulcus of each specimen; the number of lateral costae ranges from 6–8 on one specimen to 8–10 on the other. The shoulder angles are 120 and 125 degrees. The specimens of this species that are discussed and illustrated by Sartenaer (1969) range in size from 16.1 to 24.0 mm long, 18.2 to 28.8 mm wide, and 7.7 to 21.8 mm thick, and the variation of costal formulae includes the range shown in our specimens. It is likely that the Alaskan shells are juveniles or young adults of this species.

CYRTOSPIRIFERIDS

There are more than 30 reasonably complete specimens of cyrtospirifers from the Alaskan collections. These fall naturally into two groups: a narrow-hinged form with length and width about equal, and a wider-hinged form with the width almost twice the length of the shell. Both seem to be true *Cyrtospirifer*; each can be related to previously described species from North America.

In his discussion of early Famennian faunas in the *Eoparaphorhynchus* Zone, Sartenaer (1969) lists other elements of the assemblages, including Cyrtospirifers. For example, in Nevada the zone contains at least two species, one referred to *C. portae* Merriam and the other to *C. whitneyi* (Hall). The fauna of the Three Forks Formation of western Montana also includes *C. monticola* (Haynes) at about this same level. In New York State, *C. preshoensis* Greiner characterizes the lower part of the Canadaway Group (early Famennian) (Rickard, 1975) and resembles many of the Alaskan specimens. It is clear that there is a great deal of variation among the species in this genus, but those of the early Famennian are quite similar in shape and costal patterns. For the purposes of this analysis, we refer the two Alaskan forms to *C. portae* Merriam and *C. monticola* (Haynes).

Cyrtospirifer cf. *C. portae* Merriam (fig. 4*A–H*, *K–N*). This is by far the more abundant form in the Alaskan material. It is the narrower hinged, more nearly equidimensional shell with a well-differentiated fold and sulcus. Average dimensions are about 22 mm wide, 18 mm long, and 14 mm thick. The widest part of the shell is about one-fifth the distance from the hinge to the anterior. The subangular fold has two distinct parts: a central third that has 8 to 10 fine costae and two outer thirds with six costae each. Lateral costae vary from about 16 to 18 on each flank. One specimen shows several lateral costae that split near the anterior margin (see fig. 4*E*). The large triangular area is slightly incurved and the middle third is occupied by an open delthyrium. Internally, long, subparallel dental plates are present in the ventral valve, and a comblike process is present in the dorsal valve (see internal mold, fig. 4*L–M*).

Cyrtospirifer cf. *C. monticola* (Haynes) (fig. 4*I–J*). This slightly wider, more rectangular form is less common than the other and bears more costae. The illustrated specimen is about 26 mm wide, 16 mm long, and 16 mm thick. The gently rounded fold and sulcus contain about 12 costae at the anterior margin. There are more than 20 costae on each flank; 28 were counted on a particularly well preserved specimen. The large triangular area is generally apsaclinal, with the inclination of the ventral area reaching nearly 180 degrees in a few specimens. This form also has an open delthyrium that occupies about one-third of the area.

ATHYRIDACEAN

Crinisarina sp. (fig. 3*A–D*). There is a single specimen of this genus in the Alaskan material. This brachiopod is closely related to *C. angelicoides* (Merriam) which was reassigned to this genus when it was established by Cooper and Dutro (1982). Most specimens of this genus are slightly worn, as is this one, so that the distinctive microornament is not preserved. Nevertheless, this closely related group of species is characteristically Famennian in age, mostly early Famennian. The shell is subpentagonal in outline and has a broad fold and sulcus; otherwise it appears smooth. There is a narrow depression in the sulcus that extends from about mid-length to the anterior margin. There appears to be no counterpart to this feature on the fold. The shell is about 16.6 mm wide, 12.0 mm long, and 11.0 mm thick; the apical angle is about 120 degrees.

SUMMARY

Five species of Late Devonian brachiopods are described from an outcrop of beds provisionally mapped as the Noatak Sandstone in the Killik River quadrangle, northern Alaska. Two species of the rhynchonellid genus *Eoparaphorhynchus*, two species of the spiriferid genus *Cyrtospirifer*, and an athyrid *Crinisarina* are representative of the early Famennian *Eoparaphorhynchus* Zone of Sartenaer (1969). Conodonts identified by Anita Harris are of this same age, assigned by her to the interval from the Lower *triangularis* to the Lower *crepida* Subzones in the early Famennian. Strata of this age are found across the Brooks Range in the upper part of the Hunt Fork Shale and the Noatak Sandstone and their lateral equivalents.

Acknowledgments.—The authors thank R.R. Reifenstuhl and E.E. Harris for assistance in the field, and W.P. Brosgé and I.L. Tailleur for pioneering work in the region, and for continued encouragement to unravel the Paleozoic history of the central Brooks Range. Brosgé, W.A. Oliver, Jr., and Thomas E. Moore provided helpful technical reviews of the manuscript. We also thank Anita Harris for her identifications and interpretations of the conodonts associated with the megafossils. It is heartening but, of course, not unexpected to find such close agreement on the age significance of the megafauna and the conodonts. All conclusions, however, are those of the authors, who share any blame for errors or inadequacies of interpretation in this report.

REFERENCES CITED

Brosgé, W.P., Reiser, H.N., Dutro, J.T., Jr., and Detterman, R.L., 1979a, Bedrock geologic map of the Philip Smith Mountains

quadrangle, Alaska: U.S. Geological Survey Miscellaneous Field Studies MF–879–B, scale 1:250,000, 2 sheets.

Brosgé, W.P., Reiser, H.N., Dutro, J.T., Jr., and Nilsen, T.N., 1979b, Geologic map of the Devonian rocks in parts of the Chandler Lake and Killik River quadrangles, Alaska: U.S. Geological Survey Open-File Report 79-1224, scale 1:200,000.

Cooper, G.A., and Dutro, J.T., Jr., 1982, Devonian brachiopods of New Mexico: Bulletins of American Paleontology, v. 82 and 83, no. 316, 215 p., 45 plates.

Greiner, Hugo, 1957, "*Spirifer disjunctus*": Its evolution and paleoecology in the Catskill Delta: Peabody Museum of Natural History, Yale University, Bulletin 11, 75 p., 13 plates.

Merriam, C.W., 1940, Devonian stratigraphy and paleontology of the Roberts Mountains region, Nevada: Geological Society of America Special Papers No. 25, 114 p., 16 plates.

Nilsen, T.N., and Moore, T.E., 1984, Stratigraphic nomenclature of the Upper Devonian and Lower Mississippian (?) Kanayut Conglomerate, Brooks Range, Alaska: U.S. Geological Survey Bulletin 1529–A, 64 p.

Rickard, L.V., 1975, Correlation of the Silurian and Devonian rocks in New York State: New York State Museum and Science Service Map and Chart Series No. 24, 16 p., 4 plates.

Sartenaer, Paul, 1969, Late Upper Devonian (Famennian) rhynchonelloid brachiopods from western Canada: Geological Survey of Canada Bulletin 169, 269 p., 19 plates.

Ziegler, Willi, and Sandberg, C.A., 1990, The Late Devonian Standard Conodont Zonation: Courier Forschunginstitut Senckenberg 121, 115 p.

Reviewers: W.P. Brosgé and W.A. Oliver, Jr.

Figure 3. Brachiopods from Ivotuk Creek area. All specimens are deposited in the U.S. National Museum (U.S.N.M.).

Crinisarina sp.

A–D, Dorsal, ventral, anterior, and posterior views of U.S.N.M. 483746, ×3.

Eoparaphorhynchus cf. *E. walcotti* (Merriam)

E–I, Posterior, dorsal, ventral, anterior, and side views of U.S.N.M. 483747, ×2.

O–S, Side, posterior, dorsal, ventral, and anterior views of U.S.N.M. 483748, ×2.

Eoparaphorhynchus cf. *E. maclareni* Sartenaer

J–N, Posterior, dorsal, side, ventral, and anterior views of U.S.N.M. 483749, ×2.

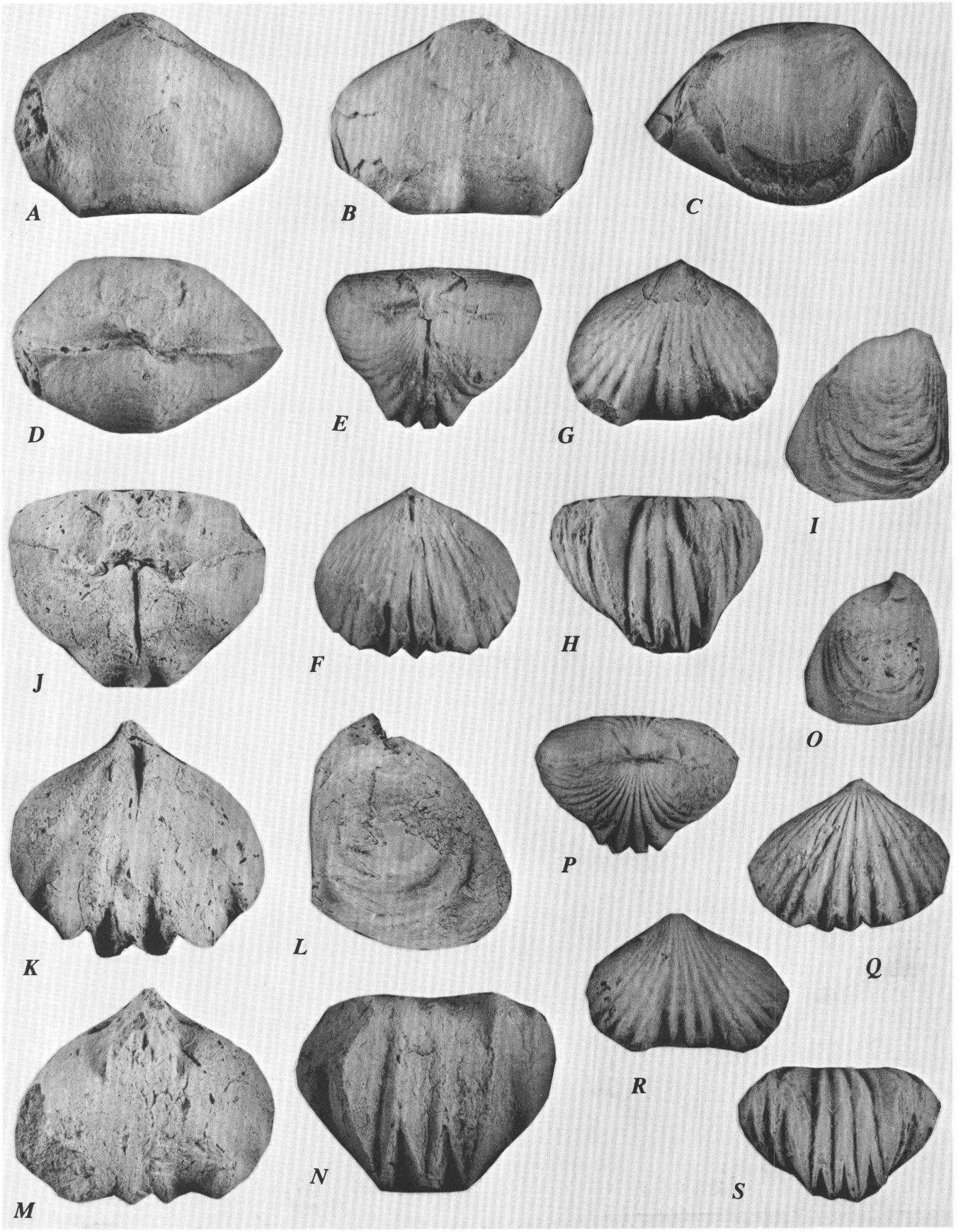
A
B
C
D
E
G
I
J
F
H
O
K
L
P
Q
M
N
R
S

Figure 4. Cyrtospirifers from the Ivotuk Creek area.

Cyrtospirifer cf. *C. portae* Merriam

A–C, Dorsal, ventral, and side views of U.S.N.M. 483750, ×2.

D, Anterior view of U.S.N.M. 483751, ×2.

E, *F*, Anterior and side views of U.S.N.M. 483752, ×2.

G, *H*, Dorsal and posterior views of U.S.N.M. 483753, ×2.

K–N, Side, posterior, anterior, and ventral views of U.S.N.M. 483754, ×2.

Cyrtospirifer cf. *C. monticola* (Haynes)

I, *J*, Dorsal and anterior views of U.S.N.M. 483755, ×2.

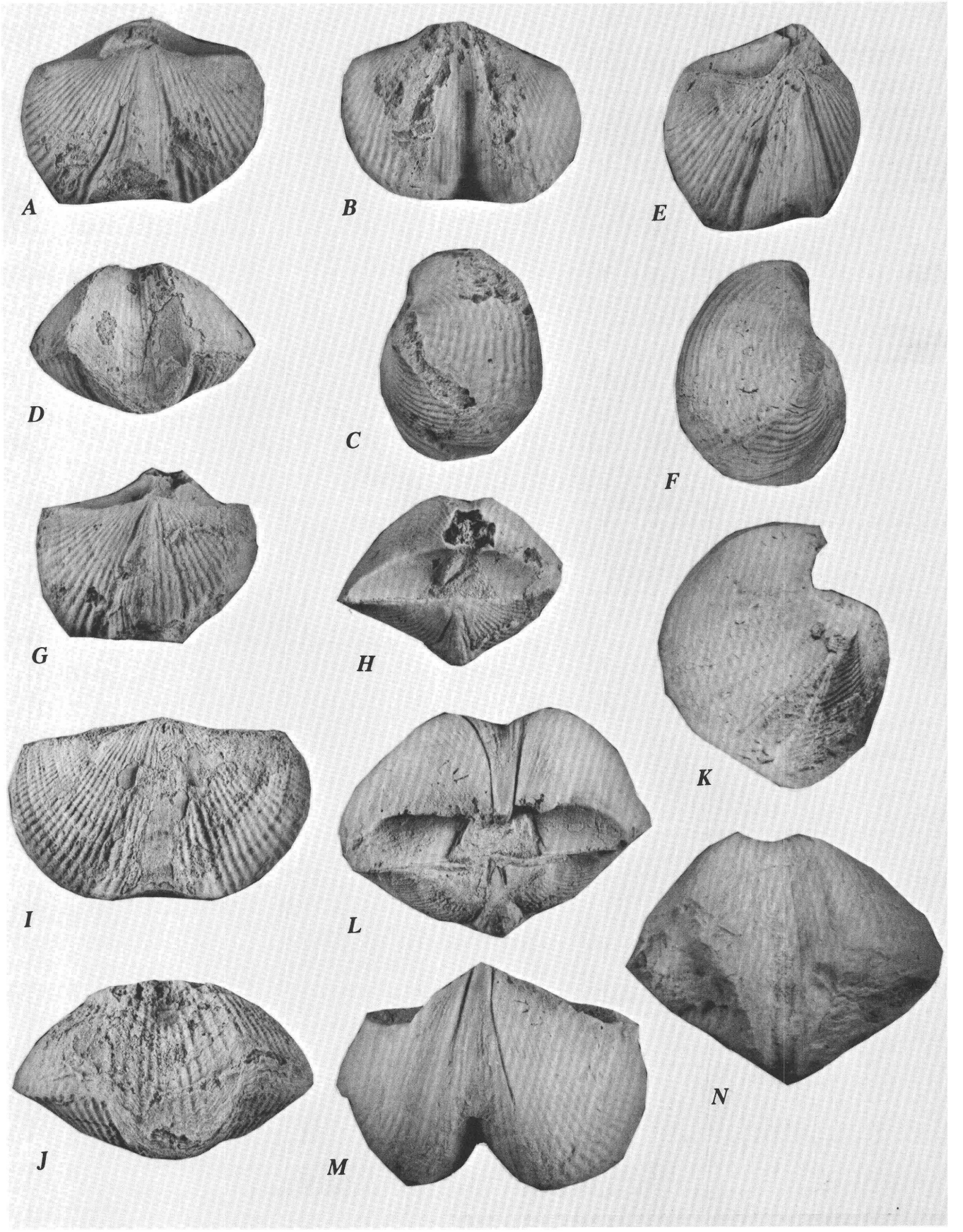
A
B
E
D
C
F
G
H
K
I
L
N
J
M

New Late(?) Proterozoic-Age Formations in the Vicinity of Lone Mountain, McGrath Quadrangle, West-Central Alaska

By Loren E. Babcock, Robert B. Blodgett, *and* James St. John

ABSTRACT

Four new formations of Late(?) Proterozoic age having a cumulative thickness of 618 m are herein proposed in the vicinity of Lone Mountain, McGrath C-4 quadrangle, west-central Alaska. The lowest unit is the lithically heterogeneous Windy Fork Formation, which consists of interbedded siliciclastic redbeds and thin beds of carbonate rocks. The Big River Dolostone, which is a lithically homogeneous dolostone unit containing coated grains and fenestral fabric, conformably overlies the Windy Fork Formation. The lithically heterogeneous Lone Formation, which consists of interbedded siliciclastic redbeds containing abundant sedimentary features and thin beds of carbonate rocks, conformably overlies the Big River Dolostone. The lithically homogeneous Khuchaynik Dolostone, which largely consists of coated grains and contains abundant gossan, conformably overlies the Lone Formation. These four new formations are interpreted to represent supratidal to shallow subtidal marine lithofacies. They are part of the Nixon Fork subterrane of the Farewell terrane and constitute the oldest sedimentary rocks recognized in west-central Alaska. Lithologically similar or equivalent strata are also present in the Holitna basin of southwestern Alaska, where they are exposed in a west-trending anticlinorium in the Sleetmute A-2 quadrangle.

INTRODUCTION

This paper describes four new formations from west-central Alaska. These units are recognized on the basis of field mapping and stratigraphic investigations by the authors in the vicinity of Lone Mountain, McGrath B-4 and C-4 quadrangles, Alaska (figs. 1–4). Much of the field work was completed during July 1993. The named units are all regarded herein as Late(?) Proterozoic in age.

Few Proterozoic units have been formally described from Alaska. Recognition of the formations described herein adds substantially to the knowledge of the Proterozoic in the North American Arctic region and paves the way for future studies of the geologic framework of west-central and southwestern Alaska. The type sections of the four new formations are exposed along a single ridge that is structurally uncomplicated with the exception of the top and possibly the base. Beds along this ridge (figs. 2, 3, 5) strike between N. 30° E. and N. 56° E., and dip 49° to 72° SE. This stratigraphic interval of more than 600 m can be used to help unravel the Proterozoic stratigraphy in some other areas that are structurally more complex. In particular, we expect that the Proterozoic formations described here from the Lone Mountain region will be useful for better understanding the stratigraphy of the southeastern part of the Sleetmute quadrangle to the southwest (see Miller and others, 1989), where a nearly identical stratigraphic succession is exposed.

Strata discussed here are the first of Late(?) Proterozoic age to be described from the Nixon Fork subterrane of the Farewell terrane (fig. 1). As originally defined by Patton (1978), the Nixon Fork is characterized primarily by a distinctive succession of lower and middle Paleozoic platform carbonate rocks. To the east this assemblage grades into stratigraphically equivalent, deeper water basinal rocks (Blodgett, 1983; Blodgett and Gilbert, 1983, 1992a, 1992b; Bundtzen and Gilbert, 1983; Gilbert and Bundtzen, 1983; Blodgett and Clough, 1985) that have been mapped as belonging to other terranes, namely the Dillinger, East Fork, and Minchumina terranes. Decker and others (in press) recognize that the units that previously have been called the Nixon Fork, Dillinger, East Fork, and Minchumina tectonostratigraphic terranes (Jones and others, 1987) are genetically related. They proposed the name Farewell terrane to embrace these entities, and reduced each of them in rank to subterranes of the Farewell. The four new formations defined here constitute the oldest recognized sedimentary rocks of the Nixon Fork subterrane.

LOCATION

The new stratigraphic units reported herein are nearly continuously exposed in rubble crops (surficial rubble

overlying buried, in situ rocks) and minor outcrops along a north-trending ridge that lies in the eastern half of section 14, T. 28 N., R. 30 W., McGrath C-4 quadrangle, directly west of the true Lone Mountain (figs. 2, 3). A GPS measurement taken at the base of the Lone Formation (new) at the type section while aboard the helicopter that transported the authors into the field was 62°30.97′ N., 154°46.74′ W. (accurate to within about 100 m during July 1993). The new formations also have been mapped in the field extending into adjacent areas of the McGrath C-4 and McGrath B-4 quadrangles.

The name "Lone Mountain" as it appears on the current McGrath C-4 1:63,360-scale topographic map (1953) and the McGrath 1:250,000-scale topographic map (1958;

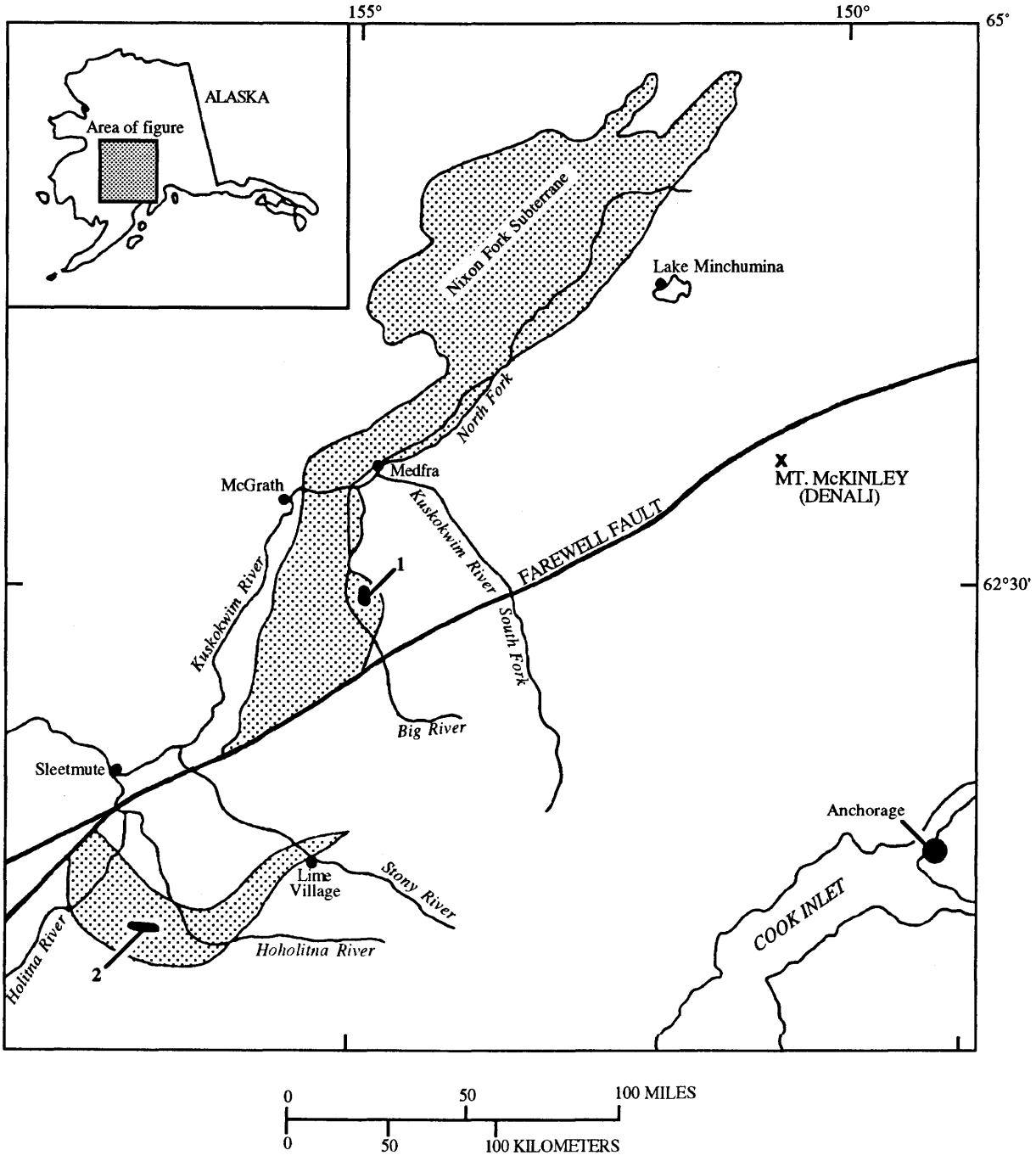

Figure 1. Index map of part of west-central and southwestern Alaska showing location of Nixon Fork subterrane of the Farewell terrane (stippled areas); modified from Blodgett and Gilbert (1992a). Map symbols: 1, area of Proterozoic sedimentary rock exposures in the vicinity of Lone Mountain, McGrath B-4 and C-4 quadrangles; 2, area of Proterozoic sedimentary rock exposures in an west-trending anticlinorium in the Sleetmute A-2 quadrangle.

limited revision 1984) is in conflict with long-standing local usage. On the McGrath C-4 topographic sheet, the name "Lone Mountain" is applied to a low north-trending ridge that lies two ridges west of VABM 2646 (triangulation station Lone), which is the highest topographic feature in the area (fig. 2). The latter feature, which is underlain by the Paleocene Lone Mountain pluton (Reed and Lanphere, 1972, 1973), is markedly higher than the low ridges to the west, and is the only geographic feature in the area that is clearly visible from a distance. Rocks from the pluton were included in previous investigations, having been dated as 58.3±1.6 Ma using K-Ar dating techniques on biotite (Reed and Lanphere, 1972, 1973). Recalculation using the constants of Steiger and Jäger (1977) yields an age of 59.7±1.6 Ma (F.H. Wilson, oral commun., 1993).

STRATA IN THE LONE MOUNTAIN AREA AND HISTORY OF NOMENCLATURE

Sedimentary rocks belonging to the Nixon Fork subterrane of the Farewell terrane that are exposed in the ridges just west of the true Lone Mountain are interpreted to range in age from Late(?) Proterozoic to Ordovician. The four formations described here comprise 618 m of continuous section as measured using a Jacob's staff (fig. 4). Strata were closely examined for evidence of bedding plane faults such as slickensides, repetition of internal stratigraphy, fault breccia, and significant changes in strikes or dips, but no such evidence was found. Moreover, strikes and dips through the measured section do not vary much (fig. 3), suggesting that the rocks have not been internally disrupted. The only fault identified in the measured section (figs. 4, 5*D*) truncates the Khuchaynik Dolostone (new). It was identified by extensive brecciation, introduction of another rock unit (a black platy lime mudstone), and truncation of individual beds.

The rocks comprising the four new formations were previously described and referred to using numerical designations by Babcock and others (1993) but have been otherwise unrecognized in published literature. The formations were identified and mapped based on internal lithic homogeneity or unity compared to adjacent rock units, and distinctive lithic features. Rocks comprising unit 1 of Babcock

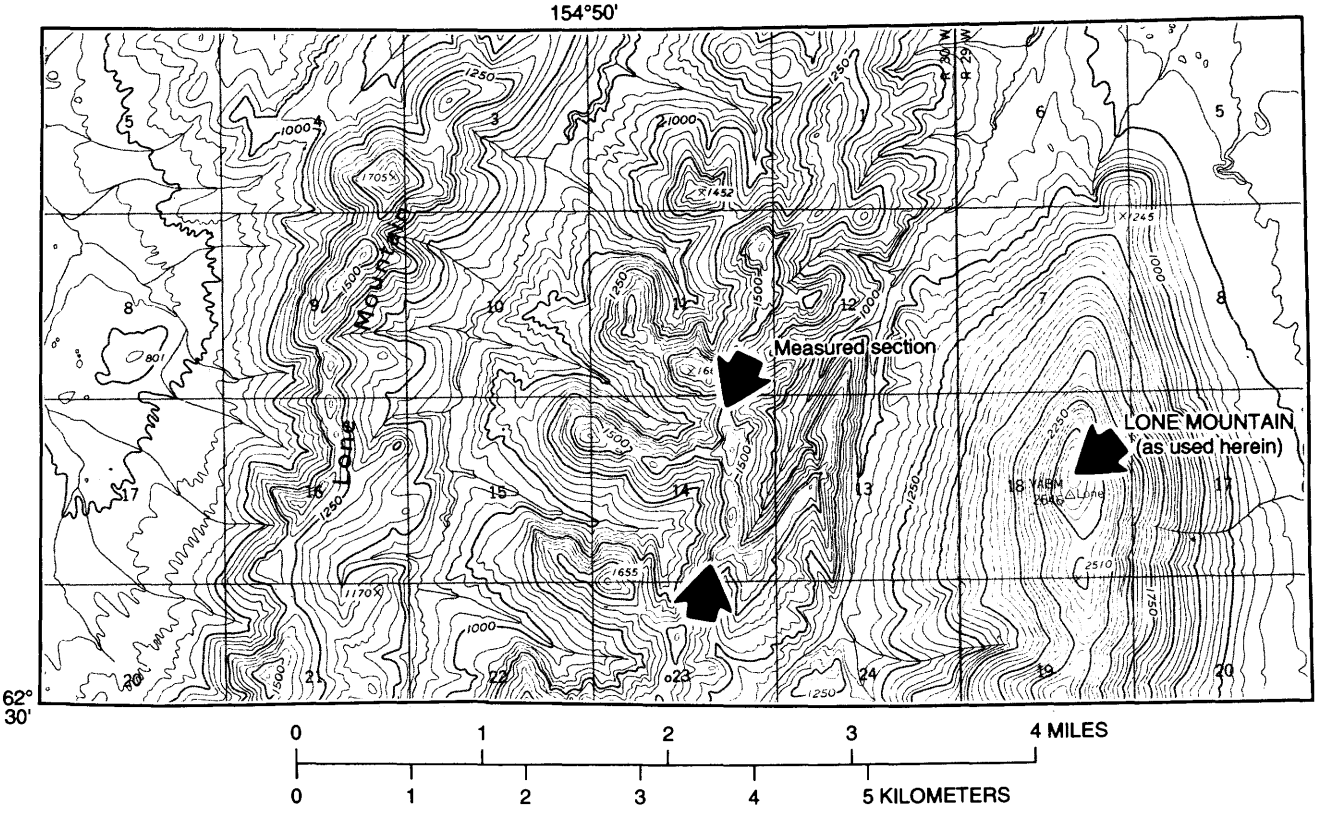

Figure 2. Topographic map showing current and corrected usage of Lone Mountain, as well as location of measured section discussed in text. Map includes part of T. 28 N. from the McGrath C-4 1:63:360 topographic quadrangle (U.S. Geological Survey, 1953). On the map, Lone Mountain is identified by uppercase and lowercase lettering as a low ridge principally through sections 3, 4, 9, 16, and 21 in T. 28 N., R. 30 W. (left). Lone Mountain, as used locally and herein, is the large mountain identified as VABM 2646 (triangulation station Lone) and centered in section 18, T. 28 N., R. 29 W. (right). Measured section described herein is located on ridge between the arrows in section 14, T. 28 N., R. 30 W. (near middle of figure).

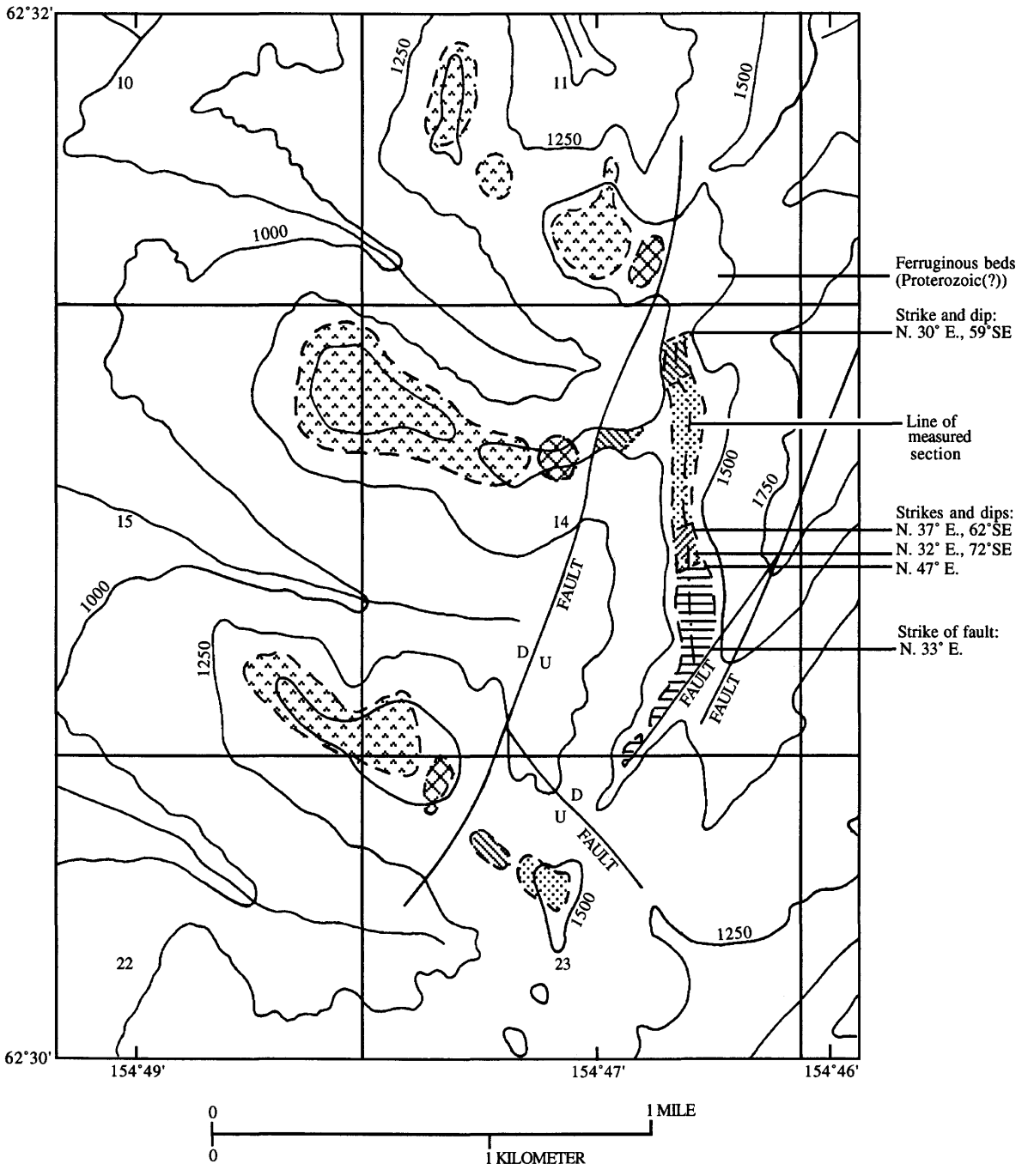

EXPLANATION

- Platy black lime mudstone (Lower Ordovician to Upper Cambrian(?))
- Gray to variegated lime mudstone and siltstone (Middle Cambrian)
- Khuchaynik Dolostone (Late(?) Proterozoic)
- Lone Formation (Late(?) Proterozoic)
- Big River Dolostone (Late(?) Proterozoic)
- Windy Fork Formation (Late(?) Proterozoic)
- Fault--D, downthrown side; U, upthrown side
- Contact--Approximately located

and others (1993) are equivalent to the Windy Fork Formation as defined herein; rocks comprising unit 2 are equivalent to the Big River Dolostone; rocks comprising unit 3 are equivalent to the Lone Formation; and rocks comprising unit 4 are equivalent to the Khuchaynik Dolostone. The authors have mapped other sedimentary rocks of Proterozoic(?) age in the Lone Mountain area, but because of uncertain structural and stratigraphic relations with the coherent succession described herein, they will not be discussed in detail.

An unnamed unit consisting of interbedded lime mudstones and siltstones is present along three northwest-trending ridges that lie to the west of, and are in fault contact with, our measured section. The ridges are mostly located in sections 11, 14, 15, and 23, T. 28 N., R. 30 W., McGrath C-4 quadrangle (fig. 3). The lime mudstones, which are gray to variegated in color and highly stylolitized, contain trilobites and other fossils of Middle Cambrian age (Babcock and others, 1993; St. John, 1994). Gray to gray-green siltstones are sporadically exposed, mostly below the lime mudstones. Based on their close stratigraphic proximity to the Middle Cambrian lime mudstones, the underlying siltstones are also presumed to be of Middle Cambrian age. The lower part of the lime mudstone-siltstone unit is faulted out.

Thick successions of unnamed platy black lime mudstones (weathering to dark gray) conformably overlie the interbedded lime mudstone-siltstone unit of Middle Cambrian age in all three northwest-trending ridges that lie just west of our measured section. Near the base of the dark lime mudstone succession on each ridge is an interval, approximately 20 m thick, that contains several discontinuous carbonate breccia beds ranging up to about 10 m in thickness. The thickest breccia beds form distinctive marker beds for this interval that can be traced by eye to nearby ridges. The platy black lime mudstones that overlie the Middle Cambrian limestones are Late Cambrian(?) and Early Ordovician in age (R.B. Blodgett, unpublished data). They appear to be equivalent to the platy dark lime mudstones that are in fault contact with the Khuchaynik Formation at the top of the measured section (figs. 3, 4).

Beds comprising a ferruginous siltstone to sandstone, dolomudstone, and quartz-pebble conglomerate succession are sporadically exposed in rubble outcrops near the southern end of the hilltop in the SW¼SE¼SE¼ sec. 11, T. 28 N., R. 30 W., McGrath C-4 quadrangle, to the east of the fault (labelled "Ferruginous beds (Proterozoic(?))" in figure 3). Gossan is locally present within the siltstone lithology. Because of limited outcrop, the limits of the unit are not illustrated in figure 3. The stratigraphic relations of this succession to other rock units in the Lone Mountain area are unknown partly because this unit is in fault contact with Middle Cambrian rocks to the northwest. The ferruginous beds have unknown structural and stratigraphic relations with the type section of the Windy Fork Formation because the base of the Windy Fork Formation is covered. The age of the ferruginous beds is unknown; no fossils were discovered in this succession. It is possible that these beds conformably underlie the Windy Fork Formation.

◄ **Figure 3.** Geologic map of ridges to the west of true Lone Mountain showing location of measured section (see fig. 4) of type sections of the Windy Fork Formation, Big River Dolostone, Lone Formation, and Khuchaynik Dolostone. Base is at north end of measured section. Map includes all or parts of sections 10-12, 13-15, and 22-24 of T. 28 N., R. 30 W., McGrath C-4 quadrangle (some section numbers are indicated on map). Contour interval 250 ft. Base map from U.S. Geological Survey, 1953, McGrath C-4 1:63,360 topographic map.

WINDY FORK FORMATION (NEW NAME)

The name "Windy Fork Formation" is here assigned to a succession of siliciclastic redbeds and carbonate rocks that is at least 84 m thick at the unit's type section (fig. 4). Outcrops of the Windy Fork Formation (fig. 5*A*) are dominated by thin- to medium-bedded siltstone and fine- to coarse-grained sandstone; beds range from about 2 to 19 m thick and weather to an earthy yellow or orange-brown color; on fresh surfaces these rocks are various shades of gray. Some sandstone beds show planar cross-beds (see fig. 6*A*). Interbeds of lime mudstone or dolomudstone are up to 6 m thick and weather to a gray or tan color. Small coated grains (2 mm or less in diameter) are sparsely distributed in dolomudstone near the base of the measured section. Pyrite is finely disseminated throughout the formation. The total thickness of the formation is unknown; its base is covered. The top of the formation is defined as the last up-section appearance of siltstone; its upper contact with the Big River Dolostone (new) is sharp and conformable. The position of the contact at 84 m in the measured section was determined by trenching because it was covered.

The Windy Fork Formation is readily distinguished from the lithologically similar and stratigraphically higher Lone Formation (new) by its internal stratigraphy, sedimentary features, and color. The Windy Fork Formation contains proportionately much more siltstone and much less sandstone and dolostone than does the Lone Formation. The distinctive sandstone-siltstone couplets found near the middle of the Lone Formation have no counterpart in the Windy Fork Formation (fig. 4). Although planar cross-beds are found in sandstone intervals of both formations, they are much more common in the Lone Formation. The Windy Fork Formation has not been observed to have symmetrical ripple marks, load casts, and siltstone intraclasts, all of which are common in the Lone Formation. The Windy Fork Formation contains dolostone beds

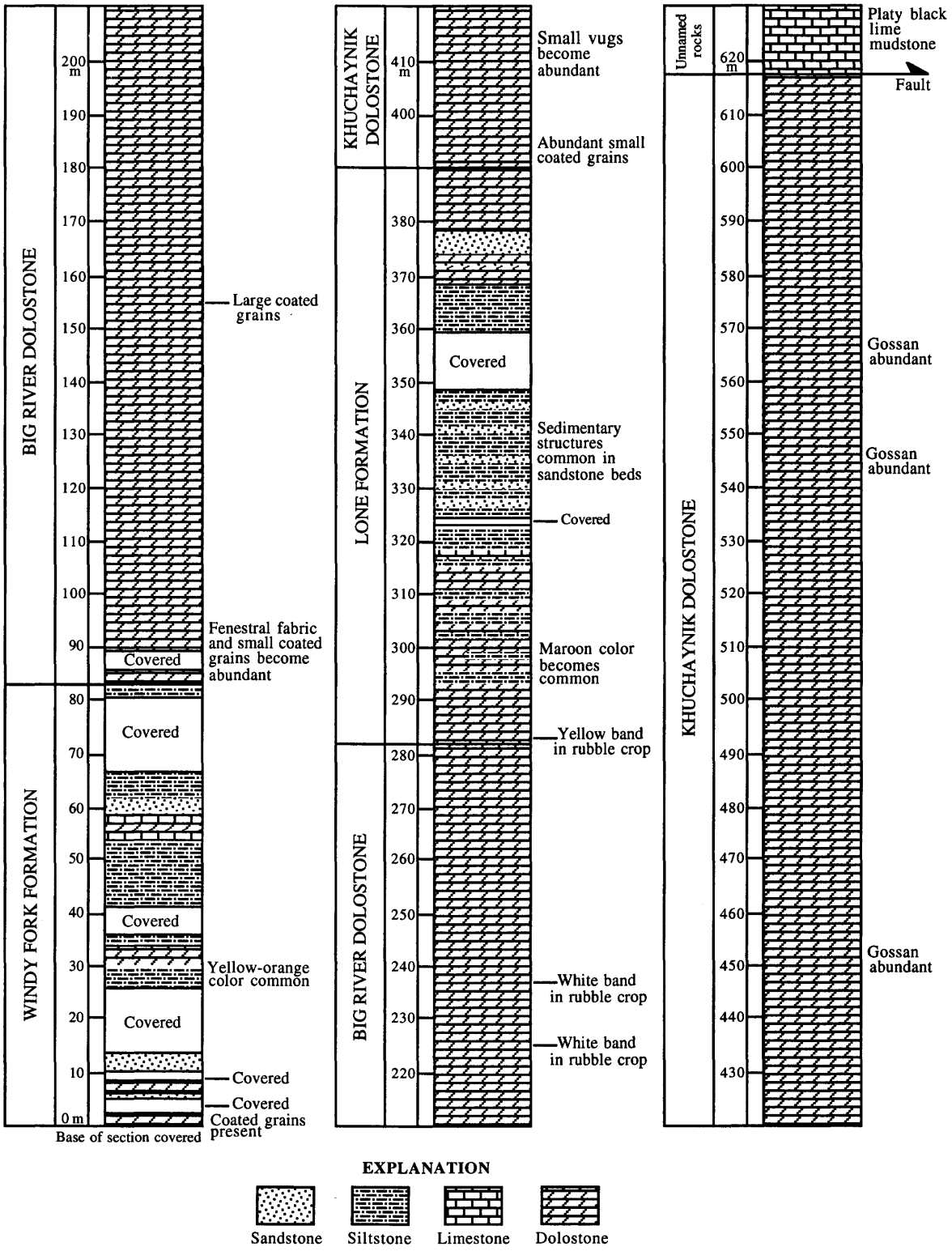

Figure 4. Columnar measured section showing type sections of the Windy Fork Formation, Big River Dolostone, Lone Formation, and Khuchaynik Dolostone. Location of measured section shown on figures 2 and 3. Thickness above base of section given in meters.

having some small coated grains, but coated grains are not present in the Lone Formation. In terms of color, siliciclastic beds of the Windy Fork Formation tend to be earthy yellow or orange-brown in color, whereas siliciclastic beds of the Lone Formation are more strongly reddish (maroon) in color. This distinct color difference facilitates easy distinction of the two formations at all exposures in the area of Lone Mountain.

The Windy Fork Formation can also be determined in the field based on its stratigraphic position underlying the Big River Dolostone (new). Although lithically heterogeneous, the strata of the Windy Fork Formation constitute a form of unity when compared to those of the overlying Big River Dolostone. The lower beds of the overlying Big River Dolostone are conspicuous, being gray dolostones containing small coated grains and abundant fenestral fabric.

The type section is located at the northern end of the north-trending ridge 3.0 km west of the Lone Mountain of long-established local usage and usage herein (fig. 2). The

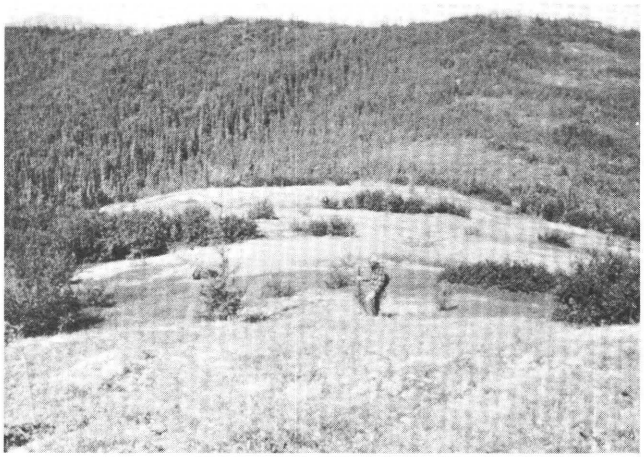

A

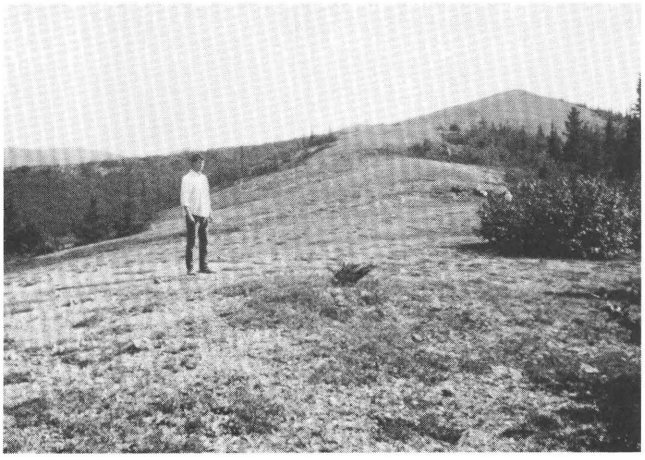

B

C

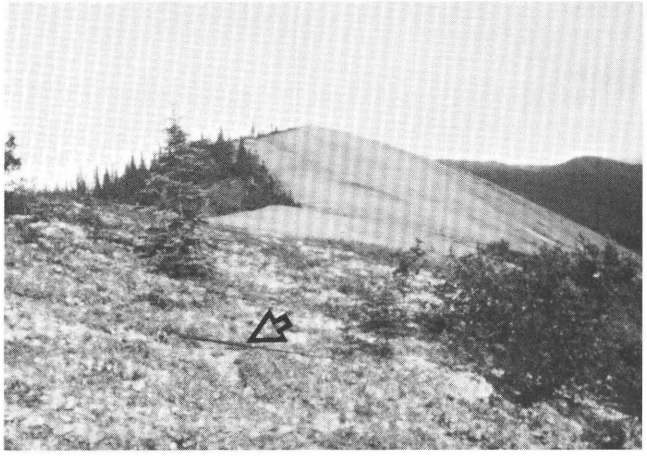

D

Figure 5. Outcrops of new Late(?) Proterozoic-age formations in the area of Lone Mountain, McGrath C-4 quadrangle; photographs were taken along measured section shown in figure 3. *A*, View looking north (down-section) showing upper part of the Windy Fork Formation (middle of photograph) and lowermost part of the Big River Dolostone (foreground). Person near middle of photograph is standing at the contact between the two formations. *B*, View looking south (up-section) showing uppermost part of the Big River Dolostone (foreground) and Lone Formation (middle of photograph); Khuchaynik Dolostone is exposed along hill in the distance. Person in foreground is standing at contact between the Big River Dolostone and the Lone Formation. Base of the Lone Formation is located at 62°30.97′ N., 154°46.74′ W., as determined from helicopter using GPS (accurate to within about 100 m during July 1993). *C*, View looking north (down-section) showing upper part of the Big River Dolostone in the distance, the Lone Formation (middle of the photograph; tents are pitched on lower part of the Lone Formation), and lowermost part of the Khuchaynik Dolostone (foreground). Person is standing at the contact between the Lone Formation and the Khuchaynik Dolostone. *D*, View looking north (down-section) showing upper part of the Khuchaynik Dolostone in background and unnamed Upper Cambrian(?) and Lower Ordovician platy black lime mudstone in foreground. Jacob's staff (arrow) marks fault trace between the two formations.

type section is located in the NW¼NE¼ sec. 14, T. 28 N., R. 30 W., McGrath C-4 quadrangle (fig. 3). The formation is mapped through several ridges in the vicinity of Lone Mountain, in both the McGrath C-4 and McGrath B-4 quadrangles. A well-exposed reference section for this unit is present along the west-trending ridge in the NW¼SW¼NE¼ sec. 14, T. 28 N., R. 30 W., McGrath C-4 quadrangle. The Windy Fork Formation derives its name from the nearby Windy Fork of the Kuskokwim River, which lies to the east of Lone Mountain.

BIG RIVER DOLOSTONE (NEW NAME)

The name "Big River Dolostone" is here assigned to a dolostone succession that is 198.5 m thick at the unit's type section (fig. 4). Outcrops of the Big River Dolostone (fig. 5*A–C*) are characterized by dolomudstone showing fenestral fabric (see fig. 6*C*) and numerous packstone to grainstone beds composed of coated grains. Fenestrae (birdseye structures) are commonly infilled by spar. Through most of the formation, the coated grains are small (generally less than 2 mm in diameter) and well-sorted, but locally they are large (up to about 10 mm in width), poorly sorted, and irregularly shaped (see fig. 6*B*). The dolostone largely weathers light to medium gray; however, two key beds, which are distinctive as white-weathering dolostone bands less than a meter thick, occur in rubble crop in the upper half of the unit (fig. 4). On fresh surfaces the dolostone, except for the white-weathering beds, varies in color from medium to dark gray. Pyrite is finely disseminated throughout the formation. Its lower contact with the Windy Fork Formation (new) is sharp and conformable; the base of the Big River Dolostone is placed at the last up-section appearance of continuous siltstone beds. Its upper contact with the Lone Formation (new) is also sharp and conformable; the top of the Big River Dolostone at the type section is marked by the base of a distinctive band (key bed) of earthy-yellow-weathering dolomitic lime mudstone that lacks coated grains (fig. 4). Dolostone beds are present above and below the contact; coated grains are present only below the contact.

The Big River Dolostone differs lithologically from the stratigraphically higher Khuchaynik Dolostone (new) by its internal stratigraphy, sedimentary features, and lack of major sulfide deposits. The Big River Dolostone, like the Khuchaynik Dolostone, consists entirely of dolostone. However, the Big River Dolostone is less than half the thickness of the Khuchaynik Dolostone in the area of the type section. Unlike the Khuchaynik Dolostone, the Big River Dolostone has two distinctive white-weathering key beds of dolostone in the upper third of the formation (fig. 4). Coated grains are present in both units but only the Big River Dolostone has been observed to contain large, irregularly shaped coated grains that are presumably oncolites. The Big River Dolostone contains abundant fenestral fabric (birdseye structures) through its entire thickness in the Lone Mountain area. The Khuchaynik Dolostone lacks fenestral fabric at the type section. Fenestral fabric is a pervasive characteristic of the Big River Dolostone in the type section; this implies that depositional environments conducive to the development of laminar stromatolites that produced the fenestral fabric had great lateral extent. For this reason, fenestral fabric in this formation is expected to have value for mapping purposes outside of the Lone Mountain area. In the Lone Mountain area, the Khuchaynik Dolostone is secondarily vuggy in places and the formation contains gossan that mostly crops out in bands paralleling the bedding; the Big River Dolostone is rarely vuggy and lacks gossan deposits.

The Big River Dolostone can also be determined in the field based on its stratigraphic position overlying the Windy Fork Formation (new) and underlying the Lone Formation (new). The strata of the Big River Dolostone are lithically homogeneous; the underlying Windy Fork Formation and the overlying Lone Formation are lithically heterogeneous. The contact between the underlying Windy Fork Formation and the Big River Dolostone is placed between the last up-section siltstone bed and the first gray dolostone bed containing small coated grains and fenestral fabric. The base of the overlying Lone Formation is a conspicuous yellow-weathering band in a dolostone succession.

The type section is located between 84 and 282.5 m in the measured section directly south (up-section) of the type section of the Windy River Formation (new) along the north-trending ridge in the NE¼ sec. 14, T. 28 N., R. 30 W., McGrath C-4 quadrangle (fig. 3). The Big River Dolostone

---

► **Figure 6.** Lithologic samples from new Late(?) Proterozoic-age formations in the area of Lone Mountain, McGrath C-4 quadrangle; all figures ×2; specimens are deposited in Orton Geological Museum of The Ohio State University (OSU). *A*, Weathered slab, broken perpendicular to bedding, showing planar cross-laminations of ferruginous quartz sandstone; Windy Fork Formation, 61 m above base of measured section; OSU 46342. *B*, Weathered slab, broken across bedding, showing large coated grains; Big River Dolostone, 155 m above base of measured section (71 m above base of formation); OSU 46343. *C*, Polished slab showing well-developed fenestral fabric and some small coated grains; upper part of the Big River Dolostone; OSU 46344. *D*, Weathered slab, broken perpendicular to bedding, showing planar laminations of ferruginous quartz sandstone; Lone Formation, 363 m above base of measured section (80.5 m above base of formation); OSU 46345. *E*, Polished slab, cut across bedding, showing abundant small coated grains; lower part of the Khuchaynik Dolostone; OSU 46346. *F*, Weathered slab, broken across bedding, showing vuggy character; Khuchaynik Dolostone, 513 m above base of measured section (123 m above base of formation); OSU 46347.

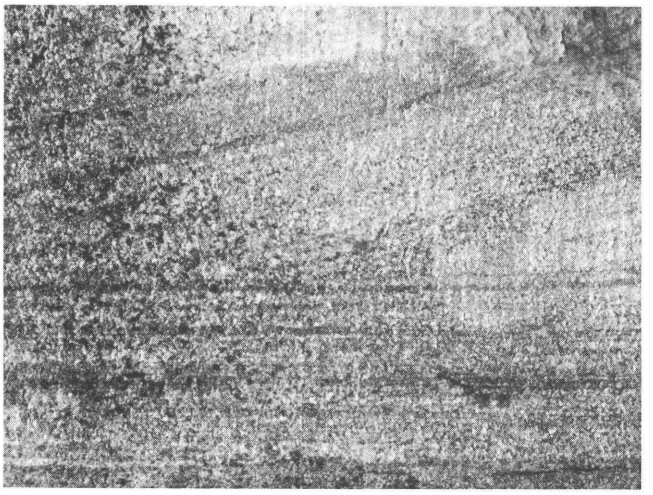

A

B

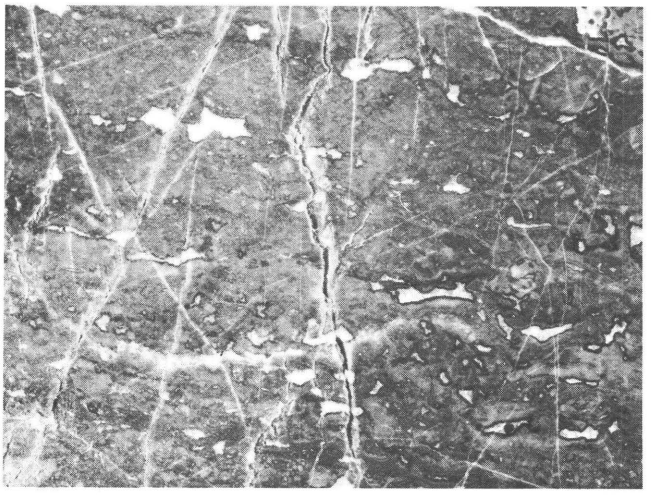

C

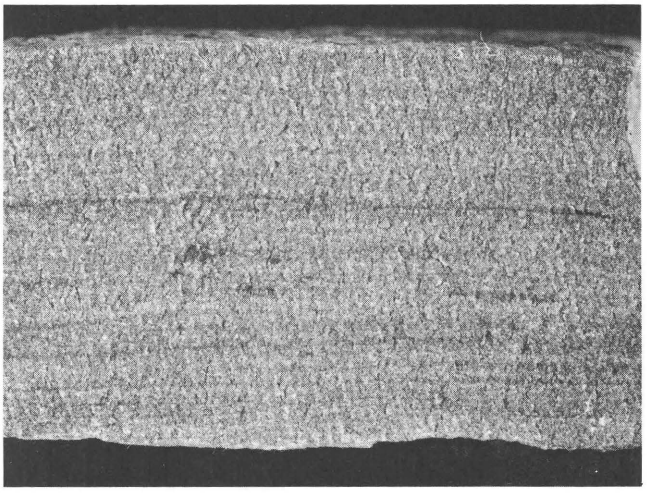

D

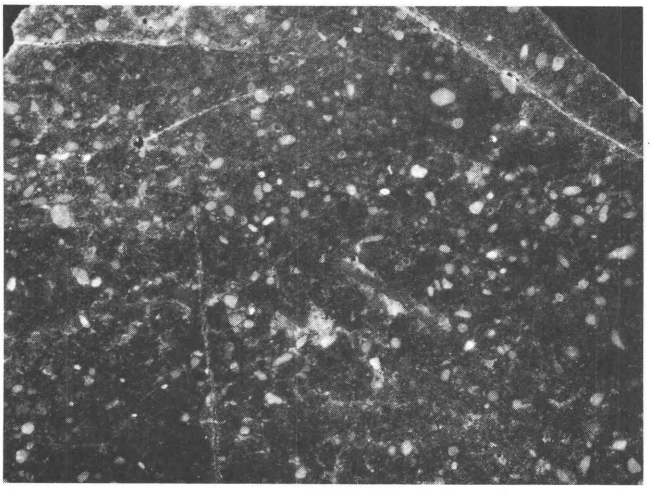

E

F

is mapped through several ridges in the vicinity of Lone Mountain, in both the McGrath C-4 and McGrath B-4 quadrangles. This formation derives its name from the nearby Big River, which lies to the west of Lone Mountain.

LONE FORMATION (NEW NAME)

The name "Lone Formation" is here assigned to a siliciclastic red bed succession that has interbedded carbonate rocks and is 107.5 m thick at the unit's type section (fig. 4). Outcrops of the Lone Formation (fig. 5*B*, *C*) are dominated by thin- to medium-bedded siltstone and fine- to coarse-grained sandstone that usually weathers to a maroon color, but locally weathers to variegated colors, including earthy yellow, tan, white, gray, gray-green, or reddish-brown. Sedimentary features present in the sandstones include planar cross-beds, symmetrical ripple marks, load casts, and siltstone intraclasts. Interbeds of lime mudstone or dolomudstone are up to 12 m thick and weather to various colors, including gray, tan, earthy yellow, orange, and pink. Siltstone intraclasts are present in some siltstone beds. A series of sandstone-siltstone couplets, each of which is approximately 1 to 5 m thick, is present near the middle of the formation. Pyrite is finely disseminated throughout the formation. The unit's lower contact with the Big River Dolostone (new) is conformable and sharp; the base of the formation is marked by the base of a distinctive band (key bed) of earthy-yellow-weathering dolomitic lime mudstone that lacks coated grains. Its upper contact with the Khuchaynik Dolostone (new) is sharp and conformable; the top of the formation is defined as the base of the first up-section dolostone bed containing coated grains. Dolostone beds are present above and below the contact.

The Lone Formation is distinguished from the stratigraphically lower Windy Fork Formation (new) by its internal stratigraphy, sedimentary features, and color. The Lone Formation contains proportionately much more sandstone and dolostone, and much less siltstone, than does the Windy Fork Formation. A distinctive set of sandstone-siltstone couplets is found near the middle of the Lone Formation, but there is no such succession in the Windy Fork Formation (fig. 4). Planar cross-beds are found in sandstone intervals of both formations, but they are much more common in the Lone Formation. The Lone Formation contains beds showing symmetrical ripple marks, load casts, and siltstone intraclasts at the outcrop, but these features have not been observed in the Windy Fork Formation. Coated grains have not been observed in the Lone Formation but dolostone beds near the base of the Windy Fork Formation have some small coated grains. Siliciclastic beds of the Lone Formation are strongly reddish (maroon) in color. Siliciclastic beds of the Windy Fork Formation, by contrast, tend to be more orange-brown in color. This distinct color difference facilitates easy distinction of the two formations at all exposures in the area of Lone Mountain.

The Lone Formation can also be determined in the field based on its stratigraphic position overlying the Big River Dolostone (new) and underlying the Khuchaynik Dolostone (new). Although lithically heterogeneous, the strata of the Lone Formation constitute a form of unity when compared to those of the underlying Big River Dolostone and those of the overlying Khuchaynik Dolostone. The top of the underlying Big River Dolostone is placed in a dolostone succession at the base of a conspicuous yellow-weathering band. The base of the overlying Khuchaynik Dolostone is placed in a gray dolostone succession at the first bed showing abundant small coated grains and lacking fenestral fabric.

The type section is located between 282.5 and 390 m in the measured section directly south (up-section) of the type section of the Big River Dolostone (new) along the north-trending ridge situated 3.0 km west of Lone Mountain, in the NW¼NE¼SE¼ sec. 14, T. 28 N., R. 30 W., McGrath C-4 quadrangle (fig. 3). The Lone Formation is mapped through several ridges in the vicinity of Lone Mountain, in both the McGrath C-4 and McGrath B-4 quadrangles. An excellent reference section for this formation is present along the northwest-trending ridge in the SW¼NE¼NW¼ sec. 23, T. 28 N., R. 30 W., McGrath C-4 quadrangle. The Lone Formation derives its name from Lone Mountain, which is located to the east of the type section.

KHUCHAYNIK DOLOSTONE (NEW NAME)

The name "Khuchaynik Dolostone" is here assigned to a dolostone succession that is at least 228 m thick at the unit's type section (fig. 4). Outcrops of the Khuchaynik Dolostone (fig. 5*B-D*) contain numerous packstone or grainstone beds composed of small coated grains (generally up to 1 mm in diameter; see fig. 6*E*) and, locally, small vugs where the grains have been dissolved away (see fig. 6*F*). At the type section, vugs tend to be better developed in the upper part of the unit. Locally, the dolostone has been strongly recrystallized to a sugary texture, and numerous discontinuous bands of gossan are present (fig. 4). The dolostone is medium gray in color on fresh surfaces and weathers light to medium gray. Pyrite is finely disseminated throughout the formation. The total thickness of the formation is not known because its top is faulted out at the type section (figs. 4, 5*D*). Its lower contact with the Lone Formation (new) is sharp and conformable; the base of the Khuchaynik Dolostone is placed at the base of the first up-section dolostone bed above the Lone Formation that contains coated grains. Dolostone beds are present above and below the contact.

The Khuchaynik Dolostone is distinguished from the stratigraphically lower Big River Dolostone (new) by its

internal stratigraphy, sedimentary features, and major sulfide deposits. The Khuchaynik Dolostone, like the Big River Dolostone, consists entirely of dolostone. However, the Khuchaynik Dolostone is more than twice as thick as the Big River Dolostone in the area of the type section. The Big River Dolostone has two distinctive white-weathering key beds in the upper third of the formation (fig. 4). Such white-weathering beds are not present in the Khuchaynik Dolostone. Coated grains are present in both units but only the Big River Dolostone has been observed to contain large, irregularly shaped coated grains. The Big River Dolostone contains abundant fenestral fabric (birdseye structures) through its entire thickness, but the Khuchaynik Dolostone lacks fenestral fabric, at least in the Lone Mountain area. In the area of the type section, the Khuchaynik Dolostone is locally vuggy. Also, it contains much gossan that tends to crop out in bands paralleling the bedding. The Big River Dolostone lacks both vugs and gossan deposits.

The Khuchaynik Dolostone can also be distinguished in the field by its stratigraphic position overlying the Lone Formation (new). The strata of the Khuchaynik Dolostone are lithically homogeneous; the underlying Lone Formation is lithically heterogeneous. The top of the underlying Lone Formation is placed in a tan-to-gray dolostone succession at the base of a bed containing abundant small coated grains and lacking fenestral fabric.

The type section is located between 390 and 618 m in the measured section directly south (up-section) of the type section of the Lone Formation along the north-trending ridge situated 3.0 km west of Lone Mountain, in the SE¼ sec. 14, T. 28 N., R. 30 W., McGrath C-4 quadrangle (fig. 3). The Khuchaynik Dolostone is mapped through several ridges in the vicinity of Lone Mountain, in both the McGrath C-4 and McGrath B-4 quadrangles. This formation derives its name from the nearby Khuchaynik Creek, a tributary of the Middle Fork of the Kuskokwim River, which lies to the east of Lone Mountain.

AGE OF NEW FORMATIONS

The Windy Fork Formation, Big River Dolostone, Lone Formation, and Khuchaynik Dolostone are here considered to be of Late(?) Proterozoic age. At present we do not have any direct, positive evidence for this age assignment; the aggregate of evidence, however, is consistent with this age determination. Macrofossils and trace fossils have not been recognized in the Windy Fork, Big River, Lone, or Khuchaynik units. Based on fossil evidence, most of the other sedimentary units in the area have early Paleozoic ages (Middle Cambrian to Early Ordovician) and appear to be in fault contact with the top or sides of the stratotype section containing the exposures of the four units named herein. The Big River Dolostone and Khuchaynik Dolostone both contain abundant coated grains (fig. 6*B*, *C*, *E*). Although not conclusive evidence of a Late Proterozoic age for the four new units, coated-grain-bearing carbonate units are present elsewhere in Late Proterozoic-age rocks of Alaska (Brabb and Churkin, 1969; Dutro, 1970; Young, 1982; Clough and others, 1988; Dumoulin, 1988; Eberlein and Lanphere, 1988). Large coated grains ("giant ooids" according to Sumner and Grotzinger, 1993) have been cited as occurring predominantly in Late Proterozoic-age rocks (Sumner and Grotzinger, 1993), but we have reservations about the use of such sedimentary features as chronostratigraphic tools. Our skepticism stems primarily from our interpretation of some of these "giant ooids" as oncolites, which are present in Archean, Proterozoic, and Phanerozoic rocks. More convincing evidence of a probable Late Proterozoic age for these units is that none of the many observed specimens of coated grains had shelly fossils at their cores, based on microscopic examination of broken and weathered specimens (see fig. 6*B*, *E*). This suggests that the Big River and Khuchaynik Dolostones were deposited after the evolution of microbial life but before the appearance of shell-secreting organisms on earth. This infers an age older than the earliest Cambrian. Numerous slabs of the Windy Fork and Lone Formations were searched for the possible presence of shelly fossils, Ediacaran-type fossils, and trace fossils; however, no fossils of any kind were found. The lack of any trace fossils or other evidence of bioturbation such as stratigraphic mixing implies a pre-latest Proterozoic age (see Landing, 1994, for discussion of trace fossils near the Proterozoic-Cambrian boundary) for these new units. No lithic units (redbeds or dolostones) such as comprise the four new formations have been heretofore recognized regionally in either west-central or southwestern Alaska among undisputed Paleozoic rocks. Unless profound facies changes are recorded in the Paleozoic succession of the Nixon Fork subterrane, this lack of lithologic similarity implies that the four new formations are pre-Middle Cambrian in age. A pre-Middle Cambrian age for these units is also implied by the presence of strikingly similar (probably lithologically equivalent) strata to the southwest in the Holitna basin, which stratigraphically underlie beds containing Middle Cambrian trilobites (Palmer and others, 1985; Babcock and Blodgett, 1992; Babcock and others, 1993; St. John, 1994) in a west-trending anticlinorium in the Sleetmute A-2 quadrangle. The fact that thick redbed successions are present in the Windy Fork and Lone Formations places a lower limit on the age of these units; they must be 2.6 Ga or younger in age because hematite (oxidized iron) is not known from older sedimentary rocks (Walker and others, 1983; Retallack, 1986).

DEPOSITIONAL ENVIRONMENTS OF NEW FORMATIONS

In the area of their type sections, the Windy Fork Formation, Big River Dolostone, Lone Formation, and

Khuchaynik Dolostone are interpreted to represent sedimentation on a shallow-marine shelf or platform. Each of the units, however, represents a distinct major lithofacies, which is the philosophical basis for describing them as separate formations. Each of the formations has a distinctive lithology or set of lithologies, and a distinctive set of sedimentary features, which together comprise the practical means by which the formations can be identified and mapped.

Thick carbonate successions of the Big River and Khuchaynik Dolostones contain abundant coated grains, which suggests that the deposition of these units took place in or adjacent to warm, shallow, tropical marine water (see Wilson, 1975). The Big River Dolostone, however, is characterized by abundant fenestral fabric (birdseye structures), which is indicative of the presence of laminar stromatolites developed in supratidal to intertidal conditions in a carbonate-dominated environment (Wilson, 1975; Friedman and Sanders, 1978, p. 334). Large coated grains (presumably oncolites) in the Big River Dolostone are additional indicators of the presence of stromatolites locally, as well as the presence of shallow subtidal conditions in places. The Big River Dolostone is thus interpreted to have been deposited under supratidal-intertidal to shallow subtidal conditions. The presence of small coated grains (presumably including ooids) in the Khuchaynik Dolostone suggests that this formation was entirely deposited under shallow subtidal conditions, probably where strong bottom currents and agitated-water conditions were present (see Boggs, 1987, p. 224).

The carbonate factory responsible for the deposition of the Big River and Khuchaynik Dolostones and the carbonate interbeds in the Windy Fork and Lone Formations, was intermittently, or perhaps cyclically, interrupted by siliciclastic input that is recorded by redbed successions in the Windy Fork and Lone Formations (Babcock and others, 1993). The siltstones and sandstones of the Windy Fork Formation are interpreted to have been deposited under predominantly low to moderate energy conditions in an intertidal to shallow subtidal setting. Sedimentary structures in the Lone Formation, particularly the symmetrical ripple marks and the intraclasts, are consistent with sedimentation in lagoonal(?) to intertidal and shallow subtidal marine environments (see Friedman and Sanders, 1978). Occasional storms may have been responsible for the deposition of some beds of abundant intraclasts. Abundant planar cross-bed sets near the middle of the Lone Formation suggest that this interval was deposited under shoreface to shallow submarine bar conditions.

Acknowledgments.—Field work was primarily supported by a grant from the National Geographic Society. St. John's participation was also supported by grants from Sigma Xi and the Friends of Orton Hall fund of The Ohio State University. Laboratory preparation of rock samples was undertaken at the National Center of the U.S. Geological Survey in Reston, Virginia. We are grateful to Bill Beebe, Area Forester, Alaska Department of Natural Resources, Division of Forestry, McGrath, Alaska, for arranging helicopter support that permitted us to conduct our field study in the Lone Mountain area during the summer of 1993. J.G. Clough, Alaska Division of Geological & Geophysical Surveys, provided helpful information about Proterozoic carbonate units in Alaska that lie outside of our study area. I.M. Whillans, Department of Geological Sciences, The Ohio State University, provided helpful information about GPS. Karen Tyler, The Ohio State University, assisted with the drafting of figures.

REFERENCES CITED

Babcock, L.E., and Blodgett, R.B., 1992, Biogeographic and paleogeographic significance of Middle Cambrian trilobites of Siberian aspect from southwestern Alaska [abs.]: Geological Society of America Abstracts with Programs, v. 24, no. 5, p. 4.

Babcock, L.E., Blodgett, R.B., and St. John, James, 1993, Proterozoic and Cambrian stratigraphy and paleontology of the Nixon Fork terrane, southwestern Alaska, *in* Ortega-Gutiérrez, F., Coney, P.J., Centeno-García, E., and Gómez-Caballero, A., eds., Proceedings of the First Circum-Pacific and Circum-Atlantic Terrane Conference: Universidad Nacional Autónoma de Mexico, Guanajuato, Mexico, p. 5-7.

Blodgett, R.B., 1983, Paleobiogeographic affinities of Devonian fossils from the Nixon Fork terrane, southwestern Alaska, *in* Stevens, C.H., ed., Pre-Jurassic rocks in western North American suspect terranes: Los Angeles, Calif., Society of Economic Paleontologists and Mineralogists, Pacific Section, p. 125-130.

Blodgett, R.B., and Clough, J.G., 1985, The Nixon Fork terrane—Part of an in-situ peninsular extension of the Paleozoic North American continent [abs.]: Geological Society of America Abstracts with Programs, v. 17, no. 6, p. 342.

Blodgett, R.B., and Gilbert, W.G., 1983, The Cheeneetnuk Limestone, a new Early(?) to Middle Devonian formation in the McGrath A-4 and A-5 quadrangles, west-central Alaska: Alaska Division of Geological and Geophysical Surveys Professional Report 85, 6 p., scale 1:63,360.

———1992a, Upper Devonian shallow-marine siliciclastic strata and associated fauna and flora, Lime Hills D-4 quadrangle, southwest Alaska, *in* Bradley, D.C., and Dusel-Bacon, C., eds., Geologic studies in Alaska by the U.S. Geological Survey, 1991: U.S. Geological Survey Bulletin 2041, p. 106-113.

———1992b, Paleogeographic relations of lower and middle Paleozoic strata of southwest and west-central Alaska [abs.]: Geological Society of America Abstracts with Programs, v. 24, no. 5, p. 8.

Boggs, Sam, Jr., 1987, Principles of stratigraphy and sedimentology: Columbus, Ohio, Merrill Publishing Company, 784 p.

Brabb, E.E., and Churkin, Michael, Jr., 1969, Geologic map of the Charley River quadrangle, east-central Alaska: U.S. Geological Survey Miscellaneous Geologic Investigations Map I-573, scale 1:250,000.

Bundtzen, T.K., and Gilbert, W.G., 1983, Outline of geology and mineral resources of the upper Kuskokwim region, Alaska: Journal of the Alaska Geological Society, v. 3, p. 101-117.

Clough, J.G., Blodgett, R.B., Imm, T.A., and Pavia, E.A., 1988, Depositional environments of the Katakturuk Dolomite (Pro-

terozoic) and the Nanook Limestone (Proterozoic to Devonian), Arctic National Wildlife Refuge, Alaska [abs.]: American Association of Petroleum Geologists Bulletin, v. 72, p. 172.

Decker, John, Bergman, S.C., Blodgett, R.B., Box, S.E., Bundtzen, T.K., Clough, J.G., Coonrad, W.L., Gilbert, W.G., Miller, M.L., Murphy, J.M., Robinson, M.S., and Wallace, W.K., in press, Geology of southwestern Alaska: Boulder, Colo., Geological Society of America, Geology of North America, v. F1, chapter II-F.

Dumoulin, J.A., 1988, Stromatolite- and coated-grain-bearing carbonate rocks of the western Brooks Range, *in* Galloway, J.P., and Hamilton, T.D., eds., Geologic studies in Alaska by the U.S. Geological Survey during 1987: U.S. Geological Survey Circular 1016, p. 31-34.

Dutro, J.T., Jr., 1970, Pre-Carboniferous carbonate rocks, northeastern Alaska, *in* Adkison, W.L., and Brosgé, W.P., eds., Proceedings of the geological seminar on the North Slope of Alaska: Los Angeles, California, American Association of Petroleum Geologists, Pacific Section, p. M1-M8.

Eberlein, G.D., and Lanphere, M.A., 1988, Precambrian rocks of Alaska: U.S. Geological Survey Professional Paper 1241-B, 18 p.

Friedman, G.M., and Sanders, J.E., 1978, Principles of sedimentology: New York, John Wiley & Sons, 792 p.

Gilbert, W.G., and Bundtzen, T.K., 1983, Paleozoic stratigraphy of the Farewell area, southwest Alaska Range, Alaska [abs.]: Alaska Geological Society Symposium, New Developments in the Paleozoic Geology of Alaska and the Yukon, Anchorage, Alaska, 1983, Program and Abstracts, p. 10-11.

Jones, D.L., Silberling, N.J., Coney, P.J., and Plafker, George, 1987, Lithotectonic terrane map of Alaska (west of the 141st Meridian): U.S. Geological Survey Map MF-1874-A, 1 sheet, scale 1:250,000.

Landing, Ed, 1994, Precambrian-Cambrian boundary global stratotype ratified and a new perspective of Cambrian time: Geology, v. 22, p. 179-182.

Miller, M.L., Belkin, H.E., Blodgett, R.B., Bundtzen, T.K., Cady, J.W., Goldfarb, R.J., Gray, J.E., McGimsey, R.G., and Simpson, S.L., 1989, Pre-field study and mineral resource assessment of the Sleetmute quadrangle, southwestern Alaska: U.S. Geological Survey Open-File Report 89-363, 115 p.

Palmer, A.R., Egbert, R.M., Sullivan, R., and Knoth, J.S., 1985, Cambrian trilobites with Siberian affinities, southwestern Alaska [abs.]: American Association of Petroleum Geologists Bulletin, v. 69, p. 295.

Patton, W.W., Jr., 1978, Juxtaposed continental and oceanic-island arc terranes in the Medfra quadrangle, west-central Alaska, *in* Johnson, K.M., ed., The United States Geological Survey in Alaska: Accomplishments during 1977: U.S. Geological Survey Circular 772-B, p. B38-B39.

Reed, B.L., and Lanphere, M.A., 1972, Generalized geologic map of the Alaska-Aleutian Range batholith showing potassium-argon ages of the plutonic rocks: U.S. Geological Survey Miscellaneous Field Studies Map MF-372, 2 sheets, scale 1:1,000,000.

———1973, Alaska-Aleutian Range Batholith: geochronology, chemistry, and relation to circum-Pacific plutonism: Geological Society of America Bulletin, v. 84, p. 2583-2610.

Retallack, G.J., 1986, The fossil record of soils, *in* Wright, V.P., ed., Paleosols, their recognition and interpretation: Oxford, Blackwell Scientific Publications, p. 1-59.

St. John, James, 1994, Systematics and biogeography of some upper Middle Cambrian trilobites from the Holitna basin, southwestern Alaska: Master of Science thesis, The Ohio State University, 90 p.

Steiger, R.H., and Jäger, E., 1977, Subcommission on Geochronology: convention on the use of decay constants in geo- and cosmochronology: Earth and Planetary Science Letters, v. 36, p. 359-362.

Sumner, D.Y., and Grotzinger, J.P., 1993, Numerical modeling of ooid size and the problem of Neoproterozoic giant ooids: Journal of Sedimentary Petrology, v. 63, p. 974-982.

Walker, J.C.G., Klein, Cornelis, Schidlowski, Manfred, Schopf, J.W., Stevenson, D.J., and Walter, M.R., 1983, Environmental evolution of the Archean-early Proterozoic earth, *in* Schopf, J.W., ed., Earth's earliest biosphere: Princeton, Princeton University Press, p. 260-290.

Wilson, J.L., 1975, Carbonate facies in geologic history: New York, Springer-Verlag, 471 p.

Young, G.M., 1982, The late Proterozoic Tindir Group, east-central Alaska: Evolution of a continental margin: Geological Society of America Bulletin, v. 93, p. 759-783.

Reviewers: Wyatt G. Gilbert, Marti L. Miller, and Scott Starratt

Possible Occurrence of Lower to Middle Paleozoic Rocks South of the Denali Fault, Denali National Park, Alaska, and Implications for Denali Fault Displacement

By Béla Csejtey, Jr., Phil F. Brease,[1] Arthur B. Ford, *and* Willis H. Nelson

The purpose of this note is to report on the discovery during fieldwork in 1993 of a unit of rocks that in our view has a bearing on interpreting displacement relations of the Denali fault system. The area of study is in the Mount McKinley (1:63,360) B-1 quadrangle of the eastern part of the Mount McKinley (1:250,000) quadrangle, Denali National Park, of south-central Alaska (fig. 1). A large fault sliver along the south side of the Denali fault was found to contain sedimentary rocks that, based on lithologic similarities, we believe may correlate with rocks of Ordovician to Devonian age north of the fault. Fossils have not been found in the unit, however, and so its age is not directly known. If valid, the proposed correlation has important implications for displacement relations across the Denali fault and for the tectonic history of this part of south-central Alaska.

The fault sliver trends northeast, parallel to the Denali fault on its south side, and is exposed at and near Anderson Pass of the central Alaska Range (fig. 1). The sliver is about 14 km long and up to 2 km wide. It is bounded on its north side by the Denali fault, which is poorly exposed in this area. However, a steep dip of the fault is indicated by its generally straight trace. The sliver is bounded on its other sides by a steeply northward-dipping reverse fault with a sharply curving surface trace. The fault juxtaposed the inferred Ordovician to Devonian rocks of the sliver (shown as unit DOs? on fig. 1) against flyschlike rocks of Jurassic and Cretaceous age similar to those mapped in the adjacent Healy (1:250,000) quadrangle to the east (units KJf and KJfl, Csejtey and others, 1992).

The rocks within the sliver comprise an intercalated sequence with varying proportions of the following rock types: (1) medium- to dark-gray, thinly bedded to laminated, frequently graded-bedded, medium- to fine-grained, commonly calcareous and rusty-weathering sandstone, (2) dark-gray to black argillite, and (3) layers, as much as a few tens of meters thick, of generally thinly bedded, fine-grained, medium-gray, locally silicified limestone. The rocks of the sequence appear to be mostly shallow-water turbidite deposits, but include some limestones with relict algal laminations indicating rapid sea-level changes and deposition in a shallow-marine intertidal to supratidal environment. The lithologies of all these rocks closely resemble those of an Ordovician to Devonian sedimentary sequence that was mapped just north of the Denali fault in the adjacent Healy quadrangle (unit DOs, Csejtey and others, 1992).

No fossils were found in any of the rocks of the fault sliver. Therefore, their age assignment is tentative, as it is based only on their lithologic similarities to the Ordovician to Devonian rocks of unit DOs (Csejtey and others, 1992, and unpub. data) just across the Denali fault. The limestone bodies were sampled for conodonts at two localities (fig. 1), but the samples were found to be barren (Anita G. Harris, U.S. Geological Survey, oral and written commun., 1993). Nevertheless, we believe the correlation between the rock sequence of the fault sliver and that of unit DOs is probable because of their lithologic similarities, especially those of the limestones, and because of the unique variety of depositional environments represented by the rocks.

Most of the rocks of the fault sliver are weakly metamorphosed and in places penetratively deformed, but not to the extent that original bedding features have been obliterated. The beds consistently strike east-northeastward, paralleling the apparent surface trace of the Denali fault. Bedding dips moderately to steeply both northward and southward, which could be the result of some large but not recognized tight folding or flexing of an essentially homoclinal sequence. Major internal faults were not detected, but bedding-plane faults may be present.

The regional tectonic significance of the fault sliver depends on two factors: (1) the validity of the inferred correlation of rocks of the sliver with those of unit DOs

[1]National Park Service, Denali National Park, Alaska.

north of the Denali fault, and (2) from where and how the sliver was emplaced. If the two sequences are indeed correlative, then the rocks of unit DOs occur at the surface on both sides of this part of the Denali fault and may occur similarly elsewhere in south-central Alaska. However, if the rocks of the sliver were not brought up essentially vertically from beneath unit KJf (fig. 2), implying that rocks of the sliver do not underlie unit KJf in at least some areas along the south side of the Denali fault, then the tectonic significance of the sliver is limited.

It theoretically is possible that the fault sliver is a little-traveled fragment that was sliced off one wall of a strike-slip fault of large displacement. However, a number of structural features and considerations, discussed below, militate against such a possibility. All the bedding attitudes within the fault sliver have strikes that are parallel or subparallel with the strike of the Denali fault, which suggests compressional forces of roughly northwest-southeast orientation rather than a force couple, parallel with the Denali fault, acting on the sliver as the adjacent main fault blocks slid by each other in opposing direction. In the latter case, the occurrence of some folds or rotational features with roughly vertical axes would be expected. Furthermore, the southern boundary fault has a steeply northwestward dipping and sharply undulating surface plane as revealed in exposures along the steep mountain sides. The "lands and grooves" of the undulations also plunge northwestward. The undulations are not the result of folding because the rocks of the sliver

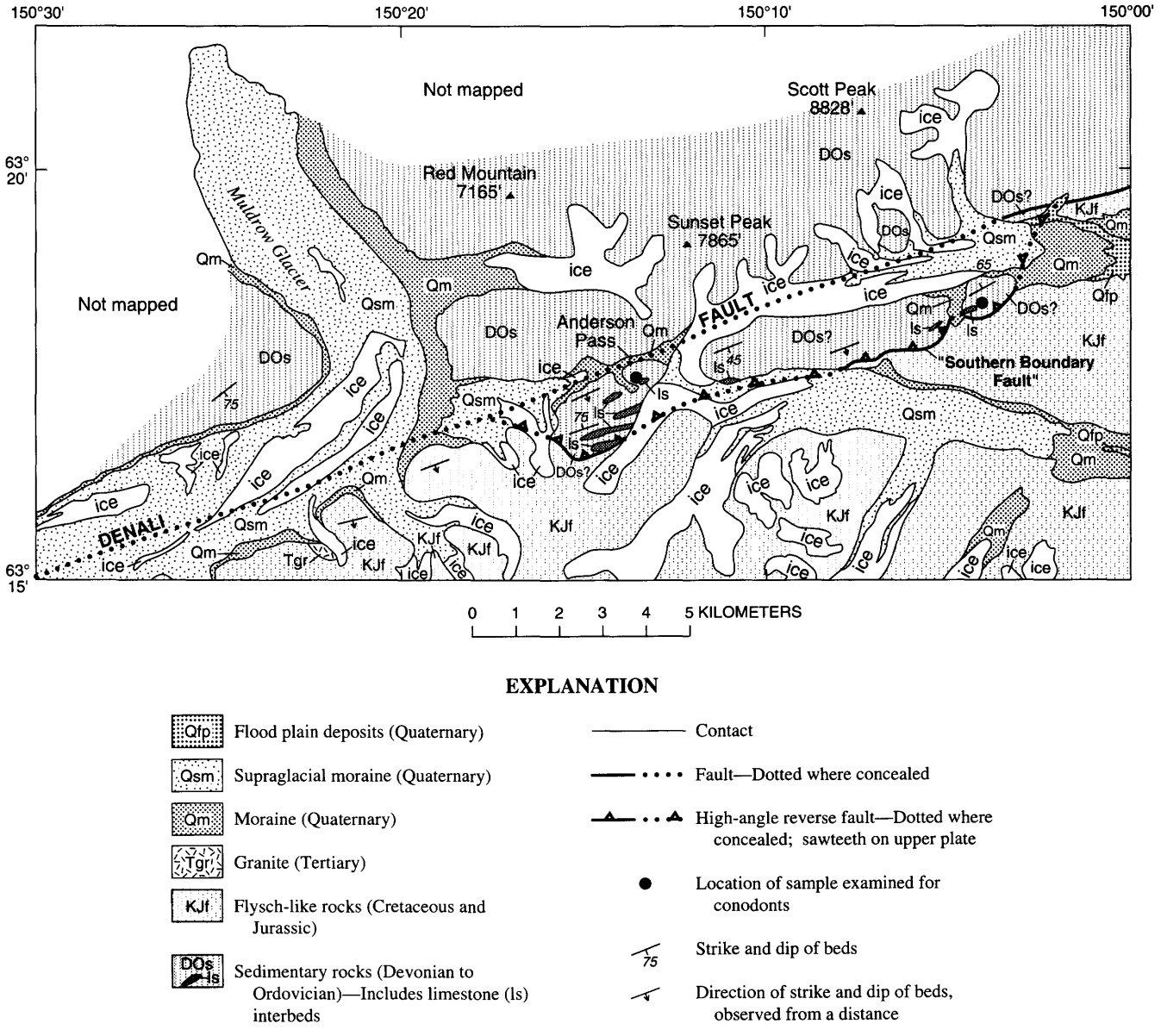

Figure 1. Generalized geologic map of Anderson Pass area of central Alaska Range, Denali National Park, Alaska.

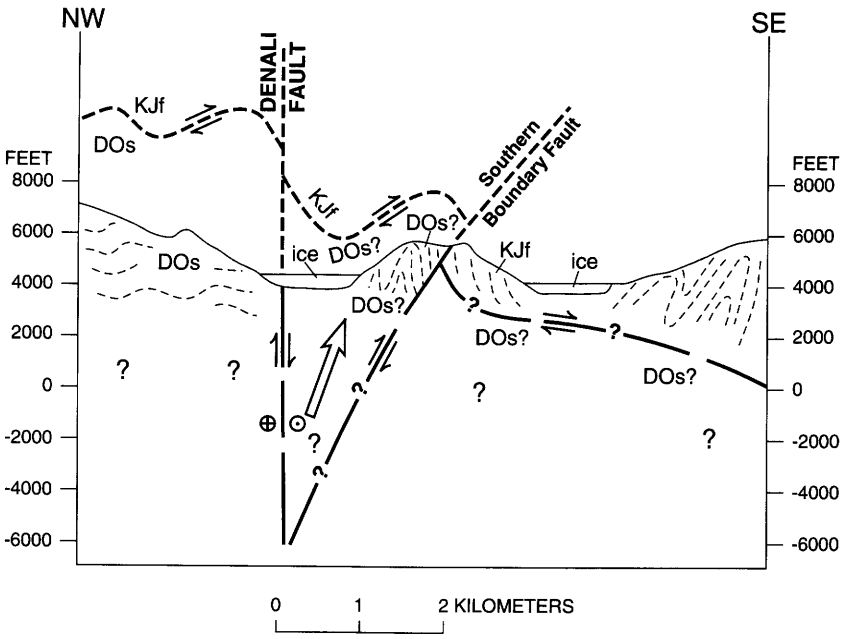

Figure 2. Schematic cross section across Denali fault, showing suggested interpretation of upward movement (open arrow) of wedge-shaped fault block of unit DOs? between southern boundary fault and Denali fault near Anderson Pass, Denali National Park, Alaska. Tectonic contact between units KJf (Cretaceous and Jurassic flysch-like rocks) and DOs (Devonian to Ordovician sedimentary rocks) is inferred from geologic mapping in adjacent Healy quadrangle (Csejtey and others, 1992). ⊕, movement toward reader; ⊙, movement away from reader.

lack folds conforming with the undulations. The above features also argue against horizontal movement along the southern boundary fault but instead argue for tectonic transport roughly perpendicular to the surface trace of the Denali fault. Accordingly, the southern boundary fault is either a high-angle reverse fault with up and southeastward tectonic transport but kinematically related to the Cenozoic Denali fault or is part of a folded and dissected older thrust fault with unknown transport direction.

According to Csejtey and others (1982, 1992), two important periods of deformation can be distinguished in south-central Alaska: (1) a mid-Cretaceous major accretionary orogeny, and (2) a comparatively less intensive late Cenozoic deformational event which modified but did not significantly alter the already existing geologic make-up of this part of Alaska. In this context, and in view of the occurrence of a number of Cenozoic faults to the east in the adjacent Healy quadrangle (Csejtey and others, 1992), with dominantly dip-slip displacements and possibly comprising flower structures (Harding, 1985), the southern boundary fault of the large tectonic sliver probably is a Cenozoic high-angle reverse fault. If so, the rocks of the fault sliver are part of a sequence of rocks which underlie the Jurassic and Cretaceous flyschlike rocks but were wedged upward against and over the flyschlike rocks by the southern boundary fault and the Denali fault (fig. 2). Furthermore, if the assumed age assignment of the rocks of the sliver is valid, then it would mean that the rocks of unit DOs north of the Denali fault also occur in the subsurface south of the fault. The foregoing interpretations and assumptions support previous tectonic concepts that in central and western Alaska, the Denali fault has had only limited horizontal displacements in Cenozoic time (Csejtey and others, 1982, 1992; Mullen and Csejtey, 1986).

The foregoing tectonic speculations are compatible with relations shown by geological mapping in Denali National Park (fig. 1). However, the lack of fossils or other evidence for dating the rocks of the fault sliver south of the Denali fault makes correlation with Ordovician to Devonian rocks (unit DOs, fig. 1) north of the fault, and thus interpretations, uncertain. We believe it is important to call attention to the presence of this hitherto unknown occurrence of rocks, possibly of early to middle Paleozoic age, in the fault sliver south of the Denali fault. Our preliminary interpretation suggests that the fault sliver may be important to our understanding the Denali fault system, as well as to the overall tectonic evolution of south-central Alaska.

REFERENCES CITED

Csejtey, Béla, Jr., Cox, D.P., Evarts, R.C., Striker, G.D., and Foster, H.L., 1982, The Cenozoic Denali fault system and the Cretaceous accretionary development of southern Alaska:

Journal of Geophysical Research, v. 87, no. B5, p. 3741–3754.

Csejtey, Béla, Jr., Mullen, M.W., Cox, D.P., and Stricker, G.D., 1992, Geology and geochronology of the Healy quadrangle, south-central Alaska: U.S. Geological Survey Miscellaneous Investigations Series Map, I–1961, 63 p., 2 plates, scales 1:250,000 and 1:360,000.

Harding, T.P., 1985, Seismic characteristics and identification of negative flower structures, positive flower structures, and positive structural inversion: The American Association of Petroleum Geologists Bulletin, v. 69, no. 4, p. 582–600.

Mullen, M.W., and Csejtey, Béla, Jr., 1986, Recognition of a Nixon Fork terrane equivalent in the Healy quadrangle, *in* Bartsch-Winkler, Susan and Reed, K.M., eds., Geologic studies in Alaska by the U.S. Geological Survey during 1985: U.S. Geological Survey Circular 978, p. 55–60.

Reviewers: Robert A. Loney, Michael W. Mullen, and William Perry

Chemical Characteristics of Major Plutonic Belts of the Coast Plutonic-Metamorphic Complex Near Juneau, Southeastern Alaska

By James L. Drinkwater, David A. Brew, *and* Arthur B. Ford

ABSTRACT

The three major plutonic belts that form part of the Coast plutonic-metamorphic complex near Juneau, Alaska, show distinctive major and minor element content and trends. The garnet- and epidote-bearing quartz diorites, tonalites, granodiorites, and quartz monzodiorites of the Late Cretaceous Admiralty-Revillagigedo belt have a wide SiO_2 range (56–69 percent), are relatively rich in alkalies (Na_2O+K_2O) and have higher FeO*/MgO ratios and Sr content, and lower aluminum saturation index than rocks of the other two belts. Foliated tonalites of the mostly Paleocene Great tonalite sill belt are characterized by their smaller SiO_2 range (59–66 percent), lower alkalies and FeO*/MgO ratios, and higher normative An content than rocks of the other belts. Eocene granodiorites and granites of the Coast Mountains belt are more acidic (64–74 percent SiO_2), have lower FeO*, MgO, and Sr contents, and higher K and Rb contents than rocks of the other belts. The compositional differences between rocks of the three belts reflect their differences in age and in the lithotectonic terranes and tectonic zones into which they were emplaced.

INTRODUCTION

Granitic rocks of Late Cretaceous to middle Tertiary age occupy a large part of the informally named Coast plutonic-metamorphic complex of Brew and Ford (1984), also referred to as the Coast Range batholith (Buddington, 1927) or Coast Mountains batholith (Gehrels and others, 1991) on the mainland of southeastern Alaska (fig. 1). We have investigated the geology, petrography, and chemistry of the plutonic rocks across part of the Coast plutonic-metamorphic complex near Juneau, which we refer to as the "Taku Inlet transect." The transect extends from the Glass Peninsula to the Canadian border between Taku Inlet and the Whiting River (fig. 2). The granitic rocks of the transect belong to three major northwest-trending plutonic belts of the Coast plutonic-metamorphic complex (fig. 1). These belts are the Admiralty-Revillagigedo belt of Late Cretaceous plutons (Brew and Morrell, 1983), and the Great tonalite sill belt and Coast Mountains belt of Brew (1988), of Tertiary age. Each belt contains plutons or plutonic units of similar age, size, modal and chemical composition, and magnetic susceptibility (Drinkwater and others, 1992) and plutons of each belt intrude different lithotectonic terranes (Berg and others, 1978; Monger and Berg, 1987; Wheeler and McFeely, 1991). Geological descriptions of plutons and country rock of the transect area are given by Brew and Ford (1977, 1986), Ford and Brew (1977, 1987), Brew and Grybeck (1984), and Drinkwater and others (1989, 1990). The study of Drinkwater and others (1992) found that individual plutons and plutonic units within the transect area are characterized by distinct magnetic susceptibilities. Brew (1988) summarized the then-available petrographic and chemical data for plutonic rocks from the transect.

This report is a product of geological investigations carried out in the Juneau region and is a preliminary account of our current study of the petrographic and chemical variations along the Taku Inlet transect (fig. 2). The purpose of the report is to define the broad petrochemical nature of the three major plutonic belts in the Coast plutonic-metamorphic complex near Juneau and to provide diagnostic chemical data that support the previously mapped delineation of plutons and plutonic belts of the transect area (Brew and Morrell, 1983; Brew and Ford, 1986). This information allows us to compare plutonic rocks of the Taku Inlet transect with other segments of the complex in southeastern Alaska and to examine the petrogenetic implications.

PLUTONIC BELTS

REGIONAL SETTING

The three major plutonic belts and intervening medium- to high-grade schist, gneiss, and migmatite make up

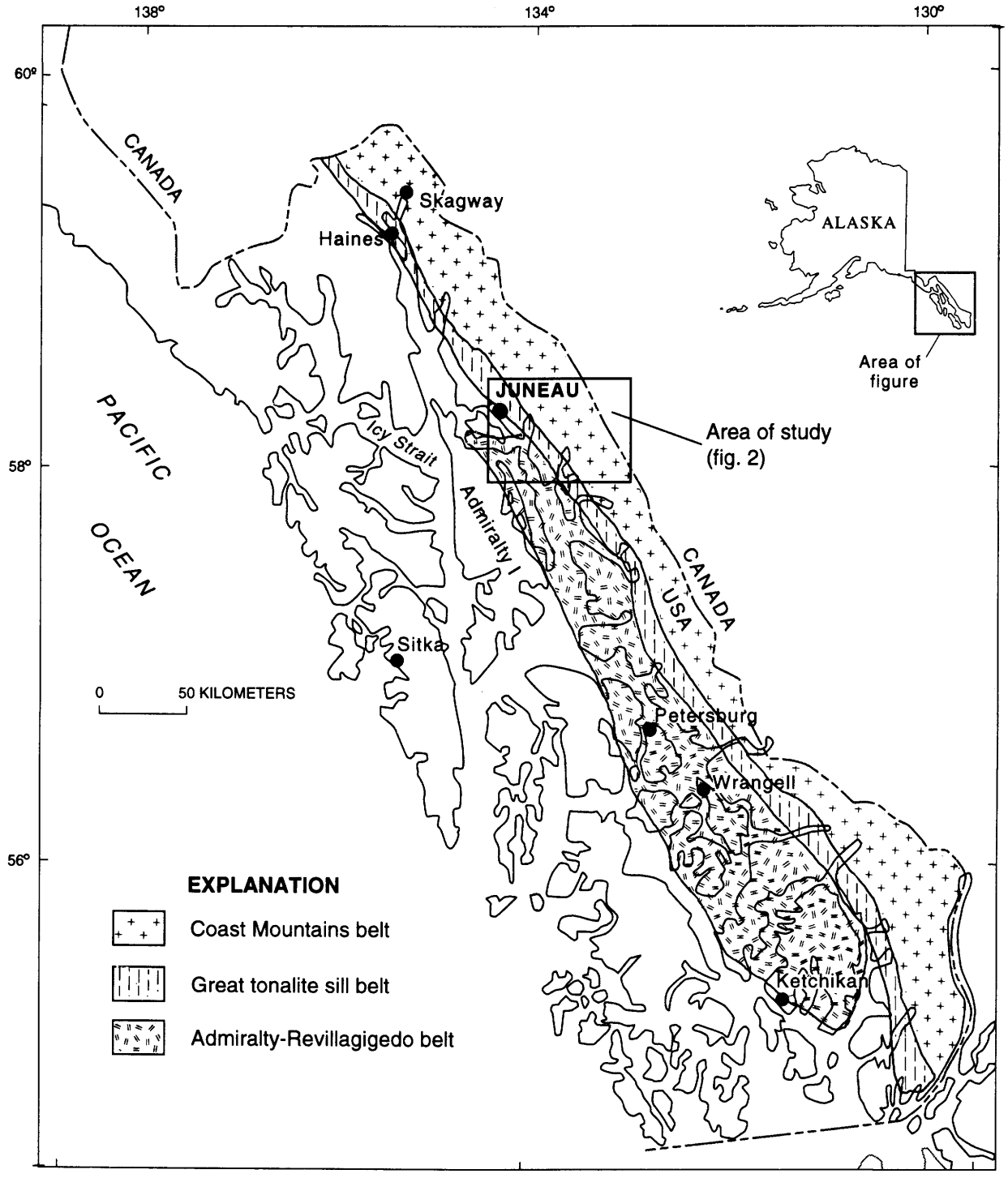

Figure 1. Index map of southeastern Alaska showing location of study area (Taku Inlet transect) and distribution of three major plutonic belts of the informally named Coast plutonic-metamorphic complex.

► **Figure 2.** Generalized geologic map of the Taku Inlet transect and adjacent area to northwest, in southeastern Alaska.

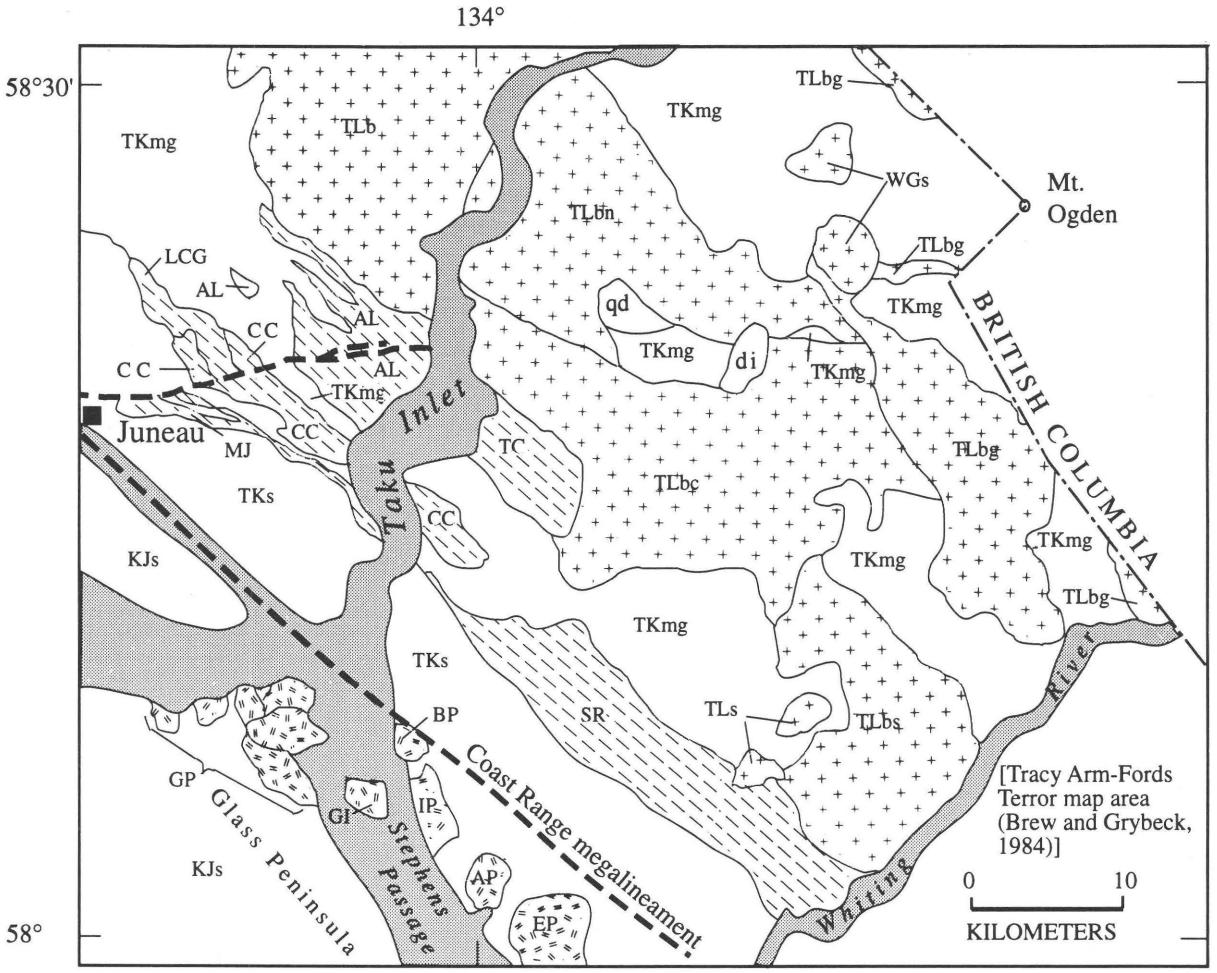

EXPLANATION

Major Plutonic Rocks of the Taku Inlet Transect

A — **Coast Mountains belt**

B — **Great tonalite sill belt**

C — **Admiralty-Revillagigedo belt**

Map Units

A
- WGs - Wright Glacier stocks
- TLbg - Turner Lake batholith, eastern unit
- TLbn - Turner Lake batholith, northern unit
- TLbc - Turner Lake batholith, central unit
- TLbs - Turner Lake batholith, southern unit
- TLb - Turner Lake batholith, undivided
- TLs - Tease Lakes stocks

B
- SR - Speel River pluton
- TC - Taku Cabin pluton
- AL - Annex Lakes pluton
- CC - Carlson Creek pluton

C
- LCG - Lemon Creek Glacier pluton
- MJ - Mount Juneau pluton
- EP - Everett Peak pluton
- AP - Arthur Peak pluton
- BP - Butler Peak pluton
- IP - Irving Peak pluton
- GI - Grand Island pluton
- GP - Glass Peninsula stocks

- TKmg - Migmatitic gneiss (Tertiary and Cretaceous)
- TKs - Schist (Tertiary and Cretaceous)
- KJs - Metasedimentary and metavolcanic rocks (Cretaceous and Jurassic)
- di - Diorite
- qd - Quartz diorite

Coast plutonic-metamorphic complex in the transect area (fig. 2). Plutons of the Coast plutonic-metamorphic complex were emplaced along the boundary of two major composite allochthonous terranes (Insular and Intermontane Superterranes of Wheeler and McFeely, 1991). This large volume of granitic rocks is believed to have been generated in response to the accretion of the Alexander-Wrangellia terrane to the Stikine terrane in Late Cretaceous time (Crawford and others, 1987; Brew, 1988; Brew and others, 1991). From west to east the major plutonic belts are (1) the Admiralty-Revillagigedo belt of Late Cretaceous tonalite, quartz diorite, and quartz monzodiorite plutons, (2) the Great tonalite sill belt of steeply dipping, foliated tonalite plutons of mostly Paleocene age, and (3) the Coast Mountains belt of large and mostly massive granodiorite and granite bodies of Eocene age. Plutons of the Admiralty-Revillagigedo belt are thought to be unrelated to the plutons of the other two plutonic belts because they differ in age (Brew and Morrell, 1983) and isotopic composition (Barker and Arth, 1990), and were emplaced in different lithotectonic terranes (Monger and Berg, 1987; Wheeler and McFeely, 1991; Brew and others, 1991; Rubin and others, 1990). Plutons of the Great tonalite sill and Coast Mountains belts were also emplaced in different terranes or tectonic regimes, but are closer in age and affinity (Brew, 1988; Barker and Arth, 1990). Because the emplacement was largely post-terrane collision, the host terranes may or may not have caused significant compositional differences; all of the belts post-date the major accretion events. Plutons of the Coast plutonic-metamorphic complex were affected by postaccretionary tectonic activity (Crawford and others, 1987; Brew and others, 1989; 1991) discussed later in this report.

The plutons within each plutonic belt are similar in size (Brew and Morrell, 1983; Brew and Ford, 1986), age (Brew and Morrell, 1983; Gehrels and others, 1990, 1991), modal composition (Brew, 1988), and magnetic susceptibility (Drinkwater and others, 1992). General characteristics of the three belts are summarized in table 1. The age, lithology, and composition of granitoids from the transect are similar to those features of other segments of the Coast plutonic-metamorphic complex (Buddington, 1927; Brew, 1988; Barker and Arth, 1990). Additional information on the timing of regional deformation, metamorphism, and pluton emplacement is given by Brew (1988), Brew and others (1989, 1991), and Gehrels and others (1991).

ADMIRALTY-REVILLAGIGEDO BELT

The plutons of the 85- to 95-Ma Admiralty-Revillagigedo belt within the transect are typically discordant bodies of well-foliated, medium-grained, porphyritic biotite and hornblende quartz diorite and tonalite that carry primary garnet and epidote, but lack primary magnetite. These plutons intrude Upper Jurassic and Lower Cretaceous metasedimentary and metavolcanic rocks of the Gravina overlap assemblage (Brew and others, 1991) on Glass Peninsula and higher-grade schist of the composite Alexander-Wrangellia terrane of Brew and others (1991) on the mainland east of Stephens Passage (Brew and Ford, 1986). Collectively, these country rocks are referred to as the western metamorphic zone of the Coast plutonic-metamorphic complex by Brew and others (1989), and are cut by the northwest-trending Coast Range megalineament (Brew and Ford, 1978).

Most plutons are partly altered, weakly metamorphosed, locally mylonitized, and exhibit very low magnetic susceptibility (Drinkwater and others, 1992). Two K-feldspar-rich plutons of this belt in the southern part of the transect (Everett Peak and Arthur Peak plutons of figure 2) consist of well-foliated, leucocratic, hornblende quartz monzodiorite that contains primary epidote and magnetite, and have moderate magnetic susceptibilities (Drinkwater and others, 1992). The hornblende geobarometry of Zen and Hammarstrom (1984), and Hammarstrom and Brew (1993) and the geothermobarometric results given by Brew and others (1992) indicate high pressures (7-9 Kbar) and corresponding deep crustal levels (>25 km) for plutons of the Admiralty-Revillagigedo belt. Mineral assemblages in the adjacent country rocks do not indicate such high pressures, however, and the contrast has not yet been explained completely (Brew and others, 1990). These plutons were emplaced in an uncertain tectonic environment (Brew and others, 1990), but were affected by post-emplacement regional compressional deformation associated with the emplacement of the Great tonalite sill belt to the east (Brew and others, 1989). Barker and Arth (1990) concluded from their Sr and Nd isotope systematics study that plutons of the Admiralty-Revillagigedo belt were derived from moderately evolved melts from a mantle source.

GREAT TONALITE SILL BELT

Plutons of the 55- to 60-Ma Great tonalite sill belt within the Taku Inlet transect (Speel River and Taku Cabin plutons, fig. 2) are concordant, thick sheet-like bodies that consist of mostly foliated equigranular biotite-hornblende tonalite, which exhibit very high magnetic susceptibility (Drinkwater and others, 1992). Plutons of the Great tonalite sill belt occur east of the Coast Range megalineament and were emplaced along a steeply dipping ductile shear zone (Hutton and Ingram, 1992) in high-grade and highly deformed metamorphic rocks within the central metamorphic zone of the Coast plutonic-metamorphic complex (Brew and Ford, 1984). This tectonic zone is interpreted as either a collision zone-terrane boundary or a within-plate rift margin (Brew, 1988). The band of metamorphic rocks between the southwest margin of the Great tonalite sill belt and the Coast Range megalineament was correlated with the Yukon Crystalline terrane by Gehrels and others (1990), but is considered

Table 1. Characteristic features of major plutonic belts from the Coast plutonic–metamorphic complex within the Taku Inlet transect area, southeastern Alaska.

Belt	Admiralty-Revillagigedo	Great tonalite sill	Coast Mountains
Country rocks	Low-grade schist, metavolcanic rocks	High-grade schist	gneiss and migmatite
Main rock types	Quartz diorite, tonalite, and quartz monzodiorite	Tonalite, and quartz diorite	Granodiorite, granite, tonalite
Texture	Foliated to gneissic, and porphyritic	Foliated, equigranular	Massive, and equigranular to porphyritic
Color Index	10 to 35	17 to 35	4 to 20
Major mafics	hornblende, biotite, and epidote	hornblende and biotite	biotite and hornblende
Major accessory	sphene, sulfides, garnet	magnetite, sphene, apatite	allanite, sphene, magnetite
Age	Late Cretaceous	Early Tertiary	Tertiary (Eocene)
FeO*	4 to 10 percent	3 to 6 percent	1 to 5 percent
K_2O	1 to 3.4 percent	1 to 2 percent	2 to 5 percent
Sr	700 to 1000 ppm	550 to 780 ppm	200 to 675 ppm
Rb	30 to 60 ppm	20 to 46 ppm	40 to 140 ppm
References	Brew and Morrell (1983), Brew and Ford (1986), Drinkwater and others (1992).	Brew and Ford (1986), Brew (1988), Drinkwater and others (1989, 1992)	Brew and Ford (1986), Brew (1988), Brew and Grybeck (1984), Drinkwater and others (1992).

to be a composite terrane consisting of a mixture of thrust slices of several different terranes (Rubin and others, 1990) including the Alexander, Wrangellia, Gravina, and Yukon Crystalline terranes (Brew and others, 1991). North of the transect, foliated granodiorite and leucotonalite of the Annex Lakes pluton (fig. 2) forms an eastern subbelt of the Great tonalite sill belt (Drinkwater and others, 1990; 1992). A group of small plutonic sills (Mount Juneau, Carlson Creek, and Lemon Creek Glacier plutons), which are spatially part of the Great tonalite sill belt, also occur just outside the transect (fig. 2) but are older than other plutons of the Great tonalite sill belt and have very low magnetic susceptibilities (Drinkwater and others, 1992).

Emplacement and crystallization of the plutons of the Great tonalite sill belt is believed to have spanned the period from 55 to 70 Ma (Brew, 1988; Barker and Arth, 1990; Wood and others, 1991). Emplacement of the tonalitic plutons was structurally controlled and concurrent with movements along the shear zone and with uplift (Crawford and others, 1987; Brew and others, 1989; Gehrels and others, 1990; Hutton and Ingram, 1992). Stowell and others (1989) concluded from their geobarometric studies on igneous hornblende and metamorphic rock assemblages, that rocks of the Great tonalite sill belt in the vicinity of the Taku Inlet area crystallized at mid-crustal depths corresponding to pressures of 5 to 6 Kbar. Studies of metamorphic-mineral assemblage by Himmelberg and others (1991) suggest that the crystallization pressures of 5 to 6 Kbar represent the final emplacement of the Great tonalite sill belt after uplift, and that initial emplacement began at greater pressures corresponding to depths of 30 to 35 km. After emplacement, plutons of the Great tonalite sill belt were affected by post-thrusting transpressional-related tectonic movements and uplift (Brew and others, 1991).

COAST MOUNTAINS BELT

The Coast Mountains belt within the transect consists of large plutons or plutonic units, and stocks (fig. 2) of the 49- to 53-Ma Turner Lake batholith (Drinkwater and others, 1992). The large granodiorite and granite units are typically homogeneous, massive, porphyritic to equigranular textured rocks. Granitic plutons of the Coast Mountains belt intrude high-grade schist, gneiss, and migmatite of Late Cretaceous to early Tertiary metamorphic age (Brew and Ford, 1986). These metamorphic country rocks are considered to have Proterozoic or Paleozoic protolith ages and may be the metamorphic equivalents of the rocks of the Alexander-Wrangellia terrane (Brew and others, 1991) or the Yukon Crystalline terrane (Gehrels and others, 1990), and which is partly equivalent to the Nisling assemblage and Stikinia terrane of Wheeler and McFeely (1991). Rocks of the Turner Lake batholith typically have moderate to high magnetic susceptibilities (Drinkwater and others, 1992). The batholith was probably emplaced at relatively shallow crustal levels as suggested by its proximity to cogenetic volcanic rocks (Ford and Brew, 1987; and Gehrels and others, 1991). The batholith as well as other Eocene plutons of the Coast Mountains belt are considered post-tectonic (post-thrusting) in nature (Brew, 1988) and were emplaced in either a slightly extensional or transtensional (Crawford and others, 1987; Barker and Arth, 1990) or transpressional to extensional (Brew and others, 1991; D.A. Brew and A.B. Ford unpubl. data, 1993) stress environment that followed the compressional crustal-thickening event associated with the emplacement of the Great tonalite sill belt (Crawford and others, 1987; Brew, 1988; Hutton and Ingram, 1992).

CHEMICAL VARIATIONS

All of the rocks of the three major belts in the Taku Inlet transect are calc-alkalic granitoids (Brew, 1988; Drinkwater and others, 1992). Major-element chemical data for representative samples from each plutonic belt are shown in table 2. Because many are similar in their modal composition, mineralogy, and textures (for instance, foliated tonalites occur in all three belts), chemical plots are useful in discriminating them. The plutonic rocks as a whole show a wide range in SiO_2 content (57–74 percent), but the major belts exhibit narrower ranges and different SiO_2 distribution patterns (fig. 3). The binary discrimination diagrams of figures 4 through 6 show the relations between rocks of the three major belts. All rocks of the three plutonic belts are metaluminous to slightly peraluminous (fig. 4) with aluminum saturation indices [$A/CNK=Al_2O_3/(CaO+Na_2O+K_2O)$ in molecular proportions] between 0.7 and 1.1. Rocks of the Coast Mountains belt are typically borderline peraluminous (A/CNK range of 0.95 to 1.1), but rocks of the Admiralty-Revillagigedo belt, which show a wide range of A/CNK values (0.7–1.1), exhibit generally lower A/CNK values than SiO_2-equivalent rocks of the Great tonalite sill and Coast Mountains belts.

Rocks of the three plutonic belts are chiefly subalkaline (fig. 5) but Admiralty-Revillagigedo belt rocks typically contain higher total alkali content (Na_2O+K_2O) than SiO_2-equivalent rocks of both the Great tonalite sill and Coast Mountains belts, and many of the Admiralty-Revillagigedo belt samples plot in or near the alkaline field of Irvine and Baragar (1971). Whether the high alkali content is a primary or secondary feature of these plutons is uncertain; because many of the rocks contain abundant sericite, either as replacement of plagioclase or as bundles intergrown with biotite that suggest possible K enrichment. The non-coherent distribution or scatter of plotted samples of Admiralty-Revillagigedo belt rocks in figure 5 may also reflect alteration. Rocks of the Great tonalite sill and Coast Mountains belts show a continuous, relatively coherent linear distribution of total alkali versus SiO_2 (fig. 5).

Rocks of the Admiralty-Revillagigedo belt are clearly separated from rocks of the Great tonalite sill and Coast Mountains belts on the FeO*/MgO versus SiO_2 diagram (fig. 6). The Admiralty-Revillagigedo belt rocks show higher FeO*/MgO ratios relative to SiO_2-equivalent rocks of the other belts (fig. 6); most of them, as volcanic-equivalents, would plot within the tholeiitic field of Miyashiro (1974). Rocks of the Great tonalite sill and Coast Mountains belts exhibit a fairly coherent semi-linear distribution within the calc-alkaline field with scatter increasing at higher SiO_2 contents (fig. 6).

Ternary diagrams (fig. 7) also clearly separate rocks of the three plutonic belts. On the AFM diagram (fig. 7*A*) rocks of the Great tonalite sill and Coast Mountains belts show a coherent linear calc-alkaline distribution, whereas the Admiralty-Revillagigedo belt rocks exhibit a separate calc-alkaline trend with more iron-rich compositions that extends into the tholeiitic field of Irvine and Baragar (1971). On the normative feldspar composition diagram

Table 2. Major element chemistry for representative plutonic rocks from the Taku Inlet Transect area.

[Samples analyzed by X-ray fluorescence spectrometry at USGS laboratories in Denver, Colorado; by J. Taggart, A. Partel, and D. Siems]

	Admiralty-Revillagigedo belt			Great tonalite sill belt			Coast Mountains belt			
Sample ---	83-6-30	87JS004	87JS005	87JS011	87JS016	87JS017	87JS012	87JS013	88SK147	88SK148
Whole rock analyses (weight percent oxide) normalized to 100 percent volatile free										
SiO_2	57.49	64.08	58.30	60.33	61.33	63.41	70.55	69.34	70.41	70.23
Al_2O_3	19.23	17.72	18.00	18.52	17.98	17.33	15.79	16.06	16.05	15.35
Fe_2O_3	2.55	2.08	2.92	2.29	1.99	1.59	1.04	1.33	0.94	0.92
FeO	4.13	1.94	3.22	3.33	3.33	3.01	1.18	1.27	0.96	1.46
MgO	2.11	1.11	1.82	2.53	2.41	2.19	0.71	0.88	0.56	0.92
CaO	7.94	5.53	7.07	7.19	7.25	6.16	3.38	4.01	3.52	2.93
Na_2O	3.81	3.99	3.87	3.87	3.75	3.58	3.95	3.86	4.17	3.86
K_2O	1.69	2.72	3.37	0.97	1.03	1.96	2.82	2.69	2.78	3.66
TiO_2	0.61	0.47	0.86	0.59	0.53	0.48	0.35	0.34	0.33	0.43
P_2O_5	0.28	0.21	0.38	0.28	0.30	0.21	0.17	0.16	0.24	0.20
MnO	0.18	0.15	0.20	0.10	0.10	0.08	0.05	0.05	0.05	0.05
LOI	0.62	0.41	0.34	0.36	0.35	0.99	0.5	0.22	0.31	0.50
FeO*	6.42	3.81	5.85	5.32	5.12	4.44	2.12	2.47	1.80	2.29

*, Total iron as FeO.

(fig. 7*B*), most rocks of the Great tonalite sill and Coast Mountains belts also show a coherent distribution within the normal alkali composition field of Irvine and Baragar (1971) with some overlap into the K-rich field, but most Admiralty-Revillagigedo belt rocks plot either in or borderline to K-rich compositions.

The relative abundances of trace-elements for plutons from the three plutonic belts are summarized in the ORG (ocean ridge granites)-normalized multi-element diagrams of figure 8. Although the geochemical patterns for the three belts are generally similar and are typical of granitic rocks from volcanic-arc environments (Pearce and

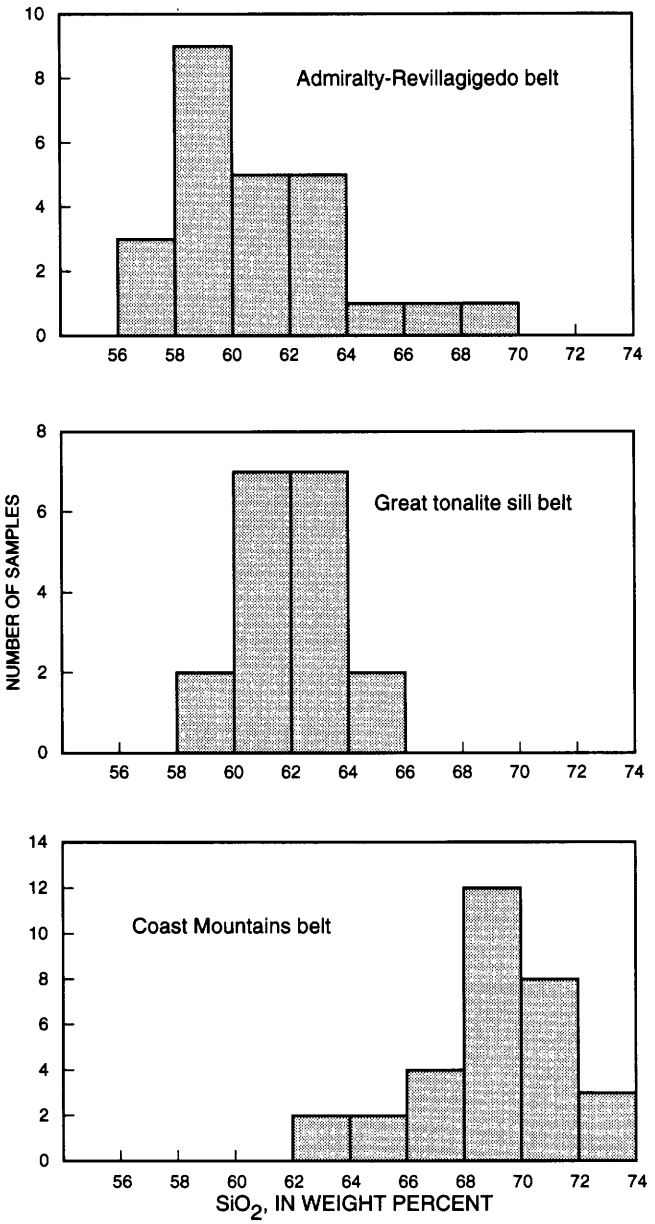

Figure 3. Distribution of SiO_2 content in plutonic rocks from three major plutonic belts of the Taku Inlet transect.

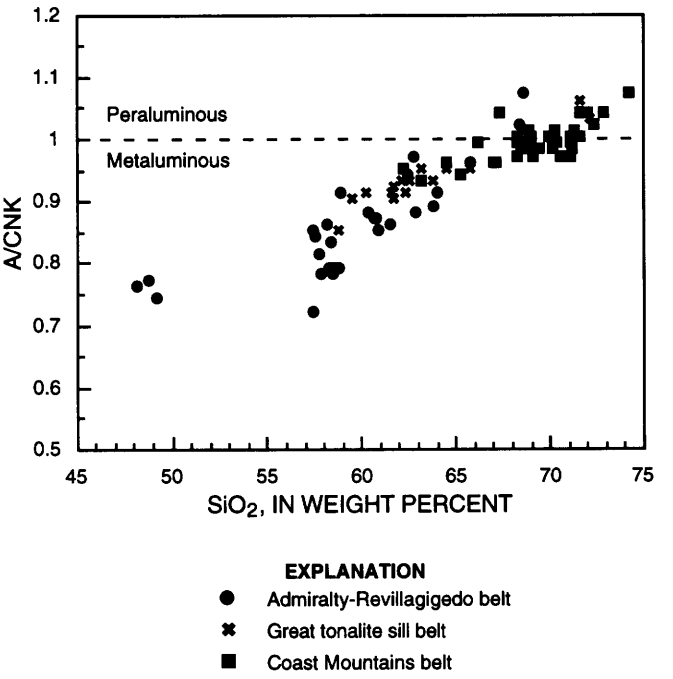

Figure 4. Variation diagram of SiO_2 versus A/CNK (molecular proportions $Al_2O_3/CaO+Na_2O+K_2O$) for granitoids from three major plutonic belts of the Taku Inlet transect.

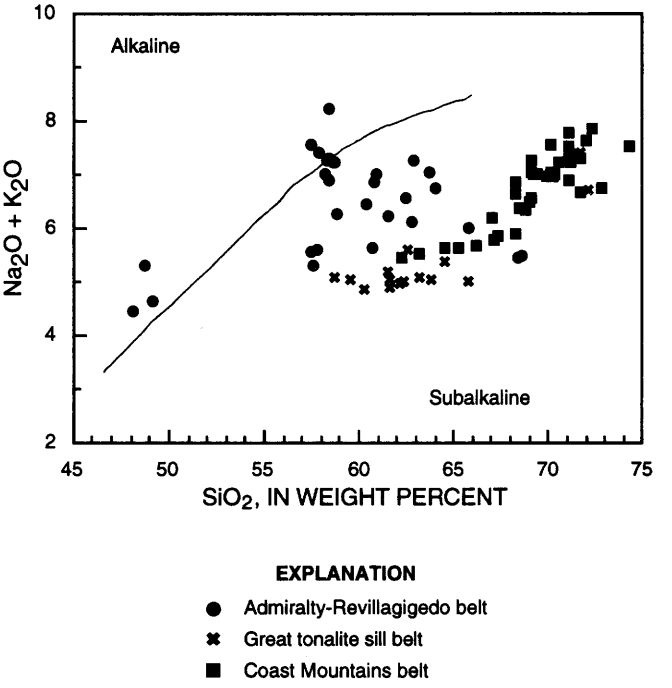

Figure 5. Variation diagram of SiO_2 versus total alkalies (Na_2O+K_2O) for plutonic rocks from three major plutonic belts of the Taku Inlet transect. Field boundary from Irvine and Baragar (1971).

others, 1984) particularly in showing relative enrichment in large-ion-lithophile elements (LILE: K-Sr-Rb-Ba-Th) in comparison to other trace elements, abundance levels for certain elements vary between belts (fig. 4). Admiralty-Revillagigedo belt rocks differ from those of the other belts in their relatively higher Sr content, slightly positive Nb spike, and lack of a positive Ce spike. Rocks from the Coast Mountains and Great tonalite sill belts show similar patterns but rocks from the Coast Mountains belt are more LILE-enriched. The elevated Ba abundance, relative to the other LILE, shown for all three belts is not typical of most volcanic arc granitic suites (Pearce and others, 1984) and may be diagnostic of rocks from the Coast plutonic-metamorphic complex.

Sr abundances (table 1) range from 200 ppm to 1000 ppm in all rocks but are consistently higher in Admiralty-Revillagigedo belt rocks and lowest in Coast Mountains belt rocks where highly evolved granites contain 200 to 250 ppm Sr. Rb content ranges from 30 ppm to 140 ppm in all rocks, but generally is higher in rocks of the Coast Mountains belt. The relative abundance of Sr and Rb is particularly useful in discriminating the three plutonic belts (fig. 9). Plots for rocks from the Great tonalite sill and Coast Mountains belts show a curvilinear distribution of increasing Rb and decreasing Sr with more silicic rocks (fig. 9) indicating a genetic relation by plagioclase fractionation. Rocks from the Admiralty-Revillagigedo belt cluster separately from rocks of the other belts because of the different relative Sr and Rb abundance (fig. 9).

The granitoids of the Coast plutonic-metamorphic complex have been ascribed to a tectonic setting of a continental-margin magmatic arc (Barker and Arth, 1990; Brew, 1988). The samples from this transect plot in the volcanic-

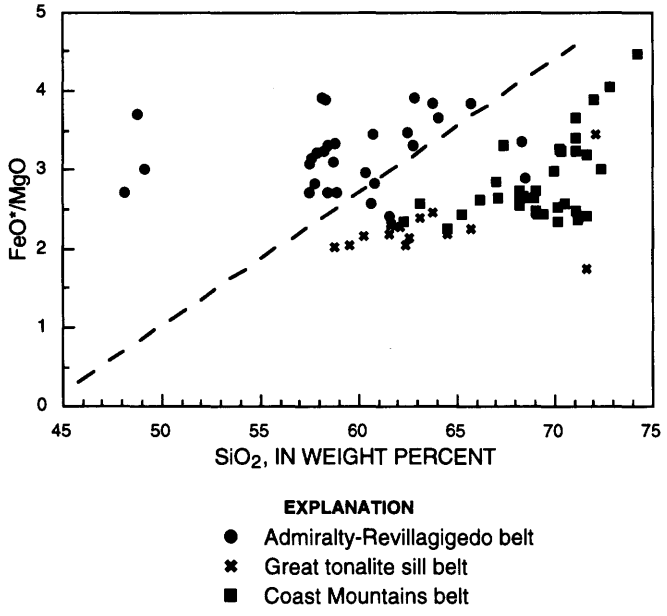

Figure 6. Variation diagram of SiO_2 versus FeO*/MgO ratios for plutonic rocks from three major plutonic belts of the Taku Inlet transect. Field boundary from Miyashiro (1974).

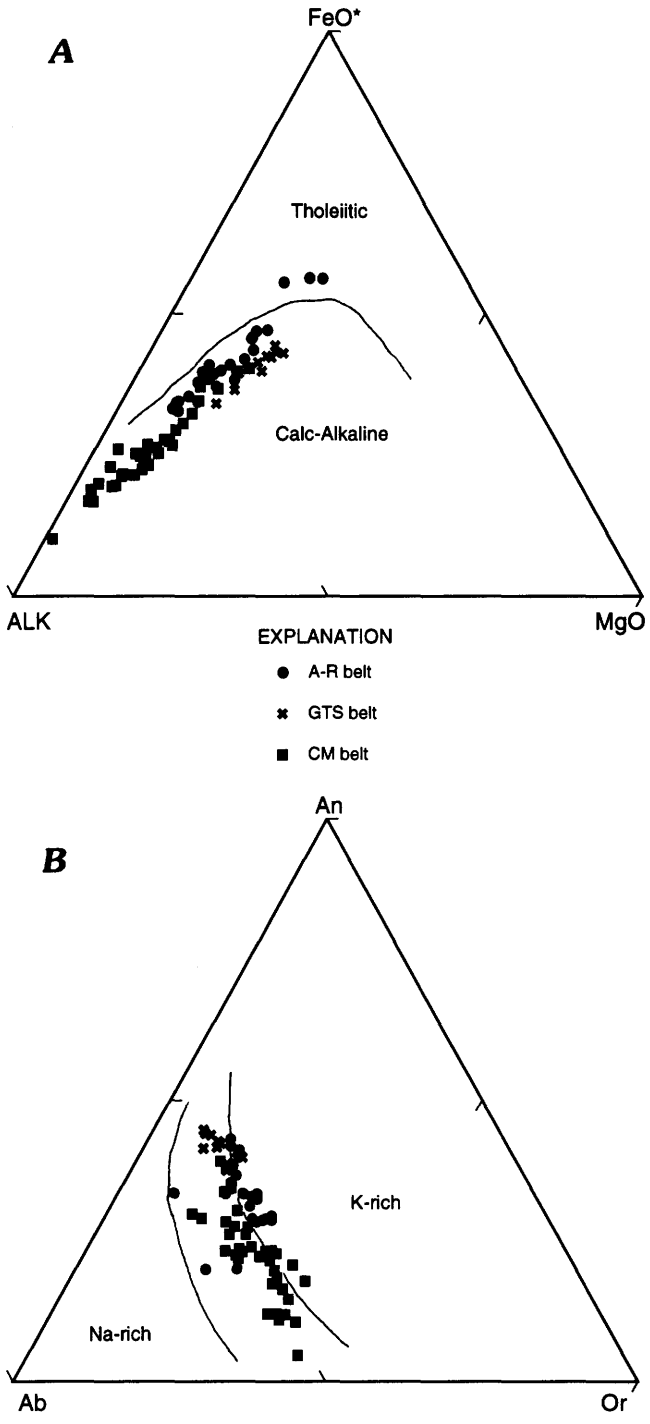

Figure 7. Ternary diagrams for plutonic rocks from three major plutonic belts of the Taku Inlet transect. A-R, Admiralty-Revillagigedo belt; GTS, Great tonalite sill belt; CM, Coast Mountains belt. *A*, AFM diagram with boundary line from Irvine and Baragar (1971). FeO*, FeO+(.8998×Fe_2O_3); Alk, Na_2O+K_2O. *B*, Normative feldspar composition diagram with boundary lines from Irvine and Baragar (1971). An, anorthite percent; Ab, albite percent; Or, orthoclase percent.

arc granite field in the Rb versus Y+Nb covariation diagram (fig. 10) of Pearce and others (1984). Rocks of the Coast Mountains belt contain higher Rb contents than rocks of the other belts, and several high-K granite samples from the eastern part of the this belt have relatively high Rb and Y+Nb contents that plot near the borderline for within-plate

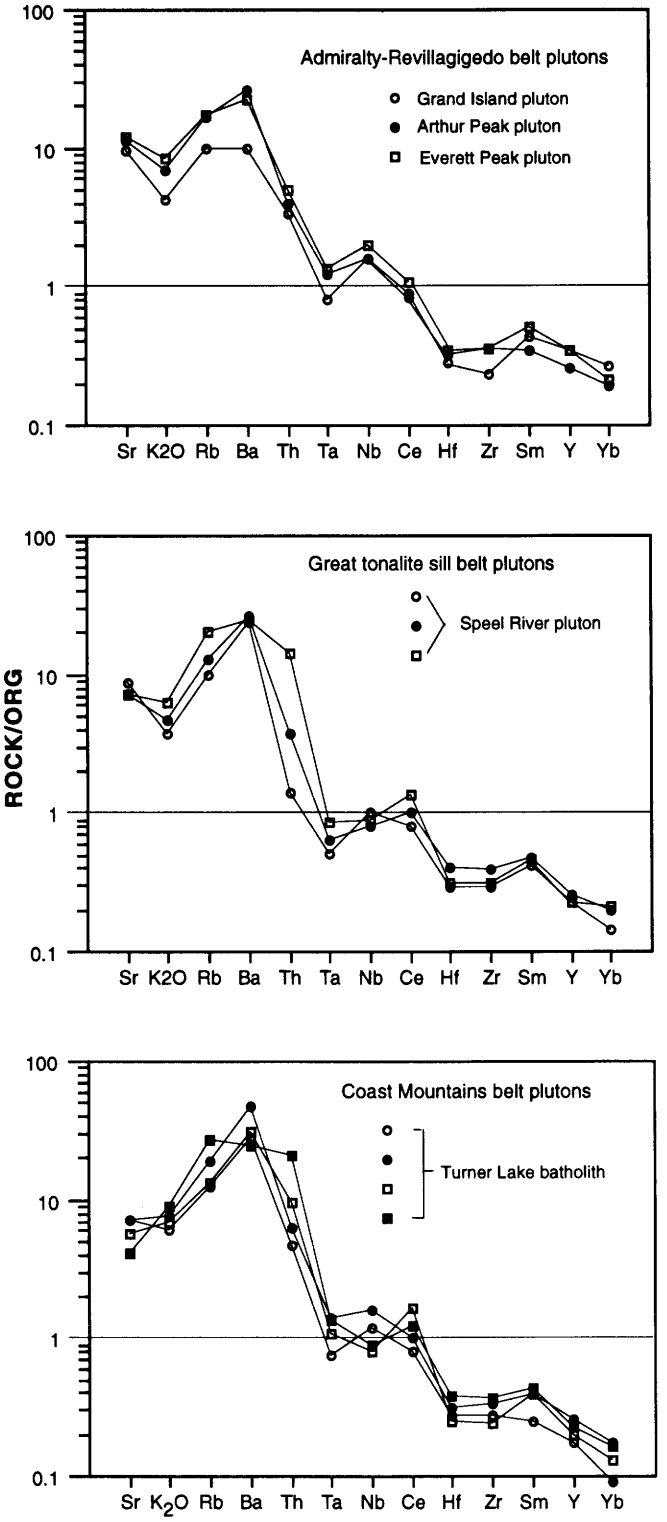

Figure 8. ORG (ocean ridge granites)-normalized multi-element plots for representative samples from three major plutonic belts of the Taku Inlet transect area. Major-element chemistry of samples shown in table 2. From method of Pearce and others (1984), and Wheatley and Rock (1988).

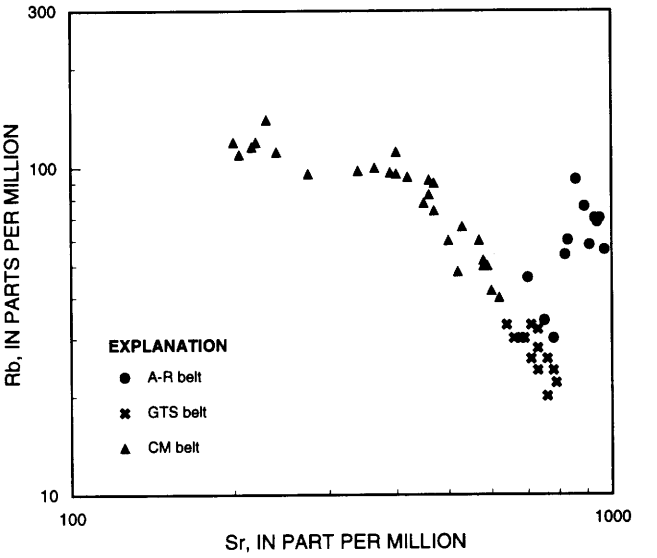

Figure 9. Variation diagram of Sr versus Rb for rocks from three major plutonic belts of the Taku Inlet transect. A-R, Admiralty-Revillagigedo belt; GTS, Great tonalite sill belt; CM, Coast Mountains belt.

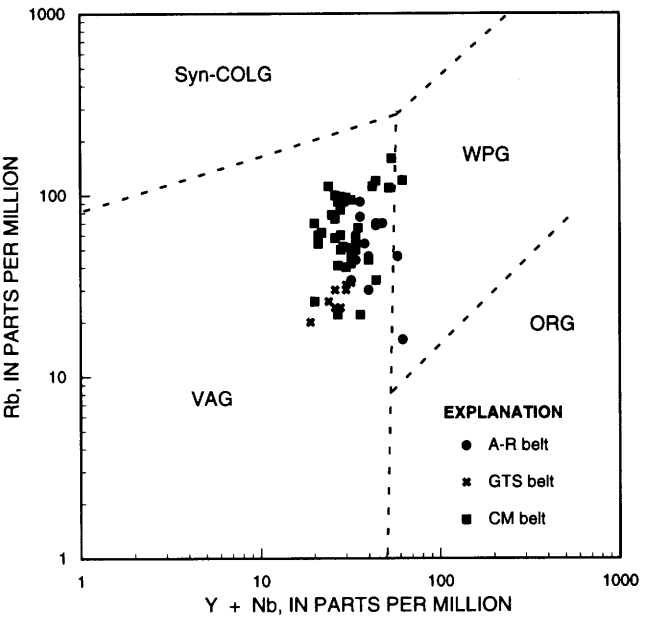

Figure 10. Variation of Y+Nb versus Rb for rocks from three major plutonic belts of the Taku Inlet transect area. Field boundaries from Pearce and others (1984). VAG, volcanic arc granitoids; ORG, ocean ridge granitoids; WPG, within plate granitoids; Syn-COLG, syn-collision granitoids; A-R, Admiralty-Revillagigedo belt; GTS, Great tonalite sill belt; CM, Coast Mountains belt.

granites (fig. 10). Although post-collision granites typically plot near the top of the VAG field (Pearce and others, 1984) such differences in Rb, Y, and Nb may indicate variations in source composition and assimilation (Arculus, 1987) rather than differences in tectonic processes. Rocks from the Great tonalite sill belt show low Rb and Y+Nb contents compared to those of other belts, but values do overlap with rocks from the Coast Mountains belt.

DISCUSSION

The three major plutonic belts in the Taku Inlet transect can be distinguished from each other by chemical trends and variations, as well as by field relations. The age and compositional trends along the Taku Inlet transect are in accord with the southwest to northwest increase in SiO_2 and K-feldspar, and decrease in mafic mineral content and age recognized in various parts of the Coast plutonic-metamorphic complex by Buddington (1927), Gehrels and others (1984), and Barker and Arth, 1990). This trend is not a continuous progression, but instead, as Barker and Arth (1990) pointed out, has abrupt or step-like changes that reflect differences in the northwest trending plutonic belts and subbelts that comprise the Coast plutonic-metamorphic complex. Additionally, Drinkwater and others (1992) showed that the Fe-oxidation state of the rocks increases and total Fe-content decreases from west to east across 6 subbelts of the Coast plutonic-metamorphic complex. Plutons of the Admiralty-Revillagigedo belt are mostly high-alkali, iron-rich, garnet- and epidote-bearing tonalites and quartz diorites of very low magnetic susceptibilities. Chemically, the rocks of the Admiralty-Revillagigedo belt are further distinguished from rocks of the other belts by their low SiO_2 content and A/CNK ratios, high FeO*/MgO ratios, high Sr content, and normative Or feldspar-rich composition, but low K-feldspar content. Plutons of the Great tonalite sill belt are low-alkali, relatively MgO-rich tonalites that have very high magnetic susceptibilities. These rocks are characterized by their restricted SiO_2 range (59–66 percent), lower Rb content and FeO*/MgO ratios, higher normative An content, and higher Ti content than rocks from the other belts. Rocks of the Coast Mountains belt are more silicic (64–74 percent SiO_2) than rocks of the other belts, and also contain higher LILE abundance, and lower FeO*, MgO, and Sr content.

Admiralty-Revillagigedo belt rocks fit the overall SW-NE trends (SiO_2 and modal composition), but they cluster separately from rocks of the other belts on most chemical variation diagrams. Their older age, chemical variations, accessory mineralogy, very low magnetic susceptibilities, and geographic position west of the Coast Range megalineament, separates them as a distinct episode of plutonism from the mainland batholith (Great tonalite sill and Coast Mountains belts) that was emplaced east of the megalineament. This is in accord with the findings of Barker and Arth (1990) who determined that the rocks of the Admiralty-Revillagigedo belt also are isotopically distinct from rocks of the other two belts. These plutons originated from deep-seated, moderately evolved, mantle-derived melts (Barker and Arth, 1990) that may be subduction related (Barker and Arth, 1990; Samson and others, 1991).

The spatially related plutons of the Great tonalite sill and Coast Mountains belts show petrologic affinity (figs. 4–7, 9); their differences in chemistry can be attributed largely to lithologic differences between the two belts. Rocks of both belts probably originated from the same source region and shared a common petrogenetic history according to Barker and Arth (1990) and the Nd and Sr isotopic studies of Samson and others (1991). In contrast, Crawford and others (1987) concluded from their studies in the Prince Rupert area of British Columbia, that Tertiary plutons equivalent to the Great tonalite sill and Coast Mountains belts did not share a common melt source or genetic link, but instead that rocks of the Great tonalite sill belt were products of mantle-derived partial melts and the Eocene plutons to the east were products of crustal anatexis. The same source models mentioned above differ in the nature of the source; Barker and Arth (1990) concluded from their results that these plutons are fractionation products from mantle-derived partial melts that assimilated crust of the accreted terranes, whereas Samson and others (1991) believed that both plutonic belts are products of crustal anatexis, being a mixture of fused juvenile terrane crust and underlying old and evolved continental crust that they correlate with the mostly Precambrian Yukon-Tanana terrane. Himmelberg and others (1991) considered the Great tonalite sill belt plutons to be in part mantle derived. Our results support a common source and petrogenetic history for the two plutonic belts, but the nature of the source region and whether the magmatic system was mantle dominated or crustal dominated is still in question. The relatively high LILE abundances and Ce anomaly support isotope evidence (Barker and Arth, 1990; Samson and others, 1991) that significant amounts of crustal component were involved in the magmatic evolution of these plutons.

Plutons of the Great tonalite sill and Coast Mountains belts were emplaced in different tectonic regimes and at least partly in different terranes. Although plutonism occurred after collision and amalgamation of the terranes, differences in composition and structural conditions between terranes could cause different histories of contamination, oxidation, fractionation, and cooling. Plutons of the Great tonalite sill belt were emplaced along the eastern margin of a complicated structural zone believed to have been the loci of major collision and thrust-fault tectonics. Plutons of the younger Coast Mountains belt were emplaced in the structurally and compositionally different Nisling and Stikinia terranes after major tectonic and accretion events, and at relatively shallow crustal levels in a

slightly extensional or transtensional tectonic environment. According to Crawford and others (1987), the generation and emplacement of plutons of the great tonalite sill belt into an active shear zone during uplift was related to the collision of the Alexander-Wrangellia and Stikinia terranes. West-directed thrusting and crustal thickening were interpreted to cause crustal weakening and decompression in the orogenic rocks to the east which resulted in partial melting of crustal terrane rocks to produce the younger plutons equivalent to those of the Coast Mountains belt (Crawford and others, 1987). Brew (1988) interpreted the age and spatial relations to suggest a close association of the two belts. Samson and others (1991) proposed a tectonic model like that of Crawford and others (1987) for the northern Coast plutonic-metamorphic complex, except that thrusting-related anatexis formed both belts of plutons largely from Yukon-Tanana type crustal rocks rather than Stikinia terrane rocks. Barker and Arth (1990) concluded that most of the plutons from these two belts are largely products of subduction-related tectonism.

Plutons of the Great tonalite sill and Coast Mountains belts from the Taku Inlet transect are genetically related and have SiO_2 and K_2O contents and AFM distributions that are similar to rocks from other parts of these belts in southeastern Alaska (Brew, 1988). The Sr content of rocks from the Great tonalite sill and Coast Mountains belts of the Taku Inlet transect falls within an intermediate range between the low Sr values of equivalent rocks from the Skagway traverse and higher values for rocks from the Ketchikan traverse reported by Barker and Arth (1990). Great tonalite sill belt rocks from the Taku Inlet transect show a lower Rb range than rocks of this unit reported by Barker and Arth (1990). These differences in Sr and Rb content correlate with the increase in average SiO_2 content and aluminum saturation indices from north to south along the Coast plutonic-metamorphic complex (Brew, 1988) that may reflect differences in source composition.

REFERENCES CITED

Arculus, R.J., 1987, The significance of source versus process in the tectonic controls of magma genesis: Journal of Volcanology and Geothermal Research, v. 32, p. 1–12.

Barker, Fred, and Arth, J.G., 1990, Two traverses across the Coast batholith, southeastern Alaska: in Anderson, J.L., ed., The nature and origin of Cordilleran magmatism: Geological Society of America Memoir 174, p. 395–404.

Berg, H.C., Jones, D.L., and Coney, P.J., 1978, Map showing pre-Cenozoic tectonostratigraphic terranes of southeastern Alaska and adjacent areas: U.S. Geological Survey Open-File Report 78-105, scale 1:1,000,000.

Brew, D.A., 1988, Latest Mesozoic and Cenozoic igneous rocks of southeastern Alaska—A synopsis: U.S Geological Survey Open-File Report 88-405, 29 p.

Brew, D.A., and Ford, A.B., 1977, Preliminary geologic and metamorphic-isograd map of the Juneau B-1 quadrangle, Alaska: U.S. Geological Survey Miscellaneous Field Studies Map MF–846, scale 1:31,680.

———1978, Megalineament in southeastern Alaska marks southwest edge of Coast Range batholithic complex: Canadian Journal of Earth Science, v. 15, no. 11, p. 1763–1772.

———1984, The northern Coast plutonic complex, southeastern Alaska and northwestern British Columbia, *in* Coonrad, W.L., and Elliott, R.L., eds., The U.S. Geological Survey in Alaska—Accomplishments during 1981: U.S. Geological Survey Circular 868, p. 120–124.

———1986, Preliminary reconnaissance geologic map of the Juneau, Taku River, Atlin, and part of the Skagway 1:250,000 quadrangles, southeastern Alaska: U.S. Geological Survey Open-File Report 85-395, 23 p.

Brew, D.A., and Grybeck, D., 1984, Geology of the Tracy Arm-Fords Terror wilderness study area and vicinity, Alaska: U.S. Geological Survey Bulletin 1525, 308 p.

Brew, D.A., Himmelberg, G.R., Douglass, S.L., Zen, E., and Sutter, J.F., 1990, Contrasting metamorphic and emplacement environment of a distinctive 95 Ma plutonic suite, southeastern Alaska [abs.]: Geological Society of America, Abstracts with Programs, v. 22, no. 3, p. 10.

Brew, D.A., Himmelberg, G.R., Loney, R.A., and Ford, A.B., 1992, Distribution and characteristics of metamorphic belts in the south-eastern Alaska part of the North American Cordillera: Journal of Metamorphic Geology, v. 10, p. 465–482.

Brew, D.A., and Morrell, R.P., 1983, Intrusive rocks and plutonic belts in southeastern Alaska, *in* Roddick, J.A., ed., Circum-Pacific plutonic terranes: Geological Society of America Memoir 159, p. 171–193.

Brew, D.A., Ford, A.B., and Himmelberg, G.R., 1989, Evolution of the western part of the Coast plutonic-metamorphic complex, southeastern Alaska, USA—A summary; *in* Daly, J.S., and others, eds., Evolution of metamorphic belts, Geological Society of America Special Publication no. 42, p. 447–452

Brew, D.A., Karl, S.M., Barnes, D.F., Jachens, R.C., Ford, A.B., and Horner, R., 1991, A northern Cordilleran ocean-continent transect: Sitka Sound, Alaska, to Atlin Lake, British Columbia: Canadian Journal of Earth Sciences, v. 28, no. 6, p. 840–853.

Buddington, A.F., 1927, Coast Range intrusives of southeastern Alaska: Journal of Geology, v. 35, no. 3, p. 224–246.

Crawford, M.L., Hollister, L.S., and Woodsworth, 1987, Crustal deformation and regional metamorphism across a terrane boundary, Coast plutonic complex, British Columbia: Tectonics, v. 6, no. 3, p. 342–361.

Drinkwater, J.L., Brew, D.A., and Ford, D.A., 1989. Petrographic and Chemical Description of the Variably Deformed Speel River Pluton, south of Juneau, southeastern Alaska; *in* Dover, J.H., and Galloway, J.P., Geologic studies in Alaska by the U.S. Geological Survey, 1988: U.S. Geological Survey Bulletin 1903, p. 104–112.

———1990, Petrographic and chemical data for the large Mesozoic and Cenozoic plutonic sills east of Juneau, southeastern Alaska: U.S. Geological Survey Bulletin 1918, 47p.

Drinkwater, J.L., Ford, D.A., and Brew, D.A., 1992, Magnetic susceptibilities and iron content of plutonic rocks across the Coast plutonic-metamorphic complex near Juneau, Alaska:

in Bradley, D., and Dusel-Bacon, C., eds., Geologic Studies in Alaska by the U.S. Geological Survey, 1991: U.S. Geological Survey Bulletin 2041, p. 125–139.

Ford, A.B., and Brew, D.A., 1977, Preliminary geologic and metamorphic-isograd map of northern parts of the Juneau A-1 and A-2 quadrangles, Alaska: U.S. Geological Survey Miscellaneous Field Studies Map MF–847, 1 sheet, scale 1:31,680.

———1987, The Wright Glacier volcanic plug and dike swarm, southeastern Alaska, *in* Hamilton, T.D., and Galloway, J.P., eds., Geologic studies in Alaska by the U.S. Geological Survey during 1986: U.S. Geological Survey Circular 998, p. 116–118.

Gehrels, G.E., Brew, D.A., and Saleeby, J.B., 1984, Progress report on U-Pb (zircon) geochronologic studies in the Coast plutonic-metamorphic complex east of Juneau, southeastern Alaska; *in* Reed, K.M., and Bartsch-Winkler, S., eds., The United States Geological Survey in Alaska: Accomplishments during 1982: U.S. Geological Survey Circular 939, p. 100–102.

Gehrels, G.E., McClelland, W.C., Samson, S.D., Patchett, P.J., and Brew, D.A., 1991, U-Pb geochronology of Late Cretaceous and early Tertiary plutons in the northern Coast Mountains batholith: Canadian Journal of Earth Science, v. 28, p. 899–911.

Gehrels, G.E., McClelland, W.C., Samson, S.D., Patchett, P.J., and Jackson, J.L., 1990, Ancient continental margin assemblage in the northern Coast Mountains, southeast Alaska and northwest Canada: Geology, v. 18, no. 3, p. 208–211

Hammarstrom, J.M., and Brew, D.A., 1993, Petrology and geobarometry of Admiralty-Revillagigedo belt granitoids near Petersburg, southeastern Alaska (abs.): Geological Society of America Abstracts with Programs, Cordilleran and Rocky Mountain Sections, v. 25, no. 5, p. 47.

Himmelberg, G.R., Brew, D.A., and Ford, A.B., 1991, Development of inverted metamorphic isograds in the western metamorphic belt, Juneau, Alaska: Journal of Metamorphic Geology, v. 9, p. 165–180.

Hutton, D.H.W., and Ingram, G.M., 1992, The Great tonalite sill of southeastern Alaska: emplacement into an active contractional high angle reverse shear zone: Transactions of the Royal Society of Edinburgh, Earth Sciences, v. 83, parts 1 and 2, p. 383–386 and The Second Hutton Symposium on the Origin of Granites and Related Rocks: Boulder, Colorado, Geological Society of America, Special Paper 272, p. 383–386.

Irvine, T.N., and Baragar, W.R., 1971, A guide to the chemical classification of the common volcanic rocks: Canadian Journal of Earth Sciences, v. 8, no. 5, p. 523–548.

Monger, J.W.H., and Berg, H.C., 1987, Lithotectonic terrane map of western Canada and southeastern Alaska: U.S. Geological Survey Miscellaneous Field Studies Map MF–1874B, scale 1: 2,500,000.

Miyashiro, Akiho, 1974, Volcanic rock series in island arcs and active continental margins: American Journal of Science, v. 274, no. 4, p. 321–355.

Pearce, J.A., Nigel, Harris, N.B.W., and Tindle, A.G., 1984, Trace element discrimination diagrams for the tectonic interpretation of granitic rocks: Journal of Petrology, v. 25, no. 4, p. 956–983.

Rubin, C.M., Saleeby, J.B., Cowan, D.S., Brandon, M.T., and McGroder, M.F., 1990, Regionally extensive mid-Cretaceous west-vergent thrust system in the northwestern Cordillera: Implications for continent-margin tectonism: Geology, v. 18, p. 276–280.

Samson, S.D., Patchett, P.J., McClelland, W.C., and Gehrels, G.E., 1991, Nd and Sr isotopic constraints on the petrogenesis of the west side of the northern Coast Mountains batholith, Alaskan and Canadian Cordillera: Canadian Journal of Earth Science, v. 28, p. 939–946.

Stowell, H.H., Onstott, T.C., and Wood, D.J., 1989, Tectonic history of the Coast plutonic complex sill and adjacent metamorphic rocks, northern Coast Ranges, SE Alaska [abs.]: Geological Society of America, Abstracts with Programs, v. 21, no. 6, p. A181.

Wheeler, J.O., McFeely, P., 1991, Tectonic Assemblage Map of the Canadian Cordillera: Geological Survey of Canada, Map 1712A, scale 1:2,000,000.

Wheatley, M.R., and Rock, N.M.S., 1988, A Macintosh program to generate normalized multi-element spidergrams: American Mineralogist, v. 73, p. 919–921.

Wood, D.J., Stowell, H.H., Onstott, T.C., and Hollister, L.S., 1991, $^{40}Ar/^{39}Ar$ constraints on the emplacement, uplift, and cooling of the Coast plutonic complex sill, southeastern Alaska: Geological Society of America Bulletin, v. 103, no. 7, p. 849–860.

Zen, E-an, and Hammarstrom, J.M., 1984, Magmatic epidote and its petrologic significance: Geology, v. 12, p. 515–518.

Reviewers: Russell C. Evarts and Allen C. Robinson

Geochemical Reconnaissance of Alkalic Plutons on Prince of Wales Island, Southeastern Alaska

By James L. Drinkwater *and* James P. Calzia

ABSTRACT

Alkalic plutons, emplaced during early Paleozoic, late Paleozoic, Jurassic, and Early Cretaceous time, form a metallogenic province on Prince of Wales island. The geochemical characteristics of these plutons are examined to help evaluate these rocks as potential hosts to U-Th and rare earth element deposits. The early Paleozoic plutons consist of metaluminous syenite, monzodiorite, and monzonite that are characterized by high K, Rb, and Ba content and low Ti and Nb content. The Middle Jurassic Dora Bay pluton is a peralkaline syenite characterized by high Nb, Zr, Ga and Y content and low Sr, Ti, and P content; the Early Cretaceous Lava Creek pluton is a calc-alkalic diorite characterized by high Rb, Ba, Th, and Nb content. The late Paleozoic plutons consist of metaluminous syenites that are chemically intermediate to the early Paleozoic and the Jurassic plutons. Light/heavy rare earth element fractionation values $(Ce/Yb)_N$ decrease from maximum values of 226 in the early Paleozoic plutons to 2.5 in the Jurassic plutons. The Dora Bay pluton shows similar chemical traits and petrologic affinity as rocks from the Bokan Mountain Granite, which are associated with U-Th and rare earth element deposits. The Paleozoic alkalic plutons show some geochemical evidence that meets the criteria for potential Th-REE vein deposits.

INTRODUCTION

Alkalic plutons of early Paleozoic to Early Cretaceous age on Prince of Wales Island in southeastern Alaska (fig. 1) are potential sites of ore deposits (Barker, 1988) and have been identified as a metallogenic province (Barker, 1988; Barker and Mardock, 1990). The Paleozoic sodium-rich alkalic plutons are potential source- and host-rocks of rare earth element (REE) deposits (Barker, 1988; Brew, 1993; Brew and others, 1991), and have been grouped as a metallogenic belt by Brew (1993, 1994). The Jurassic peralkalic Bokan Mountain Granite (MacKevett, 1963; Gehrels, 1992) is associated with U-Th, Nb, and REE deposits (MacKevett, 1963), and the Jurassic Dora Bay pluton (fig. 1) is considered to have potentially similar type of deposits (Barker, 1988; Barker and Mardock, 1990). The importance of these rocks as a potential metallogenic resource prompted us to sample mapped alkalic intrusions in southern Prince of Wales Island (Eberlein and others, 1983; Brew, 1994) and to examine their age, geologic setting, petrography, and geochemical characteristics as possible analogues to known mineralized alkalic or peralkalic plutons, of which the Bokan Mountain Granite is a prime example (fig 1.). Because the geochemical signature of host alkalic igneous rocks may indicate mineralization (Staatz, 1992) these data may aid in the evaluation of the resource potential of these plutons.

GEOLOGIC SETTING

Alkalic plutons on Prince of Wales Island were emplaced in rocks of the Alexander terrane during Late Ordovician, Late Silurian, Late Pennsylvanian to Permian, and Middle Jurassic time; calc-alkaline plutonism prevailed in the Early Cretaceous time (Eberlein and others, 1983; Gehrels and Saleeby, 1987a,b; Brew, 1994). The country rocks consist primarily of a Late Proterozoic to middle Paleozoic volcanic-arc assemblage that includes the Late Proterozoic and Early Cambrian(?) Wales Group, the Early Ordovician through Early Silurian Descon Formation, and the Devonian Karheen Formation; late Paleozoic shallow-marine sedimentary rocks occur locally (Eberlein and others, 1983; Brew, 1994). These rocks compose the Craig subterrane of Berg and others (1978) and Monger and Berg (1987) and are separated from the Wrangellia-Alexander terrane to the east by the Clarence Strait fault (Brew, 1994). Geologic descriptions and maps of Prince of Wales Island are found in Condon (1961), Eberlein and others (1983), Gehrels and Saleeby (1987b), Gehrels (1992), and Brew (1994). Table 1 summarizes the ages and general characteristics of the alkalic rocks we sampled.

Two early Paleozoic alkalic plutons lie in the southern part of Prince of Wales Island. The Late Ordovician to Early Silurian Stone Rock Bay pluton intrudes a large calc-alkalic

igneous suite (Gehrels and Saleeby, 1987b) and consists of massive, medium-grained leucocratic biotite-hornblende quartz syenite that locally contains garnet and aegerine augite (MacKevett, 1963; Gehrels, 1992). This pluton yielded a U-Pb zircon age of 438±5 Ma (Gehrels and Saleeby, 1987a). MacKevett (1963) describes a gradational brecciated contact between the pluton and a pyroxenite. This intrusive breccia contains REE-rich apatite and radioactive minerals and is interpreted as a breccia pipe (Barker, 1988). Altered andesitic dikes with radioactive prospects cut the Stone Rock Bay pluton (MacKevett, 1963). The Late Silurian pluton at Kassa Inlet intrudes the Wales Group and has a hornfels contact

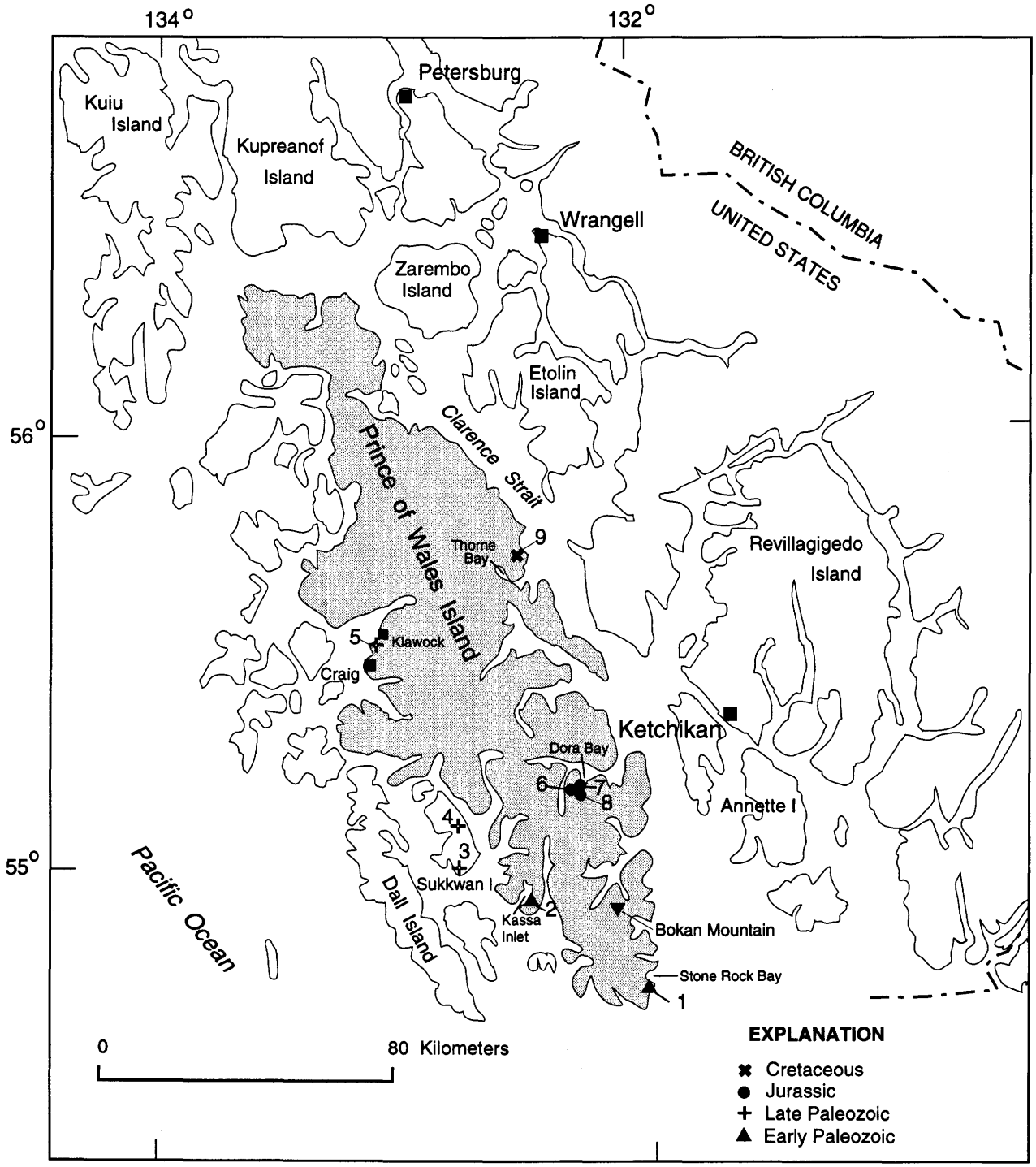

Figure 1. Index map of Prince of Wales Island showing sample locations from alkalic plutons described in this report. Numbers correspond to samples listed in tables 1 and 2.

Table 1. Summary information for alkalic plutons on Prince of Wales Island.

[MS*, magnetic susceptibility ($\times 10^{-5}$ SI units). do., ditto]

Map no.	Pluton	Age	Lithology	MS*	References
1	Stone Rock Bay	Late Ord. to Early Sil.	Quartz syenite	300	Gehrels and Saleeby (1987a & b); Gehrels (1992)
2	Kassa Inlet	Late Silurian	Monzodiorite	400	Gehrels and Saleeby (1987a & b); Gehrels (1992)
3	Sukkwan Island	Late Penn. to Early Perm.	Syenite	1240	Eberlein and others (1983); Brew (1994)
4	---- do. ----------	----- do. ----------	Monzonite	4440	Eberlein and others (1983); Brew (1994)
5	Klawock	Early Permian	Monzodiorite	60	Churkin and Eberlein (1975); Brew (1994)
6	Dora Bay	Middle Jurassic	Syenite	220	Eberlein and others (1983); Brew (1994)
7	---- do. ----------	----- do. ----------	Quartz syenite	400	Eberlein and others (1983); Brew (1994)
8	---- do. ----------	----- do. ----------	----- do. -------	20	Eberlein and others (1983); Brew (1994)
9	Lava Creek	Early Cretaceous	Diorite	200	Eberlein and others (1983); Sainsbury (1961)

aureole; it yielded a U-Pb zircon age of 418±5 Ma (Gehrels and Saleeby, 1987a). The rocks consist of massive, medium- to coarse-grained, garnet-bearing leucodiorite and minor monzodiorite, and monzonite (Gehrels, 1992); arfvedsonite is the principal mafic mineral.

Alkalic rocks of Late Pennsylvanian to Early Permian age are present on Sukkwan Island and near Klawock (fig. 1). Syenite on Sukkwan Island intrudes the Descon Formation and Ordovician to Silurian basaltic and andesitic rocks, and consists of aegerine augite and amphibole-bearing biotite leucosyenite (Eberlein and others, 1983). A K-Ar hornblende age of 283 Ma was reported by Eberlein and others (1983). The pluton near Klawock was mapped by Churkin and Eberlein (1975) as a biotite- and hornblende-bearing syenite that intrudes the Pennsylvanian Klawak Formation. This pluton yielded a K-Ar biotite age of 276 Ma (Churkin and Eberlein, 1975).

The Middle Jurassic pluton at Dora Bay was mapped by Eberlein and others (1983) as nepheline- and eudialyte-bearing syenite and associated pegmatites that intrude the Wales Group and Descon Formation. Eudialyte is a sodium and calcium zirconium-silicate mineral that commonly occurs in undersaturated rocks like syenite; a sample from the Dora Bay pluton is Y-rich (Gunter and others, 1993). Barker and Mardock (1990) investigated the radioactive mineral occurrences (REE, niobium, and yttrium) associated with this pluton; they mapped the body as a north-south trending, west-dipping sheet-like body composed mostly of hornblende syenite and peralkaline granite with minor alkalic granite, diorite, and nepheline syenite. Brew (written commun., 1990) reported that hornblende from this syenite yielded a K-Ar age of 175 Ma. Mineralized coarse-grained pegmatite dikes cut the intrusive and nearby country rocks, and mineralized veins are common in adjacent country rocks (Barker and Mardock, 1990). More recently, molybdenite was found in the hydrothermally altered northeast margin of the pluton (Philpotts and others, 1993).

The Bokan Mountain Granite (fig. 1), a zoned peralkalic pluton of Jurassic age, has been the focus of considerable geologic and geochemical investigations because of its close association with U-Th and REE deposits (Mac-Kevett, 1963; Forbes, 1980; Thompson and others, 1982; Armstrong, 1985; Warner and Barker, 1989). The granite stock, which is emplaced in quartz monzonite of Late Ordovician to Early Silurian age (Gehrels, 1992), has been mapped and described by Thompson and others (1982) as a peralkaline ring-dike complex composed of four major textural phases of aegirine and riebeckite granite. Armstrong (1985) reported a Late Jurassic age for the intrusion. Thompson and others (1982) classified the intrusion as a mantle-derived I-type (igneous) granitoid with a tectonic setting of an Andinotype-subduction zone plate margin (Pitcher, 1982). The U-Th and REE deposits occur in late-magmatic to hydrothermal pegmatitic dikes that cut the intrusion and also occur in veins and veinlets that are concentrated along the margin of the intrusion and in adjacent country rock (MacKevett, 1963).

Sainsbury (1961) reported that the pre-Tertiary pluton near Lava Creek north of Thorne Bay consists of variably altered, heterogeneous, and strongly foliated to gneissic hornblende diorite, with felsic phases of quartz monzonite and monzodiorite that contain biotite, sodic plagioclase, and perthite. Eberlein and others (1983) mapped this body as a Paleozoic or Mesozoic dioritic to granodioritic pluton, and Brew (1994) compiled it as a late Early Cretaceous pluton. Larsen and others (1958) obtained an Pb-alpha age of 103 Ma from similar plutonic rocks to the southeast. Although this pluton may contain alkalic rock phases, it is largely dioritic in composition (Sainsbury, 1961).

PETROGRAPHY AND GEOCHEMISTRY OF THE ALKALIC ROCKS

We sampled alkalic plutons of known Paleozoic age at Stone Rock Bay, Kassa Inlet, Sukkwan Island, and near Klawock, and a Jurassic pluton at Dora Bay (fig. 1). Most of the samples that we collected are syenites, quartz syenites, and monzodiorites, based on examination of stained thin sections. A diorite from the Cretaceous Lava Creek

pluton north of Thorne Bay, which was mapped and described as a possible alkalic body (Sainsbury, 1961), was also studied.

Most of these alkalic rocks yield low magnetic susceptibility values (table 1); only the two samples from the Sukkwan Island pluton yield significant positive values. The low values may be caused by hydrothermal alteration (Lapointe and others, 1986), or by mylonitic and cataclastic deformation (Drinkwater and others, 1992), or both. Magnetite-free granitoids in the plutonic-metamorphic belt of the Coast Range batholith of southeastern Alaska generally yield magnetic susceptibility values less than 300×10^{-5} SI units (Drinkwater and others, 1992); syenites and monzonites typically have low oxidation levels and low magnetic susceptibility values (Grant, 1985).

PETROGRAPHY

Stone Rock Bay pluton (Late Ordovician to Early Silurian).—Our sample of the Stone Rock Bay pluton (No. 1, fig. 1) is a homogeneous, medium-gray, massive, medium-grained, hypidiomorphic granular quartz syenite. The rock consists of abundant microperthite, saussuritized tabular plagioclase, minor intergranular quartz, and altered mafic minerals; accessory minerals include zircon, apatite, and sulfides. Microperthite occurs as stringy- and pod-textured subhedral crystals with ubiquitous dusty alteration; the mafic minerals are identified only by their amphibole and biotite morphology.

Kassa Inlet pluton (Late Silurian).—Homogeneous and weakly foliated, tannish- gray, medium-grained equigranular monzodiorite was collected from the shore of Kassa Island (No. 2, fig. 1). The rock consists of subhedral, prismatic to tabular zoned plagioclase crystals with altered cores, intergranular microcline, minor interstitial quartz, and subhedral hornblende. Garnet, titanite, allanite, and apatite are common accessory minerals and typically are clustered or intergrown with hornblende. Hornblende is pleochroic from brown to green and contains inclusions of apatite and opaque Fe-Ti oxides. Garnet occurs as light-orangish-brown skeletal crystals, titanite is present as discrete euhedral crystals up to 2 mm long, and allanite occurs as large subhedral crystals (up to 3 mm long) that are pleochroic from light to dark brown.

Sukkwan Island pluton (Late Pennsylvanian to Early Permian).—Samples of massive, medium- to coarse-grained pyroxene-bearing hornblende-biotite syenite and poorly foliated, weakly porphyritic biotite-hornblende monzonite were collected from the southern and north-central parts of the Sukkwan Island pluton, respectively (Nos. 3 and 4, fig.1). The syenite consists of abundant perthitic K-feldspar, minor intergranular quartz, recrystallized aggregates of plagioclase around margins of perthite, pleochroic brown to orange biotite, brownish green hornblende, and light green clinopyroxene; accessory minerals include Fe-Ti oxides, apatite, and rare zircon. The monzonite consists of granular to phenocrystic, inclusion-rich crystals of K-feldspar, subhedral hornblende that is pleochroic from light brown to brownish green to green, and pleochroic light orangish brown to dark brown biotite. Plagioclase occurs as partly altered, subhedral zoned crystals and as recrystallized patches and aligned blebs in K-feldspar. Titanite is relatively common and occurs as euhedral pleochroic crystals up to 3 mm long; apatite, zircon, and Fe-Ti oxides typically occur as inclusions in the mafic minerals.

Klawock pluton (Late Permian).—A massive medium-grained porphyritic monzodiorite was collected just south of Klawock (No. 5, fig. 1); it consists of subhedral twinned plagioclase phenocrysts with inclusions of euhedral apatite and zircon, and altered hornblende and biotite in a microcrystalline groundmass of plagioclase, K-feldspar, and quartz. Clots of secondary Fe-Ti oxides and sulfides are common. Plagioclase phenocrysts typically occur in clusters and are commonly saussuritized.

Dora Bay pluton (Middle Jurassic).—Three samples (Nos. 6–8, fig. 1) collected from the north end of the Dora Bay pluton are massive to weakly foliated, homogeneous, medium-grained, equigranular hornblende quartz syenite and syenite. These rocks consist of microperthite, intergranular quartz, hornblende, and pyroxene; one sample contains biotite. Apatite and zircon are the most common accessory minerals. Microperthite occurs as subhedral, prismatic to tabular crystals that show patchy alteration to sericite, calcite, and epidote; plagioclase occurs as intergranular grains and recrystallized patches in microperthite or as overgrowths on microperthite. Subhedral hornblende is pleochroic from brown and brownish green to greenish brown and is partly altered to Fe-Ti oxides, epidote, and calcite; pyroxene occurs as light brown relict crystals and as cores in hornblende. Biotite is scarce and is pleochroic from reddish brown to red. Zircon forms discrete, subhedral to anhedral crystals that are typically abraded and corroded.

Lava Creek pluton (Early Cretaceous).—A slightly foliated, medium-dark-gray, fine- to medium-grained equigranular diorite was collected (No. 9, fig 1) near Salamander Lake (Brew, 1994) at the southern end of the Lava Creek pluton. The rock is made up of tabular to microlitic plagioclase, subhedral brown hornblende, and interstitial quartz and K-feldspar. Plagioclase is reverse zoned and is commonly altered to sericite. Hornblende is twinned and pleochroic in shades of brown and greenish brown. Biotite is uncommon and occurs as relict, mostly chloritized crystals clustered or intergrown with hornblende. Apatite is the major accessory mineral and occurs as abundant euhedral acicular grains in all other constituent minerals. A few zircon grains with metamict margins and haloes were found in hornblende and plagioclase. Secondary Fe-Ti oxides occur as clots in mafic minerals and as interstitial fillings.

Table 2a. Geochemical analyses and CIPW norms of alkalic plutonic rocks, Prince of Wales Island.

[Samples analyzed by X-ray fluorescence spectrometry at USGS laboratories in Denver, Colo.; by D.F. Siems, and J.E. Taggart. The analytical methods, techniques, and precision within the USGS labs are reviewed by Baedecker (1987). BM data taken from Thompson and others (1980); BM-1 is average of 44 aegirine granites, BM-2 is average of 14 riebeckite granites. #, data from Gehrels and Saleeby (1987a). ng, not given; n.a. not applicable; nd, not determined; ---, not detected]

	Cret.	Jurassic				Paleozoic				
Pluton *-----	LC	BM-1	BM-2	DB	DB	K	SI	KI	SR	SR
Map No. ----	9			7	8	5	3	2	1	#
Major Elements (weight percent)										
SiO_2	50.20	73.67	73.02	61.70	65.80	58.00	63.90	59.90	62.70	68.7
Al_2O_3	16.50	11.02	10.15	16.20	16.30	16.90	18.10	19.30	18.00	13.8
Fe_2O_3	2.30	1.96	2.25	3.16	4.23	0.54	0.92	1.75	1.15	1.5
FeO	7.37	1.86	2.19	3.69	0.08	3.44	1.59	1.34	0.53	1.66
MgO	4.07	0.04	0.07	0.23	0.10	1.44	0.42	0.69	0.50	1.11
CaO	7.16	0.32	0.42	1.69	0.07	4.33	0.91	4.83	1.33	1.71
Na_2O	5.06	5.14	5.03	7.76	7.83	6.29	6.65	7.20	5.70	3.51
K_2O	1.02	4.08	3.98	3.33	3.86	3.11	5.89	2.36	6.59	4.58
TiO_2	2.09	0.17	0.16	0.31	0.18	0.69	0.46	0.35	0.20	0.41
P_2O_5	0.95	0.04	0.02	0.09	0.04	0.44	0.12	0.11	0.23	0.08
MnO	0.30	ng	ng	0.20	0.09	0.06	0.10	0.14	0.04	0.04
H_2O^+	1.65	ng	ng	0.47	0.57	1.30	0.19	0.36	0.37	2.06
H_2O^-	0.11	ng	ng	0.16	0.14	0.16	0.13	0.03	0.08	nd
CO_2	0.55	ng	ng	0.55	0.12	2.78	0.07	0.01	1.38	nd
Total	99.33	98.30	97.29	99.54	99.41	99.48	99.45	98.37	98.80	99.16
Normalized values										
FeO*	9.44	3.68	4.33	6.53	3.89	3.93	2.42	2.91	1.61	3.1
FeO*/MgO	2.32	92.00	60.20	28.40	38.90	2.73	5.76	4.22	3.13	2.71
total Alk#	6.27	9.38	9.26	11.27	11.86	9.87	12.70	9.76	12.23	8.33
A/CNK	0.74	0.82	0.76	0.83	0.95	0.78	0.95	0.83	0.91	1.0
Alk/CaO	0.85	28.80	21.50	6.60	n.a.	2.17	13.78	1.98	9.24	4.73
CIPW norms										
quartz	---	30.19	31.79	0.06	6.30	---	0.06	---	1.65	25.86
orthoclase	6.21	24.52	24.17	20.01	23.14	19.29	35.13	14.23	40.16	27.87
albite	44.13	34.56	30.89	65.87	63.25	55.88	56.80	61.59	49.74	30.59
anorthite	19.89	---	---	---	---	9.13	2.16	13.65	4.19	8.20
acmite	---	5.76	6.68	0.78	3.49	---	---	---	---	---
nepheline	---	---	---	---	---	---	---	0.32	---	---
wollastonite	---	---	---	---	---	---	---	1.55	---	---
diopside	8.51	1.20	1.78	6.93	0.07	8.70	1.35	5.12	0.83	---
hypersthene	1.00	2.60	3.10	1.28	0.22	1.50	1.98	---	0.90	4.10
olivine	10.47	---	---	---	---	2.23	---	---	---	---
Na-orthosil	---	0.73	1.23	---	---	---	---	---	---	---
magnetite	3.44	---	---	4.27	0.03	0.82	1.35	2.59	1.30	2.24
hematite	---	---	---	---	3.06	---	---	---	0.29	---
ilmenite	4.09	0.33	0.31	0.60	0.35	1.38	0.88	0.68	0.39	0.80
apatite	2.27	0.09	0.05	0.21	0.09	1.07	0.28	0.26	0.55	0.19
DI	50.3	89.3	86.8	85.9	92.7	75.2	92.0	76.2	84.6	84.3
Norm C.I.	27.5	4.1	5.2	13.1	3.7	14.6	5.6	8.4	4.6	7.1
Norm An%	31.1	0.0	0.0	0.0	0.0	14.1	3.7	18.0	7.8	21.1

GEOCHEMISTRY

Major-element chemistry for alkalic plutons from Prince of Wales Island are shown in table 2a, and the plutons are grouped, for ease of discussion, into three major age groups (Paleozoic, Jurassic, and Cretaceous). The Paleozoic plutons are discussed as late and early Paleozoic pluton subgroups. All of the alkalic rocks we sampled are characterized by low to moderate silica (58.0–65.8 percent SiO_2), high alumina (16.2–19.3 percent Al_2O_3), and high total alkali (9.9–12.3 percent Na_2O+K_2O) content; Na_2O exceeds K_2O in all of the rocks except the Stone Rock Bay pluton (table 2).

Table 2b. Geochemical analyses of alkalic plutonic rocks, Prince of Wales Island.

[Samples analyzed by X-ray fluorescence spectrometry (Nb-Zn); atomic emission spectrometry (Be-V); and inductive coupled plasma (ICP) mass spectrometry (rare earth elements) at USGS laboratories in Denver, Colo. and Menlo Park Calif.: by P.H. Briggs, J. Kent, and G.D. Riddle. The analytical methods, techniques, and precision within the USGS labs are reviewed by Baedecker (1987). BM data taken from Thompson and others (1980); BM-1 is average of 26 aegirine granites, BM-2 is average of 2 riebeckite granites. Note: Ag, As, Au, Bi, Cd, Ta, and U not included because they occur below detection limits. ng, not given]

	Cret.	Jurassic				Paleozoic				
Pluton* ----	LC	BM-1	BM-2	DB	DB	K	SI	KI	SR	SR
Map No. --	9			7	8	5	3	2	1	#
Trace Elements (ppm)										
Nb	58	37	35	24	70	94	28	12	24	6
Rb	32	351	325	42	100	66	40	68	144	123
Sr	820	23	9	100	10	360	22	5100	690	403
Zr	340	325	450	670	820	465	52	178	610	405
Y	44	93	110	130	186	28	18	10	28	32
Ba	380	ng	ng	960	48	590	360	2000	1600	1490
Zn	102	ng	ng	150	230	66	62	128	26	25
Be	4	4	8	4	12	4	2	4	2	ng
Co	26	ng	ng	3	<1	8	<1	6	4	ng
Cr	12	ng	ng	<1	<1	2	<1	4	<1	ng
Cu	32	ng	ng	5	1	7	<1	1	284	49
Ga	19	12	10	31	43	19	18	21	23	ng
Li	5	61	135	12	103	12	4	4	<2	7
Mo	<2	ng	ng	<2	<2	5	<2	<2	<2	ng
Ni	10	ng	ng	<2	<2	5	<2	3	<2	ng
Pb	3	ng	ng	8	56	14	8	30	15	ng
Sc	20	ng	ng	2	<2	5	6	15	3	ng
Sn	<10	ng	ng	<10	30	<10	<10	<10	<10	ng
Th	14	<50	<50	6	30	22	6	33	29	ng
V	174	<10	<10	<2	3	46	<2	42	33	ng
Rare Earth Elements (ppm)										
La	78.0	129.0	125.0	55.0	100.0	110.0	30.0	240.0	51.0	28.9
Ce	150.0	ng	ng	130.0	250.0	170.0	59.0	370.0	110.0	51.0
Pr	17.0	ng	ng	18.0	26.0	16.0	6.9	36.0	13.0	5.4
Nd	59.0	ng	ng	73.0	100.0	47.0	24.0	100.0	40.0	20.1
Sm	11.0	ng	ng	19.0	24.0	6.9	4.0	9.3	5.1	3.9
Eu	2.7	ng	ng	5.6	4.2	1.5	1.6	1.9	1.4	0.58
Gd	8.1	ng	ng	20.0	24.0	4.5	2.8	2.9	3.5	3.3
Tb	1.2	ng	ng	3.5	4.9	0.85	0.49	0.32	0.55	ng
Dy	6.8	ng	ng	22.0	32.0	4.9	2.7	1.6	2.9	1.8
Ho	1.4	ng	ng	4.2	6.6	1.1	0.48	0.25	0.67	0.44
Er	4.2	ng	ng	14.0	20.0	3.4	1.5	0.66	1.9	1.3
Tm	0.55	ng	ng	2.1	3.1	0.48	0.19	0.05	0.32	0.17
Yb	3.2	ng	ng	14.0	18.0	3.0	1.3	0.41	1.8	1.6
Total REE	343.2			380.4	612.8	369.6	135.0	763.4	232.1	118.5

*LC, Lava Creek; BM, Bokan Mountain; DB, Dora Bay; K, Klawock; SI, Sukkwan Island; KI, Kassa Inlet; SR, Stone Rock Bay.

The alkalic nature of these rocks is indicated by plots of total alkali vs. silica (fig. 2*A*) but ranges from marginal calc-alkalic to peralkaline when plotted by silica vs. alkalinity index (fig. 2*B*). The sample of diorite from the Cretaceous Lava Creek pluton shows alkalic characteristics (fig. 2*A, B*) which is probably due to Na and K metasomatism, and is considered an altered calc-alkalic rock. The Paleozoic rocks are metaluminous to borderline peraluminous; the Jurassic alkalic rocks are peralkaline, and the Cretaceous rock is metaluminous (fig. 3). Quartz syenite samples from the Dora Bay pluton are distinguished by low CaO, MgO, and P_2O_5 content, and high total iron to magnesium (FeO*/MgO) ratios, and are similar to chemical features of granitoids from anorogenic belts (A-type granite of Pitcher, 1982; Whalen and others, 1987). Samples from the late Paleozoic rocks have relatively high TiO_2 and P_2O_5 content. All of the sampled rocks are diopside-normative, and all but the Kassa Inlet rock are hypersthene-normative. The Kassa Inlet sample contains nepheline and wollastonite in the norm; the late Paleozoic plutons contain a trace of quartz and no normative feldspathoids. The Jurassic alkalic plutons contain both quartz and acmite in the norm (table 2). The Cretaceous rock

is silica-poor, olivine-normative with high FeO* (total iron as FeO), MgO, TiO_2, and P_2O_5 content.

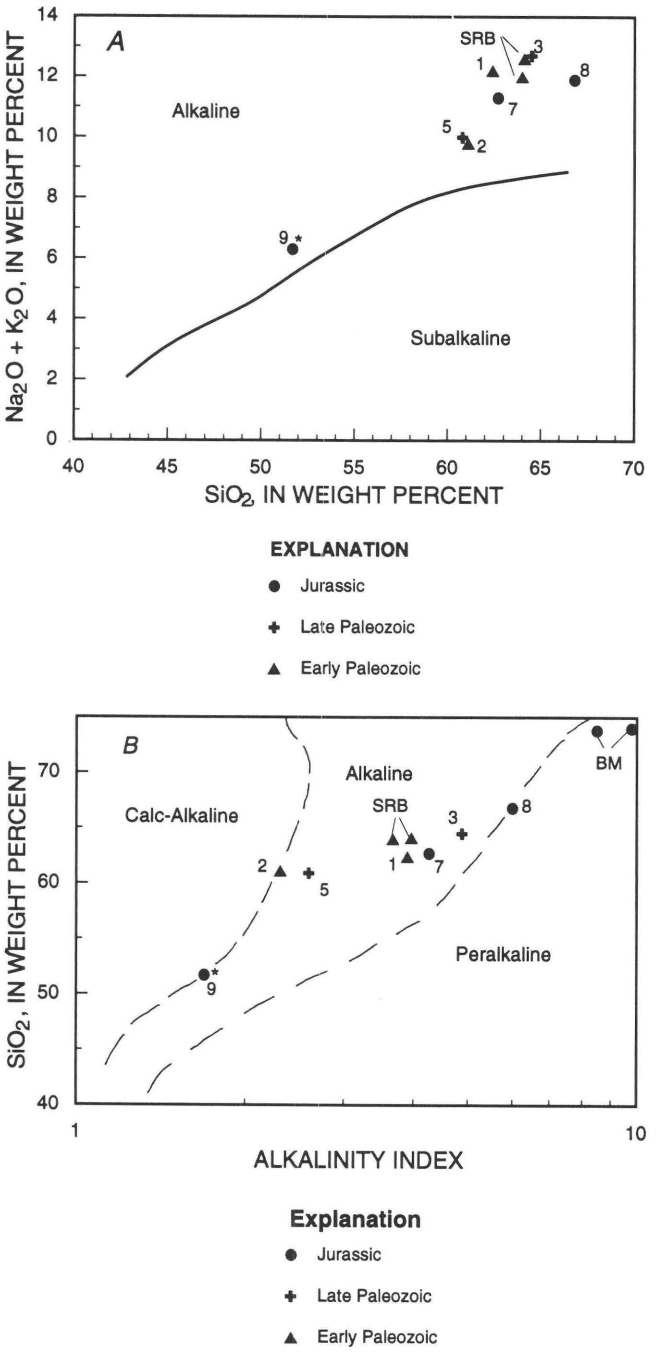

Figure 2. Chemical classification of alkalic plutons on Prince of Wales Island. *A*, Plot of total alkalies (Na_2O+K_2O) vs. SiO_2 for alkalic plutons on Prince of Wales Island; field boundary and nomenclature from Irvine and Baragar (1971). Bokan Mountain Granite not shown because it plots off scale, but consists of high SiO_2 (>72%) alkalic rocks. *B*, Plot of SiO_2 vs. alkalinity index (Al_2O_3+CaO+Alk*/Al_2O_3+CaO−Alk*) for alkalic plutons on Prince of Wales Island. Field boundary and nomenclature from Wright (1969). See figure 1 for location of sample numbers. Data for Bokan Mountain Granite (BM) and Stone Rock Bay pluton (SRB) from MacKevett (1963).

Trace element abundances vary considerably between plutons (table 2b). The problems of element mobility by hydrothermal alteration may limit the use of some trace elements for petrologic interpretation and correlations, particularly the trace alkalies and alkaline earths (Rb, Sr, Ba, and Li), which are generally the most mobilized trace elements during alteration (Arculus, 1987). Conversely, anomalous abundances of these mobile elements may also indicate mineralization. Rb, Sr, Ba, and Th abundances are higher and Nb and Y are noticeably lower in the early Paleozoic rocks (Stone Rock Bay and Kassa Inlet plutons) than in the late Paleozoic rocks (Sukkwan Island and Klawock plutons); the Late Silurian Kassa Inlet pluton is distinguished from all the other plutons by its higher Sr, Ba, Th, and light rare earth element (LREE) content (table 2b). The Jurassic Dora Bay pluton is relatively enriched in Y, Zr, Zn, Ga, and heavy rare-earth elements (HREE), and is low in Sr and Ba content; and are typical features of anorogenic (or A-type) granitoids (Whalen and others, 1987). The transition metal (Co, Cr, Cu, Ni, and V) concentrations are highest in the Cretaceous Lava Creek pluton, although the sample from the Stone Rock Bay pluton shows anomalous Cu abundance (284 ppm). The sample from the Lava Creek pluton also has relatively high concentrations of Sr, Nb, and Y. Y/Nb ratios are believed to be constant in and distinctive of alkalic suites (Eby, 1990). The Y/Nb ratios are low in the late Paleozoic rocks (.30–65), are very high in the Jurassic

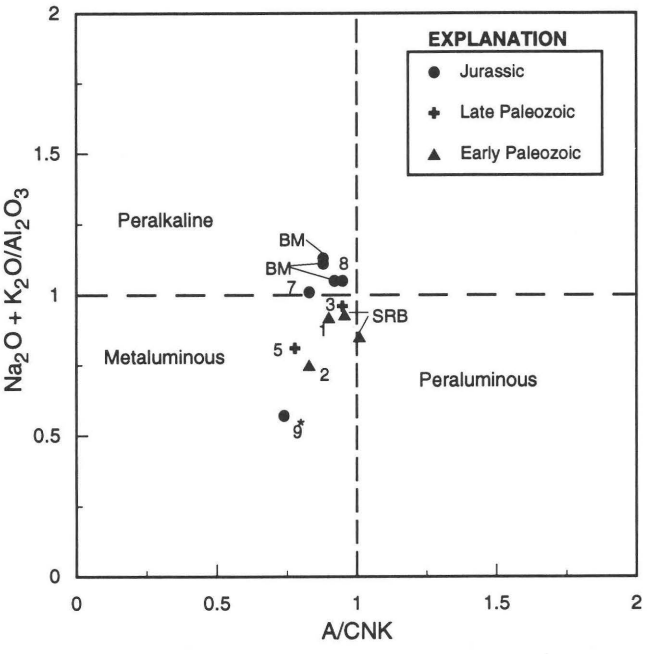

Figure 3. Plot of $(Na_2O+K_2O)/Al_2O_3$ vs. A/CNK (molecular ratio of Al_2O_3/[CaO+Na_2O+K_2O]) for alkalic rocks from Prince of Wales Island; field boundary from Shand (1951). See figure 1 for location of sample numbers. Data for Bokan Mountain Granite (BM) and Stone Rock Bay pluton (SRB) from MacKevett (1963).

rocks (2.5–5.4), and have a wide range in the early Paleozoic rocks (.83–5.3); it is less than one in the Cretaceous sample.

Chondrite-normalized rare earth element (REE) abundances in the plutonic rocks varies among age groups (fig. 4). The early Paleozoic Stone Rock Bay pluton yields relatively moderate REE abundances (La 100 times chondrite), a relatively high LREE/HREE fractionation value $(Ce/Yb=16)_N$, and a slightly curvilinear chondrite-normalized REE pattern (fig. 4). The Kassa Inlet pluton yields the highest LREE concentrations (La concentration is 700 times chondrite) and the most pronounced LREE/HREE fractionation $(Ce/Yb=226)_N$. The enriched LREE abundance in the Kassa Inlet sample may be attributed to its abundance of allanite, titanite, apatite, and garnet. Allanite and titanite generally contain high concentrations of LREE in granitic rocks (Sawka and others, 1984); apatite typically contains high LREE abundance in alkalic rocks (Cesbron, 1989). The anomalous depletion of HREE in the Kassa Inlet pluton may be due to either early fractionation of HREE-rich garnet phases, or derivation from a depleted crustal source.

The two late Paleozoic plutons yield different REE concentrations from one another (table 2), with the Klawock sample showing relatively high LREE abundances (La-Nd 300 to 100 times chondrite). Both show similar, broad U-shaped chondrite-normalized REE patterns (fig. 4) and LREE/HREE fractionation values $(Ce/Yb=12–15)_N$. The Middle Jurassic Dora Bay pluton yields highly enriched REE concentrations (LREE 150–250 times chondrite), higher HREE (Yb 60-80 times chondrite), and a slightly enriched REE fractionation pattern $(Ce/Yb=2.5–3.5)_N$ with a slight negative Eu anomaly (fig. 4). Interestingly, the diorite from the Cretaceous Lava Creek pluton yielded higher REE abundances than rocks from the Stone Rock Bay and Sukkwan Island plutons.

Multi-element diagrams (spidergrams) clearly show the relative differences in trace element distribution between the alkalic rocks of the major age groups. The Paleozoic rocks show enrichment in large-ion-lithophile (LIL) elements (Rb, Ba, and K), and pronounced enrichment in Th, but the early Paleozoic rocks are more enriched in Rb and Ba and depleted in Ti and Nb relative to the younger Paleozoic rocks; Ti and Nb depletion are characteristic signatures of subduction-related calc-alkalic magmatism (Arculus, 1987). These older plutons yield MORB-normalized spidergrams characterized by more pronounced peaks and valleys (fig. 5). The Middle Jurassic Dora Bay pluton is characterized by relative enrichment in Nb, Zr, and Y and depletion in Sr, P, and Ti. In contrast, the Cretaceous Lava Creek pluton exhibits a much smoother pattern with Rb, Ba, Th, and Nb highs. The late Paleozoic plutons yield a smooth spidergram relative to the early Paleozoic and Jurassic plutons; they lack the pronounced peaks and valleys shown by the other age groups but show the relative enrichment of LIL elements and Nb compared to other trace elements. Some of the anomalous abundance patterns may indicate selective element mobility, particularly for Sr and Ba.

In comparison to these plutons, the Bokan Mountain Granite (Thompson and others, 1980, 1982) is more sili-

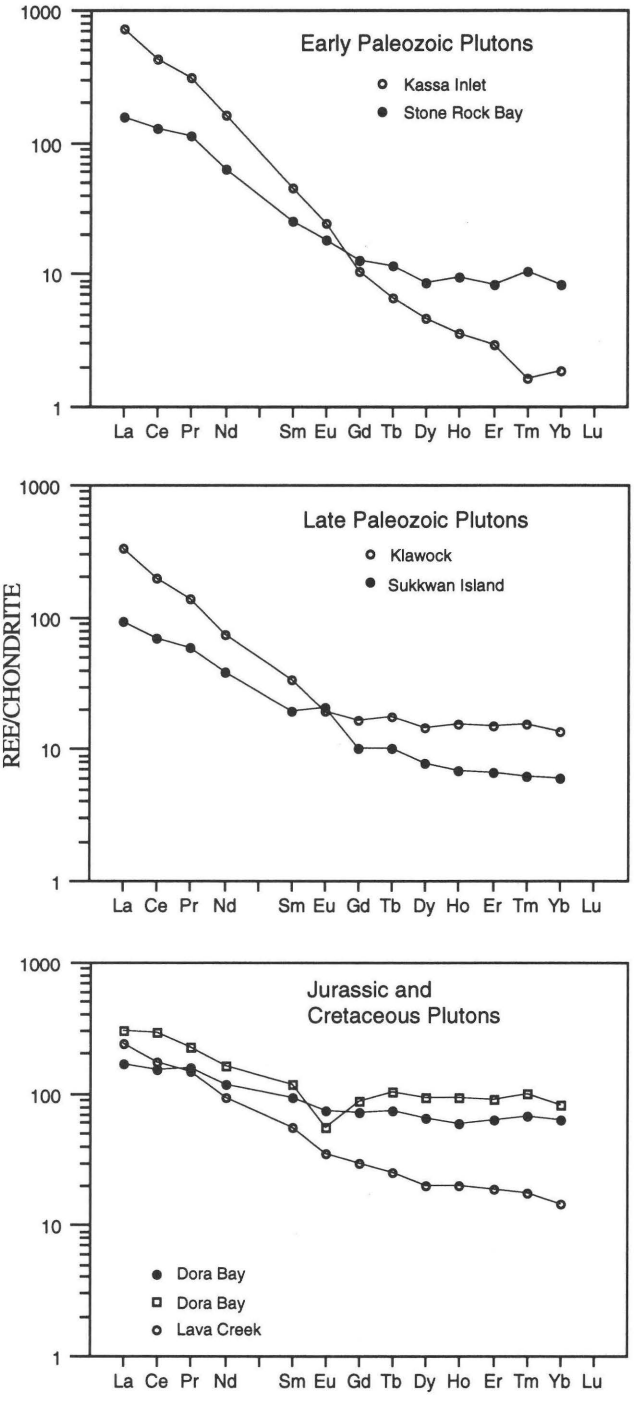

Figure 4. Chondrite-normalized rare earth element plots for alkalic plutons on Prince of Wales Island; chondrite values from Nakamura (1974).

ceous (SiO_2>70 percent) and contains lower alumina (Al_2O_3<12 percent). The TiO_2 and alkaline earth contents (CaO, MgO, Sr) of the Bokan Mountain Granite are very low (Thompson and others, 1982) and similar to rocks of the Dora Bay pluton. All the plutons we studied except the Sukkwan Island pluton have thorium concentrations within the range reported by Forbes (1980) for the Bokan Mountain Granite (10–54 ppm). The concentrations of Zr, Nb, Rb, La, and Y in the Bokan Mountain Granite (Thompson and others,1980; and table 2b) are mostly higher than the abundances of these elements in the Paleozoic alkalic rocks on Prince of Wales Island (table 2b). The exceptions are the higher Nb and Zr abundance of the Klawock pluton and higher Zr content of the Stone Rock Bay pluton. Rocks from the Jurassic Dora Bay pluton contain higher Zr and Y but lower Rb and La abundances than rocks from the Bokan Mountain Granite. The La/Y ratio of 1.4 for rocks from the Bokan Mountain Granite (Thompson and others, 1982) is less than the range of La/Y ratios for the Paleozoic alkalic rocks (1.7–24) but higher than Dora Bay rocks (.42–.54). Total REE abundances of unaltered rocks of the Bokan Mountain Granite (Warner and Barker, 1989, and fig. 6) are within the range of total REE abundances of Dora Bay rocks (table 2b), but the Bokan Mountain rocks contain higher HREE abundances (fig. 6) than Dora Bay rocks. The Bokan Mountain rocks exhibit a similar nearly flat fractionation trend $(Ce/Yb=1.3–1.9)_N$ but with a more pronounced negative Eu anomaly (fig. 6) than Dora Bay rocks.

The petrologic and tectonic affinities of the alkalic plutons are classified in figure 7*A, B*. These plots indicate that the early Paleozoic and Jurassic plutons are A-type granitoids, and the late Paleozoic plutons are transitional between A-type and fractionated I- or S-type granitoids. The early Paleozoic rocks are also chemically similar to volcanic-arc granitoids (fig. 7*B*) and their relative depletion in Ti and Nb and enrichment in LIL elements are indicators of subduction-related origin (Arculus, 1987). This is in accord with the findings of Gehrels (1987a), who interpreted

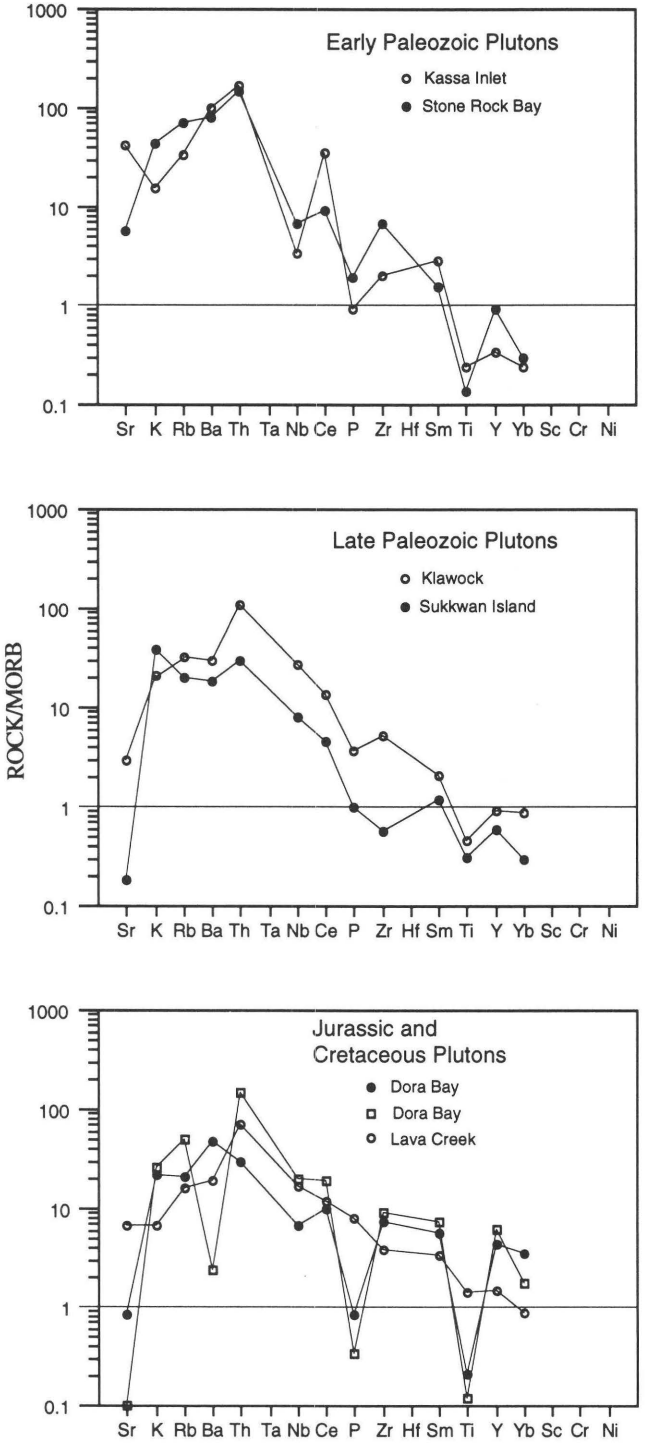

Figure 5. Mid-ocean ridge basalt (MORB) normalized multi-element diagrams (spidergrams) for alkalic plutons on Prince of Wales Island; MORB values from Pearce (1983).

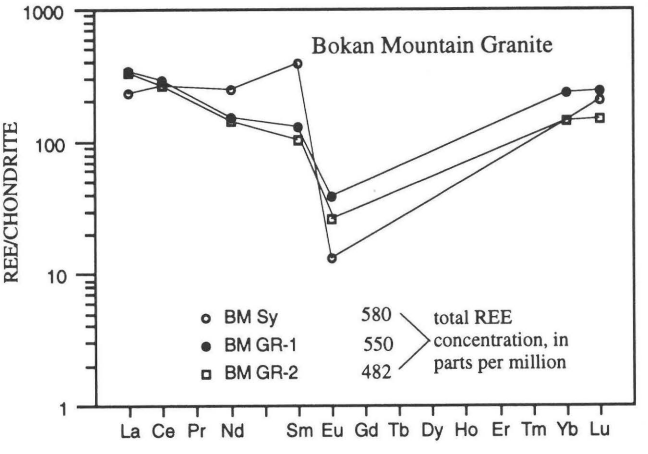

Figure 6. Chondrite-normalized rare earth element (REE) plots of Bokan Mountain Granite. Data from Warner and Barker (1989); BMSy is sample of unaltered syenite, and BMGR-1 and -2 are samples of unaltered aegirine granite. Chondrite values from Nakamura (1974).

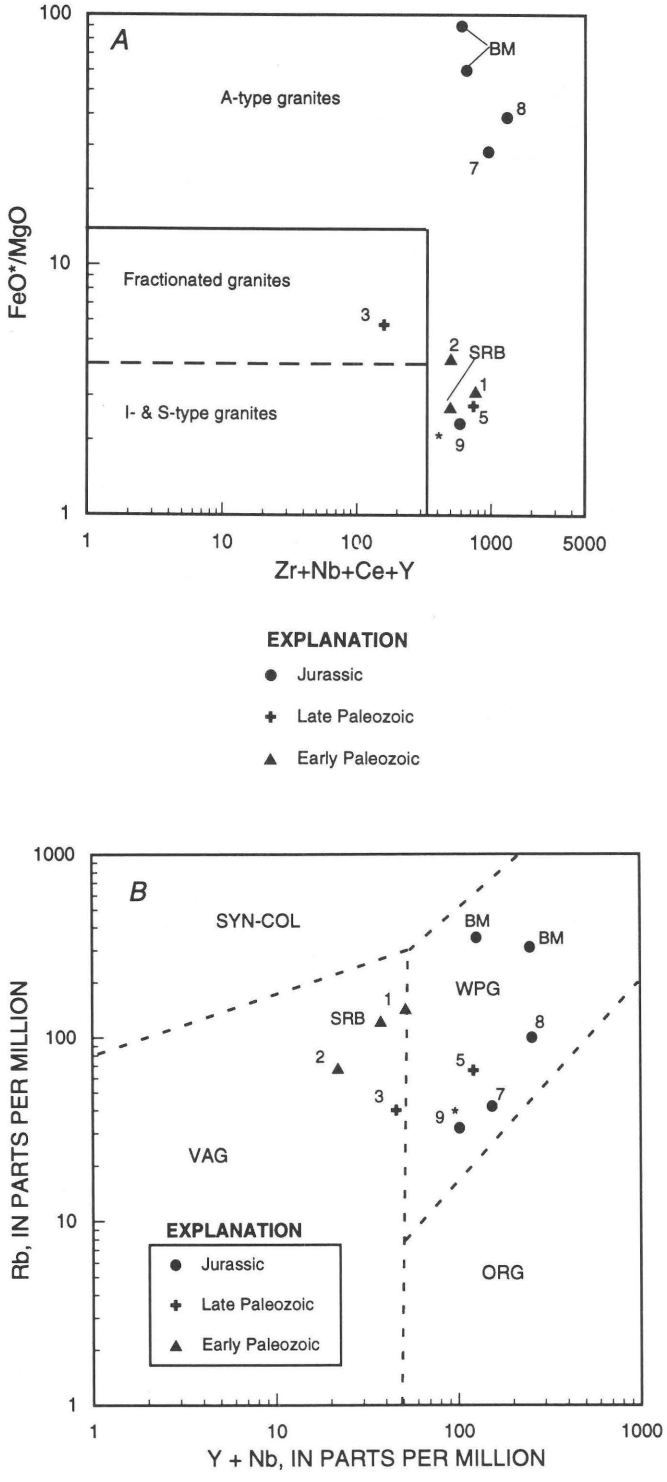

Figure 7. Trace element classification diagrams of alkalic plutons on Prince of Wales Island. *A*, Petrologic affinity classification. *B*, Tectonic classification: VAG, volcanic-arc granitoids; ORG, oceanic-ridge granitoids; WPG, within-plate granitoids; SRB, Stone Rock Bay pluton. SYN-COL, syn-collision or late tectonic granitoids. Field boundaries for *A* and *B* from Whalen and others (1987) and Pearce and others (1984), respectively. Bokan Mountain Granite (BM) data from Thompson and others (1982).

these alkalic rocks as late phases of subduction-related calc-alkalic magmatism. The Jurassic Dora Bay rocks are similar to within-plate granitoids (fig. 7*B*), and their high FeO*/MgO, low CaO and MgO, pronounced enrichment in Zr, Y, Zn, and Ga, and relatively flat REE fractionation patterns are characteristic features of A-type granitoids (Whalen and others, 1987). The Bokan Mountain Granite shows similar chemical traits and affinity as rocks from the Dora Bay pluton, but has been classified as an I-type granitoid of a Andinotype (subduction) plate margin (Thompson and others, 1982). Pitcher (1982) and Whalen and others, (1987) have argued that not all granitoids with characteristic chemical features of A-type granites are associated with continental rifts or anorogenic (tensional) environments, but some may be latest phases of orogenic activity related to plate subduction or collision environments. The high Y/Nb ratios (>1.2) of the Jurassic plutons, according to Eby (1990), indicate that significant crustal component was involved in their petrogenesis. The two late Paleozoic rocks are transitional to these tectonic settings (fig. 7*B*), although plots that straddle discriminant-tectonic fields may be caused by variations in source composition and crustal assimilation rather than by tectonic processes (Arculus, 1987). Both rocks exhibit similar multi-element and REE fractionation patterns indicating similar magmatic evolution. Their low Y/Nb ratios, according to Eby (1990), indicate that they are differentiated products of mantle-derived melts. Although the sample from the Cretaceous Lava Creek pluton has low FeO*/MgO ratios, its high incompatible trace element abundances classify it as an A-type granitoid with an affiliation to within-plate granitoids (figs 7*A*, *B*). Whether this is a primary or late magmatic-hydrothermal feature of this pluton is uncertain, but it does contrast with the mapping and classification of Cretaceous plutons on Prince of Wales island as calc-alkalic, volcanic arc intrusions (Eberlein and others, 1983; Gehrels and Saleeby, 1987a, b; Brew, 1994).

SUMMARY AND DISCUSSION

Paleozoic, Jurassic, and Early Cretaceous alkalic plutons on southern Prince of Wales Island are sites for potential U-Th and REE deposits. The early Paleozoic rocks (Stone Rock Bay and Kassa Inlet plutons) are undersaturated to oversaturated, metaluminous to borderline peraluminous granitoids that are associated with calc-alkalic plutons. The late Paleozoic rocks (Sukkwan Island and Klawock plutons) are saturated, metaluminous granitoids with uncertain petrologic and tectonic affinities. The Jurassic Dora Bay pluton is composed of oversaturated, peralkalic syenite with A-type characteristics, and its geochemical signature is very distinct from those of the Paleozoic plutons. The Cretaceous Lava Creek rock is a silica-poor, metaluminous, calc-alkalic to alkalic granitoid with relatively enriched incompatible trace element abundances.

In comparison to the Bokan Mountain Granite, only the Dora Bay pluton has a similar chemical signature. Both plutons are sodic-rich, quartz normative, peralkalic granitoids with A-type chemical characteristics. Both plutons contain mineralized dikes and veins and hydrothermally altered margins or haloes (Mackevett, 1963; Barker and Mardock, 1990). Their similarities in age, chemical composition, petrologic affinity, and hydrothermal alteration indicate that they had similar magmatic histories and that the Dora Bay pluton should be receptive to the same type of ore deposits found in the Bokan Mountain Granite.

Rocks of the Paleozoic alkalic plutons all show relative enrichment in Th and Ce (fig. 5) and most show positive Zr anomalies. Th and REE enrichment in alkalic igneous rocks may be a sign of mineralization (Staatz, 1992). All but the Sukkwan Island pluton have Th concentrations greater than average granitic igneous rocks (17 ppm, from Carmichael, 1989) but are within the range of Th abundances for syenitic rocks reported by Sorensen (1974). All but the Sukkwan Island pluton contain LREE abundances greater than average granitic igneous rocks (La, 40 ppm; Ce, 85 ppm, from Carmichael, 1989) and are much higher than LREE abundances found in the calc-alkalic plutons of the informally named Coast plutonic-metamorphic complex (Brew, 1988). The sample from the Kassa Inlet pluton contains the highest total REE, LREE and Th concentrations of the alkalic plutons. The sample from the Klawock pluton also contains relatively high Th and total REE abundances, as well as relatively high Nb and Zr. The Stone Rock Bay pluton contains relatively high concentrations of Th and Zr, and its association with a mineralized breccia pipe (Barker, 1988) warrant future investigations of this pluton; however, its moderate REE levels and potash-rich composition ($K_2O>Na_2O$) and close affinity with calc-alkalic rocks makes it unlike alkalic plutons with associated Th-REE vein deposits (Barker, 1988; Staatz, 1992). The anomalous high Cu abundance reflects the occurrence of sulfide minerals in our sample of the Stone Rock Bay pluton, which may indicate some other type of mineralization. The samples from the late Paleozoic Sukkwan Island pluton are the most deficient in Th, REE, and Zr concentrations.

The diorite sample from the Cretaceous Lava Creek pluton contains abundant apatite that probably accounts for the high P_2O_5 content (table 2a) and relatively high concentrations of Nb, Y, and REE. Sainsbury (1961) also mentions that apatite and magnetite/ilmenite are common accessory minerals in the alkalic rock phases of this pluton. Although this pluton is lithologically and geochemically different than the Paleozoic and Jurassic plutons, its relatively high REE abundances and association with heavy K-metasomatism (Sainsbury, 1961) may indicate a different type of REE mineralization, such as metasomatic-type REE deposit of Barker (1988).

Although the Paleozoic alkalic plutons are not geochemically comparable to the Jurassic peralkalic plutons, and thus probably are not subject to the same type of mineralization associated with the Bokan Mountain Granite and Dora Bay pluton, the relatively high REE and Th abundances shown by most of these plutons may indicate potential mineralization and justify their classification as a metallogenic resource. Differences in age between the four plutons does not appear to be a factor in their resource potential; samples from the early Paleozoic Stone Rock Bay and late Paleozoic Sukkwan Island plutons show the least geochemical evidence for meeting the criteria of potential Th-REE vein deposits (Barker, 1988; Staatz, 1992), whereas the samples from the early Paleozoic Kassa Inlet and late Paleozoic Klawock plutons exhibit stronger geochemical evidence for this type of mineralization. The abundance of accessory minerals, garnet, allanite, titanite, and apatite in the Kassa Inlet pluton probably account for the high LREE concentrations, and the enrichment in Sr and Ba may reflect mobility and possible hydrothermal activity, making this pluton an interesting site for future investigations.

REFERENCES CITED

Arculus, R.J., 1987, The significance of source versus process in the tectonic controls of magma genesis: Journal of Volcanology and Geothermal Research, v. 32, p. 1–12.

Armstrong, R.L., 1985, Rb-Sr dating of the Bokan Mountain granite complex and its country rocks: Canadian Journal of Earth Science, v. 22, p. 1233–1236.

Barker, J.C., 1988, Geological setting and deposit-type classification of REE in Alaska: Symposium on rare and precious metals, April 1988, Albuquerque, New Mexico, 20 p.

Barker, J.C., and Mardock, C., 1990, Rare-earth element- and yttrium-bearing pegmatite dikes near Dora Bay, southern Prince of Wales Island: United States Bureau of Mines Open-File Report 19-90, 25 p.

Baedecker, P.A., ed., 1987, Methods for geochemical analysis: U.S. Geological Survey Bulletin 1770.

Berg, H.C., Jones, D.L, and Coney, P.J., 1978, Pre-Cenozoic tectonostratigraphic terranes of southeastern Alaska and adjacent areas: U.S. Geological Survey Open-File Report 78-1085.

Brew, D.A., 1988, Latest Mesozoic and Cenozoic magmatism in southeastern Alaska—A synopsis: U.S. Geological Survey Open-File Report 88-405, 41 p.

Brew, D.A., 1993, Regional geologic setting of mineral resources in southeastern Alaska, *in* Manydeeds, S.A., and Smith, B.D., eds., Guidebook to the geology, mineral resources, and geophysics of Annette Island Tribal Lands, southeastern Alaska: U.S. Department of the Interior, Bureau of Indian Affairs, Division of Energy and Mineral Resources Publication.

Brew, D.A., 1994, Geologic map of the Craig, Dixon Entrance, and parts of the Ketchikan and Prince Rupert quadrangles, southeastern Alaska: U.S. Geological Survey Open-File Report, 55 p.

Brew, D.A., Drew, L.J., Schmidt, L.M., Root, D.H., and Huber, D.F., 1991, Undiscovered locatable mineral resources of the Tongass National Forest and adjacent areas, southeastern Alaska: U.S. Geological Survey Open-File Report 91-10, 370 p.

Carmichael, R.S., 1989, Physical properties of rocks and minerals: CRC Press, Inc., Boca Raton, Florida, 741 p.

Cesbron, F.P., 1989, Mineralogy of the rare-earth elements, *in* Moller, P., Cerny, P., and Saupe, F., eds., Lanthanides, tantalum, and niobium: Berlin, Springer-Verlag, p. 1–26

Churkin, M., Jr., and Eberlein, G.D., 1975, Geologic map of the Craig C-4 quadrangle, Alaska: U.S. Geological Survey Geologic Quadrangle Map GQ–1169, scale 1:63,360.

Condon, W.H., 1961, Geology of the Craig quadrangle, Alaska: U.S. Geological Survey Bulletin 1108–B, 43 p.

Drinkwater, J.L., Ford, A.B., and Brew, D.A., 1992, Magnetic susceptibilities and iron content of plutonic rocks across the Coast plutonic-metamorphic complex near Juneau, Alaska, *in* Bradley, D., and Dusel-Bacon, C., eds., Geological Studies in Alaska by the U.S. Geological Survey, 1991, U.S. Geological Bulletin 2041, p. 125–139.

Eby, G.N., 1990, The A-type granitoids: A review of their occurrence and chemical characteristics and speculations on their petrogenesis: Lithos, v. 26, p. 115–134.

Eberlein, G.D., Churkin, M., Carter, C., Berg, H.C., and Ovenshine, A.T., 1983, Geology of the Craig quadrangle, Alaska: U.S. Geological Survey Open-File Report 83-91, 50p

Forbes, R.B., 1980, Uranium-thorium concentrations in representative rocks from Alaskan crystalline terranes: National uranium resource evaluation: U.S. Department of Energy Report GJBX–178 (80).

Gehrels, G.E., 1992, Geologic map of the southern Prince of Wales Island, southeastern Alaska: U.S. Geological Survey Miscellaneous Investigation Map I–2169, scale 1:63,360.

Gehrels, G.E., and Saleeby, J.B., 1987a, Geologic framework, tectonic evolution, and displacement history of the Alexander terrane: Tectonics, v. 6, p. 151–173.

———1987b, Geology of southern Prince of Wales Island, southeastern Alaska: Geological Society of America Bulletin, v. 98, p. 123–137.

Grant, F.S., 1985, Aeromagnetics, geology, and ore environments; I. Magnetite in igneous, sedimentary and metamorphic rocks—An overview: Geoexploration, v. 23, p. 303–333.

Gunter, M.E., Johnson, N.E., Knowles, C.R., and Solie, D.N., 1993, Optical, X-ray, and chemical analysis of four eudialytes from Alaska: Mineralogical Magazine, v. 57, p. 743–746

Irvine, T.N., and Baragar, W.R.A., 1971, A guide to the chemical classification of the common volcanic rocks: Canadian Journal of Earth Sciences, v. 8, p. 523–548.

Lapointe, P., Morris, W.A., and Harding, K.L., 1986, Interpretation of magnetic susceptibility: A new approach to geophysical evaluation of the degree of rock alteration: Canadian Journal of Earth Science, v. 23, p. 393–401.

Larsen, E.S., Jr., Gottfried, D., Jaffe, H.W., and Waring, C.L., 1958, Lead-Alpha ages of the Mesozoic batholiths of western North America: U.S. Geological Survey Bulletin 1070–B, p. 35–58.

MacKevett, E.M., Jr., 1963, Geology and ore deposits of the Bokan Mountain uranium-thorium area, southeastern Alaska: U.S. Geological Survey Bulletin 1154, 125 p.

Monger, J.W.H., and Berg, H.C., 1987, Lithotectonic terrane map of western Canada and southeastern Alaska: U.S. Geological Survey Miscellaneous Field Studies Map MF–1874–B, scale 1:2,500,000.

Nakamura, N., 1974, Determination of REE, Ba, Mg, Na, and K in carbonaceous and ordinary chondrites: Geochemica et Cosmochimica Acta, v. 38, p. 757–775.

Pearce, J.A., 1983, Role of sub-continental lithosphere in magma genesis at active continental margins, *in* Hawkesworth, C.J., and Norry, M.J., eds., Continental basalts and mantle xenoliths: Cambridge, Birkhauser Boston, p. 230–249.

Pearce, J.A., Harris, N.B.W., and Tindle, A.G., 1984, Trace element discrimination diagrams for the tectonic interpretation of granitic rocks: Journal of Petrology, v. 25, p. 956–983.

Philpotts, J., Taylor, C., Evans, J., and Emsbo, 1993, Newly discovered molybdenite occurrences at Dora Bay, Prince of Wales Island, southeast Alaska, and preliminary scanning electron microscope studies, *in* Dusel-Bacon, Cynthia, and Till, Allison, eds., Geologic studies in Alaska by the US Geological Survey, 1992: U.S. Geological Survey Bulletin 2068, p. 187–196.

Pitcher, W.S., 1982, Granite type and tectonic environment; *in* Hsu, K.J., ed., Mountain Building Processes: Academic Press, London, p. 19–40.

Sainsbury, C.L., 1961, Geology of part of the Craig C-2 quadrangle and adjoining areas, Prince of Wales Island, southeastern Alaska: U.S. Geological Survey Bulletin 1058–H, p. 299–362.

Sawka, W.N., Chappell, B.W., and Norrish, K., 1984, Light rare-earth element zoning in sphene and allanite during granitoid fractionation: Geology, v. 12, p. 131–134.

Shand, H.S., 1951, Eruptive rocks: New York, John Wiley and Sons, 488 p.

Sorensen, H., 1974, The alkaline rocks: John Wiley and Sons, London, 622 p.

Staatz, M.H., 1992, Descriptive model of thorium-rare-earth veins, *in* Bliss, J.D., ed., Developments in mineral deposit modeling: U.S. Geological Survey Bulletin 2004, p. 13–18.

Thompson, T.B., Lyttle, T., and Pierson, J.R., 1980, Genesis of the Bokan Mountain, Alaska uranium thorium deposits: U.S. Department of Energy report GJBX–38 (80), 232 p.

Thompson, T.B., Pierson, J.R., and Lyttle, T., 1982, Geology and petrogenesis of the Bokan Mountain granite complex, southeastern Alaska: Geological Society of America Bulletin, v. 93, p. 898–908.

Warner, J.D., and Barker, J.C., 1989, Columbium- and rare-earth element-bearing deposits at Bokan Mountain, southeast Alaska: U.S. Bureau of Mines Open-File Report 33-89, 196 p.

Whalen, J.B., Currie, K.L., and Chappell, B.W., 1987, A-type granites: geochemical characteristics, discrimination, and petrogenesis: Contributions to Mineralogy and Petrology, v. 95, p. 407–419.

Wright, J.B., 1969, A simple alkalinity ratio and its application to questions of non-orogenic granite genesis: Geological Magazine, v. 106, p. 370–384

Reviewers: David A. Brew and Chester T. Wrucke, Jr.

Evaluation and Application of Garnet Amphibolite Thermobarometry, Western Metamorphic Belt Near Juneau, Alaska

By Glen R. Himmelberg, David A. Brew, *and* Arthur B. Ford

ABSTRACT

The western metamorphic belt is part of the Coast plutonic-metamorphic complex of western Canada and southeastern Alaska which was created by compressional thickening of crustal rocks during collision of the Alexander terrane and Gravina belt on the west against the Yukon prong and Stikine terranes to the east. An inverted metamorphic gradient is preserved in the western metamorphic belt near Juneau, Alaska. An earlier study of pelitic schists in the Juneau area indicated that thermal peak metamorphism occurred under pressures of 9 to 11 kbar. This study concerns thermobarometry of mafic rocks. Garnet-hornblende thermometry yields peak or near-peak temperatures that range from about 510°C for the lower garnet zone to about 765°C for the sillimanite zone, which is consistent with the range determined for pelitic schists. Plagioclase-hornblende thermometry, on the other hand, yields non-systematic results which are probably a result of compositional trends of amphiboles not accounted for by the activity model used. Pressure determinations using garnet-hornblende-plagioclase-quartz geobarometers range from 6.2 to 10.0 kbar. The higher pressure values (9.2–10.0) were determined for upper kyanite-biotite zone and sillimanite zone amphibolites that show little evidence of post-peak re-equilibration and are consistent with pressure of thermal peak metamorphism determined from pelitic schist geobarometers for these zones. However, samples that yield lower pressures occur intermixed with samples that yield higher pressures. These data suggest that equilibrium compositions were attained in the high-grade amphibolites and confirm high-pressure metamorphism (9.2–10.0 kbar) of the western metamorphic belt in the Juneau area documented by the earlier study of pelitic schists. Lower pressures (less than 9 kbar) might be attributed to continued heating of the thickened crustal block during uplift owing to intrusion of tonalite plutons. However, considering the spread of lower pressure values and the absence of a regular areal or structural distribution of pressures, one cannot rule out that the spread in calculated pressures might be related to compositional trends in amphibole that are not accounted for in the activity model used, or to non-equilibrium. Thus, we suggest that the garnet-hornblende-plagioclase-quartz geobarometer be used with caution.

INTRODUCTION

The metamorphic rocks exposed near Juneau, Alaska are part of the western metamorphic belt of the informally named Coast plutonic-metamorphic complex (Brew and Ford, 1984) of western Canada and southeastern Alaska (fig. 1). The western metamorphic belt and associated plutons developed as a result of compressional thickening of crustal rocks during the collision of the Alexander terrane and Gravina belt on the west against the Yukon prong and Stikine terranes to the east (Monger and others, 1982; Brew and Ford, 1983; Samson and others, 1989; Brew, 1990; Gehrels and others, 1990; Brew and others, 1992).

The western metamorphic belt ranges from a few kilometers to several tens of kilometers wide and is characterized by Barrovian metamorphism (Brew and others, 1989). The metamorphic grade increases to the northeast, with the highest grade adjacent to the plutonic part of the Coast plutonic-metamorphic complex. Deformational, metamorphic, and plutonic events in the western metamorphic belt span the interval from about 120 to 50 Ma (Brew and others, 1989).

At the latitude of Juneau, the western metamorphic belt is about 30 km wide. Mineral isograds, systematic changes in mineral assemblages, structural relations, and thermobarometry indicate an inverted metamorphic gradient along the easternmost part of the belt, where the metamorphic grade increases from sub-greenschist facies to kyanite- and sillimanite-bearing amphibolite facies within less than 8 km across strike (Ford and Brew, 1973; 1977; Brew and Ford, 1977; Himmelberg and others,1991). The development of the inverted metamorphic sequence, and pressures and temperatures determined from pelitic mineral assemblages were discussed in detail by Himmelberg and others (1991). Pelitic

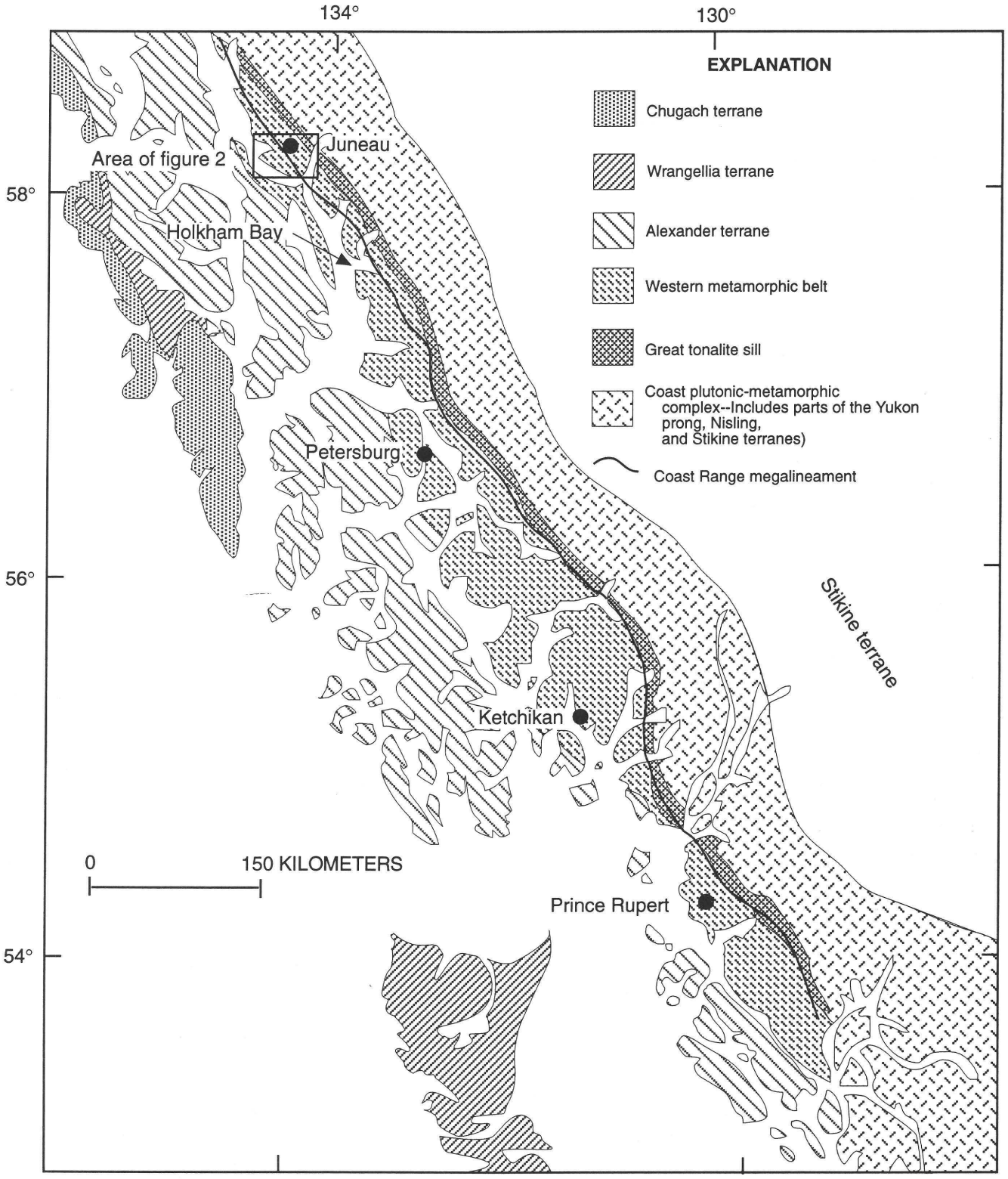

Figure 1. Index map of southeastern Alaska, showing informally named Coast plutonic-metamorphic complex (Brew and Ford 1984), Coast Range megalineament (Brew and Ford, 1978), great tonalite sill (Brew, 1988), and terrane boundaries. Modified from Brew and others (1989), Stowell (1989), and Himmelberg and others (1991).

assemblages appropriate for thermobarometry, however, are largely restricted to Heintzleman and Blackerby Ridges (fig. 2). Mafic assemblages that are appropriate to calibrated thermobarometry are more widespread. This study reports on temperatures and pressures calculated from equilibria appropriate to garnet amphibolites. The garnet amphibolite data are compared to pressures and temperatures obtained from pelitic assemblages in the Juneau area (Himmelberg and others, 1991) and along strike to the south (Stowell, 1989; McClelland and others, 1991) in order to evaluate whether garnet amphibolite thermobarometry can be used to reasonably estimate conditions of metamorphism and thereby further constrain the development of the inverted metamorphic sequence and the thermal evolution of the western metamorphic belt.

GEOLOGIC SETTING

The protoliths for the western metamorphic belt were the heterogeneous Permian and Triassic rocks of the Alexander terrane, and the Late Jurassic through early Late Cretaceous flysch and volcanic rocks of the Gravina belt (Brew and others, 1992). In the Juneau area, the metamorphic rocks consist dominantly of intermixed pelitic and semipelitic metasedimentary rocks, as well as mafic metavolcanic

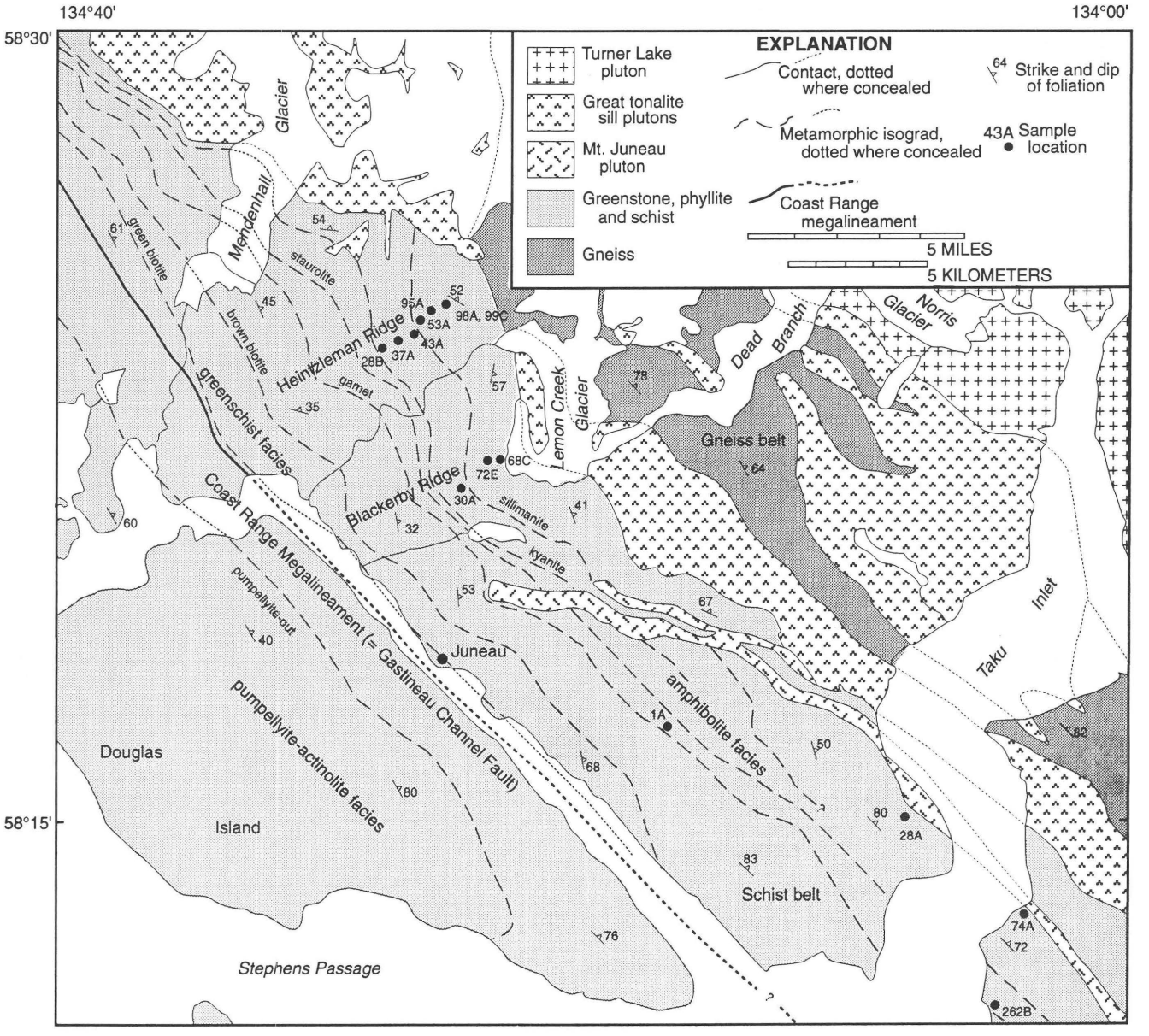

Figure 2. Geologic map of the Juneau area, southeastern Alaska (parts of A1, A2, B1, and B2 quadrangles), showing distribution of metamorphic facies, metamorphic isograds, and analyzed sample localities. Modified from Ford and Brew (1973, 1977), Brew and Ford (1977), and Himmelberg and others (1991). Sample numbers on map are the last 3 to 4 alphanumeric characters of the full sample number.

and metaintrusive rocks. Impure calcareous metasedimentary rocks, quartzite, and quartz diorite and granodioritic orthogneiss are also present.

Brew and others (1989) recognized six metamorphic events within the western metamorphic belt in southeastern Alaska. The subject of this study is metamorphic event M5. This event produced a belt of metamorphic rocks up to 10 km or more wide which are well preserved in the northern 400 km of the 700-km-long belt. Metamorphic event M5 was probably synchronous with emplacement of the tonalite to diorite plutons that make up the large composite sill (Himmelberg and others, 1991), referred to by Brew (1988) as the great tonalite sill, which extends along the east side of the western metamorphic belt (fig. 1). U-Pb radiometric studies indicate that the tonalite sill plutons were emplaced between about 83 and 55 Ma (Gehrels and others, 1991). In the Juneau area, the sub-greenschist-facies mineral assemblages, though contiguous with higher grade assemblages of the inverted metamorphic gradient, are products of the M1 metamorphic event and were not involved in the M5 metamorphism that produced the inverted metamorphic field gradient (Himmelberg and others, in press).

Mineral isograds other than garnet and staurolite have not been recognized for the southeastern part of the

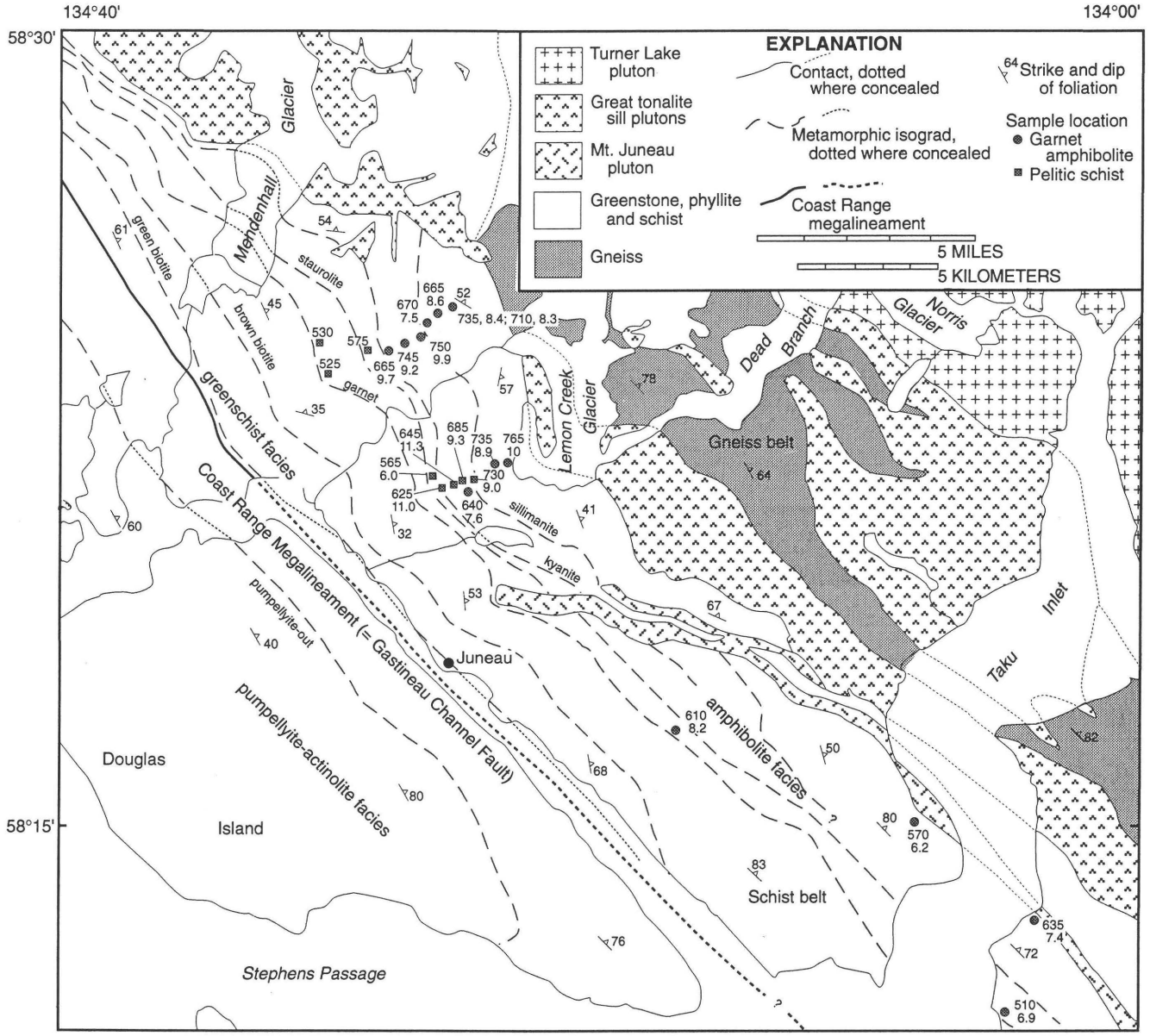

Figure 3. Geologic map of Juneau area, southeastern Alaska (parts of A1, A2, B1, and B2 quadrangles), showing distribution of metamorphic facies, metamorphic isograds, and calculated temperatures (°C) and pressures (kbar). Schist belt unpatterned for clarity. Temperatures and pressures for pelitic schists from Himmelberg and others (1991). Modified from Ford and Brew (1973, 1977), Brew and Ford (1977), and Himmelberg and others (1991). See table 6 and text for discussion of pressures and temperatures.

Table 1. Mineral assemblages of samples used for thermobarometry.

[Sample locations given of figure 2. Qtz, quartz; Pl, plagioclase; Chl, chlorite; Bt, biotite; Ep, epidote; Grt, garnet; Hbl, hornblende; Cum, cummingtonite; Mag, magnetite; Ilm, ilmenite; Rt, rutile; Ap, apatite; Ttn, titanite; Cal, calcite; St, staurolite, Ky, kyanite; Sil, sillimanite]

Sample	Qtz	Pl	Chl	Bt	Ep	Grt	Hbl	Cum	Mag/Ilm	Other	Zone	Rock type
84SK262B---------	X	X		X		X	X	X	X		Grt	grt-hbl-cum schist
83GH1A----------	X	X	X			X	X	X	X	Rt,Ap	Grt	grt amphibolite
85GH74A----------	X	X		X		X	X		X	Ap	≥St	grt-hbl-bt schist
84GH28A----------	X	X		X		X	X	X	X		≥St	grt-cum-hbl schist
79GH28B----------	X	X		X		X	X		X		Ky-Bt	grt-hbl schist
79GH37A----------	X	X		X	X	X	X		X	Ttn	Ky-Bt	grt-hbl schist
79GH43A----------	X	X		X		X	X		X	Cal, Ttn	Ky-Bt	grt-hbl schist
81DB30A----------	X	X		X		X	X		X		Ky-Bt	grt-bt-hbl schist
79GH68C----------	X	X		X		X	X		X		Sil	grt-hbl granulite
79GH53A----------	X	X		X		X	X		X	Ttn	Sil	grt-hbl-bt schist
79GH95A----------	X	X		X		X	X	X	X		Sil	grt-hbl-bt schist
79GH98A----------	X	X		X		X	X		X	Ttn	Sil	grt-hbl-bt schist
79GH99C----------	X	X		X		X	X		X		Sil	grt-hbl-bt gneiss
79GH72E----------	X	X		X		X	X		X		Sil	grt-hbl-bt schist

study area (figs. 2, 3) (Ford and Brew, 1973; 1977; Brew and Ford, 1977; this study). For this reason the maximum grade obtained in this area is uncertain.

MINERAL ASSEMBLAGES AND MINERAL CHEMISTRY

Locations of samples selected for analysis and thermobarometric calculations are plotted in figure 2, and metamorphic mineral assemblages of these samples are summarized in table 1.[1] Sample selection was based on the presence of appropriate assemblages, distribution across metamorphic grade, areal distribution, mineralogical and textural indications of equilibrium, and minimum mineralogical and textural retrograde alteration. All metamorphic assemblages include quartz-plagioclase-garnet-hornblende. Most assemblages also contain biotite, which in some samples exceeds hornblende in amount, and small amounts of magnetite/ilmenite. Other minerals present in some samples include chlorite, epidote, cummingtonite, sphene, and apatite.

Representative mineral analyses of plagioclase, hornblende, garnet, and biotite used in thermobarometric calculations are given in tables 2 through 5. Mineral analyses were obtained using the JEOL model 733 superprobe at Washington University, St. Louis, Mo. Matrix corrections were made by the method of Bence and Albee (1968), using the correction factors of Albee and Ray (1970). Structural formulas for plagioclase, garnet, and biotite, were calculated by normalizing to a fixed number of oxygens. Hornblende formulas were calculated by normalizing to 13 cations exclusive of Ca, Na, and K, and Fe^{2+} and Fe^{3+} were then calculated from charge balance. Cosca and others (1991) showed that this method, though not perfect, is the best approximation to a complete chemical analysis for Fe^{2+} and Fe^{3+} in hornblende.

Plagioclase, hornblende, and biotite analyses are for matrix grains not in contact with garnet. Plagioclase compositions range from about An_{20} to An_{50}. Most grains are compositionally zoned with a core to rim increase in anorthite component of about 2 to 5 mol percent. No significant compositional zoning nor intergrain compositional differences were detected in hornblende and biotite, although small analytical errors may cause substantial variation in the Fe^{3+}/Fe^{2+} ratio and thus the $Mg/(Mg+Fe^{2+})$ ratio of hornblende. Structural formulas of biotite calculated on the basis of 11 oxygens consistently yield octahedral site occupancy <3, and A-site occupancy <1. Dymek (1983) demonstrated that octahedral occupancy in biotite is generally <3 cations per formula as a result of Ti and Al^{vi} octahedral substitution not balanced by tetrahedral Al.

Garnet porphyroblasts are generally subhedral to euhedral. Embayed boundaries are present on some subhedral grains. Garnets in sample 83GH1A are irregularly anhedral and are interpreted to have undergone resorption. Porphyroblasts range in diameter from about 0.1 mm to 6 mm, with most being between about 0.3 mm and 1.5 mm. Most garnets analyzed are compositionally zoned from core to rim. Except for sample 83GH1A mentioned above, which shows evidence of resorption, rim points of individual garnet grains, and rim points between grains of a given sample, generally show no substantial compositional difference. The garnet analyses given in table 4 are representative, single-point, core and rim compositions. Compositional variation among rim

[1]Because isograds above staurolite have not been recognized in the southeastern part of the study area and therefore the maximum grade obtained is uncertain, samples from this area above the staurolite isograd are indicated in tables 1 and 6 as staurolite zone or greater.

Table 2. Representative analyses of plagioclase.

[Leaders (---), not detected. An, anothite; Ab, albite; Or, orthoclase]

	84SK262B	83GH1A	85GH74A	84GH28A	81SK30A	79GH28B	9GH37A	9GH43A
SiO_2	63.80	62.65	62.35	58.31	58.99	60.80	56.93	57.96
Al_2O_3	22.86	23.22	24.39	25.72	26.29	26.22	27.67	27.19
FeO*	0.04	0.02	0.07	0.16	0.06	0.22	0.14	0.03
MgO	---	---	---	---	---	---	---	---
CaO	4.28	4.88	5.91	7.67	7.87	6.60	8.96	8.64
Na_2O	9.14	8.51	8.39	7.07	6.84	7.84	6.36	6.70
K_2O	0.03	0.04	0.08	0.06	0.09	0.07	0.17	0.18
Total	100.15	99.32	101.19	98.99	100.14	101.76	100.23	100.70
Cations normalized to 8 oxygens								
Si	2.812	2.786	2.735	2.631	2.627	2.660	2.548	2.578
Al	1.187	1.217	1.261	1.368	1.380	1.352	1.459	1.425
Fe	0.002	0.001	0.003	0.006	0.002	0.008	0.005	0.001
Mg	---	---	---	---	---	---	---	---
Ca	0.202	0.233	0.278	0.371	0.376	0.309	0.430	0.412
Na	0.781	0.734	0.713	0.618	0.591	0.665	0.552	0.578
K	0.002	0.002	0.004	0.004	0.005	0.004	0.010	0.010
An	20.5	24.0	27.9	37.3	38.7	31.6	43.3	41.2
Ab	79.3	75.7	71.7	62.3	60.8	68.0	55.7	57.8
Or	0.2	0.3	0.4	0.4	0.5	0.4	1.0	1.0

	9GH53A	79GH95A	79GH98A	79GH99C	79GH72E	79GH72E†	79GH68C
SiO_2	57.81	59.81	58.39	58.13	57.55	58.12	60.12
Al_2O_3	27.18	26.10	26.61	27.16	27.40	26.58	25.82
FeO*	0.06	0.05	0.03	0.03	0.04	0.03	0.04
MgO	---	---	---	---	---	---	---
CaO	8.33	6.74	8.01	8.62	9.19	8.84	7.13
Na_2O	6.71	7.68	7.10	6.75	6.21	6.29	7.14
K_2O	0.16	0.07	0.08	0.07	0.08	0.11	0.26
Total	100.25	100.45	100.21	100.76	100.47	99.97	100.51
Cations normalized to 8 oxygens							
Si	2.580	2.651	2.604	2.582	2.565	2.599	2.662
Al	1.430	1.363	1.399	1.422	1.439	1.401	1.348
Fe	0.002	0.002	0.001	0.001	0.001	0.001	0.001
Mg	---	---	---	---	---	---	---
Ca	0.398	0.320	0.383	0.410	0.439	0.424	0.338
Na	0.581	0.660	0.614	0.581	0.537	0.545	0.613
K	0.009	0.004	0.004	0.004	0.005	0.006	0.015
An	40.3	32.5	38.2	41.2	44.8	43.4	35.0
Ab	58.8	67.1	61.3	58.4	54.8	55.9	63.5
Or	0.9	0.4	0.4	0.4	0.5	0.7	1.5

* Total iron calculated as FeO.
† Core analysis; all others are rim analyses.

points of a given sample can be qualitatively evaluated by the calculated range of pressure and temperature values (table 6).

Core to rim prograde compositional profiles for garnets in the garnet, staurolite-biotite, kyanite-biotite, and in some cases the sillimanite zone (metamorphic zonal terminology established by Himmelberg and others (1991) based on pelitic assemblages) are typical growth zoning patterns. From the garnet core toward the rim pyrope, almandine, and Mg/(Mg+Fe) ratio increase, and grossular and spessartine decrease. Two samples in the kyanite-biotite zone show

Table 3. Representative analyses of hornblende.

	84SK262B	83GH1A	85GH74A	84GH28A	81SK30A	79GH28B	79GH37A	79GH43A
SiO_2	43.42	40.87	43.13	44.86	43.60	41.13	40.68	41.84
TiO_2	0.31	0.06	0.98	0.53	0.96	0.48	0.62	1.15
Al_2O_3	14.08	17.08	11.93	13.61	12.94	15.49	12.68	13.51
FeO*	20.88	23.77	19.80	17.27	17.48	19.20	21.21	17.73
MnO	0.49	0.35	0.31	0.14	0.62	0.08	0.30	0.67
MgO	6.72	4.17	8.87	8.99	8.88	7.43	7.39	8.63
CaO	10.31	10.20	10.15	10.89	11.50	11.51	11.81	11.79
Na_2O	1.85	1.64	1.72	1.29	1.42	1.53	1.13	1.18
K_2O	0.23	0.09	0.40	0.32	0.90	0.65	1.31	1.62
Total	98.29	98.23	97.29	97.90	98.30	97.49	97.13	98.12
Formula per 13 cations exclusive of Ca, Na, K								
Si	6.402	6.075	6.372	6.532	6.442	6.148	6.213	6.258
Al^{iv}	1.598	1.925	1.628	1.468	1.558	1.852	1.787	1.742
Al^{vi}	0.851	1.068	0.450	0.868	0.697	0.878	0.496	0.641
Ti	0.034	0.007	0.109	0.058	0.107	0.054	0.071	0.129
Fe^{3+}	0.844	1.100	1.174	0.657	0.424	0.606	0.687	0.406
Fe^{2+}	1.732	1.856	1.274	1.447	1.737	1.795	2.023	1.813
Mn	0.061	0.044	0.039	0.017	0.078	0.010	0.038	0.085
Mg	1.478	0.925	1.955	1.953	1.957	1.657	1.684	1.926
Ca	1.631	1.627	1.609	1.701	1.823	1.846	1.935	1.892
Na(M4)	0.369	0.373	0.391	0.299	0.177	0.154	0.065	0.108
Na(A)	0.160	0.099	0.103	0.065	0.229	0.291	0.271	0.234
K	0.044	0.017	0.075	0.060	0.171	0.123	0.255	0.310
$\frac{Mg}{(Mg+Fe^{2+}+Mn)}$	0.45	0.33	0.60	0.57	0.52	0.48	0.45	0.50

	79GH53A	79GH95A	79GH98A	79GH99C	79GH72E	79GH72E†	79GH68C
SiO_2	44.43	44.63	41.81	43.50	44.52	42.05	40.93
TiO_2	1.11	1.28	1.54	1.60	0.95	1.25	1.42
Al_2O_3	10.46	11.65	12.85	11.80	10.91	13.24	12.75
FeO*	17.45	17.99	19.14	18.00	17.99	18.11	21.82
MnO	0.86	0.28	0.44	0.42	0.07	0.15	0.85
MgO	9.33	9.56	8.10	9.11	10.34	8.35	6.21
CaO	11.36	11.09	10.96	11.06	11.41	11.25	11.47
Na_2O	1.12	1.33	1.87	1.38	1.18	1.36	1.24
K_2O	0.96	0.57	0.81	0.82	0.54	0.89	1.75
Total	97.08	98.38	97.52	97.69	97.92	96.65	98.45
Formula per 13 cations exclusive of Ca, Na, K							
Si	6.651	6.528	6.277	6.454	6.529	6.332	6.240
Al^{iv}	1.349	1.472	1.723	1.546	1.471	1.668	1.760
Al^{vi}	0.497	0.537	0.552	0.518	0.416	0.682	0.532
Ti	0.125	0.141	0.174	0.179	0.105	0.142	0.163
Fe^{3+}	0.443	0.687	0.592	0.597	0.814	0.498	0.442
Fe^{2+}	1.743	1.515	1.812	1.638	1.393	1.784	2.342
Mn	0.109	0.034	0.056	0.053	0.009	0.018	0.110
Mg	2.083	2.086	1.814	2.016	2.262	1.875	1.412
Ca	1.824	1.740	1.765	1.760	1.795	1.817	1.876
Na(M4)	0.176	0.260	0.235	0.240	0.205	0.183	0.124
Na(A)	0.151	0.119	0.311	0.159	0.132	0.215	0.244
K	0.184	0.107	0.155	0.155	0.102	0.172	0.341
$\frac{Mg}{(Mg+Fe^{2+}+Mn)}$	0.53	0.57	0.49	0.54	0.62	0.51	0.37

*Total iron calculated as FeO; Fe^{3+} and Fe^{2+} calculated from charge balance.
†Inclusion in garnet

growth patterns where grossular increases and almandine decreases from core to rim. Most garnets in the sillimanite zone show compositional profiles typical of homogenization by high temperature intracrystalline diffusion. In places, changes caused by diffusional reequilibration during cooling are superimposed on the prograde patterns.

Table 4. Representative analyses of garnet.

[Leaders (---), not detected. Prp, pyrope; Grs, grossular; Sps, spessartine; Alm, almandine]

	84SK262B 1-4c†	84SK262B 1-1r	83GH1A 1-4c	83GH1A 1-6r	85GH74A 1-2c	85GH74A 1-1r	84GH28A 3-2c	84GH28A 3-3r	81SK30A 3-2c	81SK30A 3-3r
SiO_2 --------	37.22	37.27	37.52	37.50	38.36	38.38	37.63	38.11	38.10	38.27
TiO_2 --------	0.11	---	0.08	0.06	0.07	0.03	0.06	0.06	0.14	0.03
Al_2O_3 ------	21.35	21.49	21.43	21.64	22.08	21.90	21.70	22.12	21.64	22.24
FeO* -------	26.94	29.59	30.54	32.56	28.35	29.39	31.58	30.99	16.83	26.01
MnO -------	7.51	5.66	3.61	3.13	3.27	2.63	2.58	1.42	12.18	4.20
MgO -------	1.36	1.57	0.94	1.47	4.44	4.36	3.06	3.50	0.52	2.61
CaO --------	5.56	4.16	6.51	4.47	4.83	3.92	3.20	4.80	11.89	8.24
Total	100.05	99.74	100.63	100.83	101.40	100.61	99.81	101.00	101.30	101.60
Cations normalized to 12 oxygens										
Si ----------	2.993	3.004	3.001	2.996	2.987	3.010	3.005	2.991	2.997	2.983
Al^{iv} --------	0.007	0.000	0.000	0.004	0.013	0.000	0.000	0.009	0.003	0.017
Al^{vi} --------	2.017	2.042	2.020	2.033	2.013	2.024	2.042	2.038	2.003	2.027
Ti ----------	0.007	---	0.005	0.004	0.004	0.002	0.003	0.003	0.008	0.002
Fe ----------	1.812	1.995	2.043	2.175	1.846	1.928	2.109	2.034	1.107	1.696
Mn ---------	0.512	0.386	0.245	0.212	0.216	0.175	0.174	0.094	0.811	0.277
Mg ---------	0.163	0.188	0.111	0.175	0.515	0.509	0.364	0.409	0.061	0.303
Ca ----------	0.479	0.359	0.558	0.383	0.403	0.329	0.274	0.404	1.002	0.688
Prp ---------	5.5	6.4	3.8	5.9	17.3	17.3	12.4	13.9	2.1	10.2
Grs ---------	16.2	12.3	18.9	13.0	13.5	11.2	9.4	13.7	33.6	23.2
Sps ---------	17.3	13.2	8.3	7.2	7.2	5.9	6.0	3.2	27.2	9.4
Alm --------	61.1	68.1	69.1	73.9	62.0	65.5	72.2	69.2	37.1	57.2

	79GH28B 2-2c	79GH28B 2-1r	79GH37A 1-4c	79GH37A 1-1r	79GH43A 2-2c	79GH43A 2-1r	79GH53A 1r	79GH95A 2-4c	79GH95A 2-1r
SiO_2 --------	37.77	37.94	37.56	38.02	38.32	38.40	38.07	37.71	37.90
TiO_2 --------	0.07	0.03	0.06	0.07	0.05	0.02	0.01	0.09	---
Al_2O_3 ------	22.08	22.09	21.45	21.90	22.10	22.20	22.22	21.86	22.18
FeO* -------	28.35	28.79	26.37	26.14	21.90	21.21	20.80	23.96	27.93
MnO -------	1.28	1.01	3.53	1.64	4.32	4.46	7.83	5.32	1.36
MgO -------	2.61	2.58	3.11	2.59	2.43	2.31	2.23	1.49	3.67
CaO --------	7.98	8.24	7.52	9.87	12.06	12.62	10.09	10.54	7.28
Total	100.14	100.68	99.60	100.23	101.18	101.22	101.25	100.97	100.32
Cations normalized to 12 oxygens									
Si ----------	2.984	2.984	2.987	2.991	2.980	2.982	2.974	2.972	2.977
Al^{iv} --------	0.016	0.016	0.013	0.009	0.020	0.018	0.026	0.028	0.023
Al^{vi} --------	2.039	2.031	1.998	2.021	2.006	2.013	2.020	2.003	2.029
Ti ----------	0.004	0.002	0.004	0.004	0.003	0.001	0.001	0.006	---
Fe ----------	1.873	1.893	1.754	1.720	1.424	1.377	1.359	1.579	1.834
Mn ---------	0.086	0.067	0.238	0.109	0.285	0.293	0.518	0.355	0.090
Mg ---------	0.307	0.303	0.369	0.303	0.281	0.267	0.260	0.175	0.430
Ca ----------	0.675	0.694	0.641	0.832	1.005	1.050	0.845	0.890	0.613
Prp ---------	10.4	10.2	12.3	10.2	9.4	8.9	8.7	5.8	14.5
Grs ---------	23.0	23.5	21.4	28.1	33.6	35.1	28.3	29.7	20.6
Sps ---------	2.9	2.3	7.9	3.7	9.5	9.8	17.4	11.8	3.0
Alm --------	63.7	64.0	58.4	58.0	47.6	46.1	45.6	52.7	61.8

THERMOBAROMETRY

PROCEDURES

Temperatures and pressures for samples of Juneau garnet amphibolites were calculated from microprobe analyses and calibrated equilibria (table 6). Calculations were made for all analyzed samples using compositions of garnet rim or near-rim points (within 5 to10 micrometers of grain edge) and matrix hornblende, plagioclase, and biotite. Rim compositions were used for plagioclase. Garnet rim points in contact with hornblende or biotite were

Table 4. Representative analyses of garnet—Continued.

[Leaders (---), not detected. Prp, pyrope; Grs, grossular; Sps, spessartine; Alm, almandine]

	79GH98A 1-3c	79GH98A 1-5r	79GH99C 1-3c	79GH99C 1-6r	79GH72E 2-2 inc	79GH72E 2-3 inc	79GH72E 2-1r	79GH68C 1-4c	79GH68C 1-6r
SiO_2 --------	38.31	37.89	37.75	37.98	38.22	38.39	38.07	37.83	37.92
TiO_2 --------	0.01	0.03	0.08	0.01	0.06	0.08	0.03	0.17	0.20
Al_2O_3 ------	22.24	21.83	21.87	22.21	21.88	21.91	22.03	21.05	20.96
FeO* -------	28.05	27.43	26.91	26.76	27.48	28.06	27.15	21.18	20.49
MnO -------	2.43	2.58	3.07	3.75	0.67	0.62	0.84	8.27	8.64
MgO -------	4.33	4.21	3.85	3.40	3.86	4.14	3.61	1.70	1.56
CaO --------	6.26	6.38	6.90	6.83	8.20	7.48	8.58	10.36	10.91
Total	101.63	100.35	100.43	100.95	100.37	100.68	100.31	100.56	100.68
Cations normalized to 12 oxygens									
Si ----------	2.973	2.979	2.970	2.975	2.992	2.995	2.983	2.997	3.000
Al^{iv} --------	0.027	0.021	0.030	0.025	0.008	0.005	0.017	0.003	0.000
Al^{vi} --------	2.007	2.001	1.998	2.026	2.010	2.010	2.018	1.962	1.955
Ti ----------	0.001	0.002	0.005	0.001	0.003	0.005	0.002	0.010	0.012
Fe ----------	1.821	1.803	1.771	1.753	1.799	1.831	1.779	1.403	1.356
Mn --------	0.160	0.172	0.205	0.249	0.044	0.041	0.056	0.555	0.579
Mg --------	0.500	0.493	0.451	0.397	0.451	0.482	0.422	0.200	0.184
Ca ----------	0.521	0.537	0.582	0.573	0.688	0.625	0.720	0.879	0.925
Prp --------	16.7	16.4	15.0	13.4	15.1	16.2	14.2	6.6	6.1
Grs --------	17.3	17.9	19.3	19.3	23.1	21.0	24.2	28.9	30.4
Sps --------	5.3	5.7	6.8	8.4	1.5	1.4	1.9	18.3	19.0
Alm --------	60.7	60.0	58.9	59.0	60.3	61.5	59.8	46.2	44.5

†Garnet grain and analytical point number; c, core; r, rim; inc, at hornblende inclusion.
* Total iron calculated as FeO.

avoided and analyses of obvious retrograded garnet points are not included. Calculations of temperature and pressure were also made using garnet and plagioclase core compositions with matrix hornblende and biotite for garnets whose compositional profiles indicate intragrain diffusional homogenization. Garnet core temperature and pressure were calculated for 79GH72E using hornblende inclusions and plagioclase core composition.

For all samples temperatures were calculated using the garnet-hornblende Fe-Mg exchange equilibrium as calibrated by Graham and Powell (1984) and the hornblende-plagioclase $(Na\square_{-1})^{A}$ $(AlSi_{-1})^{T1}$ exchange thermometer calibrated by Blundy and Holland (1990). Pressures were calculated for all samples using the Fe and Mg end-member equilibria for the assemblage garnet-hornblende-plagioclase-quartz as calibrated by Kohn and Spear (1990). For those garnet amphibolites in which biotite is present, temperatures were calculated using the garnet-biotite Fe-Mg exchange equilibrium (Ferry and Spear, 1978) as recently formulated by Dasgupta and others (1991). This formulation extends the garnet-biotite thermometer to some amphibolite and granulite compositions. The garnet-biotite temperatures obtained are unreasonably high (800°–955°C), which we attribute to the Xgrs content of the garnets in the Juneau amphibolites being considerably greater than that of the garnets used in the calibration. Thus, the garnet-biotite temperatures are not reported.

Because of the uncertainty in amounts of Fe^{3+} and Fe^{2+} in the analyzed hornblende, the temperature and pressure values reported were calculated using total iron as Fe^{2+}. The assumption that all iron is present as Fe^{2+} was made by Graham and Powell (1984) in the calibration of the hornblende-garnet geothermometer, and was typically the case for hornblende used in the geobarometer calibrated by Kohn and Spear (1990). For the data set of this study, if Fe^{2+} as determined from charge balance (table 3) is used for hornblende, the calculated temperatures using the garnet-hornblende thermometer, and the calculated pressures using the Kohn and Spear barometer, are lower by about 20°C to 100°C and 0.1 to 1 kbar, respectively. The hornblende-plagioclase thermometer is not so sensitive to the Fe^{2+} and Fe^{3+} determination and resulting differences in calculated temperatures are generally less than ±10°C. Since the error in total iron determination is less than the error in calculated Fe^{3+} and Fe^{2+}, using all iron as Fe^{2+} provides a better comparison between samples.

At the 95% confidence limit, Graham and Powell (1984) report that the precision of the calibration of the garnet-hornblende geothermometer is generally less than ±30°C. The geobarometer of Kohn and Spear (1990) is

Table 5. Representative analyses of biotite.

[Leaders (---), not detected]

	79GH43A	79GH53A	79GH95A	79GH98A	79GH99C
SiO_2	36.72	36.45	36.45	36.06	35.83
TiO_2	3.23	3.78	3.57	3.17	4.01
Al_2O_3	15.99	15.33	15.75	15.55	15.62
FeO*	19.22	21.05	20.50	21.68	20.47
MnO	0.48	0.32	0.12	0.18	0.14
MgO	10.62	9.51	9.92	9.16	10.32
CaO	0.02	0.02	0.02	---	0.01
Na_2O	0.08	0.15	0.15	0.17	0.20
K_2O	9.71	9.67	9.85	9.72	9.35
Total	96.07	96.28	96.33	95.69	95.94
Cations normalized to 11 oxygens					
Si	2.782	2.783	2.773	2.780	2.735
Al^{iv}	1.218	1.217	1.227	1.220	1.265
Al^{vi}	0.210	0.163	0.185	0.193	0.141
Ti	0.184	0.217	0.204	0.184	0.230
Fe	1.218	1.344	1.304	1.398	1.307
Mn	0.031	0.021	0.007	0.012	0.009
Mg	1.199	1.082	1.125	1.053	1.174
Ca	0.002	0.001	0.002	---	0.001
Na	0.012	0.022	0.022	0.026	0.029
K	0.939	0.942	0.956	0.956	0.911
$\frac{Mg}{(Mg+Fe)}$	0.50	0.45	0.46	0.43	0.47

*Total iron calculated as FeO.

quite insensitive to temperature and analytical uncertainty; they report that application of their geobarometer yielded precisions of ±500 bars to ±1000 bars. In this study the range in temperature and pressure calculated for individual garnet points of a given sample are within the precision limits and can generally be attributed to analytical uncertainty. The precision of calculated temperatures and pressures between samples and whether or not the calculated values reflect reasonable equilibration conditions is discussed the following section.

RESULTS AND INTERPRETATION

Temperatures and pressures calculated for garnet amphibolite, using the different geothermometers and geobarometers discussed above are compared in table 6.[2] As noted below, there is a substantial range of calculated temperatures and pressures. Our purpose in this discussion is to evaluate whether the various *P-T* points determined with a geothermometer and geobarometer might represent a point on a *P-T* path that the rock followed or if they are meaningless values attributable to non-equilibrium or uncertainties in activity models used for amphibole.

Although we cannot demonstrate chemical equilibrium of the garnet amphibolite mineral assemblages, there are no obvious indications of non-equilibrium. Textural equilibrium of all analyzed samples, the generally good agreement of calculated peak metamorphic conditions for garnet amphibolites and pelitic schists (Himmelberg and others, 1991), and the relative chemical homogeneity of matrix grains and garnet rim compositions all argue favorably for an approach to chemical equilibrium.

Garnet-hornblende thermometry yields temperatures of 510°C to 610°C for the garnet zone, 570°C to 635°C for the staurolite-biotite zone, 640°C to 750°C for the kyanite-biotite zone, and 665°C to 765°C for the sillimanite zone (table 6; fig. 3). On the basis of garnet compositional profiles these temperatures are believed to reflect peak or near-peak conditions (see below). The garnet-hornblende temperatures are in general agreement with those previously determined for pelitic schists, which systematically increase from an average of 530°C in the garnet zone to an average of 705°C in the upper kyanite-biotite zone (Himmelberg and others, 1991; fig. 3; table 6). Tempera-

[2]Pressure determinations presented in table 6 are based on Mg and Fe end-member equilibria for the assemblage garnet-hornblende-plagiocalse-quartz. The pressure values given in the text and in figure 3 are for the Mg end-member equilibrium only.

Table 6. Calculated temperature (°C) and pressure (kbar) of Juneau area mafic garnet schists and garnet amphibolites.*

Sample	$T_{grt\text{-}hbl}$	P_{Mg}	P_{Fe}	$T_{pl\text{-}hbl}$		$T_{grt\text{-}hbl}$	P_{Mg}	P_{Fe}	$T_{pl\text{-}hbl}$
Garnet zone					**Sillimanite zone**				
84SK262B					79GH53A				
Average Rim (3,6)	510 (7)	6.9 (0.1)	7.1 (0.1)	710	Average Rim (8,8)	670 (20)	7.5 (0.3)	8.0 (0.2)	715
83GH1A					79GH95A				
Average Rim (2,4)	610 (11)	8.2 (0.3)	8.0 (0.3)	765	Average Rim (2,4)	665 (23)	8.6 (0.2)	8.6 (0.1)	705
Staurolite-biotite zone or greater					79GH98A				
85GH74A					Core 1 (0.3)	735	8.4	8.1	
Average Rim (2,4)	635 (13)	7.4 (0.2)	7.1(0.2)	735	Core 2 (0.3)	735	8.3	8.0	
84GH28A					Average Rim (3,6)	725 (11)	8.5 (0.1)	8.3 (0.1)	775
Average Rim (3,7)	570 (5)	6.2 (0.2)	6.3 (0.3)	755	79GH99C				
					Core 1 (0.15)	680	7.8	7.8	
Kyanite-biotite zone					Core 2 (0.15)	670	7.3	7.2	
81SK30A					Core 3 (0.15)	710	8.3	8.3	
Average Rim (3,7)	640 (11)	7.6 (0.4)	7.9 (0.3)	735	Average Rim (3,7)	670 (31)	7.6 (0.6)	7.6 (0.6)	760
79GH28B					79GH72E				
Core 2 (0.5)	665	9.7	9.7		Core-Inclusion	735	8.9	8.8	
Core 3 (0.3)	650	9.4	9.5		Average Rim (2,4)	665 (7)	7.8 (0.2)	8.0 (0.2)	750
Average Rim (3,6)	660 (9)	9.6 (0.1)	9.7 (0.1)	760					
					79GH68C				
79GH37A					Core (0.5)	765	10	10.1	
Average Rim (2,7)	745 (17)	9.2 (0.2)	9.4 (0.2)	795	Average Rim (3,6)	765 (20)	9.7 (0.3)	9.8 (0.3)	745
79GH43A									
Average Rim (3, 8)	750 (18)	9.9 (0.3)	10.4 (0.3)	740					

*$T_{grt\text{-}hbl}$ are temperatures calculated from garnet-hornblende Fe-Mg exchange equilibria as calibrated by Graham and Powell (1984). Pressure determinations are based on Fe and Mg end-member equilibria for the assemblage garnet-hornblende-plagioclase-quartz as calibrated by Kohn and Spear (1990). Average rim temperature (*T*) and pressure (*P*) were calculated using compositions of garnet-rim points, matrix plagioclase rim points, and matrix hornblende; numbers refer to number of grains and total number of garnet rim points used in average. Values in parentheses following *T* and *P* are standard deviation. Core *T* and *P* for individual garnet grains were calculated for diffusion homogenized garnets using compositions of garnet core, matrix hornblende, and matrix plagioclase core. Numbers in parentheses for cores are garnet radius in millimeters. Inclusion values were determined using composition of hornblende inclusions in garnet, composition of adjacent garnet point, and composition of matrix plagioclase core. Plagioclase-hornblende temperatures ($T_{pl\text{-}hbl}$) are temperatures calculated from $(Na\square_{-1})^{A}(AlSi_{-1})^{T1}$ exchange equilibria as calibrated by Blundy and Holland (1990) using hornblende and plagioclase rim compositions.

tures calculated for garnet amphibolite using plagioclase-hornblende thermometry range from 710°C to 795°C, with no systematic relation between temperature and metamorphic zone. With few exceptions, the plagioclase-hornblende temperatures are substantially higher (100°–200°C) than the garnet-hornblende temperatures and the temperatures determined for garnet zone and staurolite-biotite zone samples are unreasonably high. The plagioclase-hornblende thermometer of Blundy and Holland (1990) is based on a temperature dependence of Al^{iv} substitution for Si in hornblende. Furthermore, their activity-composition model for amphibole, and the calibration of the thermometer, assumes that the Al^{iv} content of amphibole is primarily a function of a $(Na\square_{-1})^{A}$ $(AlSi_{-1})^{T1}$ exchange with the albite component of plagioclase. Thus Blundy and Holland (1990) use Si^{T1} and Al^{T1} as the parameters in their amphibole activity expression. There may, however, be a bulk compositional effect imposed by the Na/K ratio of the system. The Na/K ratio of the samples used to calibrate the thermometer was very high (Blundy and Holland, 1990). However, the amphiboles in the Juneau samples have Na^{A}/K ratios generally around 1. The high K content of the Juneau garnet amphibolites is also evident from the abundant biotite in many samples. In addition, the compositions of amphiboles in the Juneau samples show substantial Tschermak exchange $[Al^{vi}Al^{iv}(Fe,Mg,Mn)_{-1}Si^{T1}{}_{-1}]$. Thus, we conclude that there are trends in Juneau amphibole compositions that are not accounted for in the activity model and that this is probably the reason for the inaccurate temperature estimates.

Thus, on the basis of the comparative thermobarometry, we believe that the garnet-hornblende thermometer of Graham and Powell (1984) yields reasonable estimates of equilibration conditions of the Juneau garnet amphibolites but that the plagioclase-hornblende thermometer of Blundy and Holland (1990) does not. As with other thermometers, however, interpretation of garnet compositional profiles are required to determine if the calculated temperatures reflect peak metamorphic conditions or reequilibration closure temperatures, but, as discussed by Spear (1991), the interpretation is not always unequivocal. Spear (1991) showed that peak temperatures are best recovered from garnet core compositions of high-grade rocks that were initially homogeneous at the peak of metamorphism and where the peak temperature was below the closure temperature. However, Spear (1991) also showed that

cores of homogenized garnets whose peak temperature was above the closure temperature may be compositionally modified owing to diffusional modification upon cooling, and that the modification may not be readily apparent from the compositional profiles. The extent of diffusional compositional change upon cooling, and thus the calculated (closure) temperature, is dependent on garnet size, ratio of garnet to biotite, and cooling rate. Spear's (1991) study was specifically for Fe-Mg exchange between garnet and biotite, but considering that intracrystalline diffusion in garnet would probably be the rate-limiting step, the results should be qualitatively applicable to garnet-hornblende pairs as well. In fact, presence of abundant biotite in nearly all garnet amphibolite samples suggests that garnet-biotite exchange would have occurred. Thus, if the closure temperature for garnet-hornblende exchange is not similar to that of garnet-biotite, or lower, then the garnet-hornblende temperatures are not valid equilibrium values.

Four of the garnet amphibolite samples from the kyanite-biotite and sillimanite zone (79GH28B, 79GH98A, 79GH99C, and 79GH68C) show high-temperature diffusional homogenized compositional profiles. Garnet core-matrix hornblende temperatures for these samples range from about 650°C to 765°C. Garnet in these samples show no, or only very slight, retrograde modification of rims, and thus the calculated core and rim temperatures are not significantly different. Without knowledge of cooling rate, an unequivocal interpretation cannot be made as to whether the calculated temperatures are peak metamorphic temperatures. On the basis of garnet size the calculated temperatures are generally higher than would be expected from Spear's (1991) garnet-biotite study unless cooling rates were substantially greater than 100°C/Ma. A high cooling rate is unlikely because the tonalite sill magma was the heat source for the metamorphism (Himmelberg and others, 1991), and emplacement of tonalite sill plutons spanned an age of about 83 to 55 Ma (Gehrels and others, 1991). The highest temperature calculated using garnet amphibolite thermobarometry is 765°C for sample 79GH68C. This temperature is the closest estimate of peak temperature of metamorphism for the sillimanite zone, although it may represent some post-peak modification. Lower temperatures for diffusionally homogenized garnets most probably do reflect post-peak diffusional modification. Temperatures calculated using garnet rim compositions and matrix hornblende for garnets having compositional profiles characteristic of growth zoning range from 510°C for the garnet zone to 750°C for the kyanite-biotite zone (table 6). Spear's (1991) study showed that growth zoned garnets that achieved peak temperatures greater than about 550°C invariably are modified by diffusion during cooling. Temperatures calculated from rim compositions would normally be several tens of degrees below peak temperatures. Thus, most of the temperatures calculated using rim compositions of growth-zoned garnets probably reflect different degrees of post-peak re-equilibration and are minimum estimates of peak conditions of metamorphism.

The garnet-hornblende-plagioclase-quartz geobarometers yield calculated pressures of metamorphism that range from about 6.2 to 10.0 kbar (table 6). The maximum pressure values (9.2–10.0 kbar) are for kyanite-biotite and sillimanite zone samples and are consistent with the pressure of peak thermal metamorphism determined for pelitic schists (Himmelberg and others, 1991). Most of the samples that yield the high pressure values yield temperatures that are interpreted to be near peak values. Some of these samples also show reasonable agreement between garnet-hornblende and plagioclase-hornblende calculated temperatures, although that agreement may be fortuitous. These data suggest that these higher grade samples retained their near-peak metamorphic equilibrium compositions and that the calculated high pressures are reasonable estimates of the pressure of thermal peak metamorphism.

The samples of garnet amphibolite that yield lower pressures (less than about 9 kbar) are essentially those that are interpreted to have experienced post-peak reequilibration upon cooling, presumably during uplift. The post-peak temperatures, however, are not necessarily substantially lower than the peak temperatures for a given metamorphic zone. Thermal modeling by England and Thompson (1984) showed that most *P-T-t* paths associated with crustal thickening lie within 50°C of the maximum temperature attained for one- third or more of their uplift history. Thus, samples may be set at a temperature near the thermal peak, but at a pressure considerably lower than the pressure of thermal peak metamorphism. High temperatures during uplift could also have been maintained by continued intrusion of tonalite sill plutons during uplift. Himmelberg and others (1991) attributed the metamorphic field gradient in the Juneau area to heat flow outward from the tonalite sill and U-Pb radiometric studies indicate that the tonalite sill plutons were emplaced between about 83 and 55 Ma (Gehrels and others, 1991). Three tonalite sill plutons, the Mendenhall pluton near Heintzleman Ridge at Juneau, the Speel River pluton in Tracy Arm near Holkham Bay, and the Quottoon pluton near Prince Rupert, B.C., range in age from 63.5 to 58.6 Ma and yield pressures of crystallization from 4.7 to about 6 kbar (Hollister and others, 1987; J.M. Hammarstrom, written commun.,1988). Whether older plutons, such as the Carlson Creek pluton (67±2 Ma, Gehrels and others, 1991), crystallized at higher pressures has not been determined.

The above considerations do not, however, explain the substantial range in calculated pressures. One would expect that if the entire area studied followed the same *P-T-t* uplift path the closure pressures would be about the same. There is no regular areal distribution of pressure values nor any structural data to suggest different *P-T-t* paths for different areas, nor is there any regular distribution of pressure values relative to proximity to the great

tonalite sill that would suggest more prolonged heating during uplift for some samples. And, as discussed previously, there does not appear to be any relation of calculated temperature and pressure to garnet grain size. Furthermore, some samples that yield lower calculated pressures occur intermixed with pelitic schist (Himmelberg and others, 1991) and garnet amphibolite samples that yield higher pressures (fig. 3).

Thus, the possibility exists that at least some of the calculated pressures do not represent any point on a *P-T-t* path that the rocks followed. Instead, some of the calculated pressures might be meaningless owing to non-equilibrium or to substantial errors in the activity models of the amphiboles. As discussed previously, equilibrium cannot be demonstrated, but there are no indications of non-equilibrium with the exception of, possibly, the range in calculated pressure. Relative to amphibole activity models, the geobarometer of Kohn and Spear (1990) is based on partitioning of calcium between garnet and plagioclase, which is a strong function of pressure. The equilibria used also involves Tschermak exchange $[Al^{vi}Al^{iv}(Fe,Mg,Mn)_{-1}Si^{T1}_{-1}]$ of amphibole in equilibrium with plagioclase, and the activity-composition model used by Kohn and Spear (1990) considers all Al^{iv} in amphibole to be result of Tschermak exchange. As mentioned previously, the compositions of amphiboles in the Juneau samples show substantial $(Na,K\square_{-1})^{A}$ $(AlSi_{-1})^{T1}$ exchange as well as variation in other components. We cannot demonstrate any relationship between amphibole composition and calculated pressure; nevertheless, components of amphiboles not accounted for in the activity models may contribute to erroneous pressure estimates and may be partly responsible for the range in calculated pressure.

CONCLUSIONS

Comparative thermobarometry of garnet amphibolites and pelitic schists near Juneau indicates that the garnet-hornblende thermometer of Graham and Powell (1984) yields reasonable estimates of equilibration temperature. Calculated peak or near-peak temperatures range from about 510°C for the lower garnet zone to about 765°C for the sillimanite zone, which is consistent with the range determined for pelitic schists by Himmelberg and others (1991). Plagioclase-hornblende thermometry (Blundy and Holland, 1990), on the other hand, yielded unreliable results which we believe is a result of compositional trends in Juneau amphiboles that are not accounted for in the activity models used. Pressure determinations using the Kohn and Spear (1990) geobarometer range from 6.2 to 10.0 kbar. The higher pressure values (9.2–10.0 kbar) were determined for upper kyanite-biotite zone and sillimanite zone amphibolites that show little evidence of post-peak reequilibration and are consistent with pressure of thermal peak metamorphism determined from pelitic schist geobarometers (Himmelberg and others, 1991). Not only does the garnet amphibolite thermobarometry confirm high-pressure metamorphism (9.2–10.0 kbar) of the western metamorphic belt in the Juneau area, but the data also document metamorphism at high pressure (10 kbar) for sillimanite-zone schists and amphibolites that was not evident in the pelitic schist study because of post-peak reequilibration. Interpretation of the spread of lower pressure values, however, is uncertain. Although the range of pressures might be attributed to continued heating of the thickened crustal block during uplift owing to continued intrusion of tonalite sill plutons, there is no regular distribution of pressure values to support this possibility. One cannot rule out that the spread in calculated pressures might be related to non-equilibrium or to compositional trends in amphibole that are not accounted for in the activity model used. Thus, we suggest that the garnet-hornblende-plagioclase-quartz geobarometer be used with caution.

Thermobarometric studies of M5 pelitic schists further to the south along the western metamorphic belt also show a range of calculated pressures. At Holkham Bay, 80 km south of Juneau (fig. 1), Stowell (1989) obtained pressures of 4.1 to 5.1 kbar at 585°C and 680°C for schists containing garnet, staurolite, and kyanite near and adjacent to the tonalite sill. Farther to the south, in the vicinity of Petersburg (fig. 1), McClelland and others (1991), using several geobarometers appropriate to pelitic schists, report pressures of metamorphism ranging from about 7.1 to 11.8 kbar. This variation may in part be a result of regional variation in time of intrusion of tonalite sill magmas and associated metamorphism relative to uplift history. However, in view of the uncertainty of the significance of pressure values determined for garnet amphibolites in the Juneau area, we suggest that comparisons of calculated temperatures and pressures obtained from different thermobarormeters may not be reliable. Where possible, the different geobarometers and geothermometers should be tested for consistency over a small, outcrop-sized area.

REFERENCES CITED

Albee, A.L., and Ray, L., 1970, Correction factors for electron probe microanalysis of silicates, oxides, carbonates, phosphates, and sulfates: Analytical Chemistry, v. 42, p. 1408–1414.

Bence, A.E., and Albee, A.L., 1968, Empirical correction factors for the electron microanalysis of silicates and oxides: Journal of Geology, v. 76, p. 382–403.

Blundy, J.D., and Holland, J.B., 1990, Calcic amphibole equilibria and a new amphibole-plagioclase geothermometer: Contributions to Mineralogy and Petrology, v. 104, p. 208–224.

Brew, D.A., 1988, Late Mesozoic and Cenozoic igneous rocks of southeastern Alaska—A synopsis: U.S. Geological Survey Open File Report, 88-405, 29 p.

———1990, The plate-tectonic setting of Glacier Bay National Park and Preserve and Admiralty Island National Monument: Second Glacier Bay Science Symposium Proceedings, USNPS Science Publications Office, Atlanta, Georgia, p. 1–5.

Brew, D.A., and Ford, A.B., 1977, Preliminary geologic and metamorphic-isograd map of the Juneau B-1 quadrangle, Alaska: U.S. Geological Survey Miscellaneous Field Studies Map MF–846, scale 1:31,680.

———1978, Megalineament in southeastern Alaska marks southwest edge of Coast Range batholithic complex: Canadian Journal of Earth Sciences, v. 15, p. 1763–1762.

———1983, Comment on "Tectonic accretion and the origin of the two major metamorphic and plutonic welts in the Canadian Cordillera": Geology, v. 11, p. 427–428.

———1984, The northern Coast plutonic complex, southeastern Alaska and northwestern British Columbia, *in* Coonrad, W.C., and Elliot, R.L., eds., The United States Geological Survey in Alaska—Accomplishments during 1981: U.S. Geological Survey Circular 868, p. 120–124.

Brew, D.A., Ford, A.B., and Himmelberg, G.R., 1989, Evolution of the western part of the Coast plutonic-metamorphic complex, southeastern Alaska, U.S.A.—A summary, *in* Daly, S.R., Cliff, R.A., and Yardley, B.W., eds., Evolution of metamorphic belts: Geological Society Special Publication 43, p. 447–451.

Brew, D.A., Himmelberg, G.R., Loney, D.A., and Ford, A.B., 1992, Distribution and characteristics of metamorphic belts in the south-eastern Alaska part of the North American Cordillera: Journal of Metamorphic Petrology, v. 10, p. 465–482.

Cosca, M.A., Essene, E.J., and Bowman, J.R., 1991, Complete chemical analyses of metamorphic hornblendes—Implications for normalizations, calculated H_2O activities, and thermobarometry: Contributions to Mineralogy and Petrology, v. 108, p. 472-484.

Dasgupta, Somnath, Sengupta, Pulak, Guha, Dipayan, and Fukuoka, M., 1991, A refined garnet-biotite Fe-Mg exchange geothermometer and its application in amphibolites and granulites: Contributions to Mineralogy and Petrology, v. 109, p. 130-137.

Dymek, R.F., 1983, Titanium, aluminum, and interlayer cation substitutions in biotite from high-grade gneisses, West Greenland: American Mineralogist, v. 68, p. 880-899.

England, P.C., and Thompson, A.B., 1984, Pressure-temperature-time paths of regional metamorphism I. Heat transfer during the evolution of regions of thickened continental crust: Journal of Petrology, v. 25, p. 894-928.

Ferry, J.M., and Spear, F.S., 1978, Experimental calibration of the partitioning of Fe and Mg between garnet and biotite: Contributions to Mineralogy and Petrology, v. 66, p. 113-117.

Ford, A.B., and Brew, D.A., 1973, Preliminary geologic and metamorphic-isograd map of the Juneau B-2 quadrangle, Alaska: U.S. Geological Survey Miscellaneous Field Studies Map MF-527, scale 1:31,680.

———1977, Preliminary geologic and metamorphic-isograd map of the Juneau A-1 and A-2 quadrangles, Alaska: U.S. Geological Survey Miscellaneous Field Studies Map MF-847, scale 1:31,680.

Gehrels, G.E., McClelland, W.C., Samson, S.D., and Patchett, P.J., 1991, U-Pb geochronology of Late Cretaceous and early Tertiary plutons in the northern Coast Mountains batholith: Canadian Journal of Earth Sciences, v. 28, p. 899-911.

Gehrels, G.E., McClelland, W.C., Samson, S.D., Patchett, P.J., and Jackson, J.L., 1990, ancient continental margin assemblage in the northern Coast Mountains, southeast Alaska and northwest Canada: Geology, v. 18, p. 208-211.

Ghent, E.D., and Stout, M.Z., 1986, Garnet-hornblende thermometry, $CaMgSi_2O_6$ activity, and the minimum pressure limits of metamorphism for garnet amphibolites: Journal of Geology, v. 94, p. 736-743.

Graham, C.M., and Powell, R., 1984, A garnet-hornblende geothermometer—Calibration, testing, and application to the Pelonas Schist, southern California: Journal of Metamorphic Geology, v. 2, p. 13-31.

Himmelberg, G.R., Brew, D.A., and Ford, A.B., 1991, Development of inverted metamorphic isograds in the western metamorphic belt, Juneau, Alaska: Journal of Metamorphic Geology, v. 9, p. 165-180.

———1995, Low-grade, M1 metamorphism of the Douglas Island Volcanics, western metamorphic belt near Juneau, Alaska, *in* Schiffman, P., and Day, H.W., eds., Low-grade metamorphism of mafic rocks: Geological Society of America Special Paper 296 (in press).

Hodges, K.V., and Crowley, P.D., 1985, Error estimation in empirical geothermometry and geobarometry for pelitic systems: American Mineralogist, v. 70, p. 702-709.

Hodges, K.V., and Royden, L., 1984, Geologic thermobarometry of retrograded metamorphic rocks—An indication of the uplift trajectory of a portion of the northern Scandinavian Caledonides: Journal of Geophysical Research, v. 89, p. 7077-7090.

Hollister, L.S., Grissom, G.C., Peters, E.K., Stowell, H.H., and Sisson, V.B., 1987, Confirmation of the empirical correlation of Al in hornblende with pressure of solidification of calc-alkaline plutons: American Mineralogist, v. 72, p. 231-239.

Kohn, M.J., and Spear, F.S., 1990. Two new geobarometers for garnet amphibolites, with applications to southeastern Vermont: American Mineralogist, v. 75, p. 89-96.

Koziol, A.M., and Newton, R.C., 1988, Redetermination of the anorthite breakdown reaction and improvement of the plagioclase-garnet-Al_2SiO_5-quartz geobarometer: American Mineralogist, v. 73, p. 216-223.

McClelland, W.C., Anovitz, L.M., and Gehrels, G.E., 1991, Thermobarometric constraints on the structural evolution of the Coast Mountains batholith, central southeastern Alaska: Canadian Journal of Earth Sciences, v. 28, p. 912-928.

Monger, J.W.H., Price, R.A., and Tempelman-Kluit, D.J., 1982, Tectonic accretion and the origin of the two major metamorphic and plutonic welts in the Canadian Cordillera: Geology, v. 10, p. 70-75.

Samson, S.D., McClelland, W.C., Patchett, W.C., Gehrels, G.E., and Anderson, R.G., 1989, Evidence from neodymium isotopes for mantle contributions to Phanerozoic crustal genesis in the Canadian Cordillera: Nature, v. 337, p. 705-709.

Spear, F.S., 1991, On the interpretation of peak metamorphic temperatures in light of garnet diffusion during cooling: Journal of Metamorphic Geology, v. 9, p. 379-378.

Stowell, H.H., 1989, Silicate and sulphide thermobarometry of low- to medium-grade metamorphic rocks from Holkham Bay, south-east Alaska: Journal of Metamorphic Geology, v. 7, p. 343-358.

Reviewers: Steven R. Bohlen and Diane E. Moore

GPS Versus Template—Simple Field and Office Experiments Concerning GPS-Determined Positions and Template-Scaled Map Locations

By David A. Brew, Arthur B. Ford, Richard D. Koch, Michael F. Diggles, James L. Drinkwater, Robert A. Loney, *and* James G. Smith

ABSTRACT

Four simple experiments were done to test the reproducibility, or precision, of latitude and longitude positions determined with low-cost Global Positioning System (GPS) instruments and of such locations scaled from a topographic map using a transparent template; and to loosely compare the results of the two systems. One experiment entailed repeated GPS position determinations using three GPS receivers simultaneously in a backyard in Los Altos, California. The second evaluated the abilities of six experienced field geologists using a latitude and longitude template to make consistent measurements of five station sites near Skagway, Alaska, that were plotted on a mylar base map. The third experiment compared the results of the second experiment with single GPS positions determined with one instrument for the same five stations. The fourth compared GPS determinations for 16 localities in Denali National Park, Alaska, with the latitudes and longitudes scaled with a template from field maps.

The first experiment (referred to here as the California experiment) produced slightly differing means and ranges. One GPS instrument had a definitely smaller range of both latitude (3 seconds) and longitude (4 seconds) than the other two, but the means of all three are within 1 second. The second experiment showed that in the Skagway area (referred to here as the office experiment) the ranges of means of the six geologists' latitude readings for each station location were generally 2 seconds and the ranges of the latitude ranges were also 2 seconds. The ranges of the means of longitude readings were generally 3 seconds or less, and the ranges of the ranges of each geologist were generally 4 seconds or less. The comparison made in the third experiment (referred to here as the Skagway experiment) showed that there are commonly 10 seconds or more difference between the GPS-determined positions for each of the five station locations and their scaled map-plotted locations, and that the discrepancies are nonsystematic and uneven. The fourth experiment in the Denali region (referred to here as the Denali experiment) showed that (1) the GPS-determined and template-scaled latitudes differed from zero to eight seconds; (2) the GPS latitudes of 13 of the 16 sites were south of the map locations; (3) the GPS-determined and template-scaled longitudes differed from one to 17 seconds; and, (4) the GPS longitudes of 15 of the 16 sites were west of the scaled-map locations. These generally systematic patterns contrast with those found in the third subexperiment.

We conclude that, although there may be discrepancies when a single GPS position is compared with a single plotted map location for a given site, the use of GPS-determined positions may be less of a problem than the combined problems involved in scaling locations from maps. We recommend that geologists continue to plot locations of field stations in the conventional way, record the GPS positions of the stations for latitude and longitude data purposes, periodically compare the scaled locations of the GPS positions with the plotted map positions, and then make appropriate adjustments as needed to deal with any discrepancies.

INTRODUCTION

This note describes some simple experiments that were designed and carried out for (1) determining the reproducibility, or precision, of Global-Positioning-System (GPS)-determined latitudinal and longitudinal positions obtained with low-cost GPS receivers; (2) determining the reproducibility of latitudinal and longitudinal locations obtained by using a clear acetate-film template (Barnes and Plouff, 1984) overlain on a mylar copy of a published topographic map; and (3) comparing the results obtained with the two methods. These three purposes were approached with four separate experiments. These experiments are not elegant, sophisticated, or totally controlled; they are, instead, the kind of thing

that a field geologist might do to decide whether or not to use GPS-determined locations.

The main goal of the experiments is to inform field geologists and others who are potential users of low-cost GPS instruments how the reproducibility of GPS-determined field positions is likely to compare with the reproducibility of template-measured locations made from conventionally plotted field stations on topographic maps. A secondary goal of the experiments is to compare GPS-determined positions with map-scaled locations for the same sites.

Some explanations of jargon are in order for those who are unfamiliar with latitude and longitude templates or with the scaling of map coordinates:

1. The templates referred to here are clear acetate sheets with latitude and longitude lines and values on them. They are commonly referred to as "graticules," even though technically they are not. Another simple definition is "latitude and longitude grid sheet." The templates are produced photomechanically from printouts of the computer program of Barnes and Plouff (1984). Each template is specific latitudinally and universal longitudinally. The accuracy, uniformity, and general quality of a template depend on the computer plotter, the paper or other material printed out, the photomechanical process used to make the acetate film sheets, the acetate itself, and how the templates are handled in the office and in the field.

2. A scaled-map location is one whose coordinates (latitude and longitude, UTM, or other system) are arrived at by finding its plotted location on a map and applying a template, a triangle and a drafting scale, proportional dividers, or parallel rulers to measure and interpolate its x and y coordinates.

Most published articles on GPS results (such as, Groten and Strauss, 1988; Davis and others, 1989; and references therein) are based on data obtained with instruments that are much more complex, much more sophisticated, and much more expensive than the low-cost receivers we used. A simple explanation of GPS and a comparison of some features of some low-cost instruments is given in popular articles (Dvorak, 1992; Naranjo and Pittman, 1993) and in brochures from different manufacturers.

Three GPS receivers, all Trimble "Ensign" models (no. 17319) and all purchased at the same time from the same commercial vendor, were used in the GPS experiments. They are referred to here as "HQO," "LBC," and "HMH" from their USGS-property-control designators. This particular make and model was selected because of its relatively low cost, light weight, ease of operation, and because its four-standard-AA-alkaline-dry-cell power pack makes it a likely candidate for purchase and use for general field geologic mapping purposes. The use of this specific make and model does not indicate its endorsement or recommendation by the U.S. Geological Survey; similar instruments are available from other manufacturers.

PROCEDURES

The California experiment was carried out at a private residence in Los Altos, California. The location was selected for its convenience to the senior author and its ready availability for determinations on weekends. The three GPS receivers were simultaneously placed side-by-side on a 0.75-m-long wooden board in the same place in the backyard of the residence, at fifteen widely and unevenly scattered times between February and October, 1993. The relative positions of two of the instruments varied on the board, but one instrument ("LBC") was always between the other two. Readings obtained at their very first deployment after being taken from the factory boxes are not included in the experimental results. At any given one of the fourteen subsequent deployments, all three instruments were read within about a three- to four-minute period. The horizon is not visible from the subexperiment locality, but either three or four transmitting satellites were acquired consistently and quickly by all three instruments. The locality was considered to be neither better nor worse for horizon visibility than most geologic mapping station localities. The simplicity of this subexperiment was intended to simulate likely actual geologic-field-mapping situations in hilly or mountainous terrain.

One of the GPS instruments ("LBC") was used in field mapping on the Klondike Highway and Dyea Road near Skagway, Alaska, in April 1993 as part of the Skagway experiment. GPS positions were determined one-time-only for several field stations. Transmissions from four to five satellites were acquired at most localities. Those stations were also plotted on a paper copy of the published U.S. Geological Survey 1:63,360-scale topographic map series Skagway B-1 map by an experienced field geologist using inspection of topographic features, the road alignment, and a small altimeter; the procedure used is standard for field mapping in Alaska, except that road alignments are rarely available. Five of the plotted locations were later transferred by overlaying the field compilation sheet with a dimensionally stable mylar map sheet, as is the usual practice in Alaskan field work, for use in the office experiment.

The Denali experiment was carried out in Denali National Park, Alaska, by the second author during a geologic mapping project in July 1993. In this experiment, the latitudes, longitudes, and altitudes of 16 different sites in the Mount McKinley A-1 and B-1 U.S. Geological Survey 1:63,360-scale topographic quadrangles were determined in the field using instrument "LBC." The site locations were plotted on paper copies of the topographic maps as described previously using a combination of inspection and altimetry. The latitudes and longitudes of the sites were scaled from the maps using a template, and then the differences between the GPS-determined positions and map-scaled locations were calculated.

The office experiment was done with the cooperation of six USGS geologist colleagues who are also authors of this article. All of them are experienced field geologists familiar with using a template overlain on a map sheet to obtain latitudinal and longitudinal locations. The acetate film template was several years old and had been in the field most of those years. The template is specific for the tier of 1:63,360-scale topographic quadrangles that includes the Skagway B-1; it consists of black north-south meridian lines approximately 0.5-mm wide, spaced at one-minute (or 60-second) longitudinal intervals, with intervening black north-south meridian lines approximately 0.2-mm wide, spaced at 10-second intervals, and black east-west parallel lines of the same dimensions spaced at one-minute (or 60-second) and 10-second latitudinal intervals. Each of the six colleagues read latitudes and longitudes for each locality five different times using the template, interpolating the values to the nearest second from the mylar map sheet. Almost all reading sessions by any one individual were spaced at least one day apart. The colleagues recorded their results on a new tally sheet each time and were instructed (1) not to record or attempt to remember their previous readings, and (2) not to be more or less careful than in a typical field situation.

RESULTS OF THE CALIFORNIA EXPERIMENT

The California experiment involved repeated GPS position determinations at the same site. The fourteen measurements made by each of the three instruments produced a slightly differing latitude mean, a consistent longitude mean, and slightly differing ranges, as shown in table 1. One of the instruments, HMH, had a definitely smaller range of latitude (3 seconds) than the other two instruments, but the means of all three are within 1 second. A second of latitude is approximately 31 m and a second of longitude at this location is about 24 m.

The mean latitude determined by the three instruments for the site differs from that of the map-scaled location by 1 second and the mean longitude differs by 4 seconds (table 1). The actual data obtained in this GPS experiment and summarized here are available in an appendix (No. 1) from the senior author.

RESULTS OF THE OFFICE EXPERIMENT

The office experiment consisted of five repeated template measurements of the five stations near Skagway made by each of the six co-authors and produced the means, ranges, and modes of latitudes and longitudes shown in table 2. Fifteen of the 300 total measurements, or five percent, were adjusted by the senior author to remove obvious 10-second interval misreadings or misposition of the template. Some of those adjustments may have been unwarranted; there are also other large ranges that may include similar 10-second problems, but they were not clearly apparent from the overall pattern and hence were not adjusted. The data obtained in this template experiment and summarized here are in an appendix (No. 2), which is available from the senior author.

Inspection of table 2 shows that the ranges of means of the six geologists' latitude readings for each station location were generally 2 seconds. One station location (93DB019) had the greatest range of means (3 seconds). The ranges of the latitude ranges were usually 2 seconds. The range of latitude modes for the five station locations is 2 seconds or less. Figure 1 presents the data for the latitude readings. A second of latitude is approximately 31 m and a second of longitude at this general location is about 19 m.

Similarly, the ranges of the means of longitude readings were generally 3 seconds or less and the ranges of the ranges of each geologist were generally 4 seconds or

Table 1. Means and ranges of latitude and longitude for GPS receivers HMH, LBC, and HQO at experiment site in Los Altos, California.

["SCALED" indicates values scaled from Mountain View 1:24,000 U.S. Geological Survey topographic series map. na, not applicable. *n*, number of observations]

Receiver	Latitude mean	Latitude range	Longitude mean	Longitude range	*n*
HMH	37°23′04″	37°23′02″–37°23′05″ = 03″	122°06′12″	122°06′10″–122°06′14″ = 04″	15
LBC	37°23′03″	37°23′00″–37°23′05″ = 05″	122°06′12″	122°06′10″–122°06′14″ = 04″	14
HQO	37°23′04″	37°23′02″–37°23′08″ = 06″	122°06′12″	122°06′09″–122°06′15″ = 06″	14
Mean of the receivers	37°23′04″	na	122°06′12″	na	na
SCALED	37°23′05″	na	122°06′08″	na	1

Table 2. Means, ranges, and modes of latitude and longitude for five stations in the Skagway B-2 quadrangle as measured with template by geologists A, B, C, D, E, and F.

[GPS denotes the receiver HMH determination for the same station. na, not applicable; *n*, number of observations]

Operator	Latitude mean	Latitude range	Longitude mean	Longitude range	Latitude mode	Longitude mode
			Station 93DB001			
A	59°27′05″	59°27′04″– 59°27′05″ = 01″	135°19′11″	135°19′09″– 135°19′12″ = 03″	59°27′05″	135°19′12″
B	59°27′04″	59°27′03″– 59°27′04″ = 01″	135°19′11″	135°19′11″– 135°19′12″ = 01″	59°27′04″	135°19′11″
C	59°27′04″	59°27′04″– 59°27′04″ = 00″	135°19′12″	135°19′10″– 135°19′15″ = 05″	59°27′04″	135°19′12″
D	59°27′04″	59°27′04″– 59°27′05″ = 01″	135°19′13″	135°19′09″– 135°19′12″ = 03″	59°27′04″	135°19′12″
E	59°27′04″	59°27′03″– 59°27′04″ = 01″	135°19′13″	135°19′12″– 135°19′14″ = 02″	59°27′04″	135°19′13″
F	59°27′04″	59°27′04″– 59°27′05″ = 01″	135°19′11″	135°19′10″– 135°19′14″ = 04″	59°27′04″	135°19′10″
GPS (*n* =3)	59°27′03″	59°27′02″– 59°27′04″ = 02″	135°19′21″	135°19′20″– 135°19′22″ = 02″	59°27′02″	135°19′20″
			Station 93DB003			
A	59°29′35″	59°29′35″– 59°29′35″ = 00″	135°16′33″	135°16′30″– 135°17′34″ = 04″	59°29′35″	135°16′33″
B	59°29′35″	59°29′34″– 59°29′35″ = 01″	135°16′33″	135°16′32″– 135°17′34″ = 02″	59°29′35″	135°16′33″
C	59°29′35″	59°29′35″– 59°29′35″ = 00″	135°16′33″	135°16′32″– 135°17′36″ = 04″	59°29′35″	135°16′33″
D	59°29′35″	59°29′34″– 59°29′35″ = 01″	135°16′33″	135°16′31″– 135°17′35″ = 04″	59°29′35″	na
E	59°29′34″	59°29′34″– 59°29′34″ = 00″	135°16′34″	135°16′34″– 135°17′36″ = 02″	59°29′34″	135°16′34″
F	59°29′35″	59°29′34″– 59°29′35″ = 01″	135°16′33″	135°16′31″– 135°17′37″ = 06″	59°29′35″	135°16′31″
GPS	59°28′59″		135°17′07″		59°28′59″	135°17′07″
			Station 93DB018			
A	59°28′53″	59°28′52″– 59°28′54″ = 02″	135°17′21″	135°17′18″– 135°17′22″ = 04″	59°28′53″	135°17′22″
B	59°28′53″	59°28′52″– 59°28′53″ = 01″	135°17′21″	135°17′21″– 135°17′22″ = 01″	59°28′53″	135°17′21″
C	59°28′53″	59°28′53″– 59°28′53″ = 00″	135°17′23″	135°17′22″– 135°17′25″ = 03″	59°28′53″	135°17′22″
D	59°28′53″	59°28′52″– 59°28′54″ = 02″	135°17′21″	135°17′20″– 135°17′23″ = 03″	59°28′53″	na
E	59°28′52″	59°28′52″– 59°28′52″ = 00″	135°17′23″	135°17′22″– 135°17′23″ = 01″	59°28′52″	135°17′23″
F	59°28′53″	59°28′52″– 59°28′53″ = 01″	135°17′22″	135°17′19″– 135°17′26″ = 07″	59°28′53″	na
GPS	59°28′52″		135°17′30″		59°28′52″	135°17′30″
			Station 93DB019			
A	59°27′45″	59°27′43″– 59°27′44″ = 01″	135°19′12″	135°19′12″– 135°19′16″ = 04″	59°27′44″	na
B	59°27′44″	59°27′43″– 59°27′44″ = 01″	135°19′16″	135°19′15″– 135°19′17″ = 02″	59°27′44″	na
C	59°27′43″	59°27′43″– 59°27′43″ = 00″	135°19′16″	135°19′14″– 135°19′18″ = 04″	59°27′43″	135°19′16″
D	59°27′43″	59°27′43″– 59°27′44″ = 01″	135°19′15″	135°19′12″– 135°19′17″ = 05″	59°27′43″	na
E	59°27′42″	59°27′42″– 59°27′43″ = 01″	135°19′17″	135°19′16″– 135°19′17″ = 01″	59°27′42″	135°19′17″
F	59°27′43″	59°27′43″– 59°27′43″ = 00″	135°19′15″	135°19′13″– 135°19′18″ = 05″	59°27′43″	135°19′13″
GPS	59°27′45″		135°19′12″		59°27′45″	135°19′12″
			Station 93DB020			
A	59°29′17″	59°29′16″– 59°29′18″ = 02″	135°20′31″	135°20′32″– 135°20′35″ = 03″	59°29′17″	135°20′32″
B	59°29′17″	59°29′16″– 59°29′17″ = 01″	135°20′32″	135°20′32″– 135°20′34″ = 02″	59°29′17″	135°20′32″
C	59°29′17″	59°29′17″– 59°29′17″ = 00″	135°20′33″	135°20′32″– 135°20′34″ = 02″	59°29′17″	na
D	59°29′18″	59°29′18″– 59°29′18″ = 00″	135°20′33″	135°20′31″– 135°20′34″ = 03″	59°29′18″	135°20′33″
E	59°29′18″	59°29′17″– 59°29′24″ = 07″	135°20′34″	135°20′33″– 135°20′34″ = 01″	59°29′17″	135°20′34″
F	59°29′18″	59°29′17″– 59°29′18″ = 01″	135°20′33″	135°20′31″– 135°20′35″ = 04″	59°29′18″	135°20′33″
GPS	59°29′32″	na	135°20′46″	na	59°29′32″	135°20′46″

less. One station location (93DB019) had the greatest range of means (5 seconds). The ranges of the longitude ranges were generally 4 seconds. One station location (93DB018) had the greatest range of ranges of means (6 seconds) and one (93DB020) had significantly fewer (3 seconds). The range of longitude modes for the five stations were 3 seconds or less, except for station location 93DB019, which gave 4 seconds for the three geologists who actually produced a mode. Figure 1 presents the aggregated data for the longitude readings.

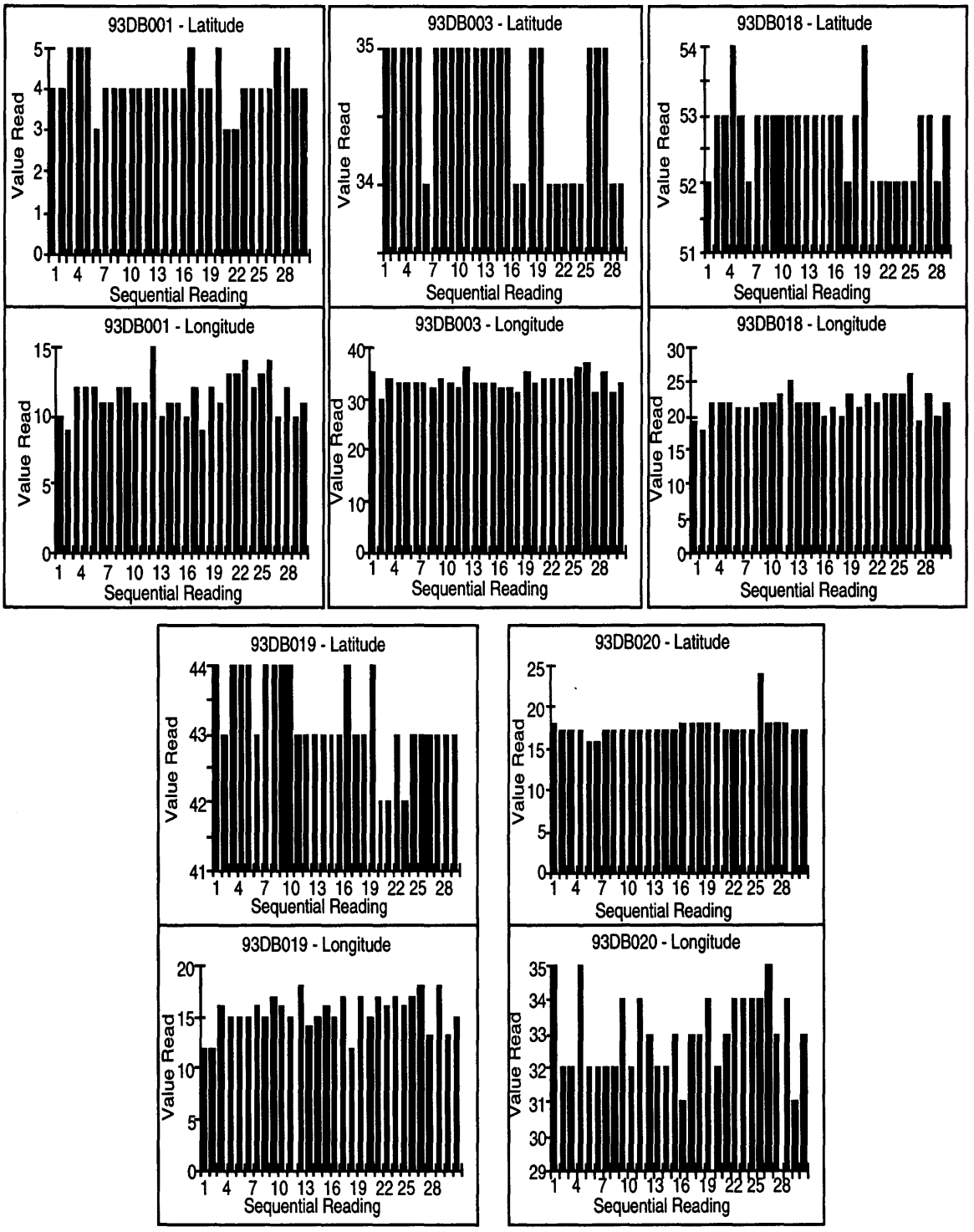

Figure 1. Histograms showing distribution of individual latitude and longitude readings made by six geologists for five sites in the Skagway area. For each site abscissas are the total number of readings; ordinates are the seconds-only values for latitudes and longitudes; data are available upon request from the senior author.

These results indicate that, at this latitude, latitudes can be scaled more precisely than longitudes; this is to be expected because of the convergence of meridians, the closer spacing of the template lines, and the resulting greater difficulty in interpolation. The results also suggest that some stations are more difficult to scale precisely than others. It is possible that this is due to a slight individual variation in the template line spacing.

COMPARISON OF THE RESULTS OF THE CALIFORNIA AND OFFICE EXPERIMENTS

Comparison of the results of the California and the office experiments indicate that the means of latitudes and longitudes as determined with a GPS instrument have slightly smaller ranges than those scaled from a map with a template. The ranges of the GPS-determined latitude and longitude positions are generally greater, however, than those scaled from a map.

RESULTS OF THE SKAGWAY EXPERIMENT

The Skagway experiment compared the results of the office experiment with the field GPS position determinations for the five Skagway area station sites. The results shown in table 2 indicate that there are commonly 10-seconds or more difference between the GPS-determined latitude and longitude positions for each of the five station locations used in this experiment and their map-plotted locations, although there are some exceptions (latitude for 93DB001, 93DB018, 93DB019, and longitude for 93DB019). There are five possible causes for these discrepancies.

1. The station locations were inaccurately determined and plotted in the field by the senior author; any inaccuracies in the published quadrangle map's cultural features, contour positions, and road alignment would contribute to such an error; as well as altimeter drift, poor location judgement, and plotting error.

2. Latitudes and longitudes of topographic features scaled precisely from published maps may not be the same as the latitudes and longitudes for those features determined by GPS; that is, the GPS-determined global positions of the features (in this case, station sites) may differ from their map locations. This type of discrepancy is caused by the different ways in which the latitudes and longitudes are measured. (a) Published topographic map positions have been established by traditional surveying methods with triangulation from distant places and the use of local baselines; and (b) GPS positions are based on a satellite system that uses a state-of-the-art global framework. Thus the latitude and longitude values for the GPS positions and map locations may not correspond; such discrepancies are common in nearby parts of southeastern Alaska (J. Taggert, U.S. National Biological Survey, Glacier Bay National Park, oral commun., 1993), and are the probable cause of the discrepancies reported in the following section for the Denali experiment.

3. The GPS positions were influenced by unrecognized instrument problems or military scrambling.

4. The template readings were inaccurate, as discussed for the office experiment.

5. A combination of the above possible causes.

It is difficult to choose one or another of the above possible alternatives as being the most likely. The first alternative cannot be dismissed, even given that all of the station locations were along roads shown on published maps and were plotted using visual inspection, altimetry, and resecting with a compass from distant, readily identifiable topographic features.

The second alternative may be equally likely, however, even given the unsystematic differences between the map-scaled locations and the GPS-determined positions. Table 2 shows that the latitudes roughly agree for three of the five station locations, the longitude roughly agrees for one of the stations, and both latitude and longitude agree roughly for only one of these (93DB019); such unsystematic differences within the small area (4.8 by 4.0 km) containing the five sites are puzzling.

The third alternative is impossible to evaluate with the information available. The fourth alternative cause should have been eliminated by the repetitive readings described in the office experiment. The fifth alternative cause may be the most likely, particularly if both alternative causes (1) and (2) are operating.

RESULTS OF THE DENALI EXPERIMENT

The Denali experiment compared the template-scaled map locations of station sites in Denali National Park with their GPS-determined positions. The results in table 3 indicate that the latitudes differed from zero to eight seconds and that the GPS latitudes of 13 of the 16 sites are south of the map locations. Fourteen of the 16 site latitudes differed 5 seconds or less and, of those, seven differed by less than 3 seconds. Ignoring two probable template-reading errors, the GPS-determined and template-scaled longitudes differed from 1 to 17 seconds; the GPS longitudes of 15 of the 16 sites are west of the scaled-map locations, and the other one differs by 1 second. A second of latitude is approximately 31 m and a second of longitude is about 16 m in this general region. These generally systematic patterns contrast with those found in the Skagway experiment and are interpreted to be due to a systematic difference between GPS-determined positions and published map locations; that is, due to the second discrepancy cause discussed for the Skagway experiment.

CONCLUSIONS

Although these experiments are simple and the results of these experiments are inconclusive in some important

Table 3. Latitudes, longitudes, and altitudes determined for station sites in Denali National Park using GPS receiver HMH and published U.S.G.S. Mt. McKinley A-1 and B-1 topographic maps, together with calculated differences.

[* indicates probable template-reading or field-location error; latitude and longitude second values were calculated from GPS receiver's decimal minute readouts that were recorded to two places]

Station	GPS latitude	GPS longitude	GPS altitude	Template latitude	Template longitude	Map altitude	GPS minus template latitude	GPS minus template longitude	GPS minus map altitude
93AF001	63°15′18″	150°05′56″	5400	63°15′23″	150°05′41″	5400	−05″	+15″	0
93AF002	63°15′07″	150°06′00″	5700	63°15′15″	150°05′51″	5700	−08″	+09″	0
93AF003	63°15′00″	150°06′00″	6000	63°15′05″	150°05′51″	5940	−05″	+09″	+60
93AF004	63°14′54″	150°06′12″	5800	63°14′57″	150°05′59″	5850	−03″	+13″	−50
93AF006	63°14′42″	150°06′42″	5800	63°14′45″	150°06′35″	5700	−03″	+07″	+100
93AF007	63°15′25″	150°05′50″	5400	63°15′26″	150°05′38″	5450	−01″	+12″	−50
93AF009	63°15′34″	150°05′40″	5960	63°15′39″	150°05′27″	5850	−05″	+13″	+110
93AF010	63°15′47″	150°05′03″	5900	63°15′47″	150°04′57″	5950	−00″	+06″	−50
93AF011	63°15′50″	150°05′02″	6300	63°15′54″	150°04′48″	6000	−04″	+04″	+300
93AF012	63°25′37″	150°22′08″	3300	63°25′36″	150°22′03″	3350	+01″	+05″	−50
93AF013	63°25′36″	150°21′32″	3800	63°25′38″	150°21′02″	3350	−02″	+30″*	+450
93AF014	63°26′01″	150°18′53″	—	63°25′53″	150°18′54″	3750	+08″	−01″	—
93AF015	63°23′42″	150°04′38″	5500	63°23′39″	150°04′27″	5550	+03″	+11″	−50
93AF017	63°25′36″	150°21′31″	3400	63°25′38″	150°21′02″	3350	−02″	+29″*	+50
ABF Camp 1	63°15′20″	150°00′53″	5500	63°15′23″	150°00′36″	5400	−03″	+17″	+100
ABF Camp 2	63°23′47″	150°04′21″	5350	63°23′48″	150°04′15″	5250	−01″	+06″	+100

ways, a few points worth emphasizing are (1) geologists can do a fairly consistent job of scaling latitudes and longitudes from a map with a template; the greatest problems are not with the template, but with careless operator error and with the actual process of locating the site on the map; (2) the best use of a GPS instrument entails repetitive recorded readings over as long a period of time as possible and the calculation of a mean value; (3) use of a hand-held GPS instrument in the field is convenient, saves time overall, and obviates the need for template use for scaling plotted locations; (4) future recovery of specific sample and other locations in the field is likely to be done with GPS instruments as their use becomes more widespread; and (5) topographic map revisions in the future will likely bring published map locations into agreement with GPS-determined locations.

From all this we conclude that, although there may be a discrepancy when a single GPS position is compared with a single plotted map location for a given site, the use of GPS-determined positions may be less of a problem than the combined problems involved in scaling locations from maps. The latter procedure includes (1) estimating the field location, (2) plotting that location on a map, and (3) scaling the latitude and longitude from the map with a template or other device; and errors can occur in each step.

We recommend that geologists continue to plot locations of field stations in the conventional way, record the GPS positions of the stations for latitude and longitude data purposes, periodically compare the scaled locations of the GPS positions with the plotted map positions, and then make appropriate adjustments as needed as needed to deal with any discrepancies. When GPS-determined positions are recorded in notes and tables, it is important to note that those positions may disagree with the map-scaled locations.

REFERENCES CITED

Barnes, D.F., and Plouff, D., 1984, Computer-generated latitude and longitude templates for rapid determination of geographic positions in Alaska, *in* Coonrad, W.L., and Elliott, R.L., eds., The United States Geological Survey in Alaska: Accomplishments during 1981: U.S. Geological Survey Circular 868, p. 10–11.

Davis, J.L., Prescott, W.H., Svarc, J.L., and Wendt, K.J., 1989, Assessment of global positioning system measurements for studies of crustal deformation: Journal of Geophysical Research, v. 94, no. B10, p. 13,635–13,650.

Dvorak, J.J., 1992, Tracking the movement of Hawaiian volcanoes: Global positioning system (GPS) measurements: Earthquakes and Volcanoes, v. 23, no. 6, p. 255–267.

Groten, E., and Strauss, R., eds., 1988, GPS-techniques applied to geodesy and surveying: Lecture Notes in Earth Sciences, v. 19, Springer Verlag, 532 p.

Naranjo, R., and Pittman, F., 1993, GPS shootout—Sail rates six hand-helds: Sail, May 1993, p. 74–82.

Reviewers: David F. Barnes, Warren E. Yeend, and William. H. Prescott

U.S. Geological Survey Reports on Alaska Released in 1993*

Compiled by Ellen R. White

*[Some reports dated 1992 did not become available until 1993: they are included in this listing.]

ABBREVIATIONS

B2068 Dusel-Bacon, Cynthia, and Till, A.B., eds., 1993, Geologic studies in Alaska by the U.S. Geological Survey, 1992: U.S. Geological Survey Bulletin 2068, 250 p.

C1086 Kelmelis, J.A., and Snow, Mitchell, eds., 1993, Proceedings of the U.S. Geological Survey Global Change Research Forum, Herndon, Virginia, March 18–20, 1991: U.S. Geological Survey Circular 1086, 121 p.

OF93-195 Jacobson, M.L., compiler, 1993, National Earthquake Hazards Reduction Program; Summaries of technical reports, v. XXXIV: U.S. Geological Survey Open-File Report 93-195, v. 1, 983 p., v. 2, 983 p.

Abers, Geoffrey, and Kim, W.Y., 1993, Determination of earthquake source parameters from regional waveforms: analysis of sparse network data in the Aleutians: OF93-195, v. 1, p. 165–170.

Ager, T.A., 1993, Late Cenozoic climates of Alaska and Yukon: A joint U.S. Geological Survey—Geological Survey of Canada global change research project [abs.]: C1086, p. 69–70.

Aleinikoff, J.N., Moore, T.E., Walter, Marianne, and Nokleberg, W.J., 1993, U-Pb ages of zircon, monazite, and sphene from Devonian metagranites and metafelsites, central Brooks Range, Alaska: B2068, p. 59–70.

Bailey, B.J., and McIntire, J.A., 1993, Levels of lakes in the north Kenai area, Alaska, 1970–1992: U.S. Geological Survey Open-File Report 93-644, 18 p.

Bohn, Diedra, and Schneider, J.L., eds., 1992 [released 1993], 1992 annual report on Alaska's mineral resources; A summary of mineral resource activities in Alaska during 1991: U.S. Geological Survey Circular 1091, 65 p.

Bond, K.R., 1993, Principal facts for gravity stations on Annette Island, southeast Alaska: U.S. Geological Survey Open-File Report 93-508–A (paper copy, 12 p.) and Open-File Report 93-508–B (5.25-inch diskette).

Box, S.E., Moll-Stalcup, E.J., Frost, T.P., and Murphy, J.M., 1993, Preliminary geologic map of the Bethel and southern Russian Mission quadrangles, southwestern Alaska: U.S. Geological Survey Miscellaneous Field Studies Map MF–2226–A, 20 p., 1 sheet, scale 1:250,000.

Boyd, T.M., 1993, Analysis of the 1957 Andreanof Islands earthquake: OF93-195, v. 1, p. 19–26.

Brabets, T.P., 1993, Glacier runoff and sediment transport and deposition, Eklutna Lake basin, Alaska: U.S. Geological Survey Water-Resources Investigations Report 92-4132, 47 p., 1 sheet, scale 1:63,360.

———1993, Hydrologic data for the lower Copper River, Alaska, May to September 1992: U.S. Geological Survey Open-File Report 93-162, 26 p.

Bradley, D.C., Haeussler, P.J., and Kusky, T.M., 1993, Timing of early Tertiary ridge subduction in southern Alaska: B2068, p. 163–177.

Brocher, T.M., and Moses, M.J., 1993, Onshore-offshore wide-angle seismic recordings of the 1989 Alaskan edge profile: Five-day recorder data: U.S. Geological Survey Open-File Report 93-238, 25 p.

Brouwers, E.M., 1993, Systematic paleontology of Quaternary ostracode assemblages from the Gulf of Alaska, Part 2: Families *Trachyleberididae, Hemicytheridae, Loxoconchidae, Paracytherideidae*: U.S. Geological Survey Professional Paper 1531, 47 p., 16 pls.

Brouwers, E.M., and Forester, R.M., 1993, Ostracode assemblages from modern bottom sediments of Vitus Lake, Bering piedmont glacier, southeast Alaska: B2068, p. 228–235.

Campbell, W.J., and Gloersen, Per, 1993, Arctic Ocean winter polynya zones during 1978–87 [abs.]: C1086, p. 73–74.

Carlson, P.R., Karl, H.A., Edwards, B.D., Gardner, J.V., and Hall, R., 1993, Mass movement related to large submarine canyons along the Beringian margin, Alaska: U.S. Geological Survey Bulletin 2002, p. 104–116.

Carlson, P.R., Powell, R.D., Cowan, E.A., and Lawson, D.E., 1993, Marine geologic investigations of Disenchantment Bay, Alaska, after breakup of 1986 Hubbard Glacier ice dam: U.S. Geological Survey Open-File Report 92-706, 41 p.

Carlson, P.R., Tagg, A.R., and Molnia, B.F., 1993, Acoustic profiles of sediment in a melt-water lake adjacent to the Bering Glacier, Alaska: U.S. Geological Survey Open-File Report 93-266, 26 p.

Carter, L.D., 1993, Late Cenozoic arctic climatic change [abs.]: C1086, p. 75.

Cathrall, J.B., Arbogast, B.F., VanTrump, George, Jr., and McDanal, S.K., 1993, Geochemical maps showing the distribution of selected elements in stream-sediment samples from the Craig, Dixon Entrance, and western edges of the Ketchikan and Prince Rupert quadrangles, southeast Alaska: U.S. Geological

Survey Miscellaneous Field Studies Map MF–2217–A, 2 sheets, scale 1:250,000.

Cathrall, J.B., McDanal, S.K., VanTrump, George, Jr., Arbogast, B.F., and Grybeck, D., 1993, Geochemical maps showing the distribution and concentration of selected elements in nonmagnetic heavy-mineral-concentrate samples from stream sediment from the Craig, Dixon Entrance, and western edges of the Ketchikan and Prince Rupert quadrangles, southeast Alaska: U.S. Geological Survey Miscellaneous Field Studies Map MF–2217–B, 2 sheets, scale 1:250,000.

Collett, T.S., 1993, Natural gas production from Arctic gas hydrates: U.S. Geological Survey Professional Paper 1570, p. 299–311.

Collett, T.S., and Kvenvolden, K.A., 1993, Interrelations between gas hydrates of northern Alaska and atmospheric methane [abs.]: C1086, p. 77–78.

Combellick, R.A., and Reger, R.D., 1993, Investigation of peat stratigraphy in estuarine flats near Anchorage, Alaska, as a means of determining recurrence intervals of major earthquakes: OF93-195, v. 1, p. 254–257.

Crock, J.G., Beck, K.A., Fey, D.L., Hageman, P.L., Papp, C.S., and Peacock, T.R., 1993, Element concentrations and baselines for moss, lichen, spruce, and surface soils, in and near Wrangell-Saint Elias National Park and Preserve, Alaska: U.S. Geological Survey Open-File Report 93-14, 98 p.

Crosson, R.S., and Creager, K.C., 1993, Earthquake hazard investigations in the Pacific Northwest and southern Alaska using network data: OF93-195, v. 1, p. 266–268.

Dorava, J.M., May, B.A., Meyer, D.F., and Myers, L.V., 1993, Channel geometry data of streams in the lower Drift River basin affected by the 1989–90 eruptions of Redoubt Volcano, Alaska: U.S. Geological Survey Open-File Report 93-94, 66 p.

Dumoulin, J.A., and Harris, A.G., 1993, Lithofacies and conodonts of carboniferous strata in the Ivotuk Hills, western Brooks Range, Alaska: B2068, p. 31–47.

Dumoulin, J.A., Harris, A.G., and Schmidt, J.M., 1993, Deepwater lithofacies and conodont faunas of the Lisburne Group, west-central Brooks Range, Alaska: B2068, p. 12–30.

Dusel-Bacon, Cynthia, Csejtey, Béla, Jr., Foster, H.L., Doyle, E.O., Nokleberg, W.J., and Plafker, George, 1993, Distribution, facies, ages, and proposed tectonic associations of regionally metamorphosed rocks in east- and south-central Alaska: U.S. Geological Survey Professional Paper 1497–C, 73 p., 2 sheets, scale 1:1,000,000.

Dusel-Bacon, Cynthia, and Till, A.B., eds., 1993, Introduction: B2068, p. 1.

Eppinger, R.G., 1993, Gold and cinnabar in heavy-mineral concentrates from stream-sediment samples collected from the western half of the Lime Hills 1°×3° quadrangle, Alaska: B2068, p. 91–100.

Flores, R.M., and Stricker, G.D., 1993, Early Cenozoic depositional systems, Wishbone Hill district, Matanuska coal field, Alaska: B2068, p. 101–117.

———1993, Reservoir framework architecture in the Clamgulchian type section (Pliocene) of the Sterling Formation, Kenai Peninsula, Alaska: B2068, p. 118–129.

Fogleman, K.A., Lahr, J.C., Stephens, C.D., and Page, R.A., 1993, Earthquake locations determined by the southern Alaska seismograph network for October 1971 through May 1989: U.S. Geological Survey Open-File Report 93-309, 54 p.

Foley, K.M., and Poore, R.Z., 1993, Planktic foraminifer census data from Northwind Ridge cores PI–88–AR P3, PI–88–AR P7, and PI–88–AR P9, Arctic Ocean: U.S. Geological Survey Open-File Report 93-218, 11 p.

Foose, M.P., and Bryant, Karen, 1993, Annotated bibliography of metallogenic maps (material mostly published between 1960 and 1987): U.S. Geological Survey Open-File Report 93-208–A (paper copy, 91 p.) and Open-File Report 93-208–B (computer diskette). [Alaska on p. 60–64.]

Ford, A.B., and Brew, D.A., 1993, Geochemical character of upper Paleozoic and Triassic greenstone and related metavolcanic rocks of the Wrangellia terrane in northern southeastern Alaska: B2068, p. 197–217.

Galloway, J.P., and Carter, L.D., 1993, Late Holocene longitudinal and parabolic dunes in northern Alaska: Preliminary interpretations of age and paleoclimatic significance: B2068, p. 3–11.

Gamble, B.M., and Till, A.B., 1993, Maps showing metallic mineral resources of the Bendeleben and Solomon quadrangles, western Alaska: U.S. Geological Survey Miscellaneous Field Studies Map MF–1838–D, 22 p., 3 sheets, scale 1:250,000.

Gaydos, L.J., 1993, Assessing the human impact of global change in western United States and Alaska [abs.]: C1086, p. 83.

Gehrels, G.E., and Barker, Fred, 1993, Reconnaissance geochemistry of Permian and Triassic basalts of the Taku and Wrangellia terranes, southeastern Alaska: B2068, p. 218–227.

Goldfarb, R.J., and Borden, J.C., 1993, Geochemical evaluation of stream-sediment data from the Bering Glacier and Icy Bay quadrangles, south-central Alaska: B2068, p. 178–186.

Grantz, Arthur, Hart, P.E., Phillips, R.L., McCormick, Michael, Perkin, R.G., Jackson, Ruth, Gagnon, Alan, Shusun, Li, Byers, Carl, and Schwartz, K.R., 1993, Cruise report and preliminary results, U.S. Geological Survey Cruise P1–93–AR Northwind Ridge and Canada basin, Arctic Ocean, aboard USCGC *Polar Star*, August 16–September 15, 1993: U.S. Geological Survey Open-File Report 93-389, 38 p.

Grantz, Arthur, Phillips, R.L., May, S.D., Mullen, M.W., Poore, R.Z., and Rieck, H.J., 1993, Climatic and paleo-oceanographic history of the Canada Basin, Arctic Ocean [abs.]: C1086, p. 84–85.

Gray, J.E., Theodorakos, P.M., Bradley, L.A., and Bullock, J.H., Jr., 1993, Favorable areas for metallic mineral resources in and near the Horn Mountains, Sleetmute quadrangle, southwestern Alaska: B2068, p. 79–90.

Haeussler, P.J., and Nelson, S.W., 1993, Structural evolution of the Chugach-Prince William terrane at the hinge of the orocline in Prince William Sound, and implications for ore deposits: B2068, p. 143–162.

Hamilton, T.D., 1993, The Old Crow tephra: A stratigraphic marker for the last interglaciation in Alaska? [abs.]: C1086, p. 87.

Hampton, M.A., 1993, Comparison of tectonic and stratigraphic control of submarine landslides on the Kodiak upper continental slope, Alaska: U.S. Geological Survey Bulletin 2002, p. 117–122.

Hampton, M.A., Lemke, R.W., and Coulter, H.W., 1993, Submarine landslides that had a significant impact on man and his activities: Seward and Valdez, Alaska: U.S. Geological Survey Bulletin 2002, p. 123–134.

Johnson, J.M., and Satake, Kenji, 1993, Source parameters of the 1957 Aleutian earthquake from tsunami waveforms: OF93-195, v. 1, p. 346–367.

Jones, S.H., and Glass, R.L., 1993, Hydrologic and mass-movement hazards near McCarthy Wrangell-St. Elias National Park and Preserve, Alaska: U.S. Geological Survey Water-Resources Investigations Report 93-4078, 55 p., 2 sheets, scale 1:25,000.

Karl, S.M., 1992 [1993], Map and table of mineral deposits on Annette Island, Alaska: U.S. Geological Survey Open-File Report 92-690, 57 p., 1 sheet, scale 1:63,360.

Karl, S.M., and Mull, C.G., 1993, Appeal for nonproliferation of escalating terrane nomenclature: B2068, p. 71–78.

Kayen, R.E., and Lee, H.J., 1993, Slope stability in regions of sea-floor gas hydrate: Beaufort Sea continental slope: U.S. Geological Survey Bulletin 2002, p. 97–103.

Kelley, J.S., Tailleur, I.L., Morin, R.L., Reed, K.M., Harris, A.G., Schmidt, J.M., Brown, F.M., and Kurtak, J.M., 1993, Barite deposits in the Howard Pass quadrangle and possible relations to barite elsewhere in the northwestern Brooks Range, Alaska: U.S. Geological Survey Open-File Report 93-215, 13 p., 9 pls., scale 1:63,360.

Kelley, K.D., Barton, H.N., Sutley, S.J., and O'Leary, R.L., 1993, Maps showing geochemistry of sediment samples from the southern part of Chandler Lake quadrangle, Alaska: U.S. Geological Survey Miscellaneous Field Studies Map MF–2144–C, 2 sheets, scale 1:250,000.

Kelley, K.D., and Sutley, S.J., 1993, Maps showing geochemistry of sediment samples from the northern part of Chandler Lake quadrangle, Alaska: U.S. Geological Survey Miscellaneous Field Studies Map MF–2144–D, 2 sheets, scale 1:250,000.

Kelley, K.D., Sutley, S.J., and Frisken, J.G., 1993, Maps showing geochemistry and mineralogy of nonmagnetic heavy-mineral-concentrate samples from the southern part of the Chandler Lake quadrangle, Alaska: U.S. Geological Survey Miscellaneous Field Studies Map MF–2144–B, 2 sheets, scale 1:250,000.

Kilburn, J.E., Goldfarb, R.J., Griscom, Andrew, and Box, S.E., 1993, Map showing metallic mineral resource potential in the Goodnews Bay, Hagemeister Island, and Nushagak Bay 1°×3° quadrangles, southwest Alaska: U.S. Geological Survey Miscellaneous Field Studies Map MF–2228, 4 sheets, scale 1:250,000.

Kistler, R.W., Newberry, R.J., and Brew, D.A., 1993, Rubidium-strontium isotopic systematics of vein minerals in the Juneau gold belt, Alaska: B2068, p. 236–240.

Kvenvolden, K.A., and Collett, T.S., 1993, Permafrost and gas hydrates as possible sources of atmospheric methane at high latitudes [abs.]: C1086, p. 92–93.

Lahr, J.C., Stephens, C.D., Page, R.A., and Fogleman, K.A., 1993, Alaska seismic studies: OF93-195, v. 1, p. 408–415.

Landis, G.P., Fitzpatrick, J.J., Hinkley, T.K., and Rye, R.O., 1993, Paleoclimate reconstructions from Alaskan ice records: Teleconnections between Pacific—North American (PNA), reverse PNA, and El Niño—Southern oscillation (ENSO) states [abs.]: C1086, p. 93.

Lockwood, Millington, Elms, J.D., Lockridge, P.A., Smith, R.H., Moore, G.W., Nishenko, S.P., Rinehart, W.A., Simkin, Tom, Siebert, Lee, and Newhall, C.G., 1990 (1992), Natural hazards map of the Circum-Pacific Region, Pacific basin sheet: U.S. Geological Survey Circum-Pacific Map Series CP–0035, 31 p., 1 sheet, scale 1:17,000,000. [Revision and reprint]

Madden-McGuire, D.J., and Tripp, R.B., 1993, Geochemical map showing the distribution of gold in the Anchorage 1°×3° quadrangle, Alaska: U.S. Geological Survey Miscellaneous Field Studies Map MF–2227, 1 sheet, scale 1:250,000.

Madden-McGuire, D.J., and Winkler, G.R., 1993, The Alaska Mineral Resources Assessment Program—Background information to accompany mineral-resource and geologic maps of the Anchorage quadrangle, south-central Alaska: U.S. Geological Survey Circular 1094, 23 p.

Mamet, B.L., Pinard, Sylvie, and Armstrong, A.K., 1993, Micropaleontological zonation (foraminifers, algae) and stratigraphy, Carboniferous Peratrovich Formation, southeastern Alaska: U.S. Geological Survey Bulletin 2031, 32 p., 16 pls., 4 sheets.

Mayo, L.R., 1993, Glacier growth and shrinkage related to climate variations and nonclimatic factors in Alaska [abs.]: C1086, p. 97–98.

McCormick, Michael, Barnes, P.W., and Reimnitz, Erk, 1993, Studies of sediment transport by Beaufort Gyre pack ice, 1992: sediment, ice & water data: U.S. Geological Survey Open-File Report 93-19, 39 p.

Menzie, W.D., and Singer, D.A., 1993, Grade and tonnage model of porphyry Cu deposits in British Columbia, Canada, and Alaska, U.S.A.: U.S. Geological Survey Open-File Report 93-275, 9 p.

Miller, T.P., 1993, Volcanic ash and aircraft: U.S. Geological Survey Yearbook, fiscal year 1992, partnership in the earth sciences: p. 57–59. [Mt. Spurr, Redoubt, and Augustine volcanoes.]

Molnia, B.F., 1993, Glacier monitoring for global change—Three case studies [abs.]: C1086, p. 99–100. [Bering, Malaspina, Mendenhall glaciers.]

Morin, R.L., 1993, Digital terrain in the Bethel, Russian Mission, and Goodnews Bay 1°×3° quadrangles, Alaska, including improved terrain for parts of these quadrangles: U.S. Geological Survey Open-File Report 93-702–A (paper copy, 9 p.) and Open-File Report 93-702–B (terrain data on diskette).

———1994, Principal facts for gravity data in the Bethel and Russian Mission 1°×3° quadrangles, Alaska: U.S. Geological Survey Open-File Report 94-14–A (paper copy, 6 p.) and Open-File Report 94-14–B (gravity data on diskette).

Murphy, J.M., Fuis, G.S., Levander, A.R., Lutter, W.J., Criley, E.E., Henrys, S.A., Asudeh, Isa, and Fowler, J.C., 1993, Data report for the 1990 seismic reflection/refraction experiment in the Brooks Range, arctic Alaska: U.S. Geological Survey Open-File Report 93-265, 128 p.

Neal, C.A., McGimsey, R.G., Doukas, M.P., and Ellersieck, Inyo, 1993, Photographs of the 1992 eruptions of Crater Peak, Spurr Volcano, Alaska: U.S. Geological Survey Open-File Report 93-707, 9 p., 20 color slides.

Nelson, S.W., and Nelson, M.S., 1993, Geochemistry of ophiolitic rocks from Knight Island, Prince William Sound, Alaska: B2068, p. 130–142.

Nokleberg, W.J., Bundtzen, T.K., Grybeck, Donald, Koch, R.D., Eremin, R.A., Rozenblum, I.S., Sidorov, A.A., Byalobzhesky, S.G., Sosunov, G.M., Shpikerman, V.I., and Gorodinsky, M.E., 1993, Metallogenesis of mainland Alaska and the Russian northeast: U.S. Geological Survey Open-File Report 93-339, 230 p., 3 sheets, scale 1:4,000,000.

O'Sullivan, P.B., Murphy, J.M., Moore, T.E., and Howell, D.G., 1993, Results of 110 apatite fission track analyses from the Brooks Range and North Slope of northern Alaska, completed in cooperation with the Trans-Alaska Crustal Transect (TACT): U.S. Geological Survey Open-File Report 93-545, 104 p.

Philpotts, John, Taylor, Cliff, Evans, John, and Emsbo, Poul, 1993, Newly discovered molybdenite occurrences at Dora Bay, Prince of Wales Island, southeast Alaska, and preliminary scanning electron microscope studies: B2068, p. 187–196.

Plafker, George, 1993, Alaska geologic earthquake hazards: OF93-195, v. 2, p. 584–587.

Power, J.A., March, G.D., Lahr, J.C., Jolly, A.D., and Cruse, G.R., 1993, Catalog of earthquake hypocenters at Redoubt Volcano and Mt. Spurr, Alaska: October 12, 1989—December 31, 1990: U.S. Geological Survey Open-File Report 93-685–A (paper copy, 57 p.) and Open-File Report 93-685–B (5.25-inch diskette).

Powers, R.B., ed., 1993, Petroleum exploration plays and resources estimates, 1989, onshore United States—Region 1, Alaska; Region 2, Pacific Coast: U.S. Geological Survey Bulletin 2034–A, 138 p.

Richter, D.H., Smith, J.G., Schmoll, H.R., and Smith, R.L., 1993, Geologic map of the Nabesna B-6 quadrangle, south-central Alaska: U.S. Geological Survey Geologic Quadrangle Map GQ–1688, 1 sheet, color, scale 1:63,360.

Rickman, R.L., 1993, Hydrologic conditions and low-flow investigations of the lower Bradley River near Homer, Alaska, October 1991 to February 1992: U.S. Geological Survey Open-File Report 93-95, 17 p.

Riehle, J.R., and Detterman, R.L., 1993, Quaternary geologic map of the Mount Katmai quadrangle and adjacent parts of the Naknek and Afognak quadrangles, Alaska: U.S. Geological Survey Miscellaneous Investigations Series Map I–2032, scale 1:250,000.

Schenk, C.J., and Bird, K.J., 1993, Depositional sequence in Lower Cretaceous rocks, Atigun syncline and Slope Mountain areas, Alaskan North Slope: B2068, p. 48–58.

Schneider, J.L., ed., 1993, 1993 annual report on Alaska's mineral resources: U.S. Geological Survey Circular 1102, 70 p.

Scholl, D.W., and Hart, P.E., 1993, Velocity and amplitude structures on seismic-reflection profiles—Possible massive gas-hydrate deposits and underlying gas accumulations in the Bering Sea basin: U.S. Geological Survey Professional Paper 1570, p. 331–351.

Schumann, R.R., 1993, Geologic radon potential of EPA region 10: Alaska, Idaho, Oregon, and Washington: U.S. Geological Survey Open-File Report 93-292–J, 146 p.

Schwab, W.C., and Lee, H.J., 1993, Processes controlling the style of mass movement in glaciomarine sediment: Northeastern Gulf of Alaska: U.S. Geological Survey Bulletin 2002, p. 135–142.

Shasby, M.B., 1993, Baseline studies for monitoring global climate change in the arctic environment: A remote sensing-spatial data base approach [abs.]: C1086, p. 109.

Shasby, [M.B.] Mark, and Eidenshink, Jeff, 1993, Arctic region—Sensitive indicator of global change: U.S. Geological Survey Yearbook, fiscal year 1992, partnership in the earth sciences: p. 76–77. [Remote sensing studies, GIS.]

Stover, C.W., and Coffman, J.L., 1993, Seismicity of the United States 1568–1989 (Revised): U.S. Geological Survey Professional Paper 1527, [Alaska] p. 19–60.

Stricker, G.D., and Affolter, R.H., 1993, Chemical characterization of Alaskan coal [abs.]: U.S. Geological Survey Open-File Report 93-680, p. 3. [Published in Tenth Annual International Pittsburgh Coal Conference Proceedings (1993), p. 1036–1037.]

Till, A.B., Yount, M.E., and Riehle, J.R., 1993, Redoubt Volcano, southern Alaska: A hazard assessment based on eruptive activity through 1968: U.S. Geological Survey Bulletin 1996, 19 p., 1 sheet, scale 1:125,000.

Trabant, D.C., 1993, Some anticipated and measured responses of glaciers to global change in Alaska [abs.]: C1086, p. 113.

Tripp, R.B., Curtin, G.C., Nokleberg, W.J., Huston, D.L., and Hampton, J.R., 1993, Mineralogical maps showing distribution of selected ore-related minerals in the nonmagnetic, heavy-mineral-concentrate fraction of stream sediment from the Mount Hayes 1°×3° quadrangle, eastern Alaska Range, Alaska: U.S. Geological Survey Miscellaneous Field Studies Map MF–1996–E, 13 p., 3 sheets, scale 1:250,000.

Tripp, R.B., and King, H.D., 1993, Maps showing distribution of selected minerals in the nonmagnetic heavy-mineral fraction of stream-sediment samples, Medfra quadrangle, Alaska: U.S. Geological Survey Miscellaneous Field Studies Map MF–2207, 1 sheet, scale 1:250,000.

White, E.R., compiler, 1993, Reports about Alaska in non-USGS publications released in 1992 that include USGS authors: B2068, p. 246–250.

———1993, U.S. Geological Survey reports on Alaska released in 1992: B2068, p. 241–245.

Winkler, G.R., and Plafker, George, 1993, Geologic map of the Cordova and Middleton Island quadrangles, southern Alaska: U.S. Geological Survey Miscellaneous Investigations Series Map I–1984, scale 1:250,000.

Wolfe, J.A., 1993, A method of obtaining climatic parameters from leaf assemblages: B2040, Alaska, p. 18–19.

Zihlman, F.N., and Ambroziak, R.A., 1992, National Energy Research Seismic Library: processed seismic data for 29 lines in the National Petroleum Reserve in Alaska: U.S. Geological Survey Digital Data Series DDS-0005, one CD-ROM disk. [For system requirements and description of data on disk, see "New Publications of the U.S. Geological Survey" List 1018, May 1993, p. 4.]

Reports about Alaska in Non-USGS Publications Released in 1993 that Include USGS Authors

Compiled by Ellen R. White

[Some reports dated 1991 and 1992 did not become available until 1993; they are included in this listing. USGS authors are marked with asterisks (*)]

ABBREVIATIONS

Eos	Eos (American Geophysical Union Transactions), v. 74, no. 43.
Eos2	Eos (American Geophysical Union Transactions), v. 73, no. 43.
GB	Glacier Bay Science Symposium, 3rd, Gustavus, Alaska, 1993, Program: U.S. National Park Service and Friends of Glacier Bay, P.O. Box 135, Gustavus, Alaska 99826, unpaged.
GSA	Geological Society of America Abstracts with Programs, v. 25, no. 5.
ICAM	International Conference on Arctic Margins, Anchorage, Alaska, 1992, ICAM Abstracts, 90 p.

Abers, G.A., Ekström, Göran, *Marlow, M.S., and *Geist, E.L., 1993, Bering Sea earthquake of February 21, 1991: Active faulting along the Bering shelf edge: Journal of Geophysical Research, v. 98, no. B2, p. 2155–2165.

*Affolter, R.H., *Stricker, G.D., *Roberts, S.B., and *Brownfield, M.E., 1992, Geochemical variation of arctic margin low-sulfur Cretaceous and Tertiary coals, North Slope, Alaska [abs.]: ICAM, p. 1.

*Ager, T.A., 1992, Biostratigraphic evidence for an early Pliocene age for Yukon River terrace gravels near Circle, Alaska [abs.]: ICAM, p. 1.

———1992, Ecosystem development in topographically complex south-central Alaska during the late Quaternary [abs.]: ICAM, p. 1.

Anderson, P., Borisova, O., Beaulieu, J.-I., de Vernal, A., Eiriksson, J., Funder, S., Gibbard, P., *Hamilton, T., Harrison, S.P., Houmark-Nielsen, M., Huntley, B., Knudsen, K.L., Larsen, E., Maher, L.J., Matthews, J.V., Jr., Miller, A., Raukas, A., Reeh, N., Robertsson, A.-M., Rutter, N., Schweger, C.E., Sejrup, H.-P., Sher, A., Telka, A., Turner, C., Velichko, A., and Ward, B., 1991, Report of 1st discussion group: The last interglacial in high latitudes of the northern hemisphere: Terrestrial and marine evidence: Quaternary International, v. 10–12, p. 9–28. [The climate and environment of the last interglacial in the Arctic and Subarctic, NATO Advanced Research Workshop, Hanstholm, Denmark, 1990.]

Ashley, G.M., and *Hamilton, T.D., 1993, Fluvial response to late Quaternary climatic fluctuations, central Kobuk Valley, northwestern Alaska: Journal of Sedimentary Petrology, v. 63, no. 5, p. 814–827.

*Attanasi, E.D., *Bird, K.J., and *Mast, R.F., 1993, Economics and the national oil and gas assessment: The case of onshore northern Alaska: American Association of Petroleum Geologists Bulletin, v. 77, no. 3, p. 491–504.

*Barnes, D.F., 1993, Small gravity changes indicate that different processes are involved in post-1964-Alaskan-earthquake elevation changes [abs.]: Eos, p. 95.

*Barnes, P.W., and *Reimnitz, Erk, 1992, Sediment entrainment and transport by ice: Influence of climate warming with observations from the Great Lakes and the Arctic [abs.]: Eos2, p. 302.

Beaudoin, B.C., Christensen, N.I., *Fuis, G.S., *Lutter, W.J., *Mooney, W.D., *Moore, T.E., and *Nokleberg, W.J., 1993, TACT refraction/wide-angle reflection profiling of the Yukon-Tanana Uplands, east-central Alaska [abs.]: GSA, p. 8.

*Belkin, H.E., and Sparck, H.M., 1993, Mercury, arsenic, antimony, and selenium contents of sediment from the Kuskokwim River, Bethel, Alaska, USA: Environmental Geology, v. 22, no. 2, p. 106–110.

*Blodgett, R.B., 1993, *Dutrochus*, a new Microdomatid (Gastropoda) genus from the Middle Devonian (Eifelian) of west-central Alaska: Journal of Paleontology, v. 67, no. 2, p. 194–197.

*Blodgett, R.B., Rohr, D.M., and Clough, J.G., 1992, Late Ordovician brachiopod and gastropod biogeography of arctic Alaska and Chukotka [abs.]: ICAM, p. 11.

Boyd, T.M., *Engdahl, E.R., and *Spence, W., 1993, Comparison of Aleutian aftershock locations: Inferences on the nature of seismic moment release [abs.]: Eos, p. 95.

*Brew, D.A., 1993, Bedrock-geologic and geophysical research in Glacier Bay National Park and Preserve: Unique opportunities of local to global significance [abs.], *in* GB.

*Brew, D.A., and *Ford, A.B., 1993, The Coast plutonic-metamorphic complex between Skagway, Alaska and Fraser, British Columbia—Geologic sketch and road log, *in* Johnston,

S.R., Hart, C.J.R., Mihalynuk, M.G., Brew, D.A., Ford, A.B., Stevens, R.A., and Gordey, S.P., The Northern Intermontane Superterrane, 1993 [Geological Association of Canada—] NUNA Conference, Lakeview Marina, Marsh Lake, Yukon Territory, Canada, [unpublished] field guide, p. 1–19.

———1993, Regional distribution and geologic context of volcanic-rock-hosted massive sulfide deposits in southeastern Alaska and adjacent parts of British Columbia [abs.]: Alaska Miner, v. 21, no. 8, p. 11.

———1993, Regional distribution and geologic context of volcanic-rock-hosted massive sulfide deposits in southeastern Alaska and adjacent parts of British Columbia [abs.], *in* Alaska Miners Association, Juneau Branch, Conference, Juneau, Alaska, 1993, Abstracts of Professional Papers, p. 33–34.

*Brew, D.A., Himmelberg, G.R., *Ford, A.B., and *Loney, R.A., 1993, Magmatic and metamorphic belts and plutonic-metamorphic complexes of southeastern Alaska [abs.]: GSA p. 13.

*Brewer, M.C., 1992, Disposal of drilling muds and cuttings resulting from petroleum exploration and development in arctic Alaska [abs.]: ICAM, p. 7.

*Brocher, T.M., *Fuis, G.S., *Fisher, M.A., *Plafker, George, *Moses, M.J., *Taber, J.J., and Christensen, N.I., 1993, Mapping the megathrust beneath the northern Gulf of Alaska using wide-angle seismic reflection/refraction profiles [abs.]: GSA, p. 13.

*Brouwers, E.M., and De Deckker, Patrick, 1993, Late Maastrichtian and Danian ostracode faunas from northern Alaska: Reconstructions of environment and paleogeography: Palaios, v. 8, no. 2, p. 140–154.

———1992, Late Maastrichtian and Danian ostracode faunas from northern Alaska: Reconstruction of environment and biogeography [abs.]: ICAM, p. 8.

*Brouwers, E.M., and Forester, R.M., 1993, Continental and shallow-marine ostracode assemblages from modern bottom sediments of Vitus Lake, Bering Glacier, southeast Alaska [abs]: Annual Arctic Workshop, 23rd, Bipolar perspectives on processes and records of environmental change, Columbus, Ohio, 1993, Abstracts: Columbus, Ohio, Byrd Polar Research Center, Ohio State University, BPRC Miscellaneous Series M–322, p. 19–20.

Brown, J., *Ferrians, O.J., Jr., Heginbottom, J.A., and Melnikov, E.S., 1992, A new Circumarctic map of permafrost and ground ice conditions [abs.], *in* Lay, L.B., and Everett, L.T., eds., International Sharing of Polar Information Resources, Polar Libraries Colloquy, 14th, Byrd Polar Research Center, The Ohio State University, Columbus, Ohio, 1992, Proceedings: Byrd Polar Research Center BPRC Report 4, p. 353–360.

Bundtzen, T.K., *Miller, M.L., *Nokleberg, W.J., Goryacheck, N.A., Shpikerman, V.I., Eremin, R.A., and Sidorov, A.A., 1993, Late Cretaceous and early Tertiary igneous-related metallogenic belts, Russian Northeast and western Alaska [abs.]: International Mining, Northwest Mining Association, annual convention, 99th, Spokane, Wash., 1993, Pros and cons, abstract booklet, p. 28.

Burkett, P.J., Bennett, R.H., *Schmoll, H.R., and *Olsen, H.W., 1992, TEM microfabric of Alaskan Bootlegger Cove Formation [abs.]: ICAM, p. 8.

Cai, Jinkui, Powell, R.D., and *Carlson, Paul [P.R.], 1993, Temperate glaciomarine depositional sequences interpreted from seismic facies analysis and models of modern depositional systems [abs]: Annual Arctic Workshop, 23rd, Bipolar perspectives on processes and records of environmental change, Columbus, Ohio, 1993, Abstracts: Columbus, Ohio, Byrd Polar Research Center, Ohio State University, BPRC Miscellaneous Series M–322, p. 23–24.

*Carlson, P.R., *Molnia, B.F., and *Post, Austin, 1993, Pre-Holocene and Holocene erosional and depositional history of Bering Trough, and Vitus Lake, Bering Glacier, Alaska [abs.]: Eos, p. 292.

*Carter, L.D., 1992, A chronostratigraphic framework for interpretations of late Quaternary climatic change on the Alaskan arctic coastal plain [abs.]: ICAM, p. 9.

*Casadevall, T., *Chouet, B., *Davies, J., *Dorava, M., *Doukas, M., *Ellersieck, I., *Gardner, C., *Hoblitt, R., *Jolly, A., *Keith, T., *Lahr, J., *Mattox, T., *May, B., *McGimsey, G., *Meyer, D., *Miller, T., *Neal, C., *Page, R., *Paskievitch, J., *Power, J., *Stephens, C., *Trabant, T., *Waitt, R., Beget, J., Dean, K., Eichelberger, J., Harbin, M., Kienle, J., McNutt, S., Swanson, S., Tytgat, G., March, G., Motyka, R.,and Nye, C., principal investigators, 1993, Mt. Spurr's 1992 eruptions: Eos (American Geophysical Union Transactions), v. 74, no. 19, p. 217, 221, and 222.

*Casadevall, T.J., Matson, M., and *Riehle, J.R., 1992, Volcano hazards and aviation safety: Minimizing the threat through improved communications [abs.]: Eos2, p. 68.

*Chouet, B.A., *Page, R.A., *Stephens, C.D., *Lahr, J.C., and *Power, J.A., 1992, Source parameters of the LP swarm preceding the December 14, 1989 eruption of Redoubt Volcano, Alaska [abs.]: Eos2, p. 342–343.

Churcher, C.S., Morgan, A.V., and *Carter, L.D., 1993, *Arctodus simus* from the Alaskan Arctic Slope: Canadian Journal of Earth Sciences, v. 30, no. 5, p. 1007–1013.

*Collett, T.S., 1993, Natural gas hydrates of the Prudhoe Bay and Kuparuk River area, North Slope, Alaska: American Association of Petroleum Geologists Bulletin, v. 77, no. 5, p. 793–812.

———1993, Natural gas production from Arctic gas hydrates [abs.]: American Association of Petroleum Geologists Bulletin, v. 77, no. 9, p. 1614.

*Collett, T.S., and *Bird, K.J., 1993, Gas hydrate surface simulating seismic reflector in the Prudhoe Bay-Kuparuk River region of northern Alaska [abs.]: American Association of Petroleum Geologists, Annual Convention, 1993, New Orleans, La., Program, p. 87.

*Collett, T.S., *Bird, K.J., and *Magoon, L.B., 1993, Subsurface temperatures and geothermal gradients on the North Slope of Alaska: Cold Regions Science and Technology, v. 21, no. 3, p. 275–293.

*Cronin, T.M., Whatley, Robin, Wood, Adrian, Tsukagoshi, Akira, Ikeya, Noriyuki, *Brouwers, E.M., and Briggs, W.M., Jr., 1993, Microfaunal evidence for elevated Pliocene temperatures in the Arctic Ocean: Paleoceanography, v. 8, no. 2, p. 161–173.

*Csejtey, Béla, Jr., *Keith, W.J., *Saltus, W.R., *Morin, R.L., and *Gray, J.E., 1993, Preassessment of the Holy Cross quadrangle, west-central Alaska [abs.]: GSA, p. 25.

*Davis, A.S., *Gunn, S.H., *Gray, L.-B., *Marlow, M.S., and *Wong, F.L., 1993, Petrology and isotopic composition of Quaternary basanites dredged from the Bering Sea continen-

tal margin near Navarin Basin: Canadian Journal of Earth Sciences, v. 30, no. 5, p. 975–984.

*Dawson, P.B., *Chouet, B.A., *Lahr, J.C., and *Page, R.A., 1992, Spatial relationship between LP earthquakes and a shallow three-dimensional velocity anomaly beneath Redoubt Volcano, Alaska [abs.]: Eos2, v. 73, no. 43, p. 343.

Deschu, N., and *Thompson, K., 1993, International gaging station established on the Alsek River [abs.], *in* GB.

*Doukas, M.P., and Bauer, C.I.,1992, Observations of the 18 August, 1992 eruption of Mount Spurr volcano, Alaska, using satellite, seismic and ground observation data [abs.]: Eos2, p. 346.

*Drinkwater, J.L., *Ford, A.B., and *Brew, D.A., 1993, Magnetic susceptibilities of plutonic rock units across the Coast plutonic-metamorphic complex near Juneau, Alaska [abs.]: GSA, p. 32.

Duba, A.G., *Plafker, George, Mathez, E.A., Peach, C.L., Leger, A., Fogel, R.A., and Shankland, T.J., 1993, Electrical conductivity and petrographic studies of Yukon-Tanana terrane rocks imply crustal conductor at depth is metamorphosed carbonaceous flysch [abs.]: Eos, p. 677.

*Dumoulin, J.A., and *Harris, A.G., 1992, Deep-water lithofacies and conodont faunas of the Lisburne Group, western Brooks Range, Alaska [abs.]: ICAM, p. 14.

———1992, Pre-Carboniferous carbonate sequences of the Seward Peninsula and western and central Brooks Range, northern Alaska [abs.]: ICAM, p. 15.

*Engdahl, E.R., Boyd, T.M., and Erich, A., 1993, Fine structure of the Aleutian subduction zone [abs.]: Seismological Research Letters, v. 64, no. 1, p. 15.

Engstrom, D.R., and *Brigham, M.E., 1993, Atmospheric mercury deposition in lakes on Glacier Bay's outer coast [abs.], *in* GB.

Epstein, S., and *Carter, L.D., 1993, The D/H ratio of hydrogen in plant remains which grew 8 to 12×10^3 years B.P. on the North Slope of Alaska [abs.]: Geological Society of America, Abstracts with Programs, v. 25, no. 6, p. A456.

Farmer, G.L., *Ayuso, Robert, and *Plafker, George, 1993, A Coast Mountains provenance for the Valdez and Orca Groups, southern Alaska, based on Nd, Sr, and Pb isotopic evidence: Earth and Planetary Science Letters, v. 116, no. 1/4, p. 9–21.

*Fierstein, Judy, 1992, Emplacement of the Valley of Ten Thousand Smokes ignimbrite from Novarupta (Alaska) on 6 June, 1912 [abs.]: Eos2, p. 636.

*Fisher, M.A., *Brocher, T.M., *Plafker, George, *Bruns, T.R., *Geist, E.L., *Page, R.A., and *Stephens, C.D., 1993, Deep seismic reflections from a young suture zone and the asperity of the great, 1964 Alaskan earthquake [abs.]: Eos, p. 95.

*Ford, A.B., *Arth, J.G., and *Csejtey, Béla, Jr., 1993, Trondhjemite of the Talkeetna Mountains: An unusually large low-K pluton in Alaska [abs.]: GSA, p. 38.

Ford, R.C., and *Snee, L.W., 1993, $^{40}Ar/^{39}Ar$ thermochronology of white mica from the Bluff area, Alaska—The first ages for lode sources of placer gold deposits in the Seward Peninsula [abs.]: Geological Society of America, Abstracts with Programs, v. 25, no. 6, p. A469.

———1993, Age and structural setting of gold-bearing veins, Bluff area, southern Seward Peninsula, Alaska [abs.]: Eos, p. 695.

*Fuis, G.S., *Lutter, W.J., Levander, A.R., and Wissinger, E.S., 1992, Wide-angle reflections help clarify interpretation of the CMP image of the Brooks Range, arctic Alaska [abs.]: Eos2, p. 371.

*Fuis, G.S., and Clowes, R.M., 1993, Comparison of deep structure along three transects of the western North American continental margin: Tectonics, v. 12, no. 6, p. 1420–1435.

*Galloway, J.P., and *Carter, D.L., 1993, Dune activity on the western Arctic Coastal Plain of Alaska coincident with neoglacial cirque-glacier expansion in the Brooks Range [abs]: Annual Arctic Workshop, 23rd, Bipolar perspectives on processes and records of environmental change, Columbus, Ohio, 1993, Abstracts: Columbus, Ohio, Byrd Polar Research Center, Ohio State University, BPRC Miscellaneous Series M–322, p. 35.

*Goldfarb, R.J., *Leach, D.L., and *Pickthorn, W.J., 1991, Source of synorogenic fluids of the northern Cordillera: Evidence from the Juneau gold belt, Alaska, *in* Robert, F., Sheahan, P.A., and Green, S.B., eds., Greenstone gold and crustal evolution, Geological Association of Canada, Mineral Deposits Division NUNA# Conference, Val d'Or, Québec, Canada, 1990, Proceedings, p. 160–161. [#Inuktituk word for "The Earth".]

*Goldfarb, R.J., and *Snee, L.W., 1993, Tectonic setting, high-T thermal events, and gold vein formation within metamorphic rocks of the Alaskan Cordillera [abs.], *in* Alaska Miners Association, Juneau Branch, Conference, Juneau, Alaska, 1993, Abstracts of Professional Papers, p. 21.

*Goldfarb, R.J., *Snee, L.W., and *Pickthorn, W.J., 1993, Orogenesis, high-T thermal events, and gold vein formation within metamorphic rocks of the Alaskan Cordillera: Mineralogical Magazine, v. 57, no. 388, p. 375–394.

*Grantz, Arthur, Chief Scientist, (1992 Arctic Summer West Scientific Party), 1993, Cruise to the Chukchi borderland, Arctic Ocean: Eos (American Geophysical Union Transactions), v. 74, no. 22, p. 240 and 253–254.

*Grantz, Arthur, *May, S.D., *Mullen, M.W., *Gray, L.B., *Lull, J.S., Clark, D.L., and Stevens, C.H., 1993, Northwind Ridge: A continental fragment isolated by Tertiary rifting in the Amerasia Basin, Arctic Ocean [abs.]: Eos, v. 74, no. 43, p. 614.

*Grantz, Arthur, *May, S.D., *Mullen, M.W., *Phillips, R.L., and *Hart, P.E., 1992, Significance of extension and convergence at Northwind Ridge for the tectonic development of the Chukchi borderland, Arctic Ocean [abs.]: ICAM, p. 23.

*Grybeck, D.J., 1993, Status of geology in the Craig and Dixon Entrance quadrangles, southeastern Alaska [abs.], *in* Alaska Miners Association, Juneau Branch, Conference, Juneau, Alaska, 1993, Abstracts of Professional Papers, p. 11.

*Hamilton, T.D., and Brigham-Grette, Julie, 1991, The last interglaciation in Alaska: Stratigraphy and paleoecology of potential sites: Quaternary International, v. 10–12, p. 49–71.

*Hamilton, T.D., and Ashley, G.M., 1993, Epiguruk: A late Quaternary environmental record from northwestern Alaska: Geological Society of America Bulletin, v. 105, no. 5, p. 583–602.

*Hamilton, T.D., Ashley, G.M., Reed, K.M., and Schweger, C.E., 1993, Late Pleistocene vertebrates and other fossils from Epiguruk, northwestern Alaska: Quaternary Research, v. 39, no. 3, p. 381–389.

*Hammarstrom, J.M., and *Brew, D.A., 1993, Petrology and geobarometry of Admiralty-Revillagigedo belt granitoids near Petersburg, southeastern Alaska [abs.]: GSA, p. 47.

*Hammond, W.R., *Lahr, J.C., Rowe, C.A., and Benoit, J.P., 1993, The Salcha seismic zone near Fairbanks, Alaska [abs.]: Eos, p. 417–418.

Harbin, M.L., Swanson, S.E., Nye, C.J., and *Miller, T.P., 1992, Glass and mineral chemistry of the June 27, 1992 eruption of Mount Spurr, Alaska [abs.]: Eos2, p. 346.

*Heinrichs, T.A., 1993, Black Rapids Glacier, Alaska—Observations during the quiescent phase of a surge-type glacier [abs.]: Eos, p. 233.

*Hildreth, Wes, and *Fierstein, Judy, 1992, Hydrothermal explosion breccia emplaced during caldera collapse of Mount Katmai, Alaska, on 6 June 1912 [abs.]: Eos2, p. 635–636.

Himmelberg, G.R., *Brew, D.A., and *Ford, A.B., 1993, Low-grade, M1 metamorphism of the western metamorphic belt near Juneau, Alaska [abs.]: GSA, p. 52.

*Horton, R.J., 1993, Airborne geophysical surveys of the Annette Islands Reserve [abs.]: International Mining, Northwest Mining Association, annual convention, 99th, Spokane, Wash., 1993, Pros and cons, abstract booklet, p. 10.

———1993, Mineral resource assessment of the Annette Islands Reserve, southeast Alaska [abs.]: International Mining, Northwest Mining Association, annual convention, 99th, Spokane, Wash., 1993, Pros and cons, abstract booklet, p. 12.

*Ishman, S.E., Polyak, L.V., and *Poore, R.Z., 1993, A benthic foraminifer record of Pleistocene deep arctic oceanographic change: Canada Basin, western Arctic Ocean [abs.]: Geological Society of America, Abstracts with Programs, v. 25, no. 6, p. A454.

Johnson, J.G., and *Blodgett, R.B., 1993, Russian Devonian brachiopod genera *Cyrtinoides* and *Komiella* in North America: Journal of Paleontology, v. 67, no. 6, p. 952–958. ["...identified from west-central Alaska..."]

*Johnsson, M.J., 1993, Unroofing and chemical/mechanical weathering as controls on sandstone composition: The Brookian sequence of northern Alaska [abs.], *in* Society of Economic Paleontology and Mineralogy, Stratigraphic record of global change, 1993 meeting, Penn State University Campus, State College, Pennsylvania: Society for Sedimentary Geology, Abstracts with Program, p. 19–20.

*Johnsson, M.J., *Howell, D.G., and *Bird, K.J., 1993, Thermal maturity patterns in Alaska: Implications for tectonic evolution and hydrocarbon potential: American Association of Petroleum Geologists Bulletin, v. 77, no. 11, p. 1874–1903.

Jolly, A.D., *Power, J.A., *Page, R.A., *Lahr, J.C., and *Stephens, C.D., 1992, A comparison of baseline and pre-eruption depths of seismicity at Mt. Spurr volcano, south-central Alaska [abs.]: Eos2, p. 342.

*Karl, S.M., 1993, The geology of Annette Island [abs.]: International Mining, Northwest Mining Association, annual convention, 99th, Spokane, Wash., 1993, Pros and cons, abstract booklet, p. 10.

———1993, Triassic volcanic and sedimentary rocks, Annette Island, southeastern Alaska [abs.], *in* Alaska Miners Association, Juneau Branch, Conference, Juneau, Alaska, 1993, Abstracts of Professional Papers, p. 37.

Kaufman, D.S., *Carter, L.D., Miller, G.H., Farmer, G.L., and Budd, D.A., 1993, Strontium isotopic composition of Pliocene and Pleistocene molluscs from emerged marine deposits, North American Arctic: Canadian Journal of Earth Sciences, v. 30, no. 3, p. 519–534.

*Kelley, J.S., *Wrucke, C.T., and Lane, L.S., 1992, Pre-Mississippian rocks in a transect in the Clarence and Malcolm Rivers area, Alaska and Yukon Territory [abs.]: ICAM, p. 64.

Knight, J., 1993, Comment on "Preliminary evidence for the involvement of budding bacteria in the origin of Alaskan placer gold": Geology, v. 21, no. 3, p. 279–280. *Watterson, J.R., 1993, Reply: Geology, v. 21, no. 3, p. 280. Original paper: Watterson, J.R., 1992, Preliminary evidence for the involvement of budding bacteria in the origin of Alaskan placer gold: Geology, v. 20, p. 315–318.

*Koch, R.D.,1993, Overview of granitic rocks in the Bradfield Canal area, southeastern Alaska [abs.]: GSA, p. 63.

Kodosky, L.G., and *Keith, T.E.C., 1993, Factors controlling the geochemical evolution of fumarolic encrustations, Valley of Ten Thousand Smokes, Alaska: Journal of Volcanology and Geothermal Research, v. 55, no. 3/4, p. 185–200.

Krumhardt, A.P., *Harris, A.G., and Watts, K.F., 1992, Conodont biostratigraphy and biofacies of the Wahoo Limestone (Carboniferous), eastern Sadlerochit Mountains, northeast Brooks Range, Alaska [abs.]: ICAM, p. 31.

Kusky, T.M., *Bradley, D.C., *Haeussler, Peter, *Karl, S.M., and Donley, D.T., 1993, The Chugach Bay thrust, a major tectonic boundary in the southern Alaska accretionary prism [abs.]: Geological Society of America, Abstracts with Programs, v. 25, no. 6, p. A282.

*Kvenvolden, K.A., *Lorenson, T.D., and Lilley, M.D., 1992, Methane in the Beaufort Sea on the continental shelf of Alaska [abs.]: Eos2, p. 309.

*Kvenvolden, K.A., *Lorenson, T.D., and Reeburgh, W.S., 1992, Methane in permafrost—Preliminary studies at the CRREL permafrost tunnel near Fox, Alaska [abs.]: Eos2, p. 119.

*Kvenvolden, K.A., 1993, Gas hydrates—Geological perspective and global change: Reviews of Geophysics, v. 31, no. 2, p. 173–187. (Refers as example to Prudhoe Bay, Beaufort Sea, Alaska.)

*Kvenvolden, K.A., *Carlson, P.R., *Threlkeld, C.N., and *Warden, Augusta, 1993, Possible connection between two Alaskan catastrophes occurring 25 yr apart (1964 and 1989): Geology, v. 21, no. 9, p. 813–816.

*Kvenvolden, K.A., Lilley, M.D., *Lorenson, T.D., *Barnes, P.W., and McLaughlin, Elizabeth, 1993, The Beaufort Sea continental shelf as a seasonal source of atmospheric methane: Geophysical Research Letters, v. 20, no. 22, p. 2459–2462.

*Lahr, J.C., *Fogleman, K.A., *Stephens, C.D., and *Page, R.A., 1993, Stresses within the Pacific plate of southern Alaska [abs.]: Eos, p. 95.

Lange, I.M., *Nokleberg, W.J., Newkirk, S.R., *Aleinikoff, J.N., *Church, S.E., and Krouse, H.R., 1993, Devonian volcanogenic massive sulfide deposits and occurrences, southern Yukon-Tanana terrane, eastern Alaska Range, Alaska: Economic Geology, v. 88, no. 2, p. 344–376.

*Light, T.D., Moll, S.H., Bie, S.W., and *Lee, G.K., 1993, Reconnaissance guidelines for gold exploration in central Alaska: Journal of Geochemical Exploration, v. 47, no. 1/3, p. 89–108.

*Lisowski, M., *Savage, J.C., *Svarc, J.L., and *Prescott, W.H., 1993, Deformation across the Alaska-Aleutian subduction zone near Kodiak, Alaska [abs.]: Eos, p. 191.

*Loney, R.A., and Himmelberg, G.R., 1993, Characteristics and petrogenesis of Alaskan-type ultramafic-gabbro intrusions, southeastern Alaska [abs.]: GSA, p. 111.

*Lutter, W.J., *Fuis, G.S., Levander, A.R., and Wissinger, E.S., 1992, A velocity structure of the northern Brooks Range/North Slope from inversion of secondary arrivals from the 1990 seismic experiment [abs.]: Eos2, p. 371.

*Marincovich, Louie, Jr., 1992, Earliest Cenozoic (Danian) paleogeography of the Arctic Ocean [abs.]: ICAM, p. 35.

*Marincovich, Louie, Jr., 1993, Danian mollusks from the Prince Creek Formation, northern Alaska, and implications for Arctic Ocean paleogeography: Journal of Paleontology, v. 67, suppl. 5, pt. III of III, Paleontological Society Memoir 35, 35 p.

———1993, Delayed extinction of Mesozoic marine mollusks in the Paleocene Arctic Ocean basin [abs.]: Geological Society of America, Abstracts with Programs, v. 25, no. 6, p. A295.

———1993, Paleogeographic implications of coeval "Mesozoic" and Paleocene mollusks, arctic Alaska [abs.]: America Association of Petroleum Geologists Bulletin, v. 77, no. 4, p. 707.

*McGimsey, R.G., and *Dorava, J.M., 1992, Eruption of Mount Spurr volcano, Alaska, August 18, 1992: Video footage [abs.]: Eos2, p. 345–346.

*Meyer, D.F., and *Trabant, D.C., 1992, Lahar-producing events and non-lahar-producing events at glacier-clad Cook Inlet volcanoes, Alaska [abs.]: Eos2, p. 346.

*Miller, C.D., *Ewert, J.W., *Lockhart, A.B., and Heyman, B.N., 1992, The USGS/OFDA volcano disaster assistance program [abs.]: Eos2, p. 68.

Miller, L.D., and *Goldfarb, R.J., 1993, Tectonic development and structural control of the auriferous vein deposits in the Juneau gold belt, southeastern Alaska [abs.], *in* Alaska Miners Association, Juneau Branch, Conference, Juneau, Alaska, 1993, Abstracts of Professional Papers, p. 19.

Miller, L.D., *Goldfarb, R.J., Gehrels, G.E., and *Snee, L.W., 1993, Genetic links between fluid cycling, vein formation, regional deformation, and plutonism in the Juneau gold belt, southeastern Alaska [abs.]: Geological Society of America, Abstracts with Programs, v. 25, no. 6, p. A78–79.

*Miller, T.P., *Power, J.A., Eichelberger, J.C., McNutt, S.R., and Davies, J.N., 1992, The 1989–90 Redoubt and 1992 Mt. Spurr volcanic eruptions: Response procedure of the Alaska Volcano Observatory [abs.]: Eos2, p. 68.

*Miller, T.P., McNutt, S.R., Eichelberger, J.C., and *Neal, C.A., 1992, The 1992 eruptions of Mt. Spurr volcano, Alaska: An overview [abs.]: Eos2, p. 342.

*Molnia, B.F., and *Trabant, D.C., 1992, Ice-thickness measurements on Bering Glacier, Alaska, and their relations to satellite and airborne SAR image patterns [abs.]: Eos2, p. 181.

*Molnia, B.F., 1993, Major glacier surge continues: Eos (American Geophysical Union Transactions), v. 74, no. 45, p. 521 and 524.

———1993, Major surge of the Bering Glacier: Eos (American Geophysical Union Transactions), v. 74, no. 29, July 20, p. 321 [Fig. 1 - photograph], p. 322 [text].

*Molnia, B.F., *Post, Austin, and *Carlson, P.R., 1993, Morphology and sedimentary processes: Ice-marginal Vitus Lake, Bering Glacier, Alaska [abs.]: Eos, p. 292.

*Molnia, B.F., *Post, Austin, *Trabant, D.C., and *Krimmel, Robert, 1993, 1993 surge of Bering Glacier, Alaska [abs.]: Eos, p. 263.

*Moore, T.E., Wallace, W.K., *Bird, K.J., *Karl, S.M., and Mull, C.G., 1992, Depositional model for the Ellesmerian sequence and tectonic history of the Brookian orogen, northern Alaska [abs.]: ICAM, p. 37.

*Moore, T.E., *Aleinikoff, J.N., and *Walter, Marianne, 1993, Middle Jurassic U-Pb crystallization for Siniktanneyak Mountain ophiolite, Brooks Range, Alaska [abs.]: GSA, p. 124.

*Morin, R.L., 1993, Mafic and ultramafic rocks of the northwestern Brooks Range of Alaska produce nearly symmetric gravity anomalies [abs.]: GSA, p. 124.

Morrissey, M.M., *Chouet, B.A., and Kieffer, S.W., 1993, Shock-pattern oscillation as the triggering mechanism for long-period seismicity at Redoubt Volcano, Alaska 1989–90 [abs.]: Eos, p. 649.

Mortera-Gutierrez, C.A., Carlson, R.L., *Scholl, D.W., and *Vallier, T.L., 1992, Azimuthal differences of fault fabric in the outer rise of the western Aleutian Trench [abs.]: Eos2, p. 527.

Motyka, R.J., and *Post, A., 1993, Taku Glacier: Influence of accumulation to total area ratio, channel geometry, and river sedimentation on the advance of a fjord-type glacier [abs.], *in* GB.

Mozley, P.S., *Carothers, W.W., and *Bird, K.J., 1993, Geochemistry of authigenic minerals in the Ivishak Formation, North Slope, Alaska [abs.]: Geological Society of America, Abstracts with Programs, v. 25, no. 6, p. A318.

*Mullen, M.W., 1992, Biostratigraphy and paleoecology of Cretaceous foraminifera from Northwind Ridge cores, Arctic Ocean [abs.]: ICAM, p. 40.

Murphy, J.M., *Patton, W.W., Jr., and *Till, A.B., 1992, Thermal structure and post-accretionary fault segmentation of west-central Alaska [abs.]: ICAM, p. 61.

*Murray, T.L., *Kleinman, J.W., *Iwatsubo, E.Y., and *Dzurisin, D., 1992, Establishment of a permanent radio-telemetered GPS network on Augustine volcano, Cook Inlet, Alaska [abs.]: Eos2, p. 124.

*Neal, C.A., *McGimsey, R.G., Braitseva, O., *Miller, T.P., Eichelberger, J.C., and Nye, C., 1992, Post-caldera eruptive history of Aniakchak caldera, Alaska [abs.]: Eos2, p. 645.

*Neal, C.A., *McGimsey, R.G., *Doukas, M.P., *Miller, T.P., *Richter, D., *Paskievitch, J.F., and *Ellersieck, I., 1992, The August 18, 1992 eruption of Mount Spurr volcano, Alaska: Tephra-fall stratigraphy, distribution and impact [abs.]: Eos2, p. 342.

Nelson, B.K., *Nelson, S.W., and *Till, A.B., 1993, Nd- and Sr-isotope evidence for Proterozoic and Paleozoic crustal evolution in the Brooks Range, northern Alaska: Journal of Geology, v. 101, no. 4, p. 435–450.

*Nelson, S.W., Foley, J.Y., and Nelson, B.K., 1992, Metal-rich lamprophyric and associated alkaline mafic, ultramafic, and intermediate to felsic rocks from composite plutons, central Alaska Range, Alaska [abs.]: ICAM, p. 43.

*Newberry, R.J., and *Brew, D.A., 1993, The alkalic connection (?) in the Juneau gold belt [abs.], *in* Alaska Miners Association, Juneau Branch, Conference, Juneau, Alaska, 1993, Abstracts of Professional Papers, p. 25–26.

*Nokleberg, W.J., *Grantz, A., *Patton, W.W., Jr., *Plafker, George, *Scholl, D.W., *Tabor, R.W., *Vallier, T.L., Fujita, K., Natal'in, B.A., Parfenov, L.M., Khanchuk, A.I., Sokolov,

S.D., Tsukanov, N.V., Natapov, L.M., Monger, J.W.H., Gordey, S.P., and Feeney, T.D., 1992, Circum-North Pacific terrane map [abs.]: ICAM, p. 44.

*Nokleberg, W.J., Lange, I.M., *Schmidt, J.M., and *Zierenberg, R.A., 1992, Metallogenesis of stratiform zinc-lead-silver and associated barite deposits, northwestern Brooks Range, Alaska, *in* Circum-Pacific Council, Symposium on Tectonics, Energy, and Mineral Resources of the Northwest Pacific, Khabarovsk, Russia, 1989, Proceedings: Khabarovsk, USSR Academy of Sciences, Far Eastern Division, Institute of Tectonics and Geophysics, v. 2, p. 65–79 [in Russian].

*Nokleberg, W.J., *Grybeck, Donald, Bundtzen, T.K., Shpikerman, V.I., Eremin, R.A., and Sidorov, A.A., 1993, Correlations of lode metallogenic belts between the Russian Northeast and mainland Alaska [abs.]: International Mining, Northwest Mining Association, annual convention, 99th, Spokane, Wash., 1993, Pros and cons, abstract booklet, p. 26.

*Nokleberg, W.J., *Moll-Stalcup, E.J., *Miller, T.P., *Brew, D.A., *Grantz, Arthur, *Plafker, George, *Moore, T.E., and *Patton, W.W., Jr., 1993, Tectono-stratigraphic terrane map of Alaska [abs.]: GSA, p. 127–128.

Nye, C.J., *Miller, T.P., Swanson, S.E., and Harbin, M.L., 1992, Major- and trace-element geochemistry of ejecta from the 1992 eruptions of Crater Peak, Mt. Spurr, Alaska [abs.]: Eos2, p. 346.

Nye, C.J., *Neal, C.A., and *McGimsey, R.G., 1993, Extreme and abrupt transition from tholeiitic to calcalkaline volcanism at Aniakchak Volcano, eastern Aleutian Arc [abs.]: Eos, p. 674.

Ort, M.H., Neal, C.A., McConnell, V.S., Wohletz, K.H., *Duffield, W.A., and Lescinsky, D.T., 1993, Effects of prevailing wind on the distribution of surge and fallout deposits at Ukinrek Maars, Alaska [abs.]: Eos, p. 639.

*Paskievitch, J.F., *Murray, T.L., *Hoblitt, R., and *Neal, C.A., 1992, Lightning associated with the 18 August, 1992 eruption of Mount Spurr [abs.]: Eos2, p. 346.

*Patton, W.W., Jr., Popeko, V.A., Burns, L.E., and *Nelson, S.W., 1992, Collaborative study of ophiolitic terranes of Alaska and NE Russia [abs.]: ICAM, p. 47.

*Patton, W.W., Jr., 1993, Ophiolitic terranes of northern and central Alaska and their correlatives in Canada and northeastern Russia [abs.]: GSA, p. 132.

*Pavlis, T.L., *Sisson, V.B., *Foster, H.L., *Nokleberg, W.J., and *Plafker, George, 1993, Mid-Cretaceous extensional tectonics of the Yukon-Tanana terrane, Trans-Alaska Crustal Transect (TACT), east-central Alaska: Tectonics, v. 12, no. 1, p. 103–122.

*Plafker, George, 1992, Tectonic evolution of Alaska: A preliminary synthesis, *in* Circum-Pacific Council, Symposium on Tectonics, Energy, and Mineral Resources of the Northwest Pacific, Khabarovsk, Russia, 1989, Proceedings: Khabarovsk, USSR Academy of Sciences, Far Eastern Division, Institute of Tectonics and Geophysics, v. 1, p. 92–121 [in Russian].

*Poore, R.Z., *Phillips, R.L., and *Rieck, H.J., 1993, Paleoclimate record for Northwind Ridge, western Arctic Ocean: Paleoceanography, v. 8, no. 2, p. 149–159.

Poulton, T.P., *Detterman, R.L., Hall, R.L., Jones, D.L., Peterson, J.A., Smith, P., Taylor, D.G., Tipper, H.W., and Westermann, G.E.G., 1992, Part III: Regional geology and stratigraphy: 4 Western Canada and the United States, *in* Westermann, G.E.G., ed., The Jurassic of the Circum-Pacific; International Geological Correlation Programme Project 171: New York, Cambridge University Press, p. 29–92.

*Power, J.A., *Jolly, A.D., *Stihler, S.D., *Page, R.A., *Lahr, J.C., and *Stephens, C.D., 1992, A comparison of baseline and pre-eruption depths of seismicity at Mt. Spurr volcano, south-central Alaska [abs.]: Eos2, p. 342.

*Reimnitz, Erk, *Barnes, P.W., and *Weber, W.S., 1993, Particulate matter in pack ice of the Beaufort Gyre: Journal of Glaciology, v. 39, no. 131, p. 186–198.

*Reimnitz, Erk, *McCormick, Michael, *McDougall, Kristin, and *Brouwers, Elisabeth, 1993, Sediment export by ice rafting from a coastal polynya, arctic Alaska, U.S.A.: Arctic and Alpine Research, v. 25, no. 2, p. 83–98.

Reiners, P.W., Nelson, B.K., and *Nelson, S.W., 1992, Nd- and Sr-isotope evidence for enriched mantle in south-central Alaska from Cretaceous-Tertiary composite plutons of the Alaska Range [abs.]: Eos2, p. 622.

———1993, Isotopic and chemical modification of the cumulate mush by partial melts of country rock: Evidence from the composite plutons of the Alaska Range [abs.]: Geological Society of America, Abstracts with Programs, v. 25, no. 6, p. A41.

*Reynolds, R.L., *Tuttle, M.L., and *Rice, C., 1992, Origins and ages of greigite in Cretaceous strata, North Slope basin, Alaska: Constraints from sulfur isotopes and petrography [abs.]: Eos2, p. 137.

———1993, Paleoenvironmental implications of early diagenetic greigite in Cretaceous marine mudstone, North Slope basin, Alaska [abs.]: Geological Society of America, Abstracts with Programs, v. 25, no. 6, p. A239–240.

*Riehle, J.R., Miller, T.F., *McGimsey, R.G., and *Keith, T.E.C., 1992, A comparative profile from the 1912 ash-flow sheet, Katmai National Park, Alaska [abs.]: Eos2, p. 636.

Roeske, S.M., *Snee, L.W., and Bunds, M.P., 1993, $^{40}Ar/^{39}Ar$ dates from the Border Ranges fault system, a hydrothermally altered brittle-ductile transition strike-slip shear zone, southern Alaska [abs.]: Geological Society of America, Abstracts with Programs, v. 25, no. 6, p. A419.

*Ryan, H.F., and *Scholl, D.W., 1993, Geologic implications of great interplate earthquakes along the Aleutian arc: Journal of Geophysical Research, v. 98, no. B12, p. 22,135–22,146.

Sainsbury, C.L., (Pete), 1993, Geology and geochemistry of volcanogenic massive sulfide deposits and related igneous rocks, Prince William Sound, south-central Alaska—A discussion: Economic Geology, v. 88, no. 5, p. 1284–1285.
Crowe, D.E., *Nelson, S.W., Brown, P.E., *Shanks, W.C., III, and Valley, J.W., 1993, Geology and geochemistry of volcanogenic massive sulfide deposits and related igneous rocks, Prince William Sound, south-central Alaska—A reply: Economic Geology, v. 88, no. 5, p. 1285–1288. Original article *in* Economic Geology, v. 87, no. 7, 1992, p. 1722–1746.

Sauber, Jeanne, and *Plafker, George, 1993, Predicted displacement field associated with the recession of glaciers in the eastern Chugach Mountains, Alaska [abs.]: Eos, p. 181.

*Schmidt, J.M., and Werdon, M.B., 1993, Clastic-hosted stratiform, vein/breccia and disseminated Zn-Pb-Ag deposits of the northwestern Brooks Range, AK: Are they different ex-

pressions of dewatering of the same source basin? [abs.]: GSA p. 143.

Sheppard, D.S., *Janik, C.J., and *Keith, T.E.C., 1993, Gas compositions from fumaroles in Katmai National Park volcanoes and in the 1912 ash flow sheet [abs.], *in* International Association of Volcanology and Chemistry of the Earth's Interior, Ancient volcanism and modern analogues, IAVCEI General Assembly, Canberra, Australia, 1993, Abstracts, p. 99.

Siok, J.P., and *Harris, A.G., 1992, Enigmatic conodonts from the uppermost Lisburne Group—Implications for Pennsylvanian reconstructions, central Brooks Range [abs.]: ICAM, p. 55.

*Sliter, R.W., *Vallier, T.L., *McCarthy, Jill, and *Geist, E.L., 1992, Multichannel seismic reflection and GLORIA images of the obliquely convergent western Aleutian Arc [abs.]: Eos2, p. 527.

*Starratt, S.W., 1993, Late Quaternary diatoms from the Canadian Basin abyssal plain east of Northwind Ridge, Chukchi Sea: Evidence for the re-establishment of the Chukchi Sea—Central Arctic Ocean connection and (or) middle Holocene warming [abs.]: Eos, p. 327.

———1993, Late Quaternary paleoceanography of the Pervenets Canyon area of the Bering Sea: Evidence from the diatom flora: Diatom Research, v. 8, no. 1, p. 159–170.

———1993, Quaternary diatoms from the Canadian basin abyssal plain east of the Northwind Ridge, Chukchi Sea: Evidence for the reconnection of the Bering Sea and the central Arctic Ocean and (or) middle Holocene warming [abs.]: Geological Society of America, Abstracts with Programs, v. 25, no. 6, p. A328.

*Stricker, G.D., 1992, Cretaceous coals in Alaska's arctic margin (North Slope)—Geology and resources [abs.]: ICAM, p. 59.

Swanson, S.E., Harbin, M.L., *Miller, T.P., and Nye, C.J., 1992, Use of tephra as a petrologic tool: An example from the 1992 eruptions of Mt. Spurr, Alaska [abs.]: Eos2, p. 346.

*Tailleur, I.L., 1993, Paleogeographic context of Brookian mafic/ultramafic rocks, Alaska [abs.]: GSA, p. 153.

*Till, A.B., *Box, S.E., Roeske, S.M., and *Patton, W.W., Jr., 1993, Comment on "Mid-Cretaceous extensional fragmentation of a Jurassic-Early Cretaceous compressional orogen, Alaska" by E.L. Miller and T.L. Hudson: Tectonics, v. 12, no. 4, p. 1076–1081. Miller, E.L., and Hudson, T.L., 1993, Reply: Tectonics, v. 12, no. 4, p. 1082–1086. Original paper: Miller, E.L., and Hudson, T.L., 1991, Mid-Cretaceous extensional fragmentation of a Jurassic-Early Cretaceous compressional orogen, Alaska: Tectonics, v. 10, p. 781–796.

*Till, A.B., and *Snee, L.W., 1993, Interpretation of complex $^{40}Ar/^{39}Ar$ age spectra from white mica in blueschist-facies rocks of the Brooks Range using combined electron microprobe quantitative analysis and backscatter imaging [abs.]: Geological Society of America, Abstracts with Programs, v. 25, no. 6, p. A172.

*Trabant, D.C., 1993, Time-lapse photography of the 1993 surge of Bering Glacier, Alaska [abs.]: Eos, p. 233.

*Tripp, R.B., and *Cathrall, J.B., 1993, Hidden gems in the NURE data: Placer exploration potential for Au, PGM, REE, and other metals in the Arctic coastal plain and foothills provinces, Alaska: Explore, Newsletter for the Association of Exploration Geochemists, no. 79, April 1993, p. 10–12.

von Hillebrandt, A., Westermann, G.E.G., Callomon, J.H., and *Detterman, R.L., 1992, Ammonites of the circum-Pacific region, *in* Westermann, G.E.G., ed., The Jurassic of the Circum-Pacific; International Geological Correlation Programme Project 171: New York, Cambridge University Press, p. 342–359. [Appendix: Biochronology and atlas with index and guide fossils: p. 381–382, Alaska: plate 1–4, 23–33, and 77.]

Watts, K.F., Krumhardt, A.P., Imm, T.A., Morgan, S.K., and *Harris, A.G., 1992, Unconformity above the Lisburne Group—A major Pennsylvanian-Permian hiatus in the northeastern Brooks Range, Alaska [abs.]: ICAM, p. 64.

*Waythomas, C.F., 1993, Geomorphic evidence of post-glacial uplift, northern Adak Island, Alaska [abs.]: Eos, p. 233.

Wissinger, E.S., Oldow, J.S., Levander, A.R., *Fuis, G.S., and *Lutter, W.J., 1992, Interpretation of near vertical incidence data from the 1990 Brooks Range seismic experiment [abs.]: Eos2, p. 371.

Wissinger, E.S., Levander, A., Holliger, K., Oldow, J.S., and *Fuis, G.S., 1993, Crustal reflectivity in the Brooks Range, arctic Alaska [abs.]: Eos, p. 415.

☆U.S. GOVERNMENT PRINTING OFFICE: 1994-683-048/10013

SELECTED SERIES OF U.S. GEOLOGICAL SURVEY PUBLICATIONS

Periodicals

Earthquakes & Volcanoes (issued bimonthly).
Preliminary Determination of Epicenters (issued monthly).

Technical Books and Reports

Professional Papers are mainly comprehensive scientific reports of wide and lasting interest and importance to professional scientists and engineers. Included are reports on the results of resource studies and of topographic, hydrologic, and geologic investigations. They also include collections of related papers addressing different aspects of a single scientific topic.

Bulletins contain significant data and interpretations that are of lasting scientific interest but are generally more limited in scope or geographic coverage than Professional Papers. They include the results of resource studies and of geologic and topographic investigations, as well as collections of short papers related to a specific topic.

Water-Supply Papers are comprehensive reports that present significant interpretive results of hydrologic investigations of wide interest to professional geologists, hydrologists, and engineers. The series covers investigations in all phases of hydrology, including hydrogeology, availability of water, quality of water, and use of water.

Circulars present administrative information or important scientific information of wide popular interest in a format designed for distribution at no cost to the public. Information is usually of short-term interest.

Water-Resource Investigations Reports are papers of an interpretive nature made available to the public outside the formal USGS publications series. Copies are reproduced on request unlike formal USGS publications, and they are also available for public inspection at depositories indicated in USGS catalogs.

Open-File Reports include unpublished manuscript reports, maps, and other material that are made available for public consultation at depositories. They are a nonpermanent form of publication that may be cited in other publications as sources of information.

Maps

Geologic Quadrangle Maps are multicolor geologic maps on topographic bases in 7 1/2- or 15-minute quadrangle formats (scales mainly 1:24,000 or 1:62,500) showing bedrock, surficial, or engineering geology. Maps generally include brief texts; some maps include structure and columnar sections only.

Geophysical Investigations Maps are on topographic or planimetric bases at various scales; they show results of surveys using geophysical techniques, such as gravity, magnetic, seismic, or radioactivity, which reflect subsurface structures that are of economic or geologic significance. Many maps include correlations with the geology.

Miscellaneous Investigations Series Maps are on planimetric or topographic bases of regular and irregular areas at various scales; they present a wide variety of format and subject matter. The series also includes 7 1/2-minute quadrangle photogeologic maps on planimetric bases that show geology as interpreted from aerial photographs. Series also includes maps of Mars and the Moon.

Coal Investigations Maps are geologic maps on topographic or planimetric bases at various scales showing bedrock or surficial geology, stratigraphy, and structural relations in certain coal-resource areas.

Oil and Gas Investigations Charts show stratigraphic information for certain oil and gas fields and other areas having petroleum potential.

Miscellaneous Field Studies Maps are multicolor or black-and-white maps on topographic or planimetric bases on quadrangle or irregular areas at various scales. Pre-1971 maps show bedrock geology in relation to specific mining or mineral-deposit problems; post-1971 maps are primarily black-and-white maps on various subjects, such as environmental studies or wilderness mineral investigations.

Hydrologic Investigations Atlases are multicolor or black-and-white maps on topographic or planimetric bases presenting a wide range of geohydrologic data of both regular and irregular areas; principal scale is 1:24,000, and regional studies are at 1:250,000 scale or smaller.

Catalogs

Permanent catalogs, as well as some others, giving comprehensive listings of U.S. Geological Survey publications are available under the conditions indicated below from the U.S. Geological Survey, Books and Open-File Reports Sales, Federal Center, Box 25286, Denver, CO 80225. (See latest Price and Availability List.)

"Publications of the Geological Survey, 1879-1961" may be purchased by mail and over the counter in paperback book form and as a set of microfiche.

"Publications of the Geological Survey, 1962-1970" may be purchased by mail and over the counter in paperback book form and as a set of microfiche.

"Publications of the Geological Survey, 1971-1981" may be purchased by mail and over the counter in paperback book form (two volumes, publications listing and index) and as a set of microfiche.

Supplements for 1982, 1983, 1984, 1985, 1986, and for subsequent years since the last permanent catalog may be purchased by mail and over the counter in paperback book form.

State catalogs, "List of U.S. Geological Survey Geologic and Water-Supply Reports and Maps For (State)," may be purchased by mail and over the counter in paperback booklet form only.

"Price and Availability List of U.S. Geological Survey Publications," issued annually, is available free of charge in paperback booklet form only.

Selected copies of a monthly catalog "New Publications of the U.S. Geological Survey" are available free of charge by mail or may be obtained over the counter in paperback booklet form only. Those wishing a free subscription to the monthly catalog "New Publications of the U.S. Geological Survey" should write to the U.S. Geological Survey, 582 National Center, Reston, VA 22092.

Note.--Prices of Government publications listed in older catalogs, announcements, and publications may be incorrect. Therefore, the prices charged may differ from the prices in catalogs, announcements, and publications.

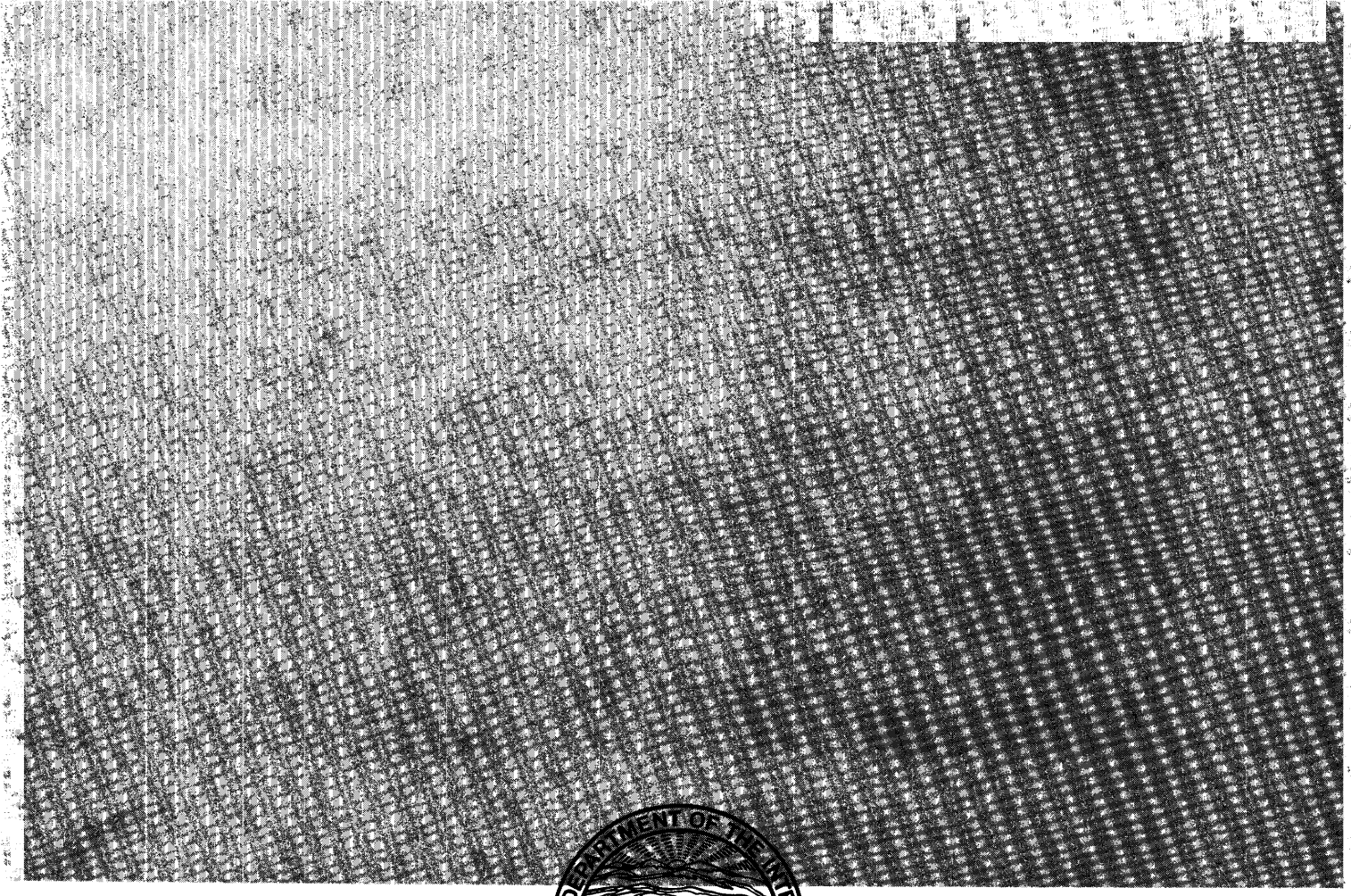


U.S. DEPARTMENT OF THE INTERIOR
MARCH 3, 1849